José J. G. Moura
Isabel Moura
Luisa B. Maia *Editors*

Enzymes for Solving Humankind's Problems

Natural and Artificial Systems in Health, Agriculture, Environment and Energy

Springer

Enzymes for Solving Humankind's Problems

José J. G. Moura • Isabel Moura •
Luisa B. Maia
Editors

Enzymes for Solving Humankind's Problems

Natural and Artificial Systems in Health, Agriculture, Environment and Energy

Springer

Editors
José J. G. Moura
LAQV, REQUIMTE
NOVA School of Science and Technology
Caparica, Portugal

Isabel Moura
LAQV, REQUIMTE
NOVA School of Science and Technology
Caparica, Portugal

Luisa B. Maia
LAQV, REQUIMTE
NOVA School of Science and Technology
Caparica, Portugal

ISBN 978-3-030-58314-9 ISBN 978-3-030-58315-6 (eBook)
https://doi.org/10.1007/978-3-030-58315-6

This Springer imprint is published by the registered company Springer Nature Switzerland AG
The registered company address is: Gewerbestrasse 11, 6330 Cham, Switzerland

Preface

This book is devoted to specific natural and artificial systems that are promising biocatalysts in the areas of health, agriculture, environment and energy. It provides a comprehensive account of the state of the art of selected systems and presents an overview of the significant progress made in the last decade to develop innovative, sustainable and environmentally friendly solutions. The potential use of enzymes for solving humankind's problems is discussed, as well as the key role they play in these processes. Nowadays, we understand well how enzymes work, in terms of structure and function. They are fragile structures made of long chains of amino acids that build up the active sites (with or without metals) and speed reactions and introduce selectivity. A wide range of reactions are carried out at room temperatures and in water, the biological solvent. They participate in a broad range of applications, from environmental to energy industries, chemical transformations, fertilisers, food processing and other significant market niches.

Fifteen chapters in this book provide important and inspiring accounts on the role of enzymes, with a lesson and a message: complex systems, such as the ones here described, can only be unrevealed by the multidisciplinary effort and consortia of many branches of science. During the last years, the ubiquitous utilisation of enzymes has dramatically improved our quality of life, by many relevant scientific discoveries and inventions. Enzymes for solving humankind's problems is a challenge, a vast and actual topic, resulting in the curiosity and the motivation of scientists to make scientific research advances and turn fundamental into applied research. The chapters, here reunited and written by experts, are aligned into four main axes, "Planet Under Carbon Attack" (Part One), "Nitrogen, Too Much of a Vital Resource" (Part Two), "Bio-powering the Future" (Part Three) and "Making Use of Biological Assets" (Part Four), and explore how natural enzymes and artificial systems tackle specific targets such as: climate change, carbon footprint and economy and carbon dioxide utilisation; nitrogen footprint and fixation and nitrous oxide mitigation; hydrogen production, fuel cells and energy from bacteria; biomass transformation and production of added-value compounds, as well as biosensor development.

Climate change, carbon footprint and economy and CO_2 conversion into added-value compounds are the opening topics of this book. Julia Seixas and Francisco Ferreira (Chapter "Carbon Economy and Carbon Footprint") made an

introduction to climate change and the global warming theme. A focus is given to the society transformation required towards carbon neutrality, which demands innovation and new technologies, and promotion of new clean processes. The three following chapters discuss carbon dioxide utilisation. Luisa B. Maia, Isabel Moura, and José J. G. Moura explore the conversion into formate, focusing on formate dehydrogenase enzymes (Chapter "Carbon Dioxide Utilisation—The Formate Route"). After a detailed discussion of the enzyme structure and mechanistic strategies, selected proof-of-concepts of formate dehydrogenase utilisation are discussed. Cristina M. Cordas, José J. G. Moura, Adrián Escapa, and Raúl Mateos explore the topic in an electrochemical perspective, with emphasis in the advantages of selecting reaction products through the applied conditions (Chapter "Carbon Dioxide Utilization—Bioelectrochemical Approaches"). A critical review is made on the economically viability, when compared with traditional industrial methods. The development of metabolically engineered acetogens as biocatalysts for the production of added-value compounds is addressed by Dennis Litty and Volker Müller (Chapter "Acetogenic Bacteria for Biotechnological Applications"), highlighting the recent made progresses towards the utilisation of these organisms as industrial biocatalysts.

Nitrogen biogeochemical cycle and nitrous oxide mitigation encompass the second part of this book. The nitrogen biogeochemical cycle plays a critical role in life on earth, providing nitrogen in available forms to be assimilated by living organism. Yet, the need to produce enough food and to meet the desired economic return is posing a serious environmental problem. In a climate change scenario, Claudia M. d. S. Cordovil, Joana Marinheiro, João Serra, Soraia Cruz, Eve Palmer, Kevin Hicks, and Jan-Willem Erisman discuss the nitrogen footprint and how soil microbial populations are affected, influencing enzyme production and activity, altering organic matter turnover and nutrient cycling (Chapter "Nitrogen Footprints and the Role of Soil Enzymes"). The assembly and function of nitrogenase, the key enzyme responsible for the atmospheric dinitrogen fixation into bioavailable ammonium, are comprehensively described by Chi-Chung Lee, Martin Tillmann Stiebritz, Yilin Hu, and Markus Walter Ribbe (Chapter "Assembly and Function of Nitrogenase"). Nitrous oxide is a greenhouse gas effect and ozone-depleting molecule, and its emission contributes significantly to the climate crises. Jörg Simon discusses nitrous oxide origin beyond denitrification and strategies to mitigate its emissions, including novel strategies for efficient nitrous oxide-respiring micro-organisms (Chapter "Mitigation of Laughing Gas Emissions by Nitrous Oxide Respiring Microorganisms").

The demand for energy in a longed-for fossil-fuel-free, "greener" planet requires the development of alternative energy sources, and bio-energy and dihydrogen production are the following topics in this book. Among the next generation of energy sources, microbial fuel cells have emerged as a promising technology using electroactive micro-organisms as catalysts and specific electron transfer chains (namely multihemecytochromes). Bacterial power, as an alternative energy source, is presented by Bruno M. Fonseca, Ricardo M. Soares, Catarina M. Paquete, and Ricardo O. Louro (Chapter "Bacterial Power: An Alternative Energy Source").

Dihydrogen is indicated as one of the most promising renewable energy sources of the future. Biology and chemistry come, hand by hand, on this important topic. The biological production of dihydrogen (hydrogenases) is discussed by Mónica Martins, Inês A. C. Pereira, Marcos Pita, and Antonio L. De Lacey, who reviewed the advances made in the last decade, including systems based on isolated hydrogenases, as well as those using micro-organisms through dark fermentation processes (Chapter "Biological Production of Hydrogen"). The detailed structural and mechanistic knowledge obtained in natural systems has been used by synthetic chemistry to generate innovative bio-inspired catalysts, as discussed by Marcetta Y. Darensbourg, Erica Lyon Oduaran, Shengda Ding, Allen M. Lunsford, K. Dilshan Kariyawasam Pathirana, Pokhraj Ghosh, and Xuemei Yang (Chapter "Organometallic Chemistry Control of Hydrogenases"). These authors present a reflection about the history of dihydrogen production/consumption that occupied, for several years, a broad range of experimentalists and theoreticians from microbiologists, enzymologists, spectroscopists, crystallographers to both synthetic and computational chemists; organometallic-like chemistry contributions, for modelling and mimicking the hydrogenase active sites and the mechanisms involved, are acknowledged.

The last five chapters are devoted to more focused biotechnological applications developed for the benefit of humankind. The potential for biocatalysts in the chemical industry is particularly exciting, also making an impact in larger-scale operations. Enzyme catalysis can provide stereospecific, most important in a wide range of fields, such as food, pharmaceutical and agricultural, chemical production and energy (besides dihydrogen, bioethanol and biodiesel), clinical diagnostics, environmental, forensic sciences and industrial processing. A great challenge is to create "new enzymes" for commercially relevant chemistries not found in nature. In addition, enzymes are extensively used in (bio)sensors as point-of-care tests, bench instruments or continuous analysis systems in a wide range of applications. Enzymes are by far the most commonly used biological element in biosensors, being typically associated with electrochemical transducers. One of the best examples for the use of enzymes is the so-called biosensors, i.e. a bioanalytical device where enzymes play a key role in the selective recognition of the analyte, as reviewed by Tiago Monteiro, Rosaceleste Zumpano, Célia M. Silveira, and M. Gabriela Almeida (Chapter "Selective Enzymes at the Core of Advanced Electroanalytical Tools: The Bloom of Biosensors"). In this chapter, the topic of enzyme-based biosensors, with special emphasis in the electrochemical ones, is undertaken for four representative classes of enzymes: oxidases, dehydrogenases, reductases and hydrolases. Jean-Pierre Mahy, Frédéric Avenier, Wadih Ghattas, Rémy Ricoux, and Michèle Salmain present current applications of artificial metalloenzymes, describing new class of hybrid catalysts, named artificial metalloenzymes, resulting from the controlled embedding of transition metal species (ions, synthetic inorganic or organometallic complexes) within natural, genetically engineered or even de novo protein scaffolds (Chapter "Current Applications of Artificial Metalloenzymes and Future Developments"). This chapter makes the state of the art on the achievements attained in artificial metalloenzyme design, with

emphasis on industrially relevant chemical reactions, including oxidations, imine reductions, C-C and C-N bond formation, and applications in cascade reactions and in vivo catalysis. New photosynthetic factories for resource recovery, using sustainable methods and circular economy, are discussed by Joana C. Fradinho, Virgínia C. F. Carvalho, and Maria A. M. Reis (Chapter "New Phototrophic Factories for Resource Recovery"). These authors highlighted how phototrophic organisms can contribute to new sustainable practices for pollutant mitigation and recovery of carbon, nitrogen and phosphorus in water treatment plants, while producing added-value products. The recent advances in enzymatic conversion of lignin to added-value products are discussed by Giang-Son Nguyen, Anna Sofia Lewin, Francesca Di Bartolomeo, and Alexander Wentzel (Chapter "Recent Advances in Enzymatic Conversion of Lignin to Value Added Products") that reviewed the microbial sources and the most important classes of ligninolytic enzymes that could be the base of more sustainable, bio-based production processes. In the last chapter of this book, some food-related questions are addressed by Alexandra F. A. Salvado, Jorge H. Leitão, and Luis P. Fonseca that extensively discussed the enzymatic production of bioactive peptides from whey proteins, their active role and potential health benefits (Chapter "Enzymatic Production of Bioactive Peptides from Whey Proteins: Their Active Role and Potential Health Benefits").

All together, fifteen chapters provide an important and inspiring account for the design of new natural and artificial systems with enhanced properties, and it appeals not only to students and researchers working in the fields of energy, health-related, food and environment topics, but also to a wider audience of educated readers that are interested in these up-to-date and exciting subjects.

As a final note, we would like to mention that the reports contained in this book were largely written and organised during the pandemic of coronavirus disease, COVID-19. An enormous acknowledgement is due to all the authors that produced the chapters under difficult times, with many constraints, facing confinement and obliged to deal with their workspaces closed.

Caparica, Portugal
June 2020

José J. G. Moura
Isabel Moura
Luisa B. Maia

Contents

Planet Under Carbon Attack

Carbon Economy and Carbon Footprint

Júlia Seixas and Francisco Ferreira

Abstract

Climate change is a global concern caused by human activities, notably since the industrial revolution. Observed climate changes and evidences of its impacts on natural and human systems have been increased in the last decades, making climate emergency a priority for a growing number of governments, businesses, organizations and individuals. From the 80s of last century, science has supported key political decisions, in particular within the multilateral framework under the United Nations Framework Convention of Climate Change. The Paris Agreement, adopted in 2015, is the central piece to strengthen the global response to tackle climate change, by keeping the global average temperature to well below 2 °C above pre-industrial levels and pursuing efforts to limit the temperature increase to 1.5 °C at the end of this century. This long-term global temperature goal requires a balance between anthropogenic emissions by sources and removals by sinks of greenhouse gases around 2050. The transformation of all human activities towards carbon neutrality demands for high innovation and dedicated instruments and tools. Carbon pricing mechanisms promoting clean technologies and processes, and carbon footprint tools quantifying and delivering emissions reduction from products, organizations, cities and individuals, are explored in this chapter.

Keywords

Climate change · Greenhouse gas emissions · Paris Agreement · Carbon footprint · Carbon pricing · Climate innovation

J. Seixas (✉) · F. Ferreira
CENSE—Center for Environmental and Sustainability Research,
School of Science and Technology, NOVA University of Lisbon, Campus de Caparica,
Caparica, Portugal
e-mail: mjs@fct.unl.pt

J. J. G. Moura et al. (eds.), *Enzymes for Solving Humankind's Problems*,
https://doi.org/10.1007/978-3-030-58315-6_1

1 Introduction

The enormous amount of scientific data on historic evidences of climatic changes and on negative impacts and vulnerabilities observed in diverse natural and human systems justifies the urgency to put the climate change issues central in the social and political agenda. The prospects about those changes for the medium to long-term call for action in all economic sectors in the next decade, making climate change a central challenge for this century. Scientific community, policy makers, business and social media have been increasingly aware of climate change and of means to deal with and solve it, in an unprecedented engagement movement. Starting in 2007, when Al Gore and the International Panel on Climate Change (IPCC) won the Nobel Peace prize, public engagement increased with the adoption of the Paris Agreement [1] in 2016 and come to the front pages in 2018, when Greta Thunberg starts to drag crowds of young people to the streets.

Climate change is a complex issue involving science, economics, society, politics and moral and ethical questions, referring to a global problem, although felt on local scales that will be around for decades and centuries to come. Currently, global average temperature has already increased approximately 1.0 °C above pre-industrial era, due to anthropogenic actions, and there is a high confidence; it likely reaches 1.5 °C between 2030 and 2052 if the current rate will persist [2]. Carbon dioxide (CO_2), methane (CH_4) and nitrous oxide (N_2O) are heat-trapping greenhouse gases (GHG) generated by many human daily activities that have driven recent global warming. Since they linger in the atmosphere for hundreds of years, and the planet, especially the oceans, takes a while to respond to warming, the effects of a changed climate system will last for many years.

Two approaches have been adopted to respond to climate change: mitigation, requiring the reduction of the flow of heat-trapping GHG into the atmosphere, either by reducing sources of these gases (e.g. the burning of fossil fuels for electricity, heat or transport) or enhancing the sinks that accumulate and store these gases (such as the oceans, forests and soil); and adaption, demanding the adjustment to current or expected future climate, in order to reduce the vulnerability of human systems to the harmful effects of climate change, like sea-level encroachment, more intense extreme weather events or food insecurity.

The pressure imposed by communities, scientists, organizations and media, at a certain extent, and especially by the increasing frequency episodes of ice cap melting and unmanageable fires in Australia, California and in Siberia near the Arctic Circle, as occurred during 2019, several countries have asked for a coordinated and timely action. Climate emergency has been propelled by several organizations and governments as a strategy to set priorities to mitigate climate change aiming to prevent, in time, high economic and ecological losses and human lives.

A wide range of options are claimed to deliver climate mitigation across all the economic sectors and human activities, and requesting innovative solutions everywhere, from engineering and technology, to economic models and behaviour changes. As a new orchestra that replaces the old fashion, climate mitigation

requires new instruments, new proficiencies, new melodies and, above all, new conductors. The magnitude and urgency of the problem requires a transformative approach instead of incremental innovation, to achieve a balance between anthropogenic emissions by sources and removals by sinks of GHG by 2050, on the basis of equity, sustainable development and poverty eradication, as stated in the Paris Agreement. That balance is known as carbon neutrality, for which countries and organizations are increasingly working to achieve, as the safe space to manage the stabilization of the climatic system.

Technological innovation is at the heart of the climate mitigation, since historically innovation has brought many low-carbon energy technologies to market readiness today, being renewable energy technologies and electric vehicles prominent examples [3]. Importantly, technological innovations and cost reductions were achieved much faster than expected by analysts. Innovation carrying by many frontrunners in scientific laboratories, start-ups and organizations is pervasive across the fields of energy, industry, health, food and agriculture, and environment. This chapter focuses the attention on the role of climate change mitigation may have as a trigger for innovation. Section 2 describes several climate changes observed, with a focus on 2019, and trends of anthropogenic carbon emissions, while Section 3 presents how carbon emissions reduction is valued through regulatory schemes, favoring non-emitting processes and technologies. Section 4 details the carbon footprint assessment as a tool to manage and reduce carbon emissions in activities, products and technologies, and Section 5 concludes by making future prospects on carbon emissions for the twenty-first century, taking uncertainties around social and technological factors.

2 Carbon Emissions at the Core of Climate Changes

2.1 Climate Changes

The most recent consolidated data [4] showed the global mean temperature for 2019 was around 1.1 ± 0.1 °C above the 1850–1900 baseline, designated as pre-industrial levels. The year 2019 is the second warmest on record, compatible with the range of 0.1–0.3 °C per decade of increasing warming, pointed out by the IPCC [2]. The year 2016 is the warmest on record, due to an exceptionally strong El Niño episode. The five warmest years on record are included in the period 2015–2019, and since the 1980s, each successive decade has been warmer than any prior one since pre-industrial level [4].

Using the global temperature indicator provided by averaging values over successive 60-month periods, Figure 1 shows the long-term trend of this indicator based on five global temperature datasets. That indicator is consistent with the five-yearly stock-take period used by countries to regularly review their progress in limiting GHG emissions under the Paris Agreement of 2015, aiming to curb the rise in global average near-surface temperatures. The 60-month period averaging

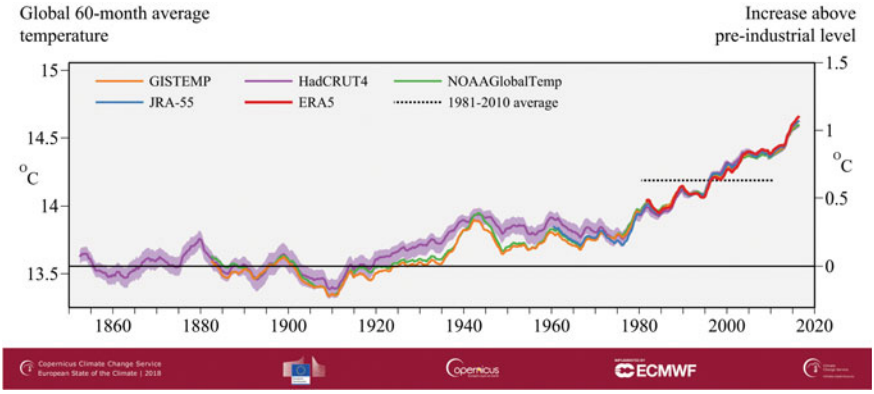

Fig. 1 Running 60-month averages of global air temperature at a height of two metres (left-hand axis) and estimated change since the pre-industrial era (right-hand axis) according to different datasets: ERA5 (Copernicus Climate Change Service (C3S), ECMWF); GISTEMP (NASA); HadCRUT4 (Met Office Hadley Centre), NOAAGlobalTemp (NOAA); and JRA-55 (JMA) Credit Copernicus Climate Change Service (C3S)/ECMWF

reduces the signal from short-term natural variability, such as that associated with El Niño events and volcanic eruptions, and also reduces the differences among the various available temperature datasets. However, longer-term variations in surface air temperature, such as those associated with decadal and multi-decadal oceanic oscillations, are still visible.

Taking the spatial variation of Earth surface temperature, there were variations across the globe in 2019 deserving to be mentioned. For Africa, the year 2019 was among the top three warmest years on record since 1950, while the US State of Alaska was exceptionally warm. Other regions around the planet like large areas of the Arctic, central and eastern Europe, southern Africa, mainland southeast Asia, north-east Asia and also some parts of Brazil were areas of notable warmth for the year. Also, some parts of Australia registered in 2019 the highest temperature and driest values on record.

These temporal and spatial increasing temperature patterns have been causing several impacts in virtually all natural systems, due to changes in ecological related temperature conditions pushing warming to high latitudes and altitude in land, and to in-depth areas in oceans. A large proportion of the heat accumulating in the climate system is embodied in the ocean heat content which contributes more than 30% of observed global mean sea-level rise through thermal expansion of sea water [4]. The occurrences of marine heat waves have substantially grown in the past three decades, increased by just over 54%, a consistent trend with declines in oceans life [5]. Marine heat waves are periods when the average water temperature of a given region is exceptionally high, and it is becoming clearer how deadly warmer temperatures are for biodiversity.

Regarding the rise in the global mean sea level, the loss of ice mass from the ice sheets is the main cause [6]. The loss of Arctic (and sub-Arctic) sea ice is of particular importance with a long-term decline in all months during the satellite monitoring period (1979–present), with the largest relative losses in late summer, September. The Arctic summer minimum daily sea-ice extent (4.15 million km^2) observed in 2019 was the second lowest on record. Antarctic sea-ice extent had shown a small long-term increase until 2016, but in late 2016, a drop in extent to extremely low values was observed and remaining at relatively low levels since then. During 2019, May, June and July were months with record-low monthly extents.

Sea level has been monitored with high-precision altimetry instrumentation since January 1993, providing accurate estimates of an average rise of 3.24 ± 0.3 mm/y, with the rate increasing over that time. In this period, the global mean sea level reached its highest in 2019. Although sea-level rise is not regionally uniform, due to geographical variations in the ocean heat content [7] and to processes involving the atmosphere, geosphere and cryosphere, its influence has been tangible in coastal flood risk areas around the world, particularly when associated with storm surges, putting human settlements and diverse ecosystems at risk of disappearance.

In the last decade, the ocean absorbed around 23% of annual CO_2 emissions [4] which helps to mitigate the impact of climate change. However, CO_2 reacts with seawater which decreases its pH and therefore the acidity of the ocean. Ocean acidity has increased by approximately 25% (decrease of 0.1pH units) since pre-industrial times [8], and observations from open-ocean sources show a clear decrease in average pH in the last 20 to 30 years [4]. This acidification process interferes with the carbonate chemistry that hampers the ability of some marine organisms, as crustacean and corals, to calcify. Marine life is suffering from these effects, with negative effects in the potential for growth and reproduction. The acidification and ocean warming have transformative impacts on coral reef ecosystems, being coral recruits more susceptible to bleaching and death during the warmest months of the year.

The changed climate system has been pushing extreme events for new records, as is the case of heatwaves. A heatwave occurs when the threshold (e.g. maximum daily temperature, P90) is exceeded for at least three consecutive days. The thresholds' value may vary from one place to another, according to the local conditions. Several major heatwaves were registered in 2019. Two heatwaves occurred in Europe in late June and late July were very significant with several records registered. The first one reached its maximum intensity in southern France (national record of 46.0 °C), while the second was more extensive, with national records set in several countries (42.6 °C in Germany, 40.7 °C in the Netherlands, 41.8 °C in Belgium, 40.8 °C in Luxembourg, 38.7 °C in United Kingdom and 33.2 °C in Finland) [4]. These temperature records pose a substantial risk to human health, particularly to elderly, fuel devastating wildfires in vast areas of Siberia, trigger the Greenland ice sheet melting at a near record rate, and increased the risk of drought across wide areas of central and eastern Europe.

Australia should also be mentioned due to an exceptionally hot summer in 2018–2019, affecting most of the country, with the most extreme anomalies occurring in inland New South Wales. January was Australia's hottest month on record, being the mean temperature summer the highest on record by almost 1 °C. A record was broken (46.6 °C) at Adelaide on January. The year 2019 was also notable due to unusual dry conditions, in comparison with long-term means, that together with high temperatures resulted in unfortunate visible impact illustrated by the Australia fires with more than 10.7 million ha of burnt area.

Monsson flooding episodes in 2019 caused high losses either in human lives and financial. India, Nepal, Bangladesh and Myanmar reported over 2 200 lives lost during the season. Also, parts of southern China were affected in June causing 83 deaths and over US$2.5 billion in economic losses, as well as the Islamic Republic of Iran in late March and early April 2019, with 76 deaths and severe economic losses [4]. A large part of the central USA was affected by heavy rainfall in the period July 2018 to June 2019, being the 12-month rainfall averaged over the contiguous USA (962 mm) the highest on record.

Slow-moving tropical cyclones can cause heavy rain because of their duration of influence, as occurred in 2019, at Beira, Mozambique on March with the tropical cyclone Idai. It was moving slowly at landfall, near almost 10 km/h, with satellite-estimated rainfall amounts in excess of 610 mm over much of central Mozambique. Huge portions of the country were submerged for days and over 1,000 people died. Damage was estimated at US$2.2 billion, mostly in Mozambique, whose GDP is just US$12 billion.

On the other hand, most of the Horn of Africa countries experienced exceptional dryness in March and April, with cumulative precipitation estimated to be about 80% below average. These conditions affected several cropping areas, with impacts on planted zones and yields, namely due to fall armyworm infestations. About 22.2 million people (6.7 million in Ethiopia, 3.1 million in Kenya, 2.1 million in Somalia, 4.5 million in South Sudan and 5.8 million in the Sudan) were estimated to be severely food insecure by 2019 [9].

According to IPCC [2], the world is on course to exceed the temperature thresholds of 1.5 °C or 2 °C above pre-industrial levels, as agreed under the Paris Agreement. This could lead the economies to a stage with an increasing risk of pervasive effects of climate change beyond what is of our knowledge. The risk of climate change impacts depends on complex interactions between climate related hazards, exposure and the adaptive capacity of human and natural systems, which differs from one country to another. However, over those global average temperature, the impacts will likely appear on many areas of our everyday lives, as on health, food and water security, human security, human subsistence and income, companies functioning, infrastructure and biodiversity. Climate change has severe implications for ecosystem services and can affect patterns of natural resource use (e.g. more energy use to tackle more frequent and severe heatwaves), as well as the distribution of resources across regions (e.g. Iberia will likely suffer from water shortage exacerbation) and also within countries.

2.2 Global Carbon Emissions

Global CO_2 concentrations in the atmosphere follow the balance between emissions, released through human activities such as deforestation and burning fossil fuels, as well as natural processes such as respiration and volcanic eruptions, and uptake by the biosphere and ocean. During the last 7000 years, prior to 1750, atmospheric CO_2 from ice cores shows only very slow changes (increase) from 260 ppm to 280 ppm, in contrast to the human-caused increase of CO_2 since pre-industrial times. The contribution of CO_2 emissions from early anthropogenic land use is unlikely sufficient to explain the CO_2 increase prior to 1750 [10]. Further back in time, during the past 800,000 years prior to 1750, atmospheric CO_2 varied from 180 ppm during glacial (cold) up to 300 ppm during interglacial (warm) periods.

The levels of heat-trapping GHG in the atmosphere have reached successive new records along the years with no sign of a reversal in this trend. Since 1990, there has been a 41% increase in total radiative forcing—the warming effect on the climate—by long-lived GHG, with CO_2 accounting for about 82% of the increase in radiative forcing over the past decade [11]. In 2018, GHG concentration in the atmosphere reached new maximum values, with globally averaged of CO_2 at 407.8 $\pm$ 0.1 ppm, CH_4 at 1869 $\pm$ 2 ppb and N_2O at 331.1 $\pm$ 0.1 ppb [11], larger than the increases in the ten-year averaged growth rates. The global averaged concentration registered in 2018 represented, 147%, 259% and 123% of pre-industrial (1750) levels for CO_2, CH_4 and N_2O, respectively [11]. The most recent data available, measured at Mauna Loa Observatory, Hawaii, with average seasonal cycle removed, pointed out to 413.03 ppm, at March 17, 2020.

CO_2 remains in the atmosphere for centuries and in the oceans for even longer, meaning future generations will be challenged with increasingly severe impacts of climate change, including rising temperatures, more extreme weather, water stress, sea level rise and disruption to marine and land ecosystems. The increase of atmospheric CO_2 above pre-industrial levels was, initially, primarily caused by the release of carbon to the atmosphere from deforestation and other land use change activities [10], while emissions from fossil fuels, started before the Industrial Era, became the dominant source of anthropogenic emissions to the atmosphere from around 1950, and their relative share has continued to increase until present, as Fig. 2 illustrates for the decade 2009–2018. Anthropogenic emissions occur on top of an active natural carbon cycle that circulates carbon between the reservoirs of the atmosphere, ocean and terrestrial biosphere on timescales from sub-daily to millennia, while exchanges with geologic reservoirs occur at longer timescales. Archer [12] showed that 20–35% of the CO_2 remains in the atmosphere after equilibration with the ocean (2–20 centuries).

The global carbon budget averaged over the last half-century (1959–2018), revealed 82% of the total emissions were caused by fossil CO_2 emissions and 18% by land use change [13]. The total CO_2 emissions were partitioned among the atmosphere, ocean and land, meaning that 24% were absorbed by the oceans, 29% by the terrestrial biosphere and 45% remained in the atmosphere, while 2% of the

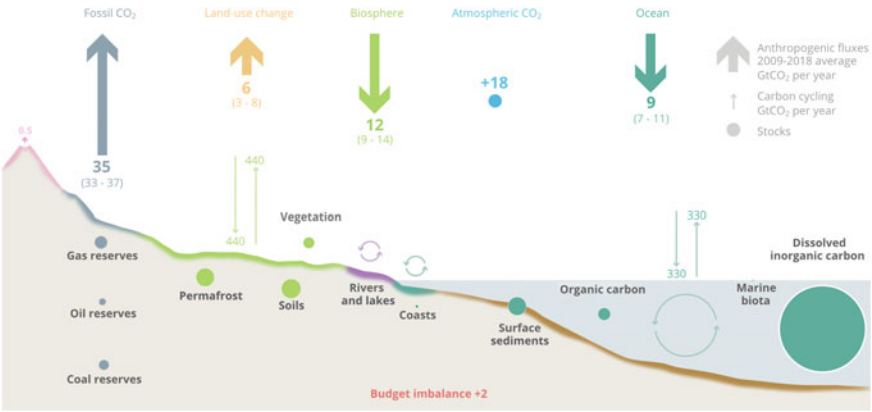

Fig. 2 Perturbation of the global carbon cycle caused by anthropogenic activities averaged globally for the decade 2009–2018 ($GtCO_2$/yr) Credit Global Carbon Project 2019

emissions does not match to any component (i.e. budget imbalance), according to the used assessment tools.

Global CO_2 emissions increased from 2 billion tonnes of carbon dioxide in 1900 to over 36 billion tonnes 115 years later [14]. Since 1960, a positive growth trend of global CO_2 emissions has been observed, as shown in Fig. 3, with the 2008 global crisis meaning nothing but a year small decrease, completely offset in the following year, mostly buy non-OECD countries. Global fossil CO_2 emissions grew at 1% per

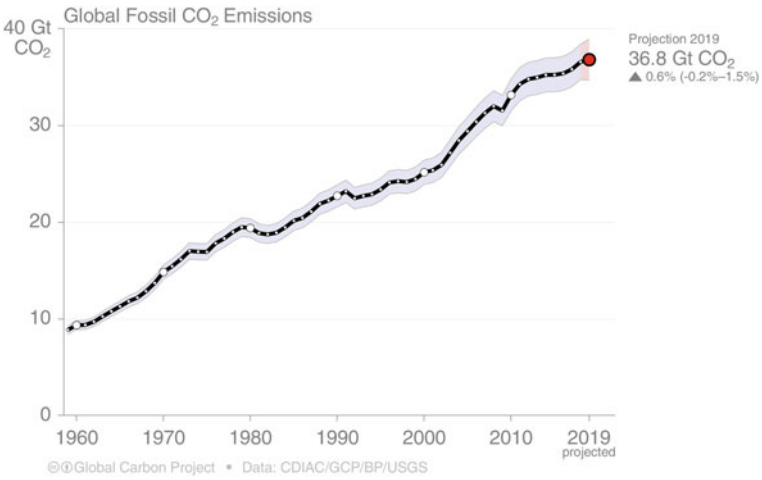

Fig. 3 Global fossil CO_2 emissions estimated for the period 1960–2018 (2019 refers to a projection estimate) *Source* Global Carbon Project (2019)

year in the 1990s, accelerated to 2.9% per year in the 2000s, but have returned to a slower growth rate of 0.9% per year since 2010 with a more pronounced slowdown from 2014 to 2016 [15].

Over the last decade (2009–2018), 42% of fossil CO_2 emissions were from coal, 34% from oil, 19% from natural gas, and the remaining 5% from cement and other smaller sources. From the perspective of the use of these fossil fuels, 45% of fossil CO_2 emissions come from the energy sector, dominated by electricity and heat production, while industry sectors, such as metals production, chemicals and manufacturing, cover 22% of global emissions, land transport combined with national shipping and aviation contribute 20% of global emissions, international shipping and aviation 40 add another 3.7%, and the remaining 10% is from buildings, agriculture, fishing and other sectors [15].

Despite modest declines in emissions in the USA and the European Union over the last decade, the growth in emissions in China, India and most developing countries has dominated global emission trends over the last 20 years. Main determinants for these trends [16] include the increasing use of coal in developing countries, pushing by increasing built infrastructures, and the increasing use of gas in developed countries, counterbalanced by low-carbon energy options, pushed by public policies. The share of fossil fuel in global primary energy consumption has remained steady since 1990.

China has become the largest CO_2 emitter in the world and presently accounts for 30% of global emissions. Major drivers of energy-related CO_2 emissions in China from 1978 when the reform and opening-up policy was launched include primarily economic growth (176%) followed by population growth (16%), while the effects of energy intensity (−79%) and carbon intensity (−13%) slowed the growth of carbon emissions over most of this period [17]. Energy intensity stands for the amount of energy per unit of GDP, while carbon intensity refers to the emissions per unit of energy consumed. Energy efficiency may condition the former while the share of renewables determines the later.

On the opposite trend, displacement of fossil fuels by renewable energy and decreases in energy use explain the decreasing CO_2 emissions in a group of 18 developed economies that have decarbonized over the period 2005–2015 [18]. Correlation analysis suggested that policies on renewable energy are supporting emissions reductions and displacing fossil fuels, while policies on energy efficiency are supporting lower energy use in those 18 countries.

Regarding the CO_2 emissions from land use change, there is no clear trend over the last decade, though the data are very uncertain [13]. The terrestrial CO_2 sink increased from 1.3±0.4 GtC yr−1 in the 1960s to 3.2±0.7 GtC yr−1 during 2009–2018, with important interannual variations, generally showing a decreased land sink during El Niño events. The total atmosphere-to-land carbon fluxes increased from a 0.2±0.8 GtC yr−1 source in the 1960s to a 1.7±0.9 GtC yr−1 sink during 2009–2018, meaning the biosphere increased its ability to sequester CO_2 from the atmosphere in that time period.

According to IPCC (2018), there is a high confidence that global warming is expected to surpass 1.5°C above pre-industrial levels with the expected GHG

emissions in 2030 from current pledges under the Paris Agreement (known as nationally determined contributions, or NDC). Limiting warming to 1.5°C requires lowering GHG emissions in 2030 down to net zero CO_2 emissions globally around 2050, as well as deep reductions in emissions of non-CO_2 forcers, particularly methane. How to transform the global economy towards this goal is the upmost important question of our time life.

3 Tackling Climate Change: From Science to Political Decisions

Climate change is a global problem with causes from all economic sectors in all countries, and therefore, it should be tackled at a global level as well. The formal process at the United Nations level started at the end of the eighties of last century, when IPCC was established in 1988 by the United Nations Environment Programme (UNEP) and the World Meteorological Organization (WMO). The goal of the IPCC was to provide up-to-date periodic assessments in the form of reports on the science, the emissions, and the current and future impacts for different mitigation scenarios that could be implemented, and the corresponding adaptation measures required. In 1992, climate change was tackled through a multilateral framework, the United Nations Framework Convention on Climate Change (UNFCCC), which entered into force in 1994 being currently with 197 Parties (i.e. nations). The Convention sets a lofty but specific goal: to stabilize greenhouse gas concentrations "at a level that would prevent dangerous anthropogenic (human induced) interference with the climate system", stating that "such a level should be achieved within a time-frame sufficient to allow ecosystems to adapt naturally to climate change, to ensure that food production is not threatened, and to enable economic development to proceed in a sustainable manner".

During the last 25 years, the UNFCCC [19] has becoming the arena welcoming the highest environmental diplomacy ever take. Specific regulatory instruments have been adopted, like the Kyoto Protocol (in force from 2005 to 2012) that launched the roots for new worldwide harmonized processes, like the national greenhouse gas national inventories based on common methodologies, the so-called carbon economy supported in market mechanisms, and the setting of climate funds to support climate adaptation in developing countries, to refer only three examples. Figure 4 presents the relationships between the science supporting information from the IPCC and the political decisions taken on the basis of the different assessment reports. The first report triggered the creation of the UNFCCC in Rio de Janeiro during ECO/92. The major Protocol of the Convention was signed two years after the second report. Unfortunately, in 2009, a global agreement with higher mitigation targets for the developed countries, with the inclusion of nations that did not ratified the Kyoto Protocol, such as the USA, was unsuccessful. Two years after the launch of the fifth assessment report, where the evidences on

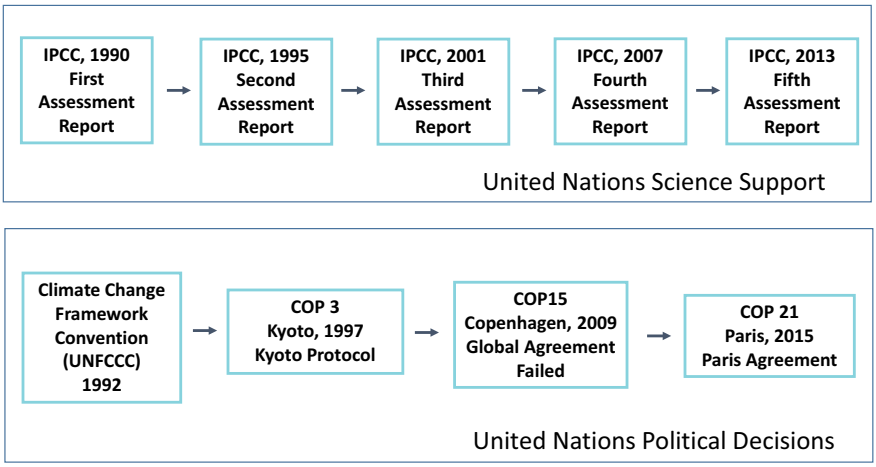

Fig. 4 Interactive progress between the United Nations political progress and the scientific support from the Intergovernmental panel on climate change until the Paris Agreement

greenhouse gas emissions trends and climate change impacts and consequences were overwhelming, the Paris Agreement was signed.

The Paris Agreement was conceptualized as a bottom-up running process, with all the countries subjected to targets previously set by each one of them (namely, the NDC), with a periodic five-year downward emission's revision. Concerning the goals of the Paris Agreement, three paragraphs are the most important: number 2 of article 2 states the main goal to "holding the increase in the global average temperature to well below 2 °C above pre-industrial levels and pursuing efforts to limit the temperature increase to 1.5 °C above pre-industrial levels, recognizing that this would significantly reduce the risks and impacts of climate change"; number 2 of article 4 states that "Parties aim to reach global peaking of greenhouse gas emissions as soon as possible, recognizing that peaking will take longer for developing country Parties, and to undertake rapid reductions thereafter in accordance with best available science, so as to achieve a balance between anthropogenic emissions by sources and removals by sinks of greenhouse gases in the second half of this century, on the basis of equity, and in the context of sustainable development and efforts to eradicate poverty"; and number 9 of the same article 4 mentions the fact that "each Party shall communicate a nationally determined contribution every five years", as part of the overall target's revision already mentioned [1].

The Paris Agreement, in force since 2016 and ratified by 189 Parties, requires all Parties to put forward their best efforts through nationally determined contributions (NDC) setting specific emission reduction goals, and every five years, a global stocktake will assess the collective progress towards achieving the purpose of the Agreement. The Agreement provides a long-term vision (until the mid of the century) which motivates and demands all nations for a long-term political goal to

achieve the balance between anthropogenic emissions by sources and removals by sinks of greenhouse gases, also referred as carbon neutrality.

Under the Paris Agreement, a particular IPCC report was scheduled for 2018 to answer if it was still viable to engage in a scenario where a limit of 1.5 °C warming compared with pre-industrial temperature level and what policies and measures would have to be applied. Four scenarios were developed showing that it is still possible to fulfil the Paris Agreement goal and that the costs of early action would pay off the costs of inaction, particularly when the costs for developing countries are considered. Also, a comparison between a 2 °C and a 1.5 °C warming impact scenarios was performed, with a clear social and economic benefit for the lower warming scenario. Figure 5 presents the timeline from the Paris Agreement to the next COP 26 in 2021, where new revised NDC will be submitted and the interactions with the scientific work conducted by the IPCC, calling for more ambitious mitigation actions [2], and expanding the climate change impacts on desertification, land degradation and terrestrial ecosystems [20], and on the ocean and cryosphere [21].

The summing up of the so-called NDC for the total number of countries, as currently submitted to UNFCCC, would lead to a global mean temperature rise between 2.9 °C and 3.4 °C by 2100 relative to pre-industrial levels, and continuing thereafter [22]. Also, based on the same data, it is clear that global emissions are not estimated to peak before 2030. The current level of NDC ambition needs to be roughly tripled for emission reduction to be in line with the 2 °C goal and increased fivefold for the 1.5 °C goal. The Emissions Gap Report [23] is the most relevant document to put into perspective the information available both from the scientific and the international policy levels from recent years concerning GHG emissions and the needs to provide a "transformational change and just transition". The total

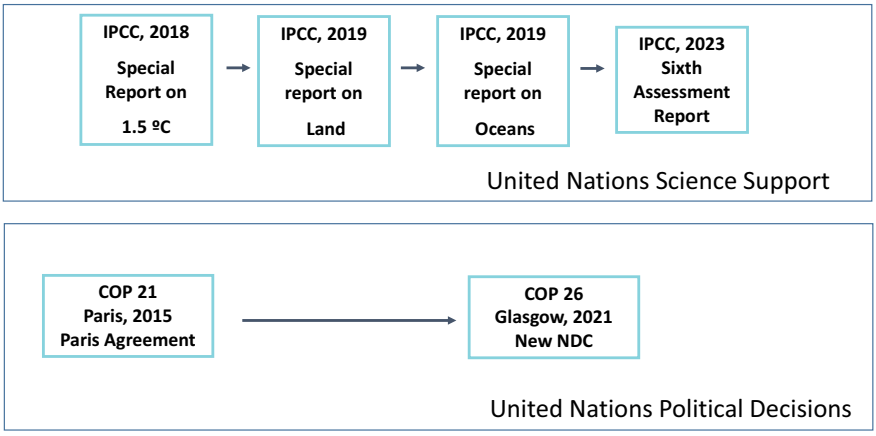

Fig. 5 Interactive progress between the United Nations political progress and the scientific support from the Intergovernmental panel on climate change after the Paris Agreement

global GHG emissions hit a new record of 55.3 $GtCO_2e$ in 2018, including land use change, being 68% from fossil fuels use. To assure that warming stays below 2 °C or 1.5 °C, emissions by 2030 have to be 25 or 55% lower than in 2018, respectively [23]. For 2030, assuming the implementation of all unconditional NDC (i.e. implementable by countries without external support), the emissions gap between estimated total global emissions a 2 °C and 1.5 °C pathways results in a gap of 15 $GtCO_2e$ and 32 $GtCO_2e$, respectively [23].

Several Parties are developing national and regional (e.g. European Union) borne instruments to deliver how carbon neutrality may be achieved up to 2050. The European Union, France, Canada, Japan, United Kingdom, Portugal and Germany among others have already delivered to the UNFCCC their long-term strategies, with the commitment to achieve a balance a balance between anthropogenic emissions by sources and removals by sinks of greenhouse gases in the second half of this century.

The European Green Deal [24] settles a sound vision for the European Union member states, asking for an economies' transition towards their carbon neutrality by 2050. A set of specific regulatory instruments are proposed to be adopted, like a climate law enshrining the 2050 climate neutrality objective, a revision of the Energy Taxation Directive, and relevant legislative measures to deliver on the increased climate ambition, like the review of the Emissions Trading System Directive; Effort Sharing Regulation; land use, land use change and forestry regulation; Energy Efficiency Directive; Renewable Energy Directive; CO_2 emissions performance standards for cars and vans. This regulatory plethora will demand for innovation in all economic sectors and processes, to deliver carbon neutrality and not an incremental emissions reduction.

Even without delivering long-term strategies yet, many countries are being implemented diverse instruments to reduce emissions, like the China national carbon pricing scheme, the India investments on renewable energy and the zero emission vehicle programs adopted by 14 states in the USA. The regulation of GHG emissions from the UNFCCC multilateral framework down to the country level is a corner stone to tackle climate change, for three reasons: it gives a long-term perspective, which is essential to secure investments; it sets the problem solving worldwide, which is a requirement to avoid carbon leakage (i.e. businesses transfer production to other countries with laxer emission constraints); and it gives a high common ambition, which stimulates innovation demanding high levels of investment for R and DD. Achieving carbon neutrality worldwide while promoting economic development and new jobs has been a common understanding of carbon regulation.

To avoid catastrophic consequences from climate change, the world has to considerably increase its efforts to reduce GHG emissions through a decarbonisation of the global economy while respecting sustainable development principles and benefiting both the humanity and the planetary system. The Paris Agreement do have moderately positive conditions to overcome the so-called effectiveness trilemma, providing participation, ambition and also compliance as a mitigation mechanism towards a global solution for climate change [25].

4 Carbon Emissions Reduction

Reducing anthropogenic GHG emissions or carbon emissions for short is key to prevent a worst future scenario, where life could become a difficult and costly task for everyone in Earth. This section presents briefly how carbon emissions are being tackled aiming to control them into a decreasing trend towards its almost disappearance at the mid of this century, which gives humanity a good chance to control the Earth climate up to an increase of 1.5 °C or 2 °C above pre-industrial levels.

4.1 Carbon Pricing and Climate Mitigation Policies

Greenhouse gas emissions are released by millions of stationary and mobile sources worldwide present in all economic sectors, from energy to manufacture industries, agriculture to forestry and fishing, buildings and transports. The release of GHG emissions has been occurred since the industrial revolution, until recently when the need to control them for the sake of climate stabilization was assumed by the UNFCCC [19]. Since there is no end-of-pipe commercial solution available to reduce carbon emissions from those million sources, the approach to value carbon emissions reductions through specific market mechanisms was adopted under the Kyoto Protocol (approved in 1997).

The rationale behind a carbon price, i.e. putting a price on the carbon emissions released from a specific activity, is to capture its external costs, related with the negative impacts of climate change like the damage to crops from droughts or floods, health effects from heatwaves, damage to properties and infrastructures from sea level rise to name few examples. Public pays these costs in other ways and carbon pricing tie them to the respective activities' sources.

A carbon price gives an economic signal and emitters decide whether to discontinue or change their activity, reduce emissions through new processes or adopting low-carbon energy sources, or continue emitting and pay for it. Put a price on carbon emissions has been revealed the most flexible and least-cost way to society, because usually the activities deciding to shift tend to be those where it is most cost-effective. The carbon price stimulates new clean technologies and new processes, and market innovation, conducting to cleaner economic production and consumption models.

There are a multitude of carbon pricing schemes, applied directly oy indirectly to carbon emissions. The most known and increasingly applied worldwide are the emissions trading systems (ETS) and carbon taxes, both usually regulated by public policies. An ETS, also referred to as a cap-and-trade system, caps the total amount of greenhouse gas emissions that can be emitted by installations covered by the system. Within the cap, companies receive or buy emission allowances, which they can trade with one another as needed, i.e. industries with low emissions may sell their extra allowances to larger emitters. By creating supply and demand for emissions allowances, an ETS establishes a market price for greenhouse gas

emissions. The cap is reduced over time so that total emissions fall, providing certainty in global emissions reduction. Usually, after each year, a company must surrender enough allowances to cover all its emissions; otherwise, heavy fines are imposed. Trading brings flexibility that ensures emissions are cut where it costs least to do so. Both the cap and the rules to attribute allowances to the installations covered by the scheme is under the responsibility of a governance body, mostly from public policies like the European Commission for the EU ETS, the Ministry for Ecology and Environment for the China National ETS, or the Regional Greenhouse Gas Initiative for the nine states of Connecticut, Delaware, Maine, Maryland, Massachusetts, New Hampshire, New York, Rhode Island and Vermont. A carbon tax sets a price on carbon by defining a tax rate on GHG emissions or on the carbon content of fossil fuels. In this case, the emission reduction outcome is not pre-defined (as in the case of a cap) but the carbon price is.

Governments are increasingly recognizing carbon pricing as a key policy instrument to meet climate mitigation targets. Of the 185 Parties that have submitted their nationally determined contributions (NDCs) to the Paris Agreement, 96 representing 55% of global GHG emissions have stated that they are planning or considering the use of carbon pricing as a tool to meet their commitments [26]. Although many jurisdictions are broadening (increasing emission coverage) and deepening (increasing prices or stringency) their carbon pricing instruments to better align with their climate goals, these efforts are insufficient, as less than 5% of global emissions covered under carbon pricing initiatives, are priced at a level consistent with achieving the goals of the Paris Agreement, i.e. US\$40/tCO_2 to US \$80/tCO_2 by 2020 and US\$50/tCO_2 to US\$100/tCO_2 by 2030. Notably, about half of the emissions covered by carbon pricing initiatives are still priced below US \$10/tCO_2 [26]. A robust carbon price may promote the investment in clean, low-carbon technologies because makes high-carbon ones more expensive and then less competitive.

There are also more indirect ways of pricing carbon, such as through fuel taxes, the removal of fossil fuel subsidies, or through payments for emission reductions. Beyond regulated or compliance markets or instruments, there are also voluntary markets where private entities can purchase emission reductions to offset their own emissions, or to support mitigation activities through results-based finance.

Experience in many countries shows that carbon pricing is cost-effective in reducing GHG emissions. However, other elements of climate mitigation policies should complement carbon pricing schemes to accelerate the transition to carbon neutrality by the mid of this century, as stated in the Paris Agreement. These may include setting fuel efficiency standards for vehicles, imposing energy-efficient building codes, promoting urban designs that encourage public transport and less use of personal vehicles, incentivizing renewables, electric vehicles and the charging infrastructure, or phasing out the use of coal as a fuel in power plants, and ultimately supporting R and D policies. The way governments choose to disburse carbon revenues has a considerable impact on reducing emissions [27], with many allocating them in varied mitigation initiatives, like subsidizing the public transportation modes.

The Paris Agreement represented a paradigm shift from cost-minimizing to opportunity-seizing, and thus from a focus on emissions to a focus on technologies [3]. With the increased competitiveness of low-carbon technologies, policymakers increasingly recognize the potential to create local industries and jobs around them, leading to strong incentives for ambitious national and subnational policies. Understanding the technology–politics feedback link may provide more realistic and transformative recommendations for climate and energy policy design, which are currently often lacking. The new technologies and processes as those tackled in this book, as hydrogen production, carbon dioxide utilization, methane utilization, biomass-based added-value compounds, fuel cells or energy from bacteria, clearly benefit from the focus on technologies, for which carbon pricing and other climate mitigation policies may condition its R and D and deployment. Therefore, assessing its carbon footprint is of upmost importance to avoid carbon burdens when entering the market.

4.2 Carbon Footprint Assessment

4.2.1 Concept

Historically, the concept of carbon footprint can be considered as a subset of the so-called ecological footprint developed by Wackernagel [28] under his PhD studies in the beginning of the 1990s. The book published afterwards by Wackernagel and Rees [29] was a key document explaining the concept and the methodology of calculation, but particularly alerting the world to the unsustainable way, humans were using their resources in relation to the production by the ecosystems to renew them. The ecological footprint applied to a certain area, with an associated number of inhabitants (from a city to the whole planet but with a particular emphasis to the country level), evaluates the amount of space required to provide the resources demand from the population, from food to infrastructure, to carbon dioxide absorption resulting from anthropogenic activities. Products require a certain area of bioproductive land. Therefore, the concept of biocapacity, stating for the area of land and sea required to supply the resources for human activity and to process its wastes, is key within the ecological footprint methodology. This area is standardized according to its biological productivity and expressed in “global hectares” [30]. Trade can be also incorporated in the methodology by taking into account the flows of resources between areas, particularly between countries. Figure 6 illustrates the rationale of the ecological footprint calculation.

The ecological impact of human activity can be assessed by calculating the balance between the biocapacity and the ecological footprint of consumption within the boundaries considered. Depending on the outcome, a country can be considered as a creditor if the result is positive, and as a debtor if the result is negative, meaning that the renewable resources provided within the established area are not sufficient to assure the amounts taken by the population. This assessment can be applied at the local level, as provided for the case of several municipalities in Portugal [31], at the country level or even for the overall planet, as shown in Fig. 7.

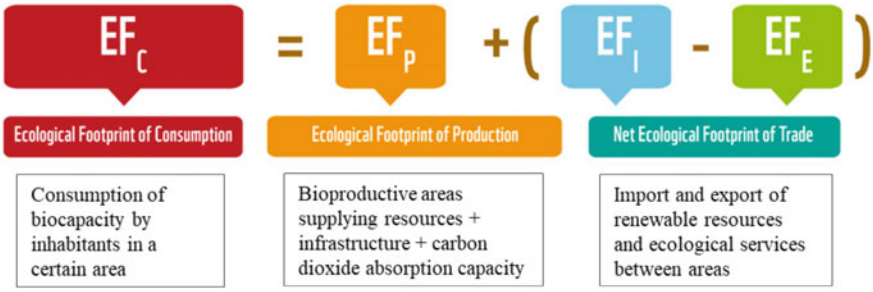

Fig. 6 Calculation of the ecological footprint of consumption (adapted with permission from [30])

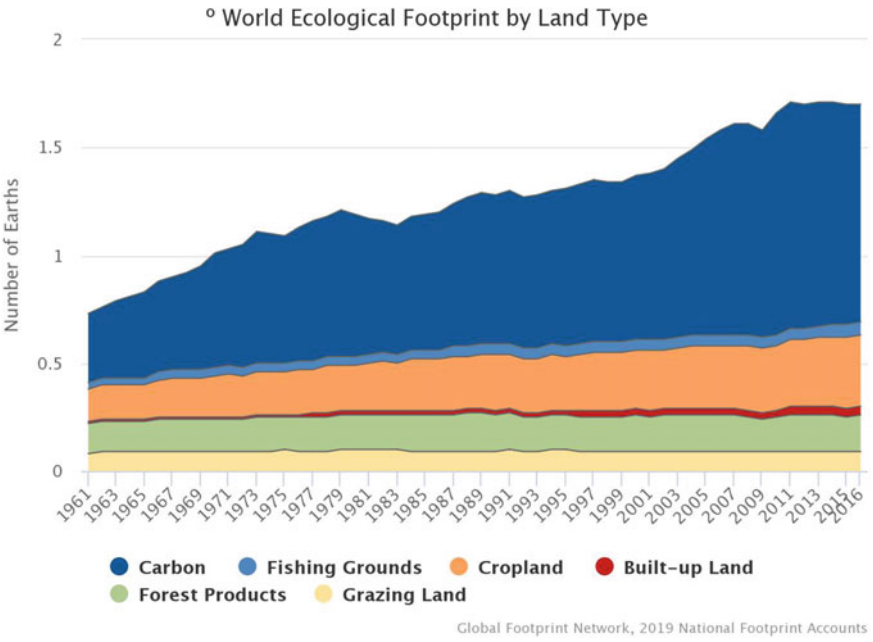

Fig. 7 Evolution of number of planets required based on the renewable resources required by the world population throughout the years based on the ecological footprint approach.(Credit GFP 2020)

Under the context of the ecological footprint approach, the carbon footprint is the area used for assimilating the carbon dioxide emitted by human activities. However, with the increased relevance of climate change along the last few decades, the concept of carbon footprint was individualized and framed into a different form. While the footprint idea remained as a key mark, it evolved to a global

warming potential contribution. A definition of carbon footprint could be "a measure of the exclusive total amount of carbon dioxide emissions that is directly and indirectly caused by an activity or is accumulated over the life stages of a product [32]". The carbon footprint may include the carbon dioxide emissions only or other greenhouse gases such as methane, nitrous oxide or fluorinated gases.

A well-structured view of the carbon footprint concept can be framed in terms of content, significance, evolution, calculation and application [33]. The carbon footprint can be defined as "the quantity of greenhouse gas expressed in terms of CO_2-equivalent, emitted into the atmosphere by an individual, organization, process, product or event from within a specified boundary [33]". The carbon footprint has been a relevant tool for organizations and businesses, more than as an object of extended research within the scientific community.

The carbon footprint calculation gained maturity throughout the time and enlarged its application. Currently, two approaches are commonly used—one based on a life-cycle assessment, based on production and/or consumption based accounting systems with inventory methods such as life-cycle analysis (LCA) and/or environmental input–output analysis (EIOA), and another where a territorial accounting system is considered, usually a city or a country, using traditional emission inventory methods with different scopes taking into account the so-called direct only and direct and indirect emissions, respectively [34].

For the first approach, a common and transparent methodology that would state how to incorporate both direct and indirect emissions and the different steps related with the production of materials or equipment (life cycle and/or use only) have been required and determinant for a proper evaluation of the emissions associated. The definition of boundaries is one of the most critical issues on evaluating the carbon footprint. The role of upstream and downstream emissions, the incorporation of direct greenhouse gas emissions associated with the operation of equipment owned by a company, and the consideration of indirect emissions from carbon dioxide associated with electricity used need clear rules to provide a proper inventory. Comparisons can only be performed if standardized calculations are performed over different products and corporations.

An extended research was recently performed on the use of the carbon footprint concept, mapping its history based on literature citation, and identifying research hotspots, frontiers and features [35]. Besides measuring the impact on global warming, the carbon footprint enables the identification of opportunities for mitigation measures, both from a product and a process view, evaluating improvement efficiencies that can be translated in considerable profit benefits from materials and energy use.

The concept of carbon footprint has been used, not only with different meanings, but also under similar names, and applied to various contexts, rising concerns of clarity, transparency of use and uncertainty issues. Therefore, under each application, the assumptions behind should be clearly stated.

4.2.2 Individual Carbon Footprint

The individual carbon footprint can be used under a customized version where each of the individual input specific information relates with his consumption options. However, at the global level, the calculation of country per capita greenhouse emissions is often used to access and compare energy use and lifestyles. Under this analysis, one cannot decouple the differences within the population of each country or identifying specificities of the role of different sectors within the footprint, from product consumption levels to mobility, food or housing. Also, the final per capita number is highly dependent on the energy sources used by each country, with higher values related with extensive use of fossil fuels.

As a curiosity, members involved in so-called grassroots initiatives, directly related with consumption and lifestyles, do show a carbon footprint 16% lower than non-members within the same sociodemographic context, particularly due to significant reduced percentages in food and clothing (43% and 86%, respectively) [36]. At the same time, those *greener* members are also reflected in a more positive life satisfaction (11–13%) compared with non-members [36]. Communicating the concept of the individual carbon footprint to others in order to make them aware of low-carbon behaviours requires credibility and transparency of the messenger or communicator [37]. In many developed countries, the footprint is already high, and then it is very difficult to achieve significant reductions. A combination of societal and individual efforts is often required to attain the desired pathway towards a lower carbon impact [37].

4.2.3 Urban Scale

The quantification of a city's carbon footprint is quite important with a roadmap for a low-carbon future, since their supply chains are responsible for considerable carbon mitigation measures. Around 70% of the worldwide population will live in urban areas by 2050, taking 80% of the energy consumption and over 60% of the greenhouse gas emissions [37]. Also, the reporting of different strategies developed by different cities can be considered an added value for benchmarking of climate policies. The Urban Carbon Footprint (UCF), with the proper accountability, inventory, and dissemination methods, is a key tool, either for decision-makers and stakeholders at the municipal level [34]. The carbon footprint at the city level can be developed based on the two approaches already described, either based on the concept of a traditional emission inventory of the direct emissions within the city or involving also the indirect emissions associated within a certain boundaries or in a more complex form where the urban system is conceptualized in a production-consumption basis [38].

Worldwide, there are several cities that have been announcing GHG reduction commitments, from a few years ago to 2020, and currently to 2030, 2050 and even up to the year 2070. These municipalities have been working under institutional platforms such as the C40 Cities Climate Leadership Group that, by May 2020, combined 96 large cities in more than 100 countries, responsible for 25% of the world GDP, the ICLEI Local Governments for Sustainability, a global network of more than 1750 local and regional governments committed to sustainable urban

development. One of the limitations of the urban level is the current lack of standardization, since there are different frameworks such as Relative Carbon Footprint —RCF, Publicly Available Specification—PAS 2070 and Global Protocol for Community scale—GPC [34].

The city's carbon footprint depends on the boundaries considered [39]. From input–output tables, calculated for both a single-regional and a multi-regional level, the incorporation of fossil fuels in the city carbon matrix can be much larger when a larger spatial scale is defined, broadening the scope of the analysis and corresponding to a more realistic application of the footprint methodology. For consistency and comparison purposes to correctly support decision-makers, it is important to establish requirements for these input–output tables, from national to regional levels, in order to capture the interlinkages of greenhouse reduction measures and avoid unacceptable errors due to inconsistent boundaries setting [40]. The calculation of the carbon footprint at the urban scale requires a difficult collection of data, increased by the complexity of allocating emissions among the different sources, from citizens to economic activities [34].

4.2.4 Country Scale

At the country level, the carbon footprint is usually based on a territorial approach where the calculations of emissions and removals of GHG within the country are compiled in an inventory that is communicated to the United Nations Framework Convention on Climate Change, to be properly assessed and compared. They have to follow strict and precise methodological rules from the Intergovernmental Panel on Climate Change, also incorporated in the inventory specifications of the European Environmental Agency and the US Environmental Protection Agency.

One of the main objectives under an inventory of the GHG emissions is the quantification of the efforts to lower carbon emissions through measures being implemented. In most cases, countries have set obligatory or indicative targets to comply with. In all these cases, a baseline year is required according to the international agreement considered. This might confuse comparisons and will give a biased perspective that requires caution and carefulness when evaluating numbers with different start and end dates.

4.2.5 Carbon Footprint for Organizations and Products

The carbon footprint of an organization or a product follows different processes. While for an organization, the calculations are based in the activities throughout different scopes, from direct emissions to a broader boundary including indirect and related emissions supporting the work of the organization, for a product, a production to consumption life-cycle analysis prevails. Two international initiatives, the "Carbon Trust" and the "Greenhouse Gas Protocol" (GHG Protocol), have been fundamental for the credibility of the application of the carbon footprint concept to products or services [41], and to organizations or businesses [42], respectively.

The Carbon Trust makes the calculation of the total global warming emissions expressed in carbon dioxide equivalents (CO_2e) of the life cycle of a product or service, from the extraction of its raw materials to end of life. They usually consider

two scopes for the carbon footprint calculation, one accounting for the emissions from the extraction of raw materials to the factory gate (known as cradle-to-gate) and another including the previous track but goes beyond the product's manufacture down to the consumer use and disposal (cradle-to-grave) [41]. Moreover, since 2007 this organization developed a process ending in certified carbon footprint labels that run from just stating that emissions were measured and certified to commitments by the manufacturer to reduce emissions, to including that the product has lower emissions compared with the average or even that the product becomes carbon neutral through the offset of its already low emissions.

The Greenhouse Gas Protocol, or GHG Protocol, was built from a partnership between World Resources Institute (WRI) and the World Business Council for Sustainable Development (WBCSD). It calculates the carbon footprint of companies and organizations through a comprehensive global standardized procedure that measures GHG emissions and enables future policies and measures to reduce them, associated with operations, value chains and mitigation actions [42].

The GHG Protocol developed the Corporate Standard in 2001 that has been updated for different scopes and to include direct and indirect emissions, such as the use of electricity. The Protocol considers three tiers: tier I includes all direct emissions, mostly onsite emissions or emissions from equipment owned by the organization; tier II refers to the energy purchased by the organization (mostly electricity but can be also steam); tier III corresponds to all the indirect emissions, from those associated with transport of input materials, products sold, disposal of products and other activities not included in the previous tiers [42]. Tier III emissions are the most difficult to be considered in a standard form because of their broadness. It is upon selection criteria such as the relevance of the emission sources or the interest of the stakeholders that those tier III components should be selected in case it is impossible n a cost-benefit basis to evaluate them all. Also, as a large part of these emissions stand further away from a direct responsibility of the organization, it is always questionable how they can be manageable by the organization. Relevant issues such as the accuracy of the emissions inventory of the organization and the consideration of data quality aspects have to be considered. As for Carbon Trust, in terms of product, the GHG Protocol also developed tools to measure the benefits of climate change policies and measures.

The environmental track record of corporations became a key factor for the selection of products and a relevant accountability criteria. As part of the market systems transparency and procurement rules, many businesses started to disclosure their carbon accounts through the Carbon Disclosure Project that developed environmental reporting rules and best-practice recommendations [43]. Activities within the context of corporate social responsibility taken by companies regarding the effort to reduce their carbon footprint can be widely communicated, ranging from the products to mobility related actions [44].

A carbon footprint label would influence the purchasing options of the consumers who are getting more concerned with climate change. However, price continues to be the main decision factor and the carbon emissions that mostly concern the consumer are the ones associated with the transportation and disposal

stages and not as much with production. Also, consumers prefer that the company takes care of the responsibility for the emissions of the product even in terms of usage, eventually through off-setting, than that responsibility being assumed by themselves [45]. Consumers may appreciate carbon footprint labels but they would be more effective when combined with lower or equal prices of conventional products [46]. Another use of the carbon footprint concept that has been broadly expanded is associated with its calculation for a large variety of services and events in different businesses and other organizations, with a higher visibility in the case of sporting events such as the Olympic Games, starting particularly with the London Olympics where a lot of measures concerning transportation of construction materials, energy use and the athlete's participation were conditioned by a low-carbon strategy effort.

4.2.6 Carbon Footprint ISO Standards and Calculators

At both the organization level and project level, an international standard was developed (ISO 14064) with two parts associated with each of the two components, respectively. ISO 14064-1:2018 includes all the "requirements for the design, development, management, reporting and verification of an organization's greenhouse gas inventory", while ISO 14064-2:2019 "specifies principles and requirements and provides guidance at the project level for the quantification, monitoring and reporting of activities intended to cause greenhouse gas emission reductions or removal enhancements". It also "includes requirements for planning a GHG project, identifying and selecting GHG sources, sinks and reservoirs (SSRs) relevant to the project and baseline scenario, monitoring, quantifying, documenting and reporting GHG project performance and managing data quality".

In 2018, and after an extended work of several years, an international standard was approved with the principles, requirements and guidelines for the overall and partial quantification and reporting of the carbon footprint of a product (ISO 14067:2018), in full and consistent articulation with the previous standards approved for life-cycle assessment (LCA). This standard was an important step forward to try to harmonize the different results that have been obtained through the application of slightly different methodologies to the calculation of product LCA and subsequently to the carbon footprint. Only climate change and in particular greenhouse emissions are included within the standard, without procedures and considerations related with carbon off-setting and communication aspects, including social, economic or other environmental concerns related with the product life cycle.

With higher concerns with the emission of GHG gases associated with personal activities and consumer options, the need for evaluation of the carbon footprint at the individual scale has been growing considerably. From food to travel, only as a curiosity or as an educational resource, a decision support tool or even as a requirement by certain organizations for tracking and eventual emissions off-setting, individual carbon footprint calculators are now a major tool extensive used [47]. Indeed, many of these online tools are used for business purposes where the main objective is to support a variety of projects, from renewable energies to forestation, where carbon emissions can be offset through the payment of such a service.

Most of the greenhouse gas emissions are calculated based on emission factors from references accepted internationally. Models and direct monitoring measurements can also be used. Better consistency and standardization in the near future will be decisive for a higher credibility of online calculators [48].

5 Final Prospects

The magnitude and pervasive climate change impacts is a threat for economic activities, human health and ecosystems as well. At the global level, there are various political and regulatory instruments in place, adopted by a vast majority of countries, being the Paris Agreement the soundest one, ratified by 189 countries. Carbon pricing schemes are becoming popular instruments adopted by an increasing number of countries, either as compliance emissions trading schemes or as carbon taxes. Its effectiveness in reducing carbon emissions is demonstrated in a multitude of examples, by turning fossil based processes costly while making clean processes and technologies, like renewables, competitive. Carbon footprint tools have been voluntarily adopted, by many organizations and companies as a way to measure its climate responsibility and to manage emissions reduction along the time. Innovation is the magical word to transform the way societies manage everyday lives, including technologies, political and economic models, individual and collective behaviours. World population is increasing and consumption per capita is growing as well. New processes and technologies are required to counteract the expected greenhouse gas emissions increase. Several prospective assessments, at global and national levels, have demonstrated it is viable to transform human systems to carbon neutral and climate resilient ones, without hamper social welfare. Governments and businesses have a serious responsibility to drive economies towards that goal, backed by science and innovation. However, new human values, inspired in solidarity and frugality in collective and individual behaviours, respectively, have to accompany novel technologies to have a chance to keep the life on Earth safe within a stable climate system.

References

1. UN (2015) The Paris Agreement. United Nations. https://unfccc.int/files/essential_background/convention/application/pdf/english_paris_agreement.pdf. Accessed 20 Abr 2020
2. IPCC (2018) Global Warming of 1.5°C. In: Masson-Delmotte V, Zhai P, Pörtner H-O, Roberts D, Skea J, Shukla PR, Pirani A, Moufouma-Okia W, Péan C, Pidcock R, Connors S, Matthews JBR, Chen Y, Zhou X, Gomis MI, Lonnoy E, Maycock T, Tignor M, Waterfield T (eds) An IPCC Special Report on the impacts of global warming of 1.5°C above pre-industrial levels and related global greenhouse gas emission pathways, in the context of strengthening the global response to the threat of climate change, sustainable development, and efforts to eradicate poverty, 2019 Intergovernmental Panel on Climate Change
3. Schmidt T, Sewerin S (2017) Technology as a driver of climate and energy politics. Nat Energ 2:17084

4. WMO (2020) Statement on the State of the Global Climate in 2019. World Meteorological Organization (ISBN 978-92-63-11248-4)
5. Smale DA, Wernberg T, Oliver ECJ et al (2019) Marine heatwaves threaten global biodiversity and the provision of ecosystem services. Nat Clim Chang 9:306–312
6. WCRP Global Sea Level Budget Group (2018) Global sea-level budget 1993–present. Earth Syst Sci Data 10:1551–1590
7. IPCC (2019) Summary for policymakers. In: Pörtner H-O, Roberts DC, Masson-Delmotte V, Zhai P, Tignor M, Poloczanska E, Mintenbeck K, Nicolai M, Okem A, Petzold J, Rama B, Weyer N (eds) IPCC special report on the Ocean and cryosphere in a changing climate, In press
8. Lacis AA, Schmidt GA, Rind D et al (2010) Atmospheric CO_2: principal control knob governing Earth's temperature. Science 330:356–359
9. FAO (2020) GIEWS special alert 347: the worst desert locust outbreak in decades threatens food security across East Africa. Food and Agriculture Organization of the United Nations (FAO), Rome
10. Ciais P, Sabine C, Bala G et al (2013) Carbon and other biogeochemical cycles. In: Stocker TF, Qin D, Plattner G-K, Tignor M, Allen SK, Boschung J, Nauels A, Xia Y, Bex V, Midgley PM (eds) Climate change 2013: the physical science basis. contribution of working group i to the fifth assessment report of the intergovernmental panel on climate change, Cambridge University Press, Cambridge, United Kingdom and New York, NY, USA
11. WMO (2019) In: greenhouse gas bulletin: the state of greenhouse gases in the atmosphere based on global observations through 2018. World Meteorological Organization and Global Atmosphere Watch. https://library.wmo.int/doc_num.php?explnum_id=10100. Accessed 20 Apr 2020
12. Archer D, Eby M, Brovkin V et al (2009) Atmospheric lifetime of fossil fuel carbon dioxide. Annu Rev Earth Pl Sc 37:117–134
13. Friedlingstein P, Jones MW et al (2019) Global carbon budget 2019. Earth Syst Sci Data 11:1783–1838
14. Ritchie H and Roser M (2019) CO_2 and Greenhouse Gas Emissions. https://ourworldindata.org/co2-and-other-greenhouse-gas-emissions. Accessed 25 Apr 2020
15. Peters GP, Andrew RM, Canadell JG et al (2020) Carbon dioxide emissions continue to grow amidst slowly emerging climate policies. Nat Clim Chang 10:3–6
16. Jiang X, Guanb D (2016) Determinants of global CO_2 emissions growth. Appl Energ 184:1132–1141
17. Zheng X, Lu Y, Yuan J et al (2020) Drivers of change in China's energy-related CO_2 emissions. PNAS 117:29–36
18. Le Quéré C, Korsbakken JI, Wilson C et al (2019) Drivers of declining CO_2 emissions in 18 developed economies. Nat Clim Chang 9:213–217
19. UN (1992) United Nations Convention on Climate Change. United Nations. https://unfccc.int/files/essential_background/background_publications_htmlpdf/application/pdf/conveng.pdf. Accessed 20 Abr 2020
20. IPCC (2019) In: Shukla PR, Skea J, Calvo Buendia E, Masson-Delmotte V, Pörtner HO, Roberts DC, Zhai P, Slade R, Connors S, van Diemen R, Ferrat M, Haughey E, Luz S, Neogi S, Pathak M, Petzold J, Portugal Pereira J, Vyas P, Huntley E, Kissick K, Belkacemi M, Malley J (eds) Climate change and land: an IPCC special report on climate change, desertification, land degradation, sustainable land management, food security, and greenhouse gas fluxes in terrestrial ecosystems, In press
21. IPCC (2019) In: Pörtner HO, Roberts DC, Masson-Delmotte V, Zhai P, Tignor M, Poloczanska E, Mintenbeck K, Alegría A, Nicolai M, Okem A, Petzold J, Rama B, Weyer NM (eds) IPCC special report on the Ocean and cryosphere in a changing climate, In press

22. WMO (2019) United in science high-level synthesis report of latest climate science information convened by the science advisory group of the UN climate action summit 2019. United Nations, New York
23. UNEP (2019) Emissions gap report 2019. United Nations Environment Programme, Nairobi
24. EC (2019) Communication from the commission to the European Parliament, the European council, the council, the European economic and social committee and the committee of the regions. In: The European green deal. European Commission, Brussels, 11.12.2019 COM (2019) 640 final
25. Tørstad VH (2020) Participation, ambition and compliance: can the Paris Agreement solve the effectiveness trilemma?—Environ politics (https://doi.org/10.1080/09644016.2019.1710322)
26. World Bank (2019). State and Trends of Carbon Pricing (2019) State and trends of carbon pricing (June). World Bank, Washington, DC
27. Bush MJ (2020) Pricing down carbon. Climate change and renewable energy. Palgrave Macmillan, Cham, pp 333–372
28. Wackernagel M (1994). Ecological footprint and appropriated carrying capacity: a tool for planning toward sustainability. Ph.D. Thesis, The University of British Columbia
29. Wackernagel M, Rees WE (1996) Our ecological footprint: reducing human impact on the earth. New Society Publishers, Gabriola Island
30. GFP (2020) Global Footprint Network https://www.footprintnetwork.org/. Accessed 18 Mar 2020
31. Galli A, Iha K, Pires SM et al (2020) Assessing the Ecological Footprint and biocapacity of Portuguese cities: critical results for environmental awareness and local management. Cities 96:102442
32. Wiedmann T, Minx J (2007) A definition of carbon footprint. ISAUK Research Report 07–01, Durham, ISAUK Research and Consulting. UK
33. Pandey D, Agrawal M, Pandey J (2011) Carbon footprint: current methods of estimation. Environ Monit Assess 178:135–160
34. Lombardi M, Laiola E, Tricase C, Rana R (2017) Assessing the urban carbon footprint: an overview. Environ Impact Assess Rev 66:43–52
35. Yang Y, Meng G (2020) The evolution and research framework of carbon footprint: based on the perspective of knowledge mapping. Ecol Indic 112:106125
36. Vitaa G, Ivanovaa A, Dumitrue R et al (2020) Happier with less? members of European environmental grassroots initiatives reconcile lower carbon footprints with higher life satisfaction and income increases. Energy Res Social Sci 60
37. Fitzpatrick JJ, McCarthy S, Byrne EP (2015) Sustainability insights and reflections from a personal carbon footprint study: the need for quantitative and qualitative change. Sustain Prod Consumption I:34–46
38. Harris S, Weinzettel J, Bigano A et al (2020) Low carbon cities in 2050? GHG emissions of European cities using production-based and consumption-based emission accounting methods. J Cleaner Prod 248:119206
39. Long Y, Yoshida Y, Liu Q, Zhang H, Wang S, Fang K (2020) Comparison of city-level carbon footprint evaluation by applying single and multi-regional input-output tables. J Environ Manage 260:110108
40. Fry J, Manfred Lenzen M, Jin Y et al (2018) Assessing carbon footprints of cities under limited information. J Cleaner Prod 176:1254–1270
41. Carbon Trust (2020) Carbon Trust https://www.carbontrust.com/. Accessed 5 Mar 2020
42. GGP (2020) Greenhouse Gas Protocol https://ghgprotocol.org/. Accessed 18 Mar 2020
43. CDP (2020) Carbon Disclosure Project https://www.cdp.net/en. Accessed 18 Mar 2020
44. Penz E, Polsa P (2018) How do companies reduce their carbon footprint and how do they communicate these measures to stakeholders? J Cleaner Prod 195:1125–1138
45. Groening C, Inman JJ, Ross WT Jr (2015) The role of carbon emissions in consumer purchase decisions. Int J Environ Policy Decis Making 1:261–296

46. Canavari M, Coderoni S (2020) Consumer stated preferences for dairy products with carbon footprint labels in Italy. Agric Econ 8:4
47. Collins A, Galli A, Hipwood T, Murthy A (2020) Living within a one Planet reality: the contribution of personal footprint calculators. Environ Res Lett 15
48. Mulrow J, Machaj K, Deanes J et al (2019) The state of carbon footprint calculators: an evaluation of calculator design and user interaction features. Sustain Prod Consumption 18:33–40

Carbon Dioxide Utilisation—The Formate Route

Luisa B. Maia, Isabel Moura, and José J. G. Moura

Abstract

The relentless rise of atmospheric CO_2 is causing large and unpredictable impacts on the Earth climate, due to the CO_2 significant greenhouse effect, besides being responsible for the ocean acidification, with consequent huge impacts in our daily lives and in all forms of life. To stop spiral of destruction, we must actively reduce the CO_2 emissions and develop new and more efficient "CO_2 sinks". We should be focused on the opportunities provided by exploiting this novel and huge carbon feedstock to produce de novo fuels and added-value compounds. The conversion of CO_2 into formate offers key advantages for carbon recycling, and formate dehydrogenase (FDH) enzymes are at the centre of intense research, due to the "green" advantages the bioconversion can offer, namely substrate and product selectivity and specificity, in reactions run at ambient temperature and pressure and neutral pH. In this chapter, we describe the remarkable recent progress towards efficient and selective FDH-catalysed CO_2 reduction to formate. We focus on the enzymes, discussing their structure and mechanism of action. Selected promising studies and successful proof of concepts of FDH-dependent CO_2 reduction to formate and beyond are discussed, to highlight the power of FDHs and the challenges this CO_2 bioconversion still faces.

Keywords

Carbon dioxide utilisation · Formic acid · Formate dehydrogenase · Molybdenum · Tungsten · Hydride transfer · Biocatalyst · Green chemistry · Energy · Biotechnology

L. B. Maia (✉) · I. Moura · J. J. G. Moura
LAQV, REQUIMTE, NOVA School of Science and Technology, Campus de Caparica, Caparica, Portugal
e-mail: luisa.maia@fct.unl.pt

J. J. G. Moura et al. (eds.), *Enzymes for Solving Humankind's Problems*,
https://doi.org/10.1007/978-3-030-58315-6_2

Abbreviations

CCS	Carbon dioxide capture and sequestration
Cys-Mo-FDH	Cysteine, molybdenum-containing formate dehydrogenase
Cys-W-FDH	Cysteine, tungsten-containing formate dehydrogenase
EPR	Electron paramagnetic resonance spectroscopic
Fe/Fe-Hase	Iron–iron hydrogenase
Fe/S	Iron–sulfur centres
FDH	Formate dehydrogenase
FMFDH	*N*-formyl-methanofuran dehydrogenase
GDE	Gas diffusion electrode
Mo-FDH	Molybdenum-containing formate dehydrogenase
Ni/Fe-Hase	Nickel/iron-containing hydrogenase
RES	Renewable energy sources
SeCys-Mo-FDH	Selenocysteine, molybdenum-containing formate dehydrogenase
SeCys-W-FDH	Selenocysteine, tungsten-containing formate dehydrogenase
XAS	X-ray absorption spectroscopy
VC	Added-value compounds or valuable compounds
W-FDH	Tungsten-containing formate dehydrogenase

1 The Relentless Rise of Carbon Dioxide

In 2018 alone, more than 36Gt of CO_2 [1] were dumped into the atmosphere as waste material from fossil resources-based energy and chemical industries! In that year, the global atmospheric CO_2 concentration reached an annual average value of 407 ppm, an increase of 150% since pre-industrial times (277 ppm in 1750) (Fig. 1) [1]. Yet, new records are being set, and a monthly average of 416 ppm was already observed this March 2020 [2]. This ever-increasing atmospheric CO_2 concentration is causing large and unpredictable impacts on the Earth climate, due to the CO_2 significant greenhouse effect, besides being responsible for the ocean acidification, with consequent huge impacts in our daily lives and in all forms of life.

Atmospheric CO_2 concentration results from the balance between CO_2 emission and uptake [3]. CO_2 is emitted from human activities, such as fossil fuel combustion and oxidation from other energy and industrial processes (10.0Gt of carbon in 2018 [1]) and deliberate activities on land, mainly deforestation (1.5Gt of carbon in 2018 [1]), as well as, from natural processes, such as volcanic eruptions and biological emissions. On the other plate of the scale, the small "CO_2 sinks" are mainly provided by physical and biological processes in oceans (2.6Gt of carbon in

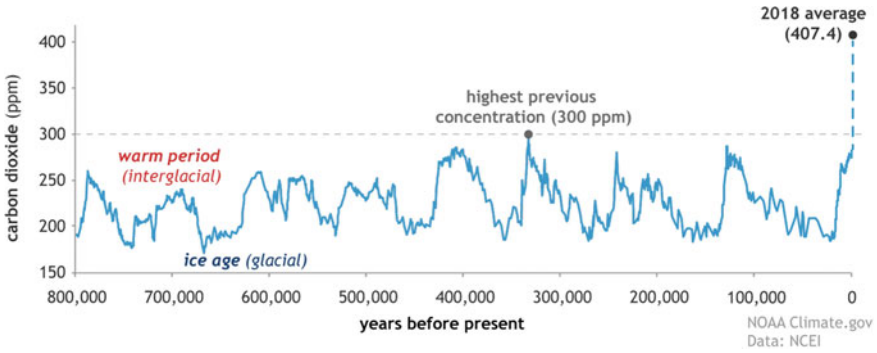

Fig. 1 Relentless rise of carbon dioxide. Global atmospheric CO_2 concentrations in parts per million (ppm) for the past 800,000 years. The peaks and valleys track ice ages (low CO_2) and warmer interglacials (higher CO_2). During these cycles, CO_2 was never higher than 300 ppm. In 2018, it reached 407.4 ppm. On the geologic time scale, the increase (blue dashed line) looks virtually instantaneous *Source* NOAA Climate.gov, based on EPICA Dome C data provided by NOAA NCEI Paleoclimatology Program (https://www.climate.gov/news-features/understanding-climate/climate-change-atmospheric-carbon-dioxide)

2018 [1]) and land (3.5Gt of carbon in 2018 [1]). To break this largely unfavourable imbalance (more than 5Gt in 2018), we must actively reduce the CO_2 emissions and develop new and more efficient "CO_2 sinks"—new individual actions and political decisions are needed, as reviewed by Seixas and Ferreira in this book [3].

Until recently, the debate often focused only on "passive CO_2 mitigation", searching for strategies for CO_2 capture and sequestration (CCS). Instead, we should be looking at the opportunities for the energy and chemical industries provided by exploiting this novel and huge carbon feedstock (Fig. 2), such as (a) storage of "intermittent" renewable energy sources (RES) (wind, solar and hydropower energy, which are now rapidly growing and becoming economically viable), (b) conversion of RES-derived electricity into fuels (mainly for mobility and transport sector, in particular aviation and heavy freight over long distances, the major polluters), (c) production of added-value compounds (VC) and feedstock chemicals for making all the modern-world chemical commodities (from bulk chemicals to plastics, fertilisers and even pharmaceuticals). Regarding atmospheric CO_2 reduction, points (a) and (b) (energy industry) are of major relevance, as the different scales of energy and chemical industries impede the VC production to function as a quantitative "sink" for the massive fossil fuels-dependent CO_2 emissions. Together, these three axes, storage/conversion/production, will certainly provide a straightforward way to actively reduce the CO_2 emissions, while actively consuming the CO_2 already released—"two-in-one solution".

But, how to direct CO_2 into the storage/conversion/production axes? Formic acid/formate[1] offers key advantages (Fig. 2)!

[1] pK_{a1} (formic acid (methanoic acid, HCOOH)/formate) = 3.77.

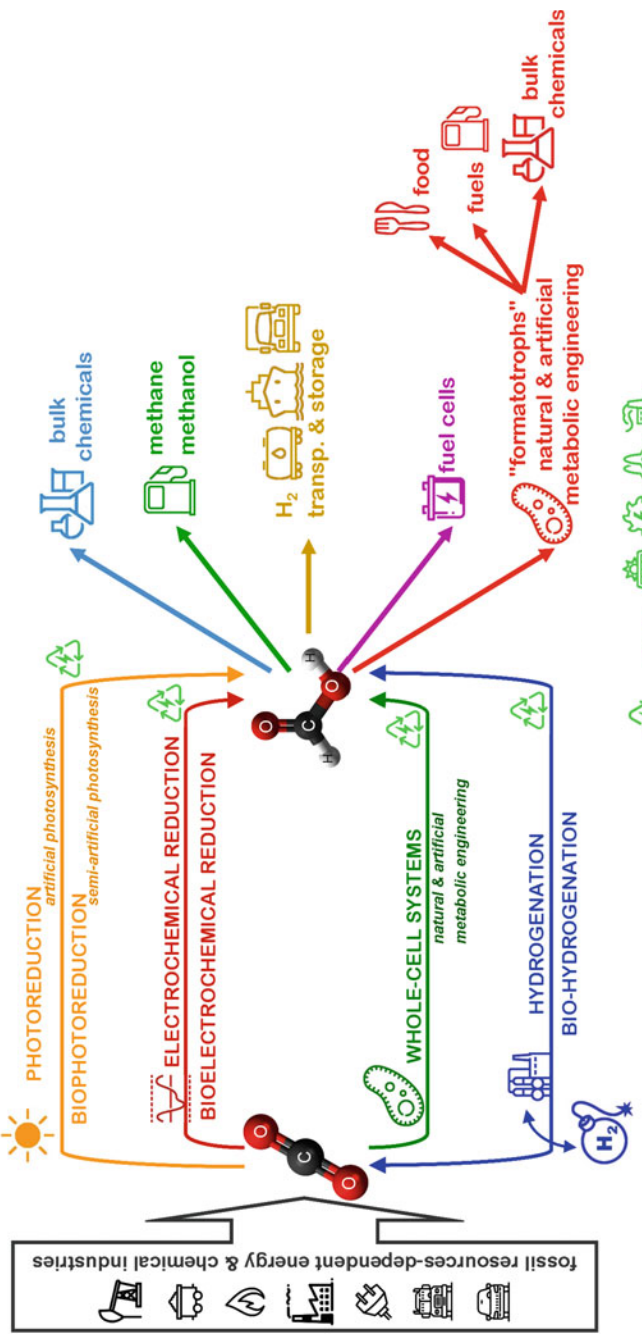

Fig. 2 Directing CO_2 into the axes storage/conversion/production through the formate route. (icons from www.icons8.com)

2 Formic Acid—The Stepping Stone Towards Carbon Dioxide Utilisation

Formic acid was identified in fifteenth century as an acidic vapour in ant hills, from where its name derivates—"formica", the Latin word for ant. It was first synthesised only in the nineteenth century from hydrocyanic acid by the famous French chemist and physicist Joseph Gay-Lussac and also from carbon monoxide by another French chemist, Marcellin Berthelot. However, formic acid received little industrial attention until the last quarter of twentieth century, when it started to be used as a preservative and antibacterial in livestock feed due to its low toxicity (LD_{50} of 1.8 g/kg). More recently, formic acid regained a new interest, due to some features that are key to the longed-for "post-fossil era" (Fig. 2).

(a) Formic acid is a stable product that can be formed by the "simple" two-electron reduction of CO_2 (Eq. 1), what, noteworthy, resulted in a considerable attention to the electrochemical CO_2 reduction in the last decade (see Sect. 3.).
(b) Besides formic acid, also carbon monoxide is a stable product of the two-electron CO_2 reduction (Eq. 2). However, its high toxicity, low solubility and low mass transfer rate make the carbon monoxide subsequent utilisation challenging. In contrast, formic acid is a highly soluble and stable liquid, easy to store and transport.
(c) Formic acid is also not explosive, what represents an important advantage relatively to dihydrogen, an ideal "clean" fuel (see below).
(d) Formic acid is already used as a "building block" in chemical industry.
(e) Formic acid can be a substrate for further reduction to a carbon-based fuel, methanol and methane, what might not be the most obvious option regarding CO_2 consumption.
(f) Formic acid, formed from CO_2 and dihydrogen (Eq. 3), can be used as a "storage form" of dihydrogen, an ideal "clean" fuel (potentially zero contribution to the global carbon cycle, with a high gravimetric energy density) [4–13]. Although formic acid is not a perfect dihydrogen "storage medium", due to its relatively small hydrogen content (4.4%(m/m) or 5.3%(m/v)), it is currently still one of the best options to circumvent the technical difficulties associated with dihydrogen handling, storage and transport. For this purpose, formic acid produced by CO_2 hydrogenation or any other approach is converted back to dihydrogen when needed.
(g) Moreover, formic acid fuel cells are being the centre of a renewed interest [14–18].
(h) From a biotechnological point of view, formate can be both produced and assimilated by many natural and biotechnologically engineered organisms and, unlike dihydrogen (that is "just" oxidised to form reducing power), act as a carbon source for "formatotrophic" organisms, thus, enabling considerably higher biomass formation and VC and fuels production yields [19].

$$CO_2 + 2e^- + 2H^+ \rightleftharpoons HCOOH \quad (1)$$

$$CO_2 + 2e^- + 2H^+ \rightleftharpoons CO + H_2O \quad (2)$$

$$CO_2 + H_2 \rightleftharpoons HCOOH \quad (3)$$

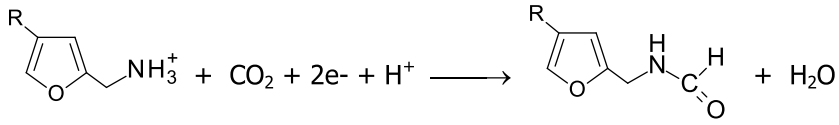

methanofuran formyl-methanofuran (4)

3 How to Convert Carbon Dioxide to Formic Acid/Formate?—The Chemical Way

CO_2 is a kinetically and thermodynamically stable molecule, with a high negative value of the reduction potential of the CO_2/HCOOH pair (highly pH dependent), what makes its activation and reduction a difficult task [8]. Hence, perhaps the first answer that comes to mind to reduce CO_2 to formate is: electrochemically [20–33]. However, the feasibility—meaning essentially the economic viability—of this process, that is currently the centre of intense research, depends on the Faradaic efficiency and energetic efficiency of CO_2 reduction (avoiding high electrochemical overpotentials) and on the rate and selectivity (purity) of formate production. The other "cost" to be considered is obviously the environmental one, and this depends on the use of a RES-derived electricity and on the sustainability of the electrodes (composition and durability).

The second answer is probably going to be photoreduction, which is the most straightforward way to use a RES to convert CO_2. Solar energy (photogenerated electrons) can be used to drive chemical reactions, and this solar-to-chemical energy conversion followed by storage in the form of chemical bonds is generally called "artificial photosynthesis" (as it is a mimic of photosynthetic process used by living organism to fix CO_2). The progress in this field has been quite remarkable, and several highly efficient and promising systems have been developed for CO_2 reduction (as well as water oxidation and hydrogen evolution), and formic acid can be produced with high rates and selectivity [34–44]. However, some problems have yet to be solved. In a very simplified way, artificial photosynthesis needs two fundamental components: an ideal light absorber/photosensitiser (for light harvest, charge separation and charge transfer) and an ideal catalyst (with high intrinsic activity and stability and low overpotential). Therefore, the heterogenisation of the molecular catalysts and engineering of applicable devices are the main challenges towards the development of effective artificial photosynthesis devices (practical

problems, such as density and exposure of the catalyst active sites, conductivity, mass transport and stability of the catalyst-derived material or electrode, all make the catalyst intrinsic activity and efficiency quite different from the device performance numbers). In addition, scale-up feasibility and whole device long-term stability (also associated with the costs of using expensive high-purity semiconductors to achieve high efficiency) have to be attained. Nevertheless, artificial photosynthesis devices might become economically viable sooner than many anticipate: considering the energy consumption forecasted for 2050, the future solar energy devices only need a ≈ 10% solar-to-fuel efficiency (already achievable in proof of concept devices!) if 1% of the Earth's surface is covered [44].

Formic acid can also be produced chemically from CO_2 and dihydrogen. This CO_2 hydrogenation is just the thermal overall CO_2 reduction by dihydrogen using molecular catalysts (Eq. 3), as an alternative to direct electrochemical or photoelectrochemical reduction of CO_2 [5, 10, 12, 13, 45–71]. Hence, here, it is the rational design of the catalytic systems (efficiency and selectivity) that must be attained and the systems that have been developed to date exhibit selectivity and yield lower than desirable, besides requiring a high temperature and/or high pressure. Dihydrogen is a "clean" fuel (potentially zero contribution to the global carbon cycle), but its real environmental impact depends on how it is produce. The industrial production of dihydrogen (primarily from methane) requires harsh temperatures and emits as much CO_2 into the atmosphere as natural gas burning [72]. To be environmentally friendly, dihydrogen must be produced by electrolysis of water using a RES and selected heterogeneous or homogeneous catalysts or biological systems [73–93]. As noted above, besides producing formic acid itself, CO_2 hydrogenation is thought as a relevant way to storage dihydrogen. Therefore, also the reversible interconversion of formic acid to CO_2 and dihydrogen must be carefully considered.

4 How to Convert Carbon Dioxide to Formic Acid/Formate?—Exploiting the Power of Formate Dehydrogenases (Enzymes for Solving Humankind's Problems)

4.1 The Biochemical Way

In contrast to purely physicochemical, biological processes are substrate and product-specific (life requires a well-defined metabolism) and occur under truly "green", sustainable conditions, at ambient temperature and pressure and close to neutral pH. Biological catalysts—enzymes—offer selectivity and specificity, coupled with high specific activity (in terms of active sites) and maximal rate (under the respective cellular context). Enzymes have evolved to become perfect catalysts[2],

[2]It should be kept in mind that enzymes did not evolve to maximise "our" VC production. Enzymes and all cellular components evolved to achieve sustained life. The statement of "perfect catalysts" must be taken within the respective context.

comprising (a) *specific* surface patches to establish contact with *specific* biomolecules (for cell localisation, integration into metabolic complexes, crosstalk or simple electron transfer), (b) channels where only (or mainly) the *correct* substrates come in and well-determined products come out, as well as, (c) highly defined active sites, assembled to promote the formation of key transition states and intermediates and, thus, lower the reaction energy barriers and energy loss. For that, active sites are built with precise steric features, electrostatic and hydrogen bonding interactions, fine-tuned reduction potentials and pK_a values and optimised (and often synchronised) electron and proton transfer paths. The power and efficiency of biological catalysis is such that enzymes cascades are the cornerstone of all metabolic pathways that sustain life on Earth. Hence, there is a growing interest in making use of all the advantages the "biochemical way" can provide. Numerous hybrid systems have been (are being) designed to merge the best of the two worlds —chemical and biochemical—and the CO_2 reduction to formate is no exception.

4.2 Formate Dehydrogenases—Enzymatic Machineries

To interconvert CO_2 and formate, living organisms use formate dehydrogenase (FDH) enzymes. FDHs are a heterogeneous and broadly distributed group of enzymes that catalyse the reversible two-electron interconversion of formate and CO_2 (Eq. 1) [94–101]. These enzymes evolved to take part in diverse metabolic pathways, being used by some prokaryotic organism to fix (reduce) CO_2 into formate, while other prokaryotes use FDHs to derive energy, by coupling the formate oxidation (which has a very low reduction potential value, $E^{\circ\prime}(CO_2/HCOO^-) = -0.43$ V) to the reduction of several terminal electron acceptors; FDHs are also broadly used by both prokaryotes and eukaryotes in C1 metabolism.

FDHs can be divided into two major classes, based on their cofactor content and the consequent chemical strategy used to carry out the formate/CO_2 interconversion. One class comprises FDHs that have no metal ions or other redox-active centres—*the metal-independent FDHs class* [102–109]. These enzymes are widespread, being found in bacteria, yeasts, fungi and plants, are all (as far as is known) NAD-dependent and belong to the *D*-specific dehydrogenases of 2-oxyacids family. The other class—*the metal-dependent FDHs class* [3]—comprises only prokaryotic enzymes that hold different redox-active centres (Table 1) and whose active site harbours one molybdenum or one tungsten centre (molybdenum-containing FDH (Mo-FDH) or tungsten-containing FDH (W-FDH), respectively) [94–101, 110–112].

[3]It should be noted that the difference between the two FDHs classes is the absence or presence of redox-active centres. All (so far known) metal-independent FDHs are NAD(P)-dependent. In contrast, there are some metal-dependent FDHs that use $NAD(P)^+$/NAD(P)H as a co-substrate, while many other use other physiological redox partners (such as membrane quinols, cytoplasmatic and periplasmatic cytochromes, ferredoxins or coenzyme F_{420}).

Table 1 Summary of the features of some representative formate dehydrogenases and *N*-formyl-methanofuran dehydrogenases

Enzyme	Active site[a]	Subunit composition	Notes
Clostridium carboxidivorans FDH	W SeCys	α W, [4Fe–4S]	• cytoplasmatic? • NAD^+-dependent
Thermoanaerobacter kivui FDH			• hydrogen-dependent CO_2 reductase
Desulfovibrio gigas FDH		αβ α: W, [4Fe–4S] β: 3 [4Fe–4S]	• periplasmatic
Desulfovibrio alaskensis FDH			
Desulfovibrio vulgaris FDH			
Moorella thermoacetica FDH		$(\alpha\beta)_2$ α: W, [4Fe–4S] β: 3 [4Fe–4S]	• cytoplasmatic • $NADP^+$-dependent
Synthrobacter fumaroxidans FDH		$(\alpha\beta\gamma)_2$ W, Fe	• periplasmatic?
Methylobacterium extorquens FDH	W Cys	αβ α: W, ≥ 1 Fe/S β: [4Fe–4S], FMN	• cytoplasmatic • NAD^+-dependent
Escherichia coli FDH H	Mo SeCys	α Mo, [4Fe–4S]	• cytoplasmatic (membrane-bound via its partners) • partner of formate-hydrogen lyase system
Acetobacterium woodii FDH			• hydrogen-dependent CO_2 reductase
Desulfovibrio desulfuricans FDH		αβγ α: Mo, [4Fe–4S] β: 3 [4Fe–4S] γ: 4 *c* haems	• periplasmatic
Desulfovibrio vulgaris FDH			
Escherichia coli FDH N		$(\alpha\beta\gamma)_3$ α: Mo, [4Fe–4S] β: 4 [4Fe–4S] γ: 2 *b* haems	• membrane-bound periplasm-faced • partner in anaerobic nitrate-formate respiratory system
Escherichia coli FDH O			• membrane-bound periplasm-faced • partner in nitrate-formate respiratory system during aerobic to anaerobic transition

(continued)

Table 1 (continued)

Enzyme	Active site[a]	Subunit composition	Notes
Pectobacterium atrosepticum FDH	Mo Cys	α Mo, [4Fe–4S]	• cytoplasmatic
Corynebacterium glutamicum FDH			
Clostridium pasteurianum FDH		αβ Mo, several Fe/S	• cytoplasmatic
Methanobacterium formicicum FDH		αβ Mo, FAD, several Fe/S, Zn	• cytoplasmatic • F_{420}-dependent
Wolinella succinogenes FDH		αβγ α: Mo, [4Fe–4S] β: 4 [4Fe–4S] γ: 4 *b* haems	• membrane-bound
Cupriavidus necator FDH		$(\alpha\beta\gamma)_2$ α: Mo, [2Fe–2S], 4 [4Fe–4S] β: [4Fe–4S], FMN γ: [2Fe–2S]	• cytoplasmatic • NAD^+-dependent
Rhodobacter capsulatus FDH			
Methylosinus trichosporium FDH			
Pseudomonas oxalatus FDH			
Methylosinus trichosporium FDH		$(\alpha\beta\gamma\delta)_2$ Mo, ≥ 1 [2Fe–2S], ≥ 1 [4Fe–4S], FMN	• cytoplasmatic • NAD^+-dependent
Methanothermobacter wolfeiir FMFDH		$(\alpha\beta\gamma\delta\varepsilon\omega)_4$ α: 2 Zn β: Mo, [4Fe–4S] γ: 2 [4Fe–4S] γ: 4 *b* haems δ ε: 8 [4Fe–4S] ω	• cytoplasmatic

[a] Active site composition, besides the two pyranopterin cofactor molecules and the terminal sulfido group

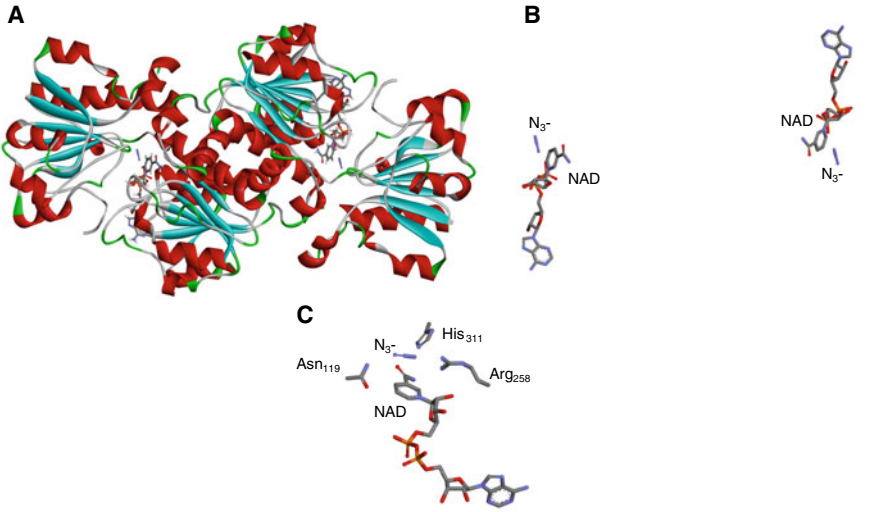

Fig. 3 *C. boidinii* formate dehydrogenase. **A** Three-dimensional structure view of the homodimer. **B** Arrangement of NAD and azide shown in the same orientation (but not same scale) as in (**A**). **C** Enzyme active site, with azide and NAD bound. The structures shown are based on the PDB file 5DN9 [109] (α helices and β sheets are shown in red and cyan, respectively)

4.2.1 The Metal-Independent Formate Dehydrogenases

Comparatively, the metal-independent FDHs are quite simple enzymes, generally forming homodimers, containing a NAD(H) and a formate-binding pockets in a close vicinity of each other (Fig. 3) [102–109]. The formate-binding site harbours a conserved arginine and asparagine residues, while an aspartate and serine residues make contacts to the nicotinamide ring, with another arginine residue binding the phosphate moiety linker of NAD(H).

4.2.2 The Metal-Dependent Formate Dehydrogenases

Because the metal-dependent FDHs are involved in diverse metabolic pathways (energy and C1 metabolism), for which different "interfaces" are needed, this class is extraordinarily heterogeneous, comprising enzymes with diverse redox-active centres, such as iron–sulfur centres (Fe/S), haems and flavins, besides the characteristic molybdenum or tungsten active sites, organised in different subunit compositions and quaternary structures (Table 1) [94–101, 110–112]. This structural diversity is well exemplified by *Escherichia coli*, that expresses one "simple" monomeric cytoplasmatic enzyme, containing only the molybdenum centre and one [4Fe–4S] centre (the FDH H; Fig. 4) [113–117], and two "complex" heteromeric ($(\alpha\beta\gamma)_3$) membrane-bound respiratory enzymes that harbour seven additional redox-active centres ([4Fe–4S] centres and b-type haems) in addition to the molybdenum centre (the FDH N [118–120] (Fig. 5) and FDH O [121–123]). Also, the sulfate-reducing bacteria of the *Desulfovibrio* genus contain diverse Mo-FDHs and W-FDHs [124–129], such as the heterodimeric ($\alpha\beta$) periplasmatic W-FDH of

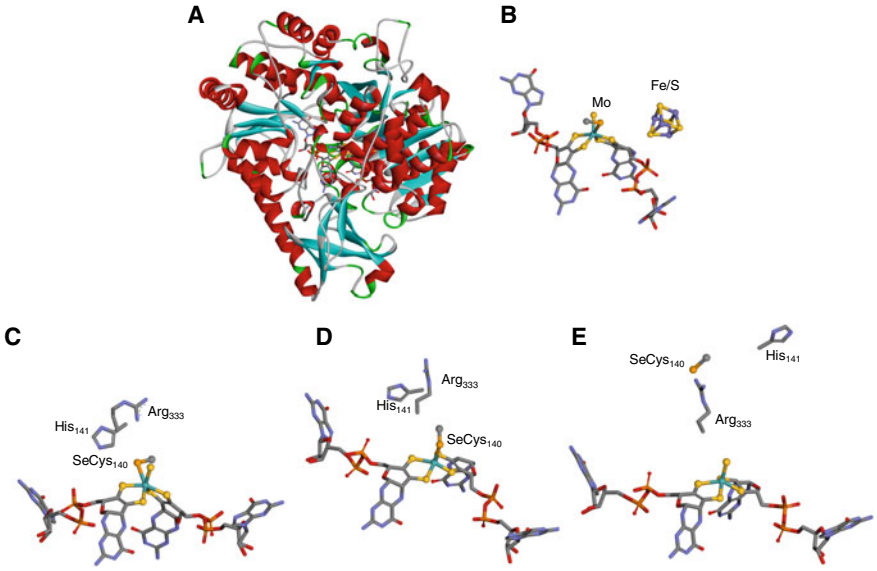

Fig. 4 *E. coli* formate dehydrogenase H. **A** Three-dimensional structure view. **B** Arrangement of the redox-active centres shown in the same orientation (but not same scale) as in (**A**). **C** Molybdenum catalytic centre of oxidised enzyme. **D** Molybdenum catalytic centre of reduced enzyme as suggested by Boyington et al. in 1997 [116]. **E** Molybdenum catalytic centre of reduced enzyme as suggested by Raaijmakers and Romão in 2006 [117]. The structures shown are based on the PDB files 1FDO (**A**, **B**, **C**), 1AA6 (**D**) [116] and 2IV2 (E) [117] (α helices and β sheets are shown in red and cyan, respectively)

D. gigas [130] or *D. vulgaris* [129, 131, 132], with "only" four [4Fe–4S] centres and one tungsten centre (Fig. 6) [133, 134], or the more "complex" heteromeric ($\alpha\beta\gamma$) Mo-FDH of *D. desulfuricans* [135–137] or *D. vulgaris* [129, 131] that contains eight redox-active centres ([4Fe–4S] centres and c-type haems) in addition to the molybdenum centre. Remarkably, the overall protein fold of the molybdenum —and tungsten-containing subunits, including the arrangement of Fe/S centre, is highly conserved[4] [116, 117, 119, 130, 132, 138–140].

The diversity of metal-dependent FDHs is also observed through their "molecular plasticity". Some FDHs take part in formate-hydrogen lyase systems, as is the case of FDH H from *E. coli* (Mo-FDH) [141], *Pectobacterium atrosepticum* (Mo-FDH) [142] or *C. carboxidovorans* (W-FDH) [143–147]. Physiologically, the *E. coli* formate-hydrogen lyase is a membrane-bound system involved in formate

[4]Presently, only five FDHs have been structurally characterised: the *E. coli* Mo-FDHs FDH H [116, 117] and FDH N [119], the *D. gigas* W-FDH [130], the *D. vulgaris* W-FDH [132] and the *Rhodobacter capsulatus* Mo-FDH [138] were crystallographically characterised; the *R. capsulatus* enzyme structure was also determined by cryo-electron microscopy [139]. In addition, also the crystallographic structure of the tungsten-containing *Methanothermobacter wolfeii N*-formyl-methanofuran dehydrogenase, a structurally related enzyme (see below), was solved [140].

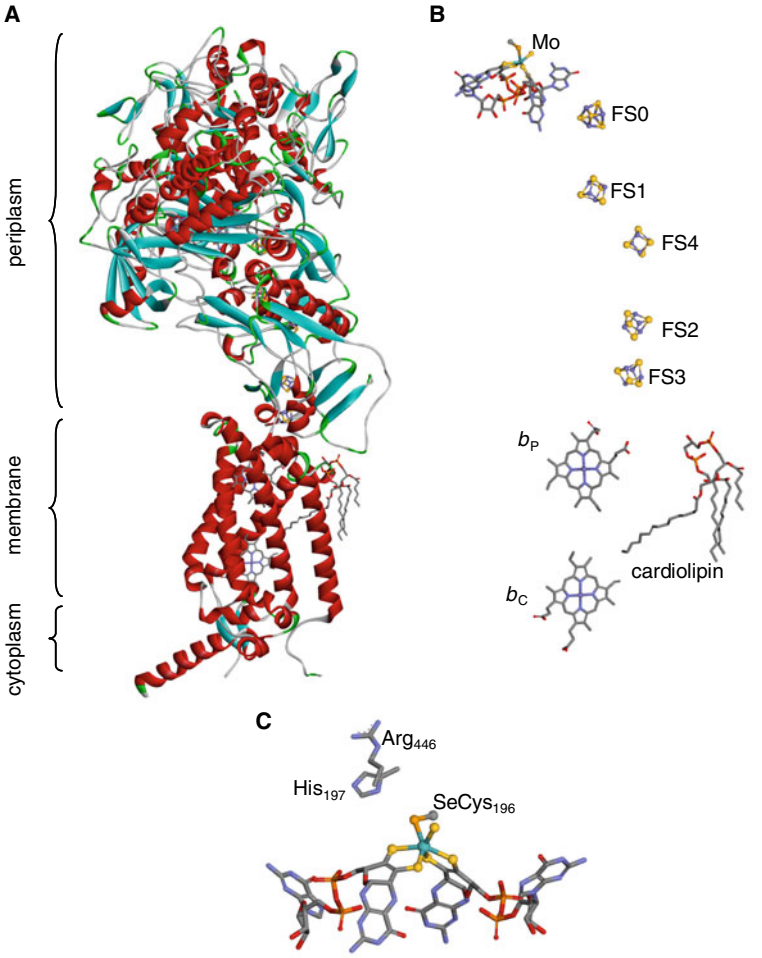

Fig. 5 *E. coli* formate dehydrogenase N. **A** Three-dimensional structure view. **B** Arrangement of the redox-active centres shown in the same orientation (but not same scale) as in (**A**). **C** Molybdenum catalytic centre of oxidised enzyme. The structures shown are based on the PDB file 1KQF [119] (α helices and β sheets are shown in red and cyan, respectively)

oxidation and dihydrogen formation under fermentative growth conditions [141, 148–151]. The system comprises two enzymes, the cytoplasmatic Mo-FDH (described above) and a membrane-bound, cytoplasm-faced nickel/iron-containing hydrogenase (Ni/Fe-Hase); FDH oxidises formate to CO_2 and the resulting reducing equivalents are transferred, through three Fe/S proteins, to the Ni/Fe-Hase that reduces protons to dihydrogen (Fig. 7).

A different rearrangement of the same basic features (FDH plus Hase) is found in cytoplasmatic dihydrogen-dependent FDHs (better denominated as CO_2 reductases), that physiologically catalyse the reduction of CO_2 to formate with the simultaneous

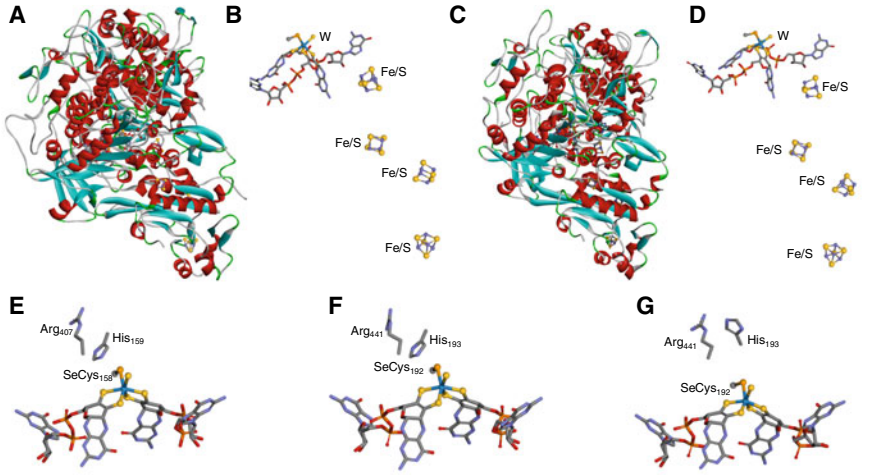

Fig. 6 *D. gigas* (**A**, **B**, **E**) and *D. vulgaris* (**C**, **D**, **F**, **G**) formate dehydrogenases. **A** Three-dimensional structure view of *D. gigas* W-FDH. **B** Arrangement of the redox-active centres of *D. gigas* W-FDH, shown in the same orientation (but not same scale) as in (**A**). **C** Three-dimensional structure view of *D. vulgaris* W-FDH. **D** Arrangement of the redox-active centres of *D. vulgaris* W-FDH, shown in the same orientation (but not same scale) as in (**C**). **E** Tungsten catalytic centre of oxidised *D. gigas* W-FDH. **F** Tungsten catalytic centre of oxidised *D. vulgaris* W-FDH. **G** Tungsten catalytic centre of formate-reduced *D. vulgaris* W-FDH. The structures shown are based on the PDB files 1H0H (**A**, **B**, **E**) [130], 6SDR (**C**, **D**, **F**) and 6SDV (**G**) [132] (α helices and β sheets are shown in red and cyan, respectively)

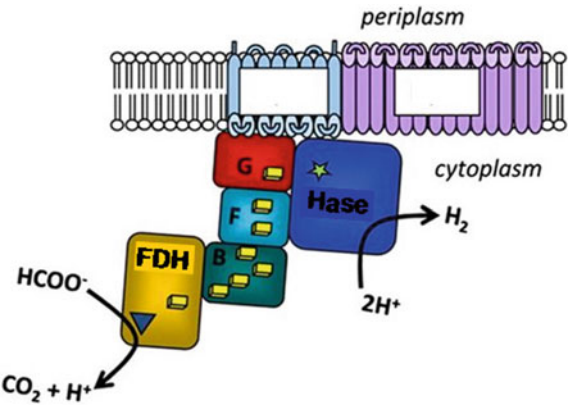

Fig. 7 Predicted architecture of the *E. coli* formate-hydrogen lyase. **B**, **F** and **G** represent three Fe/S proteins. See text for details Adapted with permission from Ref. [149]

and direct oxidation of dihydrogen, that is, without the intervention of an external electron-transfer protein or molecule, as reviewed by Litty and Müller in this Book [152] and also [153–159]. The dihydrogen-dependent CO_2 reductase of the acetogen *A. woodii* is a tetramer ($\alpha\beta\gamma\delta$), holding one FDH-like subunit comprising one molybdenum and one [4Fe–4S] centres, where CO_2 is reduced; the necessary electrons are transferred intramolecularly from an iron–iron hydrogenase-like (Fe/Fe-Hase) subunit (second active site), via two small electron-transfer subunits (each with four [4Fe–4S] centres) (Fig. 8) [153]. A tungsten-containing homologue enzyme is found in *Thermoanaerobacter kivui* [156].

A further example of the "plasticity" of FDH-like proteins is provided by *N*-formyl-methanofuran dehydrogenases (FMFDH) that also have two physically separated active sites: one catalyses the reduction of CO_2 to formate, which is then intramolecularly transferred to the second active site, where it is condensed with methanofuran to form *N*-formyl-methanofuran (Eq. 4) [140, 160, 161]. The FMFDHs are even more complex than FDHs and the enzyme from the methanogen *M. wolfeii* is a tetramer of ($\alpha\beta\gamma\delta\varepsilon\omega$) units, whose CO_2-reducing subunit shares the tungsten and [4Fe–4S] centres, as well as, the protein fold of the W-FDHs and Mo-FDHs (Fig. 9).

In contrast to the structural and organisational diversity, the active site of all presently known metal-dependent FDHs and FMFDH is very well conserved [94–101, 110–112, 140]. In the oxidised form, the active site harbours one molybdenum ion (in the case of Mo-FDHs and Mo-FMFDHs) or one tungsten ion (in W-FDHs and W-FMFDHs) coordinated by the *cis*-dithiolene (–S–C = C–S–) group of two pyranopterin cofactor molecules (Fig. 10), as is characteristic of this family of mononuclear molybdenum and tungsten enzymes [97, 110–112, 162–165]. The metal first coordination sphere is completed by one terminal sulfido group (Mo/W = S)[5] plus one sulfur or selenium atom from a cysteine or selenocysteine residue (Mo/W–S(Cys) or Mo/W–Se(SeCys)) (abbreviated as Cys–Mo–FDH, Cys–W–FDH, SeCys–Mo–FDH and SeCys–W–FDH), in a distorted trigonal prismatic. Noteworthy, there is no apparent relation (as far as is presently known) between the metal and the bound amino acid residue (examples of the four combinations Cys–Mo–FDH, Cys–W–FDH, SeCys–Mo–FDH and SeCys–W–FDH are known for long; Table 1) or the enzyme activity. The active site also comprises two other residues that are strictly conserved to all known FDHs and FMFDHs and are thought to be crucial to the catalytic cycle (as discussed below), one arginine and one histidine (this linked (C-terminal side) to the selenocysteine or cysteine that coordinates the molybdenum or tungsten ion) [116, 117, 119, 130].

[5]Although initially thought to be an oxygen [116], it is now unambiguously established that this terminal atom it is a sulfur, in both Mo-FDHs and W-FDHs, as well as in FMFDH, as established by X-ray crystallography and XAS [117, 140, 166]. In addition, it was already identified the sulfotransferase that, in conjunction with the IscS cysteine desulfurase, catalyses the insertion of this ligand in the active site [167–169].

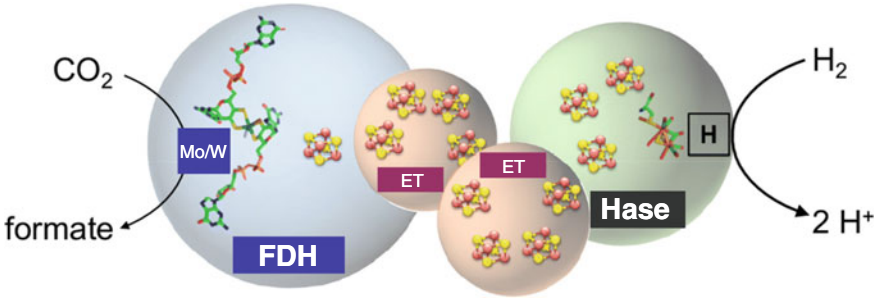

Fig. 8 Structural organisation of *A. woodii* (molybdenum-dependent) and *T. kivui* (tungsten-dependent) dihydrogen-dependent CO_2 reductases. ET represents two small electron-transfer subunits. See text for details Adapted with permission from Ref. [156]. http://creativecommons.org/licenses/by/4.0/

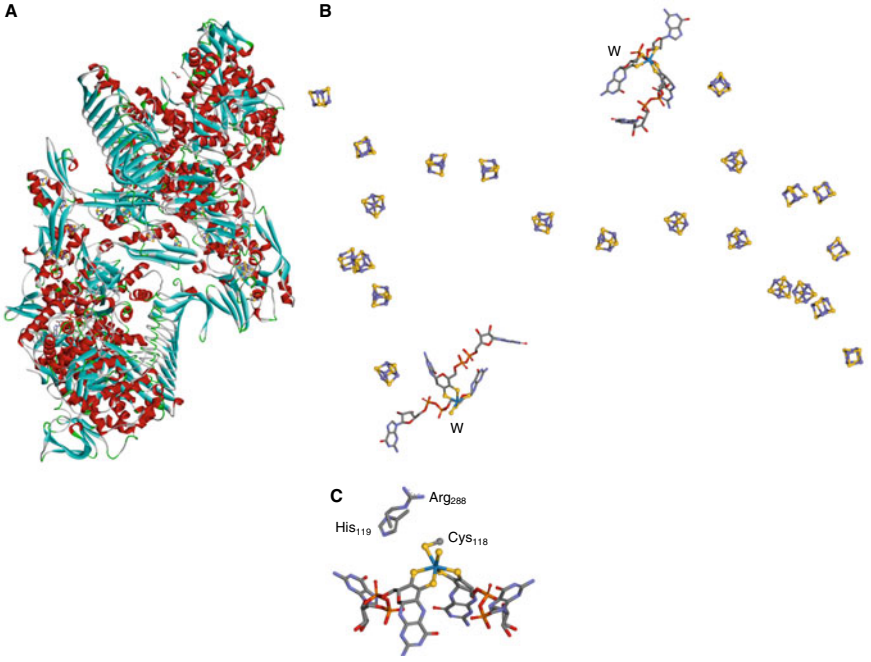

Fig. 9 *M. wolfeii N*-formyl-methanofuran dehydrogenase. **A** Three-dimensional structure view. **B** Arrangement of the redox-active centres shown in the same orientation (but not same scale) as in (**A**). **C** Tungsten catalytic centre of oxidised enzyme. The structures shown are based on the PDB file 5T5I [140] (α helices and β sheets are shown in red and cyan, respectively)

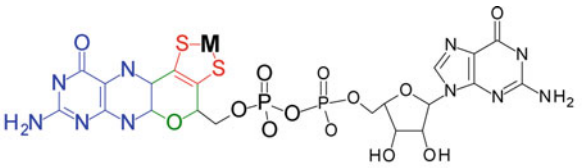

molybdenum/tungten centre in the oxidised state

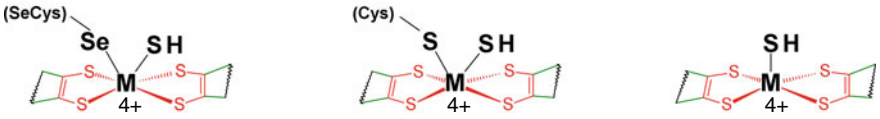

molybdenum/tungten centre in the reduced state

Fig. 10 Active site of formate dehydrogenase and *N*-formyl-methanofuran dehydrogenase. Structure of the pyranopterin cofactor (top). The pyranopterin cofactor molecule is formed by pyrano(green)-pterin(blue)-dithiolene(red)-methylphosphate(black) moieties; in all so far characterised FDHs, the cofactor is found esterified with a guanosine monophosphate (dark grey). The dithiolene (–S–C = C–S–) group forms a five-membered ene-1,2-dithiolene chelate ring with the molybdenum or tungsten ion, here indicated as M (from metal). Structure of the molybdenum/tungsten centre in the oxidised state (middle). For simplicity, only the dithiolene moiety of the pyranopterin cofactor is represented. Structure of the molybdenum/tungsten centre in the reduced state (bottom). For simplicity, only the dithiolene moiety of the pyranopterin cofactor is represented. Contrary to the oxidised state (that is consensually accepted), the structure of the reduced state is still under debate, as discussed below, under Sect. 4.3.2b. The two hypotheses under debate are represented, with the cysteine or selenocysteine residue bound to the metal and with the residue dissociated from the metal (Sect. 4.3.2b)

4.3 Formate Dehydrogenases—Mechanism of Action

4.3.1 The Metal-Independent Formate Dehydrogenases

The metal-independent FDHs are NAD-dependent enzymes, whose chemical strategy to interconvert formate and CO_2 is surprisingly simple and well established (Fig. 11) [102–109]: the enzyme binds formate and NAD^+ in close proximity of each other (1.4 Å distance between H-(formate) and C4-(pyridine ring)) and makes NAD^+ acquire a bipolar conformation, which increases its electrophilicity and, thus, facilitates the hydride transfer. The reaction, then, proceeds by straightforward hydride transfer from formate to NAD^+. In accordance, the rate-limiting step of the

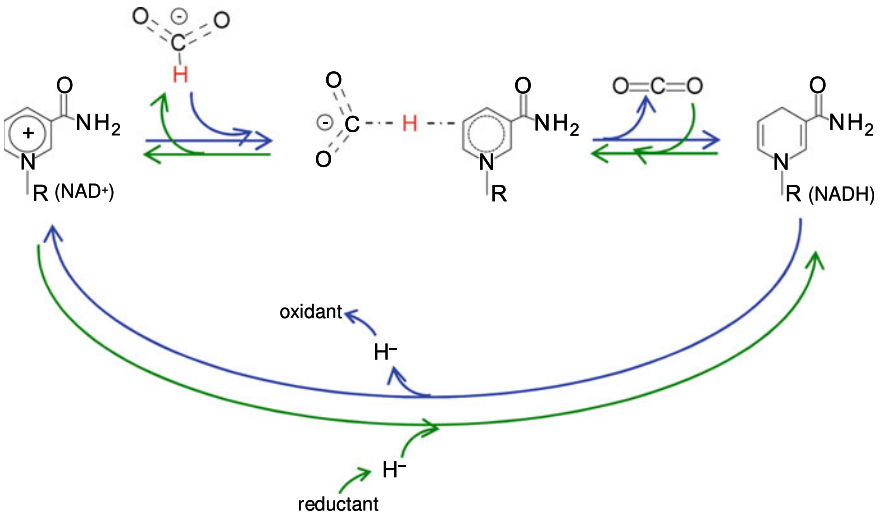

Fig. 11 Hydride transfer mechanism proposed for metal-independent NAD-dependent formate dehydrogenases

catalytic cycle is the formate C–H bond cleavage, as shown by kinetic studies of the ^{2}H-labelled formate isotopic effect), and the enzyme operate via a ternary complex (FDH-formate-NAD^{+}) kinetic mechanism [107, 170–178].

4.3.2 The Metal-Dependent Formate Dehydrogenases

Several experimental and some computational approaches have been exploited to elucidate how the metal-dependent FDHs carry out the formate/CO_2 interconversion and over the years a few mechanistic proposals have been put forward [116, 117, 137, 166, 169, 179–185]. Presently, several key points are well established, but two remain a matter of debate, and all are discussed below, before the currently accepted mechanistic hypotheses are introduced.

(a) ***Presently, several key points are well established***

(i) The formate/CO_2 interconversion occurs at the molybdenum or tungsten centre, in a reaction that is intermediated by the metal, which cycles between the +6 and +4 oxidation states (Eq. 5a–5d), as demonstrated by numerous spectroscopic and kinetic studies. The electrons necessary to carry out CO_2 reduction or released from formate oxidation are intramolecularly transferred from the physiological partner (electron donor or electron acceptor), through the different redox centres of each enzyme (Fe/S centres, haems, FAD (see above)) that act like a "wire" to facilitate the fast and effective electron transfer. Therefore, the intramolecular electron transfer is, thus, an integral aspect of the global reaction. Depending on the enzyme (on the biochemical pathway where the enzyme is involved in), the physiological redox partner can be membrane

quinols, cytoplasmatic and periplasmatic cytochromes, ferredoxins, NAD(P) or coenzyme F_{420} [94–101]. For those enzymes like the dihydrogen-dependent CO_2 reductase (see above), the electrons are directly provided by the co-substrate oxidation (dihydrogen in this case) that occurs in the enzyme second active site. As a consequence of the physical separation of the oxidation and reduction half-reactions (that occur at different enzyme centres), all these enzymes operate via a ping-pong kinetic mechanism, as observed experimentally.

$$HCOO^- + Mo/W^{6+} \rightleftharpoons CO_2 + H^+ + Mo/W^{4+} \quad (5a)$$

$$Mo/W^{4+} + \text{Physiol. Partner}^{\text{oxidised}} \rightleftharpoons Mo/W^{6+} + \text{Physiol. Partner}^{\text{reduced}} \quad (5b)$$

$$CO_2 + H^+ + Mo/W^{4+} \rightleftharpoons HCOO^- + Mo/W^{6+} \quad (5c)$$

$$Mo/W^{6+} + \text{Physiol. Partner}^{\text{reduced}} \rightleftharpoons Mo/W^{4+} + \text{Physiol. Partner}^{\text{oxidised}} \quad (5d)$$

(ii) Although the formate/CO_2 interconversion occurs at the molybdenum or tungsten centre, the reaction is not one of oxygen atom transfer, as is characteristic of many molybdoenzymes and tungstoenzymes (Fig. 12) [94, 97, 110–112, 162–165]: the substrate for "CO_2 reduction" is in fact CO_2 and not hydrogencarbonate (Eq. 6) [186], and the product of formate oxidation is CO_2 and not hydrogencarbonate (Eq. 7), as was clearly demonstrated by the formation of $^{13}C^{16}O_2$ gas during the oxidation of ^{13}C-labelled formate in ^{18}O-enriched water [166]. Therefore, to catalyse the formate oxidation, FDH has to abstract one proton plus two electrons (Eq. 8) or one hydride (Eq. 9) from the formate molecule (or the reverse for CO_2 reduction).

$$HOCOO^- + 2e^- + 2H^+ \not\longrightarrow HCOO^- + H_2O \quad (6)$$

$$HCOO^- + H_2O \not\longrightarrow HOCOO^- + 2e^- + 2H^+ \quad (7)$$

$$HCOO^- \rightleftharpoons CO_2 + 2e^- + H^+ \quad (8)$$

$$HCOO^- \rightleftharpoons CO_2 + H^- \quad (9)$$

(iii) A simple chemical reasoning, based on the pK_a values of formic acid ($HCOOH/HCOO^-$ = 3.77; $HCOO^-/CO_2^{2-} \gg 14$), demonstrates that it is

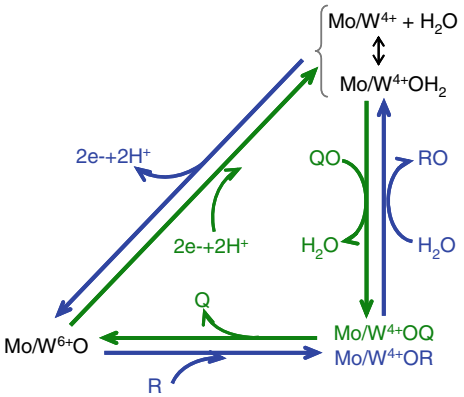

Fig. 12 Oxygen atom transfer in molybdo—and tungstoenzymes. Typically, these enzymes catalyse the transfer of an oxygen atom from water to product—oxygen atom insertion (blue arrows)—or from substrate to water—oxygen atom abstraction (green arrows)—in reactions that entail a net exchange of two electrons, in which the molybdenum/tungsten atom cycle between Mo/W^{6+} and Mo/W^{4+}, and, most importantly, where the metal is the direct oxygen atom acceptor or donor. This feature was coined by Holm and others in the 1980s as the "oxo transfer hypothesis"

much more difficult to abstract the Cα proton from formate (Eq. 8) than abstract a hydride (Eq. 9), which, in addition, lead to the formation of a stable product (CO_2), instead of a carbonanion (CO_2^{2-}) (Scheme 1). The simple mechanistic strategy followed by the metal-independent FDHs (Sect. 4.3.1.), that is, direct reaction with NAD^+, with no enzyme cofactors involved, further confirms that it must be exceptionally facile (thermodynamics) to abstract a hydride from the formate molecule. On its turn, CO_2, with an electronic structure $O\ {}^{-\delta}C^{+2\delta}\ O^{-\delta}$ and a carbon-localised LUMO, is susceptible to attack by nucleophiles and to reduction, being a good hydride acceptor, as supported by the chemistry of several synthetic transition metal-hydride complexes that mimic the FDH catalysis [65, 67, 187–192].

(iv) The terminal sulfido group of the active site (Fig. 10) is well documented as a hydride acceptor/donor. Since the 1970s, the sulfido group is established as the hydride acceptor in the oxidised molybdenum centre (Mo^{6+}=S) of xanthine oxidase and aldehyde oxidase[6] [110–112, 162–165, 193–202], as well

[6] Xanthine oxidase catalyses the hydroxylation of xanthine to urate. To carry out this reaction, xanthine oxidase promotes the cleavage of the C8–H bond of xanthine, with the hydride being transferred from the xanthine moiety to the active site sulfido group (Mo^{6+}=S → Mo^{4+}–SH); simultaneously, the active site catalyses the insertion of an oxygen atom in the xanthine moiety to produce urate (Mo^{6+}–O^- → Mo^{4+}). Aldehyde oxidase catalyses the conversion of aldehydes into the respective carboxylates, following the same chemical strategy: cleavage of the C–H bond, with transfer of hydride to the sulfido group, and subsequent insertion of an oxygen atom.

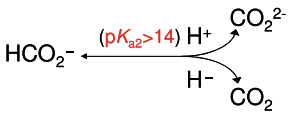

Scheme 1 Products formed by proton abstraction (ruled by a $pK_{a2} >> 14$) or hydride abstraction from formate

as, the hydride donor in the reduced centre (Mo^{4+}–SH) of hydroxybenzoyl-CoA reductase[7] [203, 204]. This "twin" behaviour (oxidised/hydride acceptor *versus* reduced/hydride donor) is supported by a remarkable characteristic of the Mo/W-ligands: the pK_a values of the coordinated ligands change dramatically with the oxidation state of the metal and determine that the higher oxidation states should hold deprotonated ligands, that is Mo/W^{6+}=S, while the lower oxidation states should hold protonated ligands, that is Mo/W^{4+}–SH [205–207]. This behaviour (Eq. 10) enables the metal-sulfido to act as a hydride acceptor/donor and is supported by the high covalency of the terminal sulfur atom in the metal sulfido group, with an available S π-bond well suited to accept a hydride.

$$Mo/W^{6+} = S + (2e^- + H^+) \rightleftharpoons Mo/W^{4+} - SH \tag{10}$$

The involvement of the sulfido group as the hydride acceptor during FDH catalysis was demonstrated by electron paramagnetic resonance (EPR) spectroscopic studies that showed that, in formate-reduced FDH, the formate Cα hydrogen atom is transferred to an acceptor group located within magnetic contact to the molybdenum atom of FDHs from different sources (*E. coli* [166], *D. desulfuricans* [136] or *Cupriavidus necator* (previously known as *Ralstonia eutropha*) [184]). The observation of a strongly coupled, solvent-exchangeable and substrate-derived proton, with a hyperfine constant of 20–30 MHz, is consistent with the hydrogen atom being transferred to a ligand in the first coordination sphere of the molybdenum atom upon its reduction [196, 197, 200, 201, 208]. Similar hyperfine constant values were determined in model complexes [209] and also in real enzymes, as in xanthine oxidase, where the strong coupled hydrogen is originated from the xanthine C8 hydrogen atom (the position that is hydroxylated by that enzyme (see Footnote 6) [196–198, 200–202, 208]. It should be noted that a hyperfine interaction of this magnitude could not arise from the transfer of the formate Cα hydrogen atom to an acceptor in the second coordination sphere of the metal, for example, transfer to the conserved histidine residue, as initially proposed [116, 117, 166, 169, 180–183], or transfer to the selenocysteine/cysteine residue if it had been dissociated from the

[7] Hydroxybenzoyl-CoA reductase catalyses the reverse reaction of the xanthine oxidase one, with insertion of a hydride and abstraction of an oxygen atom.

molybdenum/tungsten ion [117, 169, 180–183]—an hypothesis discussed below in point (vi). Photolysis assays with ^{77}Se-enriched FDH, described below in point (vi) and Footnote 8, further confirmed that the selenocysteine residue cannot be the hydrogen atom acceptor [166].

Further evidence that the sulfido group becomes protonated upon reduction was also provided by a recent X-ray absorption spectroscopy (XAS) study with the *R. capsulatus* Mo-FDH [210].

(v) The terminal sulfido group is essential to both formate oxidation and CO_2 reduction. It is well established, by numerous spectroscopic and kinetic studies, that cyanide reacts with the active site sulfido group of different molybdoenzymes, such as xanthine oxidase, and abstracts it in the form of thiocyanate, yielding a desulfo enzyme form that harbours an oxo group in the place of the native sulfido group [110–112, 193–195, 198, 199, 202]. The sulfido by oxo replacement renders xanthine oxidase and other enzymes inactive, because its active site is no longer able to accept a hydride (see Footnote 6). The same and complete cyanide inhibition is observed in several FDH, such as the ones from *Methanobacterium formicicum* [211], *Alcaligenes eutrophus* [212], *E. coli* [167], *R. capsulatus* (where the sulfido was observed to be replaced by an oxo group) [210], or *D. desulfuricans* (where thiocyanate formation accounted to 0.87 per molybdenum atom) [137]. Together with the experimental evidences that support the involvement of the sulfido group as a hydrogen atom acceptor during FDH catalysis (described above), these inhibitory results demonstrate that the sulfido group acts as a hydride acceptor/donor in FDH catalysis.

(b) ***Two interrelated points are not yet consensual***

(vi) Does the active site cysteine or selenocysteine residue dissociate from the metal during catalysis?

If the configuration of the oxidised active site is consensually accepted, the reduced form still finds a few contradictory experimental evidences (Fig. 10).

X-ray crystallography: In a reinterpretation of the crystallographic data of the reduced *E. coli* SeCys–Mo–FDH H originally obtained by Boyington et al. in 1997 [116], Raaijmakers and Romão in 2006 [117] suggested that the polypeptide loop containing the selenocysteine was not properly traced in the original work and that the selenocysteine residue is not bound to the metal, but, instead, is found dissociated from the molybdenum ion and shifted away (12 Å) (Fig. 4). Therefore, those authors suggested that, while in the oxidised state the selenocysteine residue is coordinated to the metal, the enzyme reduction triggers the residue dissociation, resulting in a square pyramidal penta-coordinated centre, where the molybdenum ion is coordinated by the *cis*-dithiolene (–S–C = C–S–) group of two pyranopterin cofactor molecules (in the equatorial positions) plus the terminal sulfido group (in the axial position) (Fig. 10). Regardless of this reinterpretation, all other

crystallographic structures so far available, for FDH and FMFDH (Figs. 4, 5, 6 and 9, and references herein), show a stable hexa-coordination, with the cysteine or selenocysteine always bound to the molybdenum/tungsten ion. This is also the case of the recently solved structure of the formate-reduced *D. vulgaris* SeCys–W–FDH [132] and also of the NADH-reduced *R. capsulatus* Cys–Mo–FDH, whose structure was determined by cryo-electron microscopy [139].

XAS: Two recent XAS studies at the Mo K-edge suggested that, in *R. capsulatus* Cys–Mo–FDH, the Mo^{5+} state holds the cysteine residue bound to the metal, as the oxidised Mo^{6+} one, with a Mo-S(Cys) bond of 2.63 Å, while the Mo^{4+} state of formate-reduced enzyme has its cysteine displaced form the metal [169, 210]. However, contrary results were obtained with SeCys–Mo–FDHs from *E. coli* [213] and *D. desulfuricans* [214], which showed a metal bound residue in all oxidised and reduced states: the *E. coli* enzyme EXAFS data at both the Mo and Se K-edges were interpreted as indicating the presence of one Mo–Se bond of 2.62 Å, plus one Se–S bond of 2.19 Å (between the sulfido group and the selenocysteine selenium) [213].

EPR spectroscopy: Further experimental evidence for the stable molybdenum/tungsten hexa-coordination came from EPR spectroscopy that clearly showed that the selenocysteine/cysteine must remain bound to the Mo^{5+} centre of formate-reduced enzyme [208]. When the EPR spectrum is obtained from ^{77}Se-enriched enzyme, a very strong and anisotropic interaction with selenium is observed ($A_{1,2,3}(^{77}Se)$ = 13.2, 75, 240 MHz) [166]. This interaction and the observation of the expected ^{95,97}Mo hyperfine coupling confirms that the selenium atom of the selenocysteine is directly coordinated to the Mo^{5+} and further suggests that the unpaired electron is delocalised over the selenium (17–27%) and molybdenum atoms (73–83%) [166]. Also, the hydrogen atoms of the β-methylene carbon of the selenocysteine residue are thought to be in the close proximity of the molybdenum atom, being responsible for an interaction with a not solvent-exchangeable protons (A_1 = 35.1 MHz) [136]. Photolysis assays additionally confirmed that the selenium/sulfur ligation is retained in the FDH Mo^{5+} centre (the light beam did not affect the strong selenium–molybdenum EPR interaction observed in ^{77}Se-enriched FDH)[8] [166]. The Mo^{5+} hexa-coordination (resulting from having the selenocysteine/cysteine residue bound to the molybdenum ion) was also supported by theoretical calculations on the signals-giving species of FDHs [215].

Inhibition assays: A different type of experimental evidence came from inhibition studies with iodoacetamide, an alkylating agent that reacts with "free" ionised selenocysteine or cysteine residues (carboxamidomethylation). Native *E. coli* SeCys–Mo–FDH H and its cysteine mutant [216] and native *R. capsulatus* Cys–Mo–FDH [183] are not inhibited by iodoacetamide treatment. However, when the preliminary iodoacetamide treatment (incubation) is carried out in the presence of formate (not under turnover), both native and cysteine-containing mutant *E. coli*

[8] These photolysis assays also demonstrate that the selenocysteine residue is not the formate Cα hydrogen acceptor [166]: while the light beam did not affect the ^{77}Se interaction, it induced the photolysis of the solvent-exchangeable formate-derived proton, showing that the selenocysteine residue does not bind the strongly coupled proton mentioned above.

FDHs are inhibited [216]. Inhibition is also observed in the *R. capsulatus* FDH, but only when the iodoacetamide treatment (incubation) is carried out in the presence of nitrate; in this case, the cysteine carboxamidomethylation was confirmed by mass spectroscopy [183]. On the other hand, native *D. vulgaris* SeCys–W–FDH is inhibited by iodoacetamide, but mass spectroscopy clearly showed that the inhibition is not due to the carboxamidomethylation of the active site selenocysteine residue (but of 9 other cysteine residues not present in the active site) [132]. In addition, other FDHs are not at all affected by iodoacetamide [135, 136]. Hence, the inhibition results available were not obtained under formate/CO_2 turnover conditions and the inconsistency of the results, once more, do not contribute to provide a definitive answer.

Overall, the majority of experimental evidences points towards a molybdenum/tungsten stable hexa-coordination, with the cysteine/selenocysteine residue always bound to the metal. Regarding the results showing a metal penta-coordination, with unbound cysteine/selenocysteine residue, it is possible that the crystallisation/irradiation had induced some artefacts that are not relevant to the enzyme activity; but it is also possible that the species crystallographically characterised, being catalytically relevant, bear no relation to the species observed by XAS and EPR (with these being not catalytically relevant). Certainly, high-resolution structures are needed to confirm the existence of the two alternating conformations of the selenocysteine/cysteine-containing polypeptide loop and to discuss the catalytic relevance of each conformation.

(vii) Do formate/CO_2 bind directly to the molybdenum/tungsten ion during catalysis?

Inspired by the oxotransfer chemistry displayed by several molybdenum—and tungsten-dependent enzymes (Fig. 12) [110–112, 162–165], and in particular by periplasmatic nitrate reductases[9], it was suggested that FDH catalysis necessarily involves the formate/CO_2 direct binding to the molybdenum/tungsten ion [180, 218].

To begin the discussion of this point, it should be noted that the direct formate/CO_2 binding would involve an unprecedented hepta-coordinated

[9] The *C. necator* periplasmatic nitrate reductase catalyses the reduction of nitrate to nitrite ($ONO_2^- + 2e^- + 2H^+ \rightarrow NO_2^- + H_2O$), and it was described to share with FDHs the same molybdenum coordination sphere, with the *cis*-dithiolene (–S–C = C–S–) group of two pyranopterin cofactor molecules, one terminal sulfido group and one sulfur atom from a cysteine residue [217]. The similarity in the active site metal centre led some authors to suggest similar mechanistic strategies for nitrate reductases and FDHs—leading to the so-called sulfur-shift mechanism [180, 218].

To give further support to the hypothesis of a similar mechanistic strategy, the nitrate reductase activity of different FDHs was investigated. The *R. capsulatus* Cys-Mo-FDH was described to be able to catalyse the nitrate reduction to nitrite, even though at an extremely low catalytic constant (k_{cat}(nitrate) = 0.21 min^{-1} [183] that compares very poorly with k_{cat}(formate) = 2124 min^{-1} and $k_{cat}(CO_2)$ = 89 min^{-1} [182]), and the catalysis was suggested by XAS to involve the dissociation of the cysteine residue from the molybdenum ion, with the subsequent nitrate binding [183]. However, other FDHs failed to reduce nitrate (such as the ones from *D. desulfuricans* [135, 136], *D. vulgaris* [132]).

molybdenum/tungsten centre or it would depend on the dissociation of the cysteine/selenocysteine residue from the metal, in order to create a vacant position (penta-coordinated centre) for substrate binding. While the hypothesis of the hepta-coordinated metal centre was (so far) never perused, the dissociation of the cysteine/selenocysteine is, as discussed above, controversial.

The two recent XAS studies mentioned above in point (vi) suggested that, in the presence of formate, the cysteine ligation of (active) *R. capsulatus* Cys–Mo–FDH is replaced by a long Mo–O bond of 2.15 Å, which was interpreted as arising from the Mo–OCO(H) complex [169, 210]. The strong and competitive inhibition of *E. coli* SeCys–Mo–FDH H-catalysed formate oxidation by azide, cyanate, thiocyanate, nitrite and nitrate (1–00 μM range) was also evoked to support that formate, as well as those inhibitors, bind directly to the molybdenum ion [219]. Yet, competitive inhibition can arise if the inhibitor binds in the active site, but not directly to the metal[10] [220]; this seems to be the case at least of azide, a well documented inhibitor of both metal-independent [104, 171, 177] and metal-dependent [136, 166] FDHs (as suggested by EPR [136, 215]) and nitrite (as suggested by crystallography[11]). Regarding nitrate, (once more) several other FDH enzymes are not inhibited or the inhibition constants are 2–3 orders of magnitude higher than K_m(formate) [132, 135, 136, 166], or it is though as a substrate (even though a very poor one; see Footnote 9 [182]). Moreover, the same study [219] showed that the inhibition of the *E. coli* SeCys-Mo-FDH H-catalysed CO_2 reduction by those anions is very weak (in the range of 1–50 mM) and not competitive in nature, results that are contradictory to the hypothesis that the reduced active site (the one that reacts with CO_2) becomes penta-coordinated, with an unbound selenocysteine residue, and with an available position to bind inhibitors and CO_2.

Therefore, except from the abovementioned XAS data, there are no other direct experimental evidences of the direct formate or CO_2 binding to the FDH molybdenum/tungsten ion; namely, there are no crystallographic structures showing the formate molecule in the active site and there are no EPR signals showing the presence of formate in the first coordination sphere of molybdenum/tungsten [136, 166, 184].

[10] The active site conserved arginine residue, below suggested to be key to "anchor" formate and CO_2 during turnover, could also be involved in the binding of these inhibitory anions through electrostatic interactions—to have a strong and competitive inhibition of the formate oxidation, it is not necessary that those anions bind directly to the molybdenum/tungsten ion it self.

The observed very weak inhibition of the CO_2 reduction by those anions (mentioned below in this point (vii)) could be explained by subtle conformational changes involving the conserved histidine residue upon reduction of the active site. Such conformational changes were described for *D. vulgaris* FDH [132] and could explain why those inhibitory anions would not be stabilised at the arginine spot within the reduced active site. Therefore, both the formate oxidation (strong inhibition) and the CO_2 reduction (weak inhibition) could be inhibited without evoking the direct binding of the inhibitory anions to the metal or the dissociation of the selenocysteine residue.

[11] Boyington et al. [116] described the structure of *E. coli* SeCys-Mo-FDH treated with the inhibitor nitrite as showing the selenocysteine bound to the molybdenum ion and the nitrite molecule with one of its oxygen atoms at 2.58Å from the molybdenum.

Theoretically, it can be argued that, since the FDH-catalysed reaction does not involve the transfer of an oxygen atom (as explained above in point (ii)), there is no need to form the otherwise expected Mo/W^{6+}–OCO(H) or Mo/W^{4+}–OCO complexes (follow Mo^{4+}–OR and Mo^{4+}–OQ in Fig. 12). It can also be argued in the opposite way: if formate/CO_2 binds directly to the molybdenum/tungsten ion, why there is no oxygen atom transfer to form hydrogencarbonate (Eq. 7)? Overall, in the absence of more definitive experimental evidences, we must continue to ask: Does the direct formate/CO_2 binding to the metal occur? Is it necessary or desirable to interconvert formate and CO_2? Is the penta-coordinated metal centre with unbound cysteine/selenocysteine catalytically relevant?

(c) ***Currently accepted mechanistic hypotheses***

In accordance with the well-established points (i) to (v) highlighted above, the FDH-catalysed formate oxidation and CO_2 reduction are presently recognised to occur through hydride transfer (Eq. 9), with the oxidised and reduced active site sulfido group, Mo/W^{6+}=S and Mo/W^{4+}–SH, acting as the direct hydride acceptor and donor, respectively. Yet, points (vi) and (vii) still raise questions to some authors regarding the coordination of the active site and substrates binding during FDH catalysis.

As originally proposed by Niks et al. [184] for formate oxidation and shortly after also for CO_2 reduction [137], we suggest that FDH catalysis proceeds as follows (the reaction mechanism is suggested to be identical in Mo–FDH and W–FDH, as well as in FMFDH):

Formate oxidation (Fig. 13, blue arrows) is initiated with the formate binding to the oxidised active site, but not directly to the molybdenum/tungsten atom. Following the example provided by the metal-independent FDH, where the formate-binding site harbours arginine and asparagine residues [102–109], it is suggested that the conserved arginine residue is essential to drive the formate Cα hydrogen towards the sulfido ligand, by establishing hydrogen bond(s) with its oxygen atom(s). Also, azide (N_3^-, isoelectronic with CO_2) is suggested to bind (tightly) to the same site and not directly to the molybdenum/tungsten ion (as had been previously suggested for the *D. desulfuricans* FDH inhibition by azide [136, 215]). The binding of azide and formate to the same site, and not to the molybdenum/tungsten atom itself, explains why azide is a powerful inhibitor of both metal-independent (K_i = 40 nM for *Candida boidinii*) [104, 171, 177] and metal-dependent FDHs [136, 166]. A similar reasoning applies to the inhibitor nitrite (isoelectronic with formate). Formate oxidation, then, proceeds by a straightforward hydride transfer from formate to the sulfido group of the oxidised molybdenum/tungsten centre, Mo/W^{6+}=S, leading to the formation of Mo/W^{4+}–SH and CO_2. The re-oxidation of Mo/W^{4+} to Mo/W^{6+} (via intramolecular electron transfer to the enzyme other(s) redox centre(s) and, eventually, to the physiological partner) and the release of CO_2 close the catalytic cycle. The now oxidised Mo/W^{6+} favours the sulfido group deprotonation (dictated by the ligand pK_a [205–207]), and the initial oxidised

molybdenum/tungsten centre, Mo/W^{6+}=S, is regenerated. Under non-steady-state catalytic conditions (as the ones created in EPR experiments) the molybdenum/tungsten one-electron oxidation should be favoured ($Mo/W^{4+} \rightarrow Mo/W^{5+}$), leading to the formation of the EPR detectable Mo^{5+}–SH species.

CO_2 reduction is suggested to follow the reverse reaction mechanism (Fig. 13, green arrows). First, CO_2 binds to the reduced active site, not directly to the molybdenum/tungsten ion, but at the same site as formate (and azide), with the conserved arginine anchoring its oxygen atom(s) through hydrogen bond(s) and orienting its carbon atom towards the protonated sulfido ligand. In an approximated way, based on the inhibition and Michaelis–Menten constants for the *D. desulfuricans* FDH, the "binding strength" is suggested to follow the order CO_2 ($K_m \approx 15$ μM [137]) > azide ($K_i \approx 30$ μM [136]) > formate ($K_m \approx 60$ μM [137]). Then, the reaction proceeds through straightforward hydride transfer from the protonated sulfido group of the reduced molybdenum/tungsten centre, Mo/W^{4+}–SH, to the CO_2 carbon, whose LUMO have predominant C–π orbital character, prone to nucleophile attack and reduction. This yields a formate moiety and Mo/W^{6+}=S. The subsequent re-reduction of Mo/W^{6+} to Mo/W^{4+} (via intramolecular electron transfer from the enzyme physiological partner, through its redox centre(s)) and formate release closes the catalytic cycle. The now reduced Mo/W^{4+} favours the sulfido group protonation and the initial reduced molybdenum/tungsten centre, Mo/W^{4+}–SH, is regenerated.

The FDH-catalysed reaction is reversible and the equilibrium between formate oxidation *versus* CO_2 reduction is determined by the availability of formate *versus* CO_2 and the ability to maintain the active site oxidised (Mo/W^{6+}) *versus* reduced (Mo/W^{4+}), which, in its turn, determines the protonation state of the metal sulfido group in a concerted and straightforward way.

Overall, the chemical strategy herein suggested is exactly the same as the one proposed for the metal-independent FDHs: both bind formate in a close proximity to an oxidised, electrophilic, hydride acceptor, which in metal-independent enzymes is a NAD^+ molecule and in metal-dependent enzymes is the M^{6+}=S group; both bind CO_2 in a close proximity of a reduced, nucleophilic, hydride donor, a NADH molecule or the M^{4+}–SH group.

As expected, this mechanistic proposal faces some criticism and the most relevant one concerns the role of the active site selenocysteine/cysteine residue. In fact, although the mechanism is suggested to operate in a hexa-coordinated metal centre (Fig. 13), it can also take place in a penta-coordinated centre (Fig. 10), with an unbound selenocysteine/cysteine—the sixth ligand does not seem to interfere with the hydride transfer[12]. Even though there are experimental evidences (as discussed above) and mechanistic arguments can be envisaged to support the necessity of having a bound selenocysteine/cysteine (as discussed in [96, 98]), in the absence of

[12] It should be noted that, xanthine oxidase, for example, that also uses a terminal sulfido group as the hydride acceptor in the conversion of xanthine to urate, has a molybdenum penta-coordinated active site, with no amino acid residues bound to it (the molybdenum ion is coordinated by the *cis*-dithiolene (–S–C = C–S–) group of one pyranopterin cofactor molecule, the terminal sulfido group plus two oxo groups (see previous Footnotes and references in the text).

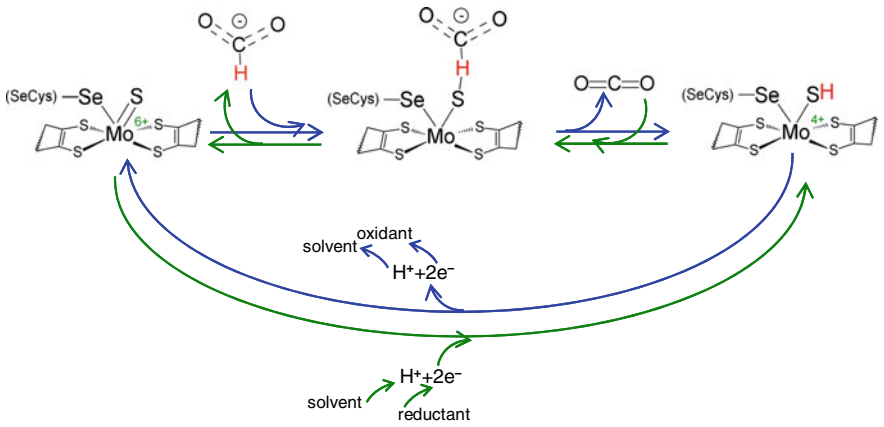

Fig. 13 Reversible hydride transfer mechanism proposed for metal-dependent formate dehydrogenase and *N*-formyl-methanofuran dehydrogenase [137, 184]. Reaction mechanism proposed for formate oxidation (blue arrows) and CO_2 reduction (green arrows). For simplicity, the mechanism is represented only for a molybdenum, selenocysteine-containing enzyme, but it should be similar for tungsten and cysteine-containing enzymes. See text for details. A similar hydride transfer mechanism can also take place with a penta-coordinated reduced metal centre, with a dissociated selenocysteine/cysteine residue (see text for details)

clear and definitive experimental evidences, both scenarios—*dissociated and bound selenocysteine/cysteine*—seem to be possible and this is an aspect that will remain in open for now. Certainly, future research will shed light in these aspects of the FDH reaction, allowing a critic evaluation of this mechanistic proposal.

4.4 Formate Dehydrogenases in the Context of Carbon Dioxide Utilisation

The majority of currently known FDHs function in vivo to oxidise formate, with only a few participating in metabolic pathways to reduce (fix) CO_2—the reaction direction that is interesting to "solve humankind's problem" with atmospheric CO_2. However, the CO_2/formate interconversion is thermodynamically reversible ($E^{\circ\prime}$ (CO_2/$HCOO^-$) = −0.43 V) and in vitro there is no a priori reason for a FDH to be unable to catalyse the CO_2 reduction, as long as there is sufficient reducing power available[13]. Regarding the metal-independent FDHs, this simply means the adequate NADH/NAD^+ ratio (Eq. 11); in what concerns the metal-dependent FDHs,

[13] *In vivo*, in the great majority of the cases, the reaction is tuned to operate only in one direction; this is determined by the reduction potential of the enzyme redox centres, by the available physiological electron partners and substrates and by the redox status of the subcellular location where the reaction takes place. The few exceptions are mainly related with regulation points of the metabolism.

this means that the molybdenum/tungsten active site centre must be kept reduced at the proper reduction potential (Eq. 12). Although at first sight obvious, the necessity to keep the enzyme active site reduced is most often overlooked, what may explain why there are so many reports in the literature of FDHs unable to reduce CO_2. This is particularly true for metal-dependent FDHs: if the reduction potential of one (or more) of the FDH redox centres is (are) relatively high, it could be difficult to "push" the electrons into the active site (the centre with the higher reduction potential could stay reduced, "blocking" the electron transfer to the other (s) centre(s) with lower reduction potentials and the active site in particular). In addition to thermodynamics, also the kinetics has to be taken into account to evaluate if the CO_2 reduction is going to be efficient, or too slow relatively to the formate oxidation to be relevant (rate of formate oxidation versus CO_2 reduction, Eqs. 13, 14). The key point here is that FDH kinetics is determined by four parameters, the K_m and k_{cat} for the two substrates (CO_2 and formate), and the reaction can be run under different regimes (mainly forward, mainly reverse and equilibrium, as determined by k_{cat}/K_m and imposed conditions). However, except for protein engineering (a difficult task on its own), there is not much that can be done to modify the kinetic parameters to further favour the CO_2 reduction.

$$CO_2 + NADH \rightarrow HCOO^- + NAD^+ \tag{11}$$

$$CO_2 + FDH\left(Mo/W^{4+}\right) \rightarrow HCOO^- + FDH\left(Mo/W^{6+}\right) \tag{12}$$

$$CO_2 + A_{red} \overset{k^{CO_2}}{\rightarrow} HCOO^- + A_{ox} \tag{13}$$

$$HCOO^- + A_{ox} \overset{k^{HCCO-}}{\rightarrow} CO_2 + A_{red} \tag{14}$$

Also, the enzymes stability and potential interfering compounds must be well thoughtout. The lifetime of a CO_2 converter device is a critical issue, and it would greatly depend on the time the enzyme maintains its full activity. In this respect, it should be emphasised that the purifying processes often decrease the enzymes stability and even make them unstable (while taken out of their biological environment), thus hampering their usage in a sustained ("real life") way or just making the scale up process unviable. The inhibition and inactivation by compounds that might be present in the "substrate reaction mixture"; for example, dioxygen or carbon monoxide, are pitfalls that must be considered to avoid the need (additional cost) of using purified CO_2. The inhibition or inactivation (or, on the contrary, improved stability) by the materials used to build the device cannot be overlook also.

The enzyme–material "communication" is another major challenge in hybrid systems. It is necessary to properly orient and "link" the enzyme to the material (for example, electrode or light absorber), via electrostatic or covalent interactions to maximise the charge transfer. In this respect, features as the enzyme size (in the

nanoscale) and local-specific surface charge/hydrophilicity/hydrophobicity must be taken into consideration when choosing the materials and its functionalisations.

Having these general points tackled, any FDH could be used to build a device to promote the CO_2 reduction. The same would be true for whole-cell devices, but considering in that case the organism whole metabolism (carbon and energy needs).

4.5 Formate Dehydrogenases in Action

The use of enzymes and whole-cells systems to convert CO_2 into VC is growing exponentially due to the "green" advantages the "biochemical way" can offer, namely substrate and product specificity (ability to discriminate the substrate in a complex mixture and to produce only the product of interest) in reactions at ambient temperature and pressure and neutral pH. Numerous hybrid systems are currently being exploited to convert CO_2 into formate, following the same master lines as described in Sect. 3 (Fig. 2). Like electrochemistry, bioelectrochemistry is currently under intense research, as is reviewed in [221–227] and references herein (below). Most interest is also being focused on the biophotoreduction of CO_2, as solar light represents the most straightforward way to use a RES to convert CO_2. Semi-artificial photosynthesis systems have been devised, where enzymes and also entire metabolic pathways within cells are interfaced with synthetic materials to develop new solar-to-VC and solar-to-fuel devices, which would not be feasible with natural or artificial systems alone [228 and references herein (below)]. The direct CO_2 hydrogenation is also getting enormous attention, mimicking metabolic pathways, where the formate-hydrogen lyase systems are the most explored examples, but using also whole-cells systems. Most important are the breakthroughs achieved by exploiting the recently identified metabolic pathways of acetogens and its dihydrogen-dependent CO_2 reductase enzymes (Sect. 4.2.2.), as is reviewed by Litty and Müller in this Book [152] and also [153–159] and references herein (below).

Herein (below), a few promising studies and successful proof of concepts of FDH-dependent CO_2 reduction to formate and beyond are discussed, to highlight the power of FDHs and the challenges this CO_2 bioconversion still faces.

One of the most efficient CO_2 reducers so far described (along with the *T. kivui* enzyme described below) is a SeCys–W–FDH from the *Synthrobacter fumaroxidans* that displays an impressive rate of CO_2 reduction of $\approx 2.5 \times 10^3 s^{-1}$ (reported as $900 U mg^{-1}$; K_m^{CO2} not determined, assays with 10 mM hydrogencarbonate), with a slightly lower formate oxidation rate ($\approx 1.9 \times 10^3 s^{-1}$ (reported as $700 U mg^{-1}$); $K_m^{HCOO^-}$ of 40 μM) [229–231]. This enzyme is also a good electrocatalyst to carry out the electrochemical reduction of CO_2 to formate, using mild conditions and applying small overpotentials, with a maximum current density of $\approx 80\ \mu A cm^{-2}$ that corresponds to $\approx 110\ s^{-1}$ (from a monolayer of enzyme) [232]. Intriguingly, while in homogeneous catalysis in solution the CO_2 reduction is slightly faster than the formate oxidation, in the electrochemical-assisted reduction/oxidation is the formate oxidation that is more than 2 times

faster (with a current density of $\approx$ 200 μAcm^{-2} [232]). *S. fumaroxidans* expresses another very fast CO_2 reducer SeCys-W-FDH, with a rate of $\approx$ 200 s^{-1} (reported as 90Umg^{-1}) [229–231], but its CO_2 reduction activity cannot kinetically compete with its highly efficient formate oxidation, rate of $\approx 5.6 \times 10^3 s^{-1}$ (value reported as 2700Umg^{-1}) and $K_m^{HCOO^-}$ of 10 μM. Unfortunately, these enzymes are extremely oxygen-sensitive, and no further studies towards a biotechnological application were pursuit, as far as we know.

Several other FDHs have been described to be able to reduce CO_2, but at considerably lower rates. Numerous studies have been conducted with metal-independent FDHs, many of which relying on sacrificial electron donors [233–248]. This is the case of the *C. boidinii* NAD-dependent metal-independent FDH, that, in spite of its considerably low $k_{cat}^{HCO3^-}$ value of only 0.009 s^{-1} ($K_m^{HCO3^-} \approx$ 27.3 mM [240]; $k^{HCO3^-} \approx 0.3\ M^{-1}s^{-1}$; $k_{cat}^{HCOO^-} \approx 5.0\ s^{-1}$; $K_m^{HCOO^-} \approx 5.0$ mM; $k^{HCOO^-} \approx 1.0 \times 10^3 M^{-1}s^{-1}$ [109]), has been largely exploited for its ability to reduce CO_2. To push the reaction in the desired, but thermodynamically unfavourable, direction[14] is important to remove NAD^+/regenerate NADH (also essential for the process to become cost-effective, since NADH is a very expensive reducing agent). Four selected examples of different strategies to force the reaction towards the CO_2 reduction are: (a) an electroenzymatic cell where NADH is electrochemically regenerated through a rhodium complex, with which a formate formation rate of $\approx 3.2 \times 10^{-4}$ μmolmin^{-1}mg^{-1} was achieved [240]; (b) electrochemical NADH regeneration, but with an electropolymerised mediator-regenerator (neutral red) in a novel cathode with immobilised FDH, which is able to produce formate at a rate of $\approx$ 60 μMmin^{-1}) [249]; (c) photocatalytical NADH regeneration using a rhodium complex and a visible light-active photocatalyst) that enabled a formate formation rate of $\approx$ 1 μmolmin^{-1} [250]; (d) and enzymatic regeneration, using glutamate dehydrogenase with NAD(H) being covalently attached to micro-particles, to be easily recovered and reused, in an approach that allowed to improve the reaction yield from 0.12 to 1.27 methanol formed/NADH consumed (in this study, formate was further reduced to methanol) [251]. The *Thiobacillus* sp KNK65MA NAD-dependent metal-independent FDH exhibit an as well low k_{cat} value ($k_{cat}^{HCO3^-} \approx 0.32\ s^{-1}$; $K_m^{HCO3^-} \approx 9.2$ mM; $k^{HCO3^-} \approx 35\ M^{-1}s^{-1}$), but its specificity for formate is only 3 times superior ($k_{cat}^{HCOO^-} \approx 1.8\ s^{-1}$; $K_m^{HCOO^-} \approx 16$ mM; $k^{HCOO^-} \approx 110\ M^{-1}s^{-1}$) [252]. This *Thiobacillus* enzyme was successfully used to reduce CO_2 by coupling it with a NADH photoelectrochemical regeneration system (Fig. 14), with a formate production rate of 2 μMmin^{-1} (current density $\approx$ 3.5mAcm^{-2}) [245].

The metal-dependent FDHs display a wide range of CO_2 reduction rates. The *Clostridium carboxidivorans* NAD-dependent SeCys-W-FDH exhibits a considerably low $k_{cat\,2}^{CO}$ value (only 0.08 s^{-1}; $K_m^{HCO3^-} \approx 50$ μM) [144, 145, 147].

[14] The reduction potential values of the $NAD(P)^+$/NAD(P)H (−0.32 V) and CO_2/$HCOO^-$ (−0.43 V) pairs indicate that the NADH-dependent CO_2 reduction (Eq. 11) is thermodynamically highly unfavourable. To force the reaction towards the CO_2 reduction is important to remove the product (NAD^+) and maintain (regenerate) the substrate (NADH) concentration.

Nevertheless, it enabled the photoelectrochemical CO_2 reduction to formate within an enzyme cascade that led to the methanol production at $\approx$ 4 μMmin^{-1}) [253]. The *Methylobacterium extorquens* AM1 NAD-dependent Cys-W-FDH has also been exploited with different approaches to drive the electrochemical CO_2 reduction [242, 254–258]. Using mediated enzymatic bioelectrocatalysis with gas diffusion electrodes[15], current densities of 15–20mAcm^{-2} were attained [254, 255]; in a whole-cell catalyst, *M. extorquens* was able to electrochemically produced formate concentrations of up to 60 mM [242].

The *R. capsulatus* [182] and *Cupriavidus oxalaticus* [259] NAD-dependent Cys–Mo–FDH enzymes, on the other hand, have $k_{cat\,2}^{CO}$ values, of 1.5 s^{-1} and $\approx$ 3 s^{-1}, respectively, but $\approx$ 25 and $\approx$ 30 times (respectively) lower than the one for formate oxidation (*R. capsulatus* $K_m^{HCOO-} \approx 280$ μM and $K_{m\,2}^{CO}$ not determined, assays with 100 mM hydrogencarbonate; *C. oxalaticus* $K_m^{HCOO-} \approx 100$ μM and $K_m^{HCO3-} \approx 40$ mM). The *C. necator* NAD-dependent Cys–Mo–FDH, on the contrary, catalyses the reduction of CO_2 with a $k_{cat\,2}^{CO} \approx 11$ s^{-1} ($K_{m\,2}^{CO} \approx 2.7$ mM; $K_m^{NADH} \approx 45$ μM) [260, 261]. To fulfil the potential industry application of this oxygen-tolerant and robust enzyme, it is necessary to implement a NADH regenerating system that pushes the reaction towards CO_2 reduction (as discussed above; see Footnote 14) [262]. With the *C. necator* FDH, this was successfully achieved with the inclusion of glucose dehydrogenase in the system (Fig. 15), which, while catalysing the re-reduction of NAD^+ to NADH, enabled the continuous electron delivery to drive the CO_2 reduction and, therefore, improved the reaction yield from 0.2 to 1.8 formate formed/NADH consumed [262].

The *E. coli* SeCys-Mo-FDH H was also shown to be able to reduce CO_2 [263], but at rates considerably lower than the ones of formate oxidation, < 1 *versus* 160 s^{-1} [263]. Interestingly, when the reaction is driven electrochemically (protein film voltammetry), the formate oxidation was only two times higher than the CO_2 reduction, with current densities of 180 *versus* 80 μAcm^{-2}, respectively [263]. This *E. coli* enzyme feature has been exploited in fuel cell devices (FDH immobilised in redox mediators-functionalised redox polymers) [15, 16], where CO_2 could be reduced with a very high Faradaic efficiency (99%) and a current density of $\approx$ 60 μAcm^{-2} ($K_m^{HCO3-} \approx 2.5$ mM) [16]. Thanks to the FDH H-containing formate-hydrogen lyase system (Sect. 4.2.2.)[16], engineered *E. coli* whole cells were also used as a "cell factory" to very efficiently produce formate from a gaseous mixture of CO_2 and dihydrogen (56:44; up to 10 bar) (Fig. 16); an 100% of CO_2 conversion was achieved, with formate (more than 500 mM) being accumulated outside the bacterial cells [264]. Intact *E. coli* cells were also used in a microbial

[15] Gas diffusion electrodes (GDE) promote electrochemical reactions between the liquid and the gaseous phase, thus eliminating the limitations arising from slow mass transport when hydrogencarbonate/carbonate is used as CO_2 source.

[16] Under physiological conditions the *E. coli* formate-hydrogen lyase system catalyses the formate oxidation to CO_2 coupled to the reduction of protons to dihydrogen (Sect. 4.2.2.); yet, under a pressurised (up to 10 bar) atmosphere of CO_2 and dihydrogen, engineered *E. coli* (with abolished "respiratory" FDH, pyruvate-formate lyase and all major hydrogenases) whole cells efficiently catalyse the reverse reaction of formate formation.

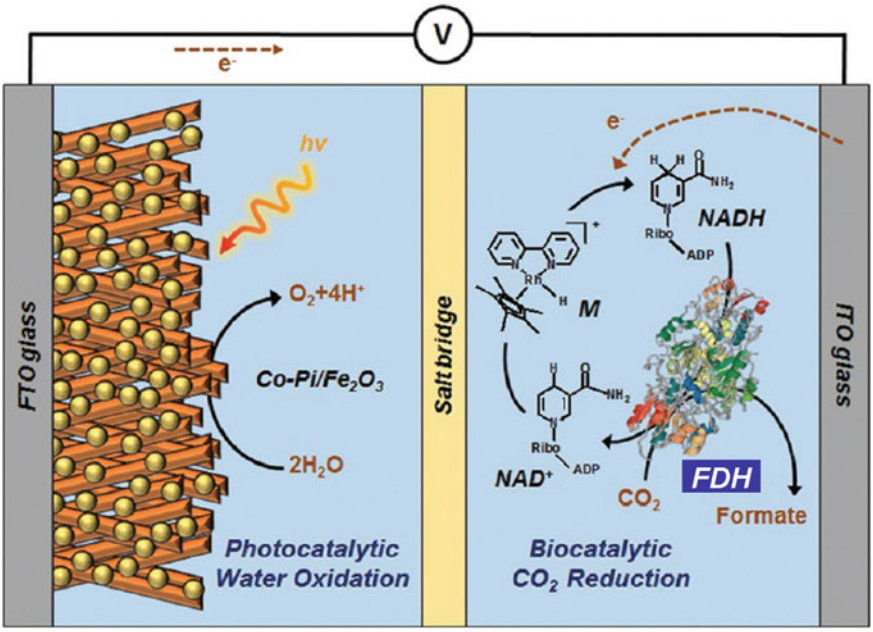

Fig. 14 Schematic diagram of enzymatic photosynthesis of formic acid using *Thiobacillus* FDH coupled with photoelectrochemical regeneration of nicotinamide cofactors. Co-Pi, cobalt phosphate. See text and Ref. [245] for details. Reproduced (from Ref. [245]) by permission of the Royal Society of Chemistry. All rights reserved. https://doi.org/10.1039/c6gc02110g

electrolysis system using an iron-modified carbon cathode, with which a formate production rate of $\approx 10\ \mu\text{Mmin}^{-1}$, with a Faradaic efficiency of $\approx 60\%$, was attained [265].

FDHs from sulfate-reducing bacteria constitute other very interesting systems to exploit, exhibiting high rates of CO_2 reduction. The *D. desulfuricans* SeCys–Mo–FDH is a strikingly efficient CO_2 reducer. With a $k_{cat}^{CO_2} \approx 50\ s^{-1}$ and particularly low $K_m^{CO_2} \approx 15\ \mu M$, this enzyme has a superior specificity for CO_2 ($k^{CO_2} \approx 3.3 \times 10^6 M^{-1}s^{-1}$) [137]. The high K_m value for formate ($K_m^{HCOO^-} \approx 55\ \mu M$; $k_{cat}^{HCOO^-} \approx 550\ s^{-1}$; $k^{HCOO^-} \approx 10 \times 10^6 M^{-1}s^{-1}$) enables *D. desulfuricans* SeCys–Mo–FDH to be a powerful CO_2 reducer, as long as the formate concentration is kept low (is removed from the system). In addition, once the catalysis is initiated (occurring at steady-state rates), this enzyme robustness allows the reaction to fully proceed even in the presence of dioxygen [139]. Moreover, the *D. desulfuricans* SeCys–Mo–FDH is also a good electrocatalyst (unmediated electrochemistry) to carry out the electrochemical reduction of CO_2 with good catalytic currents being attained [266]. The ability of *D. desulfuricans* to produce formate was also demonstrated in whole-cells catalysis, where the continuous formate production exhibited a maximum specific formate production rate of 14 mM formate/g_{dcw}h, and more than 45 mM of formate were obtained with a production rate of 0.40mMh^{-1} [267].

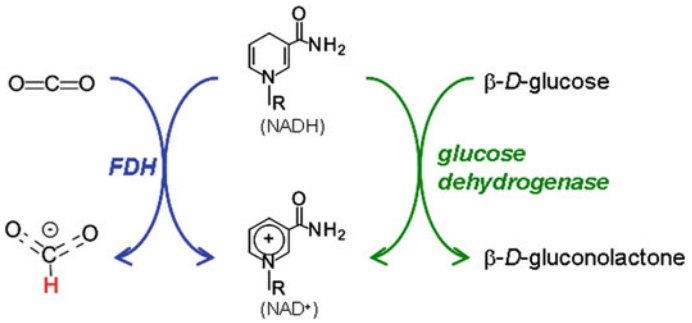

Fig. 15 Schematic diagram of the enzymatic cascade reaction *C. necator* FDH and glucose dehydrogenase. See text and Ref. [262] for details

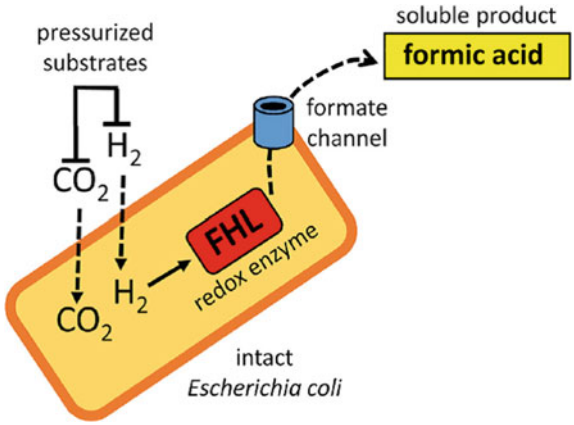

Fig. 16 Schematic diagram of a "cell factory" to produce formate using *E. coli* whole-cells. FHL, formate-hydrogen lyase. See text and Ref. [264] for details Adapted with permission from Ref. [264]. http://creativecommons.org/licenses/by/4.0/

The *D. vulgaris* contains also several interesting FDHs. One SeCys–Mo–FDH is able to catalyse the CO_2 reduction at a rate of $\approx$ 3.4 s^{-1} (reported as 1Umg^{-1}) [129, 131, 268]. However, its extremely low K_m value for formate ($K_m^{HCOO^-}$ of 8 μM) and higher rate of formate oxidation ($k_{cat}^{HCOO^-} \approx 260\ s^{-1}$) makes this enzyme a very interesting biocatalyst to oxidise formate instead, namely to be coupled to dihydrogen production. The proof of concept that *D. vulgaris* is able to produce dihydrogen at high volumetric and specific rates (0.125 dm^3 H_2/dm^3h^1 and 2.5 dm^3 $H_2/g_{dcw}h$) was obtained recently, with the demonstration that whole cells are able to grow by catalysing the oxidation of formate to hydrogencarbonate and dihydrogen, in the absence of sulfate or a syntrophic partner [268, 269].

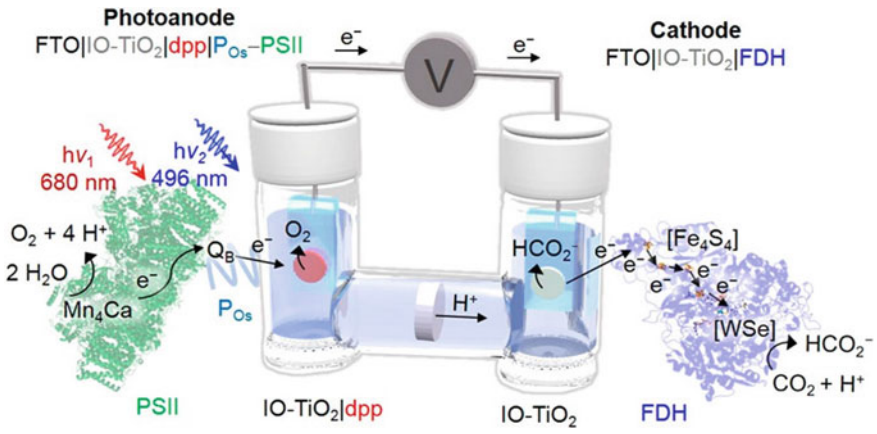

Fig. 17 Schematic diagram of a semi-artificial photosynthetic tandem PEC cell coupling water oxidation to CO_2 reduction by *D. vulgaris* FDH. dpp, phosphonated diketopyrrolopyrrole dye, P_{Os}, [poly(1-vinylimidazole-coallylamine)-[Os(bipy)$_2$Cl]Cl redox polymer], PS II, photosystem II. See text and Ref. [270] for details Adapted with permission from Ref. [270]

The *D. vulgaris* SeCys–W–FDH, on the other hand, is better suited for CO_2 reduction, with a $k_{\text{cat}\,2}^{\text{CO}} \approx 315\ \text{s}^{-1}$ ($K_m^{\text{CO}_2} \approx 420\ \mu\text{M}$; $k^{\text{CO}_2} \approx 0.75 \times 10^6\text{M}^{-1}\text{s}^{-1}$) [132]. Even though the CO_2 specificity of this enzyme is considerably lower (100 times) than that for formate ($k_{\text{cat}}^{\text{HCOO}^-} \approx 1310\ \text{s}^{-1}$; $K_{\text{m}}^{\text{HCOO}^-} \approx 17\ \mu\text{M}$; $k^{\text{HCOO}^-} \approx 77.5 \times 10^6\text{M}^{-1}\text{s}^{-1}$ [132]), this *D. vulgaris* W-FDH is at the base of several very well succeeded proof-of-principle devices for semi-artificial photosynthesis and production/storage of dihydrogen. A *D. vulgaris* W-FDH-containing cathode wired to a *T. elongatus* photosystem II-containing photoanode with a synthetic dye with complementary light absorption was successfully employed to drive light-dependent CO_2 conversion to formate, using water as an electron donor (Fig. 17) [270]. In this photoelectrochemical tandem device, electrons are photo-generated in the photosystem II, which oxidises water to dioxygen, and transferred to the FDH cathode (this biocathode catalyses the formate formation with a current density of 240 μAcm^{-2} (at—0.6 V versus SHE) and a Faradaic efficiency of 80%). The whole system is able to efficiently produce formate at 0.185 μmolcm^{-2}, with Faradaic efficiency of $\approx$ 70%, but progressive photosystem II photodegradation (due to prolonged irradiation) resulted in an irreversible decrease in the CO_2 photoreduction. A different *D. vulgaris* W-FDH-material configuration was recently devised, based on a ruthenium dye [271]. The employment of this dye-sensitised TiO_2-adsorped FDH enable the visible light-driven CO_2 reduction to formate with a turnover frequency of 11 s^{-1}, in the absence of a soluble redox mediator (Fig. 18) [271] (comparatively, this bioelectrode reached a current density of 100 μAcm^{-2} (at −0.6 V versus SHE), with a Faradaic efficiency of 92.5%). Furthermore, the *D. vulgaris* FDH-mediated electroenzymatic CO_2 reduction to formate was attained using a redox viologen-based polymer/enzyme-modified gas diffusion electrode

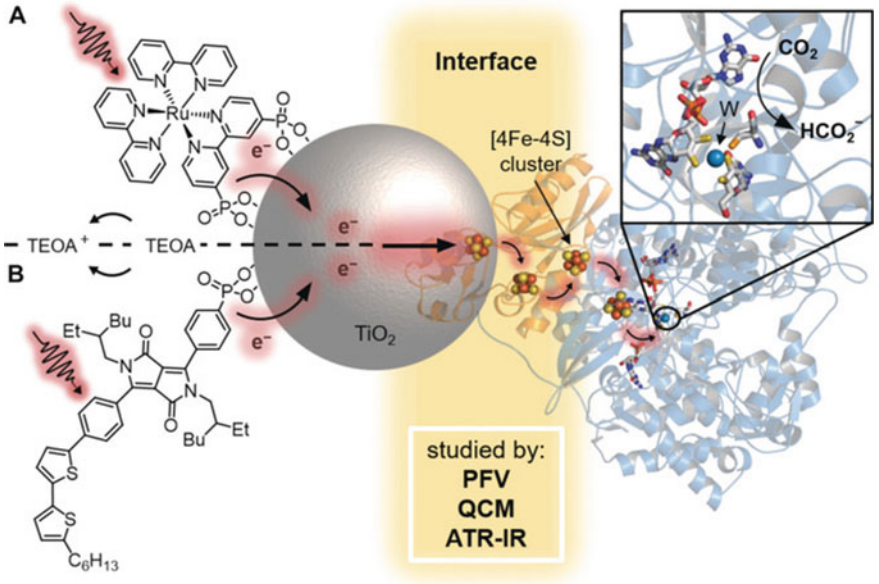

Fig. 18 Schematic diagram of a photocatalyst system for CO_2 conversion using a dye-semiconductor-*D. vulgaris* FDH arrangement. ATR-IR, attenuated total reflection infrared, PFV, protein film voltammetry, QCM, quartz crystal microbalance, TEOA, triethanolamine. See text and Ref. [271] for details Adapted with permission from Ref. [271]

[272]. The *D. vulgaris* W-FDH has also been exploited to drive the dihydrogen formation/storage in a system that mimics the natural formate-hydrogen lyase systems (see Sect. 4.2.2.) [273]. The semi-artificial formate-hydrogen lyase system consists of the *D. vulgaris* W-FDH and *D. vulgaris* Ni/Fe-Hase immobilised on a conductive scaffold of indium tin oxide that acts as an electron relay. This configuration enables the overall reaction to proceed reversibly towards formate conversion into CO_2 plus dihydrogen or towards formate formation, with minimal bias in either direction (Fig. 19), thus allowing the longed-for dihydrogen storage and release on demand. The system is able to produce dihydrogen (upon formate addition) at a rate of 4nmolmin^{-1} (turnover number of 23 $\times$ 10^3 and turnover frequency of 6.4 s^{-1} for the Hase) or to produce formate (in the presence of dihydrogen) at a rate of 22nmolmin^{-1} (turnover number of 16 $\times$ 10^3 and turnover frequency of e.4 s^{-1} for the FDH) for 8 h (this bioelectrode system reached current densities of 185 and 450 μAcm^{-2}, for CO_2 and H^+ reduction, respectively (at −0.6 V versus SHE) and of 300 and 440 μAcm^{-2} for formate and H_2 oxidation, respectively (at −0.2 V versus SHE), with Faradaic efficiencies for H_2 and formate production of 77 and 76%, respectively). Moreover, this semi-artificial formate-hydrogen lyase concept can be deployed in either an electrochemical cell or a self-assembled colloidal suspension, thus providing versatility for applications in different contexts.

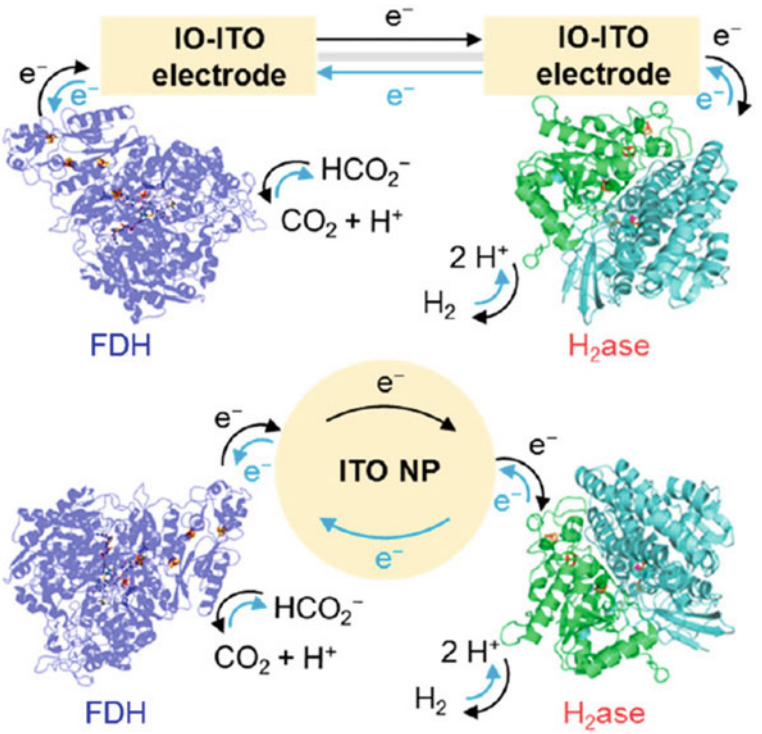

Fig. 19 Schematic diagram of a semi-artificial formate-hydrogen lyase system for the reversible and selective interconversion of dihydrogen and CO_2 into formate using *D. vulgaris* FDH. The concept can be deployed in either an electrochemical cell (top) or a self-assembled colloidal suspension (bottom). H_{2ase}, hydrogenase, ITO. indium tin oxide, NP, nanoparticle. See text and Ref. [273] for details Adapted with permission from Ref. [273]

Acetogens and methanogens are organisms that reduce (fix) CO_2 in vivo [274, 275], and, as such, they have been the focus of intense research to develop new CO_2 converter devices, enzymatic and whole-cell systems, as is reviewed by Litty and Müller in this Book [152] and also [153–159]. Herein, we only highlight the dihydrogen-dependent CO_2 reductases (Sect. 4.2.2.) from *Acetobacterium woodii* and *T. kivui*: the former is a SeCys–Mo–FDH that catalyses the CO_2 hydrogenation with a k_{cat} of 28 s^{-1} (reported as 10Umg^{-1}; $K_m^{HCO3-} \approx 37$ mM) and displays slightly higher rates of formate oxidation (CO_2 plus dihydrogen formation with a $k_{cat} \approx 39$ s^{-1}, reported as 14Umg^{-1}; $K_m^{HCOO-} \approx 1$ mM) [153, 154]; the second is a outstanding Cys–W–FDH that catalyses the CO_2 hydrogenation with a k_{cat} of 2.5 $\times$ $10^3 s^{-1}$ (900 µmol formate min^{-1}mg^{-1}; $K_m^{H2} \approx 130$ μM—one of the fastest CO_2 reducers so far described), with the reverse reaction being catalysed with a k_{cat} of 2.7 $\times$ $10^3 s^{-1}$ (930 µmol dihydrogen min^{-1}mg^{-1}; $K_m^{HCOO-} \approx 550$ μM) [156]. The CO_2 hydrogenation equilibrium constant close to one ($\Delta G^{o\prime}$ = 3.5KJmol^{-1}) makes these systems ideal biocatalysts for dihydrogen storage and production. *A. woodii*

was successfully used as a whole-cell biocatalyst to produce dihydrogen from formate, reaching a specific dihydrogen formation rate of ≈ 70 mmol $g^{-1}_{protein}1h^{-1}$ (≈ 30 mmol $g^{-1}_{cdw}h^{-1}$) and a volumetric dihydrogen evolution rate of ≈ 80 mMh^{-1}, with yields up to 1 mol dihydrogen per mol formate [155]. *T. kivui* was successfully exploited in a whole-cell system to convert dihydrogen plus CO_2 (hydrogencarbonate) into formate, achieving a specific formate formation rate of ≈ 235 mmol $g^{-1}_{protein}1h^{-1}$ (≈ 150 mmol $g^{-1}_{cdw}h^{-1}$) and a volumetric formate production rate of $270mMh^{-1}$; high titres up to 130 mM of formate were reached, with the key advantage of having the unwanted acetate formation abolished [159].

5 Outlook

The global energy demand and the present high dependence on fossil fuels have caused the increase in the atmospheric CO_2 concentration for the highest values since records began. Due to its significant greenhouse effect, CO_2 rise is responsible for large and unpredictable impacts on the Earth climate, besides being responsible for ocean acidification (its major sink). While some authors defend that these alterations are no longer reversible, the CO_2 emissions must be greatly decelerate and new and more efficient "CO_2 sinks" must be developed to avoid worsen this (already huge) "carbon crisis". The three axes, storage/conversion/production, are envisaged by many authors as the best strategy to actively reduce the CO_2 emissions, while actively consuming the CO_2 already released—"two-in-one solution". Along with chemical strategies, the "biochemical way" is proving is high value in different hybrid and biological systems to convert CO_2 into fuels and VC. FDHs are efficient catalysts to reduce CO_2 to formate and are in the right way to became key partners in the longed-for safe energy/stable climate solution.

Acknowledgements This work was supported by the Associate Laboratory for Green Chemistry —LAQV, which is financed by national funds from Fundacão para a Ciência e a Tecnologia, MCTES (FCT/MCTES; UIDB/50006/2020). LBM thanks to FCT/MCTES for the CEEC-Individual 2017 Program Contract.

References

1. Friedlingstein P, Jones MW, O'Sullivan M et al (2019) Global carbon budget 2019. Earth Syst Sci Data 11:1783–1838
2. CO_2 Earth (2020). https://www.co2.earth/monthly-co2. Accessed 15 Apr 2020
3. Seixas J, Ferreira F (2020) Carbon economy and carbon footprint. In: Moura JJG, Moura I, Maia L (ed) Enzymes for solving humankind's problems, Springer Nature Switzerland AG (in press
4. Loges B, Boddien A, Junge H, Beller M (2008) Controlled generation of hydrogen from formic acid amine adducts at room temperature and application in H_2/O_2 fuel cells. Angew Chem 47:3962–3965

5. Enthaler S, Langermann J, Schmidt T (2010) Carbon dioxide and formic acid-the couple for environmental-friendly hydrogen storage? Energy Environ Sci 3:1207–1217
6. Jiang HL, Singh SK, Yan JM, Zhang XB, Xu Q (2010) Liquid-phase chemical hydrogen storage: catalytic hydrogen generation under ambient conditions. Chemsuschem 3:541–549
7. Yadav M, Xu Q (2012) Liquid-phase chemical hydrogen storage materials. Energy Environ Sci 5:9698–9725
8. Appel AM, Bercaw JE, Bocarsly AB, Dobbek H, DuBois DL, Dupuis M, Ferry JG, Fujita E, Hille R, Kenis PJA, Kerfeld CA, Morris RH, Peden CHF, Portis AR, Ragsdale SW, Rauchfuss TB, Reek JNH, Seefeldt LC, Thauer RK, Waldrop GL (2013) Frontiers, opportunities, and challenges in biochemical and chemical catalysis of CO_2 fixation. Chem Rev 113:6621–6658
9. Kuehnel MF, Wakerley DW, Orchard KL, Reisner E (2015) Photocatalytic formic acid conversion on cds nanocrystals with controllable selectivity for H_2 or CO. Angew Chem 54:9627–9631
10. Wang W, Himeda Y, Muckerman JT, Manbeck G, Fujita E (2015) CO_2 Hydrogenation to formate and methanol as an alternative to photo—and electrochemical CO_2 reduction. Chem Rev 115:12936–12973
11. Preuster P, Papp C, Wasserscheid P (2017) Liquid organic hydrogen carriers (LOHCs): toward a hydrogen-free hydrogen economy. Acc Chem Res 50:74–85
12. Sordakis K, Tang CH, Vogt LK, Junge H, Dyson PJ, Beller M, Laurenczy G (2018) Homogeneous catalysis for sustainable hydrogen storage in formic acid and alcohols. Chem Rev 118:372–433
13. Zhong H, Iguchi M, Chatterjee M, Himeda Y, Xu Q, Kawanami H (2018) Formic acid-based liquid organic hydrogen carrier system with heterogeneous catalysts. Adv Sustain Syst 2:1700161
14. Yu X, Pickup PG (2008) Recent advances in direct formic acid fuel cells (DFAFC). J Power Sources 182:124–132
15. Sahin S, Cai R, Milton RD, Abdellaoui S, Macazo FC, Minteer SD (2018) Molybdenum-dependent formate dehydrogenase for formate bioelectrocatalysis in a formate/O_2 enzymatic fuel cell. J Electrochem Soc 165:109–113
16. Yuan M, Sahin S, Cai R, Abdellaoui S, Hickey DP, Minteer SD, Milton RD (2018) Creating a low-potential redox polymer for efficient electroenzymatic CO_2 reduction. Angew Chem 57:6582–6586
17. EPFL News (2020). https://actu.epfl.ch/news/the-world-s-first-formic-acid-based-fuel-cell/. Accessed 15 Apr 2020
18. BBC News (2020). https://www.bbc.com/news/business-40403351. Accessed 15 Apr 2020
19. Bar-Even A, Noor E, Flamholz A, Milo R (2013) Design and analysis of metabolic pathways supporting formatotrophic growth for electricity-dependent cultivation of microbes. Biochim Biophys Acta 1827:1039–1047
20. Benson EE, Kubiak CP, Sathrum AJ, Smieja JM (2009) Electrocatalytic and homogeneous approaches to conversion of CO_2 to liquid fuels. Chem Soc Rev 38:89–99
21. DuBois MR, DuBois DL (2009) Development of molecular electrocatalysts for CO_2 reduction and H_2 production/oxidation. Acc Chem Res 42:1974–1982
22. Whipple DT, Kenis PJA (2010) Prospects of CO_2 utilization via direct heterogeneous electrochemical reduction. J Phys Chem Lett 1:3451–3458
23. Agarwal AS, Zhai Y, Hill D, Sridhar N (2011) The electrochemical reduction of carbon dioxide to formate/formic acid: engineering and economic feasibility. Chemsuschem 4:1301–1310
24. Schneider J, Jia HF, Muckerman JT, Fujita E (2012) Thermodynamics and kinetics of CO_2, CO, and H + binding to the metal centre of CO_2 reduction catalysts. Chem Soc Rev 41:2036–2051
25. Costentin C, Robert M, Saveant JM (2013) Catalysis of the electrochemical reduction of carbon dioxide. Chem Soc Rev 42:2423–2436

26. Jhong HR, Ma S, Kenis PJA (2013) Electrochemical conversion of CO_2 to useful chemicals: current status, remaining challenges, and future opportunities. Curr Opin Chem Eng 2:191–199
27. Clark ML, Grice KA, Moore CE, Rheingold AL, Kubiak CP (2014) Electrocatalytic CO_2 reduction by M(bpy–R) $(CO)_4$ (M = Mo, W; R = H, tBu) complexes. electrochemical, spectroscopic and computational studies and comparison with group 7 catalysts. Chem Sci 5:1894–1900
28. Kopljar D, Inan A, Vindayer P, Wagner N, Klemm E (2014) Electrochemical reduction of CO_2 to formate at high current density using gas diffusion electrodes. J Appl Electrochem 44:1107–1116
29. Lu X, Leung DY, Wang H, Leung MK, Xuan J (2014) Electrochemical reduction of carbon dioxide to formic acid. ChemElectroChem 1:836–849
30. Qiao J, Liu Y, Hong F, Zhang J (2014) A review of catalysts for the electroreduction of carbon dioxide to produce low carbon fuels. Chem Soc Rev 43(2):631–675
31. Martín AJ, Larrazábal GO, Pérez-Ramírez J (2015) Towards sustainable fuels and chemicals through the electrochemical reduction of CO_2: lessons from water electrolysis. Green Chem 17:5114–5130
32. Pletcher D (2015) The cathodic reduction of carbon dioxide—what can it realistically achieve? a mini review. Electrochem Commun 61:97–101
33. Yoo JS, Christensen R, Vegge T, Nørskov JK, Studt F (2016) Theoretical Insight into the trends that guide the electrochemical reduction of carbon dioxide to formic acid. Chemsuschem 9:358–363
34. Morris AJ, Meyer GJ, Fujita E (2009) Molecular approaches to the photocatalytic reduction of carbon dioxide for solar fuels. Acc Chem Res 42:1983–1994
35. Doherty MD, Grills DC, Muckerman JT, Polyansky DE (2010) Toward more efficient photochemical CO_2 reduction: Use of $scCO_2$ or photogenerated hydrides. Coord Chem Rev 254:2472–2482
36. Takeda H, Ishitani O (2010) Development of efficient photocatalytic systems for CO2 reduction using mononuclear and multinuclear metal complexes based on mechanistic studies. Coord Chem Rev 254:346–354
37. Tamaki Y, Morimoto T, Koike K, Ishitani O (2012) Photocatalytic CO_2 reduction with high turnover frequency and selectivity of formic acid formation using Ru(II) multinuclear complexes. Proc Natl Acad Sci U S A 109:15673–15678
38. Izumi Y (2013) Recent advances in the photocatalytic conversion of carbon dioxide to fuels with water and/or hydrogen using solar energy and beyond. Coord Chem Rev 257:171–186
39. Navalon S, Dhakshinamoorthy A, Garcia AMH (2013) Photocatalytic CO_2 reduction using non-titanium metal oxides and sulfides. Chemsuschem 6:562–577
40. Oh Y, Hu X (2013) Organic molecules as mediators and catalysts for photocatalytic and electrocatalytic CO_2 reduction. Chem Soc Rev 42:2253–2261
41. Das S, Daud WMAW (2014) Photocatalytic CO_2 transformation into fuel: a review on advances in photocatalyst and photoreactor. Renew Sustain Energy Rev 39:765–805
42. Zhou X, Liu R, Sun K, Chen Y, Verlage E, Francis SA, Lewis NS, Xiang C (2016) Solar-driven reduction of 1 atm of CO_2 to formate at 10% energy-conversion efficiency by use of a TiO_2-protected III-V tandem photoanode in conjunction with a bipolar membrane and a Pd/C cathode. ACS Energy Lett 1:764–770
43. Nocera DG (2017) Solar fuels and solar chemicals industry. Acc Chem Res 50:616–619
44. Zhang B, Sun L (2019) Artificial photosynthesis: opportunities and challenges of molecular catalysts. Chem Soc Rev 48:2216–2264
45. Graf E, Leitner W (1992) Direct formation of formic-acid from carbon-dioxide and dihydrogen using the $[(Rh(Cod)Cl)_2]Ph_2P\text{-}(CH2)_4PPh_2$ catalyst system. J Chem Soc Chem Commun 1992:623–624
46. Jessop PG, Ikariya T, Noyori R (1994) Homogeneous catalytic-hydrogenation of supercritical carbon-dioxide. Nature 368:231–233

47. Gassner F, Leitner W (1993) Hydrogenation of carbon-dioxide to formic-acid using water-soluble rhodium catalysts. J Chem Soc Chem Commun 1993:1465–1466
48. Jessop PG, Ikariya T, Noyori R (1995) Homogeneous hydrogenation of carbon-dioxide. Chem Rev 95:259–272
49. Leitner W (1995) Carbon dioxide as a raw material: synthesis of formic acid and its derivatives from CO_2. Angew Chem 34:2207–2221
50. Munshi P, Main AD, Linehan JC, Tai CC, Jessop PG (2002) Hydrogenation of carbon dioxide catalyzed by ruthenium trimethylphosphine complexes: the accelerating effect of certain alcohols and amines. J Am Chem Soc 124:7963–7971
51. Jessop PG, Joó F, Tai CC (2004) Recent advances in the homogeneous hydrogenation of carbon dioxide. Coord Chem Rev 248:2425–2442
52. Enthaler S (2008) Carbon dioxide—the hydrogen-storage material of the future? Chemsuschem 1:801–804
53. Fukuzumi S (2008) Bioinspired energy conversion systems for hydrogen production and storage. Eur J Inorg Chem 2008:1351–1362
54. Federsel C, Jackstell R, Boddien A, Laurenczy G, Beller M (2010) Ruthenium-catalyzed hydrogenation of bicarbonate in water. Chemsuschem 3:1048–1050
55. Loges B, Boddien A, Gartner F, Junge H, Beller M (2010) Catalytic generation of hydrogen from formic acid and its derivatives: useful hydrogen storage materials. Top Catal 53:902–914
56. Himeda Y, Miyazawa S, Hirose T (2011) Interconversion between formic acid and H_2/CO_2 using rhodium and ruthenium catalysts for CO_2 fixation and H_2 storage. Chemsuschem 4:487–493
57. Langer R, Diskin-Posner Y, Leitus G, Shimon LJW, Ben-David Y, Milstein D (2011) Low-pressure hydrogenation of carbon dioxide catalyzed by an iron pincer complex exhibiting noble metal activity. Angew Chem 50:9948–9952
58. Schmeier TJ, Dobereiner GE, Crabtree RH, Hazari N (2011) Secondary coordination sphere interactions facilitate the insertion step in an iridium(iii) CO_2 reduction catalyst. J Am Chem Soc 133:9274–9277
59. Wang W, Wang S, Ma X, Gong J (2011) Recent advances in catalytic hydrogenation of carbon dioxide. Chem Soc Rev 40:3703–3727
60. Hull JF, Himeda Y, Wang W-H, Hashiguchi B, Periana R, Szalda DJ, Muckerman JT, Fujita E (2012) Reversible hydrogen storage using CO_2 and a proton-switchable iridium catalyst in aqueous media under mild temperatures and pressures. Nat Chem 4:383–388
61. Maenaka Y, Suenobu T, Fukuzumi S (2012) Catalytic interconversion between hydrogen and formic acid at ambient temperature and pressure. Energy Environ Sci 5:7360–7367
62. Yadav M, Xu Q (2012) Liquid-phase chemical hydrogen storage materials Energy. Environ Sci 5:9698–9725
63. Wesselbaum S, Hintermair U, Leitner W (2012) Continuous-flow hydrogenation of carbon dioxide to pure formic acid using an integrated $scCO_2$ process with immobilized catalyst and base. Angew Chem 51:8585–8588
64. Huff CA, Sanford MS (2013) Catalytic CO_2 hydrogenation to formate by a ruthenium pincer complex. ACS Catal 3:2412–2416
65. Jeletic MS, Mock MT, Appel AM, Linehan JCA (2013) Cobalt-based catalyst for the hydrogenation of CO_2 under ambient conditions. J Am Chem Soc 135:11533–11536
66. Muller K, Sun Y, Thiel WR (2013) Ruthenium(II) phosphite complexes as catalysts for the hydrogenation of carbon dioxide. ChemCatChem 5:1340–1343
67. Wang W-H, Muckerman JT, Fujita E, Himeda Y (2013) Mechanistic insight through factors controlling effective hydrogenation of CO_2 catalyzed by bioinspired proton-responsive iridium(iii) complexes. ACS Catal 3:856–860
68. Bays JT, Priyadarshani N, Jeletic MS, Hulley EB, Miller DL, Linehan JC, Shaw WJ (2014) The influence of the second and outer coordination spheres on $Rh(diphosphine)_2$ CO_2 hydrogenation catalysts. ACS Catal 4:3663–3670

69. Filonenko GA, van Putten R, Schulpen EN, Hensen EJM, Pidko E (2014) A highly efficient reversible hydrogenation of carbon dioxide to formates using a ruthenium PNP-Pincer catalyst. ChemCatChem 6:1526–1530
70. Hsu S-F, Rommel S, Eversfield P, Muller K, Klemm E, Thiel WR, Plietker BA (2014) Rechargeable hydrogen battery based on Ru catalysis. Angew Chem 53:7074–7078
71. Moret S, Dyson PJ, Laurenczy G (2014) Direct synthesis of formic acid from carbon dioxide by hydrogenation in acidic media. Nat Commun 5:5017
72. Barelli L, Bidini G, Gallorini F, Servili S (2008) Hydrogen production through sorption-enhanced steam methane reforming and membrane technology: a review. Energy 33:554–570
73. Fihri A, Artero V, Razavet M, Baffert C, Leibl W, Fontecave M (2008) Cobaloxime-based photocatalytic devices for hydrogen production. Angew Chem 47:564–567
74. Gloaguen F, Rauchfuss TB (2009) Small molecule mimics of hydrogenases: hydrides and redox. Chem Soc Rev 38:100–108
75. Losse S, Vos JG, Rau S (2010) Catalytic hydrogen production at cobalt centres. Coord Chem Rev 254:2492–2504
76. Artero V, Chavarot-Kerlidou M, Fontecave M (2011) Splitting water with cobalt. Angew Chem 50:7238–7266
77. Kilgore UJ, Roberts JAS, Pool DH, Appel AM, Stewart MP, DuBois MR, Dougherty WG, Kassel WS, Bullock RM, DuBois DL (2011) [Ni(PPh2NC6H4X2)2]2 + complexes as electrocatalysts for H_2 production: effect of substituents, acids, and water on catalytic rates. J Am Chem Soc 133:5861–5872
78. Du P, Eisenberg R (2012) Catalysts made of earth-abundant elements (Co, Ni, Fe) for water splitting: recent progress and future challenges. Energy Environ Sci 5:6012–6021
79. Tran PD, Barber J (2012) Proton reduction to hydrogen in biological and chemical systems. Phys Chem Chem Phys 14:13772–13784
80. Wang M, Chen L, Sun LC (2012) Recent progress in electrochemical hydrogen production with earth-abundant metal complexes as catalysts. Energy Environ Sci 5:6763–6778
81. Chen WF, Iyer S, Sasaki K, Wang CH, Zhu YM, Muckerman JT, Fujita E (2013) Biomass-derived electrocatalytic composites for hydrogen evolution. Energy Environ Sci 6:1818–1826
82. Eckenhoff WT, McNamara WR, Du PW, Eisenberg R (2013) Cobalt complexes as artificial hydrogenases for the reductive side of water splitting. Biochim Biophys Acta—Bioenerg 1827:958–973
83. Thoi VS, Sun YJ, Long JR, Chang CJ (2013) Complexes of earth-abundant metals for catalytic electrochemical hydrogen generation under aqueous conditions. Chem Soc Rev 42:2388–2400
84. Faber MS, Jin S (2014) Earth-abundant inorganic electrocatalysts and their nanostructures for energy conversion applications. Energy Environ Sci 7:3519–3542
85. Liu YM, Yu HT, Quan X, Chen S, Zhao HM, Zhang YB (2014) Efficient and durable hydrogen evolution electrocatalyst based on nonmetallic nitrogen doped hexagonal carbon. Sci Rep 4:6843
86. McKone JR, Marinescu SC, Brunschwig BS, Winkler JR, Gray HB (2014) Earth-abundant hydrogen evolution electrocatalysts. Chem Sci 5:865–878
87. Pan LF, Li YH, Yang S, Liu PF, Yu MQ, Yang HG (2014) Molybdenum carbide stabilized on graphene with high electrocatalytic activity for hydrogen evolution reaction. Chem Commun 50:13135–13137
88. Xiao P, Sk MA, Thia L, Ge XM, Lim RJ, Wang JY, Lim KH, Wang X (2014) Molybdenum phosphide as an efficient electrocatalyst for the hydrogen evolution reaction. Energy Environ Sci 7:2624–2629
89. Clough AJ, Yoo JW, Mecklenburg MH, Marinescu SC (2015) Two-dimensional metal-organic surfaces for efficient hydrogen evolution from water. J Am Chem Soc 137:118–121

90. Cui W, Liu Q, Xing ZC, Asiri AM, Alamry KA, Sun X (2015) MoP nanosheets supported on biomass-derived carbon flake: One-step facile preparation and application as a novel high-active electrocatalyst toward hydrogen evolution reaction. Appl Catal B 164:144–150
91. Morozan A, Goellner V, Zitolo A, Fonda E, Donnadieu B, Jones D, Jaouen F (2015) Synergy between molybdenum nitride and gold leading to platinum-like activity for hydrogen evolution. Phys Chem Chem Phys 17:4047–4053
92. Darensbourg MY, Eduaran EL, Ding S, Lunsford AL, Pathirana KD, Ghosh P, Yang X (2020) Hydrides, carbonyls, and metal—metal bonds: organometallic chemistry control of hydrogenases. In: Moura JJG, Moura I, Maia L (eds) Enzymes for solving humankind's problems, Springer Nature Switzerland AG (in press)
93. Martins M, Pereira IAC, Pita M, De Lacey AL (2020) Biological production of hydrogen. In: Moura JJG, Moura I, Maia L (eds) Enzymes for solving humankind's problems, Springer Nature Switzerland AG (in press)
94. Grimaldi S, Schoepp-Cothenet B, Ceccaldi P, Guigliarelli B, Magalon A (2013) The prokaryotic Mo/W-bisPGD enzymes family: a catalytic workhorse in bioenergetic. Biochim Biophys Acta 1827:1048–1085
95. Hartmann T, Schwanhold N, Leimkühler S (2015) Assembly and catalysis of molybdenum or tungsten-containing formate dehydrogenases from bacteria. Biochim Biophys Acta 1854:1090–1100
96. Maia LB, Moura JJG, Moura I (2015) Molybdenum and tungsten-dependent formate dehydrogenases. J Biol Inorg Chem 20:287–309
97. Magalon A, Ceccaldi P, Schoepp-Cothenet B (2017) The Prokaryotic Mo/W-bisPGD Enzymes Family. In: Hille R, Schulzke C, Kirk M (eds) Molybdenum and tungsten enzymes: biochemistry, RSC Metallobiology Series No. 5, The Royal Society of Chemistry, Cambridge, Chap. 5, p 143–191
98. Maia LB, Moura I, Moura JJG (2017) Molybdenum and tungsten-containing formate dehydrogenases: aiming to inspire a catalyst for carbon dioxide utilization. Inorg Chim Acta 455:350–363
99. Niks D, Hille R (2018) Reductive activation of CO_2 by formate dehydrogenases. Methods Enzymol 613:277–295
100. Niks D, Hille R (2019) Molybdenum—and tungsten-containing formate dehydrogenases and formylmethanofuran dehydrogenases: structure mechanism, and cofactor insertion. Ptot Sci 28:111–122
101. Nielsen CF, Lange L, Meyer AS (2019) Classification and enzyme kinetics of formate dehydrogenases for biomanufacturing via CO_2 utilization. Biotechnol Adv 37:107408
102. Kato N (1990) Formate dehydrogenase from methylotrophic yeasts. Methods Enzymol 188:459–462
103. Vinals C, Depiereux E, Feytmans E (1993) Prediction of structurally conserved regions of D-specific hydroxy acid dehydrogenases by multiple alignment with formate dehydrogenase. Biochem Biophys Res Commun 192:182–188
104. Popov VO, Lamzin VS (1994) NAD + -dependent formate dehydrogenase. Biochem J 301:625–643
105. Filippova EV, Polyakov KM, Tikhonova TV, Stekhanova TN, Boiko KM, Popov KO (2005) Structure of a new crystal modification of the bacterial NAD-dependent formate dehydrogenase with a resolution of 2.1 Å. Crystallogr Rep 50:796–800
106. Schirwitz K, Schmidt A, Lamzin VS (2007) High resolution structures of formate dehydrogenase from Candida boidinii. Protein Sci 16:1146–1156
107. Shabalin IG, Polyakov KM, Tishkov VI, Popov VO (2009) Atomic resolution crystal structure of NAD(+)-dependent formate dehydrogenase from bacterium moraxella Sp. C-1. Acta Nat 1:89–93
108. Alekseeva AA, Savin SS, Tishkov VI (2011) NAD (+) -dependent formate dehydrogenase from plants. Acta Nat 3:38–54

109. Guo Q, Gakhar L, Wickersham K, Francis K, Vardi-Kilshtain A, Major DT, Cheatum CM, Kohen A (2016) Structural and kinetic studies of formate dehydrogenase from candida boidinii. Biochemistry 55:2760–2771
110. Hille R, Hall J, Basu P (2014) The mononuclear molybdenum enzymes. Chem Rev 114:3963–4038
111. Maia L, Moura I, Moura JJG (2017) Molybdenum and tungsten-containing enzymes: an overview. In: Hille R, Schulzke C, Kirk M (eds) Molybdenum and *Tungsten Enzymes: Biochemistry*, RSC Metallobiology Series No. 5, The Royal Society of Chemistry, Cambridge, Chap. 1, p 1–80
112. Maia L, Moura JJG (2018) Mononuclear molybdenum-containing enzymes. Reference module in chemistry, molecular sciences and chemical engineering, pp 1–19. https://doi.org/10.1016/B978-0-12-409547-2.13932-0
113. Zinoni F, Birkmann A, Stadtman TC, Böck A (1986) Nucleotide sequence and expression of the selenocysteine-containing polypeptide of formate dehydrogenase (Formate-Hydrogen-Lyase-Linked) from *Escherichia coli*. Proc Natl Acad Sci USA 83:4650–4654
114. Axley MJ, Grahame DA, Stadtman TC (1990) *Escherichia coli* formate-hydrogen Lyase. J Biol Chem 265:18213–18218
115. Gladyshev VN, Boyington JC, Khangulov SV, Grahame DA, Stadtman TC, Sun PD (1996) Characterization of crystalline formate dehydrogenase h from *Escherichia coli*. J Biol Chem 271:8095–8100
116. Boyington JC, Gladyshev VN, Khangulov SV, Stadtman T, Sun PD (1997) Crystal structure of formate dehydrogenase H: catalysis involving Mo, molybdopterin, selenocysteine and an Fe_4S_4 cluster. Science 275:1305–1308
117. Raaijmakers HCA, Romão MJ (2006) Formate-reduced E coli formate dehydrogenase H: the reinterpretation of the crystal structure suggests a new reaction mechanism. J Biol Inorg Chem 11:849–854
118. Jormakka M, Tornroth S, Abramson J, Byrne B, Iwata S (2002) Purification and crystallization of the respiratory complex formate dehydrogenase-N from *Escherichia coli*. Acta Crystallogr D Biol Crystallogr 58:160–162
119. Jormakka M, Törnroth S, Byrne B, Iwata S (2002) Molecular basis of proton motive force generation: structure of formate dehydrogenase-N. Science 2295:1863–1868
120. Wang H, Gunsalus RP (2003) Coordinate regulation of the *Escherichia coli* formate dehydrogenase fdnGHI and fdhF genes in response to nitrate, nitrite and formate: roles fro NarL and NarP. J Bacteriol 185:5076–5085
121. Pommier J, Mandrand MA, Holt SE, Boxer DH, Giodano G (1992) A second phenazine methosulphate-linked formate dehydrogenase isoenzyme in *Escherichia coli*. Biochim Biophys Acta 1107:305–313
122. Plunkett G, Burland V, Daniels DL, Blattner FR (1993) Analysis of the *Escherichia coli* genome. Nucleic Acids Res 21:3391–3398
123. Abaibou H, Pommier J, Benoit JP, Giordano G, Mandrand M (1995) Expression and characterization of the *Escherichia coli* fdo locus and a possible physiological role for aerobic formate dehydrogenase. J Bacteriol 177:7141–7149
124. Bursakov S, Liu M-Y, Payne WJ, LeGall J, Moura I, Moura JJG (1995) Isolation and preliminary characterization of a soluble nitrate reductase from the sulfate reducing organism *Desulfovibrio desulfuricans* ATCC 27774. Anaerobe 1:55–60
125. Sebban C, Blanchard L, Bruschi M, Guerlesquin F (1995) Purification and characterization of the formate dehydrogenase from *Desulfovibrio vulgaris* hildenborough. FEMS Microbiol Lett 133:143–149
126. Brondino CD, Passeggi MCG, Caldeira J, Almendra MJ, Feio MJ, Moura JJG, Moura I (2004) Incorporation of either molybdenum or tungsten into formate dehydrogenase from *Desulfovibrio alaskensis* NCIMB 13491. J Biol Inorg Chem 9:145–151

127. Heidelberg JF, Seshadri R, Haveman SA, Hemme CL, Paulsen IT, Kolonay JF, Eisen JA, Ward N, Methe B, Brinkac LM, Daugherty SC, Deboy RT, Dodson RJ, Durkin AS, Madupu R, Nelson WC, Sullivan SA, Fouts D, Haft DH, Selengut J, Peterson JD, Davidsen TM, Zafar N, Zhou L, Radune D, Dimitrov G, Hance M, Tran K, Khouri H, Gill J, Utterback TR, Feldblyum TV, Wall JD, Voordouw G, Fraser CM (2004) The genome sequence of the anaerobic, sulfate-reducing bacterium *Desulfovibrio vulgaris* hildenborough. Nat Biotechnol 22:554–559
128. Mota CS, Valette O, Gonzalez PJ, Brondino CD, Moura JJG, Moura I, Dolla A, Rivas MG (2011) Effects of molybdate and tungstate on expression levels and biochemical characteristics of formate dehydrogenases produced by *Desulfovibrio alaskensis* NCIMB 13491. J Bacteriol 193:2917–2923
129. Silva SM, Pimentel C, Valente FMA, Rodrigues-Pousada C, Pereira IAC (2011) Tungsten and molybdenum regulation of formate dehydrogenase expression in *Desulfovibrio vulgaris* hildenborough. J Bacteriol 193:2908–2916
130. Raaijmakers H, Macieira S, Dias JM, Texierira S, Bursakov S, Huber R, Moura JJG, Moura I, Romão MJ (2002) Gene sequence and the 18Å crystal structure of the tungsten-containing formate dehydrogenase from *Desulfovibrio gigas*. Structure 10:1261–1272
131. da Silva SM, Voordouw J, Leitão C, Martins M, Voordouw G, Pereira IAC (2013) Function of formate dehydrogenases in *Desulfovibrio vulgaris* hildenborough energy metabolism. Microbiology 159:1760–1769
132. Oliveira AR, Mota C, Mourato C, Domingos RM, Santos MFA, Gesto D, Guigliarelli B, Santos-Silva T, Romão MJ, Pereira IAC (2020) Toward the mechanistic understanding of enzymatic CO_2 reduction. ACS Catal 10:3844–3856
133. Almendra MJ, Brondino CD, Gavel O, Pereira AS, Tavares P, Bursakov S, Duarte R, Caldeira J, Moura JJ, Moura I (1999) Purification and characterization of a tungsten-containing formate dehydrogenase from *Desulfovibrio gigas*. Biochemistry 38:16366–16372
134. Raaijmakers H, Teixeira S, Dias JM, Almendra MJ, Brondino CD, Moura I, Moura JJ, Romão MJ (2001) Tungsten-containing formate dehydrogenase from *Desulfovibrio gigas*: metal identification and preliminary structural data by multi-wavelength crystallography. J Biol Inorg Chem 6:398–404
135. Costa C, Teixeira M, LeGall J, Moura JJG, Moura I (1997) Formate dehydrogenase from *Desulfovibrio desulfuricans* ATCC 27774: isolation and spectroscopic characterization of the active sites. J Biol Inorg Chem 2:198–208
136. Rivas M, Gonzalez P, Brondino CD, Moura JJG, Moura I (2007) EPR characterization of the molybdenum(V) forms of formate dehydrogenase from *Desulfovibrio desulfuricans* ATCC 27774 upon formate reduction. J Inorg Biol 101:1617–1622
137. Maia L, Fonseca L, Moura I, Moura JJG (2016) Reduction of carbon dioxide by a molybdenum-containing formate dehydrogenase: a kinetic and mechanistic study. J Am Chem Soc 138:8834–8846
138. Young T, Niks D, Hakopian S, Tam TK, Yu X, Hille R, Blaha GM (2020) Crystallographic and kinetic analyses of the FdsBG subcomplex of the cytosolic formate dehydrogenase FdsABG from *Cupriavidus necator*. J Biol Chem 295:6570–6585
139. Radon C, Mittelstädt G, Duffus BR, Bürger J, Hartmann T, Mielke T, Teutloff C, Leimkühler S, Wendler P (2020) Cryo-EM structures reveal intricate Fe-S cluster arrangement and charging in *Rhodobacter capsulatus* formate dehydrogenase. Nat Commun 11:1912
140. Wagner T, Ermler U, Shima S (2016) The methanogenic CO2 reducing-and-fixing enzyme is bifunctional and contains 46 [4Fe-4S] clusters. Science 354:114–117
141. Trchounian K, Poladyan A, Vassilian A, Trchounian A (2012) Multiple and reversible hydrogenases for hydrogen production by *Escherichia coli*. Crit Rev Biochem Mol Biol 47:236–249

142. Babujee L, Apodaca J, Balakrishnan V, Liss P, Kiley PJ, Charkowski AO, Glasner JD, Perna NT (2012) Evolution of the metabolic and regulatory networks associated with oxygen availability in two phytopathogenic enterobacteria. BMC Genom 13:110
143. Liou JS-C, Balkwill DL, Drake GR, Tanner RS (2005) Clostridium carboxidivorans Sp. Nov., a solvent-producing clostridium isolated from an agricultural settling lagoon, and reclassification of the acetogen clostridium scatologenes strain SL1 as clostridium drakei Sp Nov. Int J Syst Evol Microbiol 55:2085–2091
144. Ragsdale SW, Pierce E (2008) Acetogenesis and the wood-Ljungdahl pathway of CO_2 fixation. Biochim Biophys Acta 1784:1873–1898
145. Bruant G, Levesque M-J, Peter C, Guiot SR, Masson L (2010) Genomic analysis of carbon monoxide utilization and butanol production by clostridium carboxidivorans strain P7T. PLoS One 5:e13033
146. Paul D, Austin FW, Arick T, Bridges SM, Burgess SC, Dandass YS, Lawrence ML (2010) Genome sequence of the solvent-producing bacterium clostridium carboxidivorans strain P7T. J Bacteriol 192:5554–5555
147. Alissandratos A, Kim HK, Matthews HK, Hennessey JE, Philbrook A, Easton CJ (2013) Clostridium carboxidovorans strain P7T recombinant formate dehydrogenase catalyzes reduction of CO_2 to formate. Appl Environ Micorobiol 79:741–744
148. Bagramyan K, Trchounian A (2003) Structural and functional features of formate hydrogen lyase, an enzyme of mixed-acid fermentation from *Escherichia coli*. Biochem Moscow 68:1159–1170
149. McDowall JS, Murphy BJ, Haumann M, Palmer T, Armstrong FA, Sargent F (2014) Bacterial formate hydrogenlyase complex. Proc Natl Acad Sci U S A 111:E3948–E3956
150. Mcdowall JS, Hjersing MC, Palmer T, Sargent F (2015) Dissection and engineering of the *Escherichia coli* formate hydrogenlyase complex. FEBS Lett 589:3141–3147
151. Pinske C, Sargent F (2016) Exploring the directionality of *Escherichia coli* formate hydrogenlyase: a membrane-bound enzyme capable of fixing carbon dioxide to organic acid. MicrobiologyOpen 5:721–737
152. Litty D, Müller V (2020) Acetogenic bacteria for biotechnological applications. In: Moura JJG, Moura I, Maia L (eds) Enzymes for solving humankind's problems, Springer Nature Switzerland AG (in press)
153. Schuchmann K, Müller V (2013) Direct and reversible hydrogenation of CO2 to formate by a bacterial carbon dioxide reductase. Science 342:1382–1385
154. Schuchmann K, Vonck J, Müller V (2016) A bacterial hydrogen-dependent CO_2 reductase forms filamentous structures. FEBS J 283:1311–1322
155. Kottenhahn P, Schuchmann K, Müller V (2018) Efficient whole cell biocatalyst for formate-based hydrogen production. Biotechnol Biofuels 11:93
156. Schwarz FM, Schuchmann K, Müller V (2018) Hydrogenation of CO_2 at ambient pressure catalyzed by a highly active thermostable biocatalyst. Biotechnol Biofuels 11:237
157. Müller V (2019) New horizons in acetogenic conversion of one-carbon substrates and biological hydrogen storage. Trends Biotechnol 37:1344–1354
158. Schoelmerich MC, Müller V (2019) Energy conservation by a hydrogenase-dependent chemiosmotic mechanism in an ancient metabolic pathway. Proc Natl Acad Sci USA 116:6329–6334
159. Schwarz FM, Müller V (2020) Whole-cell biocatalysis for hydrogen storage and syngas conversion to formate using a thermophilic acetogen. Biotechnol Biofuels 13:32
160. Bertram PA, Karrasch M, Schmitz RA, Böcher R, Albracht SPJ, Thauer RK (1994) Formylmethanofuran dehydrogenases from methanogenic Archaea Substrate specificity, EPR properties and reversible inactivation by cyanide of the molybdenum or tungsten iron-sulfur proteins. Eur J Biochem 220:477–484
161. Hochheimer A, Hedderich R, Thauer RK (1998) The formylmethanofuran dehydrogenase isozymes in Methanobacterium wolfeii and Methanobacterium terhmoautotrophicum:

induction of the molybdenum isozyme by molybdate and constitutive synthesis of the tungsten isozyme. Arch Microbiol 170:389–393
162. Hille R (1996) The mononuclear molybdenum enzymes. Chem Rev 96:27575–27816
163. Johnson MK, Rees DC, Adams MWW (1996) Tungstoenzymes Chem Rev 96:2817–2839
164. Bevers LE, Hagedoorn PL, Hagen WR (2009) The bioinorganic chemistry of tungsten. Coord Chem Rev 253:269–290
165. Hagen WR (2017) Tungsten-containing enzymes. In: Hille R, Schulzke C, Kirk M (eds) Molybdenum and tungsten enzymes: biochemistry, RSC Metallobiology Series No. 5, The Royal Society of Chemistry, Cambridge, Chap 10, pp 313–342
166. Khangulov SVV, Gladyshev VN, Dismukes GC, Stadtman TC (1998) Selenium-containing formate dehydrogenase H from *Escherichia coli*: a molybdenum enzyme that catalyzes formate oxidation without oxygen transfer. Biochemistry 37:3518–3528
167. Thome R, Gust A, Toci R, Mendel R, Bittner F, Magalon A, Walburger A (2012) A sulfurtransferase is essential for activity of formate dehydrogenases in *Escherichia coli*. J Biol Chem 287:4671–4678
168. Arnoux P, Ruppelt C, Oudouhou F, Lavergne J, Siponen MI, Toci R, Mendel RR, Bittner F, Pignol D, Magalon A, Walburger A (2015) Sulphur shuttling across a chaperone during molybdenum cofactor maturation. Nat Commun 6:6148
169. Schrapers P, Hartmann T, Kositzki R, Dau H, Reshke S, Schulzke C, Leimkühler S, Haumann M (2015) Sulfido and cysteine ligation changes at the molybdenum cofactor during substrate conversion by formate dehydrogenase (FDH) from *Rhodobacter capsulatus*. Inorg Chem 54:3260–3271
170. Blanchard JS, Cleland WW (1980) Kinetic and chemical mechanisms of yeast formate dehydrogenase. Biochemistry 19:3543–3550
171. Rotberg NS, Cleland WW (1991) Secondary 15 N isotope effects on the reactions catalyzed by alcohol and formate dehydrogenases. Biochemistry 30:4068–4071
172. Lamzin VS, Dauter Z, Popov VO, Harutyunyan EH, Wilson KS (1994) High resolution structures of holo and apo formate dehydrogenase. J Mol Biol 236:759–785
173. Tishkov VI, Matorin AD, Rojkova AM, Fedorchuk VV, Savitsky PA, Dementieva LA, Lamzin VS, Mezentzev AV, Popov VO (1996) Site-directed mutagenesis of the formate dehydrogenase active centre: role of the His332-Gln313 pair in enzyme catalysis. FEBS Lett 390:104–108
174. Mesentsev AV, Lamzin VS, Tishkov VI, Ustinnikova TB, Popov VO (1997) Effect of pH on kinetic parameters of NAD + -dependent formate dehydrogenase. Biochem J 321:475–480
175. Tishkov VI, Popov VO (2004) Catalytic mechanism and application of formate dehydrogenase. Biochemistry (Mosc) 69:1252–1267
176. Castillo R, Oliva M, Marti S, Moliner V (2008) A theoretical study of the catalytic mechanism of formate dehydrogenase. J Phys Chem B 112:10012–10022
177. Bandaria JN, Cheatum CM, Kohen A (2009) Examination of enzymatic H-tunneling through kinetics and dynamics. J Am Chem Soc 131:10151–10155
178. Nilov DK, Shabalin IG, Popov VO, Svedas VK (2012) Molecular modeling of formate dehydrogenase: the formation of the Michaelis complex. J Biomol Struct Dyn 30:170–199
179. Leopoldini M, Chiodo SG, Toscano M, Russo N (2008) Reaction mechanism of molybdoenzyme formate dehydrogenase. Chemistry 14:8674–8681
180. Mota CS, Rivas MG, Brondino CD, Moura I, Moura JJG, Gonzalez PG, Cerqueira NMFSA (2011) The mechanism of formate oxidation by metal-dependent formate dehydrogenases. J Biol Inorg Chem 16:1255–1268
181. Tiberti M, Papaleo E, Russo N, Gioia L, Zampella G (2012) Evidence for the formation of a Mo-H intermediate in the catalytic cycle of formate dehydrogenase. Inorg Chem 51:8331–8339
182. Hartmann T, Leimkuhler S (2013) The oxygen-tolerant and NAD + -dependent formate dehydrogenase from *Rhodobacter capsulatus* is able to catalyze the reduction of CO_2 to formate. FEBS J 280:6083–6096

183. Hartmann T, Schrapers P, Utesch T, Nimtz M, Rippers Y, Dau H, Mroginski MA, Haumann M, Leimkühler S (2016) The molybdenum active site of formate dehydrogenase is capable of catalyzing C-H bond cleavage and oxygen atom transfer reactions. Biochemistry 55:2381–2389
184. Niks D, Duvvuru J, Escalona M, Hille R (2016) Spectroscopic and kinetic properties of the molybdenum-containing, NAD + -dependent formate dehydrogenase from *Ralstonia eutropha*. J Biol Chem 291:1162–1174
185. Dong G, Ryde U (2018) Reaction mechanism of formate dehydrogenase studied by computational methods. J Biol Inorg Chem 23:1243–1255
186. Thauer RK, Kaufer B, Fuchs G (1975) The active species of 'CO_2' utilized by reduced ferredoxin: CO_2 oxidoreductase from clostridium pasteurianum. Eur J Biochem 55:111–117
187. Arnoux P, Sabaty M, Alric J, Frangioni B, Guigliarelli B, Adriano JM, Pignol D (2003) Structural and redox plasticity in the heterodimeric periplasmic nitrate reductase. Nat Struct Biol 10:928–934
188. Tanaka R, Yamashita M, Nozaki K (2009) Catalytic hydrogenation of carbon dioxide using Ir(III)-pincer complexes. J Am Chem Soc 131:14168–14169
189. Ziebart C, Federsel C, Anbarasan P, Jackstell R, Baumann W, Spannenberg A, Beller M (2012) Well-defined iron catalyst for improved hydrogenation of carbon dioxide and bicarbonate. J Am Chem Soc 134:20701–20704
190. Filonenko GA, Hensen EJM, Pidko EA (2014) Mechanism of CO_2 hydrogenation to formates by homogeneous Ru-PNP pincer catalyst: from a theoretical description to performance optimization. Catal Sci Technol 4:3474–3485
191. Maiti BK, Maia LB, Pal K, Pakhira B, Avilés T, Moura I, Pauleta SR, Nuñez JL, Rizzi AC, Brondino CD, Sarkar S, Moura JJG (2014) One electron reduced square planar bis (benzene-1,2-dithiolato) copper dianionic complex and redox switch by O_2/HO−. Inorg Chem 53:12799–12808
192. Lothrop AP, Snider GW, Flemer S, Ruggles EL, Davidson RS, Lamb AL, Hondal RJ (2014) Compensating for the absence of selenocysteine in high-molecular weight thioredoxin reductases: the electrophilic activation hypothesis. Biochemistry 53:664–674
193. Massey V, Edmondson D (1970) On the mechanism of inactivation of xanthine oxidase by cyanide. J Biol Chem 245:6595–6598
194. Edmondson DE, Ballou D, Vanheuvelen A, Palmer G, Massey V (1973) Kinetic studies on the substrate reduction of xanthine oxidase. J Biol Chem 248:6135–6144
195. Olson JS, Ballou DP, Palmer G, Massey V (1974) The mechanism of action of xanthine oxidase. J Biol Chem 249:4363–4382
196. Gutteridge S, Tanner SJ, Bray RC (1978) The molybdenum centre of native xanthine oxidase. evidence for proton transfer from substrates to the centre and for existence of an anion-binding site. Biochem J 175:869–878
197. Gutteridge S, Tanner SJ, Bray RC (1978) Comparison of the molybdenum centres of native and desulpho xanthine oxidase. the nature of the cyanide-labile sulphur atom and the nature of the proton-accepting group. Biochem J 175:887–897
198. Bray RC, Gutteridge S, Stotter DA, Tanner SJ (1979) The mechanism of xanthine oxidase The relationship between the rapid and very rapid electron-paramagnetic-resonance signals. Biochem J 177:357–360
199. Coughlan MP, Johnson JL, Rajagopalan KV (1980) Mechanisms of inactivation of molybdoenzymes by cyanide. J Biol Chem 255:2694–2699
200. Gutteridg S, Bray RC (1980) Oxygen-17 splitting of the very rapid molybdenum(V) e.p.r. signal from xanthine oxidase. rate of exchange with water of the coupled oxygen atom. Biochem J 189:615–623
201. Malthouse JPG, Gutteridge S, Bray RC (1980) Rapid type 2 molybdenum(V) electron-paramagnetic resonance signals from xanthine oxidase and the structure of the active centre of the enzyme. Biochem J 185:767–770

202. Xia M, Dempski R, Hille R (1999) The reductive half-reaction of xanthine oxidase Reaction with aldehydes and identification of the catalytically labile oxygen. J Biol Chem 274:3323–3330
203. Boll M (2005) Key enzymes in the anaerobic aromatic metabolism catalysing birch-like reductions. Biochim Biophys Acta 1707:34–50
204. Johannes J, Unciuleac M, Friedrich T, Warkentin E, Ermler U, Boll M (2008) Inhibitors of the molybdenum cofactor containing 4-hydroxybenzoyl-CoA reductase. Biochemistry 47:4964–4972
205. Stiefel EI (1973) Proposed molecular mechanism for the action of molybedenum in enzymes: coupled proton and electron transfer. Proc Natl Acad Sci USA 70:988–992
206. Stiefel EI (1977) The coordination and bioinorganic chemistry of molybdenum Prog. Inorg Chem 22:1–223
207. Rajapakshe A, Snyder RA, Astashkin AV, Bernardson P, Evans DJ, Young CG, Evans DH, Enemark JH (2009) Insights into the nature of Mo(V) species in solution: modeling catalytic cycles for molybdenum enzymes. Inorg Chim Acta 362:4603–4608
208. Maia L, Moura I, Moura JJG (2017) EPR spectroscopy on mononuclear molybdenum-containing enzymes. In: Hanson G, Berliner LJ (eds) Future directions in metalloprotein and metalloenzyme research, Biological Magnetic Resonance, vol 33. Springer International Publishing, Cham, Chap 4, pp 55–101
209. Wilson GL, Greenwood RJ, Pilbrow JR, Spence JT, Wedd AG (1991) Molybdenum(V) sites in xanthine oxidase and relevant analogue complexes: comparison of molybdenum-95 and sulfur-33 coupling. J Am Chem Soc 113:6803–6812
210. Duffus BR, Schrapers P, Schuth N, Mebs S, Dau H, Leimkühler S, Haumann M (2020) Anion binding and oxidative modification at the molybdenum cofactor of formate dehydrogenase from *Rhodobacter capsulatus* studied by X-ray absorption spectroscopy. Inorg Chem 59:214–225
211. Barber MJ, May HD, Ferry JG (1986) Inactivation of formate dehydrogenase from methanobacterium formicicum by cyanide? Biochemistry 25(1986):8150–8155
212. Friedebold J, Bowien B (1993) Physiological and biochemical characterization of the soluble formate dehydrogenase, a molybdoenzyme from *Alcaligenes eutrophus*. J Bacteriol 175:4719–4728
213. George GN, Colangelo CM, Dong J, Scott RA, Khangulov SV, Gladyshev VN, Stadtman TC (1998) X-ray absorption spectroscopy of the molybdenum site of *Escherichia coli* formate dehydrogenase. J Am Chem Soc 120:1267–1273
214. George GN, Costa C, Moura JJG, Moura I (1999) Observation of ligand-based redox chemistry at the active site of a molybdenum enzyme. J Am Chem Soc 121:2625–2626
215. Mota CS (2011) Faculdade de Ciências e Tecnologia, Universidade Nova de Lisboa, Portugal, PhD Thesis. https://hdl.handle.net/10362/6688
216. Axley MJ, Böck A, Stadtman TC (1991) Catalytic properties of an *Escherichia coli* formate dehydrogenase in which sulfur replaces selenium. Proc Natl Acad Sci USA 88:8450–8454
217. Coelho C, Gonzalez PJ, Moura JG, Moura I, Trincao J, Joao Romao M (2011) The crystal structure of *Cupriavidus necator* nitrate reductase in oxidized and partially reduced states. J Mol Biol 408:932–948
218. Cerqueira NMFSA, Fernandes PA, Gonsalez PJ, Moura JJG, Ramos MJ (2013) The sulfur shift: an activation mechanism for periplasmic nitrate reductase and formate dehydrogenase. Inorg Chem 52:10766–10772
219. Robinson WE, Bassegoda A, Reisner E, Hirst J (2017) Oxidation-state-dependent binding properties of the active site in a mo-containing formate dehydrogenase. J Am Chem Soc 139:9927–9936
220. Cornish-Bowden A (1995) Fundamentals of enzyme kinetics. Portland Press, London
221. Silveira CM, Almeida MG (2013) Small electron-transfer proteins as mediators in enzymatic electrochemical biosensors. Anal Bioanal Chem 405:3619–3635

222. Armstrong FA, Hirst J (2011) Reversibility and efficiency in electrocatalytic energy conversion and lessons from enzymes. Proc Natl Acad Sci U S A 108:14049–14054
223. Fourmond V, Léger C (2016) Protein electrochemistry: questions and answers. In: Jeuken L (ed) Biophotoelectrochemistry: from bioelectrochemistry to biophotovoltaics. Advances in biochemical engineering/biotechnology, vol 158. Springer, Cham
224. Fourmond V, Léger C (2017) Modelling the voltammetry of adsorbed enzymes and molecular catalysts. Curr Opin Electrochem 1:110–120
225. Fourmond V (2017) Direct Electrochemistry of molybdenum and tungsten enzymes. Reference module in chemistry, molecular sciences and chemical engineering, pp 477–488 https://doi.org/10.1016/B978-0-12-409547-2.13354-2
226. Li H, Buesen D, Dementin S, Léger C, Fourmond V, Plumeré N (2019) Complete protection of O_2-sensitive catalysts in thin films. J Am Chem Soc 141:16734–16742
227. Fourmond V, Wiedner ES, Shaw WJ, Léger C (2019) Understanding and design of bidirectional and reversible catalysts of multielectron, multistep reactions. J Am ChemSoc 141:11269–11285
228. Kornienko N, Zhang JZ, Sakimoto KK, Yang P, Reisner E (2018) Semi-artificial photosynthesis: interfacing nature's catalytic machinery with synthetic materials. Nat Nanotechnol 13:890
229. Bok FA, Hagedoorn PL, Silva PJ, Hagen WR, Schiltz E, Fritsche K, Stams AJ (2003) Two W-containing Formate Dehydrogenases (CO_2-reductases) involved in syntrophic propionate oxidation by syntrophobacter fumaroxidans. Eur J Biochem 270:2476–2485
230. Bok FA, Hagedoorn PL, Silva PJ, Hagen WR, Schiltz E, Fritsche K, Stams AJ (2003) Two W-containing formate dehydrogenases (CO_2-reductases) involved in syntrophic propionate oxidation by syntrophobacter fumaroxidans. FEBS J 270:2476–2485
231. Worm P, Stams AJ, Cheng X, Plugge CM (2011) Growth- and substrate-dependent transcription of formate dehydrogenase and hydrogenase coding genes in Syntrophobacter fumaroxidans and Methanospirillum hungatei. Microbiology 157:280–289
232. Reda T, Plugge CM, Abram NJ, Hirst J (2008) Reversible interconversion of carbon dioxide and formate by an electroactive enzyme. Proc Natl Acad Sci USA 105:10654–10658
233. Kuwabata S, Tsuda R, Nishida K, Yoneyama H (1993) Electrochemical conversion of carbon dioxide to methanol with use of enzymes as biocatalysts. Chem Lett 22:1631–1634
234. Kuwabata S, Tsuda R, Yoneyama H (1994) Electrochemical conversion of carbon dioxide to methanol with the assistance of formate dehydrogenase and methanol dehydrogenase as biocatalysts. J Am Chem Soc 116:5437–5443
235. Miyatani R, Amao Y (2002) Bio-CO_2 fixation with formate dehydrogenase from saccharomyces cerevisiae and water-soluble zinc porphyrin by visible light. Biotechnol Lett 24:1931–1934
236. Tsujisho I, Toyoda M, Amao Y (2006) Photochemical and enzymatic synthesis of formic acid from CO_2 with chlorophyll and dehydrogenase. System Catal Commun 7:173–176
237. Ihara M, Kawano Y, Urano M, Okabe A (2013) Light driven CO_2 fixation by using cyanobacterial photosystem I and NADPH-dependent formate dehydrogenase. PLoS ONE 8: e71581
238. Amao Y, Shuto N (2014) Formate dehydrogenase-viologen-Immobilized Electrode for CO_2 conversion, for development of an artificial photosynthesis system. Res Chem Intermed 40:3267–3276
239. Amao Y, Takahara S, Sakai Y (2014) Visible-light induced hydrogen and formic acid production from biomass and carbon dioxide with enzymatic and artificial photosynthesis system. Int J Hydrogen Energy 39:20771–20776
240. Kim S, Kim MK, Lee SH, Yoon S, Jung KD (2014) Conversion of CO_2 to formate in an electroenzymatic cell using candida boidinii formate dehydrogenase. J Mol Catal B Enzym 102:9–15

241. Srikanth S, Maesen M, Dominguez-Benetton X, Vanbroekhoven K, Pant D (2014) Enzymatic electrosynthesis of formate through CO_2 sequestration/reduction in a bioelectrochemical system (BES). Bioresour Technol 165:350–354
242. Hwang H, Yeon YJ, Lee S, Choe H, Jang MG, Cho DH, Park S, Kim YH (2015) Electro-biocatalytic production of formate from carbon dioxide using an oxygen-stable whole cell biocatalyst. Bioresour Technol 185:35–39
243. Kim SH, Chung GY, Kim SH, Vinothkumar G, Yoon SH, Jung KD (2016) Electrochemical NADH regeneration and electroenzymatic CO_2 reduction on cu nanorods/glassy carbon electrode prepared by cyclic deposition. Electrochim Acta 210:837–845
244. Lee SY, Lim SY, Seo D, Lee JY, Chung TD (2016) Light-driven highly selective conversion of CO_2 to formate by electrosynthesized enzyme/cofactor thin film electrode. Adv Energy Mater 6:1502207
245. Nam DH, Kuk SK, Choe H, Lee S, Ko JW, Son EJ, Choi EG, Kim YH, Park CB (2016) Enzymatic photosynthesis of formate from carbon dioxide coupled with highly efficient photoelectrochemical regeneration of nicotinamide cofactors. Green Chem 18:5989–5993
246. Schlager S, Dumitru LM, Haberbauer M, Fuchsbauer A, Neugebauer H, Hiemetsberger D, Wagner A, Portenkirchner E, Sariciftci NS (2016) Electrochemical reduction of carbon dioxide to methanol by direct injection of electrons into immobilized enzymes on a modified electrode. Chemsuschem 9:631–635
247. Ikeyama S, Amao Y (2017) A Novel electron carrier molecule based on a viologen derivative for visible light-driven CO_2 reduction to formic acid with the system of zinc porphyrin and formate dehydrogenase. Sustain Energy Fuels 1:1730–1733
248. Noji T, Jin T, Nango M, Kamiya N, Amao Y (2017) CO_2 photoreduction by formate dehydrogenase and a Ru-complex in a nanoporous glass reactor. ACS Appl Mater Interfaces 9:3260–3265
249. Zhang L, Liu J, Ong J, Li SFY (2016) Specific and sustainable bioelectro-reduction of carbon dioxide to formate on a novel enzymatic cathode. Chemosphere 162:228–234
250. Yadav RK, Baeg J-O, Oh GH, Park N-J, Kong K-J, Kim J, Hwang DW, Biswas SK (2012) A photocatalyst-enzyme coupled artificial photosynthesis system for solar energy in production of formic acid from CO_2. J Am Chem Soc 134:11455–11461
251. El-Zahab B, Donnelly D, Wang P (2008) Particle-tethered NADH for production of methanol from CO_2 catalyzed by coimmobilized enzymes. Biotechnol Bioeng 99:508–514
252. Choe H, Joo JC, Cho DH, Kim MH, Lee SH, Jung KD, Kim YH (2014) Efficient CO_2-reducing activity of NAD-dependent formate dehydrogenase from thiobacillus sp KNK65MA for formate production from CO_2 gas. PLoS ONE 9:e103111
253. Kuk SK, Singh RK, Nam DH, Singh R, Lee JK, Park CB (2017) Photoelectrochemical reduction of carbon dioxide to methanol through a highly efficient enzyme cascade. Angew Chem 56:3827–3832
254. Sakai K, Kitazumi Y, Shirai O, Kano K (2016) Bioelectrocatalytic formate oxidation and carbon dioxide reduction at high current density and low overpotential with tungsten-containing formate dehydrogenase and mediators. Electrochem Commun 65:31–34
255. Sakai K, Kitazumi Y, Shirai O, Takagi K, Kano K (2016) Efficient bioelectrocatalytic CO_2 reduction on gas-diffusion-type biocathode with tungsten-containing formate dehydrogenase. Electrochem Commun 73:85–88
256. Sakai K, Kitazumi Y, Shirai O, Takagi K, Kano K (2017) direct electron transfer-type four-way bioelectrocatalysis of CO_2/ formate and NAD +/NADH redox couples by tungsten-containing formate dehydrogenase adsorbed on gold nanoparticle-embedded mesoporous carbon electrodes modified with 4-Mercaptopyridine. Electrochem Commun 84:75–79
257. Sakai K, Sugimoto Y, Kitazumi Y, Shirai O, Takagi K, Kano K (2017) Direct electron transfer-type bioelectrocatalytic interconversion of carbon dioxide/formate and NAD +/NADH redox couples with tungsten-containing formate dehydrogenase. Electrochim Acta 228:537–544

258. Sakai K, Xia H, Kitazumi Y, Shirai O, Kano K (2018) Assembly of direct-electron-transfer-type bioelectrodes with high performance. Electrochim Acta 271:305–311
259. Muller U, Willnow P, Ruschig U, Hopner T (1978) Formate dehydrogenase from *Pseudomonas oxalaticus*. Eur J Biochem 83:485–498
260. Yu X, Niks D, Mulchandani A, Hille R (2017) Efficient reduction of CO_2 by the molybdenum-containing formate dehydrogenase from *Cupriavidus necator* (*Ralstonia eutropha*). J Biol Chem 292:16872–16879
261. Walker LM, Li V, Niks D, Hille R, Elliott SJ (2019) Deconvolution of reduction potentials of formate dehydrogenase from *Cupriavidus necator*. J Biol Inorg Chem 24:889–898
262. Yu X, Niks D, Ge X, Liu H, Hille R, Mulchandani A (2019) Synthesis of formate from CO_2 gas catalyzed by an O_2-tolerant NAD-dependent formate dehydrogenase and glucose dehydrogenase. Biochemistry 58:1861–1868
263. Bassegoda A, Madden C, Wakerley DW, Reisner E, Hirst J (2014) Reversible interconversion of CO_2 and formate by a molybdenum-containing formate dehydrogenase. J Am Chem Soc 136:15473–15476
264. Roger M, Brown F, Gabrielli W, Sargent F (2018) Efficient hydrogen-dependent carbon dioxide reduction by *Escherichia coli*. Curr Biol 28:140–145
265. Singh S, Noori MT, Verm N (2020) Efficient bio-electroreduction of CO_2 to formate on a iron phthalocyanine-dispersed CDC in microbial electrolysis system. ElectrochimActa 338:135887
266. Cordas CM, Campaniço M, Baptista R, Maia LB, Moura I, Moura JJG (2019) Direct electrochemical reduction of carbon dioxide by a molybdenum-containing formate dehydrogenase. J Inorg Biochem 196:110694
267. Mourato C, Martins M, da Silva SM, Pereira IA (2017) A continuous system for biocatalytic hydrogenation of CO_2 to Formate. Bioresour Technol 235:149–156
268. Martins M, Mourato C, Pereira IAC (2015) *Desulfovibrio vulgaris* growth coupled to formate-driven H_2 production. Environ Sci Technol 49:14655–14662
269. Martins M, Mourato C, Morais-Silva FO, Rodrigues- Pousada C, Voordouw G, Wall JD, Pereira IAC (2016) Electron transfer pathways of formate-driven H_2 production in Desulfovibrio. Appl Microbiol Biotechnol 100:8135–8146
270. Sokol KP, Robinson WE, Oliveira AO, Warnan J, Nowaczyk MM, Ruff A, Pereira IAC, Reisner E (2018) Photoreduction of CO_2 with a formate dehydrogenase driven by photosystem II using a semi-artificial Z-scheme architecture. J Am Chem Soc 140:16418–16422
271. Miller M, Robinson WR, Oliveira AR, Heidary N, Kornienko N, Warnan J, Pereira IAC, Reisner E (2019) Interfacing formate dehydrogenase with metal oxides for the reversible electrocatalysis and solar-driven reduction of carbon dioxide. Angew Chem 58:4601–4605
272. Szczesny J, Ruff A, Oliveira AR, Pita M, Pereira IAC, De Lacey AL, Schuhmann W (2020) Electroenzymatic CO_2 fixation using redox polymer/enzyme-modified gas diffusion electrodes. ACS Energy Lett 5:321–327
273. Sokol KP, Robinson WE, Oliveira AR, Zacarias S, Lee C-Y, Madden C, Bassegoda A, Hirst J, Pereira IAC, Reisner E (2019) Reversible and selective interconversion of hydrogen and carbon dioxide into formate by a semiartificial formate hydrogenlyase mimic. J Chem Am Soc 141:17498–17502
274. Berg IA, Kockelkorn D, Ramos-Vera WH, Say RF, Zarzycki J, Hügler M (2010) Autotrophic carbon fixation in archaea. Nat Rev Microbiol 8:447–460
275. Martin WF, Thauer RK (2017) Energy in ancient metabolism. Cell 168:953–955

Carbon Dioxide Utilization—Bioelectrochemical Approaches

Cristina M. Cordas, José J. G. Moura, Adrián Escapa, and Raúl Mateos

Abstract

CO_2 level increase in the planet is a major concern and utilization, mitigation and transformation of CO_2 in useful compounds is of great interest. This chapter points to an alternative electrochemical approach for reducing/making use of CO_2 in a "greener" route, using electricity that may be generated from renewable sources (e.g. solar, wind). The most relevant enzymes that can utilize CO_2 are described, as well as their electrochemical behaviour. The bioelectrochemical approach (in its different possible systems and configurations) has an enormous advantage in the selection of the reaction products, in mild conditions. Carbon monoxide, hydrocarbons, alcohols, urea and formic acid are detectable products, and the last one has received particular attention in terms of its market added value. Enzymes, multi enzymatic, whole cells, and other bioelectrochemical systems, e.g. microbial fuel cells, for electrosynthesis and CO_2 mitigation, are discussed here.

C. M. Cordas (✉) · J. J. G. Moura
LAQV, REQUIMTE, NOVA School of Science and Technology, Campus de Caparica, Caparica, Portugal
e-mail: cristina.cordas@fct.ul.pt

A. Escapa (✉) · R. Mateos
Chemical and Environmental Bioprocess Engineering Group, Natural Resources Institute (IRENA), Universidad de León, León, Spain
e-mail: adrian.escapa@unileon.es

A. Escapa
Department of Electrical Engineering and Automatic Systems, Universidad de León, Campus de Vegazana, León, Spain

J. J. G. Moura et al. (eds.), *Enzymes for Solving Humankind's Problems*,
https://doi.org/10.1007/978-3-030-58315-6_3

Keywords

Carbon dioxide · Electrochemistry · Enzymes · Microorganisms · Microbial fuel cells · Electrosynthesis · Added-value compounds

Abbreviations

ADH	Alcohol dehydrogenase
A. woodi	*Acetobacterium woodie*
AldDH	Formaldehyde dehydrogenase
AEM	Anion exchange membrane
A. vinelandii	*Azotobacter vinelandii*
BES	Bioelectrochemical systems
CA	Carbonic anhydrase
C. boidinii	*Candida boidinii*
C. hydrogenoformans	*Carboxydothermus hydrogenoformans*
D. desulfuricans	*Desulfovibrio desulfuricans*
EFC	Enzymatic fuel cell
E. coli	*Escherichia coli*
EES	Enzymatic lectrosynthesis
FDH	Formate dehydrogenase
GDH	Glutamate dehydrogenase
IEM	Ion exchange membranes
M. extorquens	*Methylobacterium extorquens AM1*
M. thermoacetica	*Moorella thermoacetica*
MET	Mediated-electron transfer
MES	Microbial electrosynthesis
MDH	Methanol dehydrogenase
MFC	Microbial fuel cell
PTEF	Poly(1,1,2,2-tetrafluoroethylene)
PQQ	Pyrroloquinolinequinone
R. rubrum	*Rhododspirillum rubrum*
S. fumaroxidans	*Syntrophobacter fumaroxidans*
VFA	Volatile fatty acids

1 Introduction

1.1 Electrochemical/Bioelectrochemical Advantages

The search for solutions towards atmospheric CO_2 reduction/mitigation has increased dramatically, in recent years, driven by the global awareness of the climate change effects, including Institutional boost to find solutions, such as the 2030 Agenda for Sustainable Development, namely in its goal 13 goals (Climate Action). A multitude of past and on-going research projects propose different approaches towards the CO_2 transformation into added-value products, simultaneously reducing CO_2 atmospheric levels. Still, most of those have shown low efficiencies and the research intensively continues. Amongst the proposals, it is possible to find photochemical, biochemical, thermochemical, electrochemical and mixed methodologies [1]. The difficulties to find an efficient approach are associated to the known properties of CO_2 molecule, namely its stability and also to its low solubility in water [2, 3]. The electrochemical approach for reducing CO_2 seems to present advantages since can be considered a "greener" route by the possibility to use the excess of electricity generated by other renewable sources (considering the different demands throughout the days), such as solar or wind. Another gain is the possible estimation and selection of the reaction products through the applied conditions, namely the current density, amongst other parameters [4]. Several possible CO_2 electro-synthesized products can be formed such as carbon monoxide, hydrocarbons, alcohols, urea and formic acid. The later has received particular attention since has been considered as the most valuable (in terms of its market value) [3, 5]. Although studies have demonstrated that electroreduction of CO_2 to formic acid, for instance, can be economically viable when compared with traditional industrial methods [5], the energetics and catalysts needed are still issues to be overcome. These issues can, however, be surpassed by merging biochemical and electrochemical methods. In fact, in Nature enzymes are known to easily use (by reducing or oxidizing or by acid–base reactions) and convert CO_2 to value-added products using mild conditions (room temperature, 1 atm, physiological pH values) and some mixed methods are being pursued [6, 7]. Our ability to use Natures' solutions together with our technological developments seems to be the key to a more sustainable world.

2 Enzymatic Systems and CO_2

2.1 Enzymes Catalysing CO_2 Reactions

Currently, it is well established that human activity altered the carbon cycle, leading to perturbation in the fluxes between atmospheric, land, water and geological carbon reservoirs with consequently enhanced levels of atmospheric CO_2 [8]. The most known carbon processes/pools are related to photosynthesis, organic

decomposition and carbon dissolution in marine resources, namely the oceans, although others, such as permafrost, have been progressively recognized as important in the future regulation of atmospheric CO_2 levels [9]. Biological processes are vital in the carbon cycle. There are multiple biological processes related with CO_2 release and uptake and within these, enzymes that carry these reactions.

Brief descriptions of some of the most interesting enzymes that may be used in technological systems using CO_2 are given below.

Probably the most renowned biological process is photosynthesis, a process common to plants, algae and cyanobacteria. In the carbon cycle, one of the first enzymes whose importance was recognized is **RuBisCO** (**ribulose 1,5-bisphosphatecarboxylase/oxygenase**). This ancient enzyme allows carbon fixation and biomass accumulation through the catalysis of its initial step which is the CO_2 conversion into hydrocarbons, namely through the carboxylation of ribulose 1,5-bisphosphate (RuBP) and further cleavage, forming two molecules of 3-phospho-glycerate (3PG) [10, 11]. Although being an essential enzyme to Earth as we know it, and apparently appealing to incorporate in biotechnological systems, this enzyme presents some limitations, namely the reaction has low rate, it depends on an activation step by another enzyme, the reaction has multiple steps and it is easily inhibited [10, 12]. Also, oxygen competes with CO_2 and the specificity depends on several factors, including the ratio of CO_2 to O_2 in the vicinity of the enzyme [13]. The activation of the enzyme requires a complex mechanism depending on the presence of Mg^{2+} ion and a suitable charge distribution around this [14]. The enzyme is active when a conserved Lys201 of the large subunit binds CO_2 together with the Mg^{2+} ion-producing a carbamate [14]. RuBisCO is not easy to handle, not only due to its mechanism but also its structure, since it is a multimeric structure, presenting large (L, approx. 50 to 55 kDa) and small (S, approx. 12 to 18 kDa) subunits. The enzyme presents three forms, characteristic of organisms from, respectively, proteobacteria, cyanobacteria, algae and vascular plants (Form I, the most abundant), chemoautotrophs, proteobacteria and dinoflagellated algae (Form II) and archaea (Form III) where the main catalytic dimeric subunit, L, may present structures with L_2 to $(L_2)_5$, [12].

Another well-known enzyme class is **carbonic anhydrase** (**CA**) making a bridge between the geological and biological parts of the carbon cycle. CAs catalyse the reversible conversion of CO_2 into hydrogen carbonate ion which is very appealing to pursue its incorporation in atmospheric CO_2 mitigation systems [15]. CAs participate in several functions besides CO_2 transport and conversion to bicarbonate, namely, in respiration, pH regulation, biosynthesis, among others, and are found in all known living organisms. These are metalloenzymes, usually bearing Zn^{2+} in their active site (Fe and Cd were also found) and are observed in different families with different structures that evolved towards a common activity [16, 17]. Among those, the α-CA which are found in animals, plants, vertebrates, bacteria and algae, present high activities, and good stability, being soluble and easily expressed, making these promising to be incorporated in CO_2 mitigation systems using diverse strategies [15, 18–20].

Other reaction efficiently catalysed by enzymes is the reversible reduction of CO_2 to CO, by **carbon monoxide dehydrogenases** (**CODH**), although its main reaction is the CO oxidation to CO_2, found in bacteria and archaea, involving two electrons and two protons. This enzyme participates in the Wood-Ljungdahl pathway of Acetyl-CoA synthesis together with the acetyl-CoA synthase (ACS) enzyme [21, 22], being called as bifunctional CODH. It can also be found without ACS, called unifunctional CODH, in some anaerobic bacteria that use CO as source of growth and energy. These were isolated from anaerobes, such as, *R. rubrum or C. hydrogenoformans*, in which Ni was found in the active catalytic site. CODH is a homodimer (approx. 130 kDa) containing five metal-sulfur clusters. The active centre (the C-cluster) contains a Ni coordinated with four Fe ions, in a $[NiFe_3S_4]$ cubane-like structure with an extra-cubane Fe bond to the Ni by a sulfide bridge [23–25] for which these enzymes are frequently named as Ni-CODHs. In some aerobic bacteria, Mo (in a molybdopterin structure) is found in the active centre with a structure (and properties) similar to the one found in Mo enzymes, such as xanthine oxidase, among others [25, 26]. The enzyme also integrates other FeS clusters that play a role in the electron transfer pathway [27]. Ni-CODHs have been the subject of intense research recently aiming its integration in CO_2 mitigation systems, biofuels and H_2 production, due to its catalytic properties and the ease to purify and express them, although they also present an important disadvantage, namely its sensitivity to O_2 [22, 27–29].

Formate dehydrogenase enzymes (**FDHs**) are a particular interesting class of enzymes that have been considered to have huge potential to integrate systems using CO_2. These enzymes have the ability to catalyse the reversible 2 electrons reduction of CO_2 to formate, a reaction economically very relevant [3, 30–32]. FDHs can be divided into two classes, namely the metal-dependent (found in prokaryotes) and metal-independent enzymes (NAD-dependent, found in bacteria, fungi and plants), whether they present or not metal ions (Mo, W) in their active site, respectively [33, 34]. So far, metal-dependent enzymes have shown more activity towards the CO_2 reduction than the metal-independent [35], albeit the later has been more extensive studied, probably due to the fact of being easier to get (some are commercially available). In the metal-dependent enzymes mononuclear enzymes, Mo or W ion is coordinated in the active site by four sulfur atoms of two pyranopterin cofactors, S-Cysteine (or Se-Cysteine) and one additional S atom [33, 36]. The electrochemical control of the FDH catalysis towards CO_2 reduction has been intensively pursued and some studies have already shown the feasibility of its integration in CO_2 mitigation systems [37] or other bioelectrochemical systems (BES). This topic will be further developed in the next sections.

Nitrogenases are well-known enzymes involved in nitrogen fixation found largely in bacteria and archaea. The main catalytic reaction (reduction of N_2 to NH_3) has a chemical parallel in the high used industrial Haber–Bosch reaction, but contrarily to this later, nitrogenase works at room temperature and normal 1 atm of pressure being much more effective than the industrial reaction [38, 39]. Nitrogenase is composed by a complex that comprises two proteins, one containing the catalytic MoFe centre (where Mo may be replaced by V or Fe), with structure

[$MoFe_7S_9C$](R-homocitrate), (R can be C or N), called M-cluster (also known as FeMo cofactor) and a [Fe_8S_7] cluster (P-cluster) and a [4Fe-4S] cluster in a second protein [38, 40–42]. It was found that besides N_2, nitrogenases can catalyse the reduction of small carbon molecules (with multiple bonds) such as acetylene or cyanide, among many others [41, 43]. Interestingly, nitrogenases have also shown activity towards CO_2 and CO reduction. These enzymes were shown to reduce CO_2 to CO, formate (or formic acid) and to methane [44], displaying rates towards formic acid 10 times higher than to the two other products. This activity has made to regain the interest in nitrogenases as potential enzymes to integrate CO_2 mitigation and added-value compounds production systems.

Other enzymes have been considered aiming the same goal. These usually take advantage of other reactions in which CO_2 is a by-product of reactant and may be integrated systems in combination with other enzymes. One example is the malic enzyme (also known as malate dehydrogenase, MDH) whose catalytic reaction is the oxidation of malic acid to pyruvate releasing CO_2. This reaction is reversible being able to promote CO_2 fixation and production of malic acid, a compound with many industrial applications [45]. Some studies have also shown the feasibility of this reaction using HCO_3^- as model compound to achieve carbon fixation from it. This reaction, however, shows a low conversion rate (less than 40%) [46]. Other example was the use of isocitrate dehydrogenase to reduce CO_2 in oxoglutaric acid using electrochemistry. This reaction requires a large overpotential although conversions are reasonable (around 80%) [47].

2.2 Redox Properties of CO_2-Related Enzymes

CO_2-related enzymes use in electrochemical systems presupposes that their electrochemical properties are known allowing its electrochemical control. Highly complex enzymes, such as RuBisCO, are not easily handled and/or electrochemically studied. RuBisCO behaviour is known to be dependent on the oxidation of cysteines, with its activity decaying with the loss of cysteine sulfhydryl groups and subsequent conformational changes [48, 49]. This change from active to an inactive enzyme with the oxidation of the different cysteines corresponds to an apparent redox potential of −308 mV and further oxidation at −299 mV and implies conformational critical changes [50]. Although the redox control of RuBisCO has been considered an important factor that could help to improve the process efficiency [51], the experimental difficulties seem to have hindered the study of the isolated enzyme, though some approaches using it combined with other enzymes and structures have been reported. For instance, RuBisCO has been immobilized in multi enzymatic self-assembled synthetic amphiphilic peptide nanostructures aiming to improve the enzyme stability and activity [52]. CAs are also usually used in immobilized systems, with improved stability comparing with the free enzyme, to increase the CO_2 hydration, taking advantage of the enzyme high turnover rate [53–55]. Very often CAs are used in association with other enzymes, such as phosphoenolpyruvate carboxylase or formate dehydrogenase enhancing the

added-value compounds production yield, e.g., methanol and formate [56–58]. The mechanism of CAs is pH-dependent but not redox-dependent. The stability of the Zn^{2+} in its active centre makes difficult the direct electrochemical control of the enzyme but not its indirect control in multi enzymatic systems, free in solution or immobilized in different matrices such as polymers, hydrogels or others [55–57]. A different scenario is found with CODHs. As stated earlier, in spite the main reaction in which these enzymes are involved in the CO oxidation to CO_2, the reversible reaction is possible and can be electrochemically controlled. The formal potential of the CODH active catalytic cluster of *M. thermoacetica* (free in solution) was found to be -520 mV (at pH 7), the same theoretical value for the CO/CO_2 reduction at the same pH, with the maximum catalytic efficiency at −570 mV at pH 6.3 [59]. The CODH immobilization seems to be more efficient than its use in solution since results have shown that its immobilization on gold nanoparticles have improved the affinity for dissolved CO [60]. Immobilized CODHs from *C. hydrogenoformans* were found to efficiently catalyse the reaction in the presence of a 50:50% CO_2 and CO mixture with a catalytic potential around −520 mV closer to the thermodynamic theoretical value (−558 mV [25]). The catalysis direction was demonstrated to be controlled by the applied potential, being favorable the CO oxidation at values more positive than -520 mV and the CO_2 reduction at more negative applied values. A drawback in using Ni-CODHs is their inhibition not only by CO but also by small molecules such as cyanide and sulfide [27]; also most of Ni-CODHs are inactivated in the presence of oxygen, although some may be reactivated by reduction [29]. CODH has been recently associated with FDHs to increase the efficiency to promote the high value-added compound formate from CO and CO_2 either using all cells or the purified enzymes [61].

Similarly to CODS, FDHs can be electrochemically studied and controlled, as already stated, and the catalysis direction towards formate oxidation or CO_2 reduction can be controlled by the applied potential. The direct electrochemical behaviour of the metal-dependent FDH from *D. desulfuricans* was attained with values for the formal reduction potential of the enzyme Mo active site of −250 mV and the catalytic activity (towards CO_2 reduction) starting at values of approx. −200 mV with the maximum catalytic current observed at −250 mV [62]. The catalytic behavior is similar to other FDH enzymes of the same class, not only containing Mo, but also W [63], in spite of, in general, the W containing enzymes seem to present lower potential catalytic values, such as FDH1 from *S. fumaroxidans* or *M. extorquens* [26, 63–65], where the catalysis towards CO_2 reduction is observed at −400 mV. The last example is particularly interesting for future applications since its activity is not affected by the presence of oxygen. Also, metal-independent FDH was demonstrated to be able to efficiently catalyse the CO_2 reduction to formate, although generally presenting lower k_{cat} than the metal-dependent ones [66]. One relevant example is the *C. boidinii* FDH that has no metals in the active centre and is NAD^+ dependent (its redox co-factor). For practical uses, the need for expensive co-factors as NADH are not favourable. The use of this particular FDH has the advantages of being commercially available, and also the possible replacement of the co-factor NAD^+/NADH by other small redox

mediators, such as methyl viologen (MV) [67]. Immobilization of different FDHs classes, in diverse matrices, e.g. hydrogel, conducting polymers, nanoparticles, has been extensively pursued trying to enhance the stability and efficiency of these systems [37, 65, 68, 69].

As mentioned earlier, nitrogenases can also catalyse the CO_2 reduction along with several other small molecules. An extensive review on this multitude of nitrogenases' substrates can be found in Seefeldt et al. [41]. The potentiometric determination of the redox centres reduction potentials was possible (see Table 1) showing values of approx. −465 and −40 mV for the M-cluster (the catalytic site), −300 to −90 mV to the P-cluster and −300 to −790 mV for the [4Fe-4S] cluster [38, 42, 70]. Voltammetric determinations allowed to obtain values around -300 mV for the M-cluster [38]. Also, in solution, direct voltammetry of the nitrogenase isolated co-factors from *A. vinelandii*, was achieved allowing to observed the value of −270 mV for the M-cluster, close to the attained value of the centre reduction potential in the all protein [71]. The electrochemical studies attained, together with the knowledge that the co-factors retain its catalytic properties [72], allows expecting a possible electrochemical control of the nitrogenase activity. Studies with the immobilization of a His-tagged MoFe nitrogenase on an electrode surface with functionalized nanotubes modified with a pyrene moiety incorporated in a polypeptide shown to be efficient for the bio-electrosynthesis of ammonia from N_3 and a possible route for other catalytic routes [73]. It was also demonstrated that MoFe and FeFe nitrogenase immobilized on a polymer-modified electrode, using cobaltocene as mediator were able to reduce CO_2 through imposition of applied potentials close to −1 V. The reaction is not completely specific since there is a side reaction where protons are reduced, but opens the possibility to integrate nitrogenases in BES [74].

Table 1 shows the relevant reduction potentials associated to the main enzymes that catalyse reactions with CO_2, allowing observing the diversity of centres and potentials values found in the literature.

2.3 Bioelectrochemical Enzymatic Approaches for CO_2 Utilization

An example that illustrates the prospective use of enzymes is the case of FDH, either immobilized or as free in solution. An FDH from *M. extorquens* was immobilized using the highly conductive Ketjen Black carbon material mixed with PTFE on a waterproof carbon cloth, allowing to obtain a gas-diffusion electrode, where 1,1′-trimethylene-2,2′-bipyridinium dibromide was used as mediator. In this mediated-electron transfer (MET) system, formate was produced by the reduction of gaseous CO_2, overcoming the question of the low solubility of the molecule [75] and the dependence of the FDH activity with the pH and the different carbonic species present in solution [76]. An enzymatic (formate-based) fuel cell (EFC) based on MET using NAD^+-dependent FDH was also recently reported [67]. In this study the free in solution FDH reduces CO_2 to formate at the cathodic

Table 1 Summary of the reduction potentials of the active centres and/or catalysis for the most representative CO_2-related enzymes

Enzyme	Redox or active centre metal	Catalytic reaction	$E^{0\prime}$ or E_{cat}^{*}/mV versus NHE	Refs.
RuBisCo	Lysine-Mg^{2+}	RbBP + CO_2 + H_2O → 2(3-PGA)	−308 (inactivation)	50
CA	$Cys_2His(X)$, (X usually water)-Zn^{2+}	CO_2 + H_2O ↔ HCO_3^- + H^+	≈−1000 (in multi enzyme systems)	17; 58
CODH	[4Fe–4S]–Ni	CO_2 + H_2O ↔ CO + 2e + $2H^+$	≈0 to −100 (CO oxidation) −520 (CO_2 reduction) −520 (active site/cluster reduction)	27; 28; 59; 60
FDH	(bis-pyranoptrein)-Mo (or W)	CO_2 + H^+ + 2e ↔ $HCOO^-$	−250 (formal potential) −250; −400 (CO_2 reduction);	62; 63; 64; 65; 75
Nitrogenase	MoFe centre (M-cluster), [Fe_8S_7] (P-cluster), [4Fe-4S] cluster (in a second protein)	CO_2 + H_2O → CO + 2e + $2H^+$ CO_2 + H^+ + 2e → $HCOO^-$ CO_2 + $8H^+$ + 8e → CH_4 + $2H_2O$	−465, ≈−300 to −360; −40 $[M\text{-cluster}]^{-1/0/+1}$ −309 to −90; + 340 ($[Fe_8S_7]^{0/+1/+2/+3/+4}$) −790 to −300 ($[4Fe–4S]^{0/1+/2+}$)	38; 41; 42; 43; 70; 71

compartment, being the electron transfer mediated by an artificial co-factor, MV (that reduces FDH), replacing the NAD^+/NADH physiological redox partner. The oxidized artificial mediator is then regenerated at the electrode surface. The EFC anode is platinum where water is oxidized to oxygen. The overall system was demonstrated to be able to work continuously with a formate production yield of about 60%. In another example, a DET bi-enzymatic EFC using immobilized FDH (in both the cathode and the anode) on carbon nanotubes modified carbon felt was reported with a coulombic efficiency of 60%. In this, the cathodic compartment was continuously fed with gaseous CO_2 and NADH was added to the anodic chamber [77]. Also, a hybrid microbial fuel cell (MFC) fed with wastewater pollutants coupled with a EFC with an immobilized FDH in the cathode, converting CO_2 to formate, was successfully reported [78]. Next sections will better describe these systems.

Although several proposals have been made using free enzymes in solution, the immobilization of enzymes, by different methods, e.g. covalent binding, adsorption, encapsulation, entrapment in hydrogel or polymeric matrices, amongst others, has been the preferential approach in order to enhance the stability and possible reutilization [37, 64, 65, 68, 69, 79].

Also, and though more complex, the coupling of different enzymes in multi enzymatic systems seems to be a more efficient alternative than using a single enzyme. Within these systems, one of the first reports was the use of FDH coupled with methanol dehydrogenase (MDH) to convert CO_2 into methanol, in a system where enzymes were both in solution together with mediators such as MV and pyrroloquinolinequinone (PQQ) [80]. A bi-enzymatic system using phospho-enolpyruvate carboxylase (PEPCase) and CA was attained by the encapsulation of the enzymes in polymeric microbeads. This cascade CA/PEPCase enzymatic system allows the production of oxaloacetate by CO_2 conversion using a compartmentalized structure where PEPCase is crosslinked in an organic polymer bead and CA crosslinked in inorganic silica on the surface of the polymer [56]. The system reveals good stabilization of the enzymes and the method may be adapted to other enzymes. Interesting multi enzymatic systems were developed by immobilizing different dehydrogenases and its co-factors in multilayers of polyelectrolytes in a sandwich-type design [81, 82]. A system with a scaffold prepared with poly(allylamine hydrochloride) (PAH) and polyurethane (PU) nanofibers was used to immobilize FDH (from *C. boidinii*), formaldehyde dehydrogenase (AldDH, from *Pseudomonas sp)*, alcohol dehydrogenase (ADH) together with the cofactor NADH aiming to build a cascade multi enzymes for methanol synthesis from CO_2 reduction. Also, glutamate dehydrogenase (GDH) and carbonic anhydrase (CA) were co-assembled in the system to enhance the co-factor regeneration and CO_2 hydration [81]. This complex system presented a methanol yield of 98%, higher than the synthesis attained with the free-enzymes in solution as already observed also in other studies. A previous cascade system using FDH, AldDH and ADH in solution, where a poly(neutral red) modified electrode was used to regenerate NADH, had already shown that was possible to attain methanol. This study, however, shown that the slowest step was the initial conversion of CO_2 to formate and that CA addition improved the reaction rate [58].

The complexity and difficulty in the systems control seems directly proportional to the efficiency of the conversions and the use of CO_2 towards added-value compounds production. A step forward on complexity is the successful use of whole cells' systems. An example is the use of a BES for the direct production of methane and acetate from CO_2 using a methanogenesis and acetogenic bacteria biofilm on the cathode compartment. Although the attained efficiency could not be considered high due to requirement of the application of considerable overpotentials, this was an important proof-of-concept for future developments [83]. A system using sulfate-reducing bacteria (from *Desulfovibrio* species) that contain several FDH and hydrogenases (Hase), with no mediators added, was tested in a bioreactor where continuous CO_2 and H_2 gas was added for formate production through the hydrogenation of CO_2 [84]. Recently, a novel approach, using CO_2 as intermediate, was reported aiming to convert carbon monoxide into a polyhydroxyalkanoate biopolymer (poly-3-hydroxybutyrate, PHB) considered as a viable alternative for petroleum-based nondegradable plastic products. The system

consists in two-stage bioreactors, a first one containing *A. woodii* whole cells (that possesses CODH and FDH), that convert CO into CO_2 via CODH and where the electrons from the oxidation are transferred to reduce FDH and to produce formate and a second bioreactor fed with the produced formate, where this is the only carbon source, containing *M. extorquens* which converts it to PHB [61].

3 Microbial Electrosynthesis: Bioelectrochemical Systems for CO_2 Valorisation

Carbon capture and utilization (CCU) has aroused a notable interest within both academy and industry sectors as it can provide an efficient approach to curb carbon dioxide (CO_2) emissions, complementing the "natural carbon cycle" by converting "spent carbon" (CO_2) into "working carbon" (valuable chemicals and fuels) [85]. However, since CO_2 displays remarkable chemical stability (carbon in CO_2 is fully oxidized), its industrial conversion (usually through reduction reactions that involve high pressure and/or temperature) can turn into an energy-intensive process [86, 87].

Nature, through its evolutionary process, has developed biocatalysts able to reduce carbon dioxide (CO_2) into organic molecules at moderate (ambient) conditions of pressure and temperature [88], which enables significantly reduce the energy requirements. The importance of these biocatalysts in the biological carbon fixation can hardly be underestimated as they allow biochemical reactions to proceed at rates that make possible to sustain biological processes. Microbial electrosynthesis (MES) technology has lately been developed as somehow imitate natural carbon fixation. It evolves from conventional electrochemistry with the difference that instead of using inorganic (and many times valuable) catalysts such as novel metals, it relies on a certain type of microorganisms that are able to interact electrically with a solid surface (cathode). These microorganisms can use the electrons arriving at the cathode to convert CO_2 into organic compounds [89]. Since they somehow "catalyse" the CO_2 reduction reaction, they are usually seen as "biocatalysts" [90].

Enzymatic electrosynthesis (EES) represents an approach similar to MES for converting CO_2 into valuable products through a (bio)electrochemical process. However, instead of using living microorganisms as biocatalysts (as in MES), EES employs free enzymes [91]. ESS has several advantages over MES: it offers higher reaction selectivity, better tolerance to solvents and less complex metabolic mechanisms [91, 92]. However, MES avoids the use of costly enzymes and cofactor production/addition as microorganisms produce their own enzymes. Moreover, whole cells are more resilient to changes in reaction conditions such as pH, temperature, salinity or pressure [93].

3.1 Principles, Mechanisms and Metabolic Pathways

The MES cell is typically divided into two chambers (cathodic and anodic) that are separated by means of an ion-exchange membrane (IEM) [94] (Fig. 1). As mentioned before, the fundament of MES lies on the cathodic chamber and more specifically on the ability of cathodophilic microorganism (or electrotrophs) to

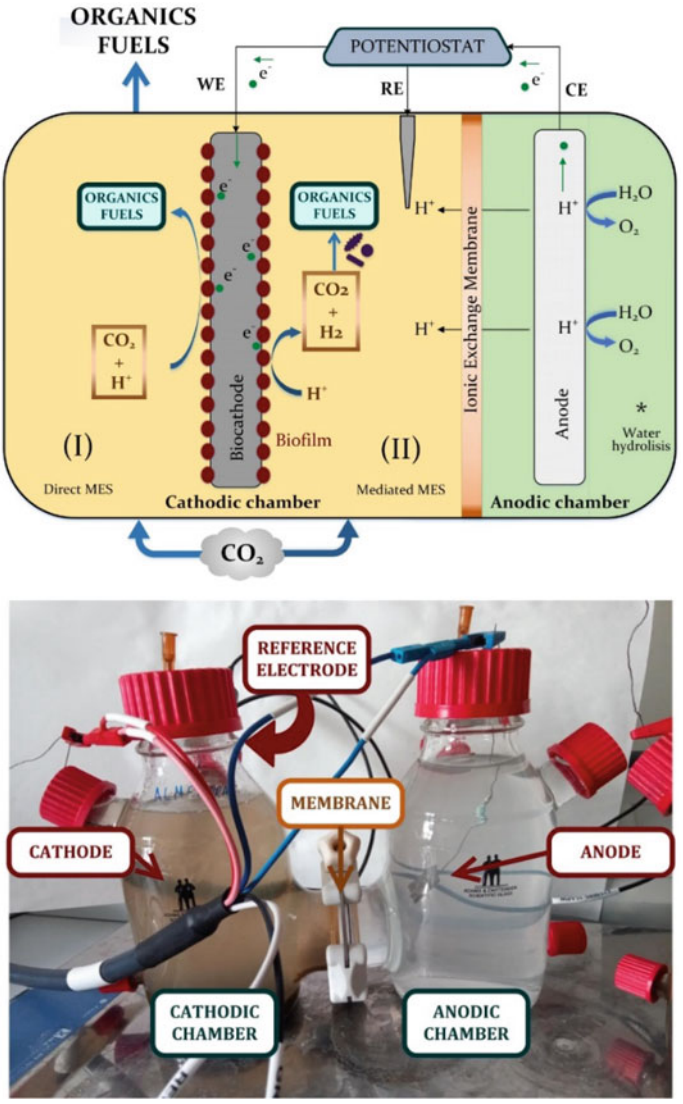

Fig. 1 Top: schematic diagram of a typical MES. Bottom: laboratory scale (0.5L) MES

transfer/accept electrons from solid surfaces (cathodes) to reduce CO_2 into organic compounds [95]. The cathode is usually made of carbonaceous materials (such as carbon felt or carbon brush) due to their high surface area, biocompatibility, conductivity and chemical stability. The interactions mechanisms between the cathode and the electrotrophs are still under discussion, though they usually are divided as direct (where microorganism directly receives electrons from the cathode) and indirect (where a chemical mediator, such as methyl viologen or neutral red, operates as an intermediary between the cathode and the microbe) [96, 97].

The anode serves as the counter-electrode and its function is to provide the necessary protons and electrons to the cathodic reaction. As MES technology has not yet moved beyond the lab, most of the current MES designs favour simplicity over efficiency. As a result, dimensionally stable electrodes are frequently used to carry out the anodic reaction. A reference electrode (which provides a well-known and stable potential) is frequently placed on the cathodic chamber to fix/control the cathode potential. Finally, the presence of the IEM is crucial because it prevents the oxygen generated in the anodic reaction from reaching the cathodophilic anaerobic microbial community on the cathode, which is quite sensitive to this gas.

Biocathodes are usually inoculated with inoculums obtained from anaerobic sludge or sediments [98]. Although the mixed microbial communities that finally develop on the bio-cathodic environment inevitably depends on the source of the inoculum, they tend to get enriched in microorganisms like *Sporomusa ovata* and *Clostridium ljungdahlii* [99]. These two microorganism belong to the group of homoacetogenic bacteria, which means that they are capable of producing acetic acid from CO_2 following the Wood-Ljungdahl pathway (this explains why acetic acid is the most common end product found in MES [100]). Sulfate-reducing bacteria and hydrogen producers are also commonly found on biocathodes, as well as hydrogenotrophic and acetoclastic archaea in the case on methane-producing systems [101–103].

When researchers perform experiments with pure cultures, they often resort to *S. ovata* and *C. ljungdahlii* [99, 103–105], precisely because of their relatively high abundance in systems inoculated with mixed cultures. To date, experiments with pure cultures have yielded the highest titers, productivities and selectivities [103], although they require sterility and fine control of reaction conditions all of which makes them not the bests candidates for future real-life applications [103]. In contrast, the use of mixed microbial consortia harvested from natural or engineered environments demand less restrictive conditions and reduces process cost [98]. As a result, most of the experiments available in the literature make use of mixed cultures, reporting moderate productivities and selectivity. Still, when enriched and acclimated following suitable procedures, mixed cultures can reach comparable results (in terms of productivity and selectivity) to those obtained with pure cultures [106–108].

The in vivo catalytic reactions for CO_2 reduction are driven by enzymes such as the carbonic anhydrase and other enzymes belonging to the oxidoreductase family, that determine the end product of their electrotrophic metabolism [88, 91, 109]. These enzymes take part in multi-enzymatic cascade reactions or in single-enzyme

processes. A relevant example of the later in MES is the conversion of CO_2 into formate by FDH enzyme. Chen and colleagues [110] studied the production of Poly 3-hydroxybutyrate (PHB) in a FDH-assisted MES system with genetically engineered *Ralstonia eutropha*, using formate production as intermediate electron carrier for further microbial conversion.

3.2 Possible Products

Volatile fatty acids (VFAs) have been the first and the most frequently reported organics obtained from CO_2 reduction in MES [111]. The production of acetate, which is the main representative product of this group, is mediated by homoacetogenic microorganisms that use, as mentioned before, the Wood-Ljungdahl route for its synthesis [87, 111]. Acetate productivities in MES can be as high as $\sim 0.8\ g{\cdot}L^{-1}{\cdot}d^{-1}$ with efficiencies near 100% in terms of current-to-acetate conversion, and achieving product titers up to 13.5 $g{\cdot}L^{-1}$ [96, 106, 107]. Butyrate is the second most frequently found VFA in MES [103], and was shown to be formed from CO_2 or to be synthetized from acetate with moderate input of energy [103]. As a result, butyrate is usually found as a by-product in acetate-producing MES [100]. Nevertheless, when butyrate is the target product, productivities can reach up to $0.16\ g{\cdot}L^{-1}{\cdot}d^{-1}$ with maximum titers of 5.5 $g{\cdot}L^{-1}$ [112]. Other co-products (VFAs and average chain fatty acids) were also found in MES systems that produce acetate but not being directly targeted to date [113].

Short-chain alcohols (such as ethanol, butanol and glycerol) is another group of easily marketable chemicals that can be found in the biocathodes of MES, although with modest productivities, selectivities and titers [114–116]. MES can be directed to the production of these organics when an excess of reducing power (as hydrogen for instance) is found in the cathodic chamber [117]. MES also make it possible to obtain alcohols from volatile fatty acids by using the cathode (instead of hydrogen) as the electron donor for the reductive process [114]. This route is thermodynamically favourable and so it is expected that alcohols production in MES would follow primarily these mechanisms.

Both, VFAs and alcohols can be used as building blocks to obtain longer chain organic compounds through chain elongation reactions (CER) [103]. As MES are commonly inoculated with mixed microbial cultures, CER can occur naturally within the catholyte as observed by several authors [112, 118].

Methane is another valuable product commonly found in the biocathodes of MES. It can be produced not only from hydrogen and/or acetate (usually present in the cathodic environment of MES) through well-known routes that involve hydrogenothophic and/or acetorophic methanogens [119] respectively, but also via direct electron transfer mechanisms from the cathode [120, 121]. These processes that ultimately comprise the reduction of CO_2 to CH_4 at a biocathode using electrical current are usually termed as electromethanogenesis [105]. Initial studies on microbial electromethanogenesis reported production rates below 5 $LCH4{\cdot}d^{-1}{\cdot}m^{-2}$ with an overall energy efficiency of $\sim 80\%$ [121]. Improved reactor designs,

together with new insights on the basic mechanisms that underlie electromethanogenesis has allowed during the past years to enhance productivity up to 30 $LCH4 \cdot d^{-1} \cdot m^{-2}$ with efficiencies near 100% [122, 123]. Here, it is important to mention that electromethanogenesis is beginning to be competitive with other methane-producing technologies that also use CO_2 as a substrate (as those that involve the use of H_2 as a reductive agent) at least in terms of energy usage [87].

3.3 Challenges and Future Perspectives. Towards Practical Application

MES is a novel technology that has not yet left the laboratory bench. Developing appropriate upscaling approaches, together with the need to find suitable electrode and membrane materials are perhaps the most important challenges that it needs to face on its way to real field application [124]. Indeed, conceiving high efficiency and cost-effective large-scale MES requires that several critical issues such as catholyte flow regimes, reactor architecture or stacking approaches (to name but a few) should be carefully considered [124]. Most of these issues are shared in common with other BES such microbial fuel cells and microbial electrolysis cells and so it seems reasonable to think that the scale-up methodologies developed for the latter [95, 125, 126] can also be applicable to MES.

Electrodes and ion exchange membranes (IEM) are two key elements that have a notable effect on the overall performance of MES. As mentioned before, the interaction between microbes and electrodes lies at the core of MES technology. Here, efforts have been made to facilitate the electron exchange by modifying the electrode surface using, for instance, carbon nanotubes, graphene or metal nanoparticles, and by pre-treating electrode surface with chemicals such as chitosan or cyanuric chloride [127–129]. The IEM are also crucial in MES. On the one hand IEM are relatively expensive and their cost may represent a significant part of the overall capital cost of MES [126]. On the other hand, IEM prevents the mixing of the electrolytes while allowing the circulation of ionic currents between electrodes (thus having an impact on the overall performance and efficiency of MES). However, IES are prone to undergo biofouling which can negatively affect their ability to exchange ions between electrolytes. That means that real-life application of MES would require periodic maintenance to prevent the excessive deterioration of these elements.

Feeding CO_2 to the biocathode is another challenging issue. Typical stationary point sources of CO_2 (e.g. off gas of combustion or fermentative process) may contain products (such as O_2) that can negatively impact on the metabolic processes of the electrotrophs. The diffusion and dispersion of those CO_2-rich gas streams on the cathodic media also deserve some attention to optimize CO_2 availability to the biofilm. Here, researchers have tried to address this question by adding excesses of inorganic carbon or recirculating the unreacted CO_2 gas [100, 130, 131]. Nevertheless, both of these approaches present significant drawbacks and more investigation is required on this topic.

Despite all these difficulties, many authors maintain that practical application of MES can become a reality in the medium term in sectors linked to waste biorefineries, or power-to-gas [132]. Here MES can contribute to the desired shift from a fossil fuel based economy to an electricity-based one, by providing a link between chemical and electrical energy. In this context, the use of MES for biogas upgrading through electromethanogenesis represents perhaps the most straightforward approach for quick market implementation of MES [123, 133, 134]. Raw biogas typically contains 30–40% CO_2 and usually needs refinement before its use as a fuel [135]. Electromethanogenesis directly converts the CO_2 present in the biogas into methane which increases the net content of the later thus avoiding the need to manage CO_2 side streams, which is one of the disadvantages of conventional methods for biogas upgrading [103]. The use of MES as a post-treatment for biogas leads to a versatile and easy-to-operate system, and recent studies reported content in CO_2 below than 10% still with high coulombic efficiencies (above 80%) [133].

The explosive growth of intermittent renewable energy sources (such as solar and wind power) has been the main drive for the increased interest in electrical energy storage systems [136]. The ability of MES to convert electrical energy into chemical energy (e.g.: methane) can make of it, at least potentially, an alternative energy storage system similar to the more mature technology of PEM electrolysers [103]. However, it is still not clear how MES would perform and how the microbial biofilms would respond to periodic power cuts (resulting from the unpredictable nature of renewable energy supplies). In this regard, a few works have already give attention to this question showing that acetate producing MES are resilient to short-term to energy fluctuations and that performance and productivities can be maintained after continuous and scheduled power disconnections, reaching titers and production rates comparable with stably powered systems [101, 102]. However, when the power cuts are relatively large (6 weeks), shifts may occur both on the microbial populations and on the final end-product [102].

Finally, another challenging question is product inhibition in batch-operated systems. The accumulation of VFA's or alcohols on the catholite can inhibit the metabolism of the electrotrophic microorganisms, leading to a decrease of the production rates thus threatening practical applicability of MES. An obvious solution to this problem is the operation of the MES in continuous mode, which prevents the accumulation of metabolites in the broth. This alternative however has its pros and cons. On the one hand, it brings the additional advantage of providing higher production rates; on the other hand it can result in lower product titers, which increases downstream post-processing costs [137]. Another approach to limit excessive product build-up in batch systems is the implementation of in-situ separation technologies such as membrane processes, distillation, adsorption/adsorption and extraction [108, 138, 139]. Gildemyn et al. [108] explored this option in a MES that incorporated an extraction compartment connected to the cathodic chamber by means of an anion exchange membrane (AEM) that allowed for the extraction and recovery of acetate. Although titers and production rates were in the range of those obtained in batch systems, the relatively high energy requirement, together with the risk of membrane fouling and the complexity of the overall set-up requires a further optimization of this approach.

4 Conclusion and Future Perspectives

Nature mimicking through bioelectrochemical approaches seems to a promising route to take advantage of the available atmospheric CO_2 as a source of added-value compounds and to reduce its current levels. From simple systems using only one enzyme, to multi enzymatic and whole cells' BES, MES and MFC, and independently of the high efficiencies, one drawback is present, that is the cost either of the enzymes purification, the co-factors or the materials to be used in these systems. Several approaches have been gaining importance to overcome those limitations, namely, the use of artificial or engineered enzymes, obtained by different methods e.g. site-directed mutagenesis, or by designing novel "enzymes" (usually using more simple molecular structures, hybrid metal–organic frameworks, proteins or polypeptides as base) mimicking the catalytic centres and activities [140–143]. Some examples include, for instance, metalloporphyrins (namely with Fe) immobilized in highly conductive materials such as carbon nanotubes that were successfully tested towards CO_2 reduction in modified electrodes and fuel cells with promising results [144]; the synthesis or isolation of iron-sulfur clusters embedded in supramolecular "artificial" structures, such as cyclodextrins or polypeptides, for example for nitrogenase complex iron-cluster mimicking [145] and the incorporation of Mo in the more simple rubredoxin protein, by substitution of the native Fe, towards mimicking the FDH catalytic centre [146]. Other approaches, using directed evolution is the activity improvement of existing enzymes, such as FDH, to obtain more efficient variants [143]. Also, the adaptation of existing microorganisms towards novel or improved functions, aiming incorporation in MES systems, such as methanogenic mixed cultures for the reduction of CO_2 to CH_4 [147].

MES is currently limited to the generation of mainly acetate, a low-value product that makes it difficult the implementation of this technology to a commercial scale. Still, the low amounts of longer chain fatty acids (such as butyric or caproic acids which are much more interesting from a commercial point of view) that have been occasionally found in the catholytes, indicates that MES has the capability for chain elongation. As advanced by LaBelle et al. [148], producing higher amounts of these (and other) organics would demand the development of means to control the regulation of the relevant genes in the electrosynthetic microbiome. An example of this is the work reported in Wu et al. [149] where the authors describe an electroactive succinate-producing cell factory engineered in *E. coli*, that harnessed the electrons arriving at the cathode to reduce fumarate. Overall, it is widely admitted that synthetic biology can help to make MES a commercially sound technology by allowing producing new organics of interest for industry [148, 150]. However, to realize its full potential, it is also recognized that synthetic biology must be supported by high-throughput electrochemical screening technologies, searchable databases of electroactive microorganisms and suitable data analysis techniques and engineering tools [150].

Acknowledgements This work was supported by the Associate Laboratory for Green Chemistry—LAQV which is financed by national funds from FCT/MCTES (UIDB/50006/2020). Adrián Escapa thanks Ente Regional de la Energía de Castilla y Leon (project ref: EREN_2019_L3_ULE).

References

1. Chen C, Khosrowabadi Kotyk JF, Sheehan SW (2018) Progress toward commercial application of electrochemical carbon dioxide reduction. Chem 4(11):2571–2586. https://doi.org/10.1016/j.chempr.2018.08.019
2. Endrődi B, Bencsik G, Darvas F, Jones R, Rajeshwar K, Janáky C (2017) Continuous-flow electroreduction of carbon dioxide. Prog Energy Combust Sci 62:133–154. https://doi.org/10.1016/j.pecs.2017.05.005
3. Finn C, Schnittger S, Yellowlees LJ, Love JB (2012) Molecular approaches to the electrochemical reduction of carbon dioxide. Chem Commun 48(10):1392–1399. https://doi.org/10.1039/c1cc15393e
4. Malkhandi S, Yeo BS (2019) Electrochemical conversion of carbon dioxide to high value chemicals using gas-diffusion electrodes. Curr Opin Chem Eng 26:112–121. https://doi.org/10.1016/j.coche.2019.09.008
5. M. Rumayor, A. Dominguez-Ramos, P. Perez, A. Irabien (2019) A techno-economic evaluation approach to the electrochemical reduction of CO_2 for formic acid manufacture. J CO_2 Util 34:490–499. https://doi.org/10.1016/j.jcou.2019.07.024
6. Franco JH, Neto SA, Hickey DP, Minteer SD, de Andrade AR (2018) Hybrid catalyst cascade architecture enhancement for complete ethanol electrochemical oxidation. Biosens Bioelectron 121:281–286. https://doi.org/10.1016/j.bios.2018.09.011
7. Schlager S, Neugebauer H, Haberbauer M, Hinterberger G, Sariciftci NS (2015) Direct electrochemical addressing of immobilized alcohol dehydrogenase for the heterogeneous bioelectrocatalytic reduction of butyraldehyde to butanol. ChemCatChem 7(6):967–971. https://doi.org/10.1002/cctc.201402932
8. Keller DP, Lenton A, Littleton EW, Oschlies A, Scott V, Vaughan NE (2018) The effects of carbon dioxide removal on the carbon cycle. Curr Clim Change Rep 4(3):250–265. https://doi.org/10.1007/s40641-018-0104-3
9. Schuur EAG, Bockheim J, Canadell JG, Euskirchen E, Field CB, Goryachkin SV, Hagemann S, Kuhry P, Lafleur PM, Lee H, Mazhitova G, Nelson FE, Rinke A, Romanovsky VE, Shiklomanov N, Tarnocai C, Venevsky S, Vogel JG, Zimov SA (2008) Vulnerability of permafrost carbon to climate change: implications for the global carbon cycle. Bioscience 58(8):701–714. https://doi.org/10.1641/b580807
10. Janssen PJD, Lambreva MD, Plumeré N, Bartolucci C, Antonacci A, Buonasera K, Frese RN, Scognamiglio V, Rea G (2014) Photosynthesis at the forefront of a sustainable life. Front Chem 2:36–36. https://doi.org/10.3389/fchem.2014.00036
11. Erb TJ, Zarzycki J (2018) A short history of RubisCO: the rise and fall (?) of Nature's predominant CO_2 fixing enzyme. Curr Opin Biotechnol 49:100–107. https://doi.org/10.1016/j.copbio.2017.07.017
12. Whitney SM, Houtz RL, Alonso H (2011) Advancing our understanding and capacity to engineer nature's CO_2-sequestering enzyme. Rubisco. Plant Physiology 155(1):27. https://doi.org/10.1104/pp.110.164814
13. Kupriyanova EV, Sinetova MA, Cho SM, Park Y-I, Los DA, Pronina NA (2013) CO_2-concentrating mechanism in cyanobacterial photosynthesis: organization, physiological role, and evolutionary origin. Photosynth Res 117(1):133–146. https://doi.org/10.1007/s11120-013-9860-z
14. Andersson I (2008) Catalysis and regulation in Rubisco. J Exp Bot 59(7):1555–1568. https://doi.org/10.1093/jxb/ern091
15. Thee H, Smith KH, da Silva G, Kentish SE, Stevens GW (2015) Carbonic anhydrase promoted absorption of CO_2 into potassium carbonate solutions. Greenhouse Gases Sci Technol 5(1):108–114. https://doi.org/10.1002/ghg.1455
16. Aspatwar A, Barker H, Tolvanen M, Emameh RZ, Parkkila S (2019) Chapter 20—Carbonic anhydrases from pathogens: protozoan CAs and related inhibitors as potential antiprotozoal

agents. In: Supuran CT, Nocentini A (eds) Carbonic Anhydrases. Academic Press, pp 449–475. https://doi.org/10.1016/B978-0-12-816476-1.00020-4
17. Rowlett RS (2010) Structure and catalytic mechanism of the β-carbonic anhydrases. Biochimica et Biophysica Acta (BBA) Proteins Proteomics 1804(2):362–373. https://doi.org/10.1016/j.bbapap.2009.08.002
18. Boone CD, Habibzadegan A, Tu C, Silverman DN, McKenna R (2013) Structural and catalytic characterization of a thermally stable and acid-stable variant of human carbonic anhydrase II containing an engineered disulfide bond. Acta Crystallographica Sect D 69 (8):1414–1422. https://doi.org/10.1107/S0907444913008743
19. Díaz-Torres NA, Mahon BP, Boone CD, Pinard MA, Tu C, Ng R, Agbandje-McKenna M, Silverman D, Scott K, McKenna R (2015) Structural and biophysical characterization of the α-carbonic anhydrase from the gammaproteobacterium Thiomicrospira crunogena XCL-2: insights into engineering thermostable enzymes for CO2 sequestration. Acta Crystallogr D Biol Crystallogr 71(Pt 8):1745–1756. https://doi.org/10.1107/s1399004715012183
20. Sundaram S, Thakur IS (2018) Induction of calcite precipitation through heightened production of extracellular carbonic anhydrase by CO2 sequestering bacteria. Biores Technol 253:368–371. https://doi.org/10.1016/j.biortech.2018.01.081
21. Lu WP, Ragsdale SW (1991) Reductive activation of the coenzyme A/acetyl-CoA isotopic exchange reaction catalyzed by carbon monoxide dehydrogenase from Clostridium thermoaceticum and its inhibition by nitrous oxide and carbon monoxide. J Biol Chem 266(6):3554–3564
22. Burton R, Can M, Esckilsen D, Wiley S, Ragsdale SW (2018) Chapter twelve—production and properties of enzymes that activate and produce carbon monoxide. In: Armstrong F (ed) Methods in enzymology, vol 613. Academic Press, pp 297–324. https://doi.org/10.1016/bs.mie.2018.10.005
23. Evans DJ (2005) Chemistry relating to the nickel enzymes CODH and ACS. Coord Chem Rev 249(15):1582–1595. https://doi.org/10.1016/j.ccr.2004.09.012
24. Wang VCC, Ragsdale SW, Armstrong FA (2014) Investigations of the efficient electrocatalytic interconversions of carbon dioxide and carbon monoxide by nickel-containing carbon monoxide dehydrogenases. Metal Ions Life Sci 14:71–97. https://doi.org/10.1007/978-94-017-9269-1_4
25. Ragsdale SW (2004) Life with carbon monoxide. Crit Rev Biochem Mol Biol 39(3):165–195. https://doi.org/10.1080/10409230490496577
26. Cordas CM, Moura JJG (2019) Molybdenum and tungsten enzymes redox properties—a brief overview. Coord Chem Rev 394:53–64. https://doi.org/10.1016/j.ccr.2019.05.005
27. Wang VCC, Ragsdale SW, Armstrong FA (2013) Investigations of two bidirectional carbon monoxide dehydrogenases from carboxydothermus hydrogenoformans by protein film electrochemistry. ChemBioChem 14(14):1845–1851. https://doi.org/10.1002/cbic.201300270
28. Wang VCC, Islam STA, Can M, Ragsdale SW, Armstrong FA (2015) Investigations by protein film electrochemistry of alternative reactions of nickel-containing carbon monoxide dehydrogenase. J Phys Chem B 119(43):13690–13697. https://doi.org/10.1021/acs.jpcb.5b03098
29. Alfano M, Cavazza C (2018) The biologically mediated water–gas shift reaction: structure, function and biosynthesis of monofunctional [NiFe]-carbon monoxide dehydrogenases. Sustain Energy Fuels 2(8):1653–1670. https://doi.org/10.1039/c8se00085a
30. Maia LB, Fonseca L, Moura I, Moura JJG (2016) Reduction of carbon dioxide by a molybdenum-containing formate dehydrogenase: a kinetic and mechanistic study. J Am Chem Soc 138(28):8834–8846. https://doi.org/10.1021/jacs.6b03941
31. Niks D, Duvvuru J, Escalona M, Hille R (2016) Spectroscopic and kinetic properties of the molybdenum-containing, NAD+-dependent formate dehydrogenase from *Ralstonia eutropha*. J Biol Chem 291(3):1162–1174
32. Bassegoda A, Madden C, Wakerley DW, Reisner E, Hirst J (2014) Reversible interconversion of CO_2 and formate by a molybdenum-containing formate dehydrogenase. J Am Chem Soc 136(44):15473–15476. https://doi.org/10.1021/ja508647u

33. Hille R, Hall J, Basu P (2014) The mononuclear molybdenum enzymes. Chem Rev 114 (7):3963–4038. https://doi.org/10.1021/cr400443z
34. Maia LB, Moura I, Moura JJG (2017) Molybdenum and tungsten-containing formate dehydrogenases: aiming to inspire a catalyst for carbon dioxide utilization. Inorg Chim Acta 455:350–363. https://doi.org/10.1016/j.ica.2016.07.010
35. Amao Y (2018) Formate dehydrogenase for CO_2 utilization and its application. J CO_2 Util 26:623–641. https://doi.org/10.1016/j.jcou.2018.06.022
36. Maia LB, Moura I, Moura JJG (2017) Chapter 1 molybdenum and tungsten-containing enzymes: an overview. In: Molybdenum and Tungsten Enzymes: Biochemistry. The Royal Society of Chemistry, pp 1–80. https://doi.org/10.1039/9781782623915-00001
37. Zhang L, Liu J, Ong J, Li SFY (2016) Specific and sustainable bioelectro-reduction of carbon dioxide to formate on a novel enzymatic cathode. Chemosphere 162:228–234. https://doi.org/10.1016/j.chemosphere.2016.07.102
38. Zanello P (2019) Structure and electrochemistry of proteins harboring iron-sulfur clusters of different nuclearities Part V. Nitrogenases. Coord Chem Rev 398:113004. https://doi.org/10.1016/j.ccr.2019.07.001
39. Vicente EJ, Dean DR (2017) Keeping the nitrogen-fixation dream alive. Proc Natl Acad Sci 114(12):3009. https://doi.org/10.1073/pnas.1701560114
40. Seefeldt LC, Peters JW, Beratan DN, Bothner B, Minteer SD, Raugei S, Hoffman BM (2018) Control of electron transfer in nitrogenase. Curr Opin Chem Biol 47:54–59. https://doi.org/10.1016/j.cbpa.2018.08.011
41. Seefeldt LC, Yang Z-Y, Duval S, Dean DR (2013) Nitrogenase reduction of carbon-containing compounds. Biochimica et Biophysica Acta (BBA) Bioenergetics 1827 (8):1102–1111. https://doi.org/10.1016/j.bbabio.2013.04.003
42. Newton WE, Dilworth MJ (2011) Assays of nitrogenase reaction products. In: Ribbe MW (ed) Nitrogen fixation: methods and protocols. Humana Press, Totowa, NJ, pp 105–127. https://doi.org/10.1007/978-1-61779-194-9_8
43. Seefeldt LC, Rasche ME, Ensign SA (1995) Carbonyl sulfide and carbon dioxide as new substrates, and carbon disulfide as a new inhibitor, of nitrogenase. Biochemistry 34 (16):5382–5389. https://doi.org/10.1021/bi00016a009
44. Khadka N, Dean DR, Smith D, Hoffman BM, Raugei S, Seefeldt LC (2016) CO_2 reduction catalyzed by nitrogenase: pathways to formate, carbon monoxide, and methane. Inorg Chem 55(17):8321–8330. https://doi.org/10.1021/acs.inorgchem.6b00388
45. Sugimura K, Kuwabata S, Yoneyama H (1990) Electrochemical fixation of carbon dioxide in pyruvic acid to yield malic acid using malic enzyme as an electrocatalyst. Bioelectrochem Bioenerg 24(2):241–247. https://doi.org/10.1016/0302-4598(90)85025-D
46. Zheng H, Ohno Y, Nakamori T, Suye S-i (2009) Production of l-malic acid with fixation of HCO3− by malic enzyme-catalyzed reaction based on regeneration of coenzyme on electrode modified by layer-by-layer self-assembly method. J Biosci Bioeng 107(1):16–20. https://doi.org/10.1016/j.jbiosc.2008.09.009
47. Sugimura K, Kuwabata S, Yoneyama H (1989) Electrochemical fixation of carbon dioxide in oxoglutaric acid using an enzyme as an electrocatalyst. J Am Chem Soc 111(6):2361–2362. https://doi.org/10.1021/ja00188a093
48. García-Ferris C, Moreno J (1993) Redox regulation of enzymatic activity and proteolytic susceptibility of ribulose-1,5-bisphosphate carboxylase/oxygenase from *Euglena gracilis*. Photosynth Res 35(1):55–66. https://doi.org/10.1007/bf02185411
49. Moreno J, García-Murria MJ, Marín-Navarro J (2008) Redox modulation of RubisCO conformation and activity through its cysteine residues. J Exp Bot 59(7):1605–1614. https://doi.org/10.1093/jxb/erm310
50. García-Murria MJ, Sudhani HPK, Marín-Navarro J, Sánchez del Pino MM, Moreno J (2018) Dissecting the individual contribution of conserved cysteines to the redox regulation of RubisCO. Photosynth Res 137(2):251–262. https://doi.org/10.1007/s11120-018-0497-9

51. Tominaga J, Takahashi S, Sakamoto A, Shimada H (2020) Arabidopsis BSD2 reveals a novel redox regulation of Rubisco physiology in vivo. Plant Signaling Behavior 15 (4):1740873. https://doi.org/10.1080/15592324.2020.1740873
52. Satagopan S, Sun Y, Parquette JR, Tabita FR (2017) Synthetic CO(2)-fixation enzyme cascades immobilized on self-assembled nanostructures that enhance CO(2)/O(2) selectivity of RubisCO. Biotechnol Biofuels 10:175–175. https://doi.org/10.1186/s13068-017-0861-6
53. Bhattacharya S, Schiavone M, Chakrabarti S, Bhattacharya SK (2003) CO_2 hydration by immobilized carbonic anhydrase. Biotechnol Appl Biochem 38(2):111–117. https://doi.org/10.1042/ba20030060
54. Zhu Y, Li W, Sun G, Tang Q, Bian H (2016) Enzymatic properties of immobilized carbonic anhydrase and the biocatalyst for promoting CO2 capture in vertical reactor. Int J Greenhouse Gas Control 49:290–296. https://doi.org/10.1016/j.ijggc.2016.03.016
55. Wanjari S, Prabhu C, Yadav R, Satyanarayana T, Labhsetwar N, Rayalu S (2011) Immobilization of carbonic anhydrase on chitosan beads for enhanced carbonation reaction. Process Biochem 46(4):1010–1018. https://doi.org/10.1016/j.procbio.2011.01.023
56. Hwang ET, Seo B-K, Gu MB, Zeng A-P (2016) Successful bi-enzyme stabilization for the biomimetic cascade transformation of carbon dioxide. Catal Sci Technol 6(19):7267–7272. https://doi.org/10.1039/c6cy00783j
57. Srikanth S, Alvarez-Gallego Y, Vanbroekhoven K, Pant D (2017) Enzymatic electrosynthesis of formic acid through carbon dioxide reduction in a bioelectrochemical system: effect of immobilization and carbonic anhydrase addition. ChemPhysChem 18(22):3174–3181. https://doi.org/10.1002/cphc.201700017
58. Addo PK, Arechederra RL, Waheed A, Shoemaker JD, Sly WS, Minteer SD (2011) Methanol production via bioelectrocatalytic reduction of carbon dioxide: role of carbonic anhydrase in improving electrode performance. Electrochem Solid-State Lett 14(4):E9–E13
59. Shin W, Lee SH, Shin JW, Lee SP, Kim Y (2003) Highly selective electrocatalytic conversion of CO_2 to CO at −0.57 V (NHE) by carbon monoxide dehydrogenase from *Moorella thermoacetica*. J Am Chem Soc 125(48):14688–14689. https://doi.org/10.1021/ja037370i
60. Reginald SS, Lee H, Lee YS, Yasin M, Chang IS (2020) Dissolved carbon monoxide concentration monitoring platform based on direct electrical connection of CO dehydrogenase with electrically accessible surface structure. Biores Technol 297:122436. https://doi.org/10.1016/j.biortech.2019.122436
61. Hwang HW, Yoon J, Min K, Kim M-S, Kim S-J, Cho DH, Susila H, Na J-G, Oh M-K, Kim YH (2020) Two-stage bioconversion of carbon monoxide to biopolymers via formate as an intermediate. Chem Eng J 389:124394. https://doi.org/10.1016/j.cej.2020.124394
62. Cordas CM, Campaniço M, Baptista R, Maia LB, Moura I, Moura JJG (2019) Direct electrochemical reduction of carbon dioxide by a molybdenum-containing formate dehydrogenase. J Inorg Biochem 196:110694. https://doi.org/10.1016/j.jinorgbio.2019.110694
63. Reda T, Plugge CM, Abram NJ, Hirst J (2008) Reversible interconversion of carbon dioxide and formate by an electroactive enzyme. Proc Natl Acad Sci 105(31):10654
64. Sakai K, Sugimoto Y, Kitazumi Y, Shirai O, Takagi K, Kano K (2017) Direct electron transfer-type bioelectrocatalytic interconversion of carbon dioxide/formate and NAD+/NADH redox couples with tungsten-containing formate dehydrogenase. Electrochim Acta 228:537–544. https://doi.org/10.1016/j.electacta.2017.01.112
65. Sakai K, Kitazumi Y, Shirai O, Takagi K, Kano K (2017) Direct electron transfer-type four-way bioelectrocatalysis of CO_2/formate and NAD+/NADH redox couples by tungsten-containing formate dehydrogenase adsorbed on gold nanoparticle-embedded mesoporous carbon electrodes modified with 4-mercaptopyridine. Electrochem Commun 84:75–79. https://doi.org/10.1016/j.elecom.2017.10.005
66. Nielsen CF, Lange L, Meyer AS (2019) Classification and enzyme kinetics of formate dehydrogenases for biomanufacturing via CO_2 utilization. Biotechnol Adv 37(7):107408. https://doi.org/10.1016/j.biotechadv.2019.06.007

67. Jayathilake BS, Bhattacharya S, Vaidehi N, Narayanan SR (2019) Efficient and selective electrochemically driven enzyme-catalyzed reduction of carbon dioxide to formate using formate dehydrogenase and an artificial cofactor. Acc Chem Res 52(3):676–685. https://doi.org/10.1021/acs.accounts.8b00551
68. Kuk SK, Gopinath K, Singh RK, Kim T-D, Lee Y, Choi WS, Lee J-K, Park CB (2019) NADH-free electroenzymatic reduction of CO_2 by conductive hydrogel-conjugated formate dehydrogenase. ACS Catalysis 9(6):5584–5589. https://doi.org/10.1021/acscatal.9b00127
69. Zhang L, Jiang Y, Jiang Z, Sun X, Shi J, Li L, Li J (2009) Biomimetic Fabrication of hydroxyapatite–polysaccharide–formate dehydrogenase composite capsules for efficient CO_2 conversion. J Biomater Sci Polym Ed 20(12):1661–1674. https://doi.org/10.1163/156856208x386255
70. Watt GD, Burns A, Lough S, Tennent DL (1980) Redox and spectroscopic properties of oxidized MoFe protein from *Azotobacter vinelandii*. Biochemistry 19(21):4926–4932. https://doi.org/10.1021/bi00562a035
71. Lydon BR, Lee CC, Tanifuji K, Sickerman NS, Newcomb MP, Hu Y, Ribbe MW, Yang JY (2020) Electrochemical characterization of isolated nitrogenase cofactors from *Azotobacter vinelandii*. ChemBioChem 21(12):1773–1778. https://doi.org/10.1002/cbic.201900425
72. Lee CC, Hu Y, Ribbe MW (2015) Catalytic reduction of CN^-, CO, and CO_2 by nitrogenase cofactors in lanthanide-driven reactions. Angew Chem Int Ed 54(4):1219–1222. https://doi.org/10.1002/anie.201410412
73. Patel J, Cai R, Milton R, Chen H, Minteer SD (2020) Pyrene-based noncovalent immobilization of nitrogenase on carbon surfaces. ChemBioChem 21(12):1729–1732. https://doi.org/10.1002/cbic.201900697
74. Hu B, Harris DF, Dean DR, Liu TL, Yang Z-Y, Seefeldt LC (2018) Electrocatalytic CO_2 reduction catalyzed by nitrogenase MoFe and FeFe proteins. Bioelectrochemistry 120:104–109. https://doi.org/10.1016/j.bioelechem.2017.12.002
75. Sakai K, Kitazumi Y, Shirai O, Takagi K, Kano K (2016) Efficient bioelectrocatalytic CO_2 reduction on gas-diffusion-type biocathode with tungsten-containing formate dehydrogenase. Electrochem Commun 73:85–88. https://doi.org/10.1016/j.elecom.2016.11.008
76. Sato R, Amao Y (2020) Can formate dehydrogenase from Candida boidinii catalytically reduce carbon dioxide, bicarbonate, or carbonate to formate? New J Chem. https://doi.org/10.1039/d0nj01183e
77. Ji C, Hou J, Wang K, Ng YH, Chen V (2017) Single-enzyme biofuel cells. Angew Chem Int Ed 56(33):9762–9766. https://doi.org/10.1002/anie.201703980
78. Zhang L, Ong J, Liu J, Li SFY (2017) Enzymatic electrosynthesis of formate from CO_2 reduction in a hybrid biofuel cell system. Renew Energy 108:581–588. https://doi.org/10.1016/j.renene.2017.03.009
79. Schoffelen S, van Hest JCM (2012) Multi-enzyme systems: bringing enzymes together in vitro. Soft Matter 8(6):1736–1746. https://doi.org/10.1039/c1sm06452e
80. Kuwabata S, Tsuda R, Yoneyama H (1994) Electrochemical conversion of carbon dioxide to methanol with the assistance of formate dehydrogenase and methanol dehydrogenase as biocatalysts. J Am Chem Soc 116(12):5437–5443. https://doi.org/10.1021/ja00091a056
81. Ji X, Su Z, Ma G, Zhang S (2018) Sandwiching multiple dehydrogenases and shared cofactor between double polyelectrolytes for enhanced communication of cofactor and enzymes. Biochem Eng J 137:40–49. https://doi.org/10.1016/j.bej.2018.05.017
82. Carvalho RNL, Almeida RM, Moura JJG, Lourenço NT, Fonseca LJP, Cordas CM (2016) Sandwich-type enzymatic fuel cell based on a new electro-conductive material—ion jelly. ChemistrySelect 1(20):6546–6552. https://doi.org/10.1002/slct.201601640
83. Jiang Y, Su M, Zhang Y, Zhan G, Tao Y, Li D (2013) Bioelectrochemical systems for simultaneously production of methane and acetate from carbon dioxide at relatively high rate. Int J Hydrogen Energy 38(8):3497–3502. https://doi.org/10.1016/j.ijhydene.2012.12.107

84. Mourato C, Martins M, da Silva SM, Pereira IAC (2017) A continuous system for biocatalytic hydrogenation of CO_2 to formate. Biores Technol 235:149–156. https://doi.org/10.1016/j.biortech.2017.03.091
85. Aresta M, Dibenedetto A, Quaranta E (2016) State of the art and perspectives in catalytic processes for CO_2 conversion into chemicals and fuels: the distinctive contribution of chemical catalysis and biotechnology. J Catal 343:2–45. https://doi.org/10.1016/j.jcat.2016.04.003
86. Desloover J, Arends Jan BA, Hennebel T, Rabaey K (2012) Operational and technical considerations for microbial electrosynthesis. Biochem Soc Trans 40(6):1233–1238. https://doi.org/10.1042/bst20120111
87. Bajracharya S, Srikanth S, Mohanakrishna G, Zacharia R, Strik DP, Pant D (2017) Biotransformation of carbon dioxide in bioelectrochemical systems: State of the art and future prospects. J Power Sources 356:256–273. https://doi.org/10.1016/j.jpowsour.2017.04.024
88. Yuan M, Kummer MJ, Minteer SD (2019) Strategies for bioelectrochemical CO_2 reduction. Chem A Euro J 25(63):14258–14266. https://doi.org/10.1002/chem.201902880
89. Halmann M, Steinberg M (1998) Chapter 12—electrochemical reduction of CO_2. Greenhouse gas carbon dioxide mitigation: science and technology, 1st edn. CRC Press, Boca Raton. https://doi.org/10.1201/9781482227833
90. Modestra JA, Mohan SV (2017) Microbial electrosynthesis of carboxylic acids through CO_2 reduction with selectively enriched biocatalyst: microbial dynamics. J CO_2 Util 20:190–199. https://doi.org/10.1016/j.jcou.2017.05.011
91. Chiranjeevi P, Bulut M, Breugelmans T, Patil SA, Pant D (2019) Current trends in enzymatic electrosynthesis for CO_2 reduction. Curr Opin Green Sustain Chem 16:65–70. https://doi.org/10.1016/j.cogsc.2019.02.007
92. Hwang H, Yeon YJ, Lee S, Choe H, Jang MG, Cho DH, Park S, Kim YH (2015) Electro-biocatalytic production of formate from carbon dioxide using an oxygen-stable whole cell biocatalyst. Biores Technol 185:35–39. https://doi.org/10.1016/j.biortech.2015.02.086
93. Wachtmeister J, Rother D (2016) Recent advances in whole cell biocatalysis techniques bridging from investigative to industrial scale. Curr Opin Biotechnol 42:169–177. https://doi.org/10.1016/j.copbio.2016.05.005
94. Sleutels THJA, ter Heijne A, Kuntke P, Buisman CJN, Hamelers HVM (2017) Membrane selectivity determines energetic losses for ion transport in bioelectrochemical systems. ChemistrySelect 2(12):3462–3470. https://doi.org/10.1002/slct.201700064
95. Escapa A, Mateos R, Martínez EJ, Blanes J (2016) Microbial electrolysis cells: an emerging technology for wastewater treatment and energy recovery. from laboratory to pilot plant and beyond. Renew Sustain Energy Rev 55:942–956. https://doi.org/10.1016/j.rser.2015.11.029
96. Kracke F, Vassilev I, Kromer JO (2015) Microbial electron transport and energy conservation—the foundation for optimizing bioelectrochemical systems. Frontiers Microbiol 6:575. https://doi.org/10.3389/fmicb.2015.00575
97. Choi O, Sang B-I (2016) Extracellular electron transfer from cathode to microbes: application for biofuel production. Biotechnol Biofuels 9(1):11. https://doi.org/10.1186/s13068-016-0426-0
98. Mateos R, Sotres A, Alonso RM, Escapa A, Morán A (2018) Impact of the start-up process on the microbial communities in biocathodes for electrosynthesis. Bioelectrochemistry 121:27–37. https://doi.org/10.1016/j.bioelechem.2018.01.002
99. Tremblay P-L, Zhang T (2015) Electrifying microbes for the production of chemicals. Frontiers Microbiol 6:201
100. Bajracharya S, Yuliasni R, Vanbroekhoven K, Buisman CJN, Strik DPBTB, Pant D (2017) Long-term operation of microbial electrosynthesis cell reducing CO_2 to multi-carbon chemicals with a mixed culture avoiding methanogenesis. Bioelectrochemistry 113:26–34. https://doi.org/10.1016/j.bioelechem.2016.09.001
101. Del Pilar Anzola Rojas M, Mateos R, Sotres A, Zaiat M, Gonzalez ER, Escapa A, De Wever H, Pant D (2018) Microbial electrosynthesis (MES) from CO_2 is resilient to

fluctuations in renewable energy supply. Energy Convers Manage. 177:272–279.https://doi.org/10.1016/j.enconman.2018.09.064
102. Mateos R, Escapa A, San-Martín MI, De Wever H, Sotres A, Pant D (2020) Long-term open circuit microbial electrosynthesis system promotes methanogenesis. J Energy Chem 41:3–6. https://doi.org/10.1016/j.jechem.2019.04.020
103. Mateos R, Escapa A, Vanbroekhoven K, Patil SA, Moran A, Pant D (2019) Microbial electrochemical technologies for CO_2 and its derived products valorization. Microbial Electrochem Technol: 777–796. https://doi.org/10.1016/B978-0-444-64052-9.00032-7
104. Nevin KP, Hensley SA, Franks AE, Summers ZM, Ou J, Woodard TL, Snoeyenbos-West OL, Lovley DR (2011) Electrosynthesis of organic compounds from carbon dioxide is catalyzed by a diversity of acetogenic microorganisms. Appl Environ Microbiol 77(9):2882. https://doi.org/10.1128/aem.02642-10
105. Rosenbaum M, Aulenta F, Villano M, Angenent LT (2011) Cathodes as electron donors for microbial metabolism: which extracellular electron transfer mechanisms are involved? Biores Technol 102(1):324–333. https://doi.org/10.1016/j.biortech.2010.07.008
106. Jourdin L, Lu Y, Flexer V, Keller J, Freguia S (2016) Biologically induced hydrogen production drives high rate/high efficiency microbial electrosynthesis of acetate from carbon dioxide. ChemElectroChem 3(4):581–591. https://doi.org/10.1002/celc.201500530
107. LaBelle EV, May HD (2017) Energy efficiency and productivity enhancement of microbial electrosynthesis of acetate. Frontiers Microbiol 8:756
108. Gildemyn S, Verbeeck K, Slabbinck R, Andersen SJ, Prévoteau A, Rabaey K (2015) Integrated production, extraction, and concentration of acetic acid from CO_2 through microbial electrosynthesis. Environ Sci Technol Lett 2(11):325–328. https://doi.org/10.1021/acs.estlett.5b00212
109. Flexer V, Brun N (2017) Fundamentals of enzymatic electrochemical systems. In: functional electrodes for enzymatic and microbial electrochemical systems. World Scientific, Europe, pp 3–50. https://doi.org/10.1142/9781786343543_0001
110. Chen X, Cao Y, Li F, Tian Y, Song H (2018) Enzyme-assisted microbial electrosynthesis of poly(3-hydroxybutyrate) via CO_2 bioreduction by engineered *Ralstonia eutropha*. ACS Catalysis 8(5):4429–4437. https://doi.org/10.1021/acscatal.8b00226
111. May HD, Evans PJ, LaBelle EV (2016) The bioelectrosynthesis of acetate. Curr Opin Biotechnol 42:225–233. https://doi.org/10.1016/j.copbio.2016.09.004
112. Batlle-Vilanova P, Ganigué R, Ramió-Pujol S, Bañeras L, Jiménez G, Hidalgo M, Balaguer MD, Colprim J, Puig S (2017) Microbial electrosynthesis of butyrate from carbon dioxide: Production and extraction. Bioelectrochemistry 117:57–64. https://doi.org/10.1016/j.bioelechem.2017.06.004
113. Annie Modestra J, Navaneeth B, Venkata Mohan S (2015) Bio-electrocatalytic reduction of CO_2: enrichment of homoacetogens and ph optimization towards enhancement of carboxylic acids biosynthesis. J CO_2 Util 10:78–87. https://doi.org/10.1016/j.jcou.2015.04.001
114. Steinbusch KJJ, Hamelers HVM, Schaap JD, Kampman C, Buisman CJN (2009) Bioelectrochemical ethanol production through mediated acetate reduction by mixed cultures. Environ Sci Technol 44:513–517
115. Blanchet E, Duquenne F, Rafrafi Y, Etcheverry L, Erable B, Bergel A (2015) Importance of the hydrogen route in up-scaling electrosynthesis for microbial CO_2 reduction. Energy Environ Sci 8(12):3731–3744. https://doi.org/10.1039/c5ee03088a
116. Soussan L, Riess J, Erable B, Delia M-L, Bergel A (2013) Electrochemical reduction of CO_2 catalysed by geobacter sulfurreducens grown on polarized stainless steel cathodes. Electrochem Commun 28:27–30. https://doi.org/10.1016/j.elecom.2012.11.033
117. Ammam F, Tremblay P-L, Zengler K, Zhang T (2015) Ethanol production in microbial electrosynthesis using Sporomusa ovata as biocatalyst. In: DTU sustain conference 2015—DTU, Lyngby, Denmark, 2015. Book of abstracts. DTU's sustain conference 2015. Technical University of Denmark, Lyngby, pp B-19

118. Ganigué R, Puig S, Batlle-Vilanova P, Balaguer MD, Colprim J (2015) Microbial electrosynthesis of butyrate from carbon dioxide. Chem Commun 51(15):3235–3238. https://doi.org/10.1039/c4cc10121a
119. Demirel B, Scherer P (2008) The roles of acetotrophic and hydrogenotrophic methanogens during anaerobic conversion of biomass to methane: a review. Rev Environ Sci Bio/Technol 7(2):173–190. https://doi.org/10.1007/s11157-008-9131-1
120. Fu Q, Kobayashi H, Kuramochi Y, Xu J, Wakayama T, Maeda H, Sato K (2013) Bioelectrochemical analyses of a thermophilic biocathode catalyzing sustainable hydrogen production. Int J Hydrogen Energy 38(35):15638–15645. https://doi.org/10.1016/j.ijhydene.2013.04.116
121. Cheng S, Xing D, Call DF, Logan BE (2009) Direct biological conversion of electrical current into methane by electromethanogenesis. Environ Sci Technol 43(10):3953–3958. https://doi.org/10.1021/es803531g
122. Kuramochi Y, Fu Q, Kobayashi H, Ikarashi M, Wakayama T, Kawaguchi H, Vilcaez J, Maeda H, Sato K (2013) Electromethanogenic CO_2 conversion by subsurface-reservoir microorganisms. Energy Procedia 37:7014–7020. https://doi.org/10.1016/j.egypro.2013.06.636
123. Van Eerten-Jansen MCAA, Veldhoen AB, Plugge CM, Stams AJM, Buisman CJN, Ter Heijne A (2013) Microbial community analysis of a methane-producing biocathode in a bioelectrochemical system. Archaea 2013:481784. https://doi.org/10.1155/2013/481784
124. Alonso RM, San-Mart, MI, Mateos R, Morán A, Escapa A (2019) Scale-up of bioelectrochemical systems for energy valorization of waste streams. Microbial Electrochem Technol
125. Krieg T, Sydow A, Schröder U, Schrader J, Holtmann D (2014) Reactor concepts for bioelectrochemical syntheses and energy conversion. Trends Biotechnol 32(12):645–655. https://doi.org/10.1016/j.tibtech.2014.10.004
126. Giddings CGS, Nevin KP, Woodward T, Lovley DR, Butler CS (2015) Simplifying microbial electrosynthesis reactor design. Frontiers Microbiol 6:468
127. Zhang T, Nie H, Bain TS, Lu H, Cui M, Snoeyenbos-West OL, Franks AE, Nevin KP, Russell TP, Lovley DR (2013) Improved cathode materials for microbial electrosynthesis. Energy Environ Sci 6:217–224. https://doi.org/10.1039/C2EE23350A
128. Jourdin L, Freguia S, Donose BC, Chen J, Wallace GG, Keller J (2014) A novel carbon nanotube modified scaffold as an efficient biocathode material for improved microbial electrosynthesis. J Mater Chem A 2.https://doi.org/10.1039/C4TA03101F
129. Aryal N, Halder A, Tremblay P-L, Chi Q, Zhang T (2016) Enhanced microbial electrosynthesis with three-dimensional graphene functionalized cathodes fabricated via solvothermal synthesis. Electrochim Acta 217:117–122. https://doi.org/10.1016/j.electacta.2016.09.063
130. Mateos R, Sotres A, Alonso MR, Morán A, Escapa A (2019) Enhanced CO_2 conversion to acetate through microbial electrosynthesis (MES) by continuous headspace gas recirculation. Energies 12(17). https://doi.org/10.3390/en12173297
131. Zaybak Z, Pisciotta JM, Tokash JC, Logan BE (2013) Enhanced start-up of anaerobic facultatively autotrophic biocathodes in bioelectrochemical systems. J Biotechnol 168(4):478–485. https://doi.org/10.1016/j.jbiotec.2013.10.001
132. Geppert F, Liu D, van Eerten-Jansen M, Weidner E, Buisman C, ter Heijne A (2016) Bioelectrochemical power-to-gas: state of the art and future perspectives. Trends Biotechnol 34(11):879–894. https://doi.org/10.1016/j.tibtech.2016.08.010
133. Van Eerten-Jansen MCAA, Heijne AT, Buisman CJN, Hamelers HVM (2012) Microbial electrolysis cells for production of methane from CO_2: long-term performance and perspectives. Int J Energy Res 36(6):809–819. https://doi.org/10.1002/er.1954
134. Xu H, Wang K, Holmes DE (2014) Bioelectrochemical removal of carbon dioxide (CO_2): an innovative method for biogas upgrading. Biores Technol 173:392–398. https://doi.org/10.1016/j.biortech.2014.09.127
135. Das Neves LC, Converti A, Vessoni Penna TC (2009) Biogas production: new trends for alternative energy sources in rural and urban zones. Chem Eng Technol 32:1147–1153

136. Gür TM (2018) Review of electrical energy storage technologies, materials and systems: challenges and prospects for large-scale grid storage. Energy Environ Sci 11(10):2696–2767. https://doi.org/10.1039/c8ee01419a
137. Prévoteau A, Carvajal-Arroyo JM, Ganigué R, Rabaey K (2020) Microbial electrosynthesis from CO_2: forever a promise? Curr Opin Biotechnol 62:48–57. https://doi.org/10.1016/j.copbio.2019.08.014
138. Bajracharya S, van den Burg B, Vanbroekhoven K, De Wever H, Buisman CJN, Pant D, Strik DPBTB (2017) In situ acetate separation in microbial electrosynthesis from CO_2 using ion-exchange resin. Electrochim Acta 237:267–275. https://doi.org/10.1016/j.electacta.2017.03.209
139. Bajracharya S, Vanbroekhoven K, De Wever H, Strik D, Buisman C, Pant D (2016) integrated product separation in bioelectrochemical CO_2 reduction for improved process efficiency. Chem Ing Tec 88(9):1255–1256. https://doi.org/10.1002/cite.201650202
140. Gutte B, Klauser S (2019) Design of catalytic polypeptides and proteins. Protein Eng Des Sel 31(12):457–470. https://doi.org/10.1093/protein/gzz009
141. Laureanti JA, Ginovska B, Buchko GW, Schenter GK, Hebert M, Zadvornyy OA, Peters JW, Shaw WJ (2020) A positive charge in the outer coordination sphere of an artificial enzyme increases CO_2 hydrogenation. Organometallics 39(9):1532–1544. https://doi.org/10.1021/acs.organomet.9b00843
142. Najafpour MM, Madadkhani S, Zand Z, Hołyńska M, Allakhverdiev SI (2016) Engineered polypeptide around nano-sized manganese–calcium oxide as an artificial water-oxidizing enzyme mimicking natural photosynthesis: toward artificial enzymes with highly active site densities. Int J Hydrogen Energy 41(40):17826–17836. https://doi.org/10.1016/j.ijhydene.2016.07.024
143. Çakar MM, Ruupunen J, Mangas-Sanchez J, Birmingham WR, Yildirim D, Turunen O, Turner NJ, Valjakka J, Binay B (2020) Engineered formate dehydrogenase from chaetomium thermophilum, a promising enzymatic solution for biotechnical CO_2 fixation. Biotech Lett. https://doi.org/10.1007/s10529-020-02937-7
144. Zhao H-Z, Chang Y-Y, Liu C (2013) Electrodes modified with iron porphyrin and carbon nanotubes: application to CO_2 reduction and mechanism of synergistic electrocatalysis. J Solid State Electrochem 17(6):1657–1664. https://doi.org/10.1007/s10008-013-2027-1
145. Martin LL, West LC, Wu B (2001) An extrusion strategy for the FeMo cofactor from nitrogenase. Eur J Biochem 268(22):5676–5686. https://doi.org/10.1046/j.0014-2956.2001.02506.x
146. Maiti BK, Maia LB, Silveira CM, Todorovic S, Carreira C, Carepo MSP, Grazina R, Moura I, Pauleta SR, Moura JJG (2015) Incorporation of molybdenum in rubredoxin: models for mononuclear molybdenum enzymes. J Biol Inorg Chem 20(5):821–829. https://doi.org/10.1007/s00775-015-1268-0
147. Schlager S, Haberbauer M, Fuchsbauer A, Hemmelmair C, Dumitru LM, Hinterberger G, Neugebauer H, Sariciftci NS (2017) Bio-electrocatalytic application of microorganisms for carbon dioxide reduction to methane. Chemsuschem 10(1):226–233. https://doi.org/10.1002/cssc.201600963
148. LaBelle EV, Marshall CW, May HD (2020) Microbiome for the electrosynthesis of chemicals from carbon dioxide. Acc Chem Res 53(1):62–71. https://doi.org/10.1021/acs.accounts.9b00522
149. Wu Z, Wang J, Liu J, Wang Y, Bi C, Zhang X (2019) Engineering an electroactive *Escherichia coli* for the microbial electrosynthesis of succinate from glucose and CO_2. Microb Cell Fact 18(1):15. https://doi.org/10.1186/s12934-019-1067-3
150. Glaven SM (2019) Bioelectrochemical systems and synthetic biology: more power, more products. Microb Biotechnol 12(5):819–823. https://doi.org/10.1111/1751-7915.13456

Acetogenic Bacteria for Biotechnological Applications

Dennis Litty and Volker Müller

Abstract

Acetogenic bacteria are a group of strictly anaerobic bacteria that employ the Wood–Ljungdahl pathway to reduce two molecules of CO_2 to acetyl-CoA, the central intermediate to various chemical compounds such as acetate, ethanol or butyrate. The capability of acetogens to utilize a wide range of substrates including industrial waste gas, methanol, formate and CO has led to a tremendous interest over the last decade to use them as industrial platform organisms to produce these valuable chemical compounds. In addition, some acetogens also possess a unique enzyme complex that directly reduces CO_2 to formate with H_2 as electron donor. This complex is superior over any chemical catalyst in hydrogenation of CO_2 and, therefore, these acetogens are also promising candidates for storage or production of hydrogen as well as carbon capture and storage. In this chapter, we discuss the biochemistry of acetogenic bacteria and give an overview of highlighted acetogenic organisms with respect to their biotechnical applications. Moreover, we discuss the progress that has been made in the development of metabolically engineered acetogens as biocatalysts for the production of valuable compounds such as acetone or biopolymers.

Keywords

Acetogens · Bioenergetics · Biofuels · Syngas

D. Litty · V. Müller (✉)
Molecular Microbiology and Bioenergetics, Institute of Molecular Biosciences, Johann Wolfgang Goethe University Frankfurt/Main, Frankfurt, Germany
e-mail: vmueller@bio.uni-frankfurt.de

J. J. G. Moura et al. (eds.), *Enzymes for Solving Humankind's Problems*,
https://doi.org/10.1007/978-3-030-58315-6_4

1 Introduction

Acetogenic bacteria are a phylogenetically very diverse group of strictly anaerobic bacteria ubiquitous in nature that employ the Wood–Ljungdahl pathway (WLP) to reduce two molecules of CO_2 to one molecule of acetyl-CoA [1–3]. Acetyl-CoA is then further reduced to mainly acetate and in some species to minor amounts of ethanol or butyrate. Although acetate is a common product in the metabolic pathway of acetogenic bacteria, it is not formed by all representatives of this group under every condition tested and their ability to produce acetate therefore does not distinguish acetogens [4, 5]. In addition, other bacterial groups, such as acetic acid bacteria or fermenting bacteria, are also able to produce acetate from organic carbon compounds such as alcohols or sugars [6]. A key feature of acetogenic bacteria is their ability to grow autotrophically on $H_2 + CO_2$ via the WLP and the CO dehydrogenase/acetyl-CoA synthase (CODH/ACS) as key enzyme [3, 7]. Several acetogens can also convert a mixture of H_2, CO_2 and CO, called synthesis gas (syngas) [8]. Syngas is a waste gas produced from steel manufacturing or from gasification of agricultural waste. Depending on the source, the composition of syngas differs [9, 10]. The capability of acetogenic bacteria to convert these gases has led to a tremendous interest to use them as biocatalysts for the production of biofuels such as ethanol or other valuable products [11, 12]. Especially in times of global warming, with the release of CO_2 from fossil fuels as one of the main causes, the call to reduce the greenhouse gas CO_2 is increasing. Therefore, the conversion of waste gases with acetogens is of special interest since it is a promising way of producing biofuels independent of carbohydrates while helping to reduce emissions of CO_2.

Acetogenic bacteria can also be used as biocatalysts to utilize one-carbon compounds (formate or methanol) as feedstocks making them also a promising alternative in a formate- or methanol-based bioeconomy [13]. In addition, some acetogens, such as *Acetobacterium woodii* and *Thermoanaerobacter kivui,* possess a unique enzyme complex capable of directly reducing CO_2 to formate with H_2 as electron donor that is superior over any chemical catalyst for a CO_2-based hydrogen storage [14, 15]. Therefore, acetogens are also promising candidates as potential catalysts for hydrogen storage or production.

2 Biochemistry of the Wood–Ljungdahl Pathway

All acetogens have in common that they reduce CO_2 to acetyl-CoA via the WLP [1, 3, 16]. Acetyl-CoA is the central intermediate for the production of various chemical compounds such as acetate, ethanol, 2,3-butanediol and more. The capability for autotrophic CO_2 assimilation via the WLP makes acetogens an important alternative for the industrial production of a variety of biofuels as well as biocommodities.

The WLP enables carbon fixation and is the only CO_2 fixing pathway that allows for energy conservation [17, 18]. During heterotrophic growth with sugars as carbon and energy source, glycolysis is coupled to the WLP via a pyruvate:ferredoxin oxidoreductase (PFOR) leading to conversion of pyruvate to acetyl-CoA. The resulting CO_2 of this reaction is then reduced in the WLP with reducing equivalents formed during glycolysis to produce additional acetyl-CoA [4]. The WLP is also well suited for the conversion of other C1 substrates such as CO, formate or methanol that enter the WLP by different routes. It consists of a methyl branch and a carbonyl branch serving for the formation of the central intermediate acetyl-CoA, starting from the reduction of one molecule of CO_2 each (Fig. 1). In the methyl branch, CO_2 is converted in several reactions to methyl-THF (tetrahydrofolate). In an initial step, CO_2 is reduced to formate. In most acetogens, this reaction is catalyzed by a formate dehydrogenase (FDH) with NADPH as electron donor [19–21], whereas in *A. woodii*, the reaction is catalyzed by recently discovered hydrogen-dependent CO_2 reductase (HDCR), where the electrons are derived directly from molecular hydrogen [15]. Formate is then bound, in a reaction driven by ATP hydrolysis, to the C1 carrier THF. Water is then split off from formyl-THF, and methenyl-THF is subsequently reduced to methenyl-THF by a methenyl-THF cyclohydrolase. The electron donor for this reaction is either NADH or NADPH [22–24]. In a second reduction step, the THF-bound methenyl group is reduced via methylene-THF to methyl-THF. The electron donor for the second reduction step, catalyzed by a methylene-THF reductase, varies among different acetogens. In some acetogens, NADH serves as electron donor [25], whereas in others, the electrons are derived via reduced ferredoxin [26]. The final step is transfer of the methyl group onto a corrinoid/FeS protein (CoFeSP) by a methyl transferase.

In the carbonyl branch of the WLP, another CO_2 is reduced to CO by the bifunctional CODH/ACS in a ferredoxin-dependent reaction. In a second reaction step, the methyl group of methyl-THF is condensed with CO of the carbonyl branch and coenzyme A (CoA) by the CODH/ACS to the central intermediate of the WLP, acetyl-CoA. The acetyl-CoA formed is then either channeled into the anabolic metabolism to provide the cell with organic material for biomass production or converted to acetate by a phosphotransacetylase and an acetate kinase. This last reaction step leads to the formation of one mol ATP per mol acetate. Since one mol ATP was also invested in the methyl branch to activate formate to formyl-THF, the WLP does not lead to a net gain of ATP. Therefore, the WLP is coupled to energy conservation by a chemiosmotic mechanism [2, 18]. Every acetogen examined to date uses reduced ferredoxin as the electron donor for an ion-translocating membrane protein complex, and acetogens can have either an Fd:NAD^+ oxidoreductase (Rnf) [27] or an Fd:H^+ oxidoreductase (Ech) complex [28] for generation of an ion motive force [18]. In both cases, the ion gradient can be either an H^+ or an Na^+ gradient. The electrochemical ion gradient thus established is then used by a membrane bound, H^+- or Na^+-translocating ATP synthase [29, 30]. For the reduction of ferredoxin with H_2 as reductant during autotrophic growth, acetogens may employ different enzymes for redox balancing [18]. One possibility of providing the reducing equivalents is by an electron-bifurcating hydrogenase.

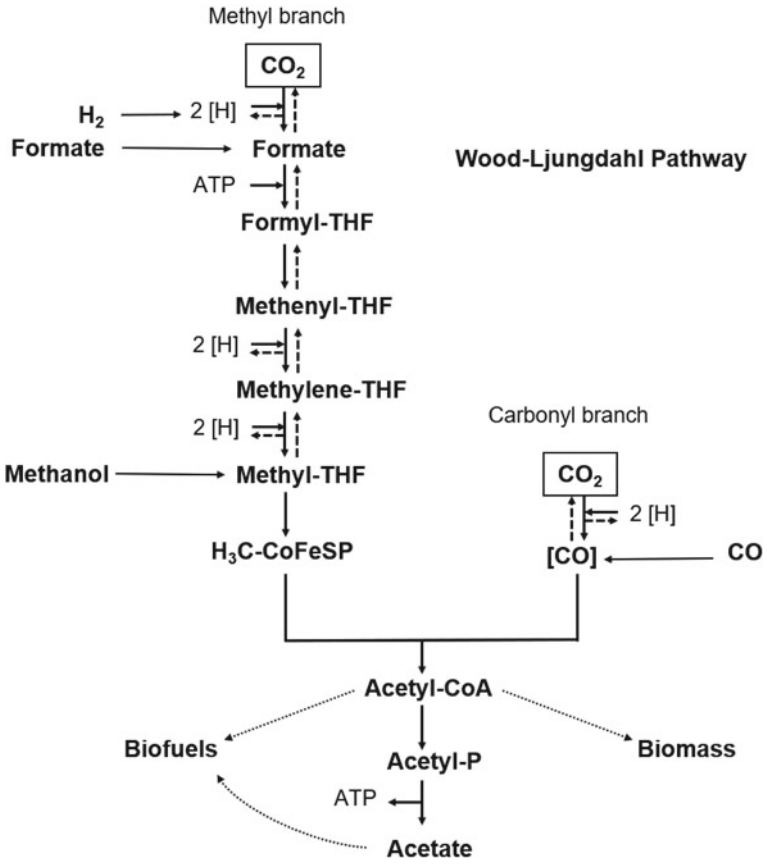

Fig. 1 The Wood–Ljungdahl pathway of CO_2 reduction. Two molecules of CO_2 are reduced to the central intermediate acetyl-CoA. Acetyl-CoA is the precursor of biomass and a wide range of natural products (dotted arrows). CoFeSP, corrinoid/iron sulfur protein; THF, tetrahydrofolate; CoA, coenzyme A; [H], reducing equivalent

In *A. woodii*, one of the best studied acetogens, this enzyme allows coupling of the exergonic reduction of NAD^+ to the endergonic reduction of ferredoxin by oxidation of H_2 [31]. In addition, during heterotrophic growth, the enzyme provides the reductant for the HDCR reaction, molecular hydrogen [32]. In *Clostridium ljungdahlii*, an acetogen also used for biotechnological applications, the reducing equivalents are provided by either the electron-bifurcating hydrogenase, as found in *A. woodii* or by a complex consisting of a formate dehydrogenase and a $NADP^+$-specific electron-bifurcating hydrogenase [19]. Depending on different modules for balancing redox equivalents, the overall ATP yield can vary. However, it is always below one ATP per mol acetate [18].

The WLP and its energetics have been studied extensively in acetogenic bacteria such as *A. woodii*, *C. ljungdahlii* or *Moorella thermoacetica* [18, 33–35]. The information obtained is not only helpful for better understanding of the mechanism of energy conservation itself but also is the foundation for further optimizations of these acetogens with respect to the production of biofuels.

3 Acetogens as Biocatalysts

The group of acetogens includes over 100 different species that are present in 23 different genera; however, more than 90% of all acetogens identified to date are only able to produce acetate as sole product [36]. Therefore, only a few are considered for the biotechnological production of biofuels and biocommodities such as ethanol, butanol and 2,3-butanediole [34, 37]. A list of acetogens currently pursued for biotechnological applications with their characteristics is summarized in Table 1. Acetogens currently considered as biocatalyst for industrial production belong mainly to the class of Clostridia including genera such as *Acetobacterium* and *Clostridium* [34, 38]. Key features of acetogenic Clostridia are their ability to grow on many different substrates and their high metabolic product diversity [39, 40], which makes them well suitable for the industrial production of a broad range of biochemicals. They can utilize a wide range of C5 (Pentose) or C6 (Hexose) sugars. However, fermentation of these sugars is not suitable for a sustainable production of biochemicals, since it offers low yields due to formation of significant amounts of CO_2 and the usage of crops (mostly sugarcane or wheat) as feedstocks competes with production of food for mankind [41, 42]. Besides sugars, they can also utilize cheap feedstocks such as glycerol and cellulose [38]. In addition, they are also able to utilize C1 compounds such as methanol, formate or as mentioned before, syngas (H_2, CO_2, CO). The natural products produced include a wide range of valuable chemicals such as acetate, ethanol, butanol, hexanol, acetone and more [8]. Clostridial acetogens considered for biotechnological applications include *A. woodii*, *Clostridium aceticum*, *Clostridium autoethanogenum*, *C. ljungdahlii* and *Clostridium ragsdalei*. *A. woodii* and *C. aceticum* are mainly considered for the production of acetate due to their high production rates, whereas the other species mentioned are mainly considered for the production of 2,3-butanediol as well as ethanol [39]. In addition, *A. woodii* offers the possibility of hydrogen storage due to its unique enzyme complex capable of directly reducing CO_2 to formate with H_2 as electron donor [15]. The same complex is found in the thermophilic acetogen *T. kivui* making it also a promising candidate for storage of hydrogen [14], a promising energy carrier that is considered as a sustainable, emission-free replacement for non-renewable fossil fuels [43, 44]. In addition to hydrogen storage, the enzyme complex can also be used for carbon capture and storage [13].

So far, we only briefly described the acetogens considered for biotechnological applications. Next, we will have a more detailed look into some highlighted acetogens with respect to their biotechnological applications in the following section.

Table 1 Characteristics of acetogenic bacteria considered for biotechnological applications

Organism	Substrates	Optimal growth temperature [°C]	Optimal growth pH	Natural products	Refs.
Acetobacterium woodii	Fructose, pyruvate, methanol, lactate, 2,3-BDO, formate, H_2+ CO_2	30	7.2	Acetate	[45]
Butyribacterium methylotrophicum	Glucose, pyruvate, methanol, H_2+ CO_2, CO	37–40	7.5	Acetate,ethanol, butyrate, butanol	[113–115]
Clostridium autoethanogenum	Fructose, rhamnose, xylose, arabinose, sucrose, malate, H_2+ CO_2, CO	37	5.8–6.0	Acetate, ethanol, 2,3-BD, lactate	[80, 81]
Clostridium carboxidivorans	Fructose, rhamnose, xylose, arabinose, sucrose, malate, H_2+ CO_2, CO	38	5.0–7.0	Acetate, butyrate, butanol, ethanol, hexanoic acid, hexanol	[90]
Clostridium coskatii	Fructose, rhamnose, xylose, arabinose, sucrose, malate, H_2+ CO_2, CO	37	5.8–6.5	Acetate, ethanol	[116]
Clostridium ljungdahlii	Fructose, rhamnose, xylose, arabinose, sucrose, malate, H_2+ CO_2, CO	37	6.0	Acetate, ethanol, 2,3-BD, lactate	[10, 117]
Thermoanaerobacter kivui	Glucose, fructose, formate, pyruvate, H_2+ CO_2, CO	66	6.4	Acetate	[70, 118, 119]

3.1 *Acetobacterium woodii*

The acetogenic bacterium *A. woodii* is a model organism to investigate the biochemistry and the energy metabolism of acetogenic bacteria. It can utilize, among others, monosaccharides such as fructose and C1 compounds such as formate, methanol or H_2 + CO_2 as substrate for growth. The major end product is always acetate [18, 45]. *A. woodii* is one of the few acetogens known to produce high amounts of acetate and therefore of special interest [46]. Acetate, a highly valuable chemical used as precursor in various chemical derivates has a global demand of approximately 18 million tons per year in 2019 [47]. Generally, acetate is produced by using petrochemical feedstocks in a methyl carbonylation process (Monsanto process) [5]. A more sustainable way to produce acetate is to use *A. woodii* as biocatalyst under autotrophic conditions. Previous strategies to improve acetate production are mainly based on process optimization [46, 48]. With 44 g/L, the

highest final acetate concentration reported so far could be achieved by using a pH-controlled, batch-operated stirred-tank bioreactor. However, problems that have to be overcome to use *A. woodii* as industrial platform with autotrophic conditions are a rather low solubility of the gaseous substrate and poor growth of biomass under these conditions [46].

A special feature of *A. woodii* is the presence of an enzyme complex that catalyzes the first step in the WLP, the reduction of CO_2 to formic acid. Typically, this reaction is catalyzed by a NADP- or ferredoxin-dependent formate dehydrogenases [19–21], whereas in *A. woodii,* as well as in *T. kivui*, this reaction is catalyzed by a novel enzyme, a hydrogen-dependent CO_2 reductase (HDCR) [14, 15]. The HDCR is composed of four subunits. Both HDCRs consist of a formate dehydrogenase module and a [FeFe] hydrogenase module (HydA2) that are connected by two small FeS-containing subunits which likely transfer electrons from the hydrogenase module to the formate dehydrogenase module and vice versa. *A. woodii* has two isoforms of the HDCR: one containing a cysteine and the other a selenocysteine. *T. kivui* only has one isoenzyme with a cysteine in the formate dehydrogenase module. In contrast to formate dehydrogenases, the HDCR directly catalyzes the reduction of CO_2 to formic acid with H_2 as electron donor with rates superior to any known chemical catalyst, thus, making it a promising candidate for storage of H_2 [14, 15]. Molecular hydrogen is an attractive future energy carrier to replace fossil fuels. The limiting problem for the technological use of H_2 is storage of the gas. However, this problem could be overcome by using the HDCR. Since the equilibrium constant for the hydrogenation of CO_2 to formate is close to one, the HDCR is an ideal biocatalyst for the storage of molecular hydrogen. In the form of formate, the so-called liquid organic hydrogen carrier (LOHC), the explosive H_2 could easily be handled and supplied by using existing infrastructure [49, 50]. The HDCRs from both acetogens are significantly more effective than the best chemical catalysts known so far [49, 51–53]. The HDCR from *A. woodii* catalyzes the hydrogenation of CO_2 with a turnover frequency (TOF) of 101 600 h^{-1} at 30 °C and 0.8 bar H_2, being significantly better than chemical catalysts. Even though the enzyme of *A. woodii* is highly stable with a temperature optimum of 40 °C, long-term stability has yet to be determined. Remarkably, the [FeFe] hydrogenase module of the HDCR is the [FeFe] hydrogenase being completely CO tolerant [54]. In contrast to other [FeFe] hydrogenases where CO leads to irreversible damage to the H-cluster [55–57], CO inhibition of the [FeFe] hydrogenase module is fully reversible, even though the enzyme is strongly inhibited by CO [54]. This feature could be a result of the metabolism of *A. woodii*, where CO is an intermediate of the WLP. However, since the HDCR requires strict anoxic conditions and/or a low redox potential, a biotechnological application is rather difficult. To overcome this problem, we established a whole-cell system for the efficient hydrogenation of CO_2 to formate [15]. The system is based on the knockout of the ATP-dependent further conversion of formate in the WLP of acetogens. Formate is transiently excreted and accumulated during autotrophic growth in *A. woodii* [58] and accumulation requires inhibition of the ATP-dependent further conversion of formate in the WLP. By reducing the cellular energy content, formate is no longer converted to acetate and

therefore is accumulated. One possibility to uncouple the pathway from ATP production is by using ionophores. Since the energy metabolism in *A. woodii* is strictly Na^+-dependent [59, 60], including a Na^+-dependent Rnf [61, 62] as well as a Na^+-dependent ATP synthase [29, 63, 64], omitting Na^+ in the medium also leads to an increased formate production.

The development of this whole-cell system paved the road for the biotechnological storage of hydrogen. However, further experiments with respect to long-term stability of the system, product toxicity and the search of low-cost, environmental-friendly uncouplers need be carried out.

The HDCR cannot only catalyze the direct hydrogenation of CO_2 to formate but also its reverse reaction and therefore is a promising candidate for a formate-based production of biohydrogen. Biohydrogen is a sustainable, environmentally friendly alternative toward a fuel-based production. Current approaches for biohydrogen production are mainly based on biophotolysis or fermentation [65, 66]. A promising alternative is to take advantage of the exceptional high activity of the HDCR of *A. woodii* and to establish an efficient whole-cell system for a formate-based biohydrogen production [14, 15]. Formate, a low-cost feedstock, can be utilized by *A. woodii* in high concentrations (<300 mM formate). Therefore, a two-step closed batch system was established [67]. In a first step, cells were grown on fructose to mid-exponential phase and then production of H_2 was initiated by addition of formate. These growing cells reached specific H_2 production rates of 66 mmol H_2 g_{CDW}^{-1} h^{-1}, one of the highest reported so far for a mesophilic organism without genetic modifications [68, 69]. One major problem that has to be overcome is to abolish production of the unwanted side-product, which mainly decreased the H_2 yield. Further optimization of biohydrogen production should therefore address this problem.

3.2 *Thermoanaerobacter kivui*

The thermophilic acetogen *T. kivui*, which was isolated from sediments of Lake Kivu (Africa), also has a HDCR and therefore, is also a promising candidate for the biotechnological storage of hydrogen [14]. In comparison to the HDCR from *A. woodii*, the enzyme from *T. kivui* is even superior to chemical catalysts for the hydrogenation of CO_2. The CO_2 hydrogenation is catalyzed with a turnover frequency of 9 556 000 h^{-1} at 60 °C and 1 bar H_2. Interestingly, even at 30 °C, the conversion rate is 18-fold higher compared to the one from *A. woodii*. The HDCR from *T. kivui* is highly thermostable, making it more flexible with respect to process parameters for a biotechnological application. However, the enzyme also requires strict anoxic conditions, thus, making applications rather difficult.

A key advantage of *T. kivui* over *A. woodii* is that it can grow on syngas/CO in mineral medium without the additional requirement for yeast extract and vitamins [28, 70], whereas *A. woodii* cannot grow on syngas at all [71, 72]. As a thermophilic acetogen, with an optimal growth temperature of 66 °C, *T. kivui* also offers several advantages in a fermentation process compared to mesophilic

biocatalysts: a reduced contamination risk, reduced costs for process cooling as well as better diffusion rates of gases at higher temperatures [73]. To take advantage of using a thermophilic acetogen as biocatalyst for hydrogen storage, our group established a whole-cell system for *T. kivui* as platform for hydrogen storage from syngas [74]. The whole-cell system for *T. kivui* is similar to that for *A. woodii* and is based on lowering the cellular ATP content by uncouplers (see Sect. 3.1). Interestingly, bicarbonate was found to be an effective inhibitor of the ATP synthase, thus, lowering the cellular ATP content. Addition of bicarbonate not only abolished formation of the unwanted side-product, acetate, but also led to a dramatic increase of the formate conversion rate. In cell suspensions experiments (closed batch), the specific formate production rates reached 234 mmol· g protein^{-1} h^{-1}, the highest rates reported so far. In addition, the conversion of syngas to formate as a sole end product could be shown for the first time. The finding of bicarbonate as an affordable, environmental-friendly inhibitor has further opened the way toward the biotechnological storage of hydrogen. Future experiments need to determine the long-term stability of the whole-cell system and should address upscaling of the process.

The HDCR of *T. kivui* also catalyzes the conversion of formate to H_2 with exceptional rates and is therefore also a promising alternative for a formate-based biohydrogen production [14]. The enzyme from T. *kivui* catalyzed conversion from formate to H_2 with a TOF of 9 892 000 h^{-1} at 60 °C. Even though a whole-cell system of *T. kivui* for the specific formate-based biohydrogen production has not been established yet, a similar whole-cell approach as in *A. woodii* (see Sect. 3.1) can be used. Due to the superior catalytic rates of the HDCR from *T. kivui*, it can be assumed that the specific H_2 production rate in a whole-cell system would be in a range of the H_2 production rate of the thermophilic archaeon *Thermoccocus onnurineus*, the highest reported so far [75, 76]. The system from *T. kivui* may be even more suited then the one from *T. onnurineus*. In contrast to *T. onnurineus* where H_2 is produced by a membrane-bound hydrogenase complex [77, 78], the HDCR is a soluble, cytoplasmatic enzyme, and therefore, the enzyme activity is energetically independent of the membrane potential.

3.3 *Clostridium autoethanogenum*

Clostridium autoethanogenum is, alongside with the closely related *C. ljungdahlii* and *C. ragsdalei*, one of the few acetogens that is currently used for the industrial production of ethanol from exhaust gases of steel manufacturing by the company LanzaTech [8, 79]. Characteristically, the wild-type strain of *C. autoethanogenum* (and their above-mentioned close relatives) produces mainly ethanol and acetate but also minor amounts of 2,3-butanediol under autotrophic conditions with an optimal pH between 5 − 5.5 (Fig. 2) [80, 81]. This rather low pH favors solventogenesis, leading to an increased yield of highly reduced products such as ethanol [82]. Ethanol production in *C. autoethanogenum* comprises two different routes. In a first route, acetyl-CoA is subsequential reduced into acetaldehyde by using the

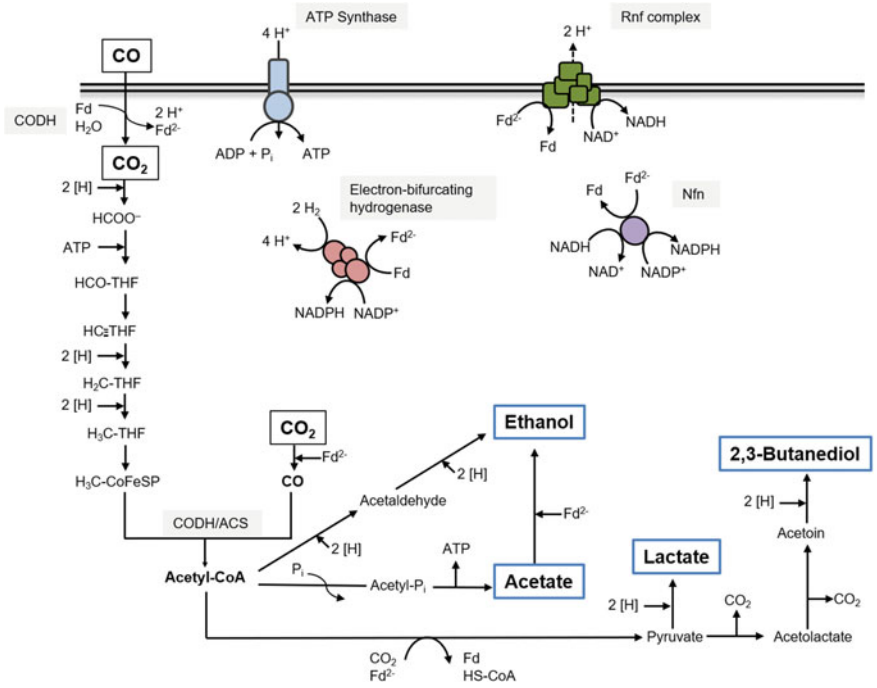

Fig. 2 Biochemistry of the Wood–Ljungdahl pathway and formation of natural products from CO_2 or CO in *C. autoethanogenum*. The membrane-bound respiratory chain for energy conservation is shown on the top, the biochemistry of the WLP and the natural products, highlighted in blue boxes, are shown below. Substrates are shown in black boxes. The principal pathways are shown, electrons are not balanced. CODH/ACS: carbon monoxide dehydrogenase/acetyl coenzyme A synthase; CM: cytoplasmic membrane; Rnf complex: ferredoxin–NAD oxidoreductase; THF, tetrahydrofolic acid

bi-functional aldehyde/alcohol dehydrogenase (AdhE) or the CoA-dependent acetaldehyde dehydrogenase (Ald). The formed acetaldehyde is then further reduced to ethanol by an alcohol dehydrogenase (Adh). In the second main route, acetate is reduced in a highly endergonic reaction with reduced ferredoxin as electron donor to acetaldehyde by an acetaldehyde:ferredoxin oxidoreductase (AOR), followed by the conversion to ethanol by Adh. *C. autoethanogenum* has a $NADP^+$-specific electron-bifurcating hydrogenase that forms a complex with a formate dehydrogenase, providing reducing equivalents for the reduction of CO_2 to formate [19]. In addition, it has an electron-bifurcating, ferredoxin-dependent transhydrogenase (Nfn) [83]. These enzyme complexes along with the presence of the AOR make *C. autoethanogenum* an ideal platform for industrial production of ethanol.

The use of *C. autoethanogenum* on an industrial scale is not only restricted to ethanol production from syngas. In 2011, it was discovered that

C. autoethanogenum is able to co-produce 2,3-butanediol in significant amounts along with the major product ethanol (with a ratio of 1:10) from CO-containing steel mill waste gas [81]. 2,3-BD is an important high-valuable chemical precursor for production of a variety of compounds such as methyl ethyl ketone (MEK) which is used in printing inks as well as in surface coatings, and 1,3-butadiene, an intermediate used for production of nylon and synthetic rubber [84, 85]. The main 2,3-BD derived products have an immense global market and are, therefore, of high economic interest.

In *C. autoethanogenum*, the production of 2,3-BD starts with the conversion of acetyl-CoA to pyruvate catalyzed by the PFOR. *C. autoethanogenum* possesses two identical genes encoding for the PFOR. In a next step, two molecules of pyruvate are then converted to acetolactate by an acetolactate synthase. *C. autoethanogenum* possesses three different genes encoding for acetolactate synthases [81]. The genes *ilvB* and *ilvIH* encoding for two of the three acetolactate synthases are most probably involved in the anabolism, whereas the gene *alsS* encodes most likely for the acetolactate synthase responsible for the catabolic formation of 2,3-butanediol. The formed acetolactate is then further split into acetoin and CO_2 by an acetolactate decarboxylase (ALDC). In a final step, acetoin is reduced to 2,3-butanediol by either a NADH-dependent 2,3-butanediol dehydrogenase or a NADPH-dependent primary-secondary alcohol dehydrogenase.

Even though *C. autoethanogenum* can naturally produce high amounts of ethanol and also significant amounts of 2,3-BD under autotrophic conditions, a problem that comes along with the industrial scaled production of both products is an undesired production of unwanted side-products such as acetate or lactate (in minor amounts). Especially, the production of lactate as side-product significantly reduces efficiency and yield of the produced 2,3-BD/ethanol. Furthermore, low concentrations of lactate (<0.5%) are toxic to *C. autoethanogenum* [81]. Another problem is that lactate can also be used as substrate by other microorganisms which increases the chances of a contamination during the fermentation process when lactate is formed. A big advantage to overcome these problems is the genetical accessibility of *C. autoethanogenum*, making metabolic engineering possible.

Strategies to improve ethanol production on a genetic level are mainly based on either overexpression or on introduction of AdhE. Another promising approach to enhance yields and production rates by metabolic engineering includes the deletion of genes via allelic exchange mutagenesis [86]. By deletion of the gene encoding for the lactate dehydrogenase in *C. autoethanogenum*, the production of 2,3-BD and ethanol was improved [87]. With the same genetic tool, the genes *adhE* and *aor2* were deleted which also resulted in an improved ethanol production (up to 180% increase) under autotrophic conditions [88].

3.4 *Clostridium carboxidivorans*

The acetogenic bacterium *C. carboxidivorans* is known to produce several solvents such as ethanol, butanol, hexanoic acid and hexanol from syngas [89]. It was

isolated from an agricultural settling lagoon in Oklahoma (USA) [90]. Along with *Butyribacterium methylotrophicum* [91], *Clostridium drakei* [90], *C. ragsdalei* [92] and *Eubacterium limosum* [93], it is one of few acetogens that is known to produce long-chained alcohols such as butanol and hexanol (Fig. 3). Butanol is an important industrial bulk chemical that is used as transport fuel. As fuel additive, butanol has better properties than ethanol. It has a higher energy content, is less explosive and is not as hygroscopic as ethanol and therefore does not lead to corrosion on metallic surfaces such as engines. While current processes for butanol production using solventogenic Clostridia such as *C. acetobutylicum* relied mostly on expensive feedstocks such as corn or sugarcane, a syngas-based butanol production could become a promising alternative [94]. Therefore, *C. carboxidivorans* is of special biotechnological interest.

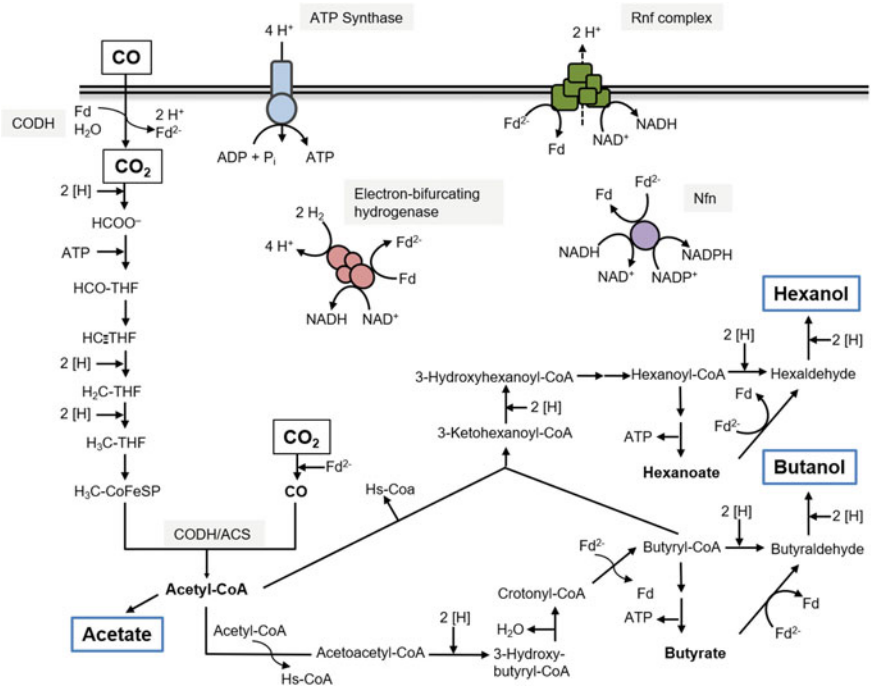

Fig. 3 Biochemistry of the Wood–Ljungdahl pathway and formation of natural products from CO_2 or CO in *C. carboxidivorans*. The membrane-bound respiratory chain for energy conservation is shown on the top, the biochemistry of the WLP and the natural products, highlighted in blue boxes, are shown below. Substrates are shown in black boxes. The formation of hexanol takes place via reverse β-oxidation. The enzymes involved in hexanol formation have not been characterized yet but are assumed to run in a similar fashion as the ones involved in the formation of the intermediate butyryl-CoA. CODH/ACS: carbon monoxide dehydrogenase/acetyl coenzyme A synthase; CM: cytoplasmic membrane; Rnf complex: ferredoxin–NAD oxidoreductase; THF, tetrahydrofolic acid

For the production of butanol, two molecules of acetyl-CoA are condensed to acetoacetyl-CoA by a thiolase (ThlA) in an initial step. Acetoacetyl-CoA is then reduced to 3-hydroxypropionyl-CoA with NADH. After water is split off by a crotonase (Crt), the formed crotonyl-CoA is then reduced to butyryl-CoA by an electron-bifurcating butyryl-CoA dehydrogenase (Bcd). The Bcd of *Clostridium kluyveri* is the prototype of a flavin-dependent, electron-bifurcating enzyme [95]. It uses the exergonic reaction of the NADH-dependent reduction of crotonyl-CoA to drive reduction of ferredoxin with NADH. Recently, we have demonstrated the presence of an electron-bifurcating Bcd in *E. limosum* KIST612, an acetogen which produces butyrate from CO [96]. Butyryl-CoA can be either reduced via butyraldehyde directly to butanol by NADH-dependent aldehyde/alcohol dehydrogenases or first converted to butyrate by a phosphotransbuturylase (Ptb) and a butyrate kinase (Buk), which is then reduced to butaraldehyde by an AOR again.

As mentioned above, *C. carboxidivorans* can also produce hexanol from syngas which makes it also a promising alternative for hexanol production. Hexanol is an interesting alternative to ethanol and is already used in the pharmaceutical and cosmetic industry as well as in the texile industry [97]. In *C. carboxidivorans,* the enzymes involved in hexanol formation have not been characterized yet but are assumed to run in a similar fashion as the enzymes involved in the formation of the intermediate butyryl-CoA. The formation of hexanol takes place via a reverse β-oxidation. In a first step, acetyl-CoA is elongated with butyryl-CoA to 3-ketohexanoyl-CoA by a thiolase (Thl2), which is then reduced to 3-hydroxyhexanoyl-CoA and subsequently converted to hexanoyl-CoA. Hexanoyl-CoA is then reduced by NADH-dependent aldehyde/alcohol dehydrogenases to hexanol, similar to the formation of butanol.

So far, butanol as well as hexanol titers from syngas are rather low due to a higher demand of reducing equivalents such as NADH or NADPH in comparison to other primary metabolites such as ethanol and a rather low solubility of H_2, CO, and CO_2 at moderate temperatures. Since *C. carboxidivorans* is not genetically accessible up to date, the main focus of research was on process optimization including parameters such as medium composition, pH and temperature. The highest concentrations of hexanol (0.94 g/L) were achieved by increasing molybdenum (to 2 mg/L) and omitting copper in the defined medium at 37 °C [89]. One important parameter for the production of these alcohols is the temperature. Generally, *C. carboxidivorans* can produce alcohols within a range of 24 − 42 °C. Even though the optimal growth temperature of *C. carboxidivorans* is at 37 °C, it is not as beneficial to produce these alcohols at 37 °C. Optimal growth temperatures come along with higher metabolic rates and thus higher production rates of acetate. However, this leads to a fast accumulation of acetate in high concentrations (>60 mmol/l) which inhibits solventogenesis. This inhibitory effect of solventogenesis, also known as “acid crash”, can be prevented by lowering the growth temperature to 25 °C which leads to lower acetate concentration and therefore to an increased yield of the produced alcohols [98].

4 Metabolic Engineering in Acetogens

Metabolic engineering offers unique opportunities to eliminate unwanted side-products, synthesize novel, high-valuable compounds and increase the yield of natural products. A prerequisite for metabolic engineering is the knowledge of the biosynthetic pathway and its bioenergetics. The biochemistry and the bioenergetics have extensively been studied in the past for acetogenic bacteria such as *A. woodii* [4, 33], *C. ljungdahlii* [34] and *C. autothenagoenum* [19, 83]. The availability of genome sequences has further developed the use of acetogenic bacteria as a production platform. However, the use of acetogens as biocatalysts for biotechnological applications requires strategies for genetic manipulation. The major challenge was to establish a genetic toolbox for acetogenic bacteria. Problems that had to be overcome in establishing a system for genetic manipulation in acetogenic bacteria included a strong restriction-modification system, efficient degradation of external DNA by nucleases and the thick outer layer of these mostly Gram-positive bacteria [99, 100]. The development of strategies to overcome these problems has drastically increased over the past decade which led to an advanced genetic toolbox for acetogens. So far, genetic systems have been reported for *A. woodii* [62, 101], *C. aceticum* [102], *C. autoethanogenum*, *C. ljungdahlii* [103], *E. limosum* [104] and *T. kivui* [105]. These acetogenic bacteria have been genetically modified to produce highly valuable chemicals such as acetone, butanol, butyrate, 2,3-BD and poly-3-hydroxybutyrate (PHB).

Strategies to enhance acetone production on a genetic level by using engineered acetogens have come into focus recently. Acetone is mainly used as an industrial solvent and serves as precursor for the generation of plastics. With a global market of estimated 4.04 billion USD in 2019 and more than 6 million tons produced, the interest of acetone is immense. These strategies are based of the implementation from the genes of the acetone pathway in *C. acetobutylicum* (*thlA*, *ctfA*, *ctfB*, and *adc*) [102, 106, 107]. In the natural acetone pathway of *C. acetobutylicum*, two molecules of acetyl-coA are converted to acetoacetyl-CoA by a thiolase A (thlA). Next, the CoA moiety from acetoacetyl-CoA is then transferred to acetate and acetoacetate as well as acetyl-CoA is formed. In a final step, the formed acetoacetate is converted into acetone and CO_2. This reaction is catalyzed by an acetoacetate decarboxylase (Adc) (Fig. 4). The successful expression of these genes in a plasmid-based approach was first shown in 2012 with a recombinant C. *aceticum* strain. In a closed batch experiment with $H_2 + CO_2$ as a sole carbon and energy source, acetone was produced up to 8 mg/l by the recombinant strain. In 2014, the successfully expression of the genes involved in the acetone pathway from *C. acetobutylicum* under control of a lactose-inducible promoter could also be shown for *C. ljungdahlii* in closed batched experiments using CO as substrate [106]. However, it was shown that *C. ljungdahlii* is converting the produced acetone to isopropanol by a NADPH-dependent primary-secondary alcohol dehydrogenase [87]. To solve this problem, the respective gene was deleted, and acetone production was further enhanced by exchanging the thiolase gene *thlA* from

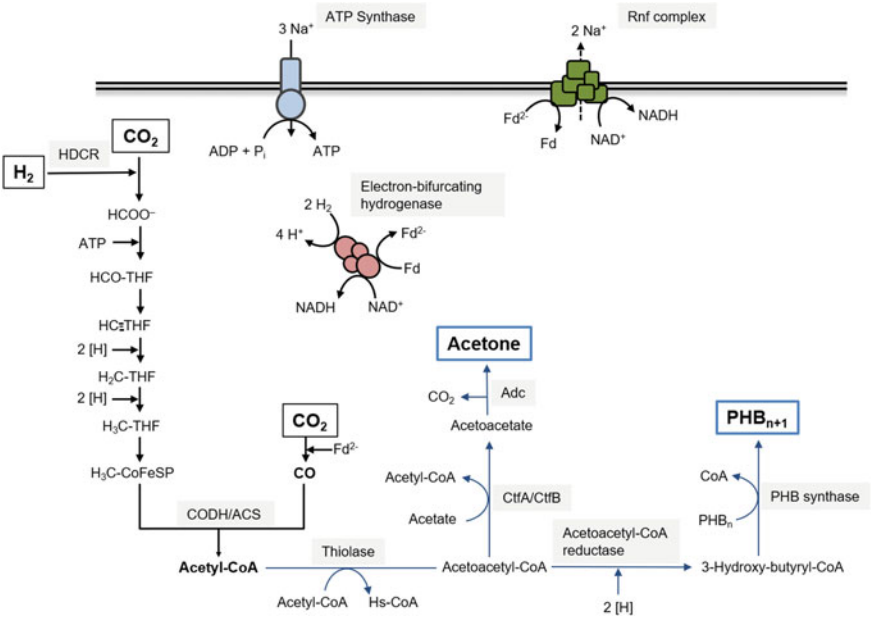

Fig. 4 Biochemistry of the Wood–Ljungdahl pathway and formation of potential recombinant products from CO_2 or CO in *A. woodii*. The membrane-bound respiratory chain for energy conservation is shown on the top. The biochemistry of the WLP and the recombinant products, highlighted in blue boxes, are shown below. Substrates are shown in black boxes. Adc: acetoacetate decarboxylase; CtfA/CtfB: acetoacetylCoA:acetate/butyrate CoA transferase; CODH/ACS: carbon monoxide dehydrogenase/acetyl coenzyme A synthase; CM: cytoplasmic membrane; HDCR, hydrogen-dependent CO_2 reductase PHB, poly-3-hydroxybutyrate; Rnf complex: ferredoxin–NAD oxidoreductase; THF, tetrahydrofolic acid

C. acetobutylicum with the one from *C. kluyveri* [108]. Successfully, acetone production was also shown for a recombinant *A. woodii* strain containing plasmids with the genes of the acetone pathway from *C. acetobutylicum* [107]. In a continuous fermentation, the production of acetone could be increased to 26.4 mg/l·h^{-1}. So far, acetone production is rather low in engineered strains and further optimizations need to be done with respect to an industrial application.

Another biosynthetic compound that has come into focus lately is poly-3-hydroxybutyrate (PHB). This biopolymer is considered as a sustainable, biodegradable replacement for non-degradable, fuel-based plastics [109]. Naturally, acetogenic bacteria are not able to produce PHB. By metabolic engineering, they could become a promising candidate for the biotechnological production of PHB. Strategies for the heterologous production of PHB are based on the implementation of codon-optimized genes from the PHB pathway in *Cupriavidus necator* (*phaA*, *phaB*, *phaC*) [110–112]. The natural PHB pathway comprises three reactions: In a first reaction, two molecules of acetyl-CoA are condensed to acetoacetyl-CoA by a

thiolase (Fig. 4.). Acetoacetyl-CoA is then reduced to 3-hydroxybutyryl-CoA by a NADPH-dependent acetoacetyl-CoA reductase, followed by the polymerization of PHB via a poly-3-hydroxybutyrate synthase. The successful heterologous expression of the PHB genes in a plasmid-based approach was recently shown in *C. autothenanogenum* [111] as well as in *C. coskatii* [112]. In a recombinant *C. ljungdahlii* strain, the same approach was without success [112]. So far, the titers of PHB are rather low. Under autotrophic conditions with syngas, the production of PHB was only 1.2% per cell dry weight in the recombinant *C. coskatii* strain, whereas in *C. autothenanogenum* a production of 5.6% PHB could be achieved. These low titers are caused by the limitation of reducing equivalents as well as ATP [111]. Future optimizations should therefore address strategies to improve the energy status of the cell. This could be achieved either by implementation of additional energy conservation modules or by implementation of ATP-yielding pathways.

5 Conclusion

Acetogens are on the advent of becoming promising candidates as catalysts toward a sustainable, bio-based economy. Their outstanding metabolic product diversity along with their wide range of substrate flexibility makes them well suited for the biotechnological production of various compounds from several feedstocks including industrial waste gas, methanol, formate and CO. With the well-studied biochemistry of the WLP and its bioenergetics for some model acetogens and a well-developed genetic toolbox for several acetogenic bacteria, the foundation for the industrial use of acetogens as biocatalysts has been laid over the past decades. A steadily increasing number of genome sequences available and additional knowledge of bioenergetics will further help to develop optimized strains in the future. Even though the metabolic engineering of acetogens is still in the beginning and the industrial use as platform organisms has been limited to the production of ethanol so far, their potential is tremendous.

References

1. Drake HL, Gößner AS, Daniel SL (2008) Old acetogens, new light. Ann NY Acad Sci 1125:100–128
2. Müller V (2003) Energy conservation in acetogenic bacteria. Appl Environ Microbiol 69:6345–6353
3. Ragsdale SW (2008) Enzymology of the Wood-Ljungdahl pathway of acetogenesis. Ann N Y Acad Sci 1125:129–136
4. Schuchmann K, Müller V (2016) Energetics and application of heterotrophy in acetogenic bacteria. Appl Environ Microbiol 82:4056–4069
5. Drake HL (1994) Acetogenesis, acetogenic bacteria, and the acetyl-CoA "Wood/Ljungdahl" pathway: Past and current perspectives. In: Drake HL (ed) Acetogenesis. Springer, US, New York, pp 3–60

6. Müller V (2008) Bacterial fermentation. In: Encyclopedia of life sciences. John Wiley & Sons Ltd., Chichester
7. Ragsdale SW, Pierce E (2008) Acetogenesis and the Wood-Ljungdahl pathway of CO_2 fixation. Biochim Biophys Acta 1784:1873–1898
8. Bengelsdorf FR, Beck MH, Erz C, Hoffmeister S, Karl MM, Riegler P, Wirth S, Poehlein A, Weuster-Botz D, Dürre P (2018) Bacterial anaerobic synthesis gas (syngas) and CO_2+H_2 fermentation. Adv Appl Microbiol 103:143–221
9. Munasinghe PC, Khanal SK (2010) Biomass-derived syngas fermentation into biofuels: opportunities and challenges. Bioresour Technol 101:5013–5022
10. Köpke M, Held C, Hujer S, Liesegang H, Wiezer A, Wollherr A, Ehrenreich A, Liebl W, Gottschalk G, Dürre P (2010) *Clostridium ljungdahlii* represents a microbial production platform based on syngas. Proc Natl Acad Sci USA 107:13087–13092
11. Dürre P, Eikmanns BJ (2015) C1-carbon sources for chemical and fuel production by microbial gas fermentation. Curr Opin Biotechnol 35:63–72
12. Humphreys CM, Minton NP (2018) Advances in metabolic engineering in the microbial production of fuels and chemicals from C1 gas. Curr Opin Biotechnol 50:174–181
13. Müller V (2019) New horizons in acetogenic conversion of one-carbon substrates and biological hydrogen storage. Trends Biotechnol 37:1344–1354
14. Schwarz FM, Schuchmann K, Müller V (2018) Hydrogenation of CO_2 at ambient pressure catalyzed by a highly active thermostable biocatalyst. Biotechnol Biofuels 11:237
15. Schuchmann K, Müller V (2013) Direct and reversible hydrogenation of CO_2 to formate by a bacterial carbon dioxide reductase. Science 342:1382–1385
16. Müller V, Inkamp F, Rauwolf A, Küsel K, Drake HL (2004) Molecular and cellular biology of acetogenic bacteria. In: Nakano M, Zuber P (eds) Strict and facultative anaerobes: medical and environmental aspects. Horizon Scientific Press, Norfolk, pp 251–281
17. Poehlein A, Cebulla M, Ilg MM, Bengelsdorf FR, Schiel-Bengelsdorf B, Whited G, Andreesen JR, Gottschalk G, Daniel R, Dürre P (2015) The complete genome sequence of *Clostridium aceticum*: a missing link between Rnf- and cytochrome-containing autotrophic acetogens. mBio 6:e01168–01115
18. Schuchmann K, Müller V (2014) Autotrophy at the thermodynamic limit of life: a model for energy conservation in acetogenic bacteria. Nat Rev Microbiol 12:809–821
19. Wang S, Huang H, Kahnt J, Müller AP, Köpke M, Thauer RK (2013) NADP-specific electron-bifurcating [FeFe]-hydrogenase in a functional complex with formate dehydrogenase in *Clostridium autoethanogenum* grown on CO. J Bacteriol 195:4373–4386
20. Yamamoto I, Saiki T, Liu SM, Ljungdahl LG (1983) Purification and properties of NADP-dependent formate dehydrogenase from *Clostridium thermoaceticum*, a tungsten-selenium-iron protein. J Biol Chem 258:1826–1832
21. Maia LB, Moura JJ, Moura I (2015) Molybdenum and tungsten-dependent formate dehydrogenases. J Biol Inorg Chem 20:287–309
22. O'Brien WE, Brewer JM, Ljungdahl LG (1973) Purification and characterization of thermostable 5,10-methylenetetrahydrofolate dehydrogenase from *Clostridium thermoaceticum*. J Biol Chem 248:403–408
23. Ragsdale SW, Ljungdahl LG (1984) Purification and properties of NAD-dependent 5,10-methylenetetrahydrofolate dehydrogenase from *Acetobacterium woodii*. J Biol Chem 259:3499–3503
24. Moore MR, O'Brien WE, Ljungdahl LG (1974) Purification and characterization of nicotinamide adenine dinucleotide-dependent methylenetetrahydrofolate dehydrogenase from *Clostridium formicoaceticum*. J Biol Chem 249:5250–5253
25. Wohlfarth G, Geerligs G, Diekert G (1990) Purification and properties of a NADH-dependent 5,10-methylenetetrahydrofolate reductase from *Peptostreptococcus productus*. Eur J Biochem 192:411–417

26. Clark JE, Ljungdahl LG (1984) Purification and properties of 5,10-methylenetetrahydrofolate reductase, an iron-sulfur flavoprotein from *Clostridium formicoaceticum*. J Biol Chem 259:10845–10849
27. Biegel E, Müller V (2010) Bacterial Na^+-translocating ferredoxin:NAD^+ oxidoreductase. Proc Natl Acad Sci USA 107:18138–18142
28. Schölmerich MC, Müller V (2019) Energy conservation by a hydrogenase-dependent chemiosmotic mechanism in an ancient metabolic pathway. Proc Natl Acad Sci USA 116:6329–6334
29. Matthies D, Zhou W, Klyszejko AL, Anselmi C, Yildiz O, Brandt K, Müller V, Faraldo-Gomez JD, Meier T (2014) High-resolution structure and mechanism of an F/V-hybrid rotor ring in a Na^+-coupled ATP synthase. Nat Commun 5:5286
30. Schölmerich MC, Katsyv A, Dönig J, Hackmann TJ, Müller V (2020) Energy conservation involving 2 respiratory circuits. Proc Natl Acad Sci USA 117:1167–1173
31. Schuchmann K, Müller V (2012) A bacterial electron bifurcating hydrogenase. J Biol Chem 287:31165–31171
32. Wiechmann A, Ciurus S, Oswald F, Seiler VN, Müller V (2020) It does not always take two to tango: "Syntrophy" via hydrogen cycling in one bacterial cell. ISME J 14:1561–1570
33. Poehlein A, Schmidt S, Kaster A-K, Goenrich M, Vollmers J, Thürmer A, Bertsch J, Schuchmann K, Voigt B, Hecker M, Daniel R, Thauer RK, Gottschalk G, Müller V (2012) An ancient pathway combining carbon dioxide fixation with the generation and utilization of a sodium ion gradient for ATP synthesis. PLoS ONE 7:e33439
34. Bengelsdorf FR, Poehlein A, Linder S, Erz C, Hummel T, Hoffmeister S, Daniel R, Dürre P (2016) Industrial acetogenic biocatalysts: a comparative metabolic and genomic analysis. Front Microbiol 7:1036
35. Huang H, Wang S, Moll J, Thauer RK (2012) Electron bifurcation involved in the energy metabolism of the acetogenic bacterium *Moorella thermoacetica* growing on glucose or H_2 plus CO_2. J Bacteriol 194:3689–3699
36. Müller V, Frerichs J (2013) Acetogenic bacteria. In: Encyclopedia of life sciences. John Wiley & Sons Ltd., Chichester
37. Daniell J, Köpke M, Simpson SD (2012) Commercial biomass syngas fermentation. Energies 5:5372–5417
38. Liew F, Martin ME, Tappel RC, Heijstra BD, Mihalcea C, Köpke M (2016) Gas fermentation-a flexible platform for commercial scale production of low-carbon-fuels and chemicals from waste and renewable feedstocks. Front Microbiol 7:694
39. Daniell J, Nagaraju S, Burton F, Köpke M, Simpson SD (2016) Low-carbon fuel and chemical production by anaerobic gas fermentation. Adv Biochem Eng Biotechnol 156:293–321
40. Dürre P (2005) Formation of solvents in clostridia. In: Dürre P (ed) Handbook on Clostridia. CRC Press-Taylor and Francis Group, Boca Raton, USA, pp 671–693
41. Naik SN, Goud VV, Rout PK, Dalai AK (2010) Production of first and second generation biofuels: A comprehensive review. Renew Sust Energ Rev 14:578–597
42. Ajanovic A (2011) Biofuels versus food production: Does biofuels production increase food prices? Energy 36:2070–2076
43. Armaroli N, Balzani V (2011) The hydrogen issue. Chem Sus Chem 4:21–36
44. Brandon NP, Kurban Z (2017) Clean energy and the hydrogen economy. Philos Trans Royal Soc A 375:20160400
45. Balch WE, Schoberth S, Tanner RS, Wolfe RS (1977) *Acetobacterium*, a new genus of hydrogen-oxidizing, carbon dioxide-reducing, anaerobic bacteria. Int J Syst Bact 27:355–361
46. Demler M, Weuster-Botz D (2010) Reaction engineering analysis of hydrogenotrophic production of acetic acid by *Acetobacterium woodii*. Biotechnol Bioeng 108:470–474

47. Karekar SC, Srinivas K, Ahring BK (2019) Kinetic study on heterotrophic growth of *Acetobacterium woodii* on lignocellulosic substrates for acetic acid production. Fermentation 5:17
48. Suzuki T, Matsuo T, Ohtaguchi K, Koide K (1993) Continuous production of acetic acid from CO_2 in repeated-batch cultures using flocculated cells of *Acetobacterium woodii*. J Chem Eng Jpn 26:459–462
49. Wang WH, Himeda Y, Muckerman JT, Manbeck GF, Fujita E (2015) CO_2 hydrogenation to formate and methanol as an alternative to photo- and electrochemical CO_2 reduction. Chem Rev 115:12936–12973
50. Preuster P, Papp C, Wasserscheid P (2017) Liquid organic hydrogen carriers (LOHCs): toward a hydrogen-free hydrogen economy. Acc Chem Res 50:74–85
51. Eppinger J, Huang KW (2017) Formic acid as a hydrogen energy carrier. ACS Energy Lett 2:188–195
52. Jeletic MS, Mock MT, Appel AM, Linehan JC (2013) A cobalt-based catalyst for the hydrogenation of CO_2 under ambient conditions. J Am Chem Soc 135:11533–11536
53. Hull JF, Himeda Y, Wang WH, Hashiguchi B, Periana R, Szalda DJ, Muckerman JT, Fujita E (2012) Reversible hydrogen storage using CO_2 and a proton-switchable iridium catalyst in aqueous media under mild temperatures and pressures. Nat Chem 4:383–388
54. Ceccaldi P, Schuchmann K, Müller V, Elliott SJ (2017) The hydrogen dependent CO_2 reductase: the first completely CO tolerant FeFe-hydrogenase. Energy Environ Sci 10:503–508
55. Baffert C, Bertini L, Lautier T, Greco C, Sybirna K, Ezanno P, Etienne E, Soucaille P, Bertrand P, Bottin H, Meynial-Salles I, De Gioia L, Leger C (2011) CO disrupts the reduced H-cluster of FeFe hydrogenase. A combined DFT and protein film voltammetry study. J Am Chem Soc 133:2096–2099
56. Foster CE, Kramer T, Wait AF, Parkin A, Jennings DP, Happe T, McGrady JE, Armstrong FA (2012) Inhibition of [FeFe]-hydrogenases by formaldehyde and wider mechanistic implications for biohydrogen activation. J Am Chem Soc 134:7553–7557
57. Goldet G, Brandmayr C, Stripp ST, Happe T, Cavazza C, Fontecilla-Camps JC, Armstrong FA (2009) Electrochemical kinetic investigations of the reactions of [FeFe]-hydrogenases with carbon monoxide and oxygen: comparing the importance of gas tunnels and active-site electronic/redox effects. J Am Chem Soc 131:14979–14989
58. Peters V, Janssen PH, Conrad R (1999) Transient production of formate during chemolithotrophic growth of anaerobic microorganisms on hydrogen. Curr Microbiol 38:285–289
59. Schmidt S, Biegel E, Müller V (2009) The ins and outs of Na^+ bioenergetics in *Acetobacterium woodii*. Biochim Biophys Acta 1787:691–696
60. Biegel E, Schmidt S, González JM, Müller V (2011) Biochemistry, evolution and physiological function of the Rnf complex, a novel ion-motive electron transport complex in prokaryotes. Cell Mol Life Sci 68:613–634
61. Hess V, Schuchmann K, Müller V (2013) The ferredoxin:NAD^+ oxidoreductase (Rnf) from the acetogen *Acetobacterium woodii* requires Na^+ and is reversibly coupled to the membrane potential. J Biol Chem 288:31496–31502
62. Westphal L, Wiechmann A, Baker J, Minton NP, Müller V (2018) The Rnf complex is an energy coupled transhydrogenase essential to reversibly link cellular NADH and ferredoxin pools in the acetogen *Acetobacterium woodii*. J Bacteriol 200:e00357-e318
63. Fritz M, Müller V (2007) An intermediate step in the evolution of ATPases - the F_1F_O-ATPase from *Acetobacterium woodii* contains F-type and V-type rotor subunits and is capable of ATP synthesis. FEBS J 274:3421–3428
64. Fritz M, Klyszejko AL, Morgner N, Vonck J, Brutschy B, Müller DJ, Meier T, Müller V (2008) An intermediate step in the evolution of ATPases: a hybrid F_1F_O rotor in a bacterial Na^+ F_1F_O ATP synthase. FEBS J 275:1999–2007

65. Amao Y (2008) Photoinduced biohydrogen production from biomass. Int J Mol Sci 9:1156–1172
66. Ergal I, Fuchs W, Hasibar B, Thallinger B, Bochmann G, Rittmann SKMR (2018) The physiology and biotechnology of dark fermentative biohydrogen production. Biotechnol Adv 36:2165–2186
67. Kottenhahn P, Schuchmann K, Müller V (2018) Efficient whole cell biocatalyst for formate-based hydrogen production. Biotechnol Biofuels 11:93
68. Rittmann S, Herwig C (2012) A comprehensive and quantitative review of dark fermentative biohydrogen production. Microb Cell Fact 11:115
69. Rittmann SK, Lee HS, Lim JK, Kim TW, Lee JH, Kang SG (2015) One-carbon substrate-based biohydrogen production: microbes, mechanism, and productivity. Biotechnol Adv 33:165–177
70. Weghoff MC, Müller V (2016) CO metabolism in the thermophilic acetogen *Thermoanaerobacter kivui*. Appl Environ Microbiol 82:2312–2319
71. Bertsch J, Müller V (2015a) CO metabolism in the acetogen *Acetobacterium woodii*. Appl Environ Microbiol 81:5949–5956
72. Bertsch J, Müller V (2015b) Bioenergetic constraints for conversion of syngas to biofuels in acetogenic bacteria. Biotechnol Biofuels 8:210
73. Taylor MP, Eley KL, Martin S, Tuffin MI, Burton SG, Cowan DA (2009) Thermophilic ethanologenesis: future prospects for second-generation bioethanol production. Trends Biotechnol 27:398–405
74. Schwarz FM, Müller V (2020) Whole-cell biocatalysis for hydrogen storage and syngas conversion to formate using a thermophilic acetogen. Biotechnol Biofuels 13:32
75. Jung HC, Lee SH, Lee SM, An YJ, Lee JH, Lee HS, Kang SG (2017) Adaptive evolution of a hyperthermophilic archaeon pinpoints a formate transporter as a critical factor for the growth enhancement on formate. Sci Rep 7:6124
76. Lim JK, Bae SS, Kim TW, Lee JH, Lee HS, Kang SG (2012) Thermodynamics of formate-oxidizing metabolism and implications for H_2 production. Appl Environ Microbiol 78:7393–7397
77. Kim YJ, Lee HS, Kim ES, Bae SS, Lim JK, Matsumi R, Lebedinsky AV, Sokolova TG, Kozhevnikova DA, Cha SS, Kim SJ, Kwon KK, Imanaka T, Atomi H, Bonch-Osmolovskaya EA, Lee JH, Kang SG (2010) Formate-driven growth coupled with H_2 production. Nature 467:352–355
78. Lim JK, Mayer F, Kang SG, Müller V (2014) Energy conservation by oxidation of formate to carbon dioxide and hydrogen via a sodium ion current in a hyperthermophilic archaeon. Proc Natl Acad Sci USA 111:11497–11502
79. Heffernan JK, Valgepea K, de Souza Pinto Lemgruber R, Casini I, Plan M, Tappel R, Simpson SD, Köpke M, Nielsen LK, Marcellin E (2020) Enhancing CO_2-valorization using *Clostridium autoethanogenum* for sustainable fuel and chemicals production. Front Bioeng Biotechnol 204
80. Abrini J, Naveau H, Nyns EJ (1994) *Clostridium autoethanogenum*, sp. nov., an anaerobic bacterium that produces ethanol from carbon monoxide. Arch Microbiol 161:345–351
81. Köpke M, Mihalcea C, Liew F, Tizard JH, Ali MS, Conolly JJ, Al-Sinawi B, Simpson SD (2011) 2,3-butanediol production by acetogenic bacteria, an alternative route to chemical synthesis, using industrial waste gas. Appl Environ Microbiol 77:5467–5475
82. Abubackar HN, Veiga MC, Kennes C (2015) Carbon monoxide fermentation to ethanol by *Clostridium autoethanogenum* in a bioreactor with no accumulation of acetic acid. Bioresour Technol 186:122–127
83. Mock J, Zheng Y, Müller AP, Ly S, Tran L, Segovia S, Nagaraju S, Köpke M, Dürre P, Thauer RK (2015) Energy conservation associated with ethanol formation from H_2 and CO_2 in *Clostridium autoethanogenum* involving electron bifurcation. J Bacteriol 197:2965–2980
84. Celinska E, Grajek W (2009) Biotechnological production of 2,3-butanediol-Current state and prospects. Biotechnol Adv 27:715–725

85. Xiu Z-L, Zeng A-P (2008) Present state and perspective of downstream processing of biologically produced 1,3-propanediol and 2,3-butanediol. Appl Microbiol Biotechnol 78:917–926
86. Heap JT, Kuehne SA, Ehsaan M, Cartman ST, Cooksley CM, Scott JC, Minton NP (2010) The ClosTron: Mutagenesis in *Clostridium* refined and streamlined. J Microbiol Methods 80:49–55
87. Köpke M, Gerth ML, Maddock DJ, Müller AP, Liew F, Simpson SD, Patrick WM (2014) Reconstruction of an acetogenic 2,3-butanediol pathway involving a novel NADPH-dependent primary-secondary alcohol dehydrogenase. Appl Environ Microbiol 80:3394–3403
88. Liew F, Henstra AM, Köpke M, Winzer K, Simpson SD, Minton NP (2017) Metabolic engineering of *Clostridium autoethanogenum* for selective alcohol production. Metab Eng 40:104–114
89. Phillips JR, Atiyeh HK, Tanner RS, Torres JR, Saxena J, Wilkins MR, Huhnke RL (2015) Butanol and hexanol production in *Clostridium carboxidivorans* syngas fermentation: Medium development and culture techniques. Bioresour Technol 190:114–121
90. Liou JS, Balkwill DL, Drake GR, Tanner RS (2005) *Clostridium carboxidivorans* sp. nov., a solvent-producing Clostridium isolated from an agricultural settling lagoon, and reclassification of the acetogen *Clostridium scatologenes* strain SL1 as *Clostridium drakei* sp. nov. Int J Syst Evol Microbiol 55:2085–2091
91. Shen GJ, Shieh JS, Grethlein AJ, Jain MK, Zeikus JG (1999) Biochemical basis for carbon monoxide tolerance and butanol production by *Butyribacterium methylotrophicum*. Appl Microbiol Biotechnol 51:827–832
92. Maddipati P, Atiyeh HK, Bellmer DD, Huhnke RL (2011) Ethanol production from syngas by *Clostridium* strain P11 using corn steep liquor as a nutrient replacement to yeast extract. Bioresour Technol 102:6494–6501
93. Chang IS, Kim BH, Kim DH, Lovitt RW, Sung HC (1999) Formulation of defined media for carbon monoxide fermentation by *Eubacterium limosum* KIST612 and the growth characteristics of the bacterium. J Biosci Bioeng 88:682–685
94. Dürre P (2016) Butanol formation from gaseous substrates. FEMS Microbiol Lett 363
95. Li F, Hinderberger J, Seedorf H, Zhang J, Buckel W, Thauer RK (2008) Coupled ferredoxin and crotonyl coenzyme A (CoA) reduction with NADH catalyzed by the butyryl-CoA dehydrogenase/Etf complex from *Clostridium kluyveri*. J Bacteriol 190:843–850
96. Jeong J, Bertsch J, Hess V, Choi S, Choi IG, Chang IS, Müller V (2015) Energy conservation model based on genomic and experimental analyses of a carbon monoxide-utilizing, butyrate-forming acetogen, *Eubacterium limosum* KIST612. Appl Environ Microbiol 81:4782–4790
97. Fernández Naveira Á, Veiga M, Kennes C (2017) H-B-E (Hexanol-Butanol-Ethanol) fermentation for the production of higher alcohols from syngas/waste gas. J Chem Technol Biotechnol 92:712–731
98. Ramió-Pujol S, Ganigué R, Bañeras L, Colprim J (2015) Incubation at 25 °C prevents acid crash and enhances alcohol production in *Clostridium carboxidivorans* P7. Bioresour Technol 192:296–303
99. Heap JT, Pennington OJ, Cartman ST, Carter GP, Minton NP (2007) The ClosTron: a universal gene knock-out system for the genus *Clostridium*. J Microbiol Methods 70:452–464
100. Papoutsakis ET (2008) Engineering solventogenic clostridia. Curr Opin Biotechnol 19:420–429
101. Strätz M, Sauer U, Kuhn A, Dürre P (1994) Plasmid transfer into the homoacetogen *Acetobacterium woodii* by electroporation and conjugation. Appl Environ Microbiol 60:1033–1037
102. Schiel-Bengelsdorf B, Dürre P (2012) Pathway engineering and synthetic biology using acetogens. FEBS Lett 586:2191–2198

103. Leang C, Ueki T, Nevin KP, Lovley DR (2013) A genetic system for *Clostridium ljungdahlii*: a chassis for autotrophic production of biocommodities and a model homoacetogen. Appl Environ Microbiol 79:1102–1109
104. Shin J, Kang S, Song Y, Jin S, Lee JS, Lee J-K, Kim DR, Kim SC, Cho S, Cho B-K (2019) Genome engineering of *Eubacterium limosum* using expanded genetic tools and the CRISPR-Cas9 system. ACS Synth Biol 8:2059–2068
105. Basen M, Geiger I, Henke L, Müller V (2018) A genetic system for the thermophilic acetogenic bacterium *Thermoanaerobacter kivui*. Appl Environ Microbiol 84:e02210-02217
106. Banerjee A, Leang C, Ueki T, Nevin KP, Lovley DR (2014) Lactose-inducible system for metabolic engineering of *Clostridium ljungdahlii*. Appl Environ Microbiol 80:2410–2416
107. Hoffmeister S, Gerdom M, Bengelsdorf FR, Linder S, Fluchter S, Oztürk H, Blumke W, May A, Fischer RJ, Bahl H, Dürre P (2016) Acetone production with metabolically engineered strains of *Acetobacterium woodii*. Metab Eng 36:37–47
108. Jones SW, Fast AG, Carlson ED, Wiedel CA, Au J, Antoniewicz MR, Papoutsakis ET, Tracy BP (2016) CO_2 fixation by anaerobic non-photosynthetic mixotrophy for improved carbon conversion. Nat Commun 7:12800
109. Mozejko-Ciesielska J, Kiewisz R (2016) Bacterial polyhydroxyalkanoates: Still fabulous? Microbiol Res 192:271–282
110. Woolston BM, Emerson DF, Currie DH, Stephanopoulos G (2018) Rediverting carbon flux in *Clostridium ljungdahlii* using CRISPR interference (CRISPRi). Metab Eng 48:243–253
111. de Souza Pinto Lemgruber R, Valgepea K, Tappel R, Behrendorff JB, Palfreyman RW, Plan M, Hodson MP, Simpson SD, Nielsen LK, Köpke M, Marcellin E (2019) Systems-level engineering and characterisation of *Clostridium autoethanogenum* through heterologous production of poly-3-hydroxybutyrate (PHB). Metab Eng 53:14–23
112. Flüchter S, Follonier S, Schiel-Bengelsdorf B, Bengelsdorf FR, Zinn M, Dürre P (2019) Anaerobic production of poly(3-hydroxybutyrate) and its precursor 3-hydroxybutyrate from synthesis gas by autotrophic clostridia. Biomacromol 20:3271–3282
113. Worden RM, Grethlein AJ, Jain MK, Datta R (1991) Production of butanol and ethanol from synthesis gas *via* fermentation. Fuel 70:615–619
114. Lynd LH, Kerby R, Zeikus JG (1982) Carbon monoxide metabolism of the methylotrophic acidogen *Butyribacterium methylotrophicum*. J Bacteriol 149:255–263
115. Lynd LH, Zeikus JG (1983) Metabolism of H_2-CO_2, methanol, and glucose by *Butyribacterium methylotrophicum*. J Bacteriol 153:1415–1423
116. Zahn JA, Saxena J (2011) Novel ethanologenic species *Clostridium coskatii*. US Patent 8143037
117. Tanner RS, Miller LM, Yang D (1993) *Clostridium ljungdahlii* sp. nov., an acetogenic species in clostridial rRNA homology Group-I. Int J Syst Bact 43:232–236
118. Daniel SL, Hsu T, Dean SI, Drake HL (1990) Characterization of the H_2-dependent and CO-dependent chemolithotrophic potentials of the acetogens *Clostridium thermoaceticum* and *Acetogenium kivui*. J Bacteriol 172:4464–4471
119. Leigh JA, Mayer F, Wolfe RS (1981) *Acetogenium kivui*, a new thermophilic hydrogen-oxidizing, acetogenic bacterium. Arch Microbiol 129:275–280

Nitrogen, Too Much of a Vital Resource

Nitrogen Footprints and the Role of Soil Enzymes

Claudia M. d. S. Cordovil, Joana Marinheiro, João Serra, Soraia Cruz, Eve Palmer, Kevin Hicks, and Jan-Willem Erisman

Abstract

In a climate change scenario soil microbial population is affected by the impacts on soil biotic and abiotic factors, with a strong influence on soil microorganisms affecting enzyme production and activity. This influences soil organic matter turnover and nutrient cycling in soil. Nitrogen is one of the most, if not the most important, nutrient for all living organisms. Besides its vital role in maintenance of life on Earth and need to maintain nitrogen availability to produce enough food for the world population, nitrogen losses into the environment cause negative effects in all environmental compartments. To quantify the impact of each individual contribution to nitrogen pollution a concept of nitrogen-footprint was created, to measure nitrogen lost as a result of food and energy consumption. Enzymes play a role in the response of soils to nitrogen pollution and the mitigation and adaptation to climate change effects on nitrogen-footprint. Enzymes are affected by abiotic factors alterations driven by climate change but may alter their activity as a result of human actions, e.g. agricultural

C. M. d. S.Cordovil (✉) · J. Marinheiro · J. Serra · S. Cruz
Centro de Estudos Florestais (CEF), Instituto Superior de Agronomia, Universidade de Lisboa, Tapada da Ajuda, Lisboa, Portugal
e-mail: cms@isa.ulisboa.pt

E. Palmer · K. Hicks
Department of Environment and Geography, Stockholm Environment Institute, University of York, York, UK

J.-W. Erisman
Louis Bolk Institute, Bunnik, The Netherlands

University Leiden, Van Steenis, Einsteinweg 2, 2333 CC Leiden, P.O.Box 9500, 2300 RA Leiden, The Netherlands

J. J. G. Moura et al. (eds.), *Enzymes for Solving Humankind's Problems*,
https://doi.org/10.1007/978-3-030-58315-6_5

management practices affecting microbial populations. Enzymes may thus be a vehicle of both increase and reduction of nitrogen availability and therefore impact on nitrogen-footprint in a positive or negative way.

Keywords

Enzymes · Footprint · Nitrogen · Soil

1 Introduction

This chapter looks at the role that soil enzymes may play in determining Nitrogen (N) Footprints. Climate change and increased global demand for food and energy are consequences of an exponential growth in the world population. The need to produce more food requires greater agricultural production which will necessarily mean higher nutrient availability requirements. Future global food demand can be met by continuing the on-going agricultural intensification and the reliance on inorganic fertilizers or alternatively through an Input–Output optimization at the farm level to increase N use efficiency (NUE). Different production paradigms have different implications in terms of N management (and N pollution) for a nutrient that indispensable for food production [1]. Furthermore, there are other pathways of N management between where N is used in food production and eventually appears "on the table" (e.g. transportation, energy production, wastewater treatment) [2]. While meeting food demand by intensifying agriculture and using more fertilizers, N pollution will also continue to increase unless action is taken to reduce losses to the environment. Although nitrogen is indispensable for food production, N losses lead to a series of negative impacts on human and environmental health. The N-footprint concept was created in 2011 as a tool to allow individuals and institutions to understand how their personal behaviour influences N losses to the environment. The quantification of the N lost as a result of food and energy consumption, as a N-footprint, allows us to take action with the objective of reducing N-footprints at different levels, with the ultimate goal of reducing the global amount of reactive N released by human activities. The calculation of N-footprint depends upon the calculation of crop- and country-specific virtual nitrogen factors (VNF) defined as the units of reactive N released to the environment per unit of reactive N consumed in the process [3]. VNFs are specific for each crop and region and the 'Applied N' is only a part of the chain of N losses considered (see example in Fig. 1). Increasing nitrogen use efficiency (NUE) in soils to reduce Applied N losses is a major challenge. For example, estimated N losses from agricultural soils to the environment for the EU28, through gaseous emissions, leaching and runoff, are approximately 50% or greater of the N inputs to agricultural soils (including atmospheric deposition) [4]. The remaining 50% being recovered by crops (field losses associated with imported crops are not considered). Increasing our understanding of the role of enzymes and

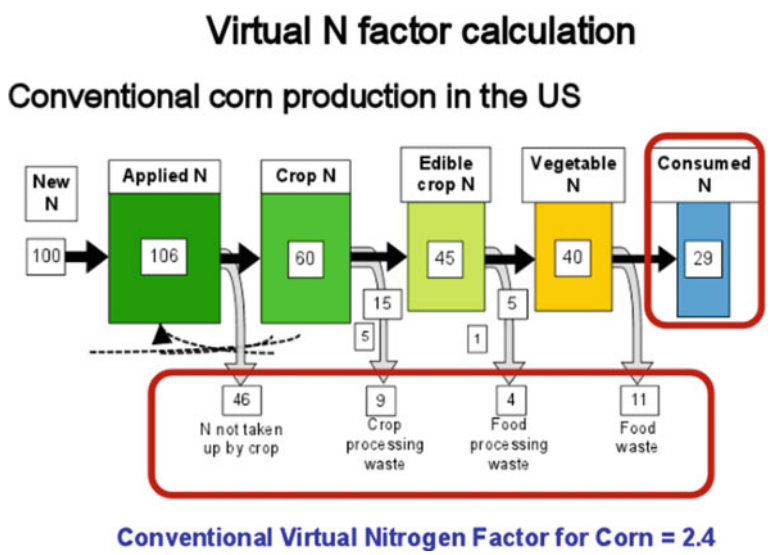

Fig. 1 Virtual nitrogen factor for maize crop in the United States (Leach et al. [3]; www.n-print.org)

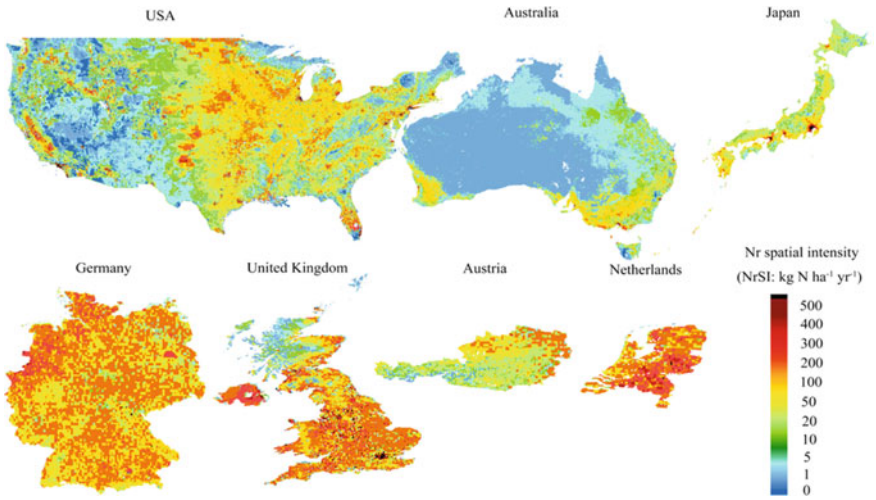

Fig. 2 Spatial variation of the anthropogenic N losses in different countries [5]

how they influence NUE and subsequent N losses to the environment is therefore essential. The spatial variation of the total anthropogenic N released to the environment following the N footprint [5] is shown in Fig. 2.

There are no current estimates given for the impacts of climate change, and enzymatic activity, on the N footprint but a simple theoretical framework can be developed based on the literature available.

2 Soil Quality, Nutrients and Crop Production

Soil quality is key to sustaining crop production in a context where the population is expected to increase up to 9.7 billion in 2050. Although soil quality is a decisive factor to ensure nutrient supply for plants' growth, current trends of soil use have led to soil quality decline, compromising soil capacity to produce enough food. Indeed, since the green revolution and the increased use of inorganic fertilizers for crop growth, it has been estimated that an exponential increase in crop production has allowed half of the world's population to be alive today [6]. The necessary increase in food production cannot be maintained for much longer due to its impactful environmental costs through the excessive mining of soil organic matter (SOM) and other nutrients from the soil, in addition to those supplied by fertilizers and by chemical pesticides to suppress diseases. Additionally, the impact of climate change in agriculture is still uncertain but already noticeable in different regions of the world through extremes in rainfall and drought. The increase in crop productivity is declining and the need for inorganic fertilizer is increasing accordingly, misleading farmers to believe that over-applying fertilizers enhance yields proportionally, thereby further decreasing the soil biological quality. The decline of soil organic matter content reduces the nutrient transformation from SOM mineralization and therefore the availability of plant nutrients in the soil solution [7]. For example, the release of N taking place during SOM breakdown and subsequent transformations are a critical part of the nitrogen (N) cycle in soil [8]. On the contrary, over-application of inorganic fertilizers leads to soil contamination, e.g. phosphorus, and water contamination or nitrate excess to the demand of plant and soil biota. Furthermore, reduction in SOM leads to poor water retention in soils enhancing the susceptibility to drought. So, for sustainable crop production today's agriculture requires appropriate management of nutrients including good soil management (light weight machinery, reduction of pesticides, crop rotation systems including grain and nitrogen fixers) and in addition the right application rate, timing, type of fertilizer and mode of application vis-a-vis plant and soil biota requirements, bearing in mind that nutrient availability is affected by climatic conditions and soil physical, chemical, and biological properties, including the effects of root exudates in the soil [9].

3 Relevance of Enzymes in Soils

Soil fertility depends upon three different but interacting components: chemical, physical and biological. Soil biological fertility regulates many functions that are beneficial to plant production: (i) releasing nutrients from soil organic matter

(SOM) (microorganisms, enzymes), (ii) fixing atmospheric N (rhizobia, bradyrhizobia), (iii) increasing phosphorus availability (mycorrhizal fungi), (iv) degrading pesticides (microorganisms, enzymes), v) controlling pathogens (microorganisms) and (vi) improving soil structure (bacteria, fungi). Soil enzymes have a major biogeochemical significance because they catalyze most of the reactions in soil chemistry processes (Fig. 3). More than 100 enzymes have been characterized in soils and are responsible for catalyzing reactions occurring in these ecosystems. Studying enzyme activity in soils is, therefore, a useful tool to assess soil functional state in environmental and ecosystem management, because any changes in soil properties will alter the activity of soil organisms and their species composition and biodiversity, including that of enzymes. In fact, enzymes play an important role in soil health as they carry out an array of crucial functions, e.g. decomposition of organic matter, production of inorganic nutrients for plant growth, nitrification, denitrification, detoxification of xenobiotics. They also have a crucial role in the biochemical cycles of essential nutrients such as C, N, P and S [10]. So, the

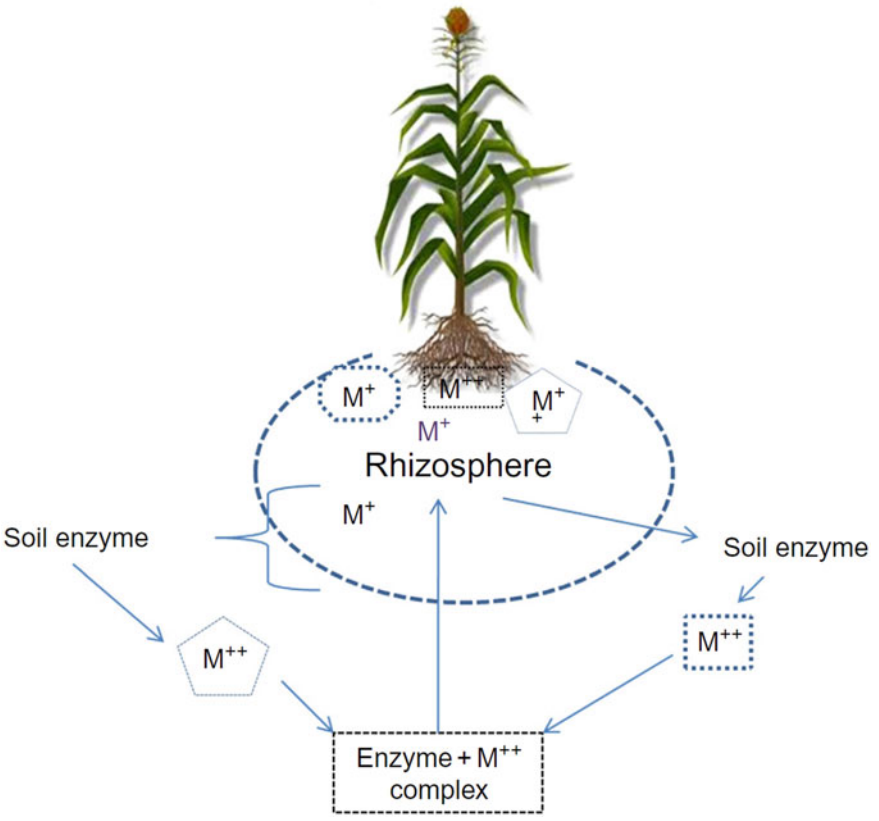

Fig. 3 Role of soil enzyme in plant nutrient dynamics [12]

management of soil enzymes can provide valuable information on microbial community functions in space and time, related to the understanding key nutrient cycles, such as nitrogen. However, only small amounts of enzymes can be directly extracted from soils, so, enzymes are mainly studied through the observation of their respective activity, which may vary with edapho-climatic conditions [11]. Seasonal variation affects microbial community responses to the environment, enzymes decrease vertically from the soil surface, vary according to microbial community distribution and also at landscape level, soil type being a major controlling factor (especially regarding soil texture and SOM content) together with soil management.

Furthermore, soil type is also a major controlling factor, particularly soil texture and SOM content. Changes in soil use and soil quality due to management affect several enzymes long before changes in soil organic matter levels can be detected [12]. This gives enzyme studies a high potential as a suitable tool for sustainable ecosystem management in the long-term. Therefore, besides the potential to anticipate soil quality depletion, enzymatic studies may show the level of degradation of highly disturbed soils and recovery in reclaimed landscapes.

Enzymes can exist on viable cells either internally or on membranes surface, but they can also be excreted into soil solution and may be found in the soil matrix and in microbial debris. Except for the case of Error! Reference source not found and a few other enzymes that exist only in viable cells, most of the other soil enzymes can be found either in viable or in complexed forms, independent of viable cells, and stabilized in the soil matrix [11]. Extracellular enzymes or exoenzymes, are secreted by cells and have the main role of hydrolyzing substrates that are too large or insoluble to be directly absorbed by microbial cells of some communities. They maybe secreted by bacteria and fungi as well and, in this case, may be used in environmental bioremediation, the ones producing hydrolases being especially useful [13]. When enzymes are found in stabilized forms on colloid surfaces and incorporated into soils, a degree of degradation of certain contaminants has been observed in soils. In fact, *enzyme activity* measurements are used as useful tools to assess certain heavy metals bioavailability in soils. Moreover, enzymes catalyze and take part in metabolism processes connected to SOM and to energy processing in soils. Therefore, the use of indicators for evaluating soil microbial diversity *and* microorganism's activity is key to understanding soil dynamics and fertility.

In summary, soil enzymes are vital not only to maintain soil fertility and health, but also to protect the environment by degrading pollutant molecules [14].

4 How Enzymes Influence Nitrogen Availability in Soils

The most important soil enzymes belong to three different classes: oxidoreductase, hydrolase, and lyase. Many of them are directly involved in the processes regulating the nitrogen cycle. Dehydrogenase (DHA) belongs to the oxidoreductase class that also includes laccases and all enzymes involved in the oxidation of different

substrates (e.g. those involved in oxidative degradation of toxic organic pollutants). DHA mediates the transfer of hydrogen atoms from organic compounds, accompanied by energy generation. DHAs are present in all microorganisms and do not exist as extracellular enzymes, being specific for different substrates. The DHA activity in the soil reflects the total oxidative metabolic capacity of microbes, being considered as a good indicator of soil biological activity [15]. DHA intervenes in the oxidation of SOM by mediating proton and electron transfer from organic matter to suitable inorganic acceptors. These enzymes are affected by soil type, moisture content, and the redox state (aeration) in the soil [12].

The dominant class of extracellular enzymes found in the soils is the hydrolase class [12]. These hydrolytic enzymes are involved in the breakdown of macromolecules to obtain smaller forms utilisable by plants and microbes but are also responsible for mediating the removal of inorganic groups or ions to allow the release of the inorganic available forms [12]. This class includes amidases, amylases, cellulases, glucosidases, phosphoesterases, sulfatases and ureases.

Lyase enzymes act without hydrolysis and mediate the removal of certain chemical species breaking covalent bonds. These enzymes include ammonia lyases, decarboxylases and dehydratases. Ammonia lyases are the most important enzymes in this class as they deaminate amino acids. Enzymes representing other classes are not so common in the soil environment and less important from the ecological point of view.

Proteases are important enzymes that act in the mineralization of organic N in soil playing a vital role in maintaining the ecosystem function and in ensuring N nutrition for plant growth. Because it is an extracellular enzyme, it is linked to both organic and inorganic colloidal substances in soil. Protease degrades protein to release short peptides through hydrolyzation of the peptide bonds. If proteins are further degraded, amino acids are released and act as N sources for the soil microbes. Amino acids may be taken up by the microbes or may be further mineralized to release ammonia for plant N nutrition [16–18].

Urease is another enzyme affecting N balance in soils and can be found both in extra and in intracellular forms in the microorganisms [16]. These enzymes are released by almost all the soil microbial groups, including fungi, bacteria, algae, yeast and even some plants roots, and have as main role to hydrolyse urea into ammonium and carbon dioxide. N dynamics are influenced by urease as it increases the ammoniacal nitrogen concentration in soils. If not taken up by the plants ammonium release leads to soil pH increase after urea fertilization, and is also volatilized as ammonia, hence negatively impacting air quality and reducing the nitrogen use efficiency (NUE) of fertilizers. The use of polymer-coated urea reduces the effect of soil urease, hence reducing N losses while increasing NUE (e.g. as now widely practiced in India—Neem coating).

β-glucosidase activity, one of the most common enzymes in soils [19], plays a key role in the breakdown of low molecular weight carbohydrates of SOM, which is strongly related to the carbon cycle in soils and the products of its enzymatic activity supplies energy to soil microorganisms. Since these enzymes are proteins and therefore very sensitive to both anthropogenic and natural variable factors,

monitoring their activity is a helpful tool to assess soil quality. This is particularly true in soils subjected to mixed organic and/or mineral fertilization included in different crop rotations [20].

Nitrogenase also plays an important role in the N cycle as it is a metalloenzyme responsible for catalyzing atmospheric nitrogen fixation, by ensuring the reduction of di-nitrogen (N_2) to ammonia (NH_3) which is a vital process for all forms of life on Earth.

Soil fertility is based on intense enzymatic and *microbial activity* and on metabolic diversity of *microorganisms*. SOM mineralization and transformation of nutrients are brought about by the microbial enzymes, both extracellular secreted enzymes as well as endogenous enzymes of microbial cells [12] (Fig. 4). Extracellular enzymes are secreted into the soil environment where they intervene in the decomposition or in the transformation of the organic and inorganic nutrient forms into plant available

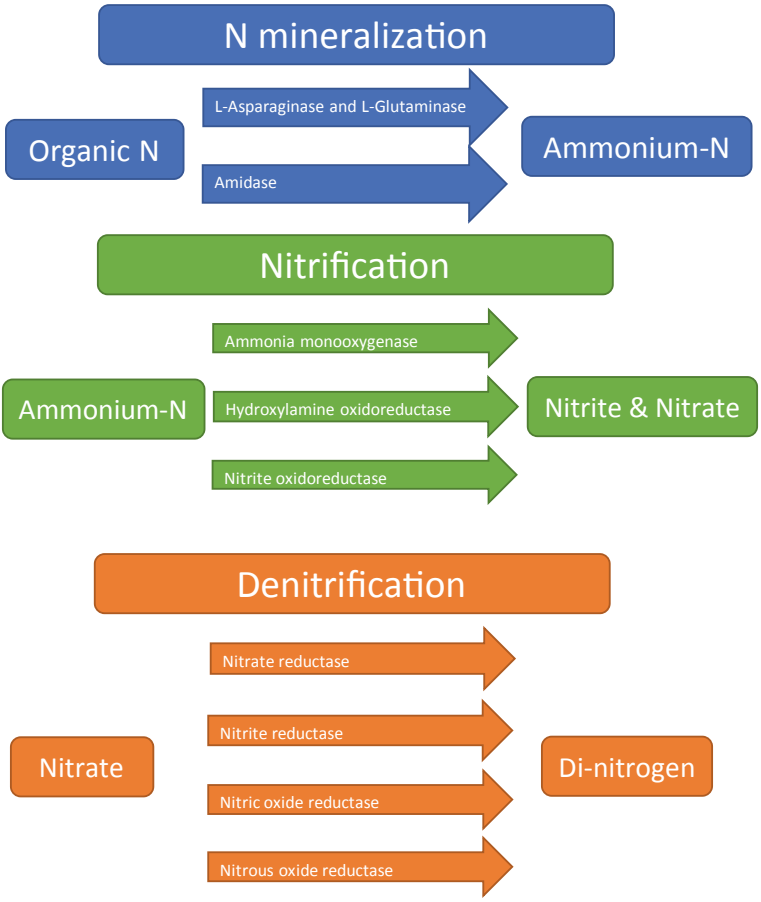

Fig. 4 Enzymes involved in the main nitrogen transformation processes in soils

forms [12]. During field application, the ammonia contained in inorganic fertilizers and animal manures is rapidly hydrolysed to the ammonium (NH_4^+) ion, ammonium compounds or nitrate (NO_3^-). This serves as a direct pathway for crop nutrient uptake, while organic amendments and SOM breakdown require depolymerization by extracellular enzymes and microbes to enhance N availability [21].

5 Soil Characteristics Influencing Enzymatic Activity

Changes in soil's physio-chemical characteristics, mostly as a result of land-use change, vegetation type and microbial status of the soil, produce a strong effect on enzymes, proving their high sensitivity to such parameters. Each soil enzyme has a specific range of pH for optimum activity at which enzymes are more stable. On the contrary, as pH deviates from optimal values, enzyme activity is reduced until becoming inactive at extremely high or low pH values where irreversible denaturation occurs. Changes in the soil concentration of H^+ ions (protons) have a strong influence on enzyme dynamics, influencing substrate degradation and acting as a co-factor in nutrients ionization and solubility properties [22]. Although this is generally true, the influence of pH in enzymatic activity is enzyme-specific and the degree of pH sensitivity is variable. For example, optimum pH for β-glucosidase is 6.0 while for urease it is 7.0 [23].

Drying and rewetting cycles in soil also affect enzyme activity to variable degrees. For example, β-glucosidase activity is reduced in dry soils showing that lower soil moisture content greatly reduces the activity of extracellular enzymes produced by microbes associated with the breakdown of SOM. The release of glucose during SOM decomposition influences the growth of soil microorganisms since glucose is the preferred carbon source for many of them [12]. β-glucosidase activity serves as one of the best predictors for evaluating the effect of crop management practices on soil health and soil quality changes. Dry conditions promote the adsorption of enzymes onto mineral surfaces where their activity is reduced as well as their access to SOM substrate. Besides reducing β-glucosidase activity, this can also reduce other enzymes rate of degradation and therefore their contribution to SOM breakdown following the next rainfall [19]. As soils dry, solutes in the water are concentrated, leading to increasingly negative osmotic potential between the inside and outside of microbes. As a response to this stress, many microbes will accumulate electrolytes and organic solutes to balance osmotic and matric potentials, which in turn may slow down the activity of enzymes within the organisms [24].

Generally, enzyme activity increases with increasing temperature, doubling the reaction rate about every 10 °C. However, beyond the enzyme-specific threshold enzymatic activity decreases drastically and becomes inactivated at high temperature. Moreover, the temperature sensitivity of the different enzymes, and thus the dynamics of nitrogen and carbon mineralization, are not the same and may be influenced by climate change in different ways [25]. As for pH, the sensitivity of enzymes to temperature varies with enzyme type and source.

6 Effect of Agricultural Management Practices (e.g. Tillage, Organic Fertilization)

Agricultural management practices and soil enzymatic activity are closely linked. On one hand, agricultural systems benefit from higher soil enzymatic activity due to an improved land management responsiveness. On the other hand, monoculture-based systems limit inter-species interactions, and thus bacteria associations, since these are influenced by root exudate components that vary in type and quantity according to different crop species [26]. Crop rotations, no-tillage, organic amendments, the use of low weight machinery and cover crops are some Conservation Agricultural (CA) practices known to favour enzyme activity [27]. A meta-analysis of 62 studies demonstrated that no till or reduced tillage promotes large microbial communities and greater enzymatic activity [28], although further study is necessary to understand the long-term (>10 years) impact on the microbial communities under CA, e.g. [28] stated till and no-till microbial activity show similar results after a 10 year period.

Tillage is performed to increase the aeration of the topsoil and provide weed control. However, conventional tillage techniques can result in soil compaction due to heavy machinery [29], which alters soil vertical structure, reducing soil organic matter, plant nutrient availability over time and microbial biomass [30]. In fact, soil compaction leads to a change in the soil atmosphere which may have negative effects on soil biological activity that, in turn, will affect soil physical properties. Therefore, plant growth may be repressed due to the negative effects on plant roots, because aeration characteristics of soil and its effects on plant growth depends mostly on the composition of air in the soil [31]. Curci et al. [32] studied the influence of tillage (shallow ploughing, deep ploughing and scarification) on enzyme activity and concluded the enzymes β-glucosidase, galactosidase, nitrate reductase and dehydrogenase were all affected negatively by tillage. These enzymes have different soil functions and different pressure responses: glucosidase activities—responsible for the hydrolysis of plant biomass—are inhibited in the presence of heavy metals (e.g. copper [33]) and when there is soil acidification; dehydrogenase activities are highly influenced by pesticides, remaining low when high doses of pesticides are traced [34]. Conversely, no-till coupled with the incorporation of crop residues increases microbial biomass as a response to an increase in SOM [32, 35, 36]. Urease is also influenced by tillage activities as it is highly influenced by SOM content. Urease catalyzes the hydrolysis of urea into carbon dioxide and ammonia and is commonly used for soil quality evaluation versus its respective management [37, 38], although enzyme activity performance is also dependent on environmental factors such as, pH, oxido-reduction potential and, in particular, temperature and moisture [39].

Crop monoculture can lead to an imbalance in the main enzymes which has a negative impact on soil function [23] subsequently causing a decline in soil quality [40]. Microbial and biochemical analyses of soil under winter wheat in a field trial with various cultivation systems (organic, conventional and monoculture) were performed during three growing seasons [41]. The activities of the tested enzymes

(dehydrogenase and phosphatases) and microbial biomass C and N contents in the monoculture soil were generally significantly lower than those in the soil from the organic and conventional–short rotation systems, indicating that substantial disturbances may occur in the microbial activity of the monoculture soil. Crop rotations are an efficient measure to enhance microbial diversity in the rhizosphere, increase soil organic carbon (SOC), total nitrogen (TN) and build up resistance to disturbance and suppress root diseases [41, 42]. Cover cropping can be a useful approach to improve diversification of soil microbial communities whether through a form of rotation diversification or through its cover crop residues [30, 43]. Indeed, [44] reported an increase in soil enzymatic activity around 20% in soils with a cover crop mixture of oat/radish/vetch, with increases also in soil C and N storage. Pasture rotated with well- managed crops can also increase enzyme activity in soil because overgrazing leads to a decrease in soil microbial biomass [45].

Irrigation, aside from its primary function, helps to determine the enzymatic activity of the soil with regard to dry conditions which limit the decomposition rate and therefore microbial biomass. Protease and urease—N-cycling enzymes—seem to be the most affected by drought [46].

It is widely reported that using organic fertilizers such as manure promotes enzyme activity. In soils that are organically farmed crop residues and rhizodeposits support higher microbial biomass, leading to enhanced enzyme activities [47]. For example, it was found that enzyme activity associated with C, N and S cycling were higher under organic farming practises compared to conventional farming [47]. More specifically, [48] demonstrated that activities of soil β-1,4-glucosidase, β-1,4-*N*-acetylglucosaminidase, and leucine aminopeptidase increased with manure application. Application of chemical fertilizers such as phosphorus and N negatively affects microbial activity, particularly with long term use [48]. For example, nitrogen application may negatively affect enzyme activity, such as nitrogenase. Nitrogenase activity provides N to the soil, through catalyzing N_2 fixation from the atmosphere into two molecules of NH_3—also known as biological nitrogen fixation and [49] recorded higher activity of this enzyme with no urea-N application and inhibition of *Stenotrophomonas* sp. population (significantly important for nitrogen and sulphur cycle) with an application of 300 mg L^{-1} urea-N. The way nitrogen-based fertilizer affect nitrifying bacteria might be associated not only to the cultivar, but also to its age and to the diazotrophs present in the environment [50]. Diazotrophs are Plant- Growth-Promoting Rhizobacteria or PGPR [51, 52], although they can colonize the interior of plants (xylem vessels and intercellular spaces) where the potential for nitrogenase activity increases [52].

7 Relation of Enzymes with N and C Cycles

Soil enzymatic activity plays a major role in key processes related to the quality of SOM which, in turn, influences the efficiency of microbial nutrient assimilation since carbon is required in microbial metabolism [54]. Moreover, soil enzymatic

activity can impact the availability and/or storage of C and N in SOM pools. Because a lot of the enzymatic activity occurs in the rhizosphere from associations between soil microorganisms and root exudates (plant-soil interaction) enzymes may be used as a proxy for potential plant growth and for nutrient availability [55], especially for nitrogen. While this may not directly promote crop nutrient uptake and thus, crop growth, it does so indirectly by improving the availability of soil microorganisms that play a key role in nutrient availability for plant nutrition. These degrade complex organic carbon compounds to release simple utilizable C compounds for microorganisms' survival and growth (e.g. sugars, organic acids). Moreover, the enzymes involved in nutrient (e.g. N, P and S) cycle processes, mineralize organic compounds of the respective nutrients into inorganic compounds, which can be readily used by microorganisms and plants. The influence of soil enzymatic activity in soil nutrient cycling is a relatively well-researched topic (e.g. [56–59]). By playing a vital role in initiating and maintaining nutrient biogeochemical cycles, enzymes play a vital role and ensure soil fertility for plants development [60, 61]. Enzyme activity is more intense in the rhizosphere than in the bulk soil due to the direct contact with plant roots and influence of root exudates, as well as with bacteria and mycorrhiza. The rhizosphere is a uniquely rich environment where enzymes and microorganisms mediate the biogeochemistry of minerals and better nourish the soil–plant ecosystems [62].

8 The Importance of Nitrogen Fertilization

Nitrogen (N) is the most important of nutrients within the structural and functional molecules that make up the plant structure, and is also essential for the *biosynthesis* of structural *molecules* such as the *nucleotides* and *amino acids* that are building blocks for plants, animals and other organisms. Despite this important role of nitrogen, fertilizer application can negatively affect the enzyme activity, such as for nitrogenase, that catalyzes atmospheric N fixation as mentioned before. Similarly, atmospheric deposition of reactive nitrogen reportedly reduces the activity of lignin-modifying enzymes and hence of C decomposition, which positively affects terrestrial C sequestration [63]. While ligninase activity increases in soils with low SOM quality under nutrient deficiencies, its activity is progressively reduced as nutrient deficiency is replenished [64]. By contrast, cellulase activity derived from N deposition was reported by [63] not to correlate with changes in soil C stocks.

One of the main anthropogenic factors affecting soil enzymatic activity is both organic and mineral fertilization that has a crucial influence on soil biological status and the enzymatic activity in soils. The application of organic fertilizers such as farmyard manure, has a positive effect by increasing organic C and N concentrations in soil and affects the quality and quantity of SOM. On the contrary, if manure is too rich in inorganic N (NH_4^+), it may promote immobilization and N losses and have a negative effect. Data shows that the impact of agricultural nutrient management practices on enzyme activity depends on the type of fertilizer (i.e.

inorganic and organic), (in)organic N content, application rate and mulching materials [65]. For instance, the application of N fertilizer and leaf mulching has significantly increased the activities of dehydrogenase and *β-glucosidase* [66]. Soil mulched with white clover and crown vetch also considerably increases the activity of soil urease, invertase and alkaline phosphatase [67, 68] observed a higher enzymatic activity from mulching when compared to mulched no-till treatments, which is a typical practice of conservation agriculture, particularly popular in drylands. Additionally, mulching can enhance enzyme activity when coupled with earthworms during rice and wheat cropping systems [68] and under bare soil [69], soil compaction [70] which can negatively impact nutrient availability and crop production [71]. Indeed, soil compaction can be arguably more important than N fertilization regarding soil enzymatic activity [29]. Red clover mulches and different levels of N fertilization were found to significantly impact the activity of different enzymes (e.g. acid phosphatase, protease) [72]. Furthermore, [20] showed a 10–26% increase in the enzymatic activity when applying lower N fertilization rates to catch crops (40 and 80 kg N ha^{-1} $year^{-1}$), while the opposite was found following the application of poultry organic manures [73, 74] also found higher enzymatic activity following the N fertilization of organic fertilizers compared to inorganic fertilizers. In addition, the application of N fertilizers over longer periods of time positively affects enzyme activity [75].

By contrast, N fertilizers can negatively affect enzyme activity such as nitrogenase. Nitrogenase enhances soil N availability by catalyzing atmospheric biological N fixation. N fertilizers also affect nitrifying bacteria that convert ammonia to nitrate (NO_3^-) according to the cultivar and to the diazotrophs present in the environment [50]. Conversely [77], observed a strong negative effect of L-asparaginase, a *N*-acquiring enzyme, to C-acquiring enzyme (BG) ratio, on total N concentration in an agricultural field previously amended with different fertilization plans. It is therefore worth mentioning that plant production is generally N limited, while soil microorganisms may be carbon (C) or N limited.

9 Climate Change Impact and Mitigation, and Related Effects on Nitrogen Footprint

The most recent concerns about climate change impacts on soil processes, along with a growing depletion of soil quality worldwide have stimulated experimental research towards the development of methods of fighting and adapting to these impacts. Improving carbon sequestration and promoting plant nutrition from bio-based sources have become priorities. In fact, the use of natural processes to restore soil quality while retaining C to decarbonize production, and monetization of microbially mediated soil nutrients resources (e.g. N) are undoubtedly the pathway for environmental recovery.

Changing conditions and reducing resources will lead to promoting adaptation strategies that allow the production of enzymes with a minimum of carbon and nutrient costs for the cell but still obtaining maximum benefits. In this sense, the enzymatic activity will be a result of the efficiency achieved by microorganisms, in terms of spending resources to produce enzymes versus the benefit of increasing the availability of assimilable mineral nutrients, energy sources and low molecular weight organic compounds. While in a climate change scenario, microbial cells face the need to reduce the energy they use to produce enzymes, they must, on the other hand, maintain a sufficiently high concentration of the reaction products to ensure the maintenance of cell function and maintain viability of their populations. The products necessary to guarantee the microbiological functions in the soil and the balance of nutrient cycles, are C and the nutrients (especially nitrogen and phosphorus) necessary to ensure the existence of energy (i.e. ATP) and the synthesis and secretion of enzymes (proteins). Therefore, N is a crucial element to maintain soil functions as well as microbial and plants survival.

Because of climate change, soil temperature is increasing, soil wetting and drying cycles are more frequent and carbon dioxide and other greenhouse gases are increasing in the atmosphere [25]. These abiotic phenomena will have marked effects in the microbial community composition and may increase biomass and enzyme activities, which can occur as a direct effect or as a result of plant growth, increases in litter deposition and root exudation. So, any attempt to mitigate the impacts of global warming in plant production and soil quality must take into account the microbial responses, including soil enzyme activity dynamics.

A good SOM turnover and balanced nutrient cycles greatly depend on enzymatic activity which in turn is dependent on soil conditions such as temperature and water content but are also influenced by enzyme pool size [19]. The rate of enzymes production by soil microbial populations versus the rate of degradation in the environment, determine pool size. Both production and turnover are affected by soil conditions that vary seasonally but are also affected by climate change, that produces temperature, moisture and atmosphere composition alterations. Enzyme production by microbes requires energy and nutrients, and an adequate stoichiometry of their biomass targeting specific C, N or P rich compounds [19]. Besides the mere maintenance of the enzymatic pool, temperature and moisture can affect both the global rate of enzyme production and the relative rate of production of the different enzymes present in soils. This is due to climatic effects on substrate availability for microbes, microbial efficiency and finally on enzyme efficiency. Therefore, whether climate changes affect environmental conditions locally and regardless of the duration and timing of the impacts, it is certain that this will affect enzyme pool sizes and will have an effect on N-footprint of plant production. Whenever the enzymatic activity increases as a consequence of higher soil temperature, in the presence of available substrate for microbes, enzyme production may be reduced if microbial biomass remains unchanged [77]. Different enzymes are differentially affected by temperature thus, climate change is enzyme-specific. Reference [78] observed that N-degrading enzymes have lower temperature sensitivity compared to C-degrading enzymes, which will lead to a higher production

of the former enzymes and consequently reducing N availability. N pool reduction in soils will require heavier fertilization for agricultural production which in turn will increase N-footprint related to crop production. If it is true that the increase in temperature has an immediate effect reducing enzyme activity, it is also true that the continued effect of climate change has a negative impact on the production of enzymes by microorganisms compromising enzyme pools and turnover rates. When enzymes activity is affected by temperature, C degradation will decrease with consequent reduction on C availability for microorganisms that will slow down N availability for plant absorption. On the contrary, as mentioned, N-degrading enzymes will still be active, with cumulative depletion effect on N pool for crop nutrition.

Diffusion of substrates, enzymes and therefore the products of enzyme activity, are affected by soil water availability. So, climate change driven drought conditions will limit diffusion of enzymes and substrates in the soil affecting enzymes contribution to nutrient balances in soils. Indeed, Burns et al. [25] predicted that the reduction of soil moisture would potentially decrease enzyme activity in response to a lower microbial biomass and enzyme production. However, the enzyme pool under drought conditions was stable, which could be explained in two ways: either mass-specific enzyme production was higher under low water availability, or enzyme turnover decreased in dry soils, which was the most probable reason to this observation. The stability of enzymatic processes was not necessarily due to enzyme activity in situ in dry soils, as reported by the same authors. If this is the case, N availability is compromised both for protein production for microbes and for plant nutrition.

Another effect of climate change is the alteration of atmosphere CO_2 content. This may not directly affect microbial activities because CO_2 concentration in soils are naturally much higher than in the atmosphere [24]. However, plant direct responses to elevated CO_2 levels may strongly affect microbial communities due to the changes in plant's metabolism and processes. These may include increased water use efficiency, increased exudation of labile C by roots and a faster nutrient uptake due to a higher plant productivity [25]. Increased rhizodeposition tends to stimulate microbial biomass, therefore increasing potential enzyme production and microbial respiration, although [79] did not observe significant effects of high free air CO_2 presence. CO_2 enrichment is also expected to positively impact nitrogenase activity and biological N fixation by leguminous plants by (i) increasing plant mass/N demand and decreasing soil N availability which limits N fixation and (ii) increased C allocation to root nodules [80, 81]. Whether this is enough to offset the higher need for N fertilization from the reduced soil N availability, with a positive impact in the N footprint by enhancing N recycling rather than through the Haber–Bosch process, remains to be seen.

The greater the knowledge on the degradation of lignin, which constitutes the recalcitrant fraction of SOM, the more evident is the relationship between C and N in the enzymatic processes in the soil, since the distribution of potentially lignin-degrading organisms in soils respond to disturbances associated with anthropic N deposition and climate change [25]. This leads to the assumption that C

sequestration and SOM are important to the maintenance of the equilibrium of C/N in soils, thus benefiting microbial activity and ensuring enough enzymes for nutrient cycling. Indeed, climate warming affects soil carbon (C) dynamics, with possible serious consequences for soil C stocks and atmospheric CO_2 concentrations but, the mechanisms underlying changes in soil C storage are not well understood, hampering long-term predictions of climate C-feedbacks [82]. A meta-analysis has shown that reductions in soil C stocks with warming are associated with increased ratios of ligninase to cellulase activity that can be used to track changes in the predominant C sources of soil microbes and can thus provide mechanistic insights into soil C loss pathways. Results suggest that warming stimulates microbial utilization of recalcitrant C pools, possibly exacerbating long-term climate-C feedbacks [82].

A long-term field manipulation experiment has provided evidence that soil aggregate size independently mediates soil microbial feedbacks to multiple climate change factors [83]. Altered microbial enzyme activities, enzyme stoichiometry, and specific enzyme activities under climate change were mainly consistent across soil aggregate size classes. An exception was that C degrading enzyme activities were greatest where C concentrations were highest, namely in the micro-aggregates. Moreover, climate change increased specific enzyme activities for C decomposition, suggesting positive feedbacks between microbial activities related to SOM decomposition and climate change. The distribution of aggregates within soils is affected by both physical and biological processes, and therefore not only affects microbial function but is also affected by it. Previous studies have found that soil aggregate size exerted strong impacts on soil C dynamics and microbial activity. For example, a study of microbial community profiles and activities among aggregates of winter fallow and cover-cropped soil has shown that microorganisms and their activities can be heterogeneously distributed among soil aggregates, and their distribution may change in response to management practices that affect aggregate [84]. Lack of community differentiation may be due to the frequent mixing of soil during cultivation and tillage events, whereby microbial communities become evenly distributed among soil aggregates.

Gong et al. [85] show the response of soil enzyme activity to warming and nitrogen addition in a meadow steppe. Soil enzyme activity, soil microclimate and soil nutrients were measured to investigate the response of soil enzyme activity to N addition and experimental warming. Warming enhanced phosphatase activity (35.8%) but inhibited the cellulase activity (30%). Nitrogen addition significantly enhanced the activities of urease (34.5%) and phosphatase (33.5%) but had no effect on cellulase activity. Significant interactive effects of warming and N addition on soil enzyme activity were observed. In addition, warming reduced soil C (7.2%) and available P (20.5%), whereas N addition increased soil total N (17.3%) and available N (19.8%) but reduced soil C (7.3%), total P (14.9%) and available P (23.5%). Cellulase and phosphatase activity was highly correlated with soil temperature and water content, whereas urease activity was determined primarily by soil N availability. It is difficult to generalize the effects of warming on enzyme pools, as they are also affected and affect other abiotic factors such as the above

mentioned frequent and intermittent drying of soils, that will originate matric and osmotic stresses with related impact on enzyme composition and activity.

The results show that climate change not only significantly affects soil enzyme activity, but also affects the mineralization of soil nutrients. These findings suggest that global change may alter grassland ecosystem C, N and P cycling by influencing soil enzyme activity.

Despite the current knowledge on enzymes activity, there is still considerable gaps requiring more information to understand the *ecology* and function of extracellular enzymes in soils because of the diversity and complexity of the soil physical and chemical environment and microbial communities. In fact, microbial and enzymatic responses to the effects of climate change are complex because they not only depend on several climatic factors and the relations among them, but are also cumulatively affected by enzymes activity and microbial turnover which in turn are dependent on the formerly mentioned climatic factors. Due to this complexity and missing information, the use of enzyme-based technology requires careful consideration for interpretation and application. This is particularly true when enzymes are used to evaluate soil quality because soil *enzyme activities* should be used in correlation with other key soil measurements. Since enzymes can be independent of soil type, further research on calibrating and interpreting soil enzyme technologies is needed.

10 Conclusion

The amounts of N applied to the soil from different sources are only a part of the chain of N losses considered by the N Footprinting methodology, but they do tend to be one of the larger ones and increasing NUE in soils is a major challenge to reduce these losses. Increasing the understanding of the role of enzymes and how they are affected by the factors listed above will help improve N Footprints. But there is a lot of uncertainty and responses will be site and crop specific. Climate change results in global warming, uncertain and erratic precipitation patterns and atmosphere composition alteration and, because the activity of enzymes in their natural environments is affected by abiotic factors and biotic processes (e.g. enzyme production and turnover) they are likely to be affected by climate change driven phenomena. These, in turn, have important consequences for ecosystem functions including those happening in the soils, such as the maintenance SOM and added organic material decomposition, nutrient cycling and plant—microbe interactions. These effects will ultimately have an impact on crop productivity, net C balance in soils, N use efficiency and N-footprint.

References

1. Liu L, Zhang X, Xu W, Liu X et al (2020) (2020) Challenges for global sustainable nitrogen management in agricultural systems. J Agric Food Chem 68(11):3354–3361. https://doi.org/10.1021/acs.jafc.0c00273
2. Westhoek H, Lesschen JP, Leip A et al (2015) Nitrogen on the table: the influence of food choices on nitrogen emissions and the European environment. (European Nitrogen Assessment Special Report on Nitrogen and Food.) Centre for Ecology & Hydrology, Edinburgh, UK
3. Leach AM, Galloway JN, Bleeker A, Erisman JW et al (2012) A nitrogen footprint model to help consumers understand their role in nitrogen losses to the environment. Environ Develop 1(1):40–66. https://doi.org/10.1016/j.envdev.2011.12.005
4. Leip et al (2011) Integrating nitrogen fluxes at the European scale.In: Sutton et al (eds) European nitrogen assessment 612 p. Cambridge University Press, Cambridge, pp 345–378
5. Liang X, Lam SK, Gu B, Galloway J et al (2018) Reactive nitrogen spatial intensity (NrSI): a new indicator for environmental sustainability. Global Environ Change 52:101–107. https://doi.org/10.1016/j.gloenvcha.2018.06.001
6. Erisman J, Sutton M, Galloway J et al (2008) How a century of ammonia synthesis changed the world. Nature Geosci 1:636–639. https://doi.org/10.1038/ngeo325
7. Angers DA, Eriksen-Hamel NS (2008) Full-inversion tillage and organic carbon distribution in soil profiles: a meta-analysis. Soil Sci Soc Am J 72:1370–1374. https://doi.org/10.2136/sssaj2007.0342
8. Cordovil CMdS, Bittman S, Brito LM, Goss MJ et al (2020) Climate-resilient and smart agricultural management tools to cope with climate change-induced soil quality decline. Chapter 22. In: Prasad MNV, Pietrzykowski M (eds) Climate change and soil interactions. 840 p, pp 613–641. Elsevier ISBN: 978-0-12-818032-7
9. Dotaniya ML, Menna VD (2013) Rhizosphere effect on nutrient availability in soil and its uptake by plants -a review. Proc Natl Acad Sci India Sec B Biol Sci 85(1):1–12. https://doi.org/10.1007/s40011-013-0297-0
10. Błońska E, Lasota J, Zwydak M (2017) The relationship between soil properties, enzyme activity and land use. For Res Pap 78:39–44. https://doi.org/10.1515/frp-2017-0004
11. Dick R, Kandeler E (eds) (2005) Enzymes in soil. Encyclopedia of soils in the environment. Elsevier, Oxford, pp 448–456
12. Dotaniya ML, Aparna K, Dotaniya CK, Singh Mahendra et al (2019) Role of soil enzymes in sustainable crop production. In Kuddus M (ed) Enzymes in food biotechnology—production, applications and future prospects. Academic Press, Elsevier. https://doi.org/10.1016/B978-0-12-813280-7.09989-8
13. Taylor RAJ (2019) Chapter 11—Other biological examples. In Taylor RAJ (ed) Taylor's power law—order and pattern in nature. Academic Press, Cambridge
14. Stirling G, Hayden H, Pattison T, Stirling M (2017) Soil health, soil biology, soil borne diseases and sustainable agriculture: a guide. Aust Plant Pathol 46(4):387. https://doi.org/10.1007/s13313-017-0493-0
15. Gu Y, Wang P, Kong C (2009) Urease, invertase, dehydrogenase and polyphenol activities in paddy soils influenced by allelophatic rice variety. Euro J Soil 45:411–436. https://doi.org/10.1016/j.ejsobi.2009.06.003
16. Burns RG (1982) Enzyme activity in soil: location and possible role in microbial ecology. Soil Biol Biochem 14:423–427. https://doi.org/10.1016/0038-0717(82)90099-2
17. Burns RG (1986) Interaction of enzymes with soil mineral and organic colloids. In: Huang PM, Schnitzer M (eds) Interactions of soil minerals with natural organics and microbes. Soil Sci Soc Am, Madison, pp 429–452
18. Ladd JN, Jackson RB (1982) Biochemistry of ammonification. In: Stevenson (ed) Nitrogen in agricultural soils. Am Soc Agron 2:173–228. Agronomy Monographs. https://doi.org/10.2134/agronmonogr22

19. Steinweg JM, Dukes JS, Paul EA, Wallenstein MD (2013) Microbial responses to multi actor climate change: effects on soil enzymes. Front Microbiol 4:146. https://doi.org/10.3389/fmicb.2013.00146
20. Piotrowska A, Koper J (2010) Soil β-glucosidase activity under winter wheat cultivated in crop rotation systems depleting and enriching the soil in organic matter. J Elementol 15(3): 593–600
21. Wallenstein MD, Weintraub MN (2008) Emerging tools for measuring and modelling the in situ activity of soil extracellular enzymes. Biochem 40(9):2098–2106. https://doi.org/10.1016/j.soilbio.2008.01.024
22. Tabatai MA (1994) Soil enzymes. In: Weaver RW, Agnelr JS, Bottomley PS (eds) Methods of soil analysis—part 2 microbiological and biochemical properties. Soil Science Society of America, WI, pp 775–833. SSSA Book Series No. 5
23. Acosta-Martinez V, Cruz L, Sotomayor-Ramirez D, Perez-Alegria L (2007) Enzyme activities as affected by soil properties and land use in a tropical watershed. App Soil Eco 35(1):35–45. https://doi.org/10.1016/j.apsoil.2006.05.012
24. Ghezzehei TA, Sulman B, Arnold CL, Bogie NA, Berhe AA (2019) On the role of soil water retention characteristic on aerobic microbial respiration. Biogeosci 16(6):1187–1209. https://doi.org/10.5194/bg-16-1187-2019
25. Burns RG, DeForest JL, Marxsen J, Sinsabaugh RL et al (2013) Soil enzymes in a changing environment: current knowledge and future directions. Soil Biol Biochem 58:216–234. https://doi.org/10.1016/j.soilbio.2012.11.009
26. Alvey S, Yang CH, Buerkert A, Crowley DE (2003) Cereal/legume rotation effects on rhizosphere bacterial community structure in West African soils. Biol Fertil Soils 37:73–82. https://doi.org/10.1007/s00374-002-0573-2
27. Habig J, Swanepoel C (2015) Effects of conservation agriculture and fertilization on soil microbial diversity and activity. Environments 2:358–384. https://doi.org/10.3390/environments2030358
28. Zuber SM, Villamil MB (2016) Meta-analysis approach to assess effect of tillage on microbial biomass and enzyme activities. Soil Biol Biochem 97:176–187. https://doi.org/10.1016/j.soilbio.2016.03.011
29. Tan X, Chang SX, Kabzems R (2008) Soil compaction and forest floor removal reduced microbial biomass and enzyme activities in a boreal aspen forest soil. Biol Fertil Soils 44:471–479. https://doi.org/10.1007/s00374-007-0229-3
30. Govaerts B, Mezzalama M, Unno Y et al (2007) Influence of tillage, residue management, and crop rotation on soil microbial biomass and catabolic diversity. Appl Soil Ecol 37:18–30. https://doi.org/10.1016/j.apsoil.2007.03.006
31. Namli A, Baran A (2000) The effect of compaction on urease enzyme activity, carbon dioxide evaluation and nitrogen mineralisation. Turkish J Agri 24(4):437–443
32. Curci M, Pizzigallo MDR, Crecchio C et al (1997) Effects of conventional tillage on biochemical properties of soils. Biol Fertil Soils 25:1–6. https://doi.org/10.1007/s003740050271
33. Makoi JHR, Ndakidemi PA (2008) Selected soil enzymes: examples of their potential roles in the ecosystem. Afr J Biotechn. 7(3):181–191
34. Riah W, Laval K, Laroche-Aizenberg E, Mougin C et al (2014) Effects of pesticides on soil enzymes: a review. Environ Chem Lett 12:257–273. https://doi.org/10.1007/s10311-014-0458-2
35. Utobo EB, Tewari L (2014) Soil enzymes as bioindicators of soil ecosystem status. Appl Ecol Environ Res 13:147–169. https://doi.org/10.15666/aeer/1301_147169
36. Pandey D, Agrawal M, Bohra JS (2015) Assessment of soil quality under different tillage practices during wheat cultivation: soil enzymes and microbial biomass. Chem Ecol 31:510–523. https://doi.org/10.1080/02757540.2015.1029462

37. Saviozzi A, Levi-Minzi R, Cardelli R, Riffaldi R (2001) A comparison of soil quality in adjacent cultivated, forest and native grassland soils. Plant Soil 233:251–259. https://doi.org/10.1023/A:1010526209076
38. Yang ZX, Liu SQ, Zheng DW, Feng SD (2006) Effects of cadium, zinc and lead on soil enzyme activities. J Environ Sci (China) 18:1135–1141. https://doi.org/10.1016/S1001-0742(06)60051-X
39. Brzezinska M, Stepniewska Z, Stepnewski W (2001) Dehydrogenase and catalase activity of soil irrigated with municipal wastewater. Pol J Environ Stud 10:307–3011
40. Gajda A, Martyniuk S (2005) Microbial biomass C and N and activity of enzymes in soil under winter wheat grown in different crop management systems. Pol J Environ Stud 14 (2):159–163
41. Mazzoncini M, Sapkota TB, Bàrberi P et al (2011) Long-term effect of tillage, nitrogen fertilization and cover crops on soil organic carbon and total nitrogen content. Soil Tillage Res 114:165–174. https://doi.org/10.1016/j.still.2011.05.001
42. Tiemann LK, Grandy AS, Atkinson EE et al (2015) Crop rotational diversity enhances belowground communities and functions in an agroecosystem. Ecol Lett 18:761–771. https://doi.org/10.1111/ele.12453
43. Mitchel DC, Castellano MJ, Sawyer JE, Pantoja J (2013) Cover crop effects on nitrous oxide emissions: role of mineralizable carbon. Soil Sci Soc Am J 77:1765. https://doi.org/10.2136/sssaj2013.02.0074
44. Chavarría DN, Verdenelli RA, Serri DL et al (2016) Effect of cover crops on microbial community structure and related enzyme activities and macronutrient availability. Eur J Soil Biol 76:74–82. https://doi.org/10.1016/j.ejsobi.2016.07.002
45. Kaschuk G, Alberton O, Hungria M (2010) Three decades of soil microbial biomass studies in Brazilian ecosystems: lessons learned about soil quality and indicators for improving sustainability. Soil Biol Biochem 42:1–3. https://doi.org/10.1016/j.soilbio.2009.08.020
46. Sardans J, Peñuelas J (2005) Drought decreases soil enzyme activity in a Mediterranean Quercus ilex L. forest. Soil Biol Biochem 37:455–461. https://doi.org/10.1016/j.soilbio.2004.08.004
47. Maharjan M, Sanaullah M, Razavi BS, Kuzyakov Y (2017) Effect of land use and management practices on microbial biomass and enzyme activities in subtropical top- and sub-soils. Appl Soil Ecol 113:22–28. https://doi.org/10.1016/j.apsoil.2017.01.008
48. Zhang Q, Zhou W, Liang GQ, Wang XB et al (2015) Effects of different organic manures on the biochemical and microbial characteristics of albic paddy soil in a short-term experiment. PLoS ONE 10:e0124096. https://doi.org/10.1371/journal.pone.0124096
49. Ayuni N, Radziah O, Naher UAA et al (2015) Effect of nitrogen on nitrogenase activity of diazotrophs and total bacterial population in rice soil. J Anim Plant Sci 25:1358–1364
50. Coelho MRR, Marriel IE, Jenkins SN et al (2009) Molecular detection and quantification of nifH gene sequences in the rhizosphere of sorghum (Sorghum bicolor) sown with two levels of nitrogen fertilizer. Appl Soil Ecol 42:48–53. https://doi.org/10.1016/j.apsoil.2009.01.010
51. Davison J (1988) Plant beneficial bacteria. Nat Biotechnol 6:282–286. https://doi.org/10.1038/nbt0388-282
52. Kloepper JW, Lifshitz R, Zablotowicz RM (1989) Free-living bacteria inocula for enhancing crop productivity. Trends Biotechnol 7:39–43. https://doi.org/10.1016/0167-7799(89)90057-7
53. Dobbelaere S, Vanderleyden J, Okon Y (2003) Plant growth-promoting effects of diazotrophs in the rhizosphere. CRC Crit Rev Plant Sci 22:107–149. https://doi.org/10.1080/713610853
54. Allison SD, Weintraub MN, Gartner TB, Waldrop MP (2010) Evolutionary-economic principles as regulators of soil enzyme production and ecosystem function. In: Shukla G, Varma A (eds) Soil enzimology. Soil Biol 22: Springer, Berlin. https://doi.org/10.1007/978-3-642-14225-3_12
55. Gianfreda L (2015) Enzymes of importance to rhizosphere processes. J Soil Sci Plant Nutr 15:283–306. https://doi.org/10.4067/s0718-95162015005000002

56. Cheeke TE, Phillips RP, Brzostek ER, Rosling A et al (2017) Dominant mycorrhizal association of trees alters carbon and nutrient cycle by selecting for microbial groups with distinct enzyme function. New Phylo 214:432–442. https://doi.org/10.1111/nph.14343
57. Chen R, Senbayram M, Blagodatsky S, Myachina O et al (2014) Effects of 11 years of conservation tillage on soil organic matter fractions in wheat monoculture in Loess Plateau of China. Soil Tillage Res 106:85–94. https://doi.org/10.1016/j.still.2009.09.009
58. Doran JW (1980) Soil microbial and biochemical changes associated with reduced tillage. Soil Sci Soc Am J 44:765–771. https://doi.org/10.2136/sssaj1980.03615995004400040022x
59. Fontaine S, Mariotti A, Abbadie L (2003) The priming effect of organic matter: a question of microbial competition? Soil Biol Biochem 35:837–843. https://doi.org/10.1016/S0038-0717(03)00123-8
60. Fang S, Xie B, Zhang H (2007) Nitrogen dynamics and mineralization in degraded agricultural soil mulched with fresh grass. Plant Soil 300:269–280. https://doi.org/10.1007/s11104-007-9414-2
61. Fang S, Liu J, Liu D (2010) Enzymatic activity and nutrient availability in the rhizosphere of poplar plantations treated with fresh grass mulch. Soil Sci Plant Nutr 56(3):483–491. https://doi.org/10.1111/j.1747-0765.2010.00480.x
62. Gobran GR, Clegg S, Courchesne F (1998) Rhizospheric processes influencing the biogeochemistry of forest ecosystems. Biogeochem 42:107–120. https://doi.org/10.1023/A:1005967203053
63. Chen J, Luo Y, van Groenigen KJ, Hungate BA et al (2018) A keystone microbial enzyme for nitrogen control of soil carbon storage. Sci Adv 4(8): eaaq1689. https://doi.org/10.1126/sciadv.aaq1689
64. Chen Y, Chen J, Luo Y (2019) Data-driven ENZYme (DENZY) model represents soil organic carbon dynamics in forests impacted by nitrogen deposition. Soil Biol Biochem 138:107575. https://doi.org/10.1016/j.soilbio.2019.107575
65. Acosta-Martínez V, Reicher Z, Bischoff M, Turco RF (1999) The role of tree leaf mulch and nitrogen fertilizer on turfgrass soil quality. In Wang X, Fan J, Xing Y, Xu G et al (2018) The effects of mulch and nitrogen fertilizer on the soil environment of crop plants. Adv Agron 153:121–173. https://doi.org/10.1016/bs.agron.2018.08.003
66. Qian X, Gu J, Pan H, Zhang K et al (2015) Effects of living mulches on the soil nutrient contents, enzyme activities, and bacterial community diversities of apple orchard soils. In: Wang X, Fan J, Xing Y, Xu G et al (eds) The effects of mulch and nitrogen fertilizer on the soil environment of crop plants. Adv Agron 153:121–173. https://doi.org/10.1016/bs.agron.2018.08.003
67. Jin K, Sleutel S, Buchan D, De Neve S et al (2009) Changes of soil enzyme activities under different tillage practices in the Chinese Loess Plateau. Soil Tillage Res 104:115–120. https://doi.org/10.1016/j.still.2009.02.004
68. Tao J, Griffiths B, Zhang S, Chen X et al (2009) Effects of earthworms on soil enzyme activity in an organic residue amended rice-wheat rotation agroecosystem. Appl Soil Ecol 42:221–226. https://doi.org/10.1016/j.apsoil.2009.04.003
69. Acosta-Martínez V, Tabatabai M (2001) Tillage and residue management effects on arylamidase activity in soils. In: In Wang X, Fan J, Xing Y, Xu G et al (eds) The effects of mulch and nitrogen fertilizer on the soil environment of crop plants. Adv Agron, vol 153, pp. 121–173. https://doi.org/10.1016/bs.agron.2018.08.003
70. Siczek A, Frac M (2012) Soil microbial activity as influenced by compaction and straw mulching. Int Agrophys 26:65–69. https://doi.org/10.2478/v10247-012-0010-1
71. Jung KY, Kitchen NR, Sudduth KA, Lee KS et al (2010) Soil compaction varies by crop management system over a claypan soil landscape. Soil Till Res 107(1):1–10. https://doi.org/10.1016/j.still.2009.12.007
72. Elfstrand S, Båth B, Mårtensson A (2007) Influence of various forms of green manure amendment on soil microbial community composition, enzyme activity and nutrient levels in leek. Appl Soil Ecol 36(1):70–82. https://doi.org/10.1016/j.apsoil.2006.11.001

73. Tejada M, Moreno JL, Hernández MT, García C (2008) Soil amendments with organic wastes reduce the toxicity of nickel to soil enzyme activities. Eur J Soil Biol 44:129–140. https://doi.org/10.1016/j.ejsobi.2007.10.007
74. Ge G, Li Z, Fan F, Chu G, Hou Z et al (2009) Soil biological activity and their seasonal variations in response to long-term application of organic and inorganic fertilizers. Plant Soil 326:31–44. https://doi.org/10.1007/s11104-009-0186-8
75. Ge GF, Li ZF, Zhang J, Wang LG et al (2009) Geographical and climatic differences in long-term effect of organic and inorganic amendments on soil enzymatic activities and respiration in field experimental stations of China. Ecol Complex 6:421–431. https://doi.org/10.1016/j.ecocom.2009.02.001
76. Moro H, Kunito T, Sato T (2015) Assessment of phosphorus bioavailability in cultivated Andisoils from a long-term fertilization field experiment using chemical extractions and soil enzyme activities. Arch Agron Soil Sci 61(8):1107–1123. https://doi.org/10.1080/03650340.2014.984697
77. Allison SD, Vitousek PM (2005) Responses of extracellular enzymes to simple and complex nutrient inputs. Soil Biol Biochem 37:937–944. https://doi.org/10.1016/j.soilbio.2004.09.014
78. Stone MM, Weiss MS, Goodale CL, Adams MB et al (2012) Temperature sensitivity of soil enzyme kinetics under N-fertilization in two temperate forests. Global Change Biol 18:1173–1184. https://doi.org/10.1111/j.1365-2486.2011.02545.x
79. Finzi AC, Moore DJP, Delucia EH, Lichter J et al (2006) Progressive nitrogen limitation of ecosystem processes under elevated CO_2 in a warm-temperate forest. Ecol 87(1):15–25. https://doi.org/10.1890/04-1748
80. Schulze J (2004) How are nitrogen fixation rates regulated in legumes? Jour Plant Nutr Soil Sci 167(2):125–137. https://doi.org/10.1002/jpln.200320358
81. Thomas RB, Skip J, Bloem V, Schlesinger WH (2006) Climate change and symbiotic nitrogen fixation in agroecosystems. Environ Sci 4: https://doi.org/10.1201/9781420003826.ch4
82. Chen J, Elsgaard L, van Groeningen J, Olesen JE et al (2020) Soil carbon loss with warming: new evidence from carbon-degrading enzymes. Glob Change Biol 26:1944–1952. https://doi.org/10.1111/gcb.14986
83. Nie M, Pendall E, Bell C, Wallenstein MD (2014) Soil aggregate size distribution mediates microbial climate change feedbacks. Soil Biol Biogeochem 68:357–365. https://doi.org/10.1016/j.soilbio.2013.10.012
84. Schutter ME, Dick RP (2002) Microbial community profiles and activities among aggregates of winter fallow and cover-cropped soil. Soil Sci Soc a J 66:142–153. https://doi.org/10.2136/sssaj2002.1420
85. Gong S, Zhang T, Guo R, Cao H et al (2015) Response of soil enzyme activity to warming and nitrogen addition in a meadow steppe. Soil Res 53:242–252. https://doi.org/10.1071/SR14140

Assembly and Function of Nitrogenase

Chi-Chung Lee, Martin Tillmann Stiebritz, Yilin Hu, and Markus Walter Ribbe

Abstract

Nitrogenase is the complex metalloenzyme responsible for the crucial process of biological nitrogen fixation, in which atmospheric dinitrogen (N_2) is converted into bioavailable ammonia (NH_3). This involves the breaking of the inert N≡N triple bond, a remarkable feat that is made possible by the unique metal clusters —the [Fe_8S_7] P-cluster and the [$MoFe_7S_9C$-*R*-homocitrate] M-cluster. Recent studies on molybdenum-dependent nitrogenase have greatly extended our understanding of how both of these fascinating metal clusters are assembled from common [Fe_4S_4] building blocks, as well as on the series of intriguing interplay between the proteins that are involved. In parallel, independent biochemical, spectroscopic, and structural investigations combine to provide unprecedented insights into the enigmatic mechanism of N_2 reduction. In this chapter, evidence that led up to these findings will be outlined and discussed in their respective contexts, followed by a brief perspective on the outlook of the nitrogenase field.

Keywords

P-cluster · M-cluster · K-cluster · L-cluster · Carbide insertion · Lowe-Thorneley scheme · Distal pathway · Alternating pathway · Reductive elimination · Belt sulfur atoms

C.-C. Lee (✉) · M. T. Stiebritz · Y. Hu (✉) · M. W. Ribbe (✉)
Department of Molecular Biology and Biochemistry, University of California, Irvine, CA, USA
e-mail: chichul@uci.edu

Y. Hu
e-mail: yilinh@uci.edu

M. W. Ribbe
e-mail: mribbe@uci.edu

J. J. G. Moura et al. (eds.), *Enzymes for Solving Humankind's Problems*,
https://doi.org/10.1007/978-3-030-58315-6_6

1 Introduction

Biological nitrogen fixation represents the conversion of atmospheric dinitrogen (N_2) into bioavailable ammonia (NH_3). It is a critical entry step in the global nitrogen cycle and is responsible for roughly half of the fixed nitrogen in our body [1–3]. This process also involves the breaking of the triple bond of N_2, one of the strongest bonds in nature, under ambient conditions and requires the highly sophisticated metalloenzyme known as nitrogenase. The most studied Mo-dependent nitrogenase (Mo-nitrogenase) catalyzes the reduction of N_2 to NH_3 using protons and electrons in an ATP-dependent manner. The reaction can be written as follows [4, 5]:

$$N_2 + 8e^- + 8H^+ + 16\,\mathrm{MgATP} \rightarrow 2\,NH_3 + H_2 + 16\,\mathrm{MgADP} + 16\,P_i \quad \left(\text{where } P_i = PO_3^{2-}\right)$$

Recently, important strides have been made in the understanding of Mo-nitrogenase—particularly in the areas regarding (i) how its complex metallocofactors are assembled [6, 7], and (ii) how it operates during catalysis [8, 9]. This article will summarize the exciting progresses in these areas and offer a brief outlook on the remaining questions in the field.

2 Structure and Properties of Nitrogenase

2.1 Structure and Properties of Mo-Nitrogenase

Nitrogenases are two-component systems, consisting of a reductase- and a catalytic component [4, 5]. During catalysis, the reductase component repeatedly binds to the catalytic component and supplies it with the electrons needed for the reduction of substrates. The reductase component of Mo-nitrogenase, NifH (also called the Fe protein), is a $\sim$60 kDa homodimer, the monomers of which are bridged by a single [Fe_4S_4] cluster between the subunit interface (Fig. 1a). Each monomeric subunit contains a Walker A motive that binds MgATP, hence NifH can bind and hydrolysis two molecules of MgATP for each electron transfer event [10–12]. The [Fe_4S_4] cluster is capable of accessing three oxidation states under different conditions: (i) the $[Fe_4S_4]^{1+}$ state in excess dithionite, (ii) the $[Fe_4S_4]^{2+}$ state upon treatment with oxidants like indigodisulfonate (IDS), and (iii) the $[Fe_4S_4]^{0}$ state upon treatment with strong reductants such as titanium(III) citrate [Ti(III) citrate] and europium(II) diethylenetriaminepentaacetate [Eu(II)-DTPA] [13–17]. The catalytic component of Mo-nitrogenase, NifDK (also called MoFe protein), is a $\sim$220 kDa $\alpha_2\beta_2$-heterotetramer, which contains two unique metal clusters in each αβ-dimer: the [Fe_8S_7] P-cluster located at the interface of the α- and β-subunits, and the [$MoFe_7S_9C$-*R*-homocitrate] M-cluster buried within a cavity in the α subunit and $\sim$14 Å away from the P-cluster (Fig. 1a) [18–23].

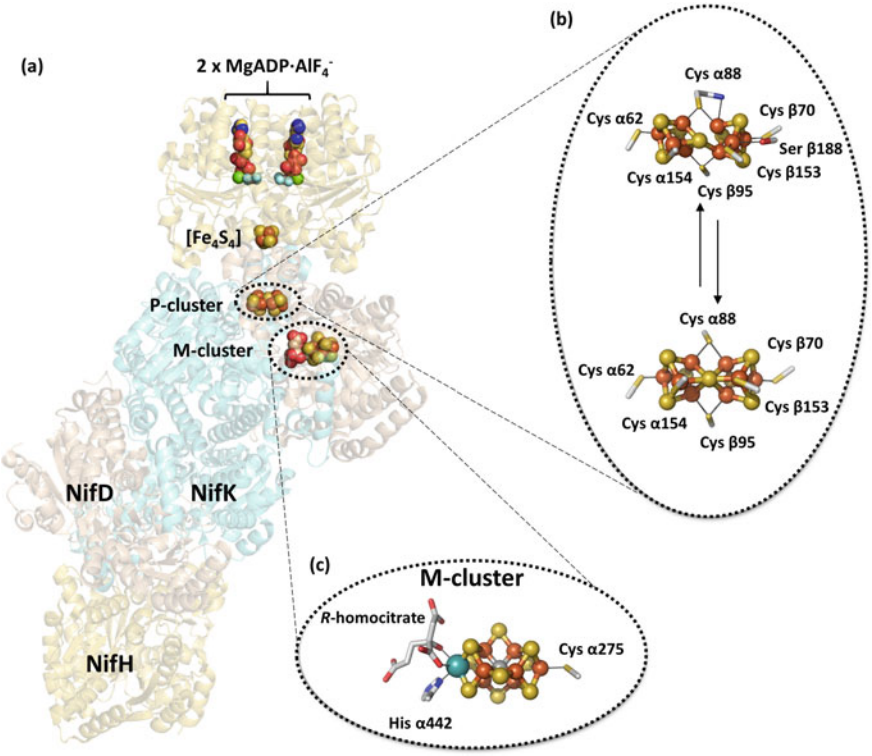

Fig. 1 *A. vinelandii* Mo-nitrogenase NifDK and the metalloclusters it contains. a) Shown is the crystal structure of *A. vinelandii* Mo-nitrogenase NifDK-NifH complex stabilized by ADP·AlF_4^-. The three essential metalloclusters ([Fe_4S_4]-, P- and M-cluster) are shown in the top half of the complex while the individual protein subunits are labeled in the bottom. Shown are the expanded molecular structure of (b) [Fe_8S_7]-core P-cluster in the interchangeable (upper) P^N and (lower) P^{OX} states; and (c) [$MoFe_7S_9C$-*R*-homocitrate] M-cluster, with indicated residues that ligate the clusters of NifDK. Atoms are depicted by spheres colored as follows: Fe, orange; S, yellow; Mo, cyan; C, light grey; N, blue; O, red; Mg, green; Al, dark grey; F, light blue. Images were generated with PYMOL (PBD IDs: 1N2C, 3MIN, 1M1N)

During catalysis, the dithionite-reduced NifH first binds two MgATP molecules which trigger a conformational change that renders the $[Fe_4S_4]^{1+}$ cluster to be more surface exposed. Subsequently, NifH docks to NifDK in such a way that the three metal clusters ([Fe_4S_4] cluster of NifH, P-cluster, and M-cluster of NifDK) are aligned for electron transfer to occur [24–26]. This is illustrated by the crystal structure of the NifH-NifDK transition-state complex that was generated by the use of the ATP analog MgADP·AlF_4 (Fig. 1a). The $[Fe_4S_4]^{1+}$ cluster then transfers one electron to the P-cluster, thus being oxidized to the $[Fe_4S_4]^{2+}$ state, and concomitantly the two MgATP are hydrolyzed to MgADP. With the release of the inorganic phosphate, the oxidized NifH dissociates from NifDK, while the electron first

passes through the P-cluster and finally reaches the M-cluster where substrates are reduced. Remarkably, this process repeats itself multiple times to successively accumulate sufficient amounts of reducing equivalents for the reduction of N_2 or other substrates [24–26].

2.2 Structures and Properties of P- and M-Cluster of Mo-Nitrogenase

Regarded among the most complex metalloclusters in nature, both the P- and the M-cluster of Mo-nitrogenase can actually be viewed as fused $[Fe_4S_4]$-like modules. The $[Fe_8S_7]$ architecture of the P-cluster is essentially two $[Fe_4S_4]$ cubanes joined by a shared S-atom-corner, resulting in a μ_6-S atom center in its final geometry (Fig. 1b). In the dithionite-reduced state (designated as P^N state), the P-cluster is ligated by six cysteinyl residues: three from the α-subunit (Cysα62, Cysα88, and Cysα154) and three from the β-subunit (Cysβ70, Cysβ95, and Cysβ153) (Fig. 1b, *top*). Each of these six cysteines coordinate with one iron atom, while the Cysα88 and Cysβ95 side chains each bridge two Fe centers (Fig. 1b, *top*). EPR spectroscopy shows that the dithionite-reduced P^N-cluster is essentially diamagnetic while Mössbauer spectroscopy demonstrated that it is an all-ferrous iron cluster [27, 28]. Upon treatment with IDS, the P^N-cluster can be oxidized by two electrons to become the P^{ox} state. The P^{ox} cluster displays a $S = 3$ or 4 integer spin state, which can be identified by a parallel-mode EPR signal at $g \sim 12$ [29]. This signal is often used as a diagnostic signature of P-cluster given that the P^N cluster is diamagnetic. This transition from P^N to P^{ox} also causes the metal cluster to conformationally rearrange. This rearrangement involves changes in the coordination spheres of two of the cluster's iron atoms: While being coordinated initially by the central sulfur atom in the P^N state, this partner is being replaced by the Oγ atom of Serβ188 and the backbone-amide N atom of Cysα88 in the P^{ox} state (Fig. 1b, *bottom*) [20, 30]. As a result, one half of the P-cluster, i.e., the half coordinated by the residues in the β-subunit, assumes a more open form. This dramatic conversion is fully reversible, and there is evidence that both states, P^N and P^{ox}, might be physiologically relevant [8, 31]. Thus, the elaborate structural rearrangement may well serve a unique purpose in nitrogenase catalysis, possibly related to P-cluster's role to relay electrons to the M-cluster.

The overall structure of the M-cluster can also be viewed as the product of the fusion of $[MoFe_3S_3]$ and $[Fe_4S_3]$ cubane-like fragments that are (i) bridged by three μ_2-sulfide atoms (also known as the "belt sulfur" atoms), and (ii) sharing a unique μ_6-carbide atom in the center of the M-cluster (Fig. 1c) [18, 32]. In addition, an organic molecule, *R*-homocitrate, coordinates the Mo atom in a bidentate fashion through one hydroxyl- and one carboxyl O atom (Fig. 1c). There is currently no consensus on the physiologically relevant oxidation states of the M-cluster. In the dithionite-reduced state, it exhibits a $S = 3/2$ EPR signal at $g = 4.7$, 3.7, and 2.0, which disappears upon enzymatic reduction [4]. Unlike the P-cluster, the M-cluster is only covalently attached to NifDK by two residues: Hisα442, which binds to the

Mo center, and Cysα275, which coordinates to the terminal Fe atom at the opposite end of the cluster (Fig. 1c) [18]. The fact that the M-cluster only requires two protein ligands is indicative of the integrity of the core structure, which likely is upheld by the central carbide and the three belt sulfur atoms. The limited ligation that tethers the M-cluster to the NifDK polypeptide also allows the metal cofactor to be chemically extracted from the protein into organic solvents such as *N*-methylformamide (NMF) [33, 34]. The extracted M-cluster (also called isolated cofactor) can reconstitute the M-cluster-deficient, but P-cluster-containing variant of NifDK (sometimes known as apo-NifDK), thereby fully restoring the substrate-reduction activity and spectroscopic features of holo-NifDK [33].

3 Assembly of Nitrogenase

The assembly of nitrogenase is a broad topic with many interesting facets: the synthesis of the catalytic and reductase components, the maturation of the unique metal clusters, the involvement of accessory proteins and the genetic regulation of all these processes [6, 7, 35–37]. This chapter focuses on the biosynthesis of the P- and M-cluster of NifDK and discusses the latest developments in this area of active research.

3.1 Overview: General Scheme and Major Players Involved

The biosynthesis of both the P- and the M-cluster starts with the assembly of a common building block: the [Fe_4S_4] cluster (Fig. 2). Its synthesis is achieved by the NifUS complex, which mobilizes cellular Fe and S to first generate [Fe_2S_2] subunits and then fuses two such subunits together into a [Fe_4S_4] cluster (Fig. 2, *top left*) [38–40]. From there, the biosynthetic path diverges. For the formation of the P-cluster, a pair of [Fe_4S_4] clusters are transferred directly to NifDK to form the P-cluster *in-situ* with the help of NifH and NifZ (Fig. 2, *bottom left*). In contrast, the assembly of the M-cluster begins with a pair of [Fe_4S_4] clusters on NifB, on which a Fe_8S_9C intermediate, known as the L-cluster, is formed (Fig. 2, *top right*). The L-cluster is subsequently transferred to NifEN, the site where Mo and homocitrate are installed—again with the participation of NifH (Fig. 2, *top right*). Finally, the matured M-cluster is inserted into the P-cluster-containing, but M-cluster-deficient "apo-NifDK" to form the competent holo-NifDK (Fig. 2, *bottom right*) [36, 37].

3.2 Assembly of P-Cluster

The identification of the P-cluster's biosynthetic precursor was made possible by two NifDK variants: one isolated in a *nifH* deletion background (which is referred to as Δ*nifH* NifDK) and one isolated in a *nifB* and *nifZ* double deletion background

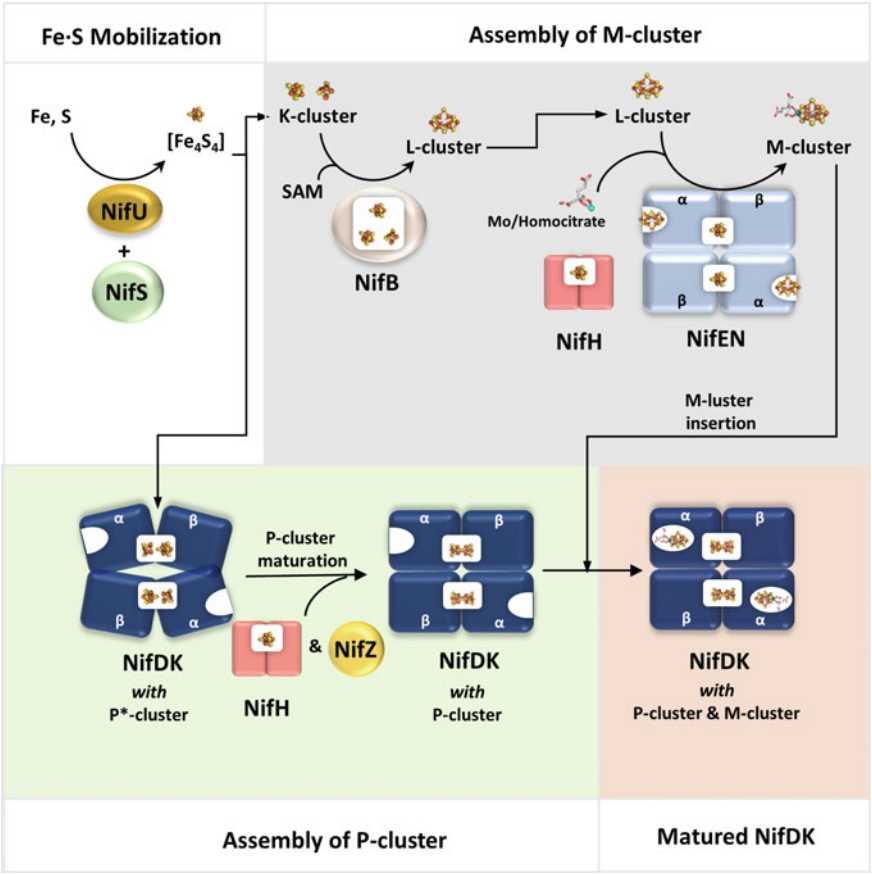

Fig. 2 Flow diagrams of the biosynthetic pathway of (top right) M- and (bottom left) P-cluster assembly. (Top Left) Biosynthesis of both M- and P-clusters shares the common components, NifU and NifS, which synthesizes the $[Fe_4S_4]$ units as the building blocks for further construction of M- and P-clusters. In the case of (top right) M-cluster assembly, two $[Fe_4S_4]$ units (designated K-cluster) are converted into a $[Fe_8S_9C]$ cluster (designated L-cluster) on NifB upon the addition of radical S-adenosyl-L-methionine-dependent (SAM). The L-cluster is then transferred to NifEN, on which Mo and homocitrate are inserted by NifH into the L-cluster to form M-cluster. In the case of (bottom left) P-cluster assembly on NifDK, a pair of $[Fe_4S_4]$-like clusters (designated P*-cluster) is coupled into P-cluster in a process that involves the actions of NifH and NifZ. All clusters shown as ball-and-stick models and atoms are colored as those in Fig. 1. PYMOL was used to generate these structural models (PBD IDs: 3U7Q, 1M1N, and 3PDI)

(which is referred to as Δ*nifBnifZ* NifDK) (Fig. 3) [41, 42]. It should be noted that both of these NifDK variants lack the M-cluster because NifH and NifB are both necessary for its biosynthesis, thereby allowing for the unambiguous assignment of spectroscopic features to the P-cluster and its precursor. EPR analysis of Δ*nifH* NifDK revealed the absence of the P^{ox}-specific $g \sim 12$ signal in the parallel mode,

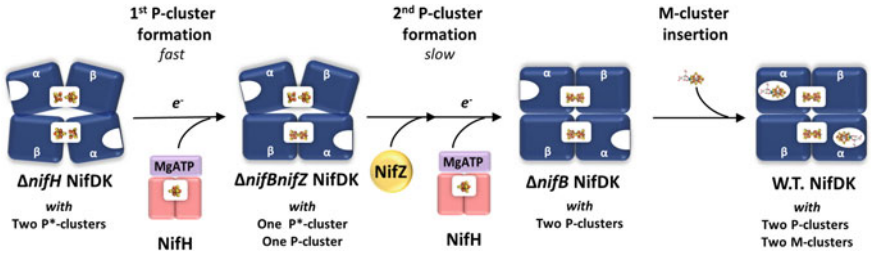

Fig. 3 The stepwise assembly of P-clusters on NifDK. The different NifDK variants representing the different stages of P-clusters assembly: (left) Δ*nifH* NifDK, which contains two P*-clusters; (middle) Δ*nifB*Δ*nifZ* NifDK, which contains one P-cluster and one P*-cluster; and (right) Δ*nifB* NifDK, which contains two P-clusters. Maturation of the first P-cluster requires NifH as well as dithionite and MgATP, whereas maturation of the second P-cluster requires first NifZ, and subsequently NifH/MgATP/dithionite. The formation of the P-cluster also induces a conformational change in NifDK that tightens the gap between α/β-subunit interface and opens up the M-cluster site in the α-subunit. The atoms of the clusters are colored as those in Fig. 1. PYMOL was used to generate this figure (PBD IDs: 1M1N and 1L5H)

but instead a $S = 1/2$ signal in the perpendicular mode was observed [41, 43]. This suggested the presence of $[Fe_4S_4]$ cluster(s) in the +1 oxidation state in place of the P-cluster. This assignment was confirmed by Fe K-edge XAS/EXAFS studies which demonstrated the presence of a typical $[Fe_4S_4]$ and an atypical $[Fe_4S_4]$ cluster that is coordinated by a light atom (N or O) [41]. In addition, magnetic circular dichroism (MCD) spectra of Δ*nifH* NifDK suggested the existence of an unbridged pair of 4Fe subclusters, with one ferredoxin-type $[Fe_4S_4]^{1+}$ cluster and one $[Fe_4S_4]$-like cluster [44, 45]. The latter was found to display an unusual paramagnetism in the +2 oxidation state, in which $[Fe_4S_4]$ clusters are typically diamagnetic [45]. Importantly, this pair of $[Fe_4S_4]$ clusters, denoted as P* cluster, could be converted to a P-cluster when Δ*NifH* NifDK was incubated with NifH, MgATP, and dithionite [46]. After re-isolation from this reaction mixture, the pre-incubated Δ*nifH* NifDK displayed no P*-specific $S = 1/2$ signal in the perpendicular mode, but instead, a P^{ox}-specific $g \sim 12$ signal in the parallel mode emerged. Additionally, XAS/EXAFS characterization of the same sample revealed an overall increase of the Fe-S backscattering distance and, more importantly, the appearance of a characteristic Fe–Fe backscattering distances which is the signature of an intact P-cluster [46]. Meanwhile, the NifH-preincubated Δ*nifH* NifDK was also found to be activatable upon addition of free M-cluster, with an activity level and profile comparable to the Δ*nifB* NifDK which contains intact P-cluster. In summation, these experiments prove that functional P-clusters are formed from P*clusters.

Although the matured NifDK is structurally symmetric, there is evidence that the maturation of the P-cluster does not occur simultaneously in both halves of the protein. Rather, an investigation into the time-dependence of the P-cluster's maturation process on Δ*nifH* NifDK revealed a biphasic pattern [47]. In this experiment, the combination of EPR, XAS/EXAFS and activity analysis were used to

monitor the progression of P-cluster maturation at different time points. The data showed that 50% of P-cluster are formed within the first 5 min, as indicated by the appearance of the $g \sim 12$ EPR signal, the characteristic Fe–Fe backscattering distances and substrate reducing activities; while the rest of the activity and P-cluster-related spectroscopic features gradually emerged in the subsequent 2 h (Fig. 3) [47]. Based on these observations, a stepwise P-cluster maturation model was proposed, in which one P-cluster is formed first in a fast step, followed by the slow maturation of the second P-cluster. In support of this model, Δ*nifBnifZ* NifDK displayed the P* cluster-specific $S = 1/2$ EPR signal (perpendicular mode) with roughly 50% intensity as compared to Δ*nifH* NifDK (which has two P* clusters) while at the same time also showed the P-cluster-specific $g \sim 12$ signal with approximately 50% intensity as compared to Δ*nifB* NifDK (which has two P-clusters). In addition, when compared to Δ*nifB,* Δ*nifBnifZ* NifDK could only be activated to a level of 50% in the presence of isolated M-cluster. Taken together, these results suggest that Δ*nifBnifZ* NifDK contains one P*-cluster in one half of NifDK and one P-cluster in the other half and could therefore represent an in vivo-intermediate in the stepwise P-cluster maturation model. Indeed, the P*-cluster on Δ*nifBnifZ* NifDK can also be matured into a P-cluster upon incubation with NifZ, NifH, MgATP, and dithionite. Interestingly, it was shown that the action of NifZ has to occur before the action of NifH/MgATP, thereby suggesting a potential role of the former as a chaperone that facilitates the action of the NifH in the maturation of the second P-cluster (Fig. 3) [47, 48].

While the molecular mechanism of P-cluster formation remains unclear, the consistent requirement of NifH, MgATP, and high concentrations of reductant (i.e., dithionite) indicates involvement of reduction of P*cluster. Reduction of P*cluster as a prerequisite of P-cluster maturation is supported by a study by Rupnik et al., in which the conversion P*- to P-cluster was achieved chemically [49]. By reducing Δ*nifH* NifDK with the strong reductant Ti(III) citrate, followed by oxidation with either dithionite or IDS, a small portion of P* cluster was shown to be matured even without NifH and MgATP. MCD characterization of the Ti(III)citrate-reduced Δ*nifH* NifDK revealed the presence of the $[Fe_4S_4]^0$ cluster, suggesting the $[Fe_4S_4]$-like sub-clusters of the P* cluster might undergo the "super reduced" all ferrous state before being fused to form the P cluster. Beyond that, the need for conformational rearrangement in NifDK in P-cluster maturation is also indicated by a small angle X-ray scattering (SAXS) [50]. In this study, comparison between Δ*nifH* NifDK and Δ*nifB* NifDK revealed a much larger gap between the αβ interface in the NifDK variant compared to the later. This may suggest that, as the P* cluster is matured, the α and β subunits of the NifDK have to move towards each other to bring the two $[Fe_4S_4]$-type modules closer to each other for a purported reductive coupling of the metal clusters to occur (Fig. 3).

3.3 Assembly of M-Cluster

3.3.1 *Formation of the [Fe_8S_9C] L-Cluster on NifB*

Like in the case of the P-cluster, the assembly of the M-cluster also begins with the fusion of two [Fe_4S_4]-like modules which occurs on NifB (Fig. 4). The investigation of NifB was historically hindered by the difficulty to express this protein in the diazotrophic model organism *A. vinelandii* [51]. Early sequence analysis revealed a number of conserved cysteine residues, indicating the presence of several putative Fe-S clusters in NifB. One of these was predicted to be a radical S-adenosyl-L-methionine (SAM)-binding [Fe_4S_4] cluster because of the occurrence of a signature CxxxCxxC motif—a sequence pattern commonly associated with cluster-ligation in radical SAM proteins—and was later referred to as the SAM cluster [52]. This intriguing [Fe_4S_4] cluster has one open coordination site that binds the sacrificial co-substrate SAM, which can either serve as methyl donor in methylation and/or as a source of a 5′ deoxyadenosyl radical (5′-dA·) in radical-mediated reactions [53]. Further analysis led to the identification of a pair of [Fe_4S_4] clusters, collectively referred to as the K-cluster, which was proposed to be the building block that makes up the 8Fe core of the M-cluster (Fig. 4) [51, 52]. This was eventually demonstrated by a series of biochemical breakthrough experiments, in which NifB was expressed as a fusion-protein with NifEN, both, in *A. vinelandii*, and, heterologously, in *E. coli* [51, 52, 54–56]. Remarkably, the different versions of NifB proteins essentially displayed identical properties and behavior, despite the different expression systems and source organisms. EPR analysis revealed a composite $S = 1/2$ signal at $g = 2.02$, 1.95, and 1.90, representing the presence of both the K- and the SAM cluster. Significantly, this signal disappeared upon addition of SAM, indicating that both metal clusters of NifB reacted with SAM molecules [51, 56]. Concomitantly, a $g = 1.94$ EPR signal, previously established to be characteristic of the [Fe_8S_9C] L-cluster, emerged and thus demonstrated a novel radical SAM-mediated biosynthetic route that fuses two [Fe_4S_4] clusters into an 8Fe cluster [51, 56]. The exact mechanism of this fascinatingly complex reaction is still a topic of ongoing research, although many details have been elucidated in the last decade. It is currently understood that the action of NifB can be roughly grouped into three stages: (i) Insertion of the methyl moiety (Fig. 4, *Step 1 & 2*); (ii) cluster rearrangement (Fig. 4, *Step 3*), and (iii) incorporation of the 9th sulfur atom (Fig. 4, *Step 4*). These events are described in the following sections.

The insertion of the methyl group from SAM. The involvement of SAM in the conversion of the K to the L cluster was initially demonstrated by detecting the cleavage products of SAM [51, 56]. HPLC analysis revealed that cleavage of SAM by NifB produces 5′-deoxyadenosine (5′-dAH) and *S*-adenosyl-L-homocysteine (SAH) (Fig. 4, *Step 1*) [51, 54]. In parallel, using [methyl-d_3] SAM instead of regular SAM, deuterated 5′-deoxyadenosine (5′-dAD) could be detected together with undeuterated SAH [54]. Interestingly, previous studies of the SAM-dependent RNA-methyltransferases RlmN and Cfr also shown a similar product profile, so

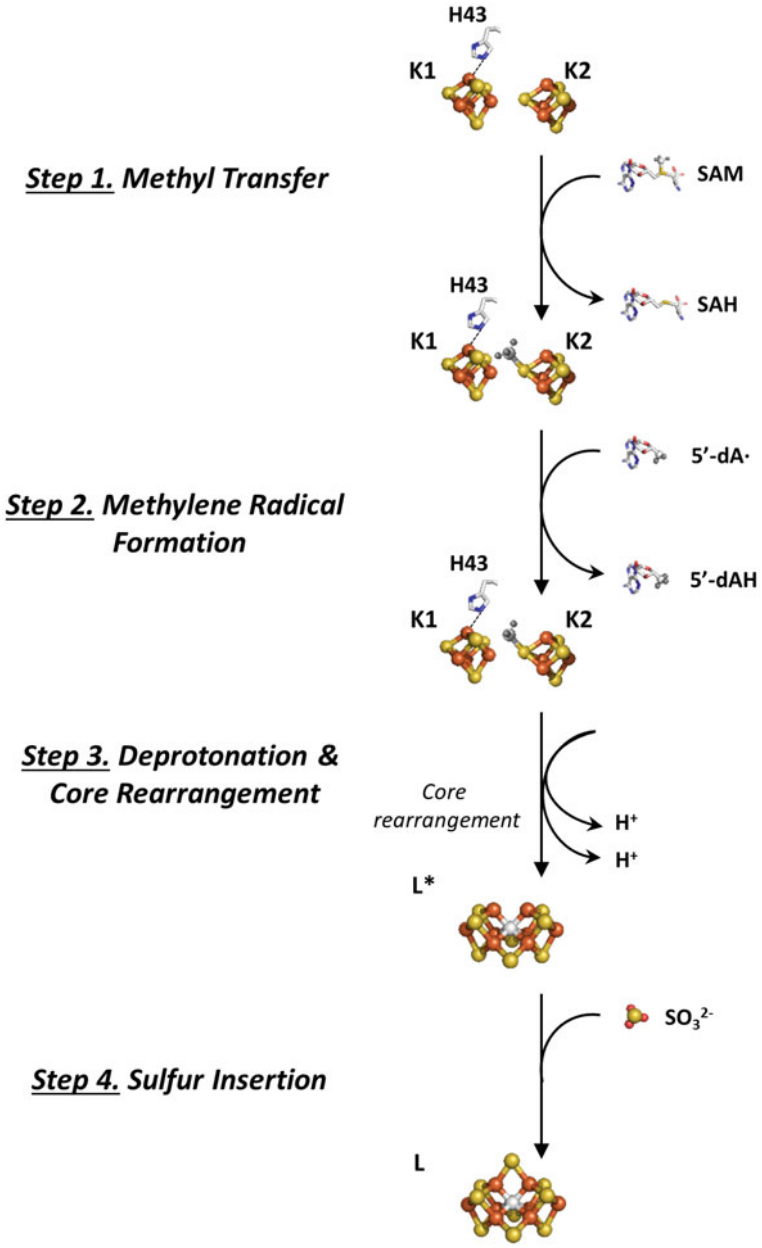
H43
K1
K2
Step 1. Methyl Transfer
SAM
SAH
H43
K1
K2
Step 2. Methylene Radical Formation
5'-dA·
5'-dAH
H43
K1
K2
Step 3. Deprotonation & Core Rearrangement
Core rearrangement
H+
H+
L*
Step 4. Sulfur Insertion
SO3 2-
L

◀

Fig. 4 The transformation of K-cluster to L-cluster on NifB. Schematic representation of K-cluster, consisting of the K1 and K2 module and the histidine-43 (H43) ligand on the K1 module are shown in the first three steps The SAM cluster of NifB is omitted for clarity. (Step 1) The methyl group from the first molecule of SAM is transferred to an S atom of the K2-cluster via an S_N2-type mechanism, producing one SAH molecule as by-product. (Step 2) An S-bound methylene radical is formed upon hydrogen atom abstraction by 5′-dA· which is generated by a second molecule of SAM, forming 5′-dAH as byproduct. (Step 3) Deprotonation of the cluster-bound methylene radical, possibly by H43, eventually gives rise to an interstitial carbide atom. Concomitantly, the two modules rearrange and fuse into a $[Fe_8S_8C]$ core known as L*-cluster, with the concomitant loss of the H43 ligand originally on K1 cluster. (Step 4) The L*-cluster is finally transformed into L-cluster through the addition of a sulfur atom, of which the source was identified in vitro to be sulfite. L-cluster is subsequently transferred to NifEN for further maturation. All clusters and molecule are shown as ball-and-stick models, with the atoms colored as those in Fig. 1. PYMOL was used to generate the structural models of the metal clusters (PDB ID: 3PDI)

based on this resemblance an analogous mechanism of methyl insertion was proposed for NifB [57, 58]. It involves an initial S_N2-type methyl transfer from one molecule of SAM (thereby generating SAH as product), followed by hydrogen abstraction from the methyl moiety by the 5′-dA· (thereby generating 5 '-dAH and 5′-dAD with regular and [methyl-d_3] SAM, respectively as products) which is derived from homolytic cleavage of a second molecule of SAM (Fig. 4, *Step 2*). However, unlike the RNA methyltransferases, in which methyl transfer is mediated by a conserved Cys residue near the substrate, the SAM-derived methyl moiety was found on the sulfur atom of the K-cluster of NifB [55]. Radiolabeling with [methyl-^{14}C] SAM resulted in the accumulation of ^{14}C on the L-cluster, which can be extracted and analyzed in isolation, but not on the NifB polypeptide. In addition, acid quenching of the methyl-transfer reaction with NifB resulted in the formation of methanethiol (CH_3SH) when regular SAM was used, or methane-d_3-thiol (CD_3SH) when [methyl-d_3] SAM was used, further confirming that the SAM-derived methyl group is donated onto an acid-labile sulfur atom of the K-cluster. A final conclusive proof of this interpretation was provided by the formation of methylselenol (CH_3SeH) in the same acid-quenching experiment using Fe/Se-reconstituted NifB, which contained Fe-Se clusters instead of Fe-S clusters [55]. Moreover, insights into the sequence of events were gained by using allyl-SAM, a SAM analog which contains an allyl group (-CH-CH=CH_2) in place of the methyl group. When NifB was incubated with allyl-SAM, only SAH (but not 5′-dA) was generated, suggesting the transfer of the allyl group from which the hydrogen cannot be abstracted. Acid quenching of this reaction resulted in the formation of allylthiol (CH_2=CH-CH-SH), which strongly suggests that the transfer of the methyl (or allyl) group precedes the abstraction of the hydrogen atom [55]. Lastly, recent mutational studies on NifB provide details on the location of this methyl-transfer step [59]. Using NifB from *M. acetivorans* (referred to as *Ma*NifB), which was heterologously expressed in *E. coli*, systematic mutagenesis of the conserved cysteines followed by biochemical and spectroscopic analysis of the mutants allows for the identification of each of the three $[Fe_4S_4]$ cluster modules:

the SAM-cluster (coordinated by Cys^{50}, Cys^{54}, and Cys^{57} in the CxxCxxxC motif), the K1-cluster (part of the K-cluster and coordinated by Cys^{30}, Cys^{63}, and Cys^{129} towards the N-terminus) and the K2-cluster (part of the K-cluster and coordinated by Cys^{264}, Cys^{274}, and Cys^{277} towards the C-terminus). Deletion of each set of cysteines, which led to the selective loss of the three [Fe_4S_4] modules, confirmed that all three modules were necessary for formation of L-cluster. More importantly, it also revealed that only the NifB mutant that misses the K1 cluster, but retains the K2- and SAM clusters, can maintain a normal SAM-cleavage-product profile and the ability to generate methanethiol upon acid quenching. Meanwhile, deletion of either the K2 or the SAM cluster led to obliteration of these activities [59]. This observation suggests that the presence of both clusters is the prerequisite for methyl transfer and the subsequent hydrogen abstraction and thus strongly points to a K2-associated sulfur atom as the target of the methyl transfer step.

Cluster rearrangement and formation of the L-cluster. The immediate events that follow the methyl transfer and hydrogen abstraction remain largely unclear at this point due to the concomitant nature of the insertion of the center carbide, the rearrangement of the K1- and K2-clusters, and the formation of the L-cluster. The following steps would need to occur in synchrony: One or both K cluster modules (K1 and K2) need to open up by breaking off the Fe-S bonds. The clusters then need to move closer to each other for the coupling reaction to occur. The methylene moiety which was originated from the methyl group transferred from SAM to the K2 cluster, and was then generated by hydrogen abstraction, needs to be deprotonated (Fig. 4, *Step 3*) [36]. These events likely involve nearby residues to either guide the rearrangement of K1 and K2 rearrangement and their fusion, or act as a base to deprotonate the K2-bound methylene moiety. One likely candidate that might simultaneously fulfill both roles could be histidine-43 of *Ma*NifB [60]. Using mutagenesis and pulse EPR, this residue was shown to coordinate to the K1 cluster, likely via an N-atom of an imidazole group on the side chain [59, 60]. Significantly, this ligation disappears as the K1- and K2-cluster is fused into the L-cluster, which highlights the importance of histidine-43 for this crucial process. Indeed, NifB with a H43A mutation (designated *Ma*$NifB^{H43A}$) was shown to be unable to form an intact L-cluster upon incubation with SAM. Moreover, the ability to *Ma*$NifB^{H43A}$ to catalyze methyl-transfer and hydrogen-abstraction was unaffected by the mutation, which was demonstrated by the detection of SAH and 5′-dA by HPLC analysis, as well as methanethiol upon acid quenching. The cluster species of the SAM-treated *Ma*$NifB^{H43A}$ could therefore be considered as an intermediate K-cluster with a methylene attachment which is on route towards its transformation to the L-cluster [59, 60]. XAS/EXAFS characterization of this supposed intermediate revealed that K1- and K2-modules become more aligned with respect to each other when compared to as original state (i.e. *Ma*$NifB^{H43A}$ without SAM treatment), while still lacks the 8Fe core arrangement which is characteristic of the L- and the M-cluster [60]. Taken together, these observations suggest the following interesting proposals: (i) the presence of histidine-43 might act as a guide to assist the structural rearrangement during the coupling of K1 and K2 cluster, (ii) histidine-43 might be

responsible for the deprotonation of the methylene moiety on the K2 cluster as the loss of histindine-43 ligation during L-cluster formation could be mediated through protonation of its side chain, and (iii) histindine-43 might thereby serve as a functional liaison that orchestrates these two events (Fig. 4, *Step 3*).

The incorporation of the 9th sulfur atom. Following the rearrangement and fusion of the two K cluster modules, a [Fe_8S_8C] core is formed. This core is referred to as the L*-cluster because of its structural similarity to the L-cluster that was deduced from spectroscopic data [61]. EPR analysis revealed that both the L*- and the L-cluster display almost identical $g = 1.94$ signals. XAS/EXAFS analysis also revealed an overall resemblance of the Fe distances between the L* and L-cluster, although detected the lack of a strong Fe–Fe interaction in L*-cluster which is present in the L-cluster [62]. This is indicative that the L*-cluster adopts a more open conformation and thereby inferring that the missing 9th sulfur atom would be located on one of the three belt positions. Activities analysis revealed the L*-cluster is incapable of undergoing the same maturation events that turn the fully matured L-cluster into the M-cluster [61]. This highlights the significance of the incorporation of the so-called "9th-sulfur" atom and raises the question of what the source of the sulfur might be. Surprisingly, the 9th-sulfur atom does not come from SAM or NifS as previously thought, but rather from inorganic sulfite (SO_3^{2-}) (Fig. 4, *Step 4*) [61–64]. In a reaction free from any S contaminations, featuring the absence of dithionite and the use a synthetic [Fe_4S_4] cluster reconstituted NifB, it could be shown that the L*-cluster can be activated (in terms of its ability to mature into the M cluster) by adding sulfite as a sulfur source (Fig. 4, *Step 4*) [61]. In stark contrast, the same could not be achieved with sulfate (SO_4^{2-}), sulfide (S^{2-}) or other common sulfur metabolites [61]. A ^{35}S-tracing experiment, finally, provided the definite proof that S from $^{35}SO_3^{2-}$ was incorporated into the L*-cluster as the radiolabel was detected on the extracted L-cluster *after* $^{35}SO_3^{2-}$ had reacted with NifB and SAM [61]. There is currently no direct evidence for the utilization of sulfite in the 9th S incorporation step inside the cell, although sulfite along with sulfate and sulfide are all essential of cellular sulfur metabolism hubs. The absence of the μ_2-belt sulfide from the L*-cluster is consistent with the labile nature of the belt region of the cofactor, as demonstrated in recent MCD studies of L cluster as well as several structures in which the belt sulfur of either M- or V-cluster are missing (see Sect. 4.3) [65].

3.3.2 Maturation of the L-Cluster on NifEN

After its formation on NifB, the L-cluster is transferred to NifEN to be further matured into the M-cluster (Fig. 5a). NifEN is a homolog of NifDK and thus contains analogous metal-cluster binding sites. Indeed, spectroscopic and structural characterization of *A. vinelandii* NifEN revealed the presence of a [Fe_4S_4] cluster in the analogous P-cluster binding site of NifDK at the interface of the α- and β-subunits [66]. When expressed in a *nifHDK*-deletion background, EPR, Fe edge XAS/EXAFS and Fe Kβ XES studies showed the accumulation of the [Fe_8S_9C] L-cluster on NifEN [67–69]. A crystal structure of this L-cluster-containing NifEN

(designated $NifEN^L$) indicated that the L-cluster is located in the analogous M-cluster-binding site as in NifDK, and yet more exposed to the surface and thereby accessible to modification [70]. Since the absence of NifH is a prerequisite for the accumulation of L-cluster on NifEN, NifH is likely involved in the conversion of L- to M cluster. This is demonstrated by a series of biochemical and spectroscopic studies which defined the exact role of NifH in the process, which is to mobilize molybdate (MoO_4^{2-}) and homocitrate at the expense of ATP hydrolysis and subsequently carries these components to NifEN for their incorporation into the L-cluster (Fig. 5a) [71–73]. This is confirmed by Mo K-edge XAS data, which points to a change in the oxidation state and/or ligation pattern of the Mo atom upon binding to NifH. EPR analysis revealed that the loading of Mo/homocitrate induces changes to NifH's Fe_4S_4 cluster that is similar to those induced by the binding of ATP or ADP [71]. For NifEN, upon incubation with dithionite, NifH, MgATP, molybdate, and homocitrate, Mo K-edge XAS/EXAFS analyses of the matured NifEN (designated as $NifEN^M$) revealed to spectral features indistinguishable from NifDK [72, 73]. In addition, the M-cluster that was matured on NifEN can be chemically extracted into solvent just like in the case of NifDK [74, 75]. Both versions of M-clusters, whether extracted from NifEN or NifDK, exhibit identical spectroscopic properties as well as the same ability to activate apo-NifDK, which proves conclusively that the M-cluster is formed on NifEN [74, 75].

After these events, $NifEN^M$ undergoes a conformational change that renders M-cluster less solvent-exposed compared to $NifEN^L$ (Fig. 5a) [75]. This change was demonstrated by metal-content analysis and chelation studies of $NifEN^L$ and $NifEN^M$. The results show that the Fe atoms in $NifEN^L$ can be completely chelated, which is supported by the solvent-exposed nature of the L-cluster observed in the crystal structure. In stark contrast, the majority of Fe atoms in $NifEN^M$, that are likely associated with the M-cluster, cannot be removed by a chelator [75]. Thus, upon maturation to the M-cluster, a conformational change must occur that embeds the cofactor within a less solvent-accessible location of the protein. This change is likely important for the subsequent events where $NifEN^M$ directly donates its fully assembled M-cluster to NifDK (Fig. 5a).

3.3.3 Insertion of M-Cluster into the NifDK Scaffold

After formation of the M-cluster, $NifEN^M$ was shown to fully activate apo-NifDK without the need for accessory chaperons or carriers (Fig. 5) [36, 37, 67, 71–74]. Moreover, results from native PAGE experiments revealed that $NifEN^M$ can form a direct protein–protein complex with apo-NifDK, in which the M-cluster can directly be transferred to NifDK [76]. Sequence analysis revealed a number of key residues in NifDK that either provide a covalent linkage or tightly pack the M-cluster within the binding pocket and are missing in NifEN. These residues include Lys426 (which anchors the homocitrate), His442 (which coordinates Mo), and Trp444 (which packs the M-cluster into the pocket with its bulky side chain) [36, 37]. Their exclusive presence on NifDK, but not on NifEN, was believed to create a high-affinity M-cluster site on NifDK and the low-affinity M-cluster site in NifEN, wherein the difference in M-cluster affinity between these two sites provide

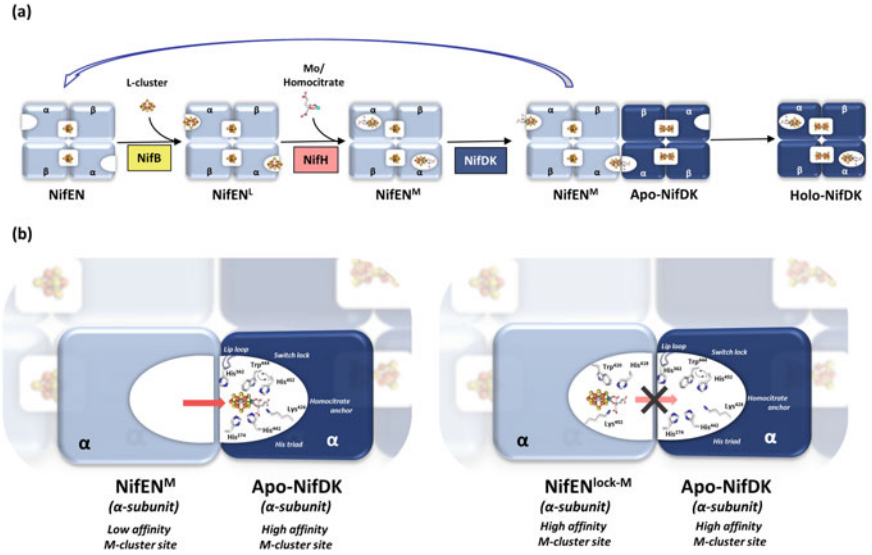

Fig. 5 Conformational changes of NifEN during the formation and subsequent transfer of M-cluster. **a** When L-cluster is delivered from NifB to apo-NifEN (designated NifEN), the metal cluster initially resides at the surface of NifEN (designated NifEN^{L}), hence available for further modification. Then Mo and homocitrate are inserted by NifH into L-cluster to form M-cluster, upon which NifEN (designated NifEN^{M}) undergoes a conformational change that buries M-cluster within the protein matrix. Subsequently, NifEN^{M} associates with apo-NifDK which triggers another structural rearrangement on NifEN^{M} that pushes out the M-cluster for its transfer to NifDK. After that, it is assumed that NifEN resumes its apo conformation and ready to receive another L-cluster. **b** (left) Close-up of the M-cluster's low- and high-affinity sites in the interacting α-subunits of NifEN and apo-NifDK respectively. Key residues for M-cluster insertion can be found along a positively charged insertion path on NifDK. These residues include (i) the lid-loop residue, Hisα362, which may help to initially bind the M-cluster in order to draw it in; (ii) the His-triad residues, Hisα274, Hisα442, and Hisα451, which may further guide the M-cluster along the path to the binding site; and (iii) the switch/lock residues, Hisα442 and Trpα444, which switch their relative positions potentially to secure the M-cluster in the correct position by the bulky side chain of Trpα444. Lastly, residue Lysα426 provide additional anchor of M-cluster through its interaction with homocitrate. These residues are only present in NifDK, but not in NifEN, thereby creating a difference in M-cluster affinity that likely drives its interprotein migration. (right) An artificial NifEN (designated NifEN^{lock}) with an engineered high-affinity M-cluster site that is consisted of residues Lysα402, Hisα418, and Trpα420 (analogous to Lysα426, Hisα442, and Trpα444 of NifDK) was shown to prevent the transfer of matured M-cluster to apo-NifDK

the driving force for the cluster to migrate from NifEN to NifDK (Fig. 5b) [36, 37]. This idea was tested by a recent study, where these three residues were engineered into NifEN (designated NifEN^{lock}) [77]. In these experiments, NifEN^{lock} was able to catalyze the maturation of an intact M-cluster like wild type NifEN. It was, however, not able to activate apo-NifDK, which indicates that the introduction of these mutations blocked the transfer of the fully assembled M-cluster from NifEN to NifDK (Fig. 5b). Subsequently, the matured NifEN^{lock} (designated NifEN^{lock-M})

was then incubated with apo-NifDK, and then re-isolated. EPR analysis of this species not only revealed the retainment of the M-cluster, it also showed the alteration of the line-shape and amplitude of the M-cluster specific signal and thus suggested a change of the cofactor environment. This observation also implies that another conformational change occurs as $NifEN^{lock-M}$ interacts with apo-NifDK, as confirmed by a Fe-chelation experiment which shows the M-cluster gained more solvent exposure after $NifEN^{lock-M}$ was incubated with apo-NifDK [77]. These findings highlight the dynamic nature of the NifEN protein, which initially presents L-cluster on the surface of the protein to allow maturation, then undergoes a first conformational change to embed the newly generated M-cluster, and finally, upon interaction with NifDK, performs a second structural rearrangement to push the M-cluster outward in order to accommodate the transfer of the cofactor (Fig. 5a).

Analogous to NifEN, apo-NifDK undergoes a conformational change of its own when it receives the M-cluster from NifEN. This was demonstrated by SAXS studies which revealed a more compact structure of holo-NifDK compared to apo-NifDK [50]. Together with the structural analysis of apo-NifDK, this indicates that as M-cluster travels down a positively charged insertion funnel at NifDK surface, the protein folds-inward to bury the cofactor within the matrix of the α-subunit [23]. The pathway of M-cluster insertion can be mapped to three specific regions of NifDK: (i) a 'lid loop' region, consisting of the residues α353 to α364; (ii) a 'His triad' region which is formed by Hisα274, Hisα442, and Hisα451; and (iii) the 'switch/lock' region composed of Hisα442 and Trpα444 (Fig. 5b) [78–80]. The positively charged residues in the 'lip/loop' region, in combination with the potential transient ligand Hisα362, likely helps to transiently bind and guide the anionic M-cluster to correctly reach its binding site. Subsequently, the 'His triad' is proposed to be a transient binding site(s) for the M-cluster as it passes along the insertion path. Finally, the 'switch/lock'-residue Hisα442 binds the cofactor within the active site and then switches position with Trpα444, of which the bulky side chain serves as a lock that fastens down the cofactor (Fig. 5b). Accordingly, the mutation of each of these residues above leads to NifDK variants with impaired M-cluster uptake and retention abilities [78–80]. The effect of Hisα442 and Trpα444 as the M-cluster-switch/lock have also been demonstrated on $NifEN^{lock}$, and it can be anticipated that further engineering using the other insertion funnel residues might eventually lead to artificial proteins that are efficient in M-cluster uptake.

4 Mechanism of Nitrogenase

4.1 Overview: Reactive Properties and the Thornley-Lowe Cycle

The basic mechanistic properties of Mo-nitrogenase is best outlined by the Lowe-Thorneley (LT) model (Fig. 6a) [81]. This model, which summarized a large body of early work on nitrogenase kinetics, was schematized by David Lowe and

Roger Thorneley in 1984, and later embellished by Hoffman and others [9, 81, 82]. While it was chiefly invented to describe the reduction of N_2, it still provides a framework for the catalytic mechanism of nitrogenase in general and is also frequently used to explain the reduction of other alternative substrates by this enzyme [4]. The model defines eight discrete stages of the catalytic cycle of NifDK, where each stage represents one of the eight electron- and proton-transfer steps that are proposed to fuel the conversion of one molecule of N_2 to two NH_3 molecules, while forming one molecule of H_2 as the obligatory side product (Fig. 6a). The individual stages are denoted as E_n, where n represents the number of electrons and protons accumulated on one αβ-dimer of NifDK—either associated with the P-cluster or the M-cluster. The first state is E_0, which is the dithionite-reduced, as isolated NifDK. It has an overall spin state of $S = 3/2$, thus indicating an odd number of unpaired electrons. Following this logic, it can be deduced that all even-numbered states (i.e. E_n where $n = 2, 4, 6$, etc.) will have an odd number of unpaired electrons as well and are hence paramagnetic. In contrast, the odd-numbered E_n states (i.e. E_n where $n = 1, 3, 5$, etc.) will have an even number of unpaired electrons and should either be diamagnetic or possess integer spin states ($S = 1, 2, 3$, etc.) which are often undetectable by EPR. Therefore, preliminary information regarding the spin state of any nitrogenase reaction intermediate species can already be very helpful in determining whether an even or odd number of electrons and protons have been added into the system [81, 82]. This feature was often being taken advantage of when a purported intermediate species is observed of which the catalytic stage it arises from is unclear.

Upon receiving electrons from the Fe protein, the E_0 state is reduced stepwise to a series of turnover states. It is believed that in the absence of suitable substrates, the states E_2 to E_4 are oxidized back to the states E_0 to E_2. This oxidation process, in which two electrons are removed, is coupled to the formation of H_2 (Fig. 6a) [83, 84]. By only cycling through the states E_0 to E_4, Mo-nitrogenase effectively becomes an ATP-dependent hydrogenase in the absence of proper substrates. Regarding the reduction of N_2, it is now commonly believed that the binding of N_2 occurs at the E_4 state, which proposedly occurs through a reductive elimination mechanism (Fig. 6) [81, 82, 85–87]. After that, NifDK can undergo five more successive proton/electron-transfer steps to cleave the N≡N triple bond and eventually yield two molecules of NH_3 (Fig. 6a). Beginning with the states E_4 to E_6, two distinct reaction pathways were proposed for the reduction of the activated N_2 to the two NH_3 products [4, 82]. In the so-called *distal pathway*, which was described in the original LT scheme, one N atom (namely the distal N) is first reduced all the way to NH_3 and released before the reduction of the second N begins. A later proposal by Seefeldt and Hoffmann, known as the *alternating pathway*, describes the alternating reduction on the two N atoms so that both NH_3 are produced and released in the last two states successively (Fig. 6a) [9, 82]. Interestingly, these two proposals predict completely different sets of reaction intermediates at the states E_4, E_5, and E_6, while still converging at a common E_7 state (Fig. 6a).

4.2 *Spectroscopic Insights into the Mechanism of N_2 Reduction*

The binding of N_2 plausibly occurs via *a reductive elimination mechanism*. Insight into N_2 binding was provided by Hoffman and co-workers who used freeze-quench trapping to accumulate an intermediate species. Its presence was first noticed in an αVal70 to αIle70 point mutant of NifDK (designated NifDK^{Ile70}) with impaired ability to reduce all known substrates except protons, but which could later also be identified in wild-type NifDK [88, 89]. For this intermediate, the presence of a paramagnetic $S = 1/2$ EPR signal indicated that NifDK is in an even-numbered state while kinetic analysis suggested that this intermediate is either three or four

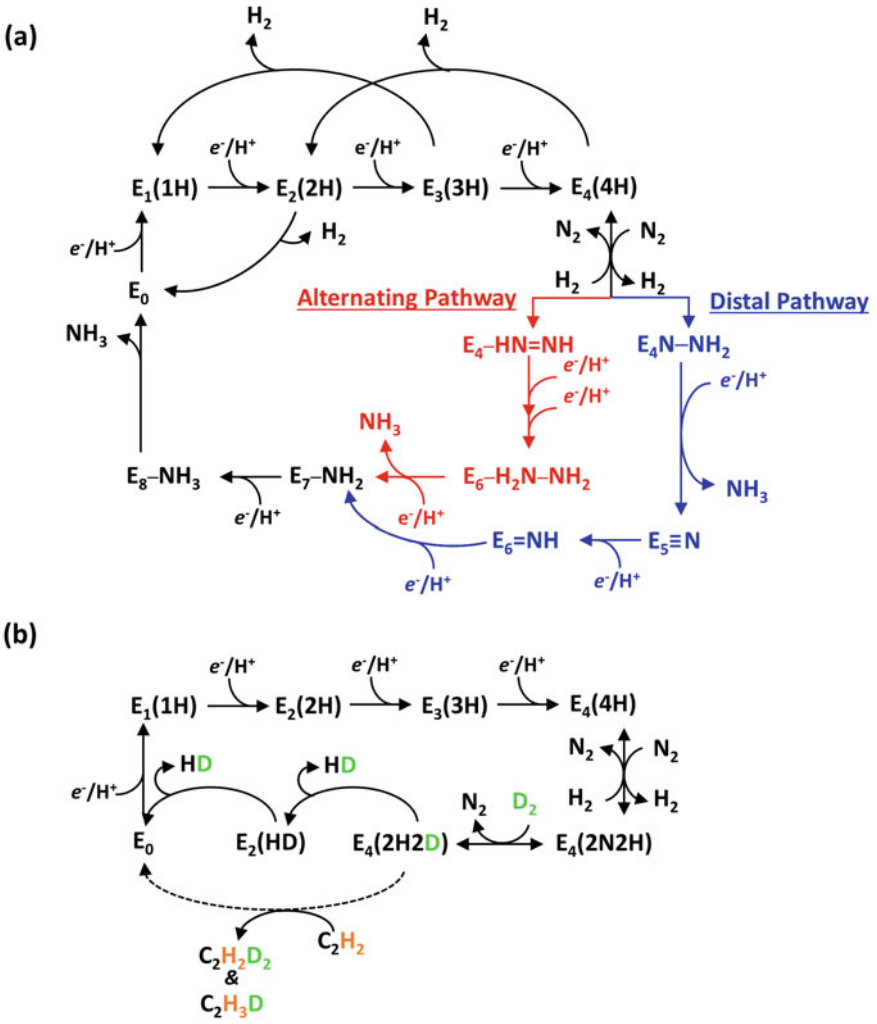

◀

Fig. 6 The modified Lowe-Thorneley scheme for N_2 reduction and the uptake of deuterium. **a** The E_n designation refers to a *n* number of protons and electrons that are loaded on to one αβ-dimer of NifDK. The states E_2 to E_4 can be two-electron oxidized back to the states E_0 to E_2, respectively, through the release of H_2. N_2 is proposed to bind at the E_4(4H) state, plausibly via a reductive elimination mechanism. After the binding of N_2, two different reduction pathways are proposed: the distal (depicted in blue) and an alternating (depicted in red) pathway. These two pathways differ in the order in which the two N atoms are reduced, the intermediates that are formed during the reaction and which of the E_n states allow for NH_3 to be released (see main text for detail). The distal and alternating pathway merges back together at the E_7 state, after that the final NH3 was released as E_8 is converted back to E_0. (b) When D_2 gas was added to the E_4(2N2H) state NifDK, the bound N_2 was displaced to generate the E_4(2H2D) state, as analogous state to E_4(4H). This reversion of catalytic states, from E_4(2N2H) to E_4(4H), is seen as demonstration of the micro-reversibility of the H_2 reductive elimination step that allows N_2 to bind. The bound hydride and deuteride can be released as HD gas as the E_4(2H2D) state relaxes back to E_2, and then E_0. Alternatively, $C_2H_2D_2$ and C_2H_3D can be observed as products of the reduction of C_2H_2, which was added to the reaction mixture to outcompete N_2 for hydride and deuteride bound on the E_4(2H2D) state

electrons more reduced than the E_0 ground state. Therefore, taken together it was recognized that the intermediate represents E_4 [89]. This interpretation was further supported by an annealing experiment, in which the warming of the freeze-trapped intermediate led to the release of two equivalents of H_2, thereby demonstrating the accumulation of four electrons/protons on M-cluster [85–87, 89]. ^{1,2}H, ^{57}Fe, and ^{95}Mo ENDOR experiments suggested that the spectroscopic features of this intermediate can be interpreted as an Fe-bound hydride fragment, plausibly in a μ_2-bridging conformation (Fe–H–Fe) [85–87, 89, 90]. This finding led to the proposal that the E_4 state of NifDK, which is represented by the freeze-trapped intermediate mentioned above, is an M-cluster having two μ_2-hydride ligands bridged between two different pairs of Fe atoms with two protons bound elsewhere on the cluster. This proposed E_4 state, also termed E_4(4H), then formed the basis for the reductive elimination mechanism of N_2 binding. Its structure was further explored in recent theoretical study, which suggests that the cleavage of an Fe-S bond, if not the entire removal of the belt sulfur atom, is an energetically feasible reaction for the M-cluster in the E_4 state [91, 92].

The binding of N_2 plausibly occurs via *a reductive elimination mechanism*. Insight into N_2 binding was provided by Hoffman and co-workers who used freeze-quench trapping to accumulate an intermediate species. Its presence was first noticed in an αVal70 to αIle70 point mutant of NifDK (designated NifDK^{Ile70}) with impaired ability to reduce all known substrates except protons, but which could later also be identified in wild-type NifDK [88, 89]. For this intermediate, the presence of a paramagnetic $S = 1/2$ EPR signal indicated that NifDK is in an even-numbered state while kinetic analysis suggested that this intermediate is either three or four electrons more reduced than the E_0 ground state. Therefore, taken together it was recognized that the intermediate represents E_4 [89]. This interpretation was further supported by an annealing experiment, in which the warming of the freeze-trapped

intermediate led to the release of two equivalents of H_2, thereby demonstrating the accumulation of four electrons/protons on M-cluster [85–87, 89]. ^{1,2}H, ^{57}Fe, and ^{95}Mo ENDOR experiments suggested that the spectroscopic features of this intermediate can be interpreted as an Fe-bound hydride fragment, plausibly in a μ_2-bridging conformation (Fe–H–Fe) [85–87, 89, 90]. This finding led to the proposal that the E_4 state of NifDK, which is represented by the freeze-trapped intermediate mentioned above, is an M-cluster having two μ_2-hydride ligands bridged between two different pairs of Fe atoms with two protons bound elsewhere on the cluster. This proposed E_4 state, also termed E_4(4H), then formed the basis for the reductive elimination mechanism of N_2 binding. Its structure was further explored in recent theoretical study, which suggests that the cleavage of an Fe-S bond, if not the entire removal of the belt sulfur atom, is an energetically feasible reaction for the M-cluster in the E_4 state [91, 92].

The two hydrides loaded on the M-cluster are thought to be the driving force for N_2 binding. Studies on synthetic compounds suggested, the binding of N_2 can be promoted by the reductive elimination of H_2 [93]. Therefore, the M-cluster in the E_4(4H) state is similarly thought to reductively eliminate one equivalent of H_2 in order to enable the transient binding of N_2. This is followed by immediate reduction, resulting in a proposed bound N_2H_2 species (known as the E_4(2N2H) state) [9, 82]. It should be mentioned that the experimentally observed stoichiometry of one H_2 per reduced N_2 can then be easily explained by the reductive elimination mechanism because in this scenario the elimination of H_2 is a prerequisite for the binding of N_2. In addition, based on the micro-reversibility principle, this proposal also predicts that exogenous H_2 can be oxidatively added to E_4(2N2H) NifDK, thereby replacing the bound N_2 on the M-cluster and generating the E_4(4H) intermediate (Fig. 6b) [9, 82]. This prediction is consistent with two previous biochemical findings. First, it was observed that NifDK produces HD gas under a deuterium D_2/N_2 atmosphere, thus suggesting the direct uptake of H_2 (or D_2) in the presence of N_2 (Fig. 6b) [94, 95]. Second, addition of H_2 was found to alleviate the inhibitory effect of N_2 on acetylene (C_2H_2) reduction observed in NifDK point-mutants, implying that H_2 might compete with N_2 for a specific binding site on the M-cluster [97]. The reversibility of the reductive elimination of H_2 was specifically tested biochemically in a recent study [98]. In this experiment, D_2 was added to the NifDK upon normal N_2 turnover in order to achieve the backward conversion of E_4(2N2H) to E_4(2H2D) as analog to E_4(4H). Subsequently, acetylene (C_2H_2) was added to this turnover mixture to outcompete N_2 for the M-cluster-bound hydrides or deuterides. Incorporation of deuterium into the product ethylene was then observed as $C_2H_2D_2$ and C_2H_3D and detected by GC–MS (Fig. 6b) [98]. This finding supports the transient presence of the E_4(2H2D) intermediate, and hence the reductive elimination proposal, although it has not directly been observed and characterized via spectroscopy.

The distal pathway versus the alternating pathway. In both the proposed distal and the alternating pathway, the steps E_1 to E_4 are thought to proceed by accumulation of reducing equivalents on M-clusters followed by the binding of N_2. Subsequently,

the two pathways diverge between the states E_4 and E_6, and then converge back into the same route for the reduction and the release of the final product ammonia (steps E_7 and E_8) (Fig. 6a) [9, 81, 82]. In the first step of the distal pathway, N_2 binds to an Fe center of the M-cluster in the E_4(4H) state and the subsequent reduction occurs by the preferential addition of protons and electrons to the N atom that is distal to the coordinated metal center. This allows for the formation of a bound hydrazido (Fe=N–NH_2) species at the E_4 state [4, 81]. In the next step (E_5), the addition of a proton and an electron, again at the distal N atom, results in the release of one equivalent of NH_3, and leaves a terminal iron nitride (Fe≡N) species behind. The reduction/protonation of this species in the E_6 state leads to the formation of an iron imido (Fe=NH) moiety which undergoes further electron/proton transfer and, via an iron amido (M-NH_2) intermediate (state E_7), is finally transformed into free NH_3 (state E_8) (Fig. 6a). In contrast, the alternating pathway starts at the N_2-bound E_4 state with the addition of one proton/electron per nitrogen atom. This generates a diazene-bound species (Fe–HN=NH) as the E_4(2N2H) intermediate. The following two electron/proton addition steps (E_5 and E_6) are also proposed to occur alternatingly on both N atoms, thus producing a hydrazine species (M–H_2N–NH_2) as the E_6 state [9, 82]. Further reduction/protonation releases NH_3, generating the same amido-bound species as described in the distal pathway in the E_7 state, followed by the reduction and release of the second equivalent of NH_3 in the final step in E_8 (Fig. 6a).

There is currently no evidence that would conclusively prove the validity of either pathway, although more recent biochemical and spectroscopic findings favor the alternating pathway. Support for the distal N_2 reduction pathway mainly stem from the early work on the synthetic, N_2-reducing, mononuclear Mo complexes by Chatt and Schrock [98, 99]. In addition, the detection of hydrazine formation upon acid- and base-quenching during the pre-steady-state turnover of N_2, was initially viewed as support for the distal pathway by Lowe and others, as this observation was interpreted as the release of the two-electron-reduced hydrazido intermediate in stage E_4 proposed in the distal pathway [100]. However, it was later realized that the same result can also be interpreted as evidence for the presence of the hydrazine bound intermediate which is proposed to be present in the E_6 state of the alternating pathway [9, 82]. On the other hand, biochemical studies revealed that hydrazine (N_2H_4) and diazene (N_2H_2) can be reduced to ammonia by nitrogenase, indicating that these nitrogenous species could be on-route intermediates of N_2 reduction along the alternating pathway [101, 102]. Subsequent spectroscopic studies identified the presence of an intermediate that is generated in the reduction of N_2H_4, N_2H_2 and N_2 [103]. This suggests the reduction of these species might share the same route, hence strongly favoring the alternating pathway. However, such intermediate was also found to only consist of one nitrogen, thus likely representing E_7 or E_8 states, which are shared by both the distal and the alternating pathway [104, 105]. In this light, future attempts to accumulate and characterize nitrogen-bound E_4, E_5 or E_6 will likely provide the definitive answer for this longstanding question in the N_2 reduction mechanism.

4.3 *Structural Insights into the Mechanism of N_2 Reduction*

In parallel to the biochemical and spectroscopic endeavors described, a series of structural studies also shed valuable insights on the workings of NifDK. It was traditionally recognized that structural characterization of any reaction intermediates is exceedingly difficult because it would require the isolation of the reactive NifDK away from the NifH/MgATP-containing reaction mixture, as well as a swift crystallization procedure to capture the reactive conformation before it relaxes back to the resting state [4, 5]. With this in mind, seminal work from the Rees group generated a CO-bound NifDK and solved its crystal structure (Fig. 7a) [106]. CO is isoelectric to N_2, and a well-known inhibitor of nitrogenase, thus it has a much higher chance to be accumulated on the M-cluster. The crystallization is also made possible by an innovated protocol developed by the team, in which substrate turnover was first initiated under an atmosphere of CO, followed by quick re-isolation from the reaction mixture by filtration. The protein was immediately crystallized with crystal seeds, and CO-bound NifDK crystals were reported to form within a matter of hours. The resulting structure had a resolution of 1.50 Å, and featured a μ_2-bridging CO, bound to Fe_2 and Fe_6 of the M-cluster (Fig. 7a). Surprisingly, analysis of the native and the sulfur anomalous data sets revealed that CO completely displaced the bridging sulfur atom (designated S2B) that was originally in the same position. This replacement of Fe ligations also results in a slight distortion of the core geometry, in which that the Mo, the interstitial carbide, and Fe1 atoms no longer align along the threefold symmetry axis, and an overall contraction of the M-cluster around the CO ligand (Fig. 7a). Significantly, the loss of the belt sulfur was demonstrated to be reversible, as recovery of S2B was demonstrated by re-dissolving the CO-bound crystalline NifDK and subjecting them again under turnover with C_2H_2. This finding, on the one hand, substantiates the idea that the loss a belt sulfur is a catalytically relevant step, but on the other hand, raises the question whether there is a nearby site that temporarily harbors the sulfur during catalysis. Inspection of the structure identified a potential sulfur binding site, albeit ~22 Å away from the S2B position, and it is unclear how the S2B sulfur should migrate back and forth across such a long distance within the time frame of substrate turnover (Fig. 7a) [106].

Despite the unanswered questions, the structure nevertheless provided the field with a novel direction of thinking about the mechanism of nitrogenase: the removal of a sulfur ligand that opens up an active Fe site for substrate activation. More recently, another structural report by the group of Einsle also revealed the presence of a light atom ligand, deemed a putative reaction intermediate, in VnfDKG of the *A. vinelandii* V-nitrogenase (Fig. 7b) [107]. In this work, the sample was directly isolated from the cells using a lower dithionite concentration than normal, followed by immediate crystallization. Throughout the process, the sample was kept under a N_2 atmosphere and the structure were resolved to 1.20 Å. Consistent with the CO-bound NifDK structure, the light atom ligand in the VnfDGK structure was also shown to displace the S2B atom of V-cluster (the V-containing analog of M-cluster). Furthermore, in this structure electron density consistent with a sulfur

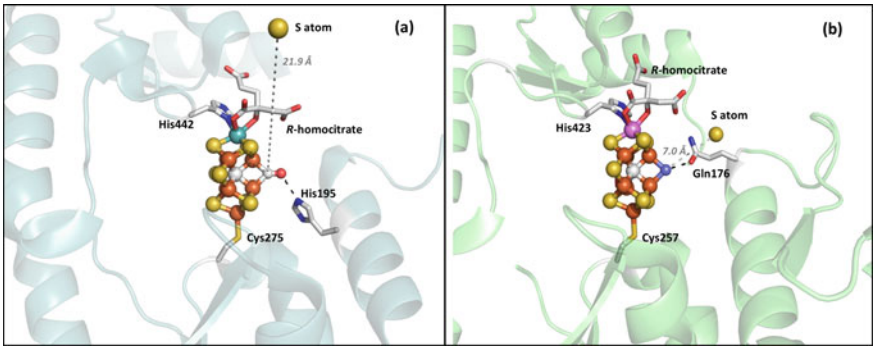

Fig. 7 Structures of the ligand bound cofactors of nitrogenases. Shown is the crystal structure of **a** NifDK with CO bound to the M-cluster; and **b** VnfDGK with a putative NH ligand (colored in light blue) bound to the V-cluster. Sulfur anomalous densities that represent putative sulfur binding sites in each structure are shown as sulfur atoms, with their distances to the light atom ligands labeled in grey. The atoms are colored as those in Fig. 1. PYMOL was used to generate this figure (PBD IDs: 4TKV and 6FEA)

atom was located about 7 Å away from the S2B site, thereby suggesting a likely site for temporary holding of the displaced sulfur (Fig. 7b). Compared to a previous structure of VnfDKG without this light atom ligand, the glutamine residue 176 (αGln176) that is in close contact with S2B is shown to reorient so that it interacts with the Fe bound light atom ligand via the residue's side-chain O atom (Fig. 7b). The movement of amido arm of αGln176 might potentially allow the sulfur to commute between the metal cluster active site and the purported sulfur binding site during catalysis. This interaction between αGln176 and the light atom also implies singly protonation of this ligand. Based on the crystallographic data, the identity of the ligand was initially assigned to be a nitrene (NH^-). However, a follow-up theoretical study in contrary suggested that hydroxide (OH^-) might be the more probable candidate, thereby casting a shadow of doubt whether the ligand might indeed be related to N_2 turnover [108].

Regardless of the identity and physiological relevance of the light atom, this ligand-bound VnfDGK structure nonetheless is a second example for the replacement of a belt sulfur by a substrate or exogenous ligand, and strongly suggests a crucial role for a labile sulfur atom in the catalytic cycle of nitrogenase. Rees and coworkers reasoned that S2B could be protonated by the nearby α-His195, generating HS^- as the leaving group (Fig. 7a) [106]. The departure of the S2B atom in turn creates a reactive diiron face on M-cluster. Theoretical calculations by Varley et al. show that the removal of sulfur from the cluster is energetically feasible and demonstrate that the activation barrier for N_2 binding is much lower when the Fe sites are freed from their original sulfur ligand. That being said, it is currently unclear whether or how the loss of the belt sulfur should be contextualized in the LT model and the proposed reductive elimination framework. Einsle suggested that

hydride accumulation in the early reactive states (i.e. E_1 to E_3) would force the sulfur ligand out of the cofactor, possibly through protonation of the sulfide, and into the nearby sulfur-holding site. It was further suggested that in VnfDGK the sulfur atom might resume its original S2B position upon after the release of the final product, a process which might be facilitated by Gln176, in order to regenerate the E_0 ground state (Fig. 7b) [107]. Based on the assumption that the assigned HN^- ligand in VnfDGK is mechanistically relevant, Einsle hypothesized that it might represent the E_6 state of the distal pathway introduced in Sect. 4.2. In this scenario, N_2 might bind symmetrically in bridging mode between Fe2 and Fe6 as a $\mu_{1,1}$-$N - NH_2$ species.

Finally, to complicate matters further, Rees and coworkers showed that all three of the sulfur atoms, not just S2B, can be lost during catalysis and thus might be mechanistically relevant [109]. First, by turnover with selenocyanate ($SeCN^-$), an alternative substrate and inhibitor of nitrogenase, it was first demonstrated in a 1.60 Å resolution crystal structure that a Se atom can be selectively incorporated into the S2B position of M-cluster [109]. Subsequently, this Se2B-containing-NifDK was then subjected to further turnover with C_2H_2 in a time-dependent structural study in order to monitor the eventual fate of the Se atom. This was achieved by terminating the reaction by freeze quenching at different time points and followed by crystallographic characterization. Remarkably, while the Se occupancy in the 2B position *decreased* during catalytic turnover, while *increasing* levels of Se were detected at the other two belt positions (3A and 5A) [109]. The observation that the Se atom can migrate from one position to another strongly suggests the structural lability of the belt sulfur atoms, although it remains unclear whether substrates or other ligands would be able to access the 3A and 5A sites. In addition, it was also shown that the total Se occupancy disappeared after 5000 turnover cycles, indicating the replenishment of S on the M-cluster [109]. The source of this sulfur has not been identified, although dithionite from the solution would be the major suspect. Taken together, these results suggest the existence of a channel within the matrix of NifDK that allows S and Se (or derivatives thereof) to migrate from the surface of the protein to the active site and vice versa.

5 Conclusion and Future Prospects

In the last decade or so, exciting advances have been made in the field of nitrogenase research which greatly extended our understanding of its assembly and function. On the biosynthesis side, we now have a complete picture of the components and conditions necessary for the synthesis of the P-cluster. Moreover, we have unraveled the once mysterious action of NifB and now have the ability to trace the individual atoms that make up the M-cluster. On the catalysis side, details of the catalytic mechanism are being filled in as an increasing number of reaction intermediates are trapped and studied spectroscopically, while the ligand-bound nitrogenase structures offer incredible insights that were unimaginable a decade ago. All

that being said, there remain a number of challenges ahead. The molecular details of the key steps of P- and M-cluster assembly are thus far missing. X-ray structures that capture snapshots of the key processes, such as the fusion of the P*-cluster or the K-cluster, will therefore be instrumental. Another formidable task is to understand the role of the belt sulfur in catalysis, and to potentially connect the structural observations with the models founded on biochemical and spectroscopic findings. Future attempts to address these questions will without a doubt yield many more exciting, and perhaps surprising, findings on this enzymatic system that has captivated scientist for many decades.

Acknowledgements We would also like to thank the funding agencies that support the work in our groups, including the NIH-NIGMS grant GM67626 (to M.W.R. and Y.H.), which funds research related to the assembly of nitrogenase; the Department of Energy grants DOE (BES) DE-SC0016510 (to Y.H. and M.W.R.) and DE-SC0014470 (to M.W.R. and Y.H.), which fund work related to the mechanistic investigation of ammonia and hydrocarbon formation, respectively, by nitrogenase and related variants; and the NSF grants CHE-1904131 (to M.W.R. and Y.H.) and CHE-1651398 (to Y.H.), which fund work related to CO and CO_2 activation by nitrogenase and its Fe protein component, respectively.

References

1. Vitousek PM, Hättenschwiler S, Olander L, Allison S (2002) Nitrogen and nature. Ambio 31 (2):97–101
2. Gruber N, Galloway JN (2008) An Earth-system perspective of the global nitrogen cycle. Nature 451(7176):293–296
3. Galloway JN, Cowling EB (2002) Reactive nitrogen and the world: 200 years of change. Ambio 31(2):64–71
4. Burgess BK, Lowe DJ (1996) Mechanism of molybdenum nitrogenase. Chem Rev 96 (7):2983–3012
5. Howard JB, Rees DC (1996) Structural basis of biological nitrogen fixation. Chem Rev 96 (7):2965–2982
6. Jasniewski AJ, Lee CC, Ribbe MW, Hu Y (2020) Reactivity, mechanism, and assembly of the alternative nitrogenases. Chem Rev. https://doi.org/10.1021/acs.chemrev.9b00704
7. Burén S, Jiménez-Vicente E, Echavarri-Erasun C, Rubio LM (2020) Biosynthesis of nitrogenase cofactors. Chem Rev. https://doi.org/10.1021/acs.chemrev.9b00489
8. Rutledge HL, Tezcan FA (2020) Electron transfer in nitrogenase. Chem Rev. https://doi.org/10.1021/acs.chemrev.9b00663
9. Seefeldt LC, Yang ZY, Lukoyanov DA et al (2020) Reduction of substrates by nitrogenases. Chem Rev. https://doi.org/10.1021/acs.chemrev.9b00556
10. Rees DC (2002) Great metalloclusters in enzymology. Annu Rev Biochem 71:221–246
11. Howard JB, Rees DC (1994) Nitrogenase: a nucleotide-dependent molecular switch. Annu Rev Biochem 63:235–264
12. Thorneley R, Lowe D (1996) Nitrogenase: substrate binding and activation. J Biol Inorg Chem 1:576–580
13. Lindahl PA, Day EP, Kent TA, Orme-Johnson WH, Münck E (1985) Mössbauer, EPR, and magnetization studies of the *Azotobacter vinelandii* Fe protein. Evidence for a $[4Fe\text{-}4S]^{1+}$ cluster with spin $S = 3/2$. J Biol Chem 260(20):11160–11173
14. Watt GD, McDonald JW (1985) Electron paramagnetic resonance spectrum of the iron protein of nitrogenase: existence of a $g = 4$ spectral component and its effect on spin quantization Biochemistry 24:7226–7231

15. Lanzilotta WN, Ryle MJ, Seefeldt LC (1995) Nucleotide hydrolysis and protein conformational changes in *Azotobacter vinelandii* nitrogenase iron protein: defining the function of aspartate 129. Biochemistry 34(34):10713–10723
16. Watt GD, Reddy KRN (1994) Formation of an all ferrous Fe_4S_4 cluster in the iron protein component of *Azotobacter vinelandii* nitrogenase. J. Inorg. Biochem 53:281–294
17. Guo M, Sulc F, Ribbe MW, Farmer PJ, Burgess BK (2002) Direct assessment of the reduction potential of the $[4Fe\text{-}4S]^{1+/0}$ couple of the Fe protein from *Azotobacter vinelandii*. J Am Chem Soc 124(41):12100–12101
18. Kim J, Rees DC (1992) Crystallographic structure and functional implications of the nitrogenase molybdenum-iron protein from *Azotobacter vinelandii*. Nature 360(6404):553–560
19. Chan MK, Kim J, Rees DC (1993) The nitrogenase FeMo-cofactor and P-cluster pair: 2.2 Å resolution structures. Science 260(5109):792–794
20. Peters JW, Stowell MH, Soltis SM, Finnegan MG, Johnson MK, Rees DC (1997) Redox-dependent structural changes in the nitrogenase P-cluster. Biochemistry 36(6):1181–1187
21. Sørlie M, Christiansen J, Lemon BJ, Peters JW, Dean DR, Hales BJ (2001) Mechanistic features and structure of the nitrogenase α-Gln195 MoFe protein. Biochemistry 40(6):1540–1549
22. Einsle O, Tezcan FA, Andrade SL et al (2002) Nitrogenase MoFe-protein at 1.16 Å resolution: a central ligand in the FeMo-cofactor. Science 297(5587):1696–1700
23. Schmid B, Ribbe MW, Einsle O et al (2002) Structure of a cofactor-deficient nitrogenase MoFe protein. Science 296(5566):352–356
24. Tezcan FA, Kaiser JT, Mustafi D, Walton MY, Howard JB, Rees DC (2005) Nitrogenase complexes: multiple docking sites for a nucleotide switch protein. Science 309(5739):1377–1380
25. Schindelin H, Kisker C, Schlessman JL, Howard JB, Rees DC (1997) Structure of ADP · AIF4–stabilized nitrogenase complex and its implications for signal transduction. Nature 387(6631):370–376
26. Schmid B, Einsle O, Chiu HJ et al (2002) Biochemical and structural characterization of the cross-linked complex of nitrogenase: comparison to the ADP · AIF4–stabilized structure. Biochemistry 41(52):15557–15565
27. Surerus KK, Hendrich MP, Christie PD, Rottgardt D, Orme-Johnson WH, Münck E (1992) Mössbauer and integer-spin EPR of the oxidized P-clusters of nitrogenase: P^{OX} is a non-Kramers system with a nearly degenerate ground doublet. J Am Chem Soc 114(22):8579–8590
28. Zimmermann R, Münck E, Brill WJ, et al (1978) Nitrogenase X: Mössbauer and EPR studies on reversibly oxidized MoFe protein from Azotobacter vinelandii OP. Nature of the iron centers. Biochim Biophys Acta 537(2):185–207
29. Pierik AJ, Wassink H, Haaker H, Hagen WR (1993) Redox properties and EPR spectroscopy of the P clusters of Azotobacter vinelandii MoFe protein. Eur J Biochem 212(1):51–61
30. Keable SM, Zadvornyy OA, Johnson LE et al (2018) Structural characterization of the P^{1+} intermediate state of the P-cluster of nitrogenase. J Biol Chem 293(25):9629–9635
31. Rutledge HL, Rittle J, Williamson LM, Xu WA, Gagnon DM, Tezcan FA (2019) Redox-dependent metastability of the nitrogenase P-cluster. J Am Chem Soc 141(25):10091–10098
32. Spatzal T, Aksoyoglu M, Zhang L et al (2011) Evidence for interstitial carbon in nitrogenase FeMo cofactor. Science 334(6058):940
33. Burgess BK (1990) The iron-molybdenum cofactor of nitrogenase. Chem Rev 90:1377–1406
34. Shah VK, Brill WJ (1977) Isolation of an iron-molybdenum cofactor from nitrogenase. Proc Natl Acad Sci U S A 74(8):3249–3253

35. Sickerman NS, Rettberg LA, Lee CC, Hu Y, Ribbe MW (2017) Cluster assembly in nitrogenase. Essays Biochem 61(2):271–279
36. Hu Y, Ribbe MW (2016a) Biosynthesis of the metalloclusters of nitrogenases. Annu Rev Biochem 85:455–483
37. Ribbe MW, Hu Y, Hodgson KO, Hedman B (2014) Biosynthesis of nitrogenase metalloclusters. Chem Rev 114(8):4063–4080
38. Smith AD, Jameson GN, Dos Santos PC et al (2005) NifS-mediated assembly of [4Fe-4S] clusters in the N- and C-terminal domains of the NifU scaffold protein. Biochemistry 44 (39):12955–12969
39. Yuvaniyama P, Agar JN, Cash VL, Johnson MK, Dean DR (2000) NifS-directed assembly of a transient [2Fe-2S] cluster within the NifU protein. Proc Natl Acad Sci U S A 97(2):599–604
40. Kennedy C, Dean D (1992) The nifU, nifS and nifV gene products are required for activity of all three nitrogenases of *Azotobacter vinelandii*. Mol Gen Genet 231(3):494–498
41. Ribbe MW, Hu Y, Guo M, Schmid B, Burgess BK (2002) The FeMoco-deficient MoFe protein produced by a nifH deletion strain of *Azotobacter vinelandii* shows unusual P-cluster features. J Biol Chem 277(26):23469–23476
42. Hu Y, Fay AW, Dos Santos PC, Naderi F, Ribbe MW (2004) Characterization of *Azotobacter vinelandii nifZ* deletion strains. Indication of stepwise MoFe protein assembly. J Biol Chem 279(52):54963–54971
43. Corbett MC, Hu Y, Naderi F, Ribbe MW, Hedman B, Hodgson KO (2004) Comparison of iron-molybdenum cofactor-deficient nitrogenase MoFe proteins by X-ray absorption spectroscopy: implications for P-cluster biosynthesis. J Biol Chem 279(27):28276–28282
44. Broach RB, Rupnik K, Hu Y et al (2006) Variable-temperature, variable-field magnetic circular dichroism spectroscopic study of the metal clusters in the Δ*nifB* and Δ*nifH* MoFe proteins of nitrogenase from *Azotobacter vinelandii*. Biochemistry 45(50):15039–15048
45. Rupnik K, Lee CC, Hu Y, Ribbe MW, Hales BJ (2011) $[4Fe4S]^{2+}$ clusters exhibit ground-state paramagnetism. J Am Chem Soc 133(18):6871–6873
46. Lee CC, Blank MA, Fay AW et al (2009) Stepwise formation of P-cluster in nitrogenase MoFe protein. Proc Natl Acad Sci U S A 106(44):18474–18478
47. Hu Y, Fay AW, Lee CC, Ribbe MW (2007) P-cluster maturation on nitrogenase MoFe protein. Proc Natl Acad Sci U S A 104(25):10424–10429
48. Rupnik K, Lee CC, Hu Y, Ribbe MW, Hales BJ (2018) A VTVH MCD and EPR spectroscopic study of the maturation of the "second" nitrogenase P-cluster. Inorg Chem 57 (8):4719–4725
49. Rupnik K, Lee CC, Wiig JA, Hu Y, Ribbe MW, Hales BJ (2014) Nonenzymatic synthesis of the P-cluster in the nitrogenase MoFe protein: evidence of the involvement of all-ferrous $[Fe_4S_4]^0$ intermediates. Biochemistry 53(7):1108–1116
50. Corbett MC, Hu Y, Fay AW et al (2007) Conformational differences between *Azotobacter vinelandii* nitrogenase MoFe proteins as studied by small-angle X-ray scattering. Biochemistry 46(27):8066–8074
51. Wiig JA, Hu Y, Ribbe MW (2011) NifEN-B complex of Azotobacter vinelandii is fully functional in nitrogenase FeMo cofactor assembly. Proc Natl Acad Sci U S A 108(21):8623–8627
52. Hu Y, Ribbe MW (2016b) Maturation of nitrogenase cofactor-the role of a class E radical SAM methyltransferase NifB. Curr Opin Chem Biol 31:188–194
53. Frey PA, Hegeman AD, Ruzicka FJ (2008) The radical SAM superfamily. Crit Rev Biochem Mol Biol 43(1):63–88
54. Wiig JA, Hu Y, Lee CC, Ribbe MW (2012) Radical SAM-dependent carbon insertion into the nitrogenase M-cluster. Science 337(6102):1672–1675
55. Wiig JA, Hu Y, Ribbe MW (2015) Refining the pathway of carbide insertion into the nitrogenase M-cluster. Nat Commun 6:8034

56. Fay AW, Wiig JA, Lee CC, Hu Y (2015) Identification and characterization of functional homologs of nitrogenase cofactor biosynthesis protein NifB from methanogens. Proc Natl Acad Sci U S A 112(48):14829–14833
57. Boal AK, Grove TL, McLaughlin MI, Yennawar NH, Booker SJ, Rosenzweig AC (2011) Structural basis for methyl transfer by a radical SAM enzyme. Science 332(6033):1089–1092
58. Grove TL, Benner JS, Radle MI et al (2011) A radically different mechanism for S-adenosylmethionine-dependent methyltransferases. Science 332(6029):604–607
59. Rettberg LA, Wilcoxen J, Lee CC et al (2018) Probing the coordination and function of Fe_4S_4 modules in nitrogenase assembly protein NifB. Nat Commun 9(1):2824
60. Rettberg LA, Wilcoxen J, Jasniewski AJ et al (2020) Identity and function of an essential nitrogen ligand of the nitrogenase cofactor biosynthesis protein NifB. Nat Commun 11 (1):1757
61. Tanifuji K, Lee CC, Sickerman NS et al (2018) Tracing the 'ninth sulfur' of the nitrogenase cofactor via a semi-synthetic approach. Nat Chem 10(5):568–572
62. Jasniewski AJ, Wilcoxen J, Tanifuji K et al (2019) Spectroscopic characterization of an eight-iron nitrogenase cofactor precursor that lacks the "9th sulfur." Angew Chem Int Ed Engl 58(41):14703–14707
63. Fugate CJ, Jarrett JT (2012) Biotin synthase: insights into radical-mediated carbon-sulfur bond formation. Biochim Biophys Acta 1824(11):1213–1222
64. Zheng L, White RH, Cash VL, Dean DR (1994) Mechanism for the desulfurization of L-cysteine catalyzed by the nifS gene product. Biochemistry 33(15):4714–4720
65. Rupnik K, Tanifuji K, Rettberg L, Ribbe MW, Hu Y, Hales BJ (2019) Electron paramagnetic resonance and magnetic circular dichroism spectra of the nitrogenase M cluster precursor suggest sulfur migration upon oxidation: a proposal for substrate and inhibitor binding. Chem BioChem. https://doi.org/10.1002/cbic.201900681
66. Goodwin PJ, Agar JN, Roll JT, Roberts GP, Johnson MK, Dean DR (1998) The Azotobacter vinelandii NifEN complex contains two identical [4Fe-4S] clusters. Biochemistry 37 (29):10420–10428
67. Hu Y, Fay AW, Ribbe MW (2005) Identification of a nitrogenase FeMo cofactor precursor on NifEN complex. Proc Natl Acad Sci U S A 102(9):3236–3241
68. Corbett MC, Hu Y, Fay AW, Ribbe MW, Hedman B, Hodgson KO (2006) Structural insights into a protein-bound iron-molybdenum cofactor precursor. Proc Natl Acad Sci U S A 103(5):1238–1243
69. Lancaster KM, Hu Y, Bergmann U, Ribbe MW, DeBeer S (2013) X-ray spectroscopic observation of an interstitial carbide in NifEN-bound FeMoco precursor. J Am Chem Soc 135(2):610–612
70. Kaiser JT, Hu Y, Wiig JA, Rees DC, Ribbe MW (2011) Structure of precursor-bound NifEN: a nitrogenase FeMo cofactor maturase/insertase. Science 331(6013):91–94
71. Hu Y, Corbett MC, Fay AW et al (2006a) Nitrogenase Fe protein: A molybdate/homocitrate insertase. Proc Natl Acad Sci U S A 103(46):17125–17130
72. Hu Y, Corbett MC, Fay AW et al (2006b) FeMo cofactor maturation on NifEN. Proc Natl Acad Sci U S A 103(46):17119–17124
73. Yoshizawa JM, Blank MA, Fay AW et al (2009) Optimization of FeMoco maturation on NifEN. J Am Chem Soc 131(26):9321–9325
74. Fay AW, Blank MA, Lee CC et al (2011) Spectroscopic characterization of the isolated iron-molybdenum cofactor (FeMoco) precursor from the protein NifEN. Angew Chem Int Ed Engl 50(34):7787–7790
75. Fay AW, Blank MA, Rebelein JG et al (2016) Assembly scaffold NifEN: a structural and functional homolog of the nitrogenase catalytic component. Proc Natl Acad Sci U S A 113 (34):9504–9508

76. Fay AW, Blank MA, Yoshizawa JM et al (2010) Formation of a homocitrate-free iron-molybdenum cluster on NifEN: implications for the role of homocitrate in nitrogenase assembly. Dalton Trans 39(12):3124–3130
77. Solomon JB, Lee CC, Jasniewski AJ, Rasekh MF, Ribbe MW, Hu Y (2020) Heterologous expression and engineering of the nitrogenase cofactor biosynthesis scaffold NifEN. Angew Chem Int Ed Engl 59(17):6887–6893
78. Hu Y, Fay AW, Ribbe MW (2007) Molecular insights into nitrogenase FeMo cofactor insertion: the role of His 362 of the MoFe protein alpha subunit in FeMo cofactor incorporation. J Biol Inorg Chem 12(4):449–460
79. Fay AW, Hu Y, Schmid B, Ribbe MW (2007) Molecular insights into nitrogenase FeMoco insertion–the role of His 274 and His 451 of MoFe protein alpha subunit. J Inorg Biochem 101(11–12):1630–1641
80. Hu Y, Fay AW, Schmid B, Makar B, Ribbe MW (2006) Molecular insights into nitrogenase FeMoco insertion: TRP-444 of MoFe protein alpha-subunit locks FeMoco in its binding site. J Biol Chem 281(41):30534–30541
81. Thorneley RN, Lowe DJ (1984) The mechanism of Klebsiella pneumoniae nitrogenase action. Pre-steady-state kinetics of an enzyme-bound intermediate in N_2 reduction and of NH_3 formation. Biochem J 224(3):887–894
82. Hoffman BM, Lukoyanov D, Yang ZY, Dean DR, Seefeldt LC (2014) Mechanism of nitrogen fixation by nitrogenase: the next stage. Chem Rev 114(8):4041–4062
83. Lowe DJ, Thorneley RN (1984) The mechanism of Klebsiella pneumoniae nitrogenase action. The determination of rate constants required for the simulation of the kinetics of N_2 reduction and H_2 evolution. Biochem J 224(3):895–901
84. Thorneley RN, Lowe DJ (1984) The mechanism of Klebsiella pneumoniae nitrogenase action. Simulation of the dependences of H_2-evolution rate on component-protein concentration and ratio and sodium dithionite concentration. Biochem J 224(3):903–909
85. Lukoyanov D, Yang ZY, Khadka N, Dean DR, Seefeldt LC, Hoffman BM (2015) Identification of a key catalytic intermediate demonstrates that nitrogenase is activated by the reversible exchange of N_2 for H_2. J Am Chem Soc 137(10):3610–3615
86. Lukoyanov D, Khadka N, Yang ZY, Dean DR, Seefeldt LC, Hoffman BM (2016a) Reversible photoinduced reductive elimination of H_2 from the nitrogenase dihydride state, the E_4(4H) Janus intermediate. J Am Chem Soc 138(4):1320–1327
87. Lukoyanov D, Khadka N, Yang ZY, Dean DR, Seefeldt LC, Hoffman BM (2016b) Reductive elimination of H_2 activates nitrogenase to reduce the N≡N triple Bond: characterization of the E_4(4H) Janus intermediate in wild-type enzyme. J Am Chem Soc 138 (33):10674–10683
88. Igarashi RY, Laryukhin M, Dos Santos PC et al (2005) Trapping H- bound to the nitrogenase FeMo-cofactor active site during H_2 evolution: characterization by ENDOR spectroscopy. J Am Chem Soc 127(17):6231–6241
89. Lukoyanov D, Barney BM, Dean DR, Seefeldt LC, Hoffman BM (2007) Connecting nitrogenase intermediates with the kinetic scheme for N2 reduction by a relaxation protocol and identification of the N_2 binding state. Proc Natl Acad Sci U S A 104(5):1451–1455
90. Lukoyanov D, Yang ZY, Dean DR, Seefeldt LC, Hoffman BM (2010) Is Mo involved in hydride binding by the four-electron reduced (E4) intermediate of the nitrogenase MoFe protein? J Am Chem Soc 132(8):2526–2527
91. Raugei S, Seefeldt LC, Hoffman BM (2018) Critical computational analysis illuminates the reductive-elimination mechanism that activates nitrogenase for N_2 reduction. Proc Natl Acad Sci U S A 115(45):E10521–E10530
92. Hoeke V, Tociu L, Case DA, Seefeldt LC, Raugei S, Hoffman BM (2019) High-resolution ENDOR spectroscopy combined with quantum chemical calculations reveals the structure of nitrogenase Janus intermediate E_4(4H). J Am Chem Soc 141(30):11984–11996

93. Yang H, Rittle J, Marts AR, Peters JC, Hoffman BM (2018) ENDOR characterization of $(N_2)Fe^{II}(\mu\text{-}H)_2Fe^{I}(N_2)^-$: A spectroscopic model for N_2 binding by the di-μ-hydrido nitrogenase Janus intermediate. Inorg Chem 57(19):12323–12330
94. Burgess BK, Wherland S, Newton WE, Stiefel EI (1981) Nitrogenase reactivity: insight into the nitrogen-fixing process through hydrogen-inhibition and HD-forming reactions. Biochemistry 20(18):5140–5146
95. Jensen BB, Burris RH (1985) Effect of high pN_2 and high pD_2 on NH_3 production, H_2 evolution, and HD formation by nitrogenases. Biochemistry 24(5):1141–1147
96. Fisher K, Dilworth MJ, Newton WE (2000) Differential effects on N_2 binding and reduction, HD formation, and azide reduction with α-195^{His}- and α-191^{Gln}-substituted MoFe proteins of Azotobacter vinelandii nitrogenase. Biochemistry 39(50):15570–15577
97. Yang ZY, Khadka N, Lukoyanov D, Hoffman BM, Dean DR, Seefeldt LC (2013) On reversible H_2 loss upon N_2 binding to FeMo-cofactor of nitrogenase. Proc Natl Acad Sci U S A 110(41):16327–16332
98. Chatt J, Pearman AJ, Richards RL (1975) The reduction of mono-coordinated molecular nitrogen to ammonia in a protic environment. Nature 253:39–40
99. Yandulov DV, Schrock RR (2003) Catalytic reduction of dinitrogen to ammonia at a single molybdenum center. Science 301(5629):76–78
100. Thorneley RNF, Eady RR, Lowe DJ (1978) Biological nitrogen fixation by way of an enzyme-bound dinitrogen-hydride intermediate. Nature 272:557–558
101. Davis LC (1980) Hydrazine as a substrate and inhibitor of *Azotobacter vinelandii* nitrogenase. Arch Biochem Biophys 204(1):270–276
102. Barney BM, McClead J, Lukoyanov D et al (2007) Diazene (HN=NH) is a substrate for nitrogenase: insights into the pathway of N_2 reduction. Biochemistry 46(23):6784–6794
103. Barney BM, Yang TC, Igarashi RY et al (2005) Intermediates trapped during nitrogenase reduction of N triple bond N, CH_3-N=NH, and H_2N–NH_2. J Am Chem Soc 127(43):14960–14961
104. Lukoyanov D, Dikanov SA, Yang ZY et al (2011) ENDOR/HYSCORE studies of the common intermediate trapped during nitrogenase reduction of N_2H_2, CH_3N_2H, and N_2H_4 support an alternating reaction pathway for N_2 reduction. J Am Chem Soc 133(30):11655–11664
105. Lukoyanov D, Yang ZY, Barney BM, Dean DR, Seefeldt LC, Hoffman BM (2012) Unification of reaction pathway and kinetic scheme for N_2 reduction catalyzed by nitrogenase. Proc Natl Acad Sci U S A 109(15):5583–5587
106. Spatzal T, Perez KA, Einsle O, Howard JB, Rees DC (2014) Ligand binding to the FeMo-cofactor: structures of CO-bound and reactivated nitrogenase. Science 345 (6204):1620–1623
107. Sippel D, Rohde M, Netzer J et al (2018) A bound reaction intermediate sheds light on the mechanism of nitrogenase. Science 359(6383):1484–1489
108. Benediktsson B, Thorhallsson AT, Bjornsson R (2018) QM/MM calculations reveal a bridging hydroxo group in a vanadium nitrogenase crystal structure. Chem Commun (Camb) 54(53):7310–7313
109. Spatzal T, Perez KA, Howard JB, Rees DC (2015) Catalysis-dependent selenium incorporation and migration in the nitrogenase active site iron-molybdenum cofactor. Elife 4:e11620

Mitigation of Laughing Gas Emissions by Nitrous Oxide Respiring Microorganisms

Jörg Simon

Abstract

Nitrous oxide (N_2O, laughing gas) is a potent greenhouse gas and ozone-depleting molecule. Since its atmospheric concentration is constantly rising, N_2O contributes significantly to the imminent climate crisis. A considerable portion of N_2O emissions has been recognized to be anthropogenic, mainly originating from extensive agriculture needed to feed an ever-increasing world population. In this context, biologically catalysed N_2O reduction to dinitrogen gas (N_2) is clearly a desirable process for humankind. Various microbial species have been described to produce the copper cluster-containing enzyme N_2O reductase (NosZ), which is the only known enzyme that converts N_2O to N_2. NosZ functions as the terminal reductase of anaerobic N_2O respiration, which conserves energy through *proton motive force* generation. In this chapter, the physiological trait of N_2O respiration is presented on the organismic, genomic and enzymatic levels including the biosynthesis of NosZ and the architecture of different kinds of dedicated electron transport chains that sustain N_2O respiration. In addition, conceivable strategies to mitigate N_2O emissions are discussed including bioaugmentation and engineering strategies for efficient and robust N_2O-respiring microorganisms.

Keywords

Anaerobic respiration · Clade I and clade II nitrous oxide reductase · Climate change · Greenhouse gas · Nitrous oxide (N_2O laughing gas) respiration · *nos* gene cluster · NosZ

J. Simon (✉)
Department of Biology, Microbial Energy Conversion and Biotechnology, Technical University of Darmstadt, Darmstadt, Germany
e-mail: simon@bio.tu-darmstadt.de

J. J. G. Moura et al. (eds.), *Enzymes for Solving Humankind's Problems*,
https://doi.org/10.1007/978-3-030-58315-6_7

1 Introduction

Nitrous oxide (laughing gas; N_2O) is the dominant nitrogenous greenhouse gas (GHG) on Earth and contributes to ozone layer depletion [1, 2]. Its current atmospheric concentration amounts to about 332 ppbv (13 nM), and its average atmospheric lifetime is 114 years. The N_2O concentration is approximately 1,250-fold lower than that of carbon dioxide (CO_2) but, noteworthily, N_2O has an almost 300-fold greater potential for global warming effects, based on radiative capacities. Hence, N_2O accounts for up to 10% of total emissions when the impact of individual GHGs on global warming is expressed in terms of CO_2 equivalents (CO_2e), a unit that has been approved by the Intergovernmental Panel on Climate Change (IPCC) [1]. For comparison, the atmospheric N_2O concentration in the year 1900 was about 277 ppbv (17% lower than today), and it has been concluded from ice core studies that the N_2O concentration was, most likely, never higher than 280 ppbv over the last 800.000 years [3, 4]. The main reason for the dramatically rising N_2O concentration is the worldwide intensification of agricultural fertilization practices that is resulting in a severe anthropogenic imbalance of the global biogeochemical nitrogen cycle [3, 5–11]. This development started with the invention of man-made nitrogen fixation by the Haber–Bosch process that allowed the ever-expanding application of synthetic nitrogen-based fertilizers [12]. Hence, agriculture and livestock farming are the main drivers of anthropogenic N_2O emissions with minor contributions from fossil fuel combustion, biomass burning and wastewater treatment [1, 3, 10]. The *IPCC Special Report Climate Change and Land* from 2019 (revised in 2020) quotes: 'Agriculture, Forestry and Other Land Use (AFOLU) activities accounted for around 13% of CO_2, 44% of methane (CH_4), and 81% of nitrous oxide (N_2O) emissions from human activities globally during 2007–2016, representing 23% (12.0 ± 3.0 $GtCO_2e$ yr^{-1}) of total net anthropogenic emissions of GHGs (*medium confidence*)'. [13]. Thus, humankind faces a severe challenge in terms of N_2O emissions since agricultural activities will have to increase further to nourish the growing world population.

At room temperature, N_2O is a rather inert, colourless and non-flammable gas that can nevertheless act as a biocide, for example, by promoting vitamin B_{12} deficiency and affecting vitamin B_{12}-dependent enzymes. N_2O is used as an anaesthetic in surgery and dentistry but also served as a recreational drug, hence its colloquial name 'laughing gas'. In natural environments, N_2O is generated by various microbial metabolic processes including nitrate or nitrite reduction via nitric oxide (NO) and N_2O to produce dinitrogen gas (N_2), the so-called denitrification pathway, as well as dissimilatory nitrate/nitrite reduction to ammonia (DNRA) (Fig. 1) [14–20].

In addition, N_2O is also produced by aerobic ammonia-oxidizing bacteria via the so-called nitrifier denitrification pathway, by ammonia-oxidizing Thaumarchaeota and by some methane-oxidizing bacteria that denitrify nitrate and/or nitrite under hypoxic conditions (Fig. 1) [17, 20–25]. Furthermore, N_2O effluxes from plants have been reported [26]. Among the microbial processes, only organisms

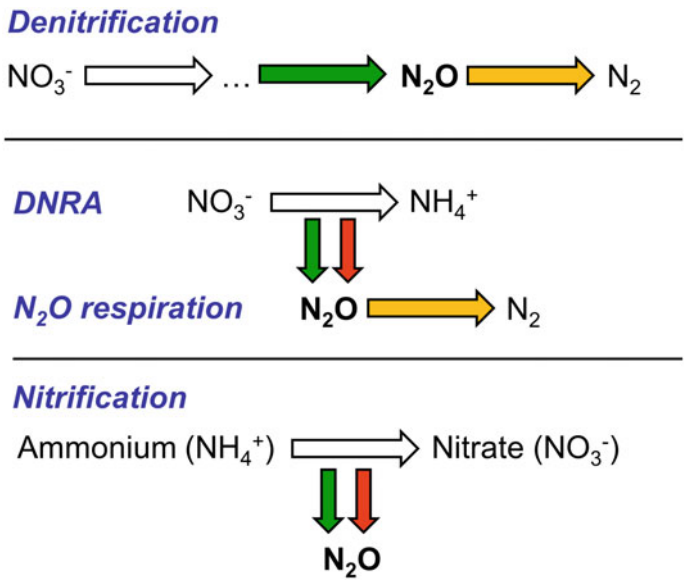

Fig. 1 Simplified presentation of energy-conserving pathways that produce or consume N_2O. Horizontal arrows show metabolic pathways (denoted in italics) and vertical arrows specify side reactions. Green and red arrows designate biotic and abiotic N_2O production respectively. Orange arrows denote N_2O reduction to N_2 catalysed by nitrous oxide reductase NosZ. Note that nitrite (NO_2^-) is an intermediate in denitrification, DNRA and nitrification. DNRA, dissimilatory nitrate reduction to ammonium

performing either denitrification or DNRA are capable to convert nitrate to N_2O [18]. However, the contribution of each of these pathways (let alone of individual species) to the release of N_2O from natural microbial communities has not been elucidated and is thought to depend on several abiotic factors such as carbon and oxygenation status, carbon-to-nitrogen ratio, pH and supply of nitrate, nitrite or bioavailable copper ions [20, 27–29]. The denitrification pathway releases intermediate N_2O when these environmental constraints or the absence of an intact N_2O reductase prevent N_2O reduction to N_2. On the other hand, the DNRA pathway is thought to produce minor amounts of N_2O as a by-product of the nitrate/nitrite ammonification process, in which nitrite is reduced directly to ammonium by a cytochrome *c* nitrite reductase called NrfA (Fig. 1) [16]. Under laboratory DNRA conditions, some NO is readily formed abiotically from (accumulated) nitrite and various enzymes have been described that catalyse non-respiratory NO detoxification [18, 30, 31]. Under anoxic conditions, some of these enzymes produce N_2O, and therefore, N_2O formation is a common feature for microbial cells that live in the presence of nitrate/nitrite. The presence of reactive nitrogenous compounds such as nitrite, NO and hydroxylamine can also give rise to the microbially mediated formation of so-called hybrid N_2O, in which only one nitrogen atom derived from nitrite, NO or hydroxylamine and the other one from another cellular N

species [25, 32]. This process, also called codenitrification or BioNitrosation, is facilitated by the presence of organics and metal ions. In addition, N_2O is produced by abiotically supported processes such as chemodenitrification [33–35].

The microbial trait of N_2O reduction to N_2 was originally assigned to denitrifying species of the phylum Proteobacteria [36]. In denitrification, the sequential reduction of nitrate via nitrite, NO and N_2O to N_2 is stepwise catalysed by dedicated enzymes. Typical denitrifiers are heterotrophs that use a variety of carbon compounds as electron and carbon source. Such electrons serve to reduce the quinone/quinol pool and are eventually transferred to terminal reductases of anaerobic respiration, namely nitrate reductase, NO-producing nitrite reductase (either cytochrome cd_1 nitrite reductase NirS or Cu-containing nitrite reductase NirK), N_2O-producing NO reductase and N_2O reductase (NosZ) [36]. NosZ is a copper-containing enzyme that is described in Sect. 4 in more detail. Over the last decade, it emerged that, based on phylogenetic analyses, each NosZ enzyme belongs to one of the two distinct clades, which are nowadays called clade I and clade II [28, 37, 38]. Furthermore, it turned out that this nomenclature can be expanded to the corresponding NosZ-encoding *nos* gene clusters (NGCs) and NosZ-harbouring microorganisms (see Table 1 for some properties of clade I and clade II N_2O reduction systems and Sects. 4 and 5 for more details).

Denitrification and DNRA (also known as respiratory nitrate/nitrite ammonification) are forms of microbial anaerobic respiration. The free energy of a redox reaction catalysed in the course of anaerobic respiration is typically conserved in the generation of a proton gradient over the cytoplasmic membrane (the proton motive force, *pmf*), which is then used to drive ADP phosphorylation by ATP synthase. According to this definition, the reduction of N_2O to N_2 qualifies as anaerobic respiration in its own right and is called here 'N_2O respiration'. N_2O-respiring microorganisms (NRBs) can be denitrifiers that catalyse N_2O respiration as part of their denitrification pathway or NosZ-containing nitrate/nitrite ammonifiers that use N_2O respiration to convert N_2O that has been produced from endogenous NO detoxification or by cells from the surrounding microbial community. Notably, some denitrifiers and DNRA-performing microbes have even been shown to grow by N_2O respiration in the laboratory using N_2O (supplied at various concentrations) as the sole electron acceptor (see Sect. 2). In general, the reduction of nitrogen oxyanions and nitrogen oxides such as nitrate, nitrite, NO and N_2O is energetically favourable, due to the rather positive midpoint redox potentials of the corresponding redox pairs (expressed in the E_0' value, i.e. under standard conditions at pH 7.0). For example, E_0' of the N_2O/N_2 couple amounts to + 1.36 V, which makes N_2O reduction by, for instance, hydrogen, formate or NAD(P)H highly exergonic (see Sect. 2).

This chapter describes the physiology of NRBs and aspects of the molecular basis of microbial N_2O reduction/respiration at different levels (Sects. 2–5). Furthermore, it presents experimental approaches that aim to apply or engineer NRBs in the context of humankind's N_2O emission problem (Sects. 6 and 7). The reader might keep the following central questions in mind throughout the chapter.

Table 1 Selected properties of clade I and II N_2O reduction systems and N_2O-reducing organisms

Property	Clade I	Clade II
General features		
Prominent phyla	Proteobacteria (classes Alpha-, Beta- and Gammaproteobacteria), Euryarchaeota	Proteobacteria (classes Beta-, Delta- and Epsilonproteobacteria), Firmicutes, Bacteroidetes, Gemmatimonadetes, Deferribacteres, Chloroflexi, Euryarchaeota, Crenarchaeota
Dissimilatory nitrate metabolism of the host cell	Often complete denitrification, i.e. N_2 formation from nitrate or nitrite	Complete or incomplete denitrification, DNRA (respiratory nitrate/nitrite ammonification)
N_2O reductase		
Type of N_2O reductase	Conventional NosZ	Conventional NosZ or cytochrome *c* NosZ (*c*NosZ)
NosZ export across the cytoplasmic membrane	Tat system	Sec system
Electron transport and maturation proteins[a]		
Components of the respiratory electron transport chain from the quinone/quinol pool to N_2O	Cytochrome bc_1 complex (Qcr), soluble monohaem cytochromes *c* and/or small copper proteins (azurins, pseudoazurins, cupredoxins)	Rieske/cytochrome *bc* complex (Qcr), soluble monohaem cytochromes *c*
Further electron transport and/or maturation proteins encoded in *nos* gene clusters	NosR, NosX, NosD, NosF, NosY, NosL	NosB, NosG, NosH, NosC, NosC1, NosC2, NosD, NosF, NosY, NosL
Miscellaneous traits		
Nos fusion proteins	-	NosB-C2, NosB-L, NosD-F
Maturation proteins not encoded in *nos* gene clusters	ApbE (functionally equivalent to NosX); Cu_A maturation proteins	Cu_A maturation proteins

[a]See Table 2 and Fig. 3 for more details
Taken from [19]

- To what extent is N_2O reduction/respiration understood at the physiological and/or molecular level?
- From the anthropocentric view: what are the best-suited N_2O-reducing/-respiring microorganisms nature has to offer to mitigate N_2O emissions?
- Is there potential to 'optimize' the physiology of NRBs and what knowledge is mandatory to do so successfully?
- Will this sort of research eventually help to mitigate N_2O emissions from different environments?

2 The Organismic Level: Physiology of Nitrous Oxide-Respiring Bacteria

By definition, laboratory cultures of axenic NRBs will grow at the expense of exogenous N_2O as (sole) electron acceptor. With formate, hydrogen gas or NADH (i.e. reducing equivalents derived from degraded carbohydrates or proteins) as exemplary electron donors, an NRB will catalyse one or more of the following exergonic reactions (Eqs. 1–3).

$$HCOO^- + H^+ + N_2O \rightarrow CO_2 + N_2 + H_2O \quad \Delta G'_0 = -345\,kJ\,mol^{-1} \tag{1}$$

$$H_2 + N_2O \rightarrow N_2 + H_2O \quad \Delta G'_0 = -342\,kJ\,mol^{-1} \tag{2}$$

$$NADH + H^+ + N_2O \rightarrow NAD^+ + N_2 + H_2O \quad \Delta G'_0 = -324\,kJ\,mol^{-1} \tag{3}$$

The few experimentally characterized NRBs are nitrate/nitrite-reducing denitrifiers or DNRA organisms although, in principle, N_2O respiration does not depend on nitrate/nitrite reduction. The known NRBs belong to the phylum Proteobacteria (e.g. the Alphaproteobacteria *Ensifer meliloti* [39] and *Bradyrhizobium japonicum* [40], members of the betaproteobacterial genera *Dechloromonas* and *Azospira* [41–43], the Gammaproteobacterium *Pseudomonas stutzeri* [44], the Deltaproteobacterium *Anaeromyxobacter dehalogenans* [37] or the Epsilonproteobacteria *Wolinella succinogenes* and *Campylobacter fetus* [45, 46]), and to the phyla Gemmatimonadetes (*Gemmatimonas aurantiaca* [47, 48], Firmicutes (*Bacillus vireti* [49] and Bacteroidetes (*Dyadobacter fermentans* [50]. Interestingly, the majority of these bacteria contain a clade II NosZ, with the exception of *E. meliloti*, *B. japonicum* and *P. stutzeri*, which are classical clade I denitrifiers. Notably, when growing these bacteria in the laboratory, the applied N_2O concentrations in the gas phase varied between a few per cent (v/v) and a pure N_2O atmosphere. The latter will result in an unphysiologically high N_2O concentration in the liquid phase of about 20–25 mM at mesophilic conditions, due the exceptionally high solubility of N_2O gas. Unfortunately, comparative knowledge of growth yields of N_2O respiration and N_2O consumption rates of the corresponding cultures is rather limited [19]. In pure cultures, the growth yields of N_2O respiration as well as the apparent cellular affinities for N_2O were reported to be higher for the clade II organisms *Dechloromonas aromatica* and *A. dehalogenans* when compared with those of the clade I bacteria *P. stutzeri* and *Shewanella loihica* [41]. For *W. succinogenes* cells that had been grown at the expense of Eq. 1, a growth yield of 9.1 ± 0.1 g dry cells per mole formate and an N_2O consumption rate of 15 mmol N_2O h^{-1} (g dry cell weight)$^{-1}$ have been reported [19, 45]. Notably, these cells grew under an atmosphere of pure N_2O provided in the headspace of the culture, a property that is thought to be facilitated by the absence of vitamin B_{12}-dependent enzymes [45, 51]. The reported yields of N_2O respiration as well as N_2O consumption rates obtained with other organisms revealed a certain variation and one should be cautious when

comparing such values since different growth media and conditions have been used [19]. The parameters did not clearly correlate with the possession of either a clade I or clade II NosZ or whether the organism is a nitrate/nitrite-reducing denitrifier or a non-denitrifying DNRA bacterium. However, the ecological significance of these findings remained unclear.

NRBs have been isolated from various, mostly anoxic or micro-oxic habitats such as soil, activated sludge or animal gut or rumen, and many of these organisms are facultatively anaerobic bacteria employing a respiratory chain involved in (micro)aerobic respiration. This feature is thought to impart a certain degree of aerotolerance on the cells and may shield N_2O reductase from inactivation by oxygen. In fact, several *P. stutzeri* strains have been described to perform N_2O reduction under microaerobic or even aerobic conditions [52–56]. This property is exceptional since N_2O reduction by NosZ usually requires anoxic conditions due to the vulnerability of the NosZ copper centres to oxygen (see Sect. 4). Interestingly, N_2O reduction under (micro)oxic conditions has also been reported for clade II organisms such as *Azospira* sp. and *G. aurantiaca* [42, 57].

3 The Genomic Level: Diversity of *nos* Gene Clusters

As stated in the Introduction, phylogenetic analyses indicated that NosZ enzymes either belong to clade I or clade II, and it appeared that this classification is also applicable to the corresponding *nos* gene clusters (NGCs). As a matter of fact, the composition of clade I and clade II NGCs differs to a large extent, reflecting the biochemical complexity of the corresponding N_2O reduction systems (see Sects. 4 and 5).

Figure 2 shows three different NGCs that are representative for (i) a clade I NGC from a denitrifier (*Paracoccus denitrificans*), (ii) a complex clade II NGC (*W. succinogenes*) and (iii) a somewhat simpler clade II NGC from a species of the phylum Firmicutes (*Bacillus vireti*) that lacks the *nosG*, *-C1*, *-C2* and *-H* gene assembly (Table 1). Note that DNRA bacteria such as *W. succinogenes* and *B. vireti* typically contain a clade II rather than a clade I NGC. The clade I core NGC comprises genes encoding NosR, -Z, -D, -F, -Y and -L, whereas the genes coding for NosC and NosX are present only in some cases [see Table 2 for an overview of the properties of different Nos proteins and their (proposed) function]. Of the core Nos proteins, only NosR is found exclusively in clade I NGCs. In contrast, multiple conserved genes that are specifically found in clade II NGCs have been described. NosB is encoded in all known clade II NGCs, whereas the cluster of four genes encoding NosG, -C1, -C2 and -H is found in many, but not all, clade II NGCs.

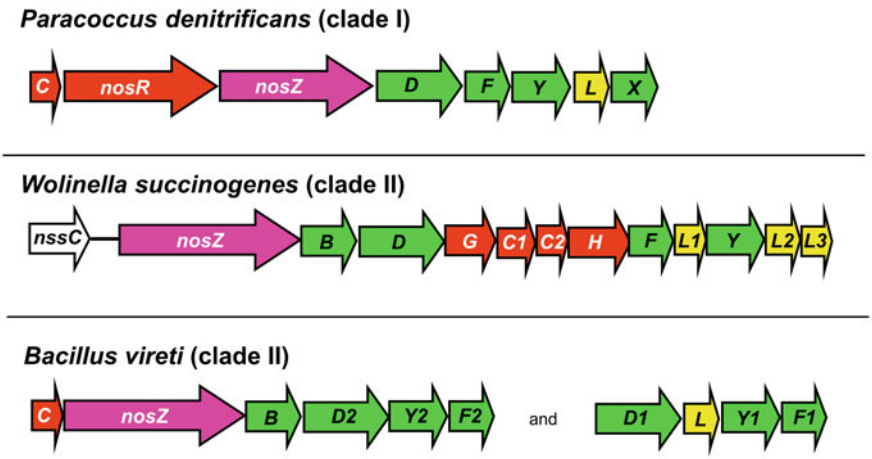

Fig. 2 Organization of representative clade I and clade II *nos* gene clusters (NGCs). Colours indicate the following functions of the respective gene products: pink, N_2O reductase; red, electron transport protein; yellow, copper chaperone; green, biogenesis and maintenance of the Nos system. The *W. succinogenes nssC* gene encodes a transcription regulator of the Crp/Fnr superfamily that is essential for N_2O respiration [51]. Note that the *B. vireti* genome encodes paralogs of *nosD*, *-Y* and *-F* [119]. See text for details and [18, 28, 37] for detailed illustrations of NGC diversity. Adapted with permission from [19]

4 The Enzymatic Level, Part I: Members of the Nitrous Oxide Reductase (NosZ) Family and Their Biogenesis

Nitrous oxide reductase catalyses the two-electron reduction of N_2O to N_2 (Eq. 4) and is located at the outer side of the cytoplasmic membrane (corresponding to the periplasm in case of gram-negative bacteria) where it receives electrons from a dedicated electron transport chain (see Sect. 5).

$$N_2O + 2e^- + 2H^+ \rightarrow N_2 + H_2O \quad (4)$$

Some DNRA-performing bacteria (predominantly Epsilonproteobacteria) produce a NosZ variant called cytochrome *c* N_2O reductase (*c*NosZ), which harbours an additional C-terminal monohaem cytochrome *c* domain that was proposed to function as an electron entry point to the copper active site [16, 58, 59]. Genes encoding *c*NosZ enzymes have been found exclusively as part of clade II *nos* gene clusters (see the NGC from *W. succinogenes* in Fig. 2 as an example). Export of clade II N_2O reductases, including *c*NosZ, to the periplasm or extracellular space is accomplished by the Sec secretion pathway (Table 1). This is in line with the view that cytochromes *c* are generally exported by the Sec pathway since covalent haem attachment is catalysed in this compartment by a dedicated biogenesis apparatus [60, 61]. In contrast, the Tat pathway is used to export clade I NosZ enzymes in denitrifiers.

Table 2 Conserved proteins encoded in representative *nos* gene clusters

Designation	Present in clade	(Predicted) cofactors	(Anticipated) properties and function
N_2O reductase			
NosZ	I, II	Binuclear Cu_A and tetranuclear Cu_Z centre	Conventional N_2O reductase
*c*NosZ	II	Binuclear Cu_A and tetranuclear Cu_Z centre; one haem *c*	Cytochrome *c* N_2O reductase
Accessory proteins serving in respiratory electron transport and/or NosZ/cNosZ activity maintenance (prevention of Cu_Z formation or Cu_Z* rescue mechanism) and/or maturation of the Nos system*			
NosD	I, II	None	Periplasmic interaction with the putative ABC transporter NosFY
NosF	I, II	None	ATP-hydrolysing cytoplasmic component of the putative ABC transporter NosDFY
NosY	I, II	None	Membrane-integral component of the putative ABC transporter NosDFY exhibiting six predicted membrane-spanning segments
NosL	I, II	Cu	Copper assembly at active site of NosZ/ *c*NosZ
NosC	I, II	One haem *c*	Periplasmic redox partner of NosZ containing a conserved haem *c* binding motif (CXXCH)
NosR	I	Covalently bound FMN and two [4Fe–4S] clusters[a]	Membrane-bound electron transport protein
NosX	I	FAD	Periplasmic FMN incorporation into NosR
NosB	II	None	Membrane-bound protein (four or six transmembrane segments) of unknown function, possibly serving as a scaffold to organize other accessory Nos proteins in the membrane
NosG	II	Four [4Fe–4S] clusters	Redox partner of NosH
NosH	II	Two [4Fe–4S] clusters[a]	Membrane-bound protein; part of a predicted NosGH complex
NosC1	II	One haem *c*	Periplasmic electron transport containing a conserved haem *c* binding motif (CXXCH)
NosC2	II	One haem *c*	Periplasmic electron transport containing a conserved haem *c* binding motif (CXXCH)

See Fig. 3 for illustrations

[a] The primary protein structure contains two additional and conserved cytoplasmic CX_3CP motifs that are potentially involved in binding a cofactor

Adapted from [19]

Purified and biochemically and/or structurally characterized NosZ enzymes generally belong to clade I with the notable exception of *W. succinogenes* *c*NosZ [62]. NosZ proteins form homodimers and consist of an N-terminal seven-bladed β-propeller domain and a C-terminal cupredoxin domain. Each monomer contains a mixed-valent binuclear Cu_A centre and a sulphide-bridged tetranuclear Cu_Z centre that harbours four more copper atoms. The four copper atoms of Cu_Z are coordinated by imidazole nitrogen atoms derived from seven conserved histidine residues. Thus, NosZ is a copper-rich enzyme that binds 12 copper atoms per homodimer. Each homodimer contains two active sites of N_2O reduction, and each active site is composed of Cu_A and Cu_Z centres that originate from different NosZ monomers. The shortest intermonomer distance between the Cu_A and Cu_Z sites is about 10 Å, whereas the two centres located in the same monomer are 40 Å apart [63–66].

Isolated NosZ enzymes showed K_M values for N_2O in the μM range, which is way above the atmospheric N_2O concentration [67, 68]. Therefore, once in the atmosphere, the chemically stable N_2O molecule evades biological turnover due to its low concentration. Usually, the N_2O reduction activity of NosZ is oxygen-sensitive and exhibits an alkaline pH optimum. The spectroscopic features of different NosZ enzyme forms isolated or incubated under different oxygen regimes have been comprehensively reviewed, and the reader is referred to these articles for details concerning the structure/function relationships of various oxidation state-dependent molecular forms of the copper centres [67–72]. Notably, the formation of an inactive (resting) state of the Cu_Z centre has been designated Cu_Z*. The Cu_Z* form corresponds to a (4Cu1S) [$1Cu^{2+}$–$3Cu^{1+}$] centre that contains one sulphur and one oxygen atom from a hydroxide ion or a water molecule [68]. This form was postulated to result from enzyme inactivation due to the absence of reductants (see Sect. 5 for putative in vivo electron donors). Furthermore, the Cu_Z* state was obtained in aerobically isolated enzymes and might thus be environmentally relevant. This raised the question as to how the Cu_Z* state can be rescued to restore a fully reduced and catalytically competent form (the [$4Cu^{1+}$] state). In vitro, this repair process has been reported to occur by *reductive activation*, for example, by donating electrons using a low-potential reductant such as methyl or benzyl viologen radicals [68, 69]. Thus, it seems mandatory that a dedicated in vivo electron transfer route to the active site of NosZ exists to enable (re-)activation of NosZ activity and/or to prevent Cu_Z* formation (see Sect. 5).

Evaluation of the literature argues that the copper content in many NosZ preparations was less than 12 copper atoms per NosZ dimer and that a mixture of different NosZ forms was present (especially in enzymes obtained from heterologous host cells) despite the fact that the cells were grown under copper-sufficient laboratory conditions [73 and references therein]. This implies that copper supply and incorporation are important features in NosZ biogenesis that are, moreover, embedded in the wider context of cellular copper homoeostasis. In prokaryotes, copper transport (import/export) and delivery/metallation systems such as cytoplasmic and periplasmic copper chaperones contribute to this tightly controlled process [74]. Copper toxicity is usually circumvented by fixing Cu(I) in the form of stable Cu(I)-thiol complexes through copper-binding proteins and/or low molecular

thiols such as glutathione. Copper chaperones often use cysteine residues arranged in a CX_2C motif as Cu(I) ligands resulting in exceptionally low K_D values in the femto- to zeptomolar (10^{-15} to 10^{-21}) range [75].

Unfortunately, knowledge on the maturation of the NosZ Cu_A and Cu_Z centres is limited. It is assumed that these centres are synthesized by mutually independent enzymes at the outside of the cytoplasmic membrane [19, 73, 76, 77]. The Cu_A site of NosZ is supposed to be functionally similar to that of respiratory haem-copper oxidases, for example, the Cu_A centre in subunit II of cytochrome *c* oxidase [72]. In both cases, electrons are transferred via Cu_A to the respective active sites of N_2O or O_2 reduction. The biogenesis of the Cu_A site has been investigated in different types of cytochrome oxidases and involves periplasmic copper chaperones of the Sco/SenC family [78, 79]. Therefore, it is likely that Sco/SenC-type proteins are also involved in NosZ Cu_A assembly [80]. However, genes encoding such chaperones are generally absent from NGCs.

Most likely, the biogenesis of the Cu_Z site involves the copper chaperone NosL, whose function might depend on the proposed NosDYF complex (Tables 1 and 2). Depending on the organism, NosL proteins are predicted to be exported by the Sec or Tat system and some of them might be membrane-anchored lipoproteins. Interaction of NosL and NosZ was indicated by a proteomic study using *Pseudomonas aeruginosa* [81]. In *P. denitrificans*, NosL was recently shown to be required for NosZ activity and Cu_Z (but not Cu_A) assembly only under copper-limited conditions [77]. This finding was in line with previous reports that characterized NosL as non-essential for cellular NosZ activity under copper-sufficent conditions [69, 76, 82]. Thus, a NosL-independent pathway of NosZ maturation is likely to exist when copper supply is sufficient. This assumption is also supported by the fact that the *nosL* gene is absent in some NGCs [28]. A soluble form of *P. denitrificans* NosL was shown to bind one Cu(I) per protein with attomolar affinity, whereas Cu(II) did not bind [77]. Therefore, it is tempting to ask whether copper centre maturation in NosZ needs a Cu(II) to Cu(I) reduction step and, if yes, whether the required electrons are donated via the same route as in Cu_Z* reactivation). Interestingly, the *W. succinogenes* NGC encodes three putative NosL-type copper chaperones (Fig. 2) [83]. Of those, NosL2 is most closely related to NosL proteins from, for example, *Achromobacter cycloclastes* and *P. denitrificans* whose NGCs encode only one NosL-type protein [84, 85]. However, the individual role of the different NosL-type proteins has not been investigated.

5 The Enzymatic Level, Part II: Electron Transport Routes, Bioenergetics and Function of Auxiliary Nos Proteins

NosZ or *c*NosZ are terminal reductases of anaerobic respiration. As such, these enzymes receive electrons from a membrane-bound and *pmf*-generating electron transport chain (ETC). Furthermore, as stated above, electron supply is possibly involved in copper centre assembly and reductive (re-)activation of NosZ in order

to restore N_2O conversion after oxygen-dependent inhibition of N_2O reduction. Since NGCs encode a multitude of electron transport enzymes (Fig. 2; Table 2), it is conceivable that these proteins serve in different dedicated and functionally non-redundant ETCs.

Figure 3 presents models of the ETCs involved in clade I and clade II N_2O respiration as well as hypotheses of the respective NosZ active site maturation and maintenance processes [19]. Notably, the deduced bioenergetic framework in clade I and clade II N_2O respiration is assumed to be equivalent. In both cases, *proton motive* quinol oxidation by N_2O is thought to be catalysed by the Q cycle mechanism of a membrane-bound Rieske/cytochrome *bc* complex (QcrABC complex) comprising a dihaem cytochrome *b* (QcrB), an iron–sulphur protein (QcrA, the so-called Rieske protein) and a mono- or dihaem cytochrome *c* named QcrC (Fig. 3) [19, 36, 45, 86–88]. QcrABC receives electrons from the membrane-bound quinone/quinol pool, which may consist of ubiquinone/ubiquinol (UQ/UQH_2) and/or menaquinone/menaquinol (MK/MKH_2). Quinone species are reduced by other *pmf*-generating enzymes such as hydrogenases, formate dehydrogenases or NADH dehydrogenases whose activity completes the reactions shown in Eqs. 1–3 (Sect. 2). The ETC between QcrC and NosZ/*c*NosZ is thought to be mediated by soluble periplasmic monohaem cytochromes *c* or, in addition for clade I NosZ enzymes and depending on the organism, by small copper proteins such as (pseudo) azurins or other cupredoxins (Fig. 3a) [45, 59, 69, 89]. The Qcr complex is usually involved in multiple ETCs, and thus, the small redox mediator proteins form a periplasmic electron transport branching point [45, 90]. In denitrifying clade I organisms, electrons are delivered to different terminal reductases including NO reductase (Nor), the NO-forming nitrite reductases NirS or NirK or the N_2O reductase NosZ [36]. In case of NosZ, it is thought that the electron entry site is the Cu_A centre. In fact, a cytochrome *c* has been shown to function as an electron donor for NosZ in denitrifying *P. pantotrophus* or *Marinobacter hydrocarbonoclasticus* cells [89, 91]. For *W. succinogenes*, interaction between a periplasmic monohaem cytochrome *c* and *c*NosZ has been shown experimentally [16, 92]. In either case, there is no indication that NosZ exchanges electrons by direct interaction with the Qcr complex, and such a feature is thought to be counterproductive for the cell in the light of the function of the Qcr complex as an electron hub. Overall, the Qcr complex would be the only coupling site within a linear electron transport chain from the quinone/quinol pool to N_2O and a proton per electron ratio (H^+/e^-) of 1 is expected.

The models put forward in Fig. 3 for the regular ETCs that connect the quinone/quinol pool and NosZ/*c*NosZ involve N_2O reductase as the only Nos protein and thereby keep the length of the highly similar *pmf*-generating ETCs to a minimum. In contrast, clade I and clade II organisms are expected to differ significantly in terms of the auxiliary electron transport processes mentioned above. Figures 3a, b depict the proposed functions for the other Nos protein, namely NosD, -Y, -F, -L, -R, -X, -C, -B, -G, -H, -C1 and -C2 (Table 2) [19]. Note that these models are in line with the absence of any functional redundancy in Nos protein inventories belonging to either clade I or clade II.

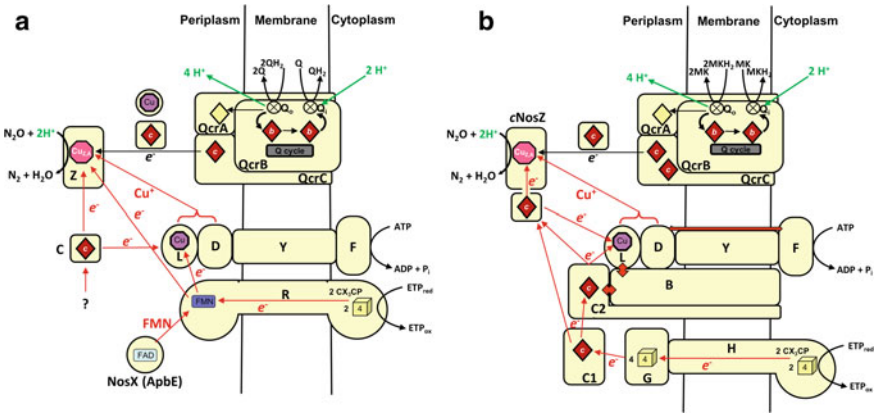

Fig. 3 Models of the electron transport chains from a quinol species to N_2O in representative N_2O-respiring bacteria containing a clade I (**a**; for example in *P. denitrificans*) or clade II (**b**; for example in *W. succinogenes*) *nos* gene cluster. In **a**, QcrA, -B and -C form a conventional cytochrome bc_1 complex that contributes to *pmf* generation via the Q cycle mechanism. QcrB is predicted to form four transmembrane segments each, whereas QcrA and QcrC are thought to be anchored to the membrane by a single hydrophobic region. Note that in Epsilonproteobacteria such as *W. succinogenes*, the QcrC subunit of the electrogenic Rieske/cytochrome *bc* complex is a dihaem cytochrome *c* (**b**). In both cases, the overall H^+/e^- ratio of QH_2 oxidation by N_2O is assumed to be 1 (green protons). NosY and NosR are predicted to form six transmembrane segments each, while NosH and NosB are predicted to form four (sometimes six in case of NosB) transmembrane segments, and NosC2 is thought to be anchored to the membrane by a single hydrophobic region. Black arrows indicate electron transport reactions involved in N_2O respiration/denitrification whereas red arrows suggest routes for reductive activation of NosZ/*c*NosZ or copper transfer reactions. Red double-headed arrows in **b** indicate that fusion protein variants connecting two usually individual Nos proteins are predicted by the genomes of some clade II organisms. Note that some clade II NRBs lack the NosG, -C1, -C2, -H proteins, for example, *B. vireti* (Fig. 2), and that NosC might functionally replace the monohaem cytochrome domain of *c*NosZ in clade II NRBs containing a conventional NosZ. For simplicity, only monomeric enzyme forms are shown. It cannot be excluded that some or all of the shown proteins form a membrane-bound supercomplex/respirasome. Q and QH_2 refer to UQ/UQH_2 and/or MK/MKH_2. *b*, haem *b*; *c*, haem *c*; $Cu_{Z,A}$, binuclear Cu_A and tetranuclear Cu_Z centres of NosZ. The yellow cube and diamond symbolize [4Fe–4S] and [2Fe–2S] centres, respectively. ETP, unknown (low potential) electron transport protein. ⊗ denotes a Q/QH_2-reactive site. See text for further details. Adapted with permission from [19]

Genes encoding NosD, -Y, -F and -L are commonly found in clade I and clade II NGCs (Fig. 2). NosD, -Y and -F possibly constitute a membrane-bound ATP-binding cassette (ABC) transporter complex [69, 70, 76]. NosY is a hydrophobic protein that is predicted to form six transmembrane segments and to interact with the putative ATP-binding and -hydrolysing subunit NosF at the cytoplasmic side of the membrane. NosD is a periplasmic protein thought to be transported by the Sec system and to interact with NosY. It is unclear whether the NosDYF complex acts as a transporter although an exporter function, presumably

of an unspecified sulphur compound, has been suggested [69, 70]. A functional cooperation of NosDYF with the copper chaperone NosL has been discussed and a function in copper delivery to NosZ was suggested, especially in the context of Cu_Z centre formation [69]. On the other hand, it cannot be excluded that cytoplasmic ATP hydrolysis is used to drive a so far unknown periplasmic process, similar to the essential role of the CcmAB complex in periplasmic cytochrome *c* biogenesis [93]. In this case, NosDYF might work as a motor rather than a transporter. NosD might interact with NosL in the way that NosD acts as a scaffold for copper centre assembly facilitated by NosL. Such a process might depend on keeping the copper atom in a reduced state upon provision of low-potential electrons (see below).

Clade I NGCs from Alpha-, Beta- and Gammaproteobacteria often encode the two flavoproteins NosR and NosX (note that *nosR* is often located upstream of *nosZ* and that the *nosX* gene is absent in some cases) [69, 70]. The membrane-bound flavin mononucleotide (FMN)- and [4Fe-4S] cluster-containing NosR protein might function in electron transfer to NosZ via its periplasmic flavoprotein domain (Fig. 3a) [94]. NosR was found to be essential for N_2O respiration and the phenotype of a corresponding *P. stutzeri* mutant was in line with a function of NosR in electron transport to NosZ and/or in the proper assembly of the Cu_Z centre (supported by the presence of Cu_Z* in NosZ) [94]. Site-directed modification of one or both CX_3CP motifs to VX_3VP indicated that each motif was important for N_2O respiration. Thus, it cannot be excluded that the two cytoplasmic iron–sulphur clusters of NosR are involved in a direct or indirect transmembrane electron transport to the FMN molecule (although the direct interaction of one of the [4Fe-4S] clusters with FMN is rather unlikely given the assumed architecture of this polytopic membrane protein). Nevertheless, this would allow transfer of low-potential electrons (putatively mediated by ETP_{red} in Fig. 3a) from the cytoplasm to periplasmic NosZ via NosR in a Qcr-independent pathway, and this could elegantly explain the phenomenon of reductive NosZ activation serving in NosZ maintenance or repair, as mentioned in Sect. 4. In such a scenario, the Qcr- and NosR-mediated electron transport pathways were separated and functionally distinct. This view is also in line with experimental evidence from studies with *P. stutzeri* and *P. aeruginosa* [81, 94]. For *P. aeruginosa*, NosR interaction with NosZ has been reported [81]. Likewise, NosR might be involved in the NosDL-dependent incorporation of copper in the process of periplasmic NosZ maturation.

NosX is a periplasmic flavin adenine dinucleotide (FAD)-binding flavoprotein of the ApbE family that was shown to be involved in NosR biogenesis [95]. Similar to the above mentioned *nosR* mutant, the absence of *nosX* promoted Cu_Z* formation in NosZ from *P. denitrificans*, indicative of a functional interaction between NosR and NosX [96]. In fact, the NosX homologue ApbE from *P. stutzeri* (an organism lacking *nosX* in its NGC) has been shown to act as a flavin donor for NosR [95].

The role of the monohaem cytochrome *c* NosC, which is encoded occasionally in clade I NGCs, is unclear. NosC might also play a dedicated and possibly accessory role in maintaining the Nos system intact. Interactions of NosC with NosZ and/or NosL are conceivable (Fig. 3a).

Nos proteins specifically encoded in clade II NGCs are NosB, -G, -C1, -C2 and -H (Table 2). The *nosB* gene is typically surrounded by *nosZ* and *nosD* (Fig. 2) [18, 37, 70]. NosB proteins are predicted to traverse the membrane four (in some cases six) times [45]. In *W. succinogenes*, characterization of a non-polar *nosB* deletion mutant demonstrated that NosB was essential for N_2O respiration [45]. Apart from this, functional studies on NosB are not available.

NosG and NosH are likely to form a membrane-bound complex involved in (transmembrane) electron transport (Fig. 3b). NosG is a periplasmic iron-sulphur protein that is exported by the Tat pathway and predicted to bind four [4Fe–4S] centres, whereas NosH is a membrane-bound protein predicted to form four transmembrane segments [45, 58]. Similar to NosR, NosH contains a C-terminal cytoplasmic domain that putatively binds two [4Fe–4S] centres and two conserved CX_3CP motifs at the cytoplasmic side of the membrane. NosG and NosH are homologues of NapG and NapH, two essential components of the periplasmic nitrate reductase system (Nap) in various Proteobacteria [97–100]. Previously, NosGH- and NapGH-type complexes have been postulated to be involved in electron transport from the quinone/quinol pool to a terminal reductase of anaerobic respiration (in this case *c*NosZ or the nitrate reductase NapA) [16, 58, 97]. However, direct biochemical evidence for quinol reactivity is lacking. NosC1 and NosC2 are monohaem cytochromes *c* located either in the periplasm or attached to the membrane via an N-terminal helix. These two cytochromes *c* might function as redox partner proteins of NosG. Non-polar *W. succinogenes* single-gene deletion mutants deficient in NosG, NosC1, NosC2 or NosH did not grow by N_2O respiration, and this phenotype was successfully complemented for each mutant upon genomic incorporation of the respective gene [45]. Thus, in principle, the NosG, -C1, -C2, -H and -B proteins could be functionally and/or structurally involved in electron transport from the QcrABC complex (which has been also shown to be essential for N_2O respiration in *W. succinogenes*) to *c*NosZ forming an elongated electron transport chain when compared to that of clade I organisms [45]. However, the experimental evidence is also in line with an alternative scenario, in which NosH, -G, -C1 and -C2 functionally replace NosR (Fig. 3b). According to this model, the absence of any of the NosH, -G, -C1 and -C2 proteins could be deleterious for N_2O respiration as the electron transport route required for reductive *c*NosZ activation and/or NosDL-dependent *c*NosZ biogenesis would be abolished. Lack of NosB could lead to the same phenotype assuming that this protein provides a membrane-bound platform for the correct assembly of the Nos system. Finally, the cytochrome *c* domain of *c*NosZ could mediate the NosGH-initiated electron transport route. This view is supported by the fact that the cytochrome *c* domain is connected to NosZ by a surprisingly large linker sequence that possibly makes this domain very flexible arguing for a transient interaction with the active site of NosZ [58, 59].

Notably, various Nos fusion proteins (NosD-F, NosB-C2, NosB-L) are predicted from (meta)genomic clade II NGC data (Table 1). In addition, NosL-D-type fusion proteins have been described, which, however, are not encoded by genes organized in NGCs [70]. The predicted multidomain proteins support the model shown in

Fig. 3b, especially with respect to NosB acting as an interaction platform. Unfortunately, none of the mentioned fusion proteins has been characterized experimentally. Nonetheless, it seems attractive to postulate a complex made up from the accessory Nos proteins that transiently interacts with NosZ and thereby facilitates copper or electron transfer reactions necessary for maturation and/or activity maintenance. The existence of a corresponding denitrification respirasome in *P. aeruginosa* cells was indicated in a recent study that also reported interaction of NosR and NosL with NosZ [81]. However, such a respirasome has not been isolated or structurally characterized and the stoichiometry of individual proteins or protein complexes has not been elucidated.

6 Mitigation of N_2O Emissions by Bioaugmentation

The use of NRBs to serve as an N_2O sink in natural or man-made environments has to be considered an attractive counteraction in addressing the problem of increasing anthropogenic N_2O emissions [19, 20, 28, 29]. In principle, many different ecosystems such as activated sludge from wastewater treatment plants, agricultural soil or digestates might be subject to microbial bioaugmentation approaches. However, it has to be kept in mind that these habitats differ significantly not only in their resident microbial communities but also in terms of environmental parameters such as carbon and nitrogen availability, carbon-to-nitrogen ratio, oxygenation, pH as well as copper content and copper complexation capability. In general, it seems advisable to augment with habitat-adapted organisms that have been isolated from the same or an ecologically similar environment to ensure cell survival and proliferation. Otherwise, the question has to be asked how long any unadapted bacteria could possibly persist in a 'foreign' environment. Moreover, it appears reasonable to use organisms for bioaugmentation that exhibit a net N_2O consumption behaviour, which would favour DNRA organsism over many denitrifiers [29]. Cells capable of N_2O reduction in the presence of ambient oxygen are desirable or, as an alternative, cells showing a fast reactivation of N_2O reduction after oxygen inhibition appear suitable.

Table 3 summarizes some representative bioaugmentation studies that used several different N_2O-reducing bacteria, including clade I and clade II bacteria as well as strains of *Pseudomonas stutzeri* capable of 'aerobic denitrification' (see Sect. 2). The reported results allowed to conclude that N_2O mitigation (i.e. reduced N_2O emissions after bioaugmentation) was indeed achievable in a laboratory scale (microcosm experiments) as well as in mesocosm and field studies, at least in the short run. At longer timescales, it remains to be seen whether any added cells will be persistent enough to sustainably affect the fine balance between N_2O production and consumption in an established natural microbial community.

Table 3 Selected bioaugmentation studies using N_2O-reducing bacteria

Organism, phylogenetic position and NosZ clade	Bioaugmented habitat	Specific aim	Special features of the study	Main result in terms of mitigation of N_2O emissions	References
Bradyrhizobium diazoefficiens (class Alphaproteobacteria); clade I NosZ	Soybean soil	Mitigation of post-harvest N_2O emissions from soybean ecosystems (due to nodule degradation)	Use of non-genetically modified mutants with increased N_2O reduction activity	Mitigation demonstrated in proof-of-principle experiments and at field scale	[101, 102]
Isolates related to *Agrobacterium/Rhizobium* (class Alphaproteobacteria), *Alcaligenes faecalis* (class Betaproteobacteria) or *Pseudomonas stutzeri* (class Gammaproteobacteria); all clade I NosZ	Wheat roots	Mitigation of N_2O emissions from cornfields	Isolates from the habitat to be augmented were used	Mitigation achieved only with the relative of *A. faecalis*	[103]
Pseudomonas stutzeri PCN-1 (class Gammaproteobacteria); clade I NosZ	Activated sludge	Mitigation of NO and N_2O emissions from wastewater	A new isolate was obtained under conditions of aerobic nitrate reduction	Mitigation demonstrated in activated sludge	[52]
Pseudomonas stutzeri TR2 (class Gammaproteobacteria); clade I NosZ	Denitrification tank of a wastewater treatment plant	Mitigation of N_2O emissions from denitrification and nitrification tanks	-	Mitigation demonstrated; the cells survived for at least 32 days	[55, 56, 104]
Dyadobacter fermentans (phylum Bacteroidetes); clade II NosZ	Different soils	Mitigation of N_2O emissions from soils with different C/N ratios and pH values	Use of a non-denitrifying organism	Mitigation demonstrated; influenced by pH and C/N ratio	[50]

(continued)

Table 3 (continued)

Organism, phylogenetic position and NosZ clade	Bioaugmented habitat	Specific aim	Special features of the study	Main result in terms of mitigation of N_2O emissions	References
Bacillus amyloliquefaciens EBL11 (phylum Firmicutes)	Acidic soil from a vegetable farm	Mitigation of N_2O emissions from acidic soils	Use of a non-denitrifying plant growth-promoting bacterium	Mitigation demonstrated in greenhouse pot and microcosm serum bottle incubation experiments; indirect effects on nitrifier and denitrifier communities	[105]

7 Engineering and Isolation Strategies for Efficient and Robust N_2O-Respiring Bacteria

In the light of the complexity of the N_2O reduction systems described above, it is quite clear that any attempt to engineer the effectiveness of NosZ activity or N_2O respiration needs to consider the respective cellular context and the physiology of the host organism. In other words, one has to take into account that the activity of any existing NosZ depends on other functional entities of the cell such as the electron transport network, the machinery ensuring copper homoeostasis and the defence systems against oxidative and nitrosative stress, caused by reactive oxygen and nitrogen species, respectively.

The following properties of a prototypic 'enhanced NRB' appear desirable:

- A high specific cellular N_2O turnover rate in natural and/or man-made N_2O-emitting environments and in the presence of N_2O concentrations in the μM or low mM range. To facilitate comparison, such activities should be given in units such as μmol N_2O min^{-1} mg^{-1} dry biomass or fmol N_2O $cell^{-1}$ h^{-1}.
- A low apparent K_M value for N_2O, for example, in the low μM range.
- Oxygen-resistant N_2O reduction or fast reactivation of N_2O reduction after inhibition due to oxygen exposure. In this context, it is notable that it is unknown so far whether oxygen-resistant N_2O reduction is due to an oxygen-insensitive NosZ enyzme or, more likely, whether the corresponding cells benefit from a superior defence system against reactive oxygen species that effectively shields NosZ from oxygen damage (see Sect. 2).
- N_2O reduction capacity over a wide range of pH values
- Functional maintenance of N_2O reduction over a wide range of copper concentrations, for example, due to the presence of efficient copper homoeostasis and/or storage systems, copper chaperones and enzymic copper centre assembly machineries.
- Efficient and fast electron transport systems delivering electrons to NosZ based on an adaequate cellular architecture that might involve an N_2O respirasome.
- Fast (and versatile) growth in cheap (minimal) media with high cell yields.
- Genetic accessibility allowing mutant construction and Metabolic Engineering. Note that only few NRBs such as *P. stutzeri*, *Bradyrhizobium* sp. and *W. succinogenes* are genetically tractable.

Given this variety of constraints, the question whether a clade I or clade II organism might be better suited as a chassis organism seems to be of secondary importance. Furthermore, it appears to be an enormous task to accomplish heterologous production of a complex metalloenzyme such as NosZ, let alone to transfer functional N_2O respiration to a non-N_2O reducing host cell, especially to cells of higher organisms such as plants. After all, an enzymatically active and copper-containing NosZ from *P. stutzeri* ZoBell has been produced recently in *Escherichia coli* upon co-production of the biosynthetic machinery for Cu_Z centre

assembly [73]. However, the enzyme was not connected to an ETC, probably hindered by the fact that *E. coli* neither forms a Rieske/cytochrome *bc* complex nor a small monohaem cytochrome *c*.

Although a lot has been learnt recently about the physiology and applicability of NRBs and their N_2O reduction systems, there are still many unknowns, especially in the context of the ecological role of clade I and clade II NRBs [106]. In natural habitats, many clade II *nos* gene clusters were found in the uncultured majority of microorganisms, based on metagenomics and metatranscriptomics data [28]. Furthermore, distinct primer sets can be applied to amplify (partial) *nosZ* genes of either clade I or clade II [106–108]. Therefore, it seems reasonable to isolate or enrich novel NRBs along the strategies mentioned above. The use of N_2O as sole electron acceptor in chemostat enrichment cultures using activated sludge samples with acetate as carbon and energy source resulted in an N_2O-reducing community, in which clade I NRBs dominated over clade II NRBs [109]. Interestingly, many enriched clade II organisms from various samples were classified as Betaproteobacteria (order Rhodocyclales) closely related to bacteria of the genera *Dechloromonas*, *Azospira*, *Thauera* or *Comamonas* ([42, 43, 109–111]; Sascha Hein and Jörg Simon, unpublished results). Therefore, another strategy to obtain efficient and resilient N_2O-respiring organisms could be the isolation or chemostat-based enrichment of new N_2O-reducing microbes under selective conditions such as permanent microaerobiosis, a growth-limiting N_2O concentration and low copper content. Sampling sites might include soil, activated sludge, digestates, the rumen and other parts of digestive systems or future hotspots of greenhouse gas emission such as thawing permafrost or marine oxygen minimum zones. Growth media should favour respiratory metabolism, for example, by offering non-fermentable carbon and electron sources (formate or acetate, for instance). Otherwise, N_2O-tolerant fermentative bacteria might outcompete NRBs.

8 Concluding Remarks and Perspectives

In the twenty-first century, humanity faces severe global challenges. Two major problems are climate change (and the need to reduce greenhouse gas emissions) and the anthropogenic disturbance of biogeochemical nutritent cycles, and it becomes increasingly clear that we cannot continue to adopt a ‘business as usual’ approach [3, 10, 112]. Practical solutions are urgently required to restore a balanced and sustainable nitrogen cycle on Earth, and climate- and nitrogen-smart food systems are needed to feed the 9–10 billion people predicted for 2050. In this context, the application potential of greenhouse gas-converting microorganisms such as methane-oxidizing or N_2O-reducing bacteria and archaea is clearly underexplored [20, 113, 114].

Perspective research in the field of NRBs might be guided based on the following knowledge gaps and thoughts.

- The detailed function of each Nos protein except NosZ needs to be elucidated.
- With the exception of NosZ and apo-NosL, structural information on Nos proteins is generally lacking. Data on Nos proteomics/complexomics and the cellular organization of the Nos system is scarce.
- Only few organisms have been described for which *nos* gene cluster mutants are available, for example, *W. succinogenes*, *P. stutzeri* and *P. denitrificans*.
- The mechanism of NosZ reactivation following oxygen inhibition is unclear.
- The ecological significance of the abundance and function of clade I and clade II systems in natural habitats is unresolved.
- Despite some indications, it is unclear whether N_2O could be sensed by clade II NRBs in order to up-regulate the Nos system [42, 51]. In denitrifying clade I organisms, nitrate and NO (but not N_2O) are known to induce the corresponding respiratory system [18].
- In soil, the combination between efficient N_2O reduction and dinitrogen fixation appears to be especially desirable and, in this respect, *Bradyrhizobium* species appear be especially useful [115, 116].
- Organisms that couple methane oxidation to N_2O reduction are yet to be described. Nonetheless, these organisms might exist as the corresponding reaction is exergonic and methane oxidation in anoxic environments has been reported [20, 117, 118].

Hopefully, future research along these points will help to find a sustainable and environmentally friendly solution to mitigate N_2O emissions from different habitats. Very likely, microbiology holds the key.

Acknowledgements The author thanks the co-workers of his cited publications for their contributions. Laboratory work is funded by the Deutsche Forschungsgemeinschaft (DFG, German Research Foundation; projects 324263958 and 418104137) and the Forum for Interdisciplinary Research (FiF) at TU Darmstadt.

References

1. IPCC (2014) Climate change 2014: synthesis report. Contribution of working groups I, II and III to the fifth assessment report of the intergovernmental panel on climate change. IPCC, Geneva, Switzerland
2. Ravishankara AR, Daniel JS, Portmann RW (2009) Nitrous oxide (N_2O): the dominant ozone-depleting substance emitted in the 21st century. Science 326:123–125
3. Rockström J, Steffen W, Noone K et al (2009) A safe operating space for humanity. Nature 461:472–475
4. Schilt A, Baumgartner M, Blunier T (2010) Glacial-interglacial and millennial scale variations in the atmospheric nitrous oxide concentration during the last 800,000 years. Quaternary Sc Rev 29:182–192

5. Smith P, Martino D, Cai Z et al (2008) Greenhouse gas mitigation in agriculture. Philos Trans R Soc Lond B Biol Sci 363:789–813
6. Smith KA, Mosier AR, Crutzen PJ et al (2012) The role of N_2O derived from crop-based biofuels, and from agriculture in general, in Earth's climate. Philos Trans R Soc Lond B Biol Sci 367:1169–1174
7. de Vries W, Kros J, Kroeze C et al (2013) Assessing planetary and regional nitrogen boundaries related to food security and adverse environmental impacts. Curr Opin Environ Sustain 5:392–402
8. Erisman JW, Galloway JN, Seitzinger S et al (2013) Consequences of human modification of the global nitrogen cycle. Philos Trans R Soc Lond B Biol Sci 368:20130116
9. Davidson EA, Kanter D (2014) Inventories and scenarios of nitrous oxide emissions. Environ Res Lett 9:105012
10. Steffen W, Richardson K, Rockström J et al (2015) Planetary boundaries: guiding human development on a changing planet. Science 347:1259855
11. Kanter DR, Zhang X, Mauzerall DL et al (2016) The importance of climate change and nitrogen use efficiency for future nitrous oxide emissions from agriculture. Environ Res Lett 11:094003
12. Erisman JW, Sutton MA, Galloway J et al (2008) How a century of ammonia synthesis changed the world. Nat Geosci 1:636–639
13. IPCC (2020) Climate change and land. An IPCC Special Report on climate change, desertification, land degradation, sustainable land management, food security, and greenhouse gas fluxes in terrestrial ecosystems. Summary for Policymakers. IPCC, Geneva, Switzerland
14. Simon J (2002) Enzymology and bioenergetics of respiratory nitrite ammonification. FEMS Microbiol Rev 26:285–309
15. Stein LY (2011) Surveying N_2O-producing pathways in bacteria. Methods Enzymol 486:131–152
16. Simon J, Klotz MG (2013) Diversity and evolution of bioenergetic systems involved in microbial nitrogen compound transformations. Biochim Biophys Acta 1827:114–135
17. Stein LY, Klotz MG (2016) The nitrogen cycle. Curr Biol 26:R94-98
18. Torres MJ, Simon J, Rowley G et al (2016) Nitrous oxide metabolism in nitrate-reducing bacteria: physiology and regulatory mechanisms. Adv Microb Physiol 68:353–432
19. Hein S, Simon J (2019) Bacterial nitrous oxide respiration: electron transport chains and copper transfer reactions. Adv Microb Physiol 75:137–175
20. Stein LY (2020) The long-term relationship between microbial metabolism and greenhouse gases. Trends Microbiol 28:500–511
21. Campbell MA, Nyerges G, Kozlowski JA et al (2011) Model of the molecular basis for hydroxylamine oxidation and nitrous oxide production in methanotrophic bacteria. FEMS Microbiol Lett 322:82–89
22. Chandran K, Stein LY, Klotz MG et al (2011) Nitrous oxide production by lithotrophic ammonia-oxidizing bacteria and implications for engineered nitrogen-removal system. Biochem Soc Trans 39:1832–1837
23. Schreiber F, Wunderlin P, Udert KM (2012) Nitric oxide and nitrous oxide turnover in natural and engineered microbial communities: biological pathways, chemical reactions and novel technologies. Front Microbiol 3:372
24. Stieglmeier M, Mooshammer M, Kitzler B et al (2014) Aerobic nitrous oxide production through N-nitrosating hybrid formation in ammonia-oxidizing archaea. ISME J 8:1135–1146
25. Kozlowski JA, Stieglmeier M, Schleper C et al (2016) Pathways and key intermediates required for obligate aerobic ammonia-dependent chemolithotrophy in bacteria and Thaumarchaeota. ISME J 10:1836–1845
26. Lenhart K, Behrendt T, Greiner S et al (2019) Nitrous oxide effluxes from plants as a potentially important source to the atmosphere. New Phytol 221:1398–1408

27. Felgate H, Giannopoulos G, Sullivan MJ et al (2012) The impact of copper, nitrate and carbon status on the emission of nitrous oxide by two species of bacteria with biochemically distinct denitrification pathways. Environ Microbiol 14:1788–1800
28. Hallin S, Philippot L, Löffler FE et al (2018) Genomics and ecology of novel N_2O-reducing microorganisms. Trends Microbiol 26:43–55
29. Yoon S, Song B, Phillips RL et al (2019) Ecological and physiological implications of nitrogen oxide reduction pathways on greenhouse gas emissions in agroecosystems. FEMS Micobiol Ecol 95: fiz066
30. Poole RK (2005) Nitric oxide and nitrosative stress tolerance in bacteria. Biochem Soc Trans 33:176–180
31. Luckmann M, Mania D, Kern M et al (2014) Production and consumption of nitrous oxide in nitrate-ammonifying *Wolinella succinogenes* cells. Microbiology 160:1749–1759
32. Spott O, Russow R, Stange CF (2011) Formation of hybrid N_2O and hybrid N_2 due to codenitrification: first review of a barely considered process of microbially mediated N-nitrosation. Soil Biol Biochem 43:1995–2011
33. Zhu-Barker X, Cavazos AR, Ostrom NE et al (2015) The importance of abiotic reactions for nitrous oxide production. Biogeochemistry 126:251–267
34. Onley JR, Ahsan S, Sanford RA et al (2017) Denitrification by *Anaeromyxobacter dehalogenans*, a common soil bacterium lacking nitrite reductase genes (*nirS*/*nirK*). Appl Environ Microbiol 4:e01985-e2017
35. Lim NYN, Frostegård Å, Bakken LR (2018) Nitrite kinetics during anoxia: the role of abiotic reactions versus microbial reduction. Soil Biol Biochem 119:203–209
36. Zumft WG (1997) Cell biology and molecular basis of denitrification. Microbiol Mol Biol Rev 61:533–616
37. Sanford RA, Wagner DD, Wu Q et al (2012) Unexpected nondenitrifier nitrous oxide reductase gene diversity and abundance in soils. Proc Natl Acad Sci USA 109:19709–19714
38. Jones CM, Graf DR, Bru D et al (2013) The unaccounted yet abundant nitrous oxide-reducing microbial community: a potential nitrous oxide sink. ISME J 7:417–426
39. Bueno E, Mania D, Frostegård Å (2015) Anoxic growth of *Ensifer meliloti* 1021 by N_2O-reduction, a potential mitigation strategy. Front Microbiol 6:537
40. Tucker KD, Neal JL (1988) Growth and respiration of Bradyrhizobium japonicum USDA143 with nitrous oxide as the terminal electron acceptor. Curr Microbiol 17:89–94
41. Yoon S, Nissen S, Park D et al (2016) Nitrous oxide reduction kinetics distinguish bacteria harboring clade I NosZ from those harboring clade II NosZ. Appl Environ Microbiol 82:3793–3800
42. Suenaga T, Riya S, Hosomi M et al (2018) Biokinetic characterization and activities of N_2O-reducing bacteria in response to various oxygen levels. Front Microbiol 9:697
43. Suenaga T, Hori T, Riya S et al (2019) Enrichment, isolation, and characterization of high-affinity N_2O-reducing bacteria in a gas-permeable membrane reactor. Environ Sci Technol 53:12101–12112
44. Strohm TO, Griffin B, Zumft WG et al (2007) Growth yields in bacterial denitrification and nitrate ammonification. Appl Environ Microbiol 73:1420–1424
45. Hein S, Witt S, Simon J (2017) Clade II nitrous oxide respiration of *Wolinella succinogenes* depends on the NosG, -C1, -C2, -H electron transport module, NosB and a Rieske/cytochrome *bc* complex. Environ Microbiol 19:4913–4925
46. Payne WJ, Grant MA, Shapleigh J et al (1982) Nitrogen oxide reduction in *Wolinella succinogenes* and *Campylobacter* species. J Bacteriol 152:915–918
47. Park D, Kim H, Yoon S (2017) Nitrous oxide reduction by an obligate aerobic bacterium, *Gemmatimonas aurantiaca* strain T-27. Appl Environ Microbiol 83:e00502-e517
48. Zhang H, Sekiguchi Y, Hanada S et al (2003) *Gemmatimonas aurantiaca* gen. nov., sp. nov., a gram-negative, aerobic, polyphosphate-accumulating micro-organism, the first cultured representative of the new bacterial phylum Gemmatimonadetes phyl. nov. Int J Syst Evol Microbiol 53:1155–1163

49. Mania D, Heylen K, van Spanning RJM et al (2016) Regulation of nitrogen metabolism in the nitrate-ammonifying soil bacterium *Bacillus vireti* and evidence for its ability to grow using N_2O as electron acceptor. Environ Microbiol 18:2937–2950
50. Domeignoz-Horta LA, Putz M, Spor A et al (2016) Non-denitrifying nitrous oxide-reducing bacteria—an effective N_2O sink in soil. Soil Biol Biochem 103:376–379
51. Kern M, Simon J (2016) Three transcription regulators of the Nss family mediate the adaptive response induced by nitrate, nitric oxide or nitrous oxide in *Wolinella succinogenes*. Environ Microbiol 18:2899–2912
52. Zheng M, He D, Ma T et al (2014) Reducing NO and N_2O emission during aerobic denitrification by newly isolated *Pseudomonas stutzeri* PCN-1. Bioresour Technol 162:80–88
53. Desloover J, Roosbroeck D, Heylen K et al (2014) Pathway of nitrous oxide consumption in isolated *Pseudomonas stutzeri* strains under anoxic and oxic conditions. Environ Microbiol 16:3143–3152
54. Zhao B, Chen DY, Tan P et al (2018) Characterization of an aerobic denitrifier *Pseudomonas stutzeri* strain XL-2 to achieve efficient nitrate removal. Bioresour Technol 250:564–573
55. Miyahara M, Kim SW, Fushinobu S et al (2010) Potential of aerobic denitrification by *Pseudomonas stutzeri* TR2 to reduce nitrous oxide emissions from wastewater treatment plants. Appl Environ Microbiol 76:4619–4625
56. Miyahara M, Kim SW, Zhou S et al (2012) Survival of the aerobic denitrifier *Pseudomonas stutzeri* strain TR2 during co-culture with activated sludge under denitrifying conditions. Biosci Biotechnol Biochem 76:495–500
57. Chee-Sanford J, Tian D, Sanford R (2020) Consumption of N_2O and other N-cycle intermediates by *Gemmatimonas aurantiaca* strain T-27. Microbiology 165:1345–1354
58. Simon J, Einsle O, Kroneck PMH et al (2004) The unprecedented *nos* gene cluster of *Wolinella succinogenes* encodes a novel respiratory electron transfer pathway to cytochrome *c* nitrous oxide reductase. FEBS Lett 569:7–12
59. Dell'Acqua S, Moura I, Moura JJG et al (2011) The electron transfer complex between nitrous oxide reductase and its electron donors. J Biol Inorg Chem 16:1241–1254
60. Stevens JM, Mavridou DA, Hamer R et al (2011) Cytochrome *c* biogenesis System I. FEBS J 278:4170–4178
61. Simon J, Hederstedt L (2011) Composition and function of cytochrome *c* biogenesis System II. FEBS J 278:4179–4188
62. Teraguchi S, Hollocher TC (1989) Purification and some characteristics of a cytochrome *c*-containing nitrous oxide reductase from *Wolinella succinogenes*. J Biol Chem 264:1972–1979
63. Brown K, Tegoni M, Prudencio M et al (2000) A novel type of catalytic copper cluster in nitrous oxide reductase. Nat Struct Biol 7:191–195
64. Haltia T, Brown K, Tegoni M et al (2003) Crystal structure of nitrous oxide reductase from *Paracoccus denitrificans* at 1.6 Å resolution. Biochem J 369:77–88
65. Paraskevopoulos K, Antonyuk SV, Sawers G et al (2006) Insight into catalysis of nitrous oxide reductase from high-resolution structures of resting and inhibitor-bound enzyme from *Achromobacter cycloclastes*. J Mol Biol 362:55–65
66. Pomowski A, Zumft WG, Kroneck PMH et al (2011) N_2O binding at a [4Cu:2S] copper-sulphur cluster in nitrous oxide reductase. Nature 477:234–237
67. Pauleta SR, Dell'Acqua S, Moura I (2013) Nitrous oxide reductase. Coord Chem Rev 257:332–349
68. Carreira C, Pauleta SR, Moura I (2017) The catalytic cycle of nitrous oxide reductase—the enzyme that catalyzes the last step of denitrification. J Inorg Biochem 177:423–434
69. Zumft WG, Kroneck PMH (2007) Respiratory transformation of nitrous oxide (N_2O) to dinitrogen by Bacteria and Archaea. Adv Microb Physiol 52:107–227
70. van Spanning RJM (2011) Structure, function, regulation and evolution of the nitrite and nitrous oxide reductases: denitrification enzymes with a beta-propeller fold. In: Moir JWB (ed) Nitrogen cycling in bacteria. Caister Academic Press, Norfolk, pp 135–161

71. Wüst A, Schneider L, Pomowski A et al (2012) Nature's way of handling a greenhouse gas: the copper-sulfur cluster of purple nitrous oxide reductase. Biol Chem 393:1067–1077
72. Kroneck PMH (2018) Walking the seven lines: binuclear copper A in cytochrome *c* oxidase and nitrous oxide reductase. J Biol Inorg Chem 23:27–39
73. Zhang L, Wüst A, Prasser B et al (2019) Functional assembly of nitrous oxide reductase provides insights into copper site maturation. Proc Natl Acad Sci USA 116:12822–12827
74. Stewart LJ, Thaqi D, Kobe B et al (2019) Handling of nutrient copper in the bacterial envelope. Metallomics 11:50
75. Hatori Y, Inouye S, Akagi R (2017) Thiol-based copper handling by the copper chaperone Atox1. IUBMB Life 69:246–254
76. Zumft WG (2005) Biogenesis of the bacterial respiratory Cu_A, Cu-S enzyme nitrous oxide reductase. J Mol Microbiol Biotechnol 10:154–166
77. Bennett SP, Soriano-Laguna MJ, Bradley JM et al (2019) NosL is a dedicated copper chaperone for assembly of the Cu_Z center of nitrous oxide reductase. Chem Sci 10:4985–4993
78. Banci L, Bertini I, Cavallaro G et al (2011) Seeking the determinants of the elusive functions of Sco proteins. FEBS J 278:2244–2262
79. Trasnea PI, Andrei A, Marckmann D et al (2018) A copper relay system involving two periplasmic chaperones drives cbb_3-type cytochrome *c* oxidase biogenesis in *Rhodobacter capsulatus*. ACS Chem Biol 13:1388–1397
80. Sullivan MJ, Gates AJ, Appia-Ayme C et al (2013) Copper control of bacterial nitrous oxide emission and its impact on vitamin B_{12}-dependent metabolism. Proc Natl Acad Sci USA 110:19926–19931
81. Borrero-de Acuña JM, Rohde M, Wissing J et al (2016) Protein network of the *Pseudomonas aeruginosa* denitrification apparatus. J Bacteriol 198:1401–1413
82. Wunsch P, Herb M, Wieland H et al (2003) Requirements for Cu(A) and Cu-S center assembly of nitrous oxide reductase deduced from complete periplasmic enzyme maturation in the nondenitrifier *Pseudomonas putida*. J Bacteriol 185:887–896
83. Eller J, Hein S, Simon J (2019) Significance of MccR, MccC, MccD, MccL and 8-methylmenaquinone in sulfite respiration of *Wolinella succinogenes*. Biochim Biophys Acta 1860:12–21
84. McGuirl MA, Bollinger JA, Cosper N et al (2001) Expression, purification, and characterization of NosL, a novel Cu(I) protein of the nitrous oxide reductase (*nos*) gene cluster. J Biol Inorg Chem 6:189–195
85. Taubner LM, McGuirl MA, Dooley DM et al (2006) Structural studies of apo NosL, an accessory protein of the nitrous oxide reductase system: insights from structural homology with MerB, a mercury resistance protein. Biochemistry 45:12240–12252
86. Dibrova DV, Cherepanov DA, Galperin MY et al (2013) Evolution of cytochrome *bc* complexes: from membrane-anchored dehydrogenases of ancient bacteria to triggers of apoptosis in vertebrates. Biochim Biophys Acta 1827:1407–1427
87. ten Brink F, Baymann F (2014) Rieske/cytochrome *b* complexes: the turbo chargers of chemiosmosis. In: Hohmann-Marriott MF (ed) The structural basis of biological energy generation, advances in photosynthesis and respiration. Springer, Dordrecht, pp 149–165
88. Cramer WA, Hasan SS, Yamashita E (2011) The Q cycle of cytochrome *bc* complexes: a structure perspective. Biochim Biophys Acta 1807:788–802
89. Dell'Acqua S, Pauleta SR, Monzani E et al (2008) Electron transfer complex between nitrous oxide reductase and cytochrome c552 from *Pseudomonas nautica*: kinetic, nuclear magnetic resonance, and docking studies. Biochemistry 47:10852–10862
90. Garg N, Taylor AJ, Kelly DJ (2018) Bacterial periplasmic nitrate and trimethylamine-N-oxide respiration coupled to menaquinol-cytochrome *c* reductase (Qcr): implications for electrogenic reduction of alternative electron acceptors. Sci Rep 8:15478
91. Rasmussen T, Brittain T, Berks BC et al (2005) Formation of a cytochrome *c*-nitrous oxide reductase complex is obligatory for N_2O reduction by *Paracoccus pantotrophus*. Dalton Trans 21:3501–3506

92. Zhang C, Hollocher TC (1993) The reaction of reduced cytochromes *c* with nitrous oxide reductase of *Wolinella succinogenes*. Biochim Biophys Acta 1142:253–261
93. Christensen O, Harvat EM, Thöny-Meyer L et al (2007) Loss of ATP hydrolysis activity by CcmAB results in loss of *c*-type cytochrome synthesis and incomplete processing of CcmE. FEBS J 274:2322–2332
94. Wunsch P, Zumft WG (2005) Functional domains of NosR, a novel transmembrane iron-sulfur flavoprotein necessary for nitrous oxide respiration. J Bacteriol 187:1992–2001
95. Zhang L, Trncik C, Andrade SL et al (2017) The flavinyl transferase ApbE of *Pseudomonas stutzeri* matures the NosR protein required for nitrous oxide reduction. Biochim Biophys Acta 1858:95–102
96. Wunsch P, Körner H, Neese F et al (2005) NosX function connects to nitrous oxide (N_2O) reduction by affecting the Cu_Z center of NosZ and its activity in vivo. FEBS Lett 579:4605–4609
97. Brondijk TH, Fiegen D, Richardson DJ et al (2002) Roles of NapF, NapG and NapH, subunits of the *Escherichia coli* periplasmic nitrate reductase, in ubiquinol oxidation. Mol Microbiol 44:245–255
98. Brondijk TH, Nilavongse A, Filenko N et al (2004) NapGH components of the periplasmic nitrate reductase of *Escherichia coli* K-12: location, topology and physiological roles in quinol oxidation and redox balancing. Biochem J 379:47–55
99. Kern M, Simon J (2008) Characterization of the NapGH quinol dehydrogenase complex involved in *Wolinella succinogenes* nitrate respiration. Mol Microbiol 69:1137–1152
100. Kern M, Simon J (2009) Electron transport chains and bioenergetics of respiratory nitrogen metabolism in *Wolinella succinogenes* and other Epsilonproteobacteria. Biochim Biophys Acta 1787:646–656
101. Itakura M, Uchida Y, Akiyama H et al (2013) Mitigation of nitrous oxide emissions from soils by *Bradyrhizobium japonicum* inoculation. Nat Clim Change 3:208–212
102. Akiyama H, Hoshino YT, Itakura M et al (2016) Mitigation of soil N_2O emission by inoculation with a mixed culture of indigenous *Bradyrhizobium diazoefficiens*. Sci Rep 6:32869
103. Usyskin-Tonne HY, Minz D (2019) Altering N_2O emissions by manipulating wheat root bacterial community. Sci Rep 9:7613
104. Ikeda-Ohtsubo W, Miyahara M, Kim SW et al (2013) Bioaugmentation of a wastewater bioreactor system with the nitrous oxide-reducing denitrifier *Pseudomonas stutzeri* strain TR2. J Biosci Bioeng 115:37–42
105. Wu S, Zhuang G, Bai Z et al (2018) Mitigation of nitrous oxide emissions from acidic soils by *Bacillus amyloliquefaciens*, a plant growth-promoting bacterium. Glob Change Biol 24:2352–2365
106. Jones CM, Spor A, Brennan FP et al (2014) Recently identified microbial guild mediates soil N_2O sink capacity. Nat Clim Change 4:801–805
107. Orellana LH, Rodriguez-R LM, Higgins S et al (2014) Detecting nitrous oxide reductase (*nosZ*) genes in soil metagenomes: method development and implications for the nitrogen cycle. mBio 5:e01193-14
108. Chee-Sanford JC, Connor L, Krichels A et al (2020) Hierarchical detection of diverse Clade II (atypical) *nosZ* genes using new primer sets for classical- and multiplex PCR array application. J Microbiol Methods 172:105908
109. Conthe M, Wittorf L, Kuenen JG et al (2018a) Growth yield and selection of *nosZ* clade II types in a continuous enrichment culture of N_2O respiring bacteria. Environ Microbiol Rep 10:239–244
110. Conthe M, Wittorf L, Kuenen JG et al (2018b) Life on N_2O: deciphering the ecophysiology of N_2O respiring bacterial communities in a continuous culture. ISME J 12:1142–1153
111. Conthe M, Kuenen JG, Kleerebezem R et al (2018) Exploring microbial N_2O reduction: a continuous enrichment in nitrogen free medium. Environ Microbiol Rep 10:102–107

112. Cavicchioli R, Ripple WJ, Timmis KN et al (2019) Scientists' warning to humanity: microorganisms and climate change. Nat Rev Microbiol 17:569–586
113. Richardson D, Felgate H, Watmough N et al (2009) Mitigating release of the potent greenhouse gas N_2O from the nitrogen cycle - could enzymic regulation hold the key? Trends Biotechnol 27:388–397
114. Thomson AJ, Giannopoulos G, Pretty J et al (2012) Biological sources and sinks of nitrous oxide and strategies to mitigate emissions. Philos Trans R Soc Lond B Biol Sci 367:1157–1168
115. Mania D, Woliy K, Degefu T et al (2019) A common mechanism for efficient N_2O reduction in diverse isolates of nodule-forming bradyrhizobia. Environ Microbiol 22:17–31
116. Woliy K, Degefu T, Frostegård Å (2019) Host range and symbiotic effectiveness of N_2O reducing *Bradyrhizobium* strains. Front Microbiol 10:2746
117. Welte CU, Rasigraf O, Vaksmaa A et al (2016) Nitrate- and nitrite-dependent anaerobic oxidation of methane. Environ Microbiol Rep 8:941–955
118. Welte CU (2018) Revival of archaeal methane microbiology. mSystems 3:e00181-e217
119. Mania D, Heylen K, van Spanning RJM et al (2014) The nitrate-ammonifying and *nosZ*-carrying bacterium *Bacillus vireti* is a potent source and sink for nitric and nitrous oxide under high nitrate conditions. Environ Microbiol 16:3196–3210

Bio-powering the Future

Bacterial Power: An Alternative Energy Source

Bruno M. Fonseca, Ricardo M. Soares, Catarina M. Paquete, and Ricardo O. Louro

Abstract

The demand for energy and the limited supply of fossil fuels and their impact in the environment have required the development of alternative energy sources. Among the next generation of energy sources, microbial fuel cells (MFCs) have emerged as a promising technology due to their ability to recover energy from wastewaters in the form of electricity using electroactive microorganisms as catalysts. Among the various factors that affect power generation performance in MFCs, the efficiency of extracellular electron transfer (EET) is one of the most important. Several enzymes, specifically multiheme cytochromes, have been implicated in this process although the electron transfer chain organization remains to be fully understood. In this chapter, we review in detail the mechanisms that support EET from electroactive microorganisms to the anode in MFCs. We focus on the model organism *Shewanella oneidensis* MR-1, due to the existence of an extensive molecular characterization of its EET processes. The recent developments in the characterization of the multiheme cytochromes involved in these mechanisms will also be reviewed.

Keywords

Alternative energy · Microbial fuel cell · Electroactive microorganism · *Shewanella oneidensis* · Extracellular electron transfer · Enzyme · Multiheme cytochrome

B. M. Fonseca · C. M. Paquete · R. O. Louro (✉)
Instituto de Tecnologia Química e Biológica Antonio Xavier, Universidade Nova de Lisboa, ITQB-NOVA, Oeiras, Portugal
e-mail: louro@itqb.unl.pt

R. M. Soares
Instituto Nacional Investigação Agrária e Veterinária, Oeiras, Portugal

J. J. G. Moura et al. (eds.), *Enzymes for Solving Humankind's Problems*,
https://doi.org/10.1007/978-3-030-58315-6_8

1 Introduction

The constant demand for energy and the limited supply of fossil fuels and their impact in the environment have required the development of alternative energy sources. Among the next generation of energy sources, microbial fuel cells (MFCs) continue to attract wide attention due to their ability to recover energy in the form of electricity using microorganisms as catalysts. This technology is among the most studied bioelectrochemical systems (BES), with these devices also being used for other eco-friendly purposes such as the production of biofuels and chemicals, biosensors, bioremediation, wastewater treatment and desalination [1–5].

MFCs employ microorganisms to produce electrical current while metabolizing nutrients available in the medium [6, 7]. The capacity of using organic waste (e.g., wastewater) as substrate has opened the possibility of producing electricity in a way that is close to carbon neutral [8, 9]. These cells consist of an anode that is kept under anoxic conditions and receives electrons from the bioenergetic metabolism of the microorganisms growing on its surface. MFCs also contain a cathode that transfers electrons to the terminal electron acceptor. It is the electron flow from the anode to the cathode through an external circuit that allows the production of electrical current. Nowadays, there are a wide variety of designs, where the anode and the cathode may coexist in a single compartment (single-chamber) or can be separated by a physical barrier that is permeable to ions (dual-chamber) (Fig. 1) [10].

In BES, electron transfer efficiency depends on several parameters, with the electron transfer processes performed by the microorganisms among the core factors that affect power generation performance [11, 12]. Microorganisms that oxidize organic compounds and transfer electrons to the anodes of BES are called electroactive but are also known under several other names in the literature, such as, electricigens, exoelectrogenic, anode-respiring or anodophilic microorganisms [13]. These electroactive microorganisms are united in their ability to perform extracellular electron transfer (EET), directly and/or mediated, to the electrode.

The concept of electric current generation by microorganisms is not new and was reported over 100 years ago [14], with research on MFCs making several advances in the last decade [7, 15]. These include different MFC architectures and construction materials for the anode and cathode, diverse microbial communities and knowledge on the biochemical characteristics of the EET performed by the microorganisms [7, 16]. Nevertheless, the commercialization of MFCs is still limited due to low performance, expensive core parts and materials, and bottlenecks in scale-up [15, 17]. Therefore, many challenges and room for improvement remain in BES, including the identification of new electroactive microorganisms with high electrochemical activities and the characterization of the electron transfer process between cells and electrodes. This has been a crucial aspect in the enhancement of MFC performance and paramount in promoting their future applications [18–20].

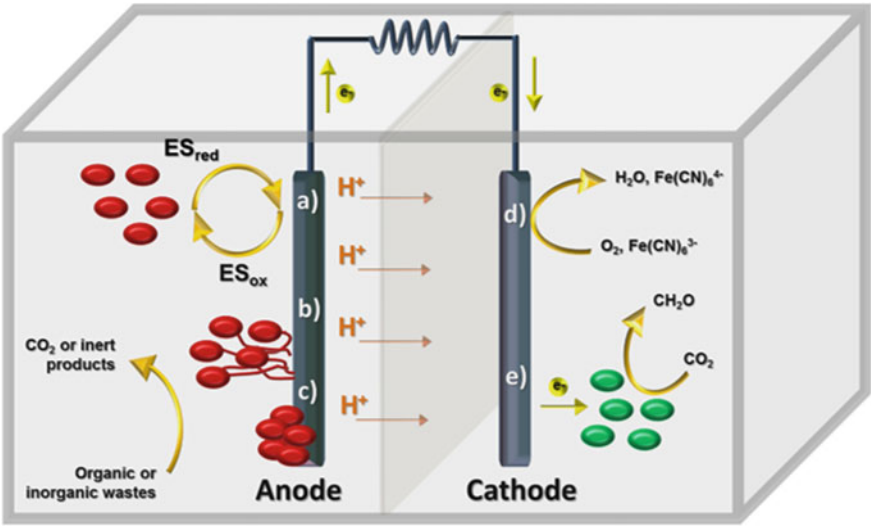

Fig. 1 Schematic representation of a MFC, where the difference between a single and double chamber design is the presence or absence of a permeable barrier that is often an ion-exchange membrane separating the anode from the cathode. Bacteria at the anode chamber (circles) feed on organic or inorganic wastes and transfer electrons to the anode through: **a** electron shuttles (ES), **b** nanowires or conductive pili, or **c** directly through cell surface redox active proteins. The protons produced flow through the selectively permeable membrane to the cathode chamber and the electrons flow through an electrical circuit to the cathode. The electrons are then transferred to the final electron acceptor. This can be **d** abiotic or **e** biotic

In this chapter, we review in detail the mechanisms that support EET from electroactive microorganisms to the anode in BES. We focus on the model organism *Shewanella oneidensis* MR-1, due to the existence of an extensive molecular characterization of its EET processes. The recent developments in the characterization of the enzymes involved in these mechanisms will also be reviewed.

2 Extracellular Electron Transfer Mechanisms

Extracellular electron transfer is defined as a metabolic process that enables electron transfer between cells and extracellular solid materials and is based on one of the oldest types of microbial respiration, the dissimilatory reduction of iron [21]. The EET process between electroactive microorganisms and electrodes is the footstone for developing MFCs and other BES, which connect the intracellular bioenergetic pathways of microorganisms with the electrochemical reactions of electrodes [22, 23].

The molecular mechanisms of electron transfer to, or from, extracellular substrates can be divided in direct and mediated EET [24] (Fig. 2). EET is a very complex phenomenon and in vivo an absolute separation between direct EET and mediated EET is often difficult since both type of EET can occur simultaneously within one single organism [23, 25]. The study and elucidation of these mechanisms have led to a better understanding on how EET occurs and provides guidance for the optimization of MFCs.

2.1 Direct EET

In direct EET, microorganisms attach to solid surfaces, to or from which they directly transfer electrons without involvement of any diffusible redox compounds. Although early studies with *S. oneidensis* MR-1 supported a mechanism of physical contact for growth on insoluble manganese oxide [26], it was only latter that the first experimental evidence for this mechanism was revealed [27]. Atomic force microscopy experiments showed that *Shewanella* cells grown anaerobically bind preferentially metal oxides in contrast to aerobically grown cells.

Direct EET is achieved through physical contact of the cells to solid surfaces, with the efficiency of this electron transfer mechanism limited by the maximum cell density in the bacterial monolayer [28]. This physical contact occurs via redox active proteins present on the outer membrane or cell envelope [29]. A high number of multiheme *c*-type cytochromes (MHCs) have been found in organisms capable of performing EET, with several of them directly implicated in direct EET [29–32]. These proteins are characterized by multiple heme cofactors that are covalently attached to the polypeptide chain and can switch between oxidized Fe(III) and reduced Fe(II) states. Their distances are typically less than 14 between closest neighbors enabling fast long-range electron transfer via electron hopping [33, 34].

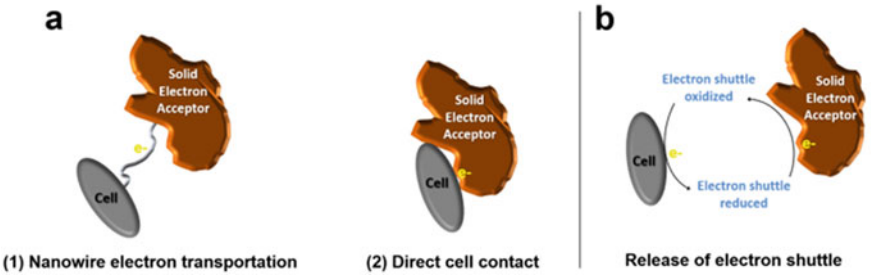

Fig. 2 Strategies employed by microorganisms for electron transfer to insoluble extracellular electron acceptors. Extracellular electron transfer can occur by direct EET. **a** through cell appendages of diverse nature called pili or nanowires (1) or through direct cell contact via cell surface redox active proteins (2); or indirect EET, **b** mediated by electron shuttling compounds

Some microorganisms can establish a thick multilayer electrochemically active biofilm, and through long-range conductive filamentous appendages, such as nanowires or pili, achieve higher electron transfer rates and densities per surface area when compared to cell monolayers [35]. Scanning tunneling microscopy images show thin filaments with about 8 nm in diameter and 10 μm in length [35]. These conductive filamentous appendages allow the bacteria to conduct electrons over a large distance within the multiple layers of a biofilm. In terms of morphology, *Shewanella* nanowires are partially composed of *c*-type cytochromes [28, 36–39]. This was demonstrated by deleting the genes coding for the outer-membrane cytochromes, MtrC and OmcA, resulting in non-conductive nanowires [38]. Also, deleting the *gspG* gene which is involved in the type II secretion pathway, that is required for the proper export of the outer-membrane cytochromes MtrC and OmcA to the cell exterior [40, 41], resulted in non-conductive nanowires. Later studies using fluorescence microscopy revealed that *Shewanella* nanowires are, in fact, extensions of the outer-membrane and periplasm [42].

Other examples of conductive filaments are the pili [43] and the more recent multiheme cytochrome OmcS filaments [44, 45] from the *Geobacter* genus. The hypothesis that the pili might function as conductive filamentous appendages resulted from the observation that pili were specifically expressed during growth on insoluble electron acceptors [46]. Studies showed that type IV pilus monomer PilA deletion mutant of *G. sulfurreducens* could not reduce Fe(III) oxide and displayed a much lower current production in MFCs [28, 47]. The NMR structure of the PilA monomer of *G. sulfurreducens* shows that it is shorter than the PilA from other microorganisms [48]. Indeed, the truncation of PilA in *G. sulfurreducens* was proposed to be essential for iron respiration, suggesting that an adaptive evolution of this organism to dissimilatory iron reduction in natural environments has been achieved with the truncation of this protein [49]. Using cryo-electron microscopy, the structure of a different conductive filament was solved, with particle reconstructions showing that only the outer surface MHC OmcS monomers alone could produce a perfect fit [44, 45]. This argues for conductive filaments in *Geobacter* to be composed entirely of OmcS and that no arrangement with PilA monomers is present, as previously proposed [50]. These observations provide a context for the fact that, whereas the mechanism by which electrons are transferred along the PilA filaments is still fiercely debated [51], the OmcS polymer provides a continuous chain of hemes at close distance for efficient conduction along the length of the whole filament [44].

2.2 Mediated EET

Besides direct EET, some bacteria can also reduce extracellular substrates through mediated electron transfer, using small organic electron shuttles. These serve as the terminal electron acceptors, and once reduced, can themselves transfer electrons to iron oxides or anodes in MFCs.

Electron shuttles are available in the media (e.g., humic acids) or can be endogenously produced (*e.g.* flavins) by microorganisms. The possible involvement of endogenous electron shuttles in reduction of poorly soluble metal minerals by *Shewanella* was first proposed by Newman and Kolter [52]. Later, Lies et al. demonstrated that iron oxide entrapped within nanoporous glass beads could be reduced by *S. oneidensis* MR-1, confirming the participation of electron shuttles in the dissimilatory iron respiration of this bacterium [53]. The ability of flavins to enhance iron reduction was first examined by Myers and Myers [54], showing that addition of flavins to the growth medium increased ferric reductase activity in *S. oneidensis* MR-1. Since then it was confirmed by numerous researchers that members of the *Shewanella* genus are capable of secreting flavins, such as riboflavin, flavin mononucleotide (FMN) and flavin adenine dinucleotide (FAD) [55–57]. Also, *S. oneidensis* MR-1 can accumulate these flavins to high concentrations in solution (250–500 nM) to be used as electron shuttles for EET to the electrodes [55].These high levels of flavins enhance the electron transfer efficiency by several fold and therefore are cost effective since the ATP used on flavin production and secretion is negligible when compared with the resulting energetic advantage.

Although, electron shuttling seems to be the primary mechanism of EET, outer membrane MHCs still play a key role in mediated EET and are responsible for at least 95% of the reduction of extracellular flavins at physiological relevant rates [58]. Indeed, the *Shewanella* Mtr complex plays an essential role in flavins' reduction, with the outer-membrane MHC MtrC accounting for approximately 50% of the activity observed [59]. Kinetic results showed that direct contact between the outer-multiheme cytochromes (*e.g.* OmcA and MtrC) and insoluble iron substrates or MFC anodes could not account for the rates of electron transfer observed when using whole cells assays [60, 61], with this gap in electron transfer rates resolved with the addition of flavins. This demonstrated that outer-membrane cytochromes are not the only elements responsible for the EET at relevant kinetic rates and that direct and mediated electron transfer occur in tandem in *S. oneidensis* MR-1 [60]. Indeed, it has been shown that mediated EET, and not direct EET, is the primary mechanism of EET employed by *S. oneidensis*, accounting for approximately 75% of its EET capacity [57].

With reduction potentials of −219 mV (FMN and FAD) and −208 mV (riboflavin) [30], flavins have the capability to act as efficient extracellular redox mediators for the reduction of metal oxides at neutral pH (redox couple ferrihydrite/Fe(II) has a reduction potential ranging from −100 to +100 mV [62]). Thus, *Shewanella* species that can secrete and utilize flavins as electron shuttles have an advantage in environments that contain poorly soluble metal oxides but lack exogenous redox mediators, such as humic acids. Another advantage of flavin secretion by *Shewanella* is their potential application in the construction of MFCs without addition of costly exogenous redox mediators [63]. Furthermore, flavin secretion by *Shewanella* may also support mediated EET by other microbial species present in the BES and thereby increase the efficiency of current generation in mixed cultures [56].

3 Electroactive Microorganisms

In Nature, there is a great diversity of microorganisms that can be used in MFCs, with more than 100 different electroactive species presently identified [16, 64]. Most of these electroactive microorganisms are Gram negative bacteria, with more than half belonging to the Proteobacteria phylum. Also, the majority of these electroactive species are: (i) mesophilic; (ii) have low tolerance to high salinity; (iii) possess motility; (iv) have biofilm formation capabilities; and (v) exhibit anodic EET activity, with most species performing EET via mediated electron transfer and only a small percentage capable of performing direct EET [64]. As MFC research advances, we expect that significantly more electroactive microorganisms will be discovered, especially those that can exist and thrive in more extreme environments [65].

Presently, it is well known that mixed microbial cultures colonizing anodes in MFCs produce greater current densities with higher columbic efficiency, compared with experiments using pure cultures [66]. Presently, the highest current densities obtained are from microbial mixed cultures that are dominated by δ-Proteobacteria of the *Geobacter* genus [16]. The reason for this is the fact that mixed cultures have a higher flexibility towards external factors due to symbiotic effects. This allows a greater diversity regarding metabolic pathways, as well as the combination of different electron transfer mechanisms that permit a complete oxidation of the organic substrates existent in the MFC reactor [67, 68].

Though mixed microbial cultures produce more current density, MFCs operating with pure cultures of electroactive bacteria are preferred for the detailed investigation of EET mechanisms as they allow a better characterization of the pathways than in mixed cultures. Understanding the processes by which electroactive organisms transfer electrons to an electrode, as well as microbial-electrode interactions will allow the enhancement of EET and ultimately benefit operational performance of the MFCs and enable their future practical applications. The Gram negative proteobacterium *S. oneidensis* MR-1 has been used as a model organism to understand EET [23, 32]. The ability to grow *Shewanella* robustly under oxygen conditions, the large quantity of sequenced genomes, and their easy genetic manipulation makes these bacteria ideal to work with, both in the laboratory and in BES applications.

3.1 *Shewanella*: A Model Organism

Organisms currently assigned to the genus *Shewanella* have been recognized for nearly 90 years, having first been isolated from the surface of rotten butter in 1931 [69]. Over the subsequent decades, these bacteria received little attention, with the exception of the name, that was frequently changed. In 1985, based on 5S rRNA sequence data a reclassification was proposed [70]. At this time the new genus *Shewanella* was created, to honor Dr. James Shewan for his contributions in the

study of these microorganisms. Although, most newly discovered *Shewanella* strains were initially classified as *S. putrefaciens*, DNA:DNA hybridization and 16S rRNA sequences resulted in the identification of more than 60 species within this genus [71].

It was only in 1988, with the discovery of members of the *Shewanella* genus with the capacity to perform EET, that these microorganisms started to find a prominent position within the scientific community [26]. These findings strongly suggested that this genus could play important roles in the biogeochemical cycles of the elements and in biotechnological applications, such as in BES [23, 32].

Members of the genus *Shewanella* are facultative anaerobic Gram negative γ-Proteobacteria. They generally possess a single polar flagellum and a rod shape with 2–3 μm in length and 0.5–0.6 μm in diameter [72]. The vast majority of the *Shewanella* isolates were obtained from marine environments, where they are sometimes found as fish pathogens with important impact in the aquaculture industry [73, 74]. *Shewanella* are also found in other habitats such as the freshwater *S. oneidensis* MR-1 [72].

Numerous *Shewanella* species are capable of growing at low temperatures (<5 °C) even though their optimal growth temperature is above 16 °C [75]. By contrast, those species found to be opportunistic human pathogens such as *S. algae* can grow at the relatively high temperature of 42 °C [76]. Another major aspect of the versatility of *Shewanella* is their ability to utilize a broad variety of organic and inorganic compounds as a final electron acceptor [77]. This allows them to thrive in a wide range of aquatic habitats, both marine and freshwater, and play a significant role in several biogeochemical redox cycles, including those of iron and manganese [26]. Since many of these organic and inorganic compounds are toxic or highly insoluble, they do not enter the bacteria and are extracellularly reduced by terminal reductases localized on the surface of the cell [31].

In 2001, the genome of *S. oneidensis MR-1* was sequenced, primarily due to its position as a model organism for dissimilatory metal reduction and its potential role in several biotechnological applications [78]. Since then, approximately 40 other *Shewanella* genomes have been sequenced [79]. Analysis of the *S. oneidensis* MR-1 genome revealed that the chromosome encodes for 41 putative *c*-type cytochromes (9 in the cytoplasmic membrane, 27 in the periplasm, and 5 in the outer membrane) [80, 81]. The capability to transfer electrons to a vast range of electron acceptors and perform EET is linked to this large number of *c*-type cytochromes, which spans from the cytoplasmic membrane to the outer membrane [82, 83]. Using a variety of genetic (e.g., knock-out studies) and biochemical techniques (e.g., protein characterization), some of the components involved have been identified and characterized in detail (Fig. 3). The so called “minimal setup” of redox proteins which are assigned to the EET process will be discussed below.

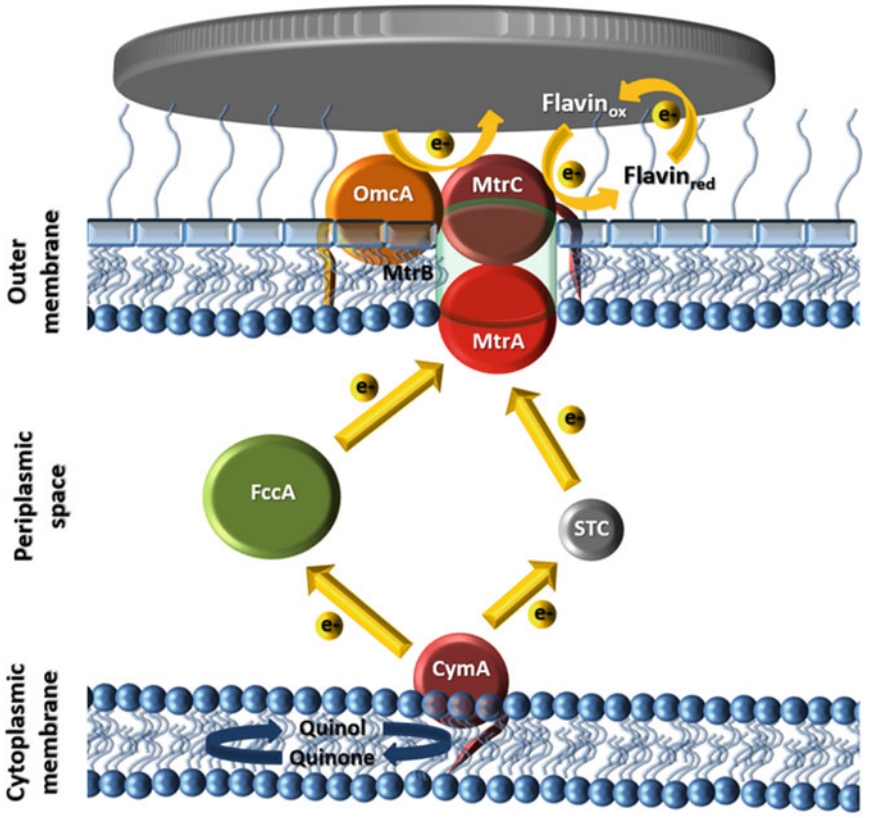

Fig. 3 Scheme of the so called "minimal setup" of redox proteins involved in the EET process of *S. oneidensis* MR-1. Arrows represent electron transfer processes

4 Extracellular Electron Transfer (EET) Pathway

MHCs play an important role in EET pathways, being critical elements for extracellular respiration and current output in electroactive microorganisms. In *S. oneidensis* MR-1, the MtrCAB pathway is the major EET pathway and is composed by several *c*-type cytochromes, that allow electrons generated from substrate oxidation to be transferred from the inner membrane, through the periplasmic space, to the outer-membrane for the reduction of terminal extracellular electron acceptors (e.g., metal oxides in the natural environment or electrodes in BES) (Fig. 3).

4.1 Cytoplasmic Membrane

Electron transfer at the cytoplasmic membrane involves the linkage of dehydrogenases responsible for oxidation of carbon sources in the cytoplasm (*e.g.* formate dehydrogenase), through a lipid soluble quinone pool, to electron transfer proteins (*e.g.* cytochromes) bound to the cytoplasmic membrane [84]. This mechanism generates a proton-electrochemical gradient that is used to produce ATP via the ATP synthase [85]. In parallel, the electron flow through the quinone pool towards extracellular electron acceptors appears to serve also as a pathway to discharge electrons without coupling to the generation of transmembrane electrochemical potential [86].

S. oneidensis MR-1 is known to produce three quinones (menaquinone, methylmenaquinone and ubiquinone) [87]. The deletion of *menD* and *menB* genes involved in the biosynthesis of menaquinone produced a phenotype incapable of iron respiration, revealing that menaquinone but not ubiquinone plays a role in metal respiration [88, 89]. This is in line with the difference in the reduction potentials of these two quinones with the ubiquinone potential more aligned to participate in aerobic respiratory chains.

4.1.1 CymA

Presently, it is well established that the linkage between the membrane quinone pool and EET chain is provided by a tetraheme *c*-type cytochrome called CymA that is attached to the periplasmic surface of the cytoplasmic membrane by a α-helical anchor [88, 90–93]. CymA from *Shewanella* has 21 kDa and is a member of the NapC/NirT protein family. It is able to bind quinol (Kd = 0.1–1 μM) [94], functioning as a quinol oxidase [88, 92, 95]. Deletion of the *cymA* gene severely hindered the reduction of a variety of substrates including Fe(III)/Mn(IV) oxides, fumarate, nitrate, nitrate, and DMSO [82, 90, 91]. This supported the proposal that CymA is one of the major hubs for electron transfer to the periplasm, being essential for EET. CymA's ability to interact with multiple periplasmic cytochrome partners has been amply demonstrated and explored [92, 96, 97]. Also, overexpression of this gene is enough to enhance electricity generation by *S. oneidensis* MR-1 in an MFC [98]. CymA's role in EET was further confirmed by cloning the gene in *E. coli* and observing that the heterologous expression of CymA is enough to make this bacterium capable of EET [99].

Although no structural characterization is presently available for CymA, it contains three low spin hemes with bis–histidine axial ligation and one high-spin heme with a histidine–water axial ligation [88, 100]. This high-spin heme forms an intrinsic part of the quinol oxidation site. Also, site-directed mutagenesis experiments revealed that the amino acid Lysine-91 is essential for quinol interaction with CymA from *Shewanella sp.* strain ANA-3 [94]. Redox properties were determined for CymA from *S. oneidensis* MR-1, with macroscopic midpoint potentials at pH 7.0 of approximately −110, −190 and −265 mV for the three low-spin hemes and −240 mV for the high-spin heme [88]. These potentials are below that of the menaquinol/menaquinone couple ($E^{o'} \approx -80$ mV), and thus electron transfer only

becomes spontaneous when the menaquinol/menaquinone balance is shifted towards menaquinol. Once the electrons enter the heme network, electron flow to the metal oxides becomes thermodynamically favorable due to progressively less negative redox potentials of the electron transfer proteins that are downstream of CymA [101].

Despite the importance of CymA for EET, the quinol dehydrogenase complex SirCD is capable of partially replacing it, restoring the capability of *Shewanella* Δ*cymA* strains to use Fe(III), fumarate or DMSO as terminal electrons acceptors [102]. *Shewanella* contains another tetraheme cytochrome attached to the inner-membrane denominated TorC [103]. Like CymA, TorC is a quinol dehydrogenase and is involved in the reduction of the terminal electron acceptor, Trimethylamine N-oxide (TMAO) to trimethylamine (TMA). This capability is the origin of the designation *putrefaciens* for the smell of rotten fish [104].

4.2 Periplasmic Space

In *S. oneidensis* MR-1, the periplasmic space has a width of approximately 235 Å [105] and contains an abundance of soluble electron transfer proteins (*e.g.* MHCs), in extremely high concentration, estimated to reach the mM range [106]. These proteins can be terminal reductases of soluble electron acceptors, or proteins that mediate electron transfer to the outer-membrane proteins for the reduction of insoluble electron acceptors. The two most abundant periplasmic cytochromes are the tetraheme flavocytochrome *c* FccA [97, 107, 108] and the small tetraheme cytochrome *c* STC [97, 107, 109].

4.2.1 FccA

Fc*c*A, a 64 kDa tetraheme *c*-type flavocytochrome, is a unidirectional fumarate reductase with a FAD cofactor in the active site [110]. This enzyme is unique in comparison to other fumarate reductases since it is a monomeric and soluble periplasmic protein. X-ray crystal structures of Fc*c*A from *S. frigidimarina* NCIMB400 and *S. oneidensis* MR-1 are available [111, 112], showing that these proteins fold into three domains: a N-terminal cytochrome domain with four bis–histidine low-spin *c*-type hemes, a C-terminal flavoprotein domain with a non-covalently bound FAD group and a clamp domain that was proposed to control the access to the active site of the enzyme. The hemes found in the N-terminal domain of Fc*c*A are arranged in a quasi-linear architecture that allows an efficient conduction of the electrons across the length of the protein to the FAD catalytic center [111–113]. Electron transfer to the active site is performed by heme IV, which is in close proximity (≈5 Å) to the FAD cofactor.

A microscopic redox characterization was obtained for Fc*c*A from *S. frigidimarina* NCIMB400 and *S. oneidensis* MR-1, revealing that despite their similar structure the details of the redox properties of the hemes are different [113, 114]. However, the differences are compatible with a common theme of internal control of the electron transfer flow that appears to direct electrons to the flavin catalytic

site only when the protein is reaching full reduction. From these observations a molecular mechanism for regulating the contribution of FccA in the EET vs fumarate reduction in *Shewanella* was proposed [114].

Fc*c*A can also transfer electrons to MtrA, the outer-membrane associated deca-heme cytochrome implicated in EET [97, 108, 115]. Binding studies performed in vitro demonstrated that Fc*c*A interacts with its redox partners, CymA and MtrA, through a single heme (heme II), avoiding the establishment of stable redox complex capable of spanning the periplasmic space [97]. Gene knock-out experiments of Fc*c*A showed defective phenotypes in several anaerobic cell growth conditions involving extracellular electron acceptors [106], which corroborates the previous studies implicating FccA as a periplasmic electron shuttle involved in the EET pathway of *Shewanella* [97, 108, 115]. Furthermore, in vitro and in vivo studies have also shown the occurrence of electron transfer between CymA and Fc*c*A [92, 97, 108].The high abundance in the periplasm, the interactions with CymA and MtrA, and the phenotypes of the deletion mutants make Fc*c*A a major player in electron shuttling in the periplasm during EET.

4.2.2 STC

STC is a highly abundant small tetraheme cytochrome *c* from the periplasm of *Shewanella* with a molecular weight of 12 kDa [116]. Based on gene knock-out experiments, STC is recognized as a key component in the EET pathway of *S. frigidimarina* NCIMB400 and *S. oneidensis* MR-1 [106, 109, 117, 118]. This was rationalized by studies with double STC and FccA knock-out experiments showing that at least one of these two cytochromes must be present in the periplasm to allow reduction of DMSO, ferric citrate or nitrate [106]. Overexpression of STC showed that it is a major component in the EET pathway of *Shewanella* [119].

High-resolution crystal structures of STC from *S. oneidensis* MR-1 and *S. algae* are available [120, 121] and a nuclear magnetic resonance (NMR) solution structure exists for STC from *S. frigidimarina* NCIMB400 [122]. Comparison of the structures from these three proteins showed that the general fold is very similar, and the relative positions of the heme groups are well conserved [121]. All four hemes are low-spin and have a bis–histidine axial ligation to the polypeptide chain [120–122]. The arrangement of the pairs of hemes in perpendicular and parallel geometries allows a short distance between the cofactors that enables a rapid intramolecular transfer of the electrons [123].

Microscopic redox properties measured for STC from *S. frigidimarina* NCIMB400, *S. oneidensis* MR-1 and *S. algae* DSM 9167 revealed similarities between these three ortholog proteins [121, 124, 125]. The microscopic reduction potentials for the four hemes of all three STCs cover similar, although not entirely overlapping reduction potential ranges: −190 to −229 mV; −171 to −243 mV; and −153 to −207 mV for *S. frigidimarina* NCIMB400, *S. oneidensis* MR-1 and *S. algae* DSM 9167, respectively. The redox potentials are in the range expected for bis-histidinyl-ligated heme groups with substantial exposure to the solvent [126]. Also, the results showed that electrostatic effects dominate the heme-heme interactions (covering a range of 8–56 mV for *S. frigidimarina*; 11–72 mV for

S. oneidensis; and 6–61 mV for *S. algae* [121, 124, 125], in agreement with the modest redox-linked structural modifications that occur in all three STCs. Furthermore, protonation has a considerable influence (redox–Bohr effect) on the redox properties of the hemes (covering a range of −4 to −36 mV for *S. frigidimarina* NCIMB400; −9 to −56 mV for *S. oneidensis* MR-1; and −1 to −51 mV for *S. algae* DSM 9167 [121, 124, 125], with heme III having in all three STCs the strongest redox-Bohr interaction, with a value similar to those reported for protonation of heme propionates [127]. In comparison, all three studied STC differ in their relative order of oxidation of the hemes due to changes that have occurred over time in their amino acid composition and/or structural arrangement. However, these three STC still possess a common feature that is heme III always presenting the highest reduction potential, and therefore is always the last heme to be oxidised [121, 124, 125].

In vitro binding studies showed that STC could interact with both inner membrane cytochrome CymA and outer-membrane protein MtrA from the MtrCAB complex [97]. These studies also showed that STC interacts with its redox partners, CymA and MtrA, through a single heme (heme IV), which forces detachment from the donor before attaching to the acceptor, preventing the formation of stable redox complexes that can span the periplasmic space of *Shewanella* [97]. Interestingly, although STC and FccA coexist and are highly abundant in the periplasmic space of *Shewanella*, they do not exchange electrons among themselves. This ensures that electron transport across the periplasmic space via these two proteins is segregated [97].

4.3 Outer Membrane

In order to reduce insoluble electron acceptors, electrons must cross the outer membrane and reach the cell exterior. Several redox proteins from *Shewanella* have been shown to be associated or bound to the outer membrane. Of these, the MtrCAB-OmcA protein complex is required to achieve maximal extracellular iron reduction rates [31, 128–130]. The genes encoding for this complex are clustered in an operon organized in the order: *omcA-mtrC-mtrA-mtrB*, where MtrC and OmcA are decaheme cytochromes present at the cell surface, MtrA is a decaheme periplasmic cytochrome and MtrB is a porin in which MtrA and MtrC are embedded on [131, 132].

4.3.1 MtrB

The outer-membrane *ß*-barrel protein MtrB is a 78 kDa protein with no cofactors but essential for EET [128]. Its pore size is estimated to be approximately 70 × 55 × 45 Å and embed MtrA and MtrC [132, 133]. The role of MtrB in metal reduction was first demonstrated by showing that a MtrB knock-out mutant strain lost its ability to reduce Fe(III) and Mn(IV) oxides [128]. MtrB knock-out mutants in *S. oneidensis* MR-1 showed mis-localization of both outer-membrane cytochromes MtrC and OmcA [134]. Furthermore, it was also demonstrated that the

decaheme cytochrome MtrA is only associated with the outer membrane when MtrB is expressed [135]. Using knock-out mutations and subsequent monitoring of complex assembly, revealed the existence of a synergetic relationship between MtrA and MtrB [136]. The assembly of the MtrAB subcomplex stabilizes MtrB, while subcomplex MtrBC does not assemble in the absence of MtrA. Three other stable modules similar to MtrAB have been identified in *S. oneidensis* MR-1. The MtrDE is proposed to be alternative to MtrAB, the DmsEF is part of porin cytochrome complex specific for DMSO reduction and SO4359-60 forms a secondary alternative iron reducing pathway to MtrAB [118, 130, 137, 138]. Moreover, gene clusters encoding for homologous MtrAB modules are phylogenetically distributed among organisms capable of electron exchange with the extracellular environment [135, 139]. Both metal-reducing (e.g., *Shewanella* and *Geobacter*) and metal-oxidizing (e.g., *Rhodopseudomonas* and *Sideroxydans*) bacteria have homologous MtrAB modules (Fig. 4) [30, 31, 135, 140–142]. This strengthens the hypothesis that the MtrAB module is essential for both outwards and inwards EET [131, 143].

4.3.2 MtrA

Decaheme cytochrome MtrA is a 37 kDa periplasmic cytochrome with 10 bis-histidine low-spin *c*-type hemes that is associated with the outer membrane via the integral membrane protein complex MtrCAB [30, 31, 135, 144, 145]. In vivo cross-linking assays showed that MtrA interacts on the periplasmic side with the outer membrane *ß*-barrel protein MtrB [144]. Also, it was shown in vitro that MtrA forms a stable protein complex with a dissociation constant stronger than 0.1 μM with its outer membrane partners, MtrB and MtrC [135]. However, under different experimental conditions MtrA was found to be present in the soluble periplasmic fraction hinting to weaker affinity for MtrB [108, 145]. In vitro studies showed that MtrA can interact and receive electrons from the periplasmic cytochrome Fc*c*A [97, 108] and also interact with the periplasmic cytochrome STC [97]. It was also revealed that MtrA can be directly reduced by CymA [96, 108]. Potentiometric redox titrations showed that MtrA is active over a potential range from −100 to −400 mV at pH 7.5 [145].

A high-resolution structure of MtrA has not been reported yet but its aminoacid sequence shows that it is likely to be evolutionarily related to the structurally characterized pentaheme cytochrome NrfB [146]. Small-angle X-ray scattering showed that MtrA is shaped like an extended molecular "wire" with overall dimensions 104 Å × 20 Å × 50 Å [133]. Given that the thickness of the

▶

Fig. 4 **a** MtrAB gene cluster in different electroactive microorganisms and their context in the genome. Cytochromes and β-barrel membrane proteins (MtrB/PioB homologues) are represented in black and gray, respectively. **b** Phylogenetic distribution of MtrAB modules in organisms known to be electroactive [16, 64]. Maximum-likelihood phylogeny with ModelFinder method (best model: LG + I + G4) of concatenated sequences of MtrA and MtrB. Bootstrap and SH-Like Test (-alrt) confidence values (from 1000 replicates each) are shown near each node of the major splits

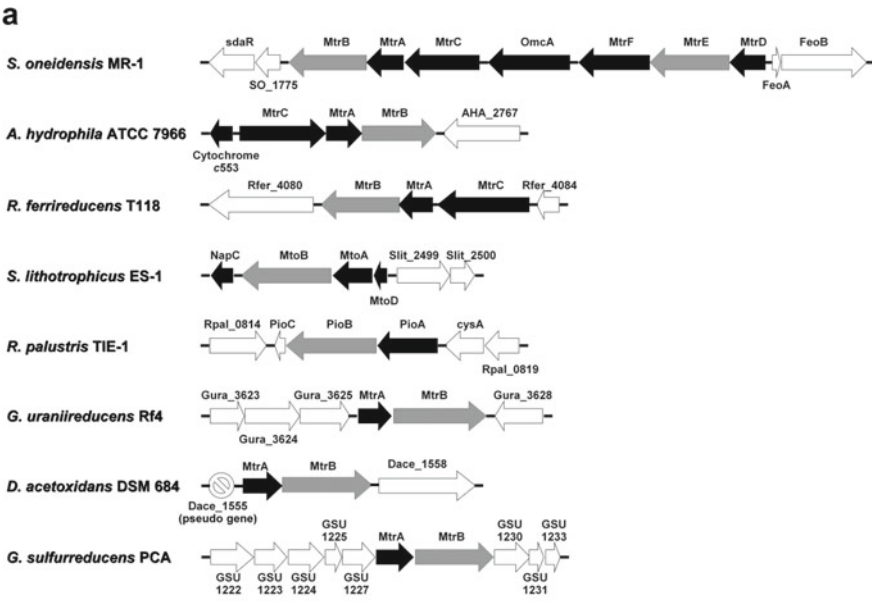
a
S. oneidensis MR-1
sdaR
MtrB
MtrA
MtrC
OmcA
MtrF
MtrE
MtrD
FeoB
SO_1775
FeoA
A. hydrophila ATCC 7966
MtrC
MtrA
MtrB
AHA_2767
Cytochrome c553
R. ferrireducens T118
Rfer_4080
MtrB
MtrA
MtrC
Rfer_4084
S. lithotrophicus ES-1
NapC
MtoB
MtoA
Slit_2499
Slit_2500
MtoD
R. palustris TIE-1
Rpal_0814
PioC
PioB
PioA
cysA
Rpal_0819
G. uraniireducens Rf4
Gura_3623
Gura_3625
MtrA
MtrB
Gura_3628
Gura_3624
D. acetoxidans DSM 684
MtrA
MtrB
Dace_1558
Dace_1555 (pseudo gene)
G. sulfurreducens PCA
GSU 1225
MtrA
MtrB
GSU 1230
GSU 1233
GSU 1222
GSU 1223
GSU 1224
GSU 1227
GSU 1231

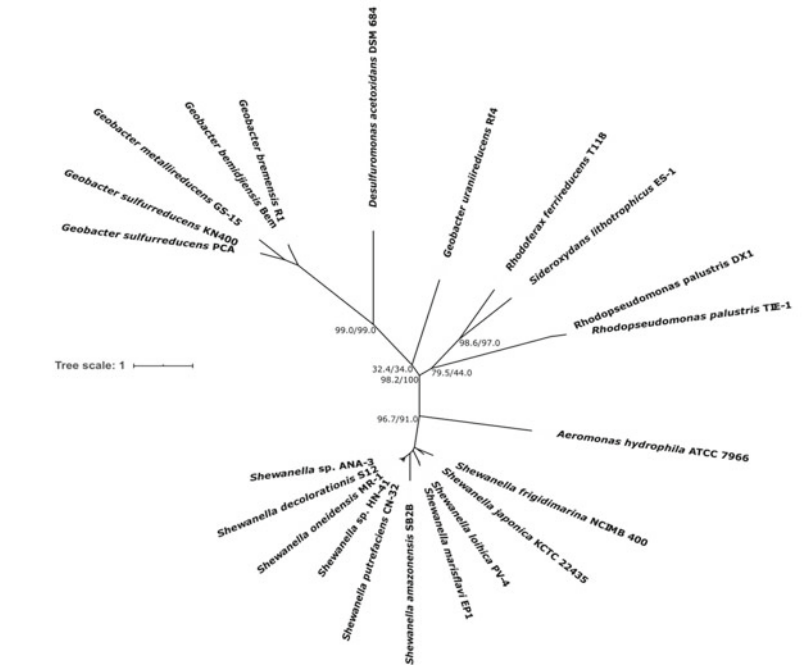
b
Desulfuromonas acetoxidans DSM 684
Geobacter bremensis R1
Geobacter bemidjiensis Bem
Geobacter metallireducens GS-15
Geobacter sulfurreducens KN400
Geobacter sulfurreducens PCA
Geobacter uraniireducens Rf4
Rhodoferax ferrireducens T118
Sideroxydans lithotrophicus ES-1
Rhodopseudomonas palustris DX1
Rhodopseudomonas palustris TIE-1
Aeromonas hydrophila ATCC 7966
Shewanella sp. ANA-3
Shewanella decolorationis S12
Shewanella oneidensis MR-1
Shewanella sp. HN-41
Shewanella putrefaciens CN-32
Shewanella amazonensis SB2B
Shewanella marisflavi EP1
Shewanella loihica PV-4
Shewanella japonica KCTC 22435
Shewanella frigidimarina NCIMB 400
99.0/99.0
98.6/97.0
32.4/34.0
98.2/100
79.5/44.0
96.7/91.0
Tree scale: 1

Gram-negative outer membrane is ≈70 Å [147], the estimated length of MtrA would be sufficient for transferring electrons heme-to-heme across the outer membrane even though the Small Angle Neutron Scattering model of the whole MtrCAB complex suggests that MtrA is only partially inserted in MtrB [143]. Indeed, the 3D-structure determination of an MtrCAB complex revealed that MtrA has very little secondary structure [132], which confer greater flexibility to the protein, allowing it to accept electrons from its various physiological partners [97, 108].

4.3.3 Decaheme Cytochromes MtrC and OmcA

Decaheme cytochromes MtrC and OmcA are two cytochromes with 75 and 85 kDa, respectively, anchored to the outer membrane via a lipidated cysteine [129, 148, 149]. Treatment by proteinase K significantly degraded MtrC and OmcA by 31 and 71%, respectively [148]. This indicates that both proteins are exposed on the outer surface of the cells and that MtrC is not as exposed to the extracellular environment as OmcA, which is coherent with the proposal that MtrC becomes partly buried upon association with the β-barrel protein MtrB [143]. The Small Angle Neutron Scattering structural data agree with previous in vivo cross-linking studies that revealed an interaction of MtrC with the β-barrel protein MtrB forming in combination with the decaheme cytochrome MtrA an outer membrane protein complex MtrCAB, with a 1:1:1 stoichiometry [144]. Cross-linking assays demonstrated that MtrC and OmcA physically interact with each other on the bacterial cells [144, 150], and in vitro studies reported a dissociation constant smaller than 0.5 μM for the MtrC-OmcA complex [151].

Several studies showed that MtrC and OmcA are highly expressed by *S. oneidensis* MR-1 under ferric iron reducing conditions [129, 130, 152] and are capable of direct electron transfer to iron oxides [153–155]. Both MtrC and OmcA polypeptides were shown to contain a putative hematite-binding motif (Ser/Thr-Pro-Ser/Thr) [156] and the physical interaction between MtrC and OmcA synergistically boosts the metal reductase activity of these outer-membrane cytochromes [151]. Disruption of the *mtrC* or *omcA* genes did not affect the growth of *S. oneidensis* MR-1 on soluble terminal electron acceptors, such as fumarate, nitrate and DMSO [149]. In contrast, reduction of insoluble iron oxides and electron transfer to MFC anodes was severely diminished [58, 82, 118, 152, 157, 158]. A series of knock-out mutations of all the outer-membrane cytochromes and subsequent expression of each one individually, showed that MtrC is critical for EET and that mutants containing only the OmcA cytochrome were not capable of transferring electrons to iron [130]. This fact suggests that while OmcA is an iron terminal reductase [60, 149], its contact with the periplasmic redox chain is mediated by MtrC [130]. Additionally, it has been shown that MtrC is responsible for most of the electron transfer to carbon electrodes, while OmcA is mainly involved in cellular attachment to solid surfaces, playing a smaller role in electron transfer [58]. This is coherent with data obtained by antibody functionalized atomic force microscopy (AFM) tips that showed OmcA in the interface between the cell and insoluble substrate, while MtrC displays a more uniform distribution across the

cell surface [158]. Purified MtrC and OmcA were reported to reduce iron oxides at much slower rates compared to measurements with intact *Shewanella* cells and that with the addition of flavins, rates were increased to values comparable to those measured with intact cells [60]. These results demonstrate a role of electron shuttle for flavins during MtrC and OmcA mediated reduction of ferric iron oxides.

Both cytochromes have 10 low-spin *c*-type hemes [95, 148, 157, 158]. Potentiometric titrations revealed that both MtrC and OmcA titrate over a broad range of redox potential from +100 mV to −500 mV and −20 mV to −320 mV, respectively [101, 151, 157]. Crystal structures of these proteins have revealed that the proteins are formed by 4 domains, two multiheme domains that are flanked by two β-barrels with β-strands arranged in Greek key motifs [159, 160]. Both MtrC and OmcA contain a conserved decaheme staggered cross cofactor arrangement, where an octaheme chain formed by hemes V, IV, III, I, VI, VIII, IX, X is crossed by a tetraheme chain consisting of hemes II, I, VI, VII. All the hemes display bis-histidine axial ligand coordination to the heme iron, with each heme within 7 Å of its nearest neighbor, ensuring rapid intra-molecular electron transfer. In vitro experiments revealed that OmcA and MtrC (as well as its homologues MtrF and UndA) are capable of transferring electrons to chemically varied soluble electron acceptors typically found in the oxic-anoxic interface habitats where *Shewanella* is found, with clear differences in the rates for different acceptors [161]. NMR and computational docking studies revealed that whereas for negatively charged FMN and AQDS binding occurs near heme II, neutral riboflavin binds near hemes IX and X and positively charged phenazine methosulphate binds near heme X in a different position. For OmcA, which plays a more important role in surface attachment than MtrC, it was observed that iron oxide particles and graphene oxides do not come into close proximity to the hemes, in agreement with experimentally observed slow electron transfer [162]. Altogether these studies reveal that the structure of these proteins appears to be designed such as the staggered cross provides different exit points for electron through different exposed hemes [161].

EET Enhancement in *Shewanella*

To increase EET in MFCs, over-expression of the MHC involved in EET of *S. oneidensis* MR-1 has been used to enhance current output. For example, it was observed that overexpression of *mtrC* in *S. oneidensis* MR-1 could generate 35% more current in MFCs than that of wild-type organism [82]. Furthermore, the co-expression of the metal-reducing biosynthesis gene cluster *mtrC-mtrA-mtrB* also exhibited an increase in maximum current density of approximately 87% [163]. More recently, the genetic manipulation of *S. oneidensis* MR-1 where the proteins that may compete with STC for EET processes in the periplasmic space were replaced by STC, led to the creation of a mutant that presented 23% higher current generation when compared with the wild-type strain [119]. These studies highlight the importance of genetic engineering to design and tailor MHC towards enhanced electron transfer processes to push forward the practical implementation of electroactive organisms in BES [18].

Genetic engineering was also shown to be crucial to increase the metabolic capacity of *S. oneidensis* MR-1. The heterologous incorporation of metabolic pathways allowed *S. oneidensis* MR-1 to use glucose, xylose or glycerol as the sole carbon and energy source for electricity production in MFC [164–166]. Furthermore, the heterologous expression of proteorhodopsin, a light-dependent proton pump, led *Shewanella* to consume lactate at an increased rate when it is illuminated which was reflected by the increase in current generation when compared with wild-type organism [167]. Recently, genetic manipulation of *S. oneidensis* MR-1 allowed the modification of this organism to use electrons from a cathode to drive reduction of acetoin to 2,3-butanediol, demonstrating the capacity to genetically engineer a microbial electrosynthesis pathway [168].

Another approach used to enhance the rate of EET in *S. oneidensis* MR-1 was the increase of the intracellular electron pool, by engineering and driving the metabolic flux toward the enhancement of intracellular NADH regeneration [169]. In this work three different modules (the de novo pathway, the salvage pathway and the universal biosynthesis pathway) were over-expressed, and the capacity for electricity production of mutated *S. oneidensis* MR-1 was evaluated. The increase in electricity generation and Coulombic efficiency showed that an increase in the NAD(H+) pool results in the transfer of more electrons from increased oxidation of the electron donor to the EET pathway, enhancing intracellular electron flux and EET rate [169].

Mediated electron transfer has been demonstrated to be one of the most important mechanism for *S. oneidensis* MR-1 in performing EET. Promoting redox shuttle biosynthesis in this organism also enhances EET efficiency in BES [163, 170]. The heterologous expression of the flavin biosynthesis pathway from *Bacillus subtilis* enhanced EET rate of *S. oneidensis* MR-1, with an increase of 13,2 times of the maximum power output when compared with wild-type strain [170]. Likewise, the homologous expression of the flavin biosynthesis gene cluster *ribA-E* in *S. oneidensis* MR-1 increased the maximum current density by approximate 110% [163]. Furthermore, overexpression of the gene *ydeH* from *E. coli* in *S. oneidensis* MR-1, responsible for the biosynthesis of c-di-GMP enhanced biofilm formation and bioelectricity generation [171]. The high levels of intracellular c-di-GMP promote the expression of adhesive matrix components, which facilitates bacterial biofilm formation. The maximum power density obtained with the engineered strain was $\sim$2.8 times higher than that achieved by the wild-type strain [171].

The recent work on the CRISPR/Cas9 approach to manipulate *S. oneidensis* MR-1 enables the precise site-directed mutagenesis of the bacterial chromosome [172]. This allows the modification of several different genes, and the introduction of various types of mutations, including individual base changes and net gene deletion in this model strain [172]. This approach will simplify the genetic manipulation of this electroactive organism facilitating the implementation of high-throughput genomic engineering technologies, contributing to the improvement of this type of organisms towards the practical implementation of BES.

5 Conclusion

MFCs have been intensively investigated over the past decades with tremendous advances. Despite all the improvements made to increment MFC power output, the low EET rate from electroactive microorganisms to the electrode surfaces remains a bottleneck that prevents the practical application of BES [173–175]. At this time, means to improve electroactivity are being explored, on the biochemical, genetic and technological fronts [121, 176–178].

EET has been observed and studied in phylogenetically diverse microorganisms [16], indicating that this microbial trait is widespread in nature. Despite the microbial diversity, only a few species have emerged as model organisms for the study of EET (e.g., *Geobacter sulfurreducens, Shewanella oneidensis* and *Thermincola spp.*). Of all the EET model organisms, *S. oneidensis* MR-1 is the most extensively studied and presently has the best characterized molecular mechanism of EET [23, 32, 179]. The extensive study of *Shewanella versus* other electroactive bacteria has to do with a number of combined factors such as robust growth under oxygen conditions, existence of sequenced genome, straightforward genetic manipulation, and robust strategies for overexpression of the relevant multiheme cytochromes which makes these bacteria ideal to work with. It is well known that *Geobacter* species are the dominant members in acetate fed BES electrode biofilms and that *Thermincola spp.* are able to grow at higher temperature, and both produce higher current densities compared to *Shewanella* [16, 176, 180–182], making them more attractive candidates for BES applications. Despite these positive aspects, several difficulties mainly involving growth and genetic manipulation have rendered these bacteria more challenging to study and fully characterize their EET pathways, with numerous gaps in the understanding of their molecular mechanisms of EET.

Using as model organism bacteria such as *S. oneidensis* MR-1, our understanding on how EET occurs has increased greatly. Here, MHCs continuously revealed themselves as key players, creating an efficient redox network that stretches from the cytoplasmic membrane, across the periplasmic space and through the outer membrane, transferring electrons directly or indirectly to their insoluble acceptors [29, 183]. The detailed functional characterization of the MHCs from microorganisms capable of EET will ultimately lead to a more rational design and optimized biotechnological applications which use these organisms. This optimization can be biological or technological, using different approaches such as molecular biology to tune the reduction potentials of hemes found in the MHC involved in the electron transfer pathway [121, 162, 184, 185], manipulation of electron mediator synthesis pathways [186] reprogramming gene regulatory circuits to enhance electron transfer pathways [187] or even surface enhancement of electrodes for improved cellular contact [188]. Either way, all stand to benefit from the full characterization of these complex electron transfer pathways.

In this chapter, the key *c*-type cytochromes for EET in *S. oneidensis* MR-1 were reviewed in order to shed light on how electrons are delivered to the cell surface during EET and possible mechanisms that could be applied to enhance the function of MFCs and other BES, bringing them closer to commercial applications.

References

1. Logan BE, Wallack MJ, Kim K, He W, Feng Y, Saikaly PE (2015) Assessment of microbial fuel cell configurations and power densities. Environ Sci Technol Lett 2:206–214. https://doi.org/10.1021/acs.estlett.5b00180
2. Prévoteau A, Carvajal-Arroyo JM, Ganigué R, Rabaey K (2020) Microbial electrosynthesis from CO_2: forever a promise? Curr Opin Biotechnol 62:48–57. https://doi.org/10.1016/j.copbio.2019.08.014
3. Rabaey K, Rozendal RA (2010) Microbial electrosynthesis - revisiting the electrical route for microbial production. Nat Rev Microbiol 8:706–716. https://doi.org/10.1038/nrmicro2422
4. Modin O, Aulenta F, Harnisch F, Patil SA, Carmona-Martinez AA, Agarwal S, Zhang Y, Sinha-Ray S, Yarin AL, Greiner A, Schröder U, Landis R, Griffith R, Shoemaker S, Smolders E, Sorensen SR, Springael D, van Breukelen BM (2017) Three promising applications of microbial electrochemistry for the water sector. Environ Sci Water Res Technol 156:1–13. https://doi.org/10.1039/C6EW00325G
5. Mohan SV, Velvizhi G, Krishna KV, Babu ML (2014) Bioresource technology microbial catalyzed electrochemical systems: a bio-factory with multi-facet applications. Bioresour Technol 165:355–364. https://doi.org/10.1016/j.biortech.2014.03.048
6. Liu H, Logan BE (2004) Electricity generation using an air-cathode single chamber microbial fuel cell in the presence and absence of a proton exchange membrane. Environ Sci Technol 38:4040–4046. https://doi.org/10.1021/ES0499344
7. Slate AJ, Whitehead KA, Brownson DAC, Banks CE (2019) Microbial fuel cells: an overview of current technology. Renew Sustain Energy Rev 101:60–81. https://doi.org/10.1016/j.rser.2018.09.044
8. Rozendal RA, Hamelers HVM, Rabaey K, Keller J, Buisman CJN (2008) Towards practical implementation of bioelectrochemical wastewater treatment. Trends Biotechnol 26:450–459. https://doi.org/10.1016/j.tibtech.2008.04.008
9. Schroder U (2007) Anodic electron transfer mechanisms in microbial fuel cells and their energy efficiency. Phys Chem Chem Phys 9:2619–2629. https://doi.org/10.1039/B703627M
10. Logan B, Cheng S, Watson V, Estadt G (2007) Graphite fiber brush anodes for increased power production in air-cathode microbial fuel cells. Environ Sci Technol 41:3341–3346. https://doi.org/10.1021/es062644y
11. Pant D, Singh A, Van Bogaert G, Irving Olsen S, Singh Nigam P, Diels L, Vanbroekhoven K (2012) Bioelectrochemical systems (BES) for sustainable energy production and product recovery from organic wastes and industrial wastewaters. RSC Adv 2:1248–1263. https://doi.org/10.1039/C1RA00839K
12. Torres CI, Marcus AK, Lee HS, Parameswaran P, Krajmalnik-Brown R, Rittmann BE (2010) A kinetic perspective on extracellular electron transfer by anode-respiring bacteria. FEMS Microbiol Rev 34:3–17. https://doi.org/10.1111/j.1574-6976.2009.00191.x
13. Schröder U, Harnisch F, Angenent LT (2015) Microbial electrochemistry and technology: terminology and classification. Energy Environ Sci 8:513–519. https://doi.org/10.1039/C4EE03359K
14. Potter MC (1911) Electrical effects accompanying the decomposition of organic compounds. Proc R Soc London B Biol Sci 84
15. Logan BE (2010) Scaling up microbial fuel cells and other bioelectrochemical systems. Appl Microbiol Biotechnol 85:1665–1671. https://doi.org/10.1007/s00253-009-2378-9

16. Logan BE, Rossi R, Ragab A, Saikaly PE (2019) Electroactive microorganisms in bioelectrochemical systems. Nat Rev Microbiol 17:307–319. https://doi.org/10.1038/s41579-019-0173-x
17. Babauta JT, Nguyen HD, Istanbullu O, Beyenal H (2013) Microscale gradients of oxygen, hydrogen peroxide, and pH in freshwater cathodic biofilms. Chemsuschem 6:1252–1261. https://doi.org/10.1002/cssc.201300019
18. Glaven SM (2019) Bioelectrochemical systems and synthetic biology: more power, more products. Microb Biotechnol 12:819–823. https://doi.org/10.1111/1751-7915.13456
19. Li F, Wang L, Liu C, Wu D, Song H (2018) Engineering exoelectrogens by synthetic biology strategies. Curr Opin Electrochem 10:37–45. https://doi.org/10.1016/j.coelec.2018.03.030
20. Teravest MA, Ajo-Franklin CM (2015) Transforming exoelectrogens for biotechnology using synthetic biology. Biotechnol Bioeng 113:687–697. https://doi.org/10.1002/bit.25723
21. Richardson DJ (2000) Bacterial respiration: A flexibe process for a changing environment. Microbiology 146:551–571. https:// doi:https://doi.org/10.1099/00221287-146-3-551
22. White GF, Edwards MJ, Gomez-Perez L, Richardson DJ, Butt JN, Clarke TA (2016) Mechanisms of bacterial extracellular electron exchange. In: Advances in microbial physiology, pp 87–138
23. Shi L, Dong H, Reguera G, Beyenal H, Lu A, Liu J, Yu HQ, Fredrickson JK (2016) Extracellular electron transfer mechanisms between microorganisms and minerals. Nat Rev Microbiol 14:651–662. https://doi.org/10.1038/nrmicro.2016.93
24. Gralnick JA, Newman DK (2007) Micro review extracellular respiration. Mol Microbiol 65:1–11. https://doi.org/10.1111/j.1365-2958.2007.05778.x
25. Kumar A, Hsu LHH, Kavanagh P, Barrière F, Lens PNL, Lapinsonnière L, Lienhard JH, Schröder U, Jiang X, Leech D (2017) The ins and outs of microorganism-electrode electron transfer reactions. Nat Rev Chem 1:1–13. https://doi.org/10.1038/s41570-017-0024
26. Myers CR, Nealson KH (1988) Bacterial manganese reduction and growth with manganese oxide as the sole electron acceptor. Science 240:1319–1321. https://doi.org/10.1126/science.240.4857.1319
27. Lower SK (2001) Bacterial recognition of mineral surfaces: nanoscale interactions between *Shewanella* and alpha -FeOOH. Science 292:1360–1363. https://doi.org/10.1126/science.1059567
28. Reguera G, McCarthy KD, Mehta T, Nicoll JS, Tuominen MT, Lovley DR (2005) Extracellular electron transfer via microbial nanowires. Nature 435:1098–1101. https://doi.org/10.1038/nature03661
29. Costa NL, Clarke TA, Philipp L-AA, Gescher J, Louro RO, Paquete CM (2018) Electron transfer process in microbial electrochemical technologies: the role of cell-surface exposed conductive proteins. Bioresour Technol 255:308–317. https://doi.org/10.1016/j.biortech.2018.01.133
30. Shi L, Rosso KM, Zachara JM, Fredrickson JK (2012) Mtr extracellular electron-transfer pathways in Fe(III)-reducing or Fe(II)-oxidizing bacteria: a genomic perspective. Biochem Soc Trans 40:1261–1267. https://doi.org/10.1042/BST20120098
31. Shi L, Rosso KM, Clarke TA, Richardson DJ, Zachara JM, Fredrickson JK (2012) Molecular underpinnings of Fe (III) oxide reduction by *Shewanella oneidensis* MR-1. Front Microbiol 3:1–10. https://doi.org/10.3389/fmicb.2012.00050
32. Shi L, Squier TC, Zachara JM, Fredrickson JK (2007) Respiration of metal (hydr)oxides by *Shewanella* and *Geobacter*: A key role for multihaem c-type cytochromes. Mol Microbiol 65:12–20. https://doi.org/10.1111/j.1365-2958.2007.05783.x
33. Page CC, Moser CC, Chen X, Dutton PL (1999) Natural engineering principles of electron tunnelling in biological oxidation–reduction. Nature 402:47–52. https://doi.org/10.1038/46972
34. Warren JJ, Ener ME, Vlček A, Winkler JR, Gray HB (2012) Electron hopping through proteins. Coord Chem Rev 256:2478–2487. https://doi.org/10.1016/j.ccr.2012.03.032

35. Harris HW, El-Naggar MY, Nealson KH (2012) *Shewanella oneidensis* MR-1 chemotaxis proteins and electron-transport chain components essential for congregation near insoluble electron acceptors. Biochem Soc Trans 40:1167–1177. https://doi.org/10.1042/BST20120232
36. Lovley DR (2008) Extracellular electron transfer: wires, capacitors, iron lungs, and more. Geobiology 6:225–231. https://doi.org/10.1111/j.1472-4669.2008.00148.x
37. El-Naggar MY, Wanger G, Leung KM, Yuzvinsky TD, Southam G, Yang J, Lau WM, Nealson KH, Gorby YA (2010) Electrical transport along bacterial nanowires from *Shewanella oneidensis* MR-1. Proc Natl Acad Sci 107:18127–18131. https://doi.org/10.1073/pnas.1004880107
38. Gorby YA, Yanina S, Mclean JS, Rosso KM, Moyles D, Dohnalkova A, Beveridge TJ, Chang IS, Kim BH, Kim KS, Culley DE, Reed SB, Romine MF, Saffarini DA, Hill EA, Shi L, Elias DA, Kennedy DW, Pinchuk G, Watanabe K, Ishii S, Logan B, Nealson KH, Fredrickson JK (2006) Electrically conductive bacterial nanowires produced by *Shewanella oneidensis* strain MR-1 and other microorganisms. Proc Natl Acad Sci 103(30):11358–11363. https://doi.org/10.1073/pnas.0604517103
39. Vargas M, Malvankar NS, Tremblay P, Leang C, Smith JA, Patel P, Synoeyenbos-West O, Nevin KP, Lovley DR (2013) Aromatic amino acids required for Pili conductivity and long-range extracellular electron transport in *Geobacter sulfurreducens*. MBio 4:1–6. https://doi.org/10.1128/mBio.00105-13
40. Shi L, Deng S, Marshall MJ, Wang Z, Kennedy DW, Dohnalkova AC, Mottaz HM, Hill EA, Gorby YA, Beliaev AS, Richardson DJ, Zachara JM, Fredrickson JK (2008) Direct involvement of type II secretion system in extracellular translocation of *Shewanella oneidensis* outer membrane cytochromes MtrC and OmcA. J Bacteriol 190:5512–5516. https://doi.org/10.1128/JB.00514-08
41. Bouhenni RA, Vora GJ, Biffinger JC, Shirodkar S, Brockman K, Ray R, Wu P, Johnson BJ, Biddle EM, Marshall MJ, Fitzgerald LA, Little BJ, Fredrickson JK, Beliaev AS, Ringeisen BR, Saffarini DA (2010) The Role of *Shewanella oneidensis* MR-1 outer surface structures in extracellular electron transfer. Electroanalysis 22:856–864. https://doi.org/10.1002/elan.200880006
42. Pirbadian S, Barchinger SE, Leung KM, Byun HS, Jangir Y, Bouhenni RA, Reed SB, Romine MF, Saffarini DA, Shi L, Gorby YA, Golbeck JH, El-Naggar MY (2014) *Shewanella oneidensis* MR-1 nanowires are outer membrane and periplasmic extensions of the extracellular electron transport components. Proc Natl Acad Sci 111:12883–12888. https://doi.org/10.1073/pnas.1410551111
43. Holmes DE, Dang Y, Walker DJF, Lovley DR (2016) The electrically conductive pili of *Geobacter* species are a recently evolved feature for extracellular electron transfer. Microb Genomics 2:e000072. https://doi.org/10.1099/mgen.0.000072
44. Wang F, Gu Y, O'Brien JP, Yi SM, Yalcin SE, Srikanth V, Shen C, Vu D, Ing NL, Hochbaum AI, Egelman EH, Malvankar NS (2019) Structure of microbial nanowires reveals stacked hemes that transport electrons over micrometers. Cell 177:361-369.e10. https://doi.org/10.1016/j.cell.2019.03.029
45. Filman DJ, Marino SF, Ward JE, Yang L, Mester Z, Bullitt E, Lovley DR, Strauss M (2019) Cryo-EM reveals the structural basis of long-range electron transport in a cytochrome-based bacterial nanowire. Commun Biol 2:219. https://doi.org/10.1038/s42003-019-0448-9
46. Childers SE, Ciufo S, Lovley DR (2002) *Geobacter metallireducens* accesses insoluble Fe (iii) oxide by chemotaxis. Nature 416:767–769. https://doi.org/10.1038/416767a
47. Reguera G, Nevin KP, Nicoll JS, Covalla SF, Woodard TL, Lovley DR (2006) Biofilm and nanowire production leads to increased current in Geobacter sulfurreducens fuel cells. Appl Environ Microbiol 72:7345–7348. https://doi.org/10.1128/AEM.01444-06
48. Reardon PN, Mueller KT (2013) Structure of the type IVa major pilin from the electrically conductive bacterial nanowires of *Geobacter sulfurreducens*. J Biol Chem 288:29260–29266. https://doi.org/10.1074/jbc.M113.498527

49. Liu X, Ye Y, Xiao K, Rensing C, Zhou S (2019) Molecular evidence for the adaptive evolution of *Geobacter sulfurreducens* to perform dissimilatory iron reduction in natural environments. Mol Microbiol 00:1–12. https://doi.org/10.1111/mmi.14443
50. Leang C, Qian X, Mester T, Lovley DR (2010) Alignment of the c-type cytochrome OmcS along pili of *Geobacter sulfurreducens*. Appl Environ Microbiol 76:4080–4084. https://doi.org/10.1128/AEM.00023-10
51. Ru X, Zhang P, Beratan DN (2019) Assessing possible mechanisms of micrometer-scale electron transfer in heme-free *Geobacter sulfurreducens* Pili. J Phys Chem B 123:5035–5047. https://doi.org/10.1021/acs.jpcb.9b01086
52. Newman DK, Kolter R (2000) A role for excreted quinones in extracellular electron transfer. 405:13–16. https://doi.org/10.1038/35011098
53. Lies DP, Hernandez ME, Kappler A, Mielke RE, Gralnick JA, Newman DK (2005) *Shewanella oneidensis* MR-1 uses overlapping pathways for iron reduction at a distance and by direct contact under conditions relevant for biofilms. Appl Environ Microbiol 71:4414–4426. https://doi.org/10.1128/AEM.71.8.4414-4426.2005
54. Myers CR, Myers JM (1993a) Ferric reductase is associated with the membranes of anaerobically grown *Shewanella putrefaciens* MR-1. FEMS Microbiol Lett 108:15–22. https://doi.org/10.1111/j.1574-6968.1993.tb06066.x
55. Marsili E, Baron DB, Shikhare ID, Coursolle D, Gralnick JA, Bond DR (2008) Shewanella secretes flavins that mediate extracellular electron transfer. Proc Natl Acad Sci 105:3968–3973. https://doi.org/10.1073/pnas.0710525105
56. Von Canstein H, Ogawa J, Shimizu S, Lloyd JR (2008) Secretion of flavins by *Shewanella* species and their role in extracellular electron transfer. Appl Environ Microbiol 74:615–623. https://doi.org/10.1128/AEM.01387-07
57. Kotloski NJ, Gralnick JA (2013) Flavin electron shuttles dominate extracellular electron transfer by *Shewanella oneidensis*. MBio 4:e00553-12. https://doi.org/10.1128/mBio.00553-12
58. Coursolle D, Baron DB, Bond DR, Gralnick JA (2010) The Mtr respiratory pathway is essential for reducing flavins and electrodes in *Shewanella oneidensis*. J Bacteriol 192:467–474. https://doi.org/10.1128/JB.00925-09
59. Okamoto A, Kalathil S, Deng X, Hashimoto K, Nakamura R, Nealson KH (2014) Cell-secreted flavins bound to membrane cytochromes dictate electron transfer reactions to surfaces with diverse charge and pH. Sci Rep 4:1–8. https://doi.org/10.1038/srep05628
60. Ross DE, Brantley SL, Tien M (2009) Kinetic characterization of OmcA and MtrC, terminal reductases involved in respiratory electron transfer for dissimilatory iron reduction in *Shewanella oneidensis* MR-1. Appl Environ Microbiol 75:5218–5226. https://doi.org/10.1128/AEM.00544-09
61. Baron D, LaBelle E, Coursolle D, Gralnick JA, Bond DR (2009) Electrochemical measurement of electron transfer kinetics by *Shewanella oneidensis* MR-1. J Biol Chem 284:28865–28873. https://doi.org/10.1074/jbc.M109.043455
62. Straub KL, Benz M, Schink B (2001) Iron metabolism in anoxic environments at near neutral pH. FEMS Microbiol Ecol 34:181–186. https://doi.org/10.1111/j.1574-6941.2001.tb00768.x
63. Kim HJ, Park HS, Hyun MS, Chang IS, Kim M, Kim BH (2002) A mediator-less microbial fuel cell using a metal reducing bacterium, *Shewanella putrefaciens*. Enzyme Microb Technol 30:145–152. https://doi.org/10.1016/S0141-0229(01)00478-1
64. Koch C, Harnisch F (2016) Is there a specific ecological Niche for electroactive microorganisms? Chem Electro Chem 3:1282–1295. https://doi.org/10.1002/celc.201600079
65. Dopson M, Ni G, Sleutels THJA (2016) Possibilities for extremophilic microorganisms in microbial electrochemical systems. FEMS Microbiol Rev 40:164–181. https://doi.org/10.1093/femsre/fuv044

66. Nevin KP, Richter H, Covalla SF, Johnson JP, Woodard TL, Orloff AL, Jia H, Zhang M, Lovley DR (2008) Power output and columbic efficiencies from biofilms of *Geobacter sulfurreducens* comparable to mixed community microbial fuel cells. Environ Microbiol 10:2505–2514. https://doi.org/10.1111/j.1462-2920.2008.01675.x
67. Pande S, Kost C (2017) Bacterial unculurability and the formation of intercellular metabolic networks. Trends Microbiol 25(5):349–361. https://doi.org/10.1016/j.tim.2017.02.015
68. Saratale RG, Saratale GD, Pugazhendhi A, Zhen G, Kumar G, Kadier A, Sivagurunathan P (2017) Microbiome involved in microbial electrochemical systems (MESs): a review. Chemosphere 177:176–188. https://doi.org/10.1016/j.chemosphere.2017.02.143
69. Derby H, Hammer B (1931) Bacteriology of butter—bacteriological studies on surface taint butter. Res Bull 145:387
70. MacDonell MT, Colwell RR (1985) Phylogeny of the *Vibrionaceae,* and recommendation for two new Genera, *Listonella* and *Shewanella*. Syst Appl Microbiol 6:171–182. https://doi.org/10.1016/S0723-2020(85)80051-5
71. Fang Y, Wang Y, Liu Z, Dai H, Cai H, Li Z, Du Z, Wang X, Jing H, Wei Q, Kan B, Wang D (2019) Multilocus sequence analysis, a rapid and accurate tool for taxonomic classification, evolutionary relationship determination, and population biology studies of the genus *Shewanella*. Appl Environ Microbiol 85:e03126-e3218. https://doi.org/10.1128/AEM.03126-18
72. Venkateswaran K, Moser DP, Dollhopf ME, Lies DP, Saffarini DA, Macgregor BJ, Ringelberg DB, White DC, Nishijima M, Sano H, Burghardt J, Stackebrandt E, Nealson KH (1999) Polyphasic taxonomy of the genus *Shewanella* and description of *Shewanella oneidensis* sp. nov . Int J Syst Bacteriol 705–724. https:// doi:https://doi.org/10.1099/00207713-49-2-705
73. Koziñska A, Pękala A (2004) First isolation of *Shewanella putrefaciens* from freshwater fish —a potential new pathogen of fish. Bull Eur Assoc Fish Pathol 24:189–193
74. Paździor E (2016) *Shewanella putrefaciens*—a new opportunistic pathogen of freshwater fish. J Vet Res 60:429–434. https://doi.org/10.1515/jvetres-2016-0064
75. Abboud R, Popa R, Souza-egipsy V, Giometti CS, Tollaksen SL, Mosher JJ, Findlay RH, Nealson KH (2005) Low-temperature growth of *Shewanella oneidensis* MR-1. Appl Environ Microbiol 71:811–816. https://doi.org/10.1128/AEM.71.2.811
76. Holt HM, Gahrn-Hansen B, Bruun B (2005) *Shewanella algae* and *Shewanella putrefaciens*: clinical and microbiological characteristics. Clin Microbiol Infect 11(5):347–352. https://doi.org/10.1111/j.1469-0691.2005.01108.x
77. Hau HH, Gralnick JA (2007) Ecology and biotechnology of the genus *Shewanella*. Annu Rev Microbiol 61:237–258. https://doi.org/10.1146/annurev.micro.61.080706.093257
78. Heidelberg JF, Paulsen IT, Nelson KE, Gaidos EJ, Nelson WC, Read TD, Eisen JA, Seshadri R, Ward N, Methe B, Clayton RA, Meyer T, Tsapin A, Scott J, Beanan M, Brinkac L, Daugherty S, DeBoy RT, Dodson RJ, Durkin AS, Haft DH, Kolonay JF, Madupu R, Peterson JD, Umayam LA, White O, Wolf AM, Vamathevan J, Weidman J, Impraim M, Lee K, Berry K, Lee C, Mueller J, Khouri H, Gill J, Utterback TR, McDonald LA, Feldblyum TV, Smith HO, Venter JC, Nealson KH, Fraser CM (2002) Genome sequence of the dissimilatory metal ion–reducing bacterium *Shewanella oneidensis*. Nat Biotechnol 20:1118–1123. https://doi.org/10.1038/nbt749
79. Thorell K, Meier-Kolthoff JP, Sjöling Å, Martín-Rodríguez AJ (2019) Whole-genome sequencing redefines *Shewanella* taxonomy. Front Microbiol 10:1861. https://doi.org/10.3389/fmicb.2019.01861
80. Romine MF, Carlson TS, Norbeck AD, McCue LA, Lipton MS (2008) Identification of mobile elements and pseudogenes in the *Shewanella oneidensis* MR-1 genome. Appl Environ Microbiol 74:3257–3265. https://doi.org/10.1128/AEM.02720-07
81. Meyer TE, Tsapin AI, Vandenberghe I, De Smet L, Frishman D, Nealson KH, Cusanovich MA, Van Beeumen JJ (2004) Identification of 42 possible cytochrome C

genes in the *Shewanella oneidensis* genome and characterization of six soluble cytochromes. Omi A J Integr Biol 8:57–77. https://doi.org/10.1089/153623104773547499
82. Bretschger O, Obraztsova A, Sturm CA, Chang IS, Gorby YA, Reed SB, Culley DE, Reardon CL, Barua S, Romine MF, Zhou J, Beliaev AS, Bouhenni R, Saffarini D, Mansfeld F, Kim B-H, Fredrickson JK, Nealson KH (2007) Current production and metal oxide reduction by *Shewanella oneidensis* MR-1 wild type and mutants. Appl Environ Microbiol 73:7003–7012. https://doi.org/10.1128/AEM.01087-07
83. Rosenbaum MA, Bar HY, Beg QK, Segrè D, Booth J, Cotta MA, Angenent LT (2012) Transcriptional analysis of *Shewanella oneidensis* MR-1 with an electrode compared to Fe (III)citrate or oxygen as terminal electron acceptor. PLoS One 7:e30827. https://doi.org/10.1371/journal.pone.0030827
84. Richardson D (2002) PMF through the redox loop. Science 295:1842–1843. https://doi.org/10.1126/science.1070366
85. Scott JH, Nealson KH (1994) A biochemical study of the intermediary carbon metabolism of *Shewanella putrefaciens*. J Bacteriol 176:3408–3411. https://doi.org/10.1128/JB.176.11.3408-3411.1994
86. Hunt KA, Flynn JM, Naranjo B, Shikhare ID, Gralnick JA (2010) Substrate-level phosphorylation is the primary source of energy conservation during anaerobic respiration of *Shewanella oneidensis* strain MR-1. J Bacteriol 192:3345–3351. https://doi.org/10.1128/JB.00090-10
87. Myers CR, Myers JM (1993b) Role of menaquinone in the reduction of fumarate, nitrate, iron(III) and manganese(IV) by *Shewanella putrefaciens* MR-1. FEMS Microbiol Lett 114:215–222. https://doi.org/10.1111/j.1574-6968.1993.tb06576.x
88. Marritt SJ, McMillan DGG, Shi L, Fredrickson JK, Zachara JM, Richardson DJ, Jeuken LJC, Butt JN (2012) The roles of CymA in support of the respiratory flexibility of *Shewanella oneidensis* MR-1. Biochem Soc Trans 40:1217–1221. https://doi.org/10.1042/bst20120150
89. Saffarini DA, Blumerman SL, Mansoorabadi KJ (2002) Role of Menaquinones in Fe (III) reduction by membrane fractions of *Shewanella putrefaciens*. J Bacteriol 184:846–848. https://doi.org/10.1128/JB.184.3.846
90. Myers CR, Myers JM (1997) Cloning and sequence of cymA, a gene encoding a tetraheme cytochrome *C* required for reduction of Iron (III), fumarate, and nitrate by *Shewanella putrefaciens* MR-1. J Bacteriol 179:1143–1152. https://doi.org/10.1128/jb.179.4.1143-1152.1997
91. Myers JM, Myers CR (2000) Role of the tetraheme cytochrome CymA in anaerobic electron transport in cells of *Shewanella putrefaciens* MR-1 with normal levels of menaquinone. J Bacteriol 182:67–75. https://doi.org/10.1128/jb.182.1.67-75.2000
92. Schwalb C, Chapman SK, Reid GA (2002) The membrane-bound tetrahaem c -type cytochrome CymA interacts directly with the soluble fumarate reductase in Shewanella. Biochem Soc Trans 30:658–662. https://doi.org/10.1042/bst0300658
93. Zhong Y, Shi L (2018) Genomic analyses of the quinol oxidases and/or quinone reductases involved in bacterial extracellular electron transfer. Front Microbiol 9:1–12. https://doi.org/10.3389/fmicb.2018.03029
94. Zargar K, Saltikov CW (2009) Lysine-91 of the tetraheme c-type cytochrome CymA is essential for quinone interaction and arsenate respiration in *Shewanella* sp. Arch Microbiol 191:797–806. https://doi.org/10.1007/s00203-009-0511-x
95. Field SJ, Dobbin PS, Cheesman MR, Watmough NJ, Thomson AJ, Richardson DJ (2000) Purification and magneto-optical spectroscopic characterization of cytoplasmic membrane and outer membrane multiheme c-type cytochromes from *Shewanella frigidimarina* NCIMB400. J Biol Chem 275:8515–8522. https://doi.org/10.1074/jbc.275.12.8515
96. Firer-Sherwood MA, Bewley KD, Mock JY, Elliott SJ (2011) Tools for resolving complexity in the electron transfer networks of multiheme cytochromes *c*. Metallomics 3:344–348. https://doi.org/10.1039/c0mt00097c

97. Fonseca BM, Paquete CM, Neto SE, Pacheco I, Soares CM, Louro RO (2013) Mind the gap: cytochrome interactions reveal electron pathways across the periplasm of *Shewanella oneidensis MR-1*. Biochem J 449:101–108
98. Vellingiri A, Song YE, Munussami G, Kim C, Park C, Jeon B-H, Lee S-G, Kim JR (2019) Overexpression of c-type cytochrome, CymA in *Shewanella oneidensis* MR-1 for enhanced bioelectricity generation and cell growth in a microbial fuel cell. J Chem Technol Biotechnol 94:2115–2122. https://doi.org/10.1002/jctb.5813
99. Gescher J, Cordova CD, Spormann AM (2008) Dissimilatory iron reduction in *Escherichia coli*: identification of CymA of Shewanella oneidensis and NapC of *E. coli* as ferric reductases. Mol Microbiol 68:706–719. https://doi.org/10.1111/j.1365-2958.2008.06183.x
100. Louro RO, Paquete CM (2012) The quest to achieve the detailed structural and functional characterization of CymA. Biochem Soc Trans 40:1291–1294. https://doi.org/10.1042/bst20120114
101. Firer-Sherwood M, Su Pulcu G, J. Elliott S, (2008) Electrochemical interrogations of the Mtr cytochromes from *Shewanella*: opening a potential window. J Biol Inorg Chem 13:849–854. https://doi.org/10.1007/s00775-008-0398-z
102. Cordova CD, Schicklberger MFR, Yu Y, Spormann AM (2011) Partial functional replacement of CymA by SirCD in *Shewanella oneidensis* MR-1. J Bacteriol 193:2312–2321. https://doi.org/10.1128/JB.01355-10
103. Breuer M, Rosso KM, Blumberger J, Butt JN (2015) Multi-haem cytochromes in Shewanella oneidensis MR-1: structures, functions and opportunities. J R Soc Interface 12. https://doi.org/10.1098/rsif.2014.1117
104. Lemaire ON, Honoré FA, Jourlin-Castelli C, Méjean V, Fons M, Iobbi-Nivol C (2016) Efficient respiration on TMAO requires TorD and TorE auxiliary proteins in *Shewanella oneidensis*. Res Microbiol 167:630–637. https://doi.org/10.1016/j.resmic.2016.05.004
105. Dohnalkova AC, Marshall MJ, Arey BW, Williams KH, Buck EC, Fredrickson JK (2011) Imaging hydrated microbial extracellular polymers: Comparative analysis by electron microscopy. Appl Environ Microbiol 77:1254–1262. https://doi.org/10.1128/AEM.02001-10
106. Sturm G, Richter K, Doetsch A, Heide H, Louro RO, Gescher J (2015) A dynamic periplasmic electron transfer network enables respiratory flexibility beyond a thermodynamic regulatory regime. ISME J 9:1802–1811. https://doi.org/10.1038/ismej.2014.264
107. Tsapin AI, Vandenberghe I, Nealson KH, Scott JH, Meyer TE, Cusanovich MA, Harada E, Kaizu T, Akutsu H, Leys D, Van BJJ (2001) Identification of a small tetraheme cytochrome c and a flavocytochrome c as two of the principal soluble cytochromes *c* in *Shewanella oneidensis* strain MR1. Appl Environ Microbiol 67:3236–3244. https://doi.org/10.1128/AEM.67.7.3236
108. Schuetz B, Schicklberger M, Kuermann J, Spormann AM, Gescher J, Kuermann J, Spormann AM, Gescher J (2009) Periplasmic electron transfer via the c-type cytochromes Mtra and Fcca of *Shewanella oneidensis* Mr-1. Appl Environ Microbiol 75:7789–7796. https://doi.org/10.1128/AEM.01834-09
109. Gordon EHJ, Pike AD, Hill AE, Cuthbertson PM, Chapman SK, Reid GA (2000) Identification and characterization of a novel cytochrome c_3 from *Shewanella frigidimarina* that is involved in Fe(III) respiration. Biochem J 349:153–158. https://doi.org/10.1042/0264-6021:3490153
110. Pealing SL, Black AC, Manson FDC, Ward FB, Chapman SK, Reid GA (1992) Sequence of the gene encoding flavocytochrome. Biochemistry 31:12132–12140. https://doi.org/10.1021/bi00163a023
111. Taylor P, Pealing SL, Reid GA, Chapman SK, Walkinshaw MD (1999) Structural and mechanistic mapping of a unique fumarate reductase. Nat Struct Biol 6:1108–1112. https://doi.org/10.1038/70045

112. Leys D, Tsapin AS, Nealson KH, Meyer TE, Cusanovich MA, Van BJJ, Van Beeumen JJ (1999) Structure and mechanism of the flavocytochrome c fumarate reductase of *Shewanella putrefaciens* MR-1. Nat Struct Biol 6:1113–1117. https://doi.org/10.1038/70051
113. Pessanha M, Rothery EL, Miles CS, Reid GA, Chapman SK, Louro RO, Turner DL, Salgueiro CA, Xavier AV (2009) Tuning of functional heme reduction potentials in *Shewanella* fumarate reductases. Biochim Biophys Acta 1787:113–120. https://doi.org/10.1016/j.bbabio.2008.11.007
114. Paquete CM, Saraiva IH, Louro RO (2014) Redox tuning of the catalytic activity of soluble fumarate reductases from *Shewanella*. Biochim Biophys Acta - Bioenerg 1837:717–725. https://doi.org/10.1016/j.bbabio.2014.02.006
115. Alves MN, Fernandes AP, Salgueiro CA, Paquete CM (2016) Biochimica et Biophysica Acta Unraveling the electron transfer processes of a nanowire protein from *Geobacter sulfurreducens*. BBA - Bioenerg 1857:7–13. https://doi.org/10.1016/j.bbabio.2015.09.010
116. Tsapin AI, Nealson KH, Meyers T, Cusanovich MA, Van Beuumen J, Crosby LD, Feinberg BA, Zhang C (1996) Purification and properties of a low-redox-potential tetraheme cytochrome c_3 from *Shewanella putrefaciens*. J Bacteriol 178:6386–6388. https://doi.org/10.1128/JB.178.21.6386-6388.1996
117. Coursolle D, Gralnick JA (2010) Modularity of the Mtr respiratory pathway of *Shewanella oneidensis* strain MR-1. Mol Microbiol 1–14. https://doi.org/10.1111/j.1365-2958.2010.07266.x
118. Coursolle D, Gralnick JA (2012) Reconstruction of extracellular respiratory pathways for iron(III) reduction in *Shewanella oneidensis* strain MR-1. Front Microbiol 3:1–11. https://doi.org/10.3389/fmicb.2012.00056
119. Delgado VP, Paquete CM, Sturm G, Gescher J (2019) Improvement of the electron transfer rate in *Shewanella oneidensis* MR-1 using a tailored periplasmic protein composition. Bioelectrochemistry 129:18–25. https://doi.org/10.1016/j.bioelechem.2019.04.022
120. Leys D, Meyer TE, Tsapin AS, Nealson KH, Cusanovich MA, Van Beeumen JJ (2002) Crystal structures at atomic resolution reveal the novel concept of "electron-harvesting" as a role for the small tetraheme cytochrome *c*. J Biol Chem 277:35703–35711. https://doi.org/10.1074/jbc.M203866200
121. Fonseca BM, Silva L, Trindade IB, Moe E, Matias PM, Louro RO, Paquete CM (2019) Optimizing electroactive organisms: the effect of orthologous proteins. Front Energy Res 7:1–13. https://doi.org/10.3389/fenrg.2019.00002
122. Paixão VB, Salgueiro CA, Brennan L, Reid GA, Chapman SK, Turner DL (2008) The solution structure of a tetraheme cytochrome from *Shewanella frigidimarina* reveals a novel family structural motif. Biochemistry 47:11973–11980. https://doi.org/10.1021/bi801326j
123. Smith DMA, Rosso KM, Dupuis M, Valiev M, Straatsma TP (2006) Electronic coupling between heme electron-transfer centers and its decay with distance depends strongly on relative orientation. J Phys Chem B 110:15582–15588. https://doi.org/10.1021/jp057068r
124. Pessanha M, Louro RO, Correia IJIJ, Rothery EL, Pankhurst KLKL, Reid GA, Chapman SK, Turner DL, Salgueiro CA (2003) Thermodynamic characterization of a tetrahaem cytochrome isolated from a facultative aerobic bacterium, *Shewanella frigidimarina* : a putative redox model for flavocytochrome c_3. Biochem J 495:489–495. https://doi.org/10.1042/BJ20021408
125. Fonseca BM, Saraiva IH, Paquete CM, Soares CM, Pacheco I, Salgueiro CA, Louro RO (2009) The tetraheme cytochrome from *Shewanella oneidensis* MR-1 shows thermodynamic bias for functional specificity of the hemes. J Biol Inorg Chem 14:375–385. https://doi.org/10.1007/s00775-008-0455-7
126. Dolla A, Blanchard L, Guerlesquin F, Bruschi M (1994) The protein moiety modulates the redox potential in cytochromes *c*. Biochimie 76:471–479. https://doi.org/10.1016/0300-9084(94)90171-6
127. Martel PJ, Soares CM, Baptista AM, Fuxreiter M, Náray-Szabó G, Louro RO, Carrondo MA (1999) Comparative redox and pK a calculations on cytochrome c_3 from several

Desulfovibrio species using continuum electrostatic methods. JBIC J Biol Inorg Chem 4:73–86. https://doi.org/10.1007/s007750050291
128. Beliaev AS, Saffarini DA (1998) *Shewanella putrefaciens* mtrB encodes an outer membrane protein required for Fe (III) and Mn (IV) reduction. J Bacteriol 180:6292–6297
129. Beliaev AS, Saffarini DA, Mclaughlin JL, Hunnicutt D (2001) MtrC, an outer membrane decahaem c cytochrome required for metal reduction in *Shewanella putrefaciens* MR-1. Mol Microbiol 39:722–730. https://doi.org/10.1046/j.1365-2958.2001.02257.x
130. Bücking C, Popp F, Kerzenmacher S, Gescher J (2010) Involvement and specificity of *Shewanella oneidensis* outer membrane cytochromes in the reduction of soluble and solid-phase terminal electron acceptors. FEMS Microbiol Lett 306:144–151. https://doi.org/10.1111/j.1574-6968.2010.01949.x
131. Richardson DJ, Butt JN, Fredrickson JK, Zachara JM, Shi L, Edwards MJ, White G, Baiden N, Gates AJ, Marritt SJ, Clarke TA (2012) The 'porin-cytochrome' model for microbe-to-mineral electron transfer. Mol Microbiol 85:201–212. https://doi.org/10.1111/j.1365-2958.2012.08088.x
132. Edwards M, White G, Butt J, Richardson DJ, Clarke TA (2019) The structure of a biological insulated transmembrane molecular wire. SSRN Electron J. https://doi.org/10.2139/ssrn.3445677
133. Firer-Sherwood MA, Ando N, Drennan CL, Elliott SJ (2011) Solution-based structural analysis of the decaheme cytochrome, MtrA, by small-angle X-ray scattering and analytical ultracentrifugation. J Phys Chem B 115:11208–11214. https://doi.org/10.1021/jp203603r
134. Myers CR, Myers JM (2002) MtrB is required for proper incorporation of the cytochromes OmcA and OmcB into the outer membrane of *Shewanella putrefaciens* MR-1. Appl Environ Microbiol 68:5585–5594. https://doi.org/10.1128/AEM.68.11.5585
135. Hartshorne RS, Reardon CL, Ross D, Nuester J, Clarke TA, Gates AJ, Mills PC, Fredrickson JK, Zachara JM, Shi L, Beliaev AS, Marshall MJ, Tien M, Brantley S, Butt JN, Richardson DJ (2009) Characterization of an electron conduit between bacteria and the extracellular environment. Proc Natl Acad Sci 106:22169–74. https://doi.org/10.1073/pnas.0900086106
136. Schicklberger M, Bücking C, Schuetz B, Heide H, Gescher J (2011) Involvement of the *Shewanella oneidensis* decaheme cytochrome MtrA in the periplasmic stability of the β-barrel protein MtrB. Appl Environ Microbiol 77:1520–1523. https://doi.org/10.1128/AEM.01201-10
137. Gralnick JA, Vali H, Lies DP, Newman DK (2006) Extracellular respiration of dimethyl sulfoxide by *Shewanella oneidensis* strain MR-1. Proc Natl Acad Sci 103:4669–4674. https://doi.org/10.1073/pnas.0505959103
138. Schicklberger M, Sturm G, Gescher J (2013) Genomic plasticity enables a secondary electron transport pathway in *Shewanella oneidensis*. Appl Environ Microbiol 79:1150–1159. https://doi.org/10.1128/AEM.03556-12
139. Richardson DJ, Fredrickson JK, Zachara JM (2012) Electron transport at the microbe-mineral interface: a synthesis of current research challenges. Biochem Soc Trans 40:1163–1166. https://doi.org/10.1042/BST20120242
140. Liu J, Wang Z, Belchik SM, Edwards MJ, Liu C, Kennedy DW, Merkley ED, Lipton MS, Butt JN, Richardson DJ, Zachara JM, Fredrickson JK, Rosso KM, Shi L (2012) Identification and characterization of MtoA: a decaheme c-type cytochrome of the neutrophilic Fe(ll)-oxidizing bacterium *Sideroxydans lithotrophicus* ES-1. Front Microbiol 3:1–11. https://doi.org/10.3389/fmicb.2012.00037
141. Jiao Y, Newman DK (2007) The pio operon is essential for phototrophic Fe(II) oxidation in *Rhodopseudomonas palustris* TIE-1. J Bacteriol 189:1765–1773. https://doi.org/10.1128/JB.00776-06
142. Gupta D, Sutherland MC, Rengasamy K, Meacham JM, Kranz RG, Bose A (2019) Photoferrotrophs produce a PioAB electron conduit for extracellular electron uptake. MBio 10. https://doi.org/10.1128/mBio.02668-19

143. Edwards MJ, White GF, Lockwood CW, Lawes MC, Martel A, Harris G, Scott DJ, Richardson DJ, Butt JN, Clarke TA (2018) Structural modeling of an outer membrane electron conduit from a metal-reducing bacterium suggests electron transfer via periplasmic redox partners. J Biol Chem 293:8103–8112. https://doi.org/10.1074/jbc.RA118.001850
144. Ross DE, Ruebush SS, Brantley SL, Hartshorne RS, Clarke TA, Richardson DJ, Tien M (2007) Characterization of protein-protein interactions involved in iron reduction by *Shewanella oneidensis* MR-1. Appl Environ Microbiol 73:5797–5808. https://doi.org/10.1128/AEM.00146-07
145. Pitts KE, Dobbin PS, Reyes-Ramirez F, Thomson AJ, Richardson DJ, Seward HE (2003) Characterization of the *Shewanella oneidensis* MR-1 decaheme cytochrome MtrA: expression in *Escherichia coli* confers the ability to reduce soluble FE(III) chelates. J Biol Chem 278:27758–27765. https://doi.org/10.1074/jbc.M302582200
146. Clarke TA, Cole JA, Richardson DJ, Hemmings AM (2007) The crystal structure of the pentahaem *c*-type cytochrome NrfB and characterization of its solution-state interaction with the pentahaem nitrite reductase NrfA. Biochem J 406:19–30. https://doi.org/10.1042/BJ20070321
147. Matias VRF, Al-Amoudi A, Dubochet J, Beveridge TJ (2003) Cryo-transmission electron microscopy of frozen-hydrated sections of *Escherichia coli* and *Pseudomonas aeruginosa*. J Bacteriol 185:6112–6118. https://doi.org/10.1128/JB.185.20.6112-6118.2003
148. Myers CR, Myers JM (2003) Cell surface exposure of the outer membrane cytochromes of *Shewanella oneidensis* MR-1. Lett Appl Microbiol 37:254–258. https://doi.org/10.1046/j.1472-765X.2003.01389.x
149. Myers JM, Myers CR (2001) Role for outer membrane cytochromes OmcA and OmcB of *Shewanella putrefaciens* MR-1 in reduction of manganese dioxide. Appl Environ Microbiol 67:260–269. https://doi.org/10.1128/AEM.67.1.260
150. Zhang H, Tang X, Munske GR, Tolic N, Anderson GA, Bruce JE (2009) Identification of protein-protein interactions and topologies in living cells with chemical cross-linking and mass spectrometry. Mol Cell Proteomics 8:409–420. https://doi.org/10.1074/mcp.M800232-MCP200
151. Shi L, Chen B, Wang Z, Elias DA, Mayer MU, Gorby YA, Ni S, Lower BH, Kennedy DW, Wunschel DS, Mottaz HM, Marshall MJ, Hill EA, Beliaev AS, Zachara JM, Fredrickson JK, Squier TC (2006) Isolation of a high-affinity functional protein complex between OmcA and MtrC: two outer membrane decaheme c-type cytochromes of *Shewanella oneidensis* MR-1. J Bacteriol 188:4705–4714. https://doi.org/10.1128/JB.01966-05
152. Borloo J, Vergauwen B, De Smet L, Brigé A, Motte B, Devreese B, Van Beeumen J, De SL, Brige A, Motte B, Devreese B, Van BJJ (2007) A kinetic approach to the dependence of dissimilatory metal reduction by *Shewanella oneidensis* MR-1 on the outer membrane cytochromes c OmcA and OmcB. FEBS J 274:3728–3738. https://doi.org/10.1111/j.1742-4658.2007.05907.x
153. Xiong Y, Shi L, Chen B, Mayer MU, Lower BH, Londer YY, Bose S, Hochella MF, Fredrickson JK, Squier TC (2006) High-affinity binding and direct electron transfer to solid metals by the *Shewanella oneidensis* MR-1 outer membrane c-type cytochrome OmcA. J Am Chem Soc 128:13978–13979. https://doi.org/10.1021/ja063526d
154. Meitl LA, Eggleston CM, Colberg PJS, Khare N, Reardon CL, Shi L (2009) Electrochemical interaction of *Shewanella oneidensis* MR-1 and its outer membrane cytochromes OmcA and MtrC with hematite electrodes. Geochim Cosmochim Acta 73:5292–5307. https://doi.org/10.1016/j.gca.2009.06.021
155. Eggleston CM, Vo J, Droubay TC, Colberg PJS (2008) Binding and direct electrochemistry of OmcA, an outer-membrane cytochrome from an iron reducing bacterium, with oxide electrodes: a candidate biofuel cell system. Inorganica Chim Acta 361:769–777. https://doi.org/10.1016/j.ica.2007.07.015
156. Lower BH, Lins RD, Oestreicher Z, Straatsma TP, Hochella MF, Shi L, Lower SK (2008) In vitro evolution of a peptide with a hematite binding motif that may constitute a natural

metal-oxide binding archetype. Environ Sci Technol 42:3821–3827. https://doi.org/10.1021/es702688c
157. Hartshorne RS, Jepson BN, Clarke TA, Field SJ, Fredrickson J, Zachara J, Shi L, Butt JN, Richardson DJ (2007) Characterization of *Shewanella oneidensis* MtrC: a cell-surface decaheme cytochrome involved in respiratory electron transport to extracellular electron acceptors. JBIC J Biol Inorg Chem 12:1083–1094. https://doi.org/10.1007/s00775-007-0278-y
158. Lower BH, Yongsunthon R, Shi L, Wildling L, Gruber HJ, Wigginton NS, Reardon CL, Pinchuk GE, Droubay TC, Boily J-F, Lower SK (2009) Antibody recognition force microscopy shows that outer membrane cytochromes OmcA and MtrC are expressed on the exterior surface of *Shewanella oneidensis* MR-1. Appl Environ Microbiol 75:2931–2935. https://doi.org/10.1128/AEM.02108-08
159. Edwards MJ, White GF, Norman M, Tome-Fernandez A, Ainsworth E, Shi L, Fredrickson JK, Zachara JM, Butt JN, Richardson DJ, Clarke TA (2015) Redox linked flavin sites in extracellular decaheme proteins involved in microbe-mineral electron transfer. Sci Rep 5:11677. https://doi.org/10.1038/srep11677
160. Edwards MJ, Baiden NA, Johs A, Tomanicek SJ, Liang L, Shi L, Fredrickson JK, Zachara JM, Gates AJ, Butt JN, Richardson DJ, Clarke TA (2014) The X-ray crystal structure of *Shewanella oneidensis* OmcA reveals new insight at the microbe-mineral interface. FEBS Lett 588:1886–1890. https://doi.org/10.1016/j.febslet.2014.04.013
161. Paquete CM, Fonseca BM, Cruz DR, Pereira TM, Pacheco I, Soares CM, Louro RO (2014) Exploring the molecular mechanisms of electron shuttling across the microbe/metal space. Front Microbiol 5:318. https://doi.org/10.3389/fmicb.2014.00318
162. Neto SE, de Melo-Diogo D, Correia IJ, Paquete CM, Louro RO (2017) Characterization of OmcA Mutants from *Shewanella oneidensis* MR-1 to investigate the molecular mechanisms underpinning electron transfer across the microbe-electrode interface. Fuel Cells 17:1–11. https://doi.org/10.1002/fuce.201700023
163. Min D, Cheng L, Zhang F, Huang X-N, Li D, Liu D, Lau T-C, Mu Y, Yu H (2017) Enhancing extracellular electron transfer of *Shewanella oneidensis* MR-1 through coupling improved flavin synthesis and metal-reducing conduit for pollutant degradation. Environ Sci Technol 51:5082–5089. https://doi.org/10.1021/acs.est.6b04640
164. Choi D, Lee SB, Kim S, Min B, Choi IG, Chang IS, Bom S, Kim S, Min B, Choi IG, Seop I (2014) Metabolically engineered glucose-utilizing *Shewanella* strains under anaerobic conditions. Bioresour Technol 154:59–66. https://doi.org/10.1016/j.biortech.2013.12.025
165. Flynn JM, Ross DE, Hunt KA, Bond DR, Gralnick JA (2010) Enabling unbalanced fermentations by using engineered electrode-interfaced bacteria. MBio 1. https://doi.org/10.1128/mBio.00190-10
166. Li F, Li Y, Sun L, Li X, Yin C, An X, Chen X, Tian Y, Song H (2017) Engineering *Shewanella oneidensis* enables xylose-fed microbial fuel cell. Biotechnol Biofuels 10:196. https://doi.org/10.1186/s13068-017-0881-2
167. Johnson ET, Baron DB, Naranjo B, Bond DR, Schmidt-Dannert C, Gralnick JA (2010) Enhancement of survival and electricity production in an engineered bacterium by light-driven proton pumping. Appl Environ Microbiol 76:4123–4129. https://doi.org/10.1128/AEM.02425-09
168. Teravest M (2019). Reversing an extracellular electron transfer pathway for electrode-driven acetoin reduction. https://doi.org/10.1021/acssynbio.8b00498
169. Li F, Li Y, Cao Y, Wang L, Liu C, Shi L, Song H (2018) Modular engineering to increase intracellular NAD(H/+) promotes rate of extracellular electron transfer of *Shewanella oneidensis*. Nat Commun 9:3637. https://doi.org/10.1038/s41467-018-05995-8
170. Yang Y, Xiang Y, Sun G, Wu WM, Xu M (2015) Electron acceptor-dependent respiratory and physiological stratifications in biofilms. Environ Sci Technol 49:196–202. https://doi.org/10.1021/es504546g

171. Liu T, Yu Y, Deng X, Ng CK, Cao B, Wang J, Rice SA, Kjelleberg S, Song H (2015) Enhanced *Shewanella* biofilm promotes bioelectricity generation. 9999:1–9. https://doi.org/10.1002/bit.25624
172. Corts AD, Thomason LC, Gill RT, Gralnick JA (2019) Efficient and precise genome editing in *Shewanella* with recombineering and CRISPR/Cas9-mediated counter-selection. ACS Synth Biol 8:1877–1889. https://doi.org/10.1021/acssynbio.9b00188
173. Rabaey K, Verstraete W (2005) Microbial fuel cells: novel biotechnology for energy generation. 23. https://doi.org/10.1016/j.tibtech.2005.04.008
174. Xu S, Jangir Y, El-Naggar MY (2016) Disentangling the roles of free and cytochrome-bound flavins in extracellular electron transport from *Shewanella oneidensis* MR-1. Electrochim Acta 198:49–55. https://doi.org/10.1016/j.electacta.2016.03.074
175. Christwardana M, Kwon Y (2017) Yeast and carbon nanotube based biocatalyst developed by synergetic effects of covalent bonding and hydrophobic interaction for performance enhancement of membraneless microbial fuel cell. Bioresour Technol 225:175–182. https://doi.org/10.1016/j.biortech.2016.11.051
176. Costa NL, Hermann B, Fourmond V, Faustino MM, Teixeira M, Einsle O, Paquete CM, Louro RO (2019) How thermophilic gram-positive organisms perform extracellular electron transfer: characterization of the cell surface terminal reductase OcwA. MBio 10:e01210. https://doi.org/10.1128/mBio.01210-19
177. Lebègue E, Costa NL, Fonseca BM, Louro RO, Barrière F (2019) Electrochemical properties of pH-dependent flavocytochrome c_3 from *Shewanella putrefaciens* adsorbed onto unmodified and catechol-modified edge plane pyrolytic graphite electrode. J Electroanal Chem 847. https://doi.org/10.1016/j.jelechem.2019.113232
178. Schievano A, Berenguer R, Goglio A, Bocchi S, Marzorati S, Rago L, Louro RO, Paquete CM, Esteve-Núñez A (2019) Electroactive biochar for large-scale environmental applications of microbial electrochemistry. ACS Sustain Chem Eng 7:18198–18212. https://doi.org/10.1021/acssuschemeng.9b04229
179. Beblawy S, Bursac T, Paquete C, Louro R, Clarke TA, Gescher J (2018) Extracellular reduction of solid electron acceptors by *Shewanella oneidensis*. Mol Microbiol 109:571–583. https://doi.org/10.1111/mmi.14067
180. Bond DR, Lovley DR (2003) Electricity production by *Geobacter sulfurreducens* attached to electrodes. Appl Environ Microbiol 69:1548–1555. https://doi.org/10.1128/AEM.69.3.1548-1555.2003
181. Wrighton KC, Thrash JC, Melnyk RA, Bigi JP, Byrne-Bailey KG, Remis JP, Schichnes D, Auer M, Chang CJ, Coates JD (2011) Evidence for direct electron transfer by a gram-positive bacterium isolated from a microbial fuel cell. Appl Environ Microbiol 77:7633–7639. https://doi.org/10.1128/AEM.05365-11
182. Carlson HK, Iavarone AT, Gorur A, Yeo BS, Tran R, Melnyk RA, Mathies RA, Auer M, Coates JD (2012) Surface multiheme *c*-type cytochromes from *Thermincola potens* and implications for respiratory metal reduction by Gram-positive bacteria. Proc Natl Acad Sci 109:1702–1707. https://doi.org/10.1073/pnas.1112905109
183. Edwards MJ, Clarke TA, Richardson DJ, Paquete CM (2019) Role of multiheme cytochromes involved in extracellular anaerobic respiration in bacteria. Protein Sci 1–13. https://doi.org/10.1002/pro.3787
184. Alves AS, Costa NL, Tien M, Louro RO, Paquete CM (2017) Modulation of the reactivity of multiheme cytochromes by site-directed mutagenesis: moving towards the optimization of microbial electrochemical technologies. J Biol Inorg Chem 22:87–97. https://doi.org/10.1007/s00775-016-1409-0
185. Voigt P, Knapp E-W (2003) Tuning heme redox potentials in the cytochrome *c* subunit of photosynthetic reaction centers. J Biol Chem 278:51993–52001. https://doi.org/10.1074/jbc.M307560200

186. Li M, Zhou M, Tian X, Tan C, McDaniel CT, Hassett DJ, Gu T (2018) Microbial fuel cell (MFC) power performance improvement through enhanced microbial electrogenicity. Biotechnol Adv 36:1316–1327. https://doi.org/10.1016/j.biotechadv.2018.04.010
187. Agapakis CM, Silver PA (2010) Modular electron transfer circuits for synthetic biology. Bioeng Bugs 1:413–418. https://doi.org/10.4161/bbug.1.6.12462
188. Wei J, Liang P, Huang X (2011) Recent progress in electrodes for microbial fuel cells. Bioresour Technol 102:9335–9344. https://doi.org/10.1016/j.biortech.2011.07.019

Biological Production of Hydrogen

Mónica Martins, Inês A. C. Pereira, Marcos Pita, and Antonio L. De Lacey

Abstract

The production of H_2 from renewable sources, such as water or biomass, is a sustainable strategy for energy supply. Hydrogenases are the only enzymes that specifically catalyze the reversible reaction of H_2 production/uptake with almost no overpotential. In this chapter, we review the advances produced in the last decade in the biocatalytic production of H_2, including systems based on isolated hydrogenases as well as those using microorganisms through dark fermentation processes.

Keywords

Hydrogenases · Hydrogen production · Dark fermentation · Bioelectrocatalysis · Photocatalysis · Photoelectrochemistry

1 Introduction

H_2 is a top candidate to substitute fossil fuels, but since there is almost no H_2 at the Earth's crust, it needs to be synthesized. Nowadays, most synthetic routes to obtain H_2 use hydrocarbons as substrate [1]. However, the most abundant source of protons to synthesize H_2 is water, and it is feasible to split water into its elements

M. Martins · I. A. C. Pereira
Instituto de Tecnologia Química e Biológica Antonio Xavier, Universidade Nova de Lisboa, ITQB-NOVA, Oeiras, Portugal

M. Pita · A. L. De Lacey (✉)
Instituto de Catálisis y Petroleoquímica, CSIC, Madrid, Spain
e-mail: alopez@icp.csic.es

J. J. G. Moura et al. (eds.), *Enzymes for Solving Humankind's Problems*,
https://doi.org/10.1007/978-3-030-58315-6_9

hydrogen and oxygen when an appropriate amount of energy is applied. In order to produce H_2 with minimal energy loss during the reduction of protons, catalysts are a must. The most used catalyst for H_2 production from water is platinum, an electrocatalyst that, when working at optimal conditions and absence of poisoning agents, produces H_2 at high rates and negligible overpotential [1]. Unfortunately, platinum is a non-abundant noble element (0.003 ppm of Pt on Earth's crust) that cannot become the solution for global problems, and thus alternative ways to reduce protons to H_2 are intensely studied. As other metallic catalysts are not as efficient as Pt for H_2 evolution, research has also focused on biocatalysts. In general, biocatalytic processes can be divided between those that employ purified enzymes and those based on whole-cells. In this chapter, we review both types of biocatalytic systems applied to H_2 production.

2 Enzymatic Production of H_2

Although some other redox metalloenzymes, such as nitrogenases, produce H_2 as a by-product, hydrogenases are the only ones that specifically catalyze the reversible reaction of H_2 production/uptake with almost no overpotential [2]. Hydrogenases are classified according to the metal content of their active site (Fig. 1), thus they either belong to the FeFe-hydrogenases, NiFe-hydrogenases or Fe-hydrogenases groups [3]. Not all hydrogenases have the same ability for catalyzing H_2-production. For instance, O_2-tolerant membrane-bound NiFe-hydrogenases are catalytically biased towards to H_2-oxidation and only are capable of H_2-production at quite acidic pH values [4]. On the other hand, FeFe-hydrogenases have very high turnover numbers for H_2-production at neutral pH and opposite to NiFe-hydrogenases they are hardly inhibited by product accumulation [5, 6]. However, FeFe-hydrogenases are very sensitive to irreversible O_2 inhibition [7, 8] or destruction of the active site by light [9], which may hamper practical applications.

2.1 Enzymatic Production of H_2 Driven by Reduced Compounds

In an early work by Zorin and coworkers, it was reported for the first time that the soluble NiFe-hydrogenase isolated from the H_2-oxidizing bacterium *Alcaligenes eutrophus* (currently named *Ralstonia eutropha*) was able to produce H_2 under air or even under 100% O_2 atmosphere using NAD(P)H as electron donor [10]. More recently, this activity under aerobic conditions has been explained in a combined spectroscopic and computational study by the capability of NAD(P)H to transfer simultaneously 2 electrons to the oxidized active site and form the active reduced state [11]. However, the rates of H_2 production are very low even under anaerobic conditions, up to 0.045 $\mu mol \times min^{-1} \times mg^{-1}$ [10], because the standard redox potential (E^0) of NAD(P)H is higher than that of H_2. Therefore, the process is only

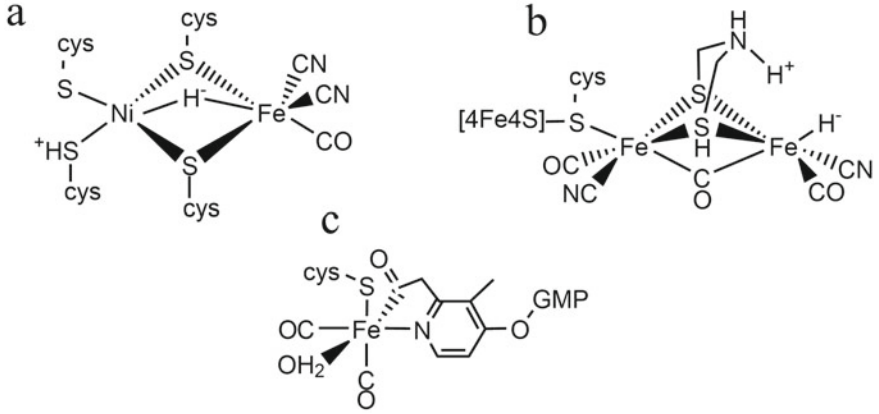

Fig. 1 Structures of the active site of NiFe- (**a**), FeFe- (**b**) and Fe-hydrogenases (**c**) in the reduced state

thermodynamically favourable at low partial pressure of H_2 and product accumulation quickly stops or reverts the reaction after a few hours. Continuous recycling of the NAD(P)H cofactor by adding glucose dehydrogenase to the system under anaerobic conditions has allowed increasing the duration of H_2 evolution using glucose as electron donor (Fig. 2) and thus the amount of accumulated H_2 (up to 10 μmoles) with the same hydrogenase [12]. The Adams group has reported using the NAD(P)H-dependent hydrogenase from the anaerobic thermophilic archaeon *Pyrococcus furiosus* in combination with other 12 enzymes to form an unnatural enzymatic pathway of H_2 production. In this way, a high yield of H_2 production from starch and water was obtained based on the principles of synthetic biology [13]. The overall thermodynamically favourable process and the separation of the gaseous products allowed measuring a maximum rate of H_2 production rate 0.5 mmoles $\times$ L^{-1} $\times$ h^{-1}. More than one order of magnitude, higher rates of H_2 production from glucose were measured by using a FeFe-hydrogenase [14, 15]. In this case, ferredoxin had to be added to shuttle electrons from NADPH to the enzyme because, as most hydrogenases, it only has iron-sulphur clusters as redox relay, which are one-electron acceptors. The increased rate of H_2 production was attributed to the higher turnover of FeFe-hydrogenases for H_2 production compared to NiFe-hydrogenases.

The use of reduced methyl viologen (MV) as electron donor for enzymatic hydrogen production has the advantage of its pH-independent low redox potential (−450 mV vs. NHE), thus favouring thermodynamically the reduction of protons to H_2, especially at acidic pH values. Another improvement is the immobilization of the hydrogenase, as immobilization of enzymes on supports is an efficient strategy used in biocatalysis in order to increase the operational stability and the reaction yield [16]. Zadvorny et al. reported the encapsulation of the NiFe-hydrogenase from *Thiocapsa roseopersecina* in a sol–gel material with multi-walled carbon nanotubes (MWCNTs), polyethylene glycol (PEG) and MV. The addition of PEG into the

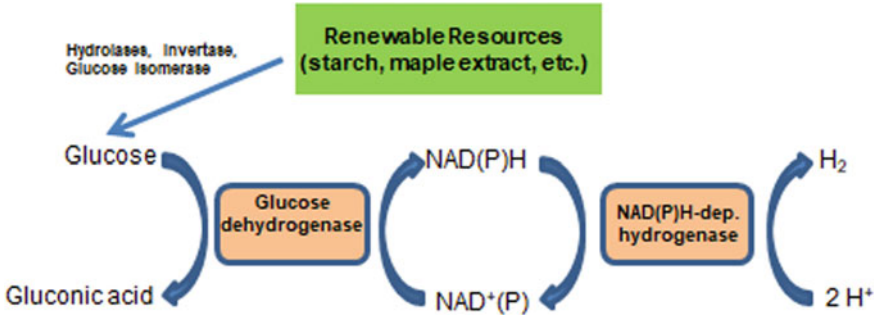

Fig. 2 Scheme of enzymatic production of H_2 from renewable resources using NAD(P)H-dependent NiFe-hydrogenases

material increased the storage stability of the encapsulated hydrogenase, while the incorporation of the MWCNTs favoured electron delivery to the enzyme from the MV reduced by sodium dithionite added to the solution. In this way, the H_2 production activity measured was equal to that measured for the enzyme in aqueous solution [17]. Another strategy developed for increasing the operational stability for in vitro evolution of H_2 has been the encapsulation of the membrane-bound hydrogenase from *P. furiosus* into water-stable discoidal nanoparticles that were formed by a lipoprotein acting as a scaffold for the self-assembly of phospholipid bilayers [18]. The aim of the work was to resemble the in vivo environment of the hydrogenase. Incorporation of the membrane enzyme into the nanolipoproteins stabilized it in an aqueous solution, while maintaining its full activity of H_2 production with reduced MV. With the same goal, the encapsulation of an *E. coli* NiFe-hydrogenase within the capsid of P22 bacteriophage led to a stabilization of its quaternary structure and a 100-fold increase of the H_2 production activity [19].

NiFeSe-hydrogenases are a subclass of the NiFe-hydrogenases in which one of the terminal cysteine ligands of Ni is replaced by a selenocysteine. This small structural change in the active site considerably alters the catalytic function of the NiFeSe-hydrogenases compared to NiFe-hydrogenases. First of all, their activity at neutral pH is strongly biased towards H_2 production, which is the opposite of most NiFe-hydrogenases [20]. The optimal H_2-production solution activity of *D. vulgaris* Hildenborough NiFeSe-hydrogenase measured with reduced MV is about one order higher than its H_2-oxidation, reaching turnover values of approximately 7,000 s^{-1} [21]. These turnover values are almost equal to the highest ones measured with FeFe-hydrogenases (about 10,000 s^{-1}), while NiFeSe-hydrogenases are more stable towards irreversible inactivation by O_2 or light than the former [21]. The high H_2-production activity of NiFeSe-hydrogenases is attributed to the lower pKa of selenocysteine compared to cysteine, thus favouring faster transfer of protons to and from the bi-metallic active site [22]. Although the active site of NiFeSe-hydrogenases reacts fast with low concentrations of O_2 and converts to the inactive oxidized active state, it can be quickly reactivated under reductive conditions [23, 24]. This fast reactivation process is an advantage compared to

anaerobic NiFe-hydrogenases, such as the one from *D. gigas* and others, because they require a long activation process (several hours at room temperature) of the oxidized enzyme in order to recover optimal activity [2]. The faster reactivation of NiFeSe-hydrogenases is explained by the fact that in the presence of O_2 the Se-Cys reacts fast with it by forming a selenoate, which can be quickly reduced back to the Se-Cys in presence of a low potential electron donor. Cys are slower to react with O_2 but sulphenates are also reduced slowly, thus if one or more of the active site Cys of NiFe-hydrogenases become oxidized it reactivation under reducing conditions will have a large kinetic barrier [25]. However, an irreversibly oxidized state has also been observed for the NiFeSe-hydrogenase from *Desulphovibrio vulgaris* Hildenborough, which is formed upon prolonged oxygen exposure during purification and crystallization [26, 27]. This oxidized species contains a terminal cysteine ligand to nickel doubly oxidized to the sulphinate state, a modification that can be prevented by blocking access of O_2 to the active site through a hydrophilic channel [28].

The powerful methodology of directed evolution for improving or obtaining new enzymatic activities has also been used with the aim of optimizing H_2-production catalyzed by hydrogenases. This strategy has been used to evolve the Fe–Fe hydrogenase genes of two species of *Clostridia* bacteria. Chimeric genes were expressed in *E. coli* and the H_2-production activity of the cell cultures with reduced MV was measured by gas chromatography. However, the best chimera mutant had only 4% of the activity of the positive control *C. acetobutylicum* [29]. High-throughput screening has also been used for simultaneous evaluation of NADPH-driven H_2 production activity by a library of more than 10,000 randomly mutated *C. pasteurianum* FeFe-hydrogenases [30].

2.2 Electroenzymatic Production of H_2

Electrodes can work directly as electron donor or acceptor of hydrogenases, replacing the natural redox proteins, co-factors or artificial redox compounds as co-substrates. In consequence, strategies for electroenzymatic H_2 production are possible [31]. A requisite for direct electron transfer (DET) of enzymes is that the redox centre located on the protein surface is at a short distance (less than 20 Å) of the electrode surface. In the case of hydrogenases, a redox relay formed by an alignment of iron-sulphur clusters connects the protein surface with the bi-metallic active site, allowing for fast intramolecular electron transfer in both directions [3]. Therefore, the most exposed iron-sulphur cluster, normally known as the distal cluster, must be facing the electrode surface in order to allow measurement of electroenzymatic H_2-production (Fig. 3a). Most of the published work in this topic is based on direct adsorption of a small amount of enzyme on rough carbon surfaces, such as carbon black or pyrolytic edge graphite [32]. These electrode materials facilitate direct electron transfer of hydrogenase, even if the orientation of the adsorbed enzyme molecules is random, because the roughness of the surface at the nanometric scale allows that a significant hydrogenase population has its distal

iron-sulphur near the electrode [33]. However, the main limitation of immobilization of hydrogenase by adsorption for biotechnological applications is that only one monolayer of enzyme is able to establish DET with the electrode, thus, the amount of produced H_2 is obviously small. Furthermore, the operational stability is very low due to enzyme desorption from the electrode [34].

In order to increase the stability of hydrogenase immobilization and to monitor the process, the adsorption of the Fe–Fe hydrogenase from *Clamydomonas reinhardtii* onto gold electrodes modified with self-assembled monolayers of thiols functionalized with a carboxylic group and of different chain length was studied. This hydrogenase was chosen because its H_2-production activity and its small size, allowing for a higher enzyme coverage over the electrode surface. The adsorption kinetics was monitored by surface-enhanced infrared absorption spectroscopy (SEIRAS), while the total amount of immobilized enzyme was measured by surface plasmon resonance (SPR). The SPR study indicated that a monolayer of hydrogenase was bound to the SAM-modified electrode, whereas the SEIRA spectra indicated that the protein film was stable. The electrocatalytic H_2-production measured in presence of MV in the solution was 1.3 $\mu mol \times min^{-1} \times mg^{-1}$, which was only 1% of the activity measured with the same enzyme in solution [35].

More recently, the adsorption of hydrogenase on nanostructured electrodes is being studied in order to improve the amount of enzyme adsorbed by geometric area and the DET. Kihara et al. reported DET of *T. roseopersicina* Ni–Fe hydrogenase on a electrode modified with a single-walled carbon nanotube (SWCNT) forest. The vertically aligned SWCNTs allowed stable confinement of the hydrogenase on their side walls and DET with the electrode. However, the maximum rate of electrocatalytic H_2-production was only 0.72 $\mu mol \times min^{-1} \times mg^{-1}$ [36]. Higher DET-based electrocatalytic currents of H_2-production up to -2 $mA \times cm^{-2}$ were measured in a study that was performed with the *C. reinhardtii* FeFe-hydrogenase

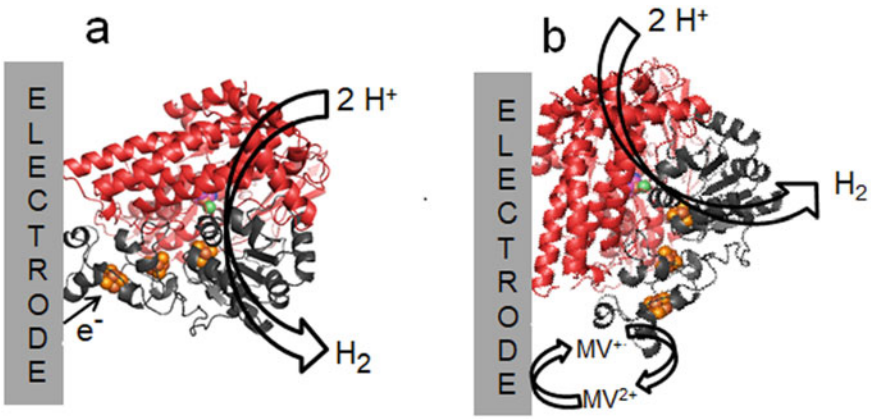

Fig. 3 Schemes for electroenzymatic H_2-production by DET (**a**) or MET (**b**) of hydrogenases immobilized on electrodes

directly adsorbed on a nanostructured TiO_2 electrode. ATR-FTIR spectroscopy was used to confirm structural integrity of the adsorbed hydrogenase. However, the quantification of the total amount of immobilized hydrogenase suggested that a high percentage of enzyme molecules were not participating on the electrocatalytic process [37]. This result could be due to incorrect orientation of hydrogenase molecules for DET with the electrode, or to protein inactivation during adsorption. Another strategy developed has been the coating of a TiO_2 with electrospun polyacrylonate fibres, to which the membrane-bound NiFe- hydrogenase from *E. coli* was bound. Current densities higher than -0.5 mA $\times$ cm^{-2} for electrocatalytic H_2-production at only −0.2 V of overpotential [38]. Electroenzymatic H_{2-} production has also been studied by co-immobilization of a NiFe-hydrogenase and a viologen polymer on a high-surface-area carbon electrode. High current densities of -100 mA/cm^{-3} were reported in this system [39].

An important issue for biocatalytic H_2-production is the effect of ambient O_2 on the activity of hydrogenases. Moreover, if H_2 is obtained from the water splitting reaction O_2 is also formed as by-product [40]. As already pointed out above, the O_2-tolerant NiFe-hydrogenases are poor catalysts for H^+ reduction to H_2. On the other hand, NiFeSe-hydrogenases, which are quickly inactivated under low concentrations of O_2 in the H_2-oxidation and H/D exchange assays, have shown to be able to produce H_2 in the presence of 1% O_2 when adsorbed on graphite electrodes [23] or covalently bound to a SAM thiol-modified gold electrode poised at low redox potentials [41]. Even if this amount of O_2 quickly oxidizes the active site of the NiFeSe-hydrogenases to the inactive state, DET from the electrode to the adequately oriented enzyme molecules allows their immediate reactivation. Moreover, it has been recently shown that the *D. desulphuricans* FeFe-hydrogenase, which belongs to the type of hydrogenases more sensitive to irreversible inactivation by either O_2 or light in spite of displaying high H_2-production activity, becomes more resistant when covalently bound to a graphite electrode poised at potentials lower than −0.46 V versus NHE. The half-live time for electrocatalytic H_2-production under at 1% O_2 increased 4 times. This effect was explained by the lower reactivity of the super reduced state of the hydrogenase active state towards the O_2 inhibitor [42]. Therefore, due to its very high turnover, this hydrogenase has potential applications in H_2-production if an excess overpotential is applied on the electrode in order to decrease the rate of O_2 inactivation.

Genetic engineering tools are also very useful for increasing biotechnological applications of hydrogenases on electrodes. A truncated mutant of the FeFe-hydrogenase from *Megasphaera elsdeini* showed the following improved properties for electroenzymatic H_2-production: (i) a smaller size that allows higher biocatalyst coverage on the electrode; (ii) an enhanced catalytic bias towards H_2 production; (iii) a less sensitivity towards O_2 inhibition compared to other FeFe-hydrogenases [43].

2.3 Enzymatic Production of H_2 Assisted by Photocatalysts

The combination of hydrogenases with electrochemical systems has been extensively researched, however, the cases for photocatalysts acting simultaneously as scaffold and electron donor for hydrogenases are, most of them, more recent. Two strategies have been regarded to achieve the photobiocatalyzed reduction of protons. The first one links the hydrogenase to an organometallic dye to form a homogeneous catalytic system, thus, requiring a sacrificial electron donor. The second strategy consists on a solid support such as a modified photoelectrode loaded with hydrogenases, yielding heterogeneous catalytic processes.

2.3.1 Homogeneous Photobiocatalytic Production of H_2

Armstrong´s group developed a colloidal system comprising TiO_2 nanoparticles modified with several hydrogenases and organometallic complexes to harvest visible light [44]. The most successful result by far was obtained using *D. baculatum* NiFeSe-hydrogenase and a ruthenium organic complex, $[Ru(bpy)_2(H_4dbpy)]^{2+}$ [45]. Upon illumination and in presence of the electron donor triethanol amine the ruthenium complex harvested the visible light and transferred the excited electrons to the conduction band of TiO_2 nanoparticles, which were further ceded to the hydrogenase to produce 50 mol $H_2 \times s^{-1}$ per mole of enzyme.

Besides TiO_2, other light harvesting semiconductors were also explored as candidates to provide high-energy electrons to hydrogenases for reduction of protons. The group of Paul King showed that CdTe is a suitable semiconductor [46]. 2.5 nm CdTe particles modified with mercaptopropionic acid (MPA) served both as energy harvester and scaffold for the FeFe-hydrogenase from *C. acetobutylicum*. After immobilization of the enzyme and the enzyme activation, the samples were illuminated with a 150 W halogen white light during 5 min, in presence of ascorbic acid acting as sacrificial electron donor. After monitoring the activity at several pH values, the authors found that maximum H_2 production was obtained at pH 4.75, obtaining 1.94 ± 0.30 μmol $\times$ $mg^{-1} \times min^{-1}$. Interestingly, at this pH value, the hydrogenase is less than half active than at pH 7 measured using MV, meaning that the interaction between the CdTe and the enzyme, and the stability of MPA on CdTe play a major role in the electron transfer. After optimization of pH (4.75) and other critical parameters such as the electron donor concentration ([Ascorbic acid] = 0.5 M) and the ratio of CdTe:Hydrogenase (4:1), the system produced at a turnover number of 25 mol H_2 per mol of hydrogenase. The efficiency of the hybrid catalyst was determined as 9% when irradiated with monochromatic light or 1.8% when irradiated with white light at 1.5 AM intensity [46]. These results using CdTe were further studied spectroscopically by FTIR, in which the hybrid CdTe-hydrogenase system was compared with that involving hydrogenase and the photosensitizer $Ru(bpy)_3^{2+}$ [47]. The differences in the interfacial interactions between either sensitizers and the hydrogenase were analysed. It was found that CdTe performed better than $Ru(bpy)_3^{2+}$ due to its possibility to host multiple photon excitation and multielectron pathways, which are not feasible for single complex molecules.

D. baculatum NiFeSe-hydrogenase was used together with Eosin Y, an organic dye, for the photocatalytic evolution of H_2 using triethanol amine as sacrificial electron donor [48]. After optimizing the concentration of hydrogenase (4.4 nM), Eosin Y (0.44 mM) and the pH = 7, the system generated 0.5 μmol of H_2 per hour under anaerobic conditions using 100 $mW{\cdot}cm^{-2}$ power light at AM 1.5 visible radiation. The oxygen tolerance of the homogeneous photobiocatalytic system was evaluated, keeping 10% of the initial H_2 production at 21% O_2 concentration, and the natural one is in air. These results using Eosin Y were compared with the ones using $[Ru(pby)_3]^{2+}$. The comparison in strict anaerobic conditions was favourable to the ruthenium complex, as it produced almost double H_2 in the same conditions. However, the former was much more sensitive to O_2 presence: at 5% O_2 the Eosin Y system kept 80% of H_2 production, whereas the ruthenium complex only kept 12% of H_2 production [48]. Another light harvester consisting of a heptazine carbon nitride polymer (CN_x) was tested in combination with either the *D. baculatum* NiFeSe-hydrogenase or a biomimetic Ni–P photocatalyst in solution, comparing the activity of the biological and the inorganic catalysts [49]. In these cases, the sacrificial electron donor used was EDTA 0.1 M. Under the optimized conditions (pH 6, anaerobic, 1 sun irradiation including UV radiation $\lambda > 300$ nm) the hydrogenase (16.7 nM) with CN_x (5 mg) yielded 55 ± 5 μmol $H_2 \times (g\ CN_x \times h)^{-1}$. The production was linear during at least 4 h before showing a rate decrease. On the other hand, the biomimetic compound was able to produce H_2, although in rates tenfold lower than the hydrogenase system. This work was extended by immobilizing the hydrogenase and the CN_x on the surface of anatase TiO_2 nanoparticles, smaller than 10 nm [50]. Addition of TiO_2 to the system yielded 1.46 μmol H_2 using pH 6, EDTA 0.1 M, 5 mg of TiO_2 and 50 pmol of NiFeSe-hydrogenase. The TiO_2-based system showed a lower initial activity than the direct combination of CN_x with the hydrogenase, although it may be stable under working conditions a longer time, as the experiments were run up to 72 h instead of cutting after 50 h.

Genetic engineering has also been tested to improve the assembly of hybrid biologic-inorganic catalysts for H_2 production. One example is the re-engineering of an *E. coli* NiFe-hydrogenase for its selective surface through its distal [4Fe4S] cluster attachment to silver nanoclusters stabilized in aqueous solution with approximately m5kDa polymethacrylic acid (PMAA) [51]. Whereas silver managed to harvest some energy from light, the system performed much better when including TiO_2 P-25 particles in the mixture. The best mutant (Y'222C) with Ag and PMAA yielded 7.2 μmol $H_2 \times h^{-1}$, the same mutant mixed with Ag, PMAA and TiO_2 particles yielded 134 μmol $H_2 \times h^{-1}$. The Y'222C mutation consisted on exchanging tyrosine 222 for a cysteine. Other mutants showed lower or no activity at all.

Some sulphides are interesting materials as semiconductors, mainly those on which the bandgap is close to 2–2.5 eV and therefore absorb visible light irradiation. One example of suitable sulphide is indium sulphide, In_2S_3. This n-type semiconductor material has a 2.2–2.3 eV bandgap and can be prepared solvothermally in such a way that provides a highly porous surface suitable to host

nanocatalysts. An example of micron-size In_2S_3 particles with an average pore diameter of 16 nm hosting *D. vulgaris* Hildenborough NiFeSe-hydrogenase and producing H_2 upon only visible light illumination, using sulphide anions as sacrificial electron donor has been reported [52]. The authors optimized the incubation time to 6 h; in that case, the In_2S_3-hydrogenase complex produced about 800 μmol $H_2 \times$ mg (hydrogenase)$^{-1} \times$ min^{-1}. Compared to the activity of the system measured with MV instead of illumination, the later one kept 89% of the activity measured chemically. The turnover frequency (TOF) of the hydrogenase under photobioproduction was 986 s^{-1}. These values match the ones obtained for another sulphide, cadmium sulphide capped with mercaptopropionic acid (CdS-MPA), a few years earlier [53]. In that case, the hydrogenase selected was the FeFe-hydrogenase I from *C. acetobutylicum*, which provided a maximum 900 s^{-1} turnover frequency for H_2 conversion using ascorbic acid as electron donor.

CdS is a very good semiconductor from this perspective, as its bandgap is 2.4 eV, and its conduction band is well aligned with the $2H^+/H_2$ redox couple. One challenge to use sulphides to provide high-energy electrons to hydrogenases in an aqueous solution is its lack of stability, needing capping agents to stabilize them in the aqueous phase. The capping agents must attract the hydrogenase in an oriented fashion to catalyze the H_2 production successfully. Mercaptoacids are suitable for this purpose, as its thiol group can be attached to the sulphide surface via either a M-S bond or a S–S bridge; and the carboxylic functionalities allow oriented electrostatic orientation of *C. acetobutylicum* FeFe-hydrogenase with the distal [4Fe4S] cluster facing the semiconductor surface. The influence of the mercaptocarboxylic derivative's chain length was studied [54], finding that the shorter the chain the more efficient was the electron transfer between the semiconductor and the enzyme. The most efficient capping agent was 2-mercaptoacetic acid, and an exponential decay upon longer chain was observed.

2.3.2 Heterogeneous Photobiocatalytic Production of H_2

The combination of the hydrogenases for photoproduction of H_2 with solid supports has interesting advantages. Firstly, the sacrificial electron donor needed in homogeneous photobiocatalytic systems may be substituted and provided by the electrode or the photo-harvesting material. Secondly, a successful immobilization of the biocatalysts provides higher stability and longer operational periods. Moreover, it gives flexibility for the design of photobioelectrochemical cells, facilitates flow systems and allows reutilization.

The most popular and material used for photon harvesting is TiO_2. A very interesting work anodizes a TiO_2 film to generate a nanosized tubular material that can be loaded with hydrogenases [55]. After a careful selection of anodization conditions to form the tubular TiO_2 and its modification with dithiothreitol, hydrogenase from *P. furiosus* was linked via disulphide bonds. Further, the electrode protection was added by electropolymerization of polypyrrole. The resulting electrode produced 140 μmol $\times$ cm$^{-2} \times$ h^{-1} of H_2, upon illumination with 75 mW/cm^2 light power and using 3.66 units of hydrogenase.

Another material tested as semiconducting photocatode was the nanoporous black silicon together with a FeFe-hydrogenase [56]. This precise preparation of silicon brings advantages such as absorbing more light than bright silicon and suppressing the attachment of H_2 bubbles due to its lower surface tension. A nanoporous structure was implemented to the Si by a several step process including the formation of Ag nanoparticles and its further etching in acidic solution, yielding pores ranging from 30 to 100 nm in diameter. The nanoporous structure allowed a high loading of the hydrogenase. The hydrogenase-modified electrode showed an onset potential of −0.22 versus Ag/AgCl at pH 6.8, much more positive than the onset potential of the bare Si electrode, starting at −0.50 and equal to that of platinum nanoparticles. The photobioelectrode delivered hydrogen production under low irradiation power, starting at 10 mW × cm^{-2}, although an increase on the light intensity yielded a photocurrent increase. The photocurrents measured were correlated to the hydrogen production, yielding a TOF of 1,300 s^{-1} for a photocurrent density of 3 mA × cm^{-2} at −0.5 V versus Ag/AgCl, pH 6.8 and 50 mW × cm^{-2} irradiation.

Silicon can also be covered with a protective layer of TiO_2 and still work as support for hydrogenases for the H_2 evolution [57]. Such TiO_2 layer prevents silicon from oxidation and facilitates the excited electron transport through its conductive band to the immobilized hydrogenase, which reduces the protons to H_2. The initial control tested if a FTO electrode modified with amorphous TiO_2 and hydrogenase was suitable, instead of crystalline TiO_2. This configuration was able to reduce protons to H_2 when a potential of −0.35 V versus SHE was applied at pH 6. After 1 h, it produced 90 nmol of H_2 with a Faradaic yield of 96%, demonstrating that amorphous TiO_2 with hydrogenase was suitable. The next experiment transferred the construction to the surface of a p–Si semiconductor. The p–Si–TiO_2-hydrogenase electrode was set to 1 h of white light illumination, producing 25 nmol of H_2 with a Faradaic yield of 95%. Control experiments demonstrated that lacking any of the components yielded negligible amounts of H_2. This photobioelectrochemical approach allowed avoiding the use of sacrificial electron donors. After determining the p–Si–TiO_2 as a successful combination of materials to develop a suitable photoelectrode to host hydrogenase, the next step was its nanostructuring. A hierarchical structure of inverse opal TiO_2 was built on the top of the silicon. The structure showed a high pore control and cavities, where the NiFeSe-hydrogenase from *D. baculatum* was immobilized. This construction showed an onset potential of +0.35 V versus RHE. The experiments of controlled potential photoelectrolysis (0 V vs. RHE) without enzyme yielded 0.5 μmol H_2 cm^{-2} with a Faradaic efficiency of 45% during 5 h, whereas the addition of hydrogenase yielded 17 μmol $H_2 \cdot cm^{-2}$ with a Faradaic efficiency of 86% during 5 h. The electrode was coupled to a $BiVO_4$ photoanode to assemble a whole 2-compartment photoelectrochemical cell including a Nafion membrane to separate them. As a result of 5 h illumination, 0.46 μmol H_2 and 0.20 μmol of O_2 were synthesized in absence of an external bias; the Faradaic efficiencies were 98 and 84%, respectively. Reisner's group has very recently established the benchmark for photoelectroenzymatic H_2 production by integrating the TiO_2-hydrogenase

construction in a lead halide perovskite photocathode, producing a photocurrent of −5 mA/cm^3 at 0 V versus RHE [58].

There are other oxides besides TiO_2 able to harvest photons and work as photocathodes, for instance, Cu_2O and ZnO. The bandgap of ZnO is too high and works only in the UV, whereas Cu_2O has a suitable bandgap but is prone to oxidation. However, their layer-by-layer combination allows harvesting of light energy within the visible range and protection against corrosion, as well as hosting hydrogenases to perform the hydrogen production [59]. The oxide layers were deposited on the surface of a FTO electrode. First, Cu_2O was deposited by alkaline electrodeposition and then ZnO by the spin coating of precursors with further annealing. On its top, a histidine-tagged hydrogenase from *E. coli* was drop-casted for its physical adsorption during 15 min. The biocathode delivered 0.8 mA × cm^{-2} upon illumination with 100 mW·cm^{-2} VIS LED light (1 Sun equivalent), which is tenfold higher than the photocurrent provided by a hydrogenase-less photocathode. The hydrogen produced was measured with a unisense H_2 external sensor, delivering 0.68 nmol of H_2 after accumulation during 200 s. Such H_2 amount measured was compared to the charge measured in the circuit, rendering a Faradaic efficiency of 1%.

Another set of photobiocathodes has recently been developed in the absence of the classical semiconductors, by combining photosystem I (PSI) and hydrogenase on the top of an electrode and connecting them with two redox polymers: one Os-modified polymer for collecting the excited electrons from PSI and another cobaltocene-derived polymer to connect the hydrogenase to the electrode [60]. The key in this first proof-of-concept work was substituting a viologen-derived polymer by the cobaltocene-derived polymer, which has a much lower redox potential and therefore providing a larger driving force to push the catalytic cycle of the *D. gigas* NiFe-hydrogenase towards H_2 production. A following work using layer-by-layer controlled strategies to connect PSI and another hydrogenase, increasing the H_2 production, has been recently published [61].

3 Microbial Production of H_2

The use of microbial whole-cells as catalysts for H_2 production has obvious advantages over the use of enzymes, which have a short lifetime and require lengthy and expensive processes to be isolated. Microbial cells are much more robust and are capable of growth and self-repair, and the corresponding bioprocesses are easily scaled up and provide an opportunity for the use of sustainable substrates, such as sunlight or wastes. Several kinds of bioprocesses have been explored to produce hydrogen biologically (biohydrogen, BioH_2), namely bio-photolysis of water by algae, photo-fermentation by photosynthetic bacteria and dark fermentation by anaerobic bacteria and archaea [62–65]. Here, we will focus specifically on dark fermentation, which is regarded as the most promising approach due to the simplicity of the process, ease of scale-up, high rates of BioH_2

production, and feasibility of using a versatile range of organic molecules, including organic wastes [66]. Therefore, the dark fermentation offers not only an environmentally friendly way to produce a value-added product but can also contribute to waste recycling. This section reviews the progress of $BioH_2$ production through dark fermentation processes using microorganisms as whole-cell catalysts to produce H_2 from organic wastes and one-carbon substrates.

3.1 Biohydrogen Production from Organic Wastes

From a realistic and economical point of view, dark fermentation is the most promising approach to produce $BioH_2$ from industrial wastewaters. Dark fermentation is carried out by anaerobic microorganisms (facultative or obligate) in the absence of light. The metabolic pathways responsible for fermentative H_2 production are diverse and depend on the microorganism and substrate used. Generally, H_2 is not the only product of the fermentation process, and various other by-products such as ethanol, acetate, propionate and butyrate will be also originated according to the pathway involved. In dark fermentation, the electrons produced from the oxidation of organic substrates are used to reduce protons to $BioH_2$. The reduction process is catalyzed by a hydrogenase, which can be a FeFe- or a NiFe-hydrogenase [67, 68].

Several organic wastes were investigated as substrates for H_2 production through dark fermentation namely distillery effluent, beverage wastewater, cheese whey, palm oil mill wastewater and sugar-rich effluents [69]. In general, wastes contain a complex mixture of molecules that are first hydrolyzed to hexoses, which are then metabolized to H_2. Lignocellulosic biomass is also an attractive substrate for hydrogen production due to its wide availability. However, this complex material composed by cellulose, hemicellulose and lignin, requires a pretreatment such as enzymatic, chemical or thermochemical hydrolysis to release simple sugars that can be readily used by most H_2-producing microorganisms [69, 70]. Another interesting substrate is glycerol that is a by-product of biodiesel producing industries. Glycerol is not only an abundant and low cost substrate but it also provides more reducing equivalents than sugars, making it an attractive raw material for the biological production of different fuels, including H_2 [71].

For the bioconversion of complex substrates like organic wastes to H_2, it is essential to find the most suitable microbial catalysts. Many microorganisms have been reported to be able to produce hydrogen through dark fermentation using organic wastes as substrate, namely *Clostridium butyricum*, *Clostridium pasteurianum*, *Enterobacter asburiae*, *Enterobacter aerogenes*, *Thermoanaerobium*, *Citrobacter* spp. and *Bacillus* spp. [66, 69, 72, 73]. Fermentative organisms can be divided in two groups according to their catabolism: saccharolytic fermenting bacteria which ferment the complex sugars such as oligosaccharides, cellulose and simple sugars, and the proteolytic bacteria that hydrolyze proteins and further ferment the amino acids [64]. Among all H_2-producing microorganisms, *Clostridium* spp., which are saccharolytic fermenting bacteria, are the most widely

used and show the highest H_2 production efficiency [66, 72]. Studies have shown that *Clostridium* sp. are able to produce the maximum H_2 yield of 4 mol H_2/mol hexose, while 2 mol H_2/mol hexose is achieved by *Enterobacter* species [74]. Moreover, some *Clostridium* species like *Clostridium thermocellum* are able to effectively break down cellulose in a single-step fermentation process [75], which make these microorganisms potential biocatalysts to produce H_2 from lignocellulosic biomass.

Clostridium species produce H_2 fermentatively through the glycolytic pathway [72]. Organic molecules, mainly sugars, are oxidized originating pyruvate, ATP and NADH. Pyruvate is subsequently converted into acetyl-CoA and CO_2 through the pyruvate-ferredoxin oxidoreductase, which also catalyzes the reduction of ferredoxin. The reduced ferredoxin is used by the electron bifurcation or monomeric Fd-dependent FeFe-hydrogenase to reduce protons to H_2. Furthermore, H_2 can be also produced by the oxidation of NADH produced by glycolysis through electron bifurcation. The acetyl-coA produced is also used in several lateral metabolic pathways originating acetate or butyrate. Since the regeneration of NAD^+ is required for the glycolysis process, several other by-products namely ethanol and butanol can be also formed [72]. Therefore, the H_2 production yield is dependent on the pathway involved. In the case of hydrogen production by *Enterobacter* spp., this process is also performed through the glycolytic pathway, but in these microorganisms, H_2 can be also produced from formate. In *Enterobacter* spp., the pyruvate is not only converted to acetyl-CoA but can also originate formate that is further oxidized into H_2 and CO_2 by the formate-hydrogen lyase [66, 69].

Although high H_2 production is possible by dark fermentation, this process has two mains drawbacks: low substrate conversion to H_2 and accumulation of by-products [65]. Theoretically, the conversion of 1 mol glucose will give 12 mol H_2. However, according with the fermentative pathway, the maximum H_2 yield is restricted to 4 mol H_2/mol glucose for acetate-type fermentation, 2 mol H_2/mol glucose for butyrate and ethanol-type fermentation and 1 mol H_2/mol glucose for propionate-type fermentation [64, 66]. When organic wastes are used as substrate, the BioH_2 yield rarely exceeds 2 mol H_2/mol hexose [64, 66]. Therefore, several strategies have been investigated to enhance the H_2 yield, namely metabolic engineering, development of integrated processes, whole-cell immobilization and incorporation of metal additives in the bioprocess [64, 65, 69, 74].

Metabolic engineering strategies reported to improve the H_2 production yield include the construction of innovative metabolic routes and/or enhancing the main metabolic pathway by overexpressing hydrogen-producing genes and knockout of competitive pathways [65, 69, 76, 77]. A synthetic pyruvate:H_2 pathway with additional co-expression of the *Bacillus subtilis* AmyE was constructed in *E. coli* allowing the recombinant strain to became able to produce H_2 from potato starch [76]. In addition, overexpressing the enzymes directly involved in hydrogen production also resulted in increase in the H_2 production [77]. It was reported the overexpression of a gene encoding the HydA hydrogenase in *Clostridium paraputricum* enhanced an increase in the H_2 yield from 1.4 to 2.4 mol H_2/mol glucose from rich synthetic wastewaters [77]. Furthermore, the gene coding for a xylose

isomerase from *Thermoanaerobacter ethanolicus* was introduced in *Clostridium thermocellum*, making the recombinant strain able to ferment simultaneously xylose, glucose, cellobiose and cellulose [78].

Another strategy that has been studied to improve H_2 production yields is the development of integrated processes such as combining dark fermentation with photo-fermentation or with a microbial electrochemical cell (MEC) [69, 74, 79, 80]. In these integrated processes, the by-products produced during dark fermentation are utilized as substrate by the photo-fermentative organisms, in the case of photo-fermentation, or by electroactive organisms in MEC, which increases the H_2 yield. Integration of a MEC with dark fermentation was shown to be an efficient solution to improve H_2 production and substrate bioconversion [79, 80]. A substrate conversion of 90% could be achieved using this hybrid system [79]. Nevertheless, the combination of dark and photo-fermentations is more widely studied [64, 69, 71]. In fact, the integrated approach of dark-photo-fermentation has many advantages and allows the maximum conversion of substrate to H_2 (12 mol H_2/mol glucose) [64, 81]. The integration of dark and photo-fermentation processes can be carried out in sequential two-stage or in single stage (co-culture) systems. The two-stage system has been applied to produce H_2 from several organic wastes [64, 69, 71]. An example is the two-stage process applied for BioH_2 production from palm oil mill wastewater, which allowed the increase of H_2 production from 0.8 to 3 ml H_2/ml waste. In this process, the fermentative bacterium *Clostridium butyricum* and the photo-fermentative organism *Rhodopseudomonas palustris* were used [82]. The integrated dark-photo-fermentation was also applied for production of H_2 from molasses with a H_2 yield of 5.65 mol H_2/mol hexose [83]. High H_2 production yield was also attained from beet molasses (13.7 mol/mol hexose) when a two-stage sequential dark-photo-fermentation was applied [81]. The single stage co-culture reactors provide an alternative solution to maximize H_2 yield in a cost-effective approach [64]. A co-culture of *Clostridium acetobutylicum* and *Rhodobacter sphaeroides* was used in a fed-batch process to enhance the H_2 production from starch [84]. This process allowed to reach a H_2 yield of 2.62 mol/mol hexose. In addition, a higher H_2 yield (5.2 mol/mol glucose) was obtained from starch by a co-culture *Clostridium butyricum* and *Rhodobacter sphaeroides* in a repeated batch process [85].

Concerning whole-cell immobilization, it was found that immobilized cells are more effective for hydrogen production than free cells [86]. Immobilization has several advantages as it can help to reduce by-product inhibition, protect the microorganism against the adverse impacts of organic wastes and prevent biomass washout. *Clostridium butyricum* immobilized in polyethylene glycol was used for H_2 production from palm oil mill effluent reaching the maximum hydrogen yield of 0.35 L/H_2/g COD [87]. *Clostridium* sp. immobilized in fungal mycelia pellets was used for H_2 production from corn stalk hydrolysate [85]. This strategy led to a maximum H_2 production of 14 mmol H_2/L/h which is 2.6 times higher than when free cells were used. The hydrogen production yield was also improved (3.5 mol H_2/mol lactose) when the fermentative organism *Enterobacter aerogenes* was immobilized in calcium alginate and used to produce H_2 from cheese whey [88].

Another strategy to improve H_2 productivity of dark fermentation is the addition of metals. These are required as enzyme co-factors improving their activity and consequently leading to an increase of H_2 production. The improvement of microbial growth and enzyme activity by supplementation of certain metals like Cu, Fe and Ni has been documented in several studies [69, 71]. Moreover, the incorporation of metal nanoparticles (NPs) to improve dark fermentation has been investigated in the last years [69, 70, 89, 90]. It was demonstrated that the presence of nanoparticles of silver, iron, titanium oxide and nickel enhance the efficiency, yield and rate of hydrogen production [69, 70, 89]. The incorporation of FeO NPs in a dark fermentation process was shown to increase the hydrogen production yield up to 17% [91]. This improvement was explained by the zero valency of the NPs that can react with oxygen promoting the decrease of dissolved oxygen levels in the media, which may increase the efficiency of the oxygen sensitive hydrogenases. A highly significant enhancement of hydrogen yield from dark fermentation of dairy wastewater was also reported when Ni NPs were added [89]. Moreover, the combination of Fe and Ni NPs allowed an increase of more than 200% in H_2 production from lignocellulosic wastes [92]. Significant improvements were achieved for H_2 production from industrial wastewaters when a nickel-graphene nanocomposite was also incorporated in the bioprocess (reaching an improvement of more than 100%) [93]. TiO_2 NPs-enhanced $BioH_2$ production by pretreatment of organic wastes. TiO_2 nanoparticles can degrade the polysaccharides and proteins into smaller organic compounds that are further utilized by the H_2-producing microorganisms [94].

3.2 Biohydrogen Production from One-Carbon Substrates

Another attractive class of substrates for biohydrogen production are one-carbon compounds like formate and carbon monoxide [95–97]. CO is a cheap compound that is present in syngas and several industrial waste gases. Therefore, the production of $BioH_2$ from these CO-containing gases contributes also for waste recycling and minimization of carbon emissions. On other hand, formate is an efficient H_2 carrier [97, 98] and can be easily obtained by biomass processing or hydrogenation of carbon dioxide [99–101].

Biological conversion of one-carbon substrates to H_2 is an environmentally friendly and economical approach since high specificity and high yields can be achieved with a minimum energy input [95, 97, 102].

3.2.1 Whole-Cell Biocatalysts for Formate-Driven H_2 Production

The first reports of H_2 bioproduction from formate were obtained with *E. coli* [103], and since then several microorganisms belonging to distinct phylogenetic groups have been reported as biocatalysts for formate conversion to H_2 [102]. The biological conversion of formate to H_2 proceeds according to the reaction:

$$HCOO^- + H_2O \rightarrow HCO_3^- + H_2 \quad \Delta G^o = +1.3 \text{ kJ/mol} \tag{1}$$

Formate-driven hydrogen production occurs through different enzyme systems according to the microorganism. Hydrogen production from formate has been extensively studied in *E. coli*, where it is catalyzed by the enzymatic complex formate-hydrogen lyase (FHL) composed by a formate dehydrogenase (FDH) associated to a membrane-bound hydrogenase [104]. Yoshida and coworkers reported that *E. coli* was able to produce 100 mmol/g_{cells}/h of H_2 [105]. To improve the production of H_2 by *E. coli*, several metabolic engineering approaches have been applied including overexpression of the FHL complex and deletion of uptake hydrogenases [102, 106]. The genetic modifications together with process optimization, where the products were continuously removed from the medium, allowed a substantial increase of H_2 production from formate (144.2 mmol/g_{cells}/h), whereas without product removal the yield was only 34.4 mmol/g_{cells}/h [107]. Seol and coworkers demonstrated the high formate conversion to hydrogen of an *E. coli* DJT152 strain, where the uptake hydrogenases and lactate dehydrogenase were deleted, and which has a constitutively-expressed *fhlA* gene, increasing the FHL expression. This engineered strain archived the highest activity of 195.2 mmol/g_{cells}/h under non-growing conditions [73].

Besides *E. coli,* enterobacteria *Citrobacter amalonaticus* and *Enterobacter asburiae* were also investigated as biocatalysts for formate conversion to H_2 [108, 109]. Similarly to *E. coli*, the H_2 production in these two strains proceeds through the FHL complex [73, 108]. Under non-growing conditions, Seol and coworkers investigated the potential for H_2 production of the wild-type strains *Citrobacter amalonaticus* and *Enterobacter asburiae* and two engineered *E. coli* strains. They found that the H_2 production capability of the two wild-type strains was similar to the engineered *E. coli* DJT152 strain (195.2 mmol/g_{cells}/h) demonstrating the high biotechnological potential of *Citrobacter amalonaticus* and *Enterobacter asburiae* was biocatalysts for formate-driven H_2 production [73].

Some *Clostridia* also have the capacity to produce H_2 from formate through an enzymatic system composed by separate cytoplasmic FDH and hydrogenase. *Clostridium paraputrificum* was able to produce H_2 from formate with a hydrogen production rate of 3.7 mmol/L/h, while *Clostridium diolis* JPCC isolated from a slurry solution showed a production rate of 0.43 mmol/L/h [102].

Sulphate-reducing bacteria are another interesting bacterial group that was been investigated for biological conversion of formate to H_2. Martins and coworkers demonstrated the high potential of *Desulphovibrio vulgaris* as whole-cell catalysts for formate-driven H_2 production [110]. Moreover, this microorganism was used as catalyst in a new bioprocess developed for hydrogen production where a hydrogen production rate of 100 mmol/g_{cells}/h was attained [111]. Formate-driven H_2 production in *D. vulgaris* occurs through two possible pathways: a direct one involving the periplasmic FDHAB and the periplasmic NiFeSe-hydrogenase, operating independently, and a second one that involves transmembrane electron transfer and may allow energy conservation [111, 112].

The archaeon *Thermococcus onnurineus*, also displays high activity in thermophilic conditions [91, 113–115]. Formate-driven H_2 production in this organism occurs through a membrane-bound enzyme complex composed by an Fdh, a hydrogenase and Na^+/H^+ antiporter subunits that couples H_2 formation to formate oxidation as well as energy conservation [115]. Under thermophilic conditions (80 ºC), *Thermococcus onnurineus* was able to reach the high hydrogen production of 404 mmol/g_{cells}/h, which outcompete the ones obtained by dark fermentation [91].

Another microorganism with a great capacity for H_2 production from formate is the strictly anaerobic acetogenic bacterium *Acetobacterium woodii* [96, 97, 116]. This bacterium possesses a new enzymatic system, the soluble hydrogen-dependent CO_2 reductase complex (HDCR) that catalyzes the reversible oxidation of formate to H_2 and CO_2 [116]. It was reported that whole-cells of *A. woodii* are capable of producing 66 mmol/g_{cells}/h of H_2 from formate [96].

3.2.2 Whole-Cell Biocatalysts for CO-Driven H_2 Production

Carbon monoxide-rich waste gases and syngas are considered as an interesting class of substrates for biological H_2 production, allowing the simultaneous production of fuel and the treatment of waste products. CO has a very low redox potential ($E^o = -520$ mV) which makes it as great electron donor, although CO is toxic gas to many microorganisms. Despite its toxicity, it has been reported that some microorganisms can use it as an energy and/or carbon source to produce H_2 [95, 102]. Efforts have been made to isolate H_2-producing microorganisms using CO as substrate, and over the past decade the number of microorganisms known to be able to oxidize CO duplicated [95, 102]. CO is biologically converted to H_2 according to the reaction:

$$CO + H_2O \rightarrow CO_2 + H_2 \quad \Delta G^o = -20 \text{ kJ/mol} \tag{2}$$

Biological production of H_2 from CO is catalyzed by two different metalloenzymes, the monofunctional nickel-containing carbon monoxide dehydrogenase (Ni-CODH) and an energy-conserving hydrogenase. Ni-CODH oxidizes CO to CO_2 with the production of reducing equivalents which are transferred to the hydrogenase that catalyzes the reduction of protons into hydrogen [95, 102, 117]. CO is a strong inhibitor of the hydrogenase activity, consequently, the hydrogenase that is coupled with CODH needs to have a high CO tolerance.

Significative advances have been made to identify efficient microorganisms producing H_2 from CO [95, 102]. The photosynthetic bacteria *Rubrivivax gelatinosus* (formerly *Rhodopseudomonas gelatinosa*) and *Rhodospirillum rubrum* were the first CO-oxidizing microorganisms reported [118]. *Rhodospirillum rubrum* was shown to produce 4.7 mmol/L/h of H_2 with a yield of 87%. The non-phototrophic facultative anaerobe *Citrobacter amalonaticus* Y19 was also reported as a whole-cell catalyst for CO-dependent H_2 production producing 3.5 mmol/g_{cell}/h of H_2 [119].

In thermophilic conditions, the high CO-tolerant microorganisms *Carboxydothermus hydrogenoformans*, *Carboxydocella thermautotrophica*, *Thermosinus carboxydivorans* and *Caldanaerobacter subterraneus* have been shown capable to

produce H_2 from CO [95, 102]. Moreover, Zhao and coworkers investigated the performance of *Carboxydothermus hydrogenoformans* as whole-cells catalysts in a bioprocess for conversion of CO to H_2 [120]. The bioprocess led to a maximum H_2 production of 117.7 mmol/L/h. Furthermore, two hyperthermophilic archaea, *Thermococcus* sp. AM4 and *Thermococcus onnurineus* NA1 can also grow on CO and produce H_2 [113, 121, 122]. The maximum H_2 production rate of 1.55 mmol/L/h with a yield of 100% was obtained with *Thermococcus onnurineus* NA1 grown on CO [113]. Recently, another thermophile with ability to catalyze CO-dependent H_2 production has been isolated, the facultative anaerobic bacterium *Parageobacillus thermoglucosidasius* [123]. Surprisingly, this bacterium can grow under 50% CO and 50% air, first consuming the O_2 and then utilizing the CO for the production of H_2 [123].

Anaerobic bacterial communities have also been used for the conversion of CO to H_2 [124, 125]. Recently, Sinharoy and coworkers evaluated the CO conversion by a bacterial consortium obtained from an upflow anaerobic sludge blanket reactor. This consortium was able to produce a maximum H_2 production of 29.9 mmol/L with a maximum yield of 70% from an initial CO concentration of 5 mmol/L [124].

Concerning syngas, its bioconversion to hydrogen by the photosynthetic bacterium *Rhodospirillum rubrum* has also been reported, with a production rate of 9.6 mmol/h and a maximum CO conversion efficiency of 81% [126]. A high potential for bioconversion of CO from steel mill waste gas to H_2 by a engineered *Thermococcus onnurineus* NA1 strain was documented [121].

Over the years, numerous studies have been performed to enhance activity of CO-dependent H_2 production through genetic engineering and process optimization. Ainala and coworkers developed a recombinant *Citrobacter amalonaticus* Y19 strain where the CO sensing transcriptional activator *cooA* was overexpressed. The overexpression of *cooA* improved the whole-cell CO-dependent H_2 production activity 3.4 fold [119]. BioH_2 production was also improved by the overexpressing of the CODH gene cluster in *T. onnurineus* NA1, leading to a H_2 production of 124 mmol/L/h, which was 3.8-fold higher than the one obtained by the wild-type strain [121]. In 2015, the same group manipulated the transcriptional regulatory system of *T. onnurineus* NA1 obtaining a modified strain with higher H_2 production rate (5.8-fold that the wild-type). A H_2 production rate of 191.9 mmol/L/h and a specific H_2 production rate of 249.6 mmol/g_{cell}/h were obtained with this engineered strain [127].

One of the major bottlenecks in biological CO conversion to H_2 is the low gas–liquid mass transfer. Therefore, several bioreactors have been designed to overcome this issue and it was found that the hollow fibre membrane (HFM) bioreactor is very effective in the mass transfer of CO, reaching the highest kLa for CO [120, 128]. In fact, the HFM bioreactor is considered as one of the most promising reactor configurations for syngas fermentation [128, 129]. Another approach that has been investigated to increase CO solubility is the incorporation of nanoparticles in bioreactor. This strategy is very effective even when a small amount of nanoparticles is used [130, 131]. Recently, the potential of biogenic iron nanoparticles synthesized using green-tea extract was evaluated to enhance the biohydrogen

production from CO by an anerobic bacterial consortium [125]. Compared with chemical nanoparticles, the biogenic ones are environmentally friendly and more economical [132–134]. The presence of the biogenic nanoparticles increased the CO solubility by more of 56% [125]. The CO solubility enhancement was attributed to the sorption–desorption of CO gas bubbles on the surface of the nanoparticles due to the presence of hydrophobic groups. The addition of biogenic iron nanoparticles to the bioprocess allowed the maximum H_2 production of 30 mmol/L [125].

The studies reported here reveal that hydrogen production through dark fermentation offers the best prospects for the development of a biohydrogen production process with high environmental benefits, contributing to clean energy generation and waste utilization.

References

1. Navarro RM, Peña MA, Fierro JLG (2007) Hydrogen production reactions from carbon feedstocks: fossil fuels and biomass. Chem Rev 107:4304–4330
2. De Lacey AL, Fernandez VM, Rousset M, Cammack R (2007) Activation and inactivation of hydrogenase function and the catalytic cycle: spectroelectrochemical studies. Chem Rev 107:4304–4330
3. Fontecilla-Camps JC, Volbeda A, Cavazza C, Nicolet Y (2007) Structure/function relationships of [NiFe]- and [FeFe]-hydrogenases. Chem Rev 107:4273–4303
4. Murphy BJ, Sargent F, Armstrong FA (2014) Transforming an oxygen-tolerant NiFe uptake hydrogenase into a proficient, reversible hydrogen producer. Energy Environ Sci 7:1426–1433
5. Hexter SV, Grey F, Happe T, Climent V, Armstrong FA (2012) Electrocatalytic mechanism of reversible hydrogen cycling by enzymes and distinctions between the major classes of hydrogenases. Proc Natl Acad Sci USA 109:18232–18233
6. Fourmond V, Baffert C, Sybirna K, Dementin S, Abou-Hamdan A, Meynial-Salles I, Soucaille P, Bottin H, Leger C (2013) The mechanism of inhibition by H_2 of H_2-evolution by hydrogenases. Chem Commun 49:6840–6842
7. Kubas A, De Sancho D, Best RB, Blumberger J (2014) Aerobic damage to FeFe-hydrogenases: activation barriers for the chemical attachment of O_2. Angew Chem Int Ed 53:4081–4084
8. Lu Y, Koo J (2019) O_2 sensitivity and H_2 production activity of hydrogenases—a review. Biotechnol Bioeng 116:3124–3135
9. Roseboom W, DeLacey AL, Fernandez VM, Hatchikian EC, Albracht SPJ (2006) The active site of the [FeFe]-hydrogenase from *Desulfovibrio desulfuricans*. II. Redox properties, light sensitivity and CO-ligand exchange as observed by infrared spectroscopy. J Biol Inorg Chem 11:102–118
10. Zorin NA, Gogotov IN, Kondratieva EN (1979) Hydrogen production by hydrogenase of *Alcaligenes eutrophus* z-1 in the presence of oxygen. FEMS Microbiol Lett 5:301–304
11. Horch M, Lauterbach L, Mroginski MA, Hildebrandt P, Lenz O, Zebger I (2015) Reversible active site sulfoxygenation can explain the oxygen tolerance of a NAD^+-reducing [NiFe] hydrogenase and its unusual infrared spectroscopic properties. J Am Chem Soc 137:2555–2564
12. Inoue T, Kumar SN, Kamachi T, Okura I (1999) Hydrogen evolution from glucose with the combination of glucose dehydrogenase and hydrogenase from A-eutrophus H16. Chem Lett 147–148

13. Zhang YHP, Evans BR, Mielenz JR, Hopkins RC, Adams MWW (2007) High-yield hydrogen production from starch and water by a synthetic enzymatic pathway. PLoS ONE 2: e456
14. Smith PR, Bingham AS, Swartz JR (2012) Generation of hydrogen from NADPH using an [FeFe] hydrogenase. Int J Hydrogen Energy 37:2977–2983
15. Lu F, Smith FR, Mehta K, Swartz JR (2015) Development of a synthetic pathway to convert glucose to hydrogen using cell fre extracts. Int J Hydrogen Energy 40:9113–9124
16. Mateo C, Palomo JM, Fernandez-Lorente G, Guisan JM, Fernandez-Lafuente R (2007) Improvement of enzyme activity, stability and selectivity via immobilization technique. Enzym Microb Technol 40:1451–1463
17. Zadvorny OA, Barrows AM, Zorin NA, Peters JW, Elgren TE (2010) High level of hydrogen production activity achieved for hydrogenase encapsulated in sol-gel material doped with carbon nanotubes. J Mater Chem 20:1065–1067
18. Baker SE, Hopkins RC, Blanchette CD, Walsworth VL, Sumbad R, Fischer NO, Kuhn EA, Coleman M, Chromy BA, Letant SE, Hoeprich PD, Adams MWW, Henderson PT (2009) Hydrogen production by a hyperthermophilic membrane-bound hydrogenase in water-soluble nanolipoprotein particles. J Am ChemSoc 131:7508–7509
19. Jordan PC, Patterson DP, Saboda KN, Edwards EJ, Miettinen HM, Basu G, Thielges MC, Douglas T (2016) Self-assembling biomolecular catalysts for hydrogen production. Nat Chem 8:179–185
20. Baltazar CSA, Marques MC, Soares CM, DeLacey AM, Pereira IAC, Matias PM (2011) Nickel-iron-selenium hydrogenases—an overview. Eur J Inorg Chem 948–962
21. Valente FMA, Oliveira ASF, Gnadt N, Pacheco I, Coelho AV, Xavier AV, Teixeira M, Soares CM, Pereira IAC (2005) Hydrogenases in *Desulfovibrio vulgaris* Hildenborough: Structural and physiologic characterisation of the membrane-bound [NiFeSe] hydrogenase. J Biol Inorg Chem 10:667–682
22. Stein M, Lubitz W (2001) The electronic structure of the catalytic intermediate Ni-C in [NiFe] and [NiFeSe] hydrogenases. Phys Chem Chem Phys 3:5115–5120
23. Parkin A, Goldet G, Cavazza C, Fontecilla-Camps JC, Armstrong FA (2008) The difference a Se makes? Oxygen-tolerant hydrogen production by the [NiFeSe]-hydrogenase from *Desulfomicrobium baculatum*. J Am Chem Soc 130:13410–13416
24. Gutiérrez-Sánchez C, Rüdiger O, Fernández VM et al (2010) Interaction of the active site of the Ni-Fe-Se hydrogenase from *Desulfovibrio vulgaris* Hildenborough with carbon monoxide and oxygen inhibitors. J Biol Inorg Chem 15:1285–1292
25. Maroney MJ, Hondal RJ (2018) Selenium *versus* sulfur: reversibility of chemical reactions and resistant to permanent oxidation in proteins and nucleic acids. Free Radical Biol Med 127:228–237
26. Marques MC, Coelho R, De Lacey AL, Pereira IAC, Matias PM (2010) The three-dimensional structure of [NiFeSe] hydrogenase from *Desulfovibrio vulgaris* Hildenborough: a hydrogenase without a bridging ligand in the active site in its oxidised, "as-isolated" state. J Mol Biol 396:893–907
27. Marques MC, Tapia C, Gutierrez-Sanz O, Ramos AR, Keller KL, Wall JD, De Lacey AL, Matias PM, Pereira IAC (2017) The direct role of selenocysteine in NiFeSe hydrogenase maturation and catalysis. Nat Chem Biol 13:544–550
28. Zacarias S, Temporao A, Del Barrio M, Fourmond V, Leger C, Matias PM, Pereira IAC (2019) A hydrophillic channel is involved in oxidative inactivation of a [NiFeSe] hydrogenase. ACS Catal 9:8509–8519
29. Plummer SM, Plummer MA, Merkel P, Hagen M, Biddle J, Waidner L (2016) Using directed evolution to improve hydrogen production in chimeric hydrogenases from *Clostridia* species. Enzym Microb Technol 93:132–141
30. Koo J, Schabel T, liong S, Evitt NH, Swartz JR, (2017) High-throughput screening of catalytic H_2 production. Angew Chem Int Ed 56:1012–1016

31. Armstrong FA, Belsey NA. Cracknell JA, Goldet G, Parkin A, Reisner E, Vincent KA, Wait AF (2009) Dynamic electrochemical investigations of hydrogen oxidation and production by enzymes and implications for future technology. Chem Soc Rev 38:36–51
32. Vincent K, Parkin A, Armstrong FA (2007) Investigating and exploiting the electrocatalytic properties of hydrogenases. Chem Rev 107:4366–4413
33. Hexter SV, Chung MW, Vincent KA, Armstrong FA (2014) Unusual reaction of NiFe-hydrogenases with cyanide. J Am Chem Soc 136:10470–10477
34. Fourmond V, Lautier T, Baffert C, Leroux F, Liebgott PP, Dementin S, Rousset M, Arnoux P, Pignol D, Meynial-Salles I, Soucaille P, Bertrand P, Leger C (2009) Correcting for electrocatalyst desorption and inactivation in chronoamperometry experiments. Anal Chem 81:2962–2968
35. Krassen H, Stripp S, von Abendroth G, Ataka K, Happe T, Heberle J (2009) Immobilization of the [FeFe]-hydrogenase CrHydA1 on a gold electrode: design of a catalytic surface for the production of molecular hydrogen. J Biotechnol 142:3–9
36. Kihara T, Liu XY, Nakamura C, Park KM, Han SW, Qian DJ, Kawasaki K, Zorin NA, Yasuda S, Hata K, Wakayama T, Miyake J (2011) Direct electron transfer to hydrogenase for catalytic hydrogen production using a single-walled carbon nanotube forest. Int J Hydrogen Energy 36:7523–7529
37. Morra S, Valetti F, Sarasso V, Castrignano S, Sadeghi SJ, Gilardi G (2015) Hydrogen production at high faradaic efficiency by a bio-electrode based on TiO2 adsorption of a new FeFe-hydrogenase from *Clostridium perfringens*. Bioelectrochemistry 106:258–262
38. Schlicht S, Assaud L, Hansen M, Lickleder M, Bechelany M, Perner M, Bachmann J (2016) An electrochemically functional layer of hydrogenase extract on an electrode of large and tunable specific surface area. J Mater Chem A 4:6487–6494
39. Shiraiwa S, So K, Sugimoto Y, Kitazumi Y, Shirai O, Nishikawa K, Higuchi Y, Kano K (2018) Reactivation of standard [NiFe]-hydrogenase and bioelectrochemical catalysis of proton reduction and hydrogen oxidation in a mediated-electron-transfer system. Bioelectrochemistry 123:156–161
40. Wakerley DW, Reisner E (2015) Oxygen tolerant proton reduction catalysis: much O_2 about nothing. Energy Environ Sci 8:2283–2295
41. Gutiérrez-Sanz O, Tapia C, Marques MC, Zacarías S, Vélez M, Pereira IAC, De Lacey AL (2015) Induction of a proton gradient across a gold-supported biomimetic membrane by electroenzymatic H_2 oxidation. Angew Chem Int Ed 54:2684–2687
42. Rodriguez-Macia P, Birrell J, Lubitz W, Rüdiger O (2017) Electrochemical investigations on the inactivation of the [FeFe] hydrogenase from *Desulfovibrio desulfuricans* by O_2 or light under hydrogen-producing conditions. ChemPlusChem 82:540–545
43. Caserta G, Papini C, Adamska-Venkatesh A, Pecqueur L, Sommer C, Reijerse E, Lubitz W, Gauquelin C, Meynial-Salles I, Pramanik D, Artero V, Atta M, del Barrio M, Faivre B, Fourmond V, Leger C, Fontecave M (2018) Engineering an FeFe-hydrogenase: do accessory clusters influence O_2 resistance and catalytic bias? J Am Chem Soc 140:5516–5526
44. Reisner E, Fontecilla-Camps JC, Armstrong FA (2009) Catalytic electrochemistry of a [NiFeSe]-hydrogenase on TiO_2 and demonstration of its suitability for visible-light driven H_2 production. Chem Commun 550–552
45. Reisner E, Powell DJ, Cavazza C, Fontecilla-Camps JC, Armstrong FA (2009) Visible light-driven h_2 production by hydrogenases attached to dye-sensitized TiO_2 nanoparticles. J Am Chem Soc 131:18457–18466
46. Brown KA, Dayal S, Ai X, Rumbles G, King PW (2010) Controlled assembly of hydrogenase-CdTe nanocrystal hybrids for solar hydrogen production. J Am Chem Soc 132:9672–9680
47. Greene BL, Joseph CA, Maroney MJ, Dyer RB (2012) Direct evidence of active-site reduction and photodriven catalysis in sensitized hydrogenase assemblies. J Am Chem Soc 134:11108–11111

48. Sakai T, Mersch D, Reisner E (2013) Photocatalytic hydrogen evolution with a hydrogenase in a mediator-free system under high levels of oxygen. Angew Chem Int Ed 52:12313–12316
49. Caputo CA, Gross MA, Lau VW, Cavazza C, Lotsch BV, Reisner E (2014) Photocatalytic hydrogen production using polymeric carbon nitride with a hydrogenase and a bioinspired synthetic Ni catalyst. Angew Chem Int Ed 53:11538–11542
50. Caputo CA, Wang L, Beranek R, Reisner E (2015) Carbon nitride-TiO_2 hybrid modified with hydrogenase for visible light driven hydrogen production. Chem Sci 6:5690–5694
51. Zhang L, Beaton SE, Carr SB, Armstrong FA (2018) Direct visible light activation of a surface cysteine-engineered [NiFe]-hydrogenase by silver nanoclusters. Energy Environ Sci 11:3342–3348
52. Tapia C, Zacarias S, Pereira IAC, Conesa JC, Pita M, De Lacey AL (2016) In situ determination of photobioproduction of H_2 by In_2S_3-[NiFeSe] hydrogenase from *Desulfovibrio vulgaris* Hildenborough using only visible light. ACS Catal 6:5691–5698
53. Brown K, Wilker MB, Boehm M, Dukovic G, King PW (2012) Characterization of photochemical processes for H_2 production by CdS nanorod-[FeFe] hydrogenase complexes. J Am Chem Soc 134:5627–5636
54. Wilker MB, Utterback JK, Greene S, Brown KA, Mulder DW, King PW, Dukovic G (2018) Role of surface-capping ligands in photoexcited electron transfer between CdS Nanorods and [FeFe] Hydrogenase subsequent H_2 generation. J Phys Chem C 122:741–750
55. Bae S, Shim E, Yoon J, Joo H (2008) Photoanodic and cathodic role of anodized tubular titania in light-sensitized enzymatic hydrogen production. J Power Sources 185:439–444
56. Zhao Y, Anderson NC, Ratzloff MW, Mulder DW, Zhu K, Turner JA, Neale NR, King PW, Branz HM (2016) Proton reduction using a hydrogenase-modified nanoporous black silicon photoelectrode. ACS Appl Mater Interf 8:14481–14487
57. Lee CY, Park HS, Fontecilla-Camps JC, Reisner E (2016) Photoelectrochemical H_2 evolution with a hydrogenase immobilized on a TiO_2-protected silicon electrode. Angew Chem Int Ed 55:5971–5974
58. Moore EE, Andrei V, Zacarias S, Pereira IAC, Reisner, (2020) Integration of a hydrogenase in a head halide perovskite photoelectrode for tandem solar water splitting. ACS Energy Lett 5:232–237
59. Tian L, Németh B, Berggren G, Tian H (2018) Hydrogen evolution by a photoelectrochemical cell based on a Cu_2O-ZnO-[FeFe] hydrogenase electrode. J Photochem Photobiol a: Chem 366:27–33
60. Tapia C, Milton RD, Pankratova G, Minteer SD, Akerlund HE, Leech D, De Lacey AL, Pita M, Gorton L (2017) Wiring of photosystem I and hydrogenase on an electrode for photoelectrochemical H_2 production by using redox polymers for relatively positive onset potential. ChemelectroChem 4:90–95
61. Zhao F, Wang P, Ruff A, Hartmann V, Zacarias S, Pereira IAC, Nowaczyk MM, Rögner M, Conzuelo F, Schuhmann W (2019) A photosystem I monolayer with anisotropic electron flow enables Z-scheme like photosynthetic water splitting. Energy Environ Sci 12:3133–3143
62. Boodhun BSF, Mudhoo A, Kumar G, Kim SH, Lin CY (2017) Research perspectives on constraints, prospects and opportunities in biohydrogen production. Int J Hydrogen Energy 42:27471–27481
63. Gopalakrishnan B, Khanna N, Das D (2019) Dark-fermentative biohydrogen production. In: Pandey A, Mohan SV, Chang JS, Hallenbeck PC, Larroche C (eds) Biohydrogen, 2nd edn. Elsevier, Amsterdam, pp 79–102
64. Mishra P, Krishnan S, Rana S, Singh L, Sakinah M, Ab Wahid Z (2019) Outlook of fermentative hydrogen production techniques: an overview of dark, photo and integrated dark-photo fermentative approach to biomass. Energy Strateg Rev 24:27–37
65. Stephen AJ, Archer SA, Orozco RL, Macaskie LE (2017) Advances and bottlenecks in microbial hydrogen production. Microb Biotechnol 10:1120–1127

66. Wang J, Yin Y (2019) Progress in microbiology for fermentative hydrogen production from organic wastes. Crit Rev Environ Sci Technol 49:825–865
67. Kim DH, Kim MS (2011) Hydrogenases for biological hydrogen production. Bioresour Technol 102:8423–8431
68. Lubitz W, Ogata H, Rüdiger O, Reijerse E (2014) Hydrogenases. Chem Rev 114:4081–4148
69. Banu JR, Kavitha S, Kannah RY, Bhosale RR, Kumar G (2020) Industrial wastewater to biohydrogen: possibilities towards successful biorefinery route. Bioresour Technol 298:122378
70. Srivastava N, Srivastava M, Malhotra BD, Gupta VK, Ramteke PW, Silva RN, Shukla P, Dubey KK, Mishra PK (2019) Nanoengineered cellulosic biohydrogen production via dark fermentation: a novel approach. Biotechnol Adv 37:107384
71. Trchounian K, Sawers RG, Trchounian A (2017) Improving biohydrogen productivity by microbial dark- and photo-fermentations: Novel data and future approaches. Renew Sustain Energy Rev 80:1201–1216
72. Latifi A, Avilan L, Brugna M (2019) Clostridial whole cell and enzyme systems for hydrogen production: current state and perspectives. Appl Microbiol Biotechnol 103:567–575
73. Seol E, Kim S, Raj SM, Park S (2008) Comparison of hydrogen-production capability of four different *Enterobacteriaceae* strains under growing and non-growing conditions. Int J Hydrogen Energy 33:5169–5175
74. Hallenbeck PC, Abo-Hashesh M, Ghosh D (2012) Strategies for improving biological hydrogen production. Bioresour Technol 110:1–9
75. Magnusson L, Cicek N, Sparling R, Levin D (2009) Continuous hydrogen production during fermentation of a cellulose by the thermophillic bacterium *Clostridium thermocellum*. Biotechnol Bioeng 102:759–766
76. Akhtar MK, Jones PR (2009) Construction of a synthetic YdbK-dependent pyruvate : H_2 pathway in Escherichia coli BL21 (DE3). Metab Eng 11:139–147
77. Morimoto K, Kimura T, Sakka K, Ohmiya K (2005) Overexpression of a hydrogenase gene in *Clostridium paraputrificum* to enhance hydrogen gas production. FEMS Microbiol Lett 246:229–234
78. Xiong W, Reyes LH, Michener WE, Maness PC, Chou KJ (2018) Engineering cellulolytic bacterium *Clostridium thermocellum* to co-ferment cellulose- and hemicellulose-derived sugars simultaneously. Biotechnol Bioeng 115:1755–1763
79. Sharma Y, Li B (2010) Optimizing energy harvest in wastewater treatment by combining anaerobic hydrogen producing biofermentor (HPB) and microbial fuel cell (MFC). Int J Hydrogen Energy 35:3789–3797
80. Zhang Y, Liu M, Zhou M, Yang H, Liang L, Gu T (2019) Microbial fuel cell hybrid systems for wastewater treatment and bioenergy production: Synergistic effects, mechanisms and challenges. Renew Sustain Energy Rev 103:13–29
81. Özgür E, Mars AE, Peksel B, Louwerse A, Yücel M, Gündüz U, Claassen PA, Eroğlu İ (2010) Biohydrogen production from beet molasses by sequential dark and photofermentation. Int J Hydrogen Energy 35:511–517
82. Mishra P, Thakur S, Singh L, Ab Wahid Z, Sakinah M (2016) Enhanced hydrogen production from palm oil mill effluent using two stage sequential dark and photo fermentation. Int J Hydrogen Energy 41:18431–18440
83. Morsy FM (2017) Synergistic dark and photo-fermentation continuous system for hydrogen production from molasses by *Clostridium acetobutylicum* ATCC 824 and *Rhodobacter capsulatus* DSM 1710. J Photochem Photobiol B Biol 169:1–6
84. Zagrodnik R, Łaniecki M (2017) Hydrogen production from starch by co-culture of *Clostridium acetobutylicum* and *Rhodobacter sphaeroides* in one step hybrid dark- and photofermentation in repeated fed-batch reactor. Bioresour Technol 224:298–306

85. Laurinavichene T, Laurinavichius K, Shastik E, Tsygankov A (2017) Long-term H_2 photoproduction from starch by co-culture of *Clostridium butyricum* and *Rhodobacter sphaeroides* in a repeated batch process. Biotechnol Lett 40:309–314
86. Kumar G, Mudhoo A, Sivagurunathan P, Nagarajan D, Ghimire A, Lay CH, Lin CY, Lee DJ, Chang JS (2016) Recent insights into the cell immobilization technology applied for dark fermentative hydrogen production. Bioresour Technol 219:725–737
87. Singh L, Wahid ZA, Siddiqui MF, Ahmad A, Rahim MHA, Sakinah M (2013) Biohydrogen production from palm oil mill effluent using immobilized *Clostridium butyricum* EB6 in polyethylene glycol. Process Biochem 48:294–298
88. Rai PK, Singh SP, Asthana RK (2012) Biohydrogen production from cheese whey wastewater in a two-step anaerobic process. Appl Biochem Biotechnol 167:1540–1549
89. Kumar G, Mathimani T, Rene ER, Pugazhendhi A (2019) Application of nanotechnology in dark fermentation for enhanced biohydrogen production using inorganic nanoparticles. Int J Hydrogen Energy 44:13106–13113
90. Taherdanak M, Zilouei H, Karimi K (2016) The effects of Fe^0 and Ni^0 nanoparticles versus Fe^{2+} and Ni^{2+} ions on dark hydrogen fermentation. Int J Hydrogen Energy 41:167–173
91. Lim JK, Bae SS, Kim TW, Lee JH, Lee HS, Kang SG (2012) Thermodynamics of formate-oxidizing metabolism and implications for H_2 production. Appl Environ Microbiol 78:7393–7397
92. Zilouei H, Taherdanak M (2015) Biohydrogen from lignocellulosic wastes. In: Karimi K (ed) Lignocellulose-based bioproducts. Springer, Heidelberg, pp 253–288
93. Elreedy A, Ibrahim E, Hassan N, El-Dissouky A, Fujii M, Yoshimura C, Tawfik A (2017) Nickel-graphene nanocomposite as a novel supplement for enhancement of biohydrogen production from industrial wastewater containing mono-ethylene glycol. Energy Convers Manag 140:133–144
94. Zhao Y, Chen Y (2011) Nano-TiO_2 enhanced photofermentative hydrogen produced from the dark fermentation liquid of waste activated sludge. Environ Sci Technol 45:8589–8595
95. Fukuyama Y, Inoue M, Omae K, Yoshida T, Sako Y (2020) Anaerobic and hydrogenogenic carbon monoxide-oxidizing prokaryotes: versatile microbial conversion of a toxic gas into an available energy. Adv Appl Microbiol (in press)
96. Kottenhahn P, Schuchmann K, Müller V (2018) Efficient whole cell biocatalyst for formate-based hydrogen production. Biotechnol Biofuels 11:1–9
97. Müller V (2019) New horizons in acetogenic conversion of one-carbon substrates and biological hydrogen storage. Trends Biotechnol 37:1344–1354
98. Eppinger J, Huang KW (2017) Formic acid as a hydrogen energy carrier. ACS Energy Lett 2:188–195
99. Boddien A, Gärtner F, Federsel C, Sponholz P, Mellmann D, Jackstell R, Junge H, Beller M (2011) CO_2-"neutral" hydrogen storage based on bicarbonates and formates. Angew Chem Int Ed 50:6411–6414
100. Enthaler S, von Langermann J, Schmidt T (2010) Carbon dioxide and formic acid—the couple for environmental-friendly hydrogen storage? Energy Environ Sci 3:1207
101. Jhong HRM, Ma S, Kenis PJA (2013) Electrochemical conversion of CO2 to useful chemicals: current status, remaining challenges, and future opportunities. Curr Opin Chem Eng 2:191–199
102. Rittmann SKMR, Lee HS, Lim JK, Kim TW, Lee JH, Kang SG (2015) One-carbon substrate-based biohydrogen production: microbes, mechanism, and productivity. Biotechnol Adv 33:165–177
103. Pakes WCC, Jollyman WH (1901) The collection and examination o f the gases produced by bacteria. J Chem Soc Trans 79:322–329
104. Pinske C, Sargent F (2016) Exploring the directionality of *Escherichia coli* formate hydrogenlyase: a membrane-bound enzyme capable of fixing carbon dioxide to organic acid. Microbiology (United Kingdom) 5:721–737

105. Yoshida A, Nishimura T, Kawaguchi H, Inui M, Yukawa H (2005) Enhanced hydrogen production from formic acid by formate hydrogen lyase-overexpressing *Escherichia coli* strains. Appl Environ Microbiol 71:6762–6768
106. Maeda T, Sanchez-Torres V, Wood TK (2012) Hydrogen production by recombinant *Escherichia coli* strains. Microb Biotechnol 5:214–225
107. Yoshida A, Nishimura T, Kawaguchi H, Inui M, Yukawa H (2007) Efficient induction of formate hydrogen lyase of aerobically grown *Escherichia coli* in a three-step biohydrogen production process. Appl Microbiol Biotechnol 74:754–760
108. Kim S, Seol E, Mohan Raj S, Park S, Oh YK, Ryu DDY (2008) Various hydrogenases and formate-dependent hydrogen production in *Citrobacter amalonaticus* Y19. Int J Hydrogen Energy 33:1509–1515
109. Shin JH, Yoon JH, Lee SH, Park TH (2010) Hydrogen production from formic acid in pH-stat fed-batch operation for direct supply to fuel cell. Bioresour Technol 101:53–58
110. Martins M, Pereira IAC (2013) Sulfate-reducing bacteria as new microorganisms for biological hydrogen production. Int J Hydrogen Energy 38:12294–12301
111. Martins M, Mourato C, Pereira IAC (2015) *Desulfovibrio vulgaris* growth coupled to formate-driven H_2 production. Environ Sci Technol 49:14655–14662
112. Martins M, Mourato C, Morais-Silva FO, Rodrigues-Pousada C, Voordouw G, Wall JD, Pereira IAC (2016) Electron transfer pathways of formate-driven H_2 production in *Desulfovibrio*. Appl Microbiol Biotechnol 100:8135–8146
113. Bae SS, Kim TW, Lee HS, Kwon KK, Kim YJ, Kim MS, Lee JH, Kang SG (2012) H_2 production from CO, formate or starch using the hyperthermophilic archaeon. Thermococcus Onnurineus Biotechnol Lett 34:75–79
114. Bae SS, Lee HS, Jeon JH, Lee JH, Kang SG, Kim TW (2015) Enhancing bio-hydrogen production from sodium formate by hyperthermophilic archaeon, thermococcus onnurineus NA1. Bioprocess Biosyst Eng 38:989–993
115. Kim YJ, Lee HS, Kim ES, Bae SS, Lim JK, Matsumi R, Lebedinsky AV, Sokolova TG, Kozhevnikova DA, Cha SS, Kim SJ, Kwon KK, Imanaka T, Atomi H, Bonch-Osmolovskaya EA, Lee JH, Kang SG (2010) Formate-driven growth coupled with H_2 production. Nature 467:352–355
116. Schuchmann K, Muller V (2013) Direct and reversible hydrogenation of CO_2 to formate by a bacterial carbon dioxide reductase. Science 342:1382–1386
117. Alfano M, Cavazza C (2018) The biologically mediated water–gas shift reaction: structure, function and biosynthesis of monofunctional [NiFe]-carbon monoxide dehydrogenases. Sustain Energy Fuels 2:1653–1670
118. Uffen RL (1976) Anaerobic growth of a *Rhodopseudomonas* species in the dark with carbon monoxide as sole and energy substrate. Proc Natl Acad Sci USA 73:3298–3302
119. Ainala SK, Seol E, Sekar BS, Park S (2014) Improvement of carbon monoxide-dependent hydrogen production activity in Citrobacter amalonaticus Y19 by over-expressing the CO-sensing transcriptional activator, CooA. Int J Hydrogen Energy 39:10417–10425
120. Zhao Y, Haddad M, Cimpoia R, Liu Z, Guiot SR (2013) Performance of a *Carboxydothermus hydrogenoformans*-immobilizing membrane reactor for syngas upgrading into hydrogen. Int J Hydrogen Energy 38:2167–2175
121. Kim MS, Bae SS, Kim YJ, Kim TW, Lim JK, Lee SH, Choi AR, Jeon JH, Lee JH, Lee HS, Kang SG (2013) CO-dependent H_2 production by genetically engineered *Thermococcus onnurineus* NA1. Appl Environ Microbiol 79:2048–2053
122. Sokolova TG, Jeanthon C, Kostrikina NA, Chernyh NA, Lebedinsky AV, Stackebrandt E, Bonch-Osmolovskaya EA (2004) The first evidence of anaerobic CO oxidation coupled with H_2 production by a hyperthermophilic archaeon isolated from a deep-sea hydrothermal vent. Extremophiles 8:317–323
123. Mohr T, Aliyu H, Küchlin R, Polliack S, Zwick M, Neumann A, Cowan D, Maayer P (2018) CO-dependent hydrogen production by the facultative anaerobe *Parageobacillus thermoglucosidasius*. Microb Cell Fact 17:1–12

124. Sinharoy A, Baskaran D, Pakshirajan K (2019) Sustainable biohydrogen production by dark fermentation using carbon monoxide as the sole carbon and energy source. Int J Hydrogen Energy 44:13114–13125
125. Sinharoy A, Pakshirajan K (2020) A novel application of biologically synthesized nanoparticles for enhanced biohydrogen production and carbon monoxide bioconversion. Renew Energy 147:864–873
126. Ismail KSK, Najafpour G, Younesi H, Mohamed AR, Kamaruddin AH (2008) Biological hydrogen production from CO: bioreactor performance. Biochem Eng J 39:468–477
127. Kim MS, Choi AR, Lee SH, Jung HC, Bae SS, Yang TJ, Jeon JH, Lim JK, Youn H, Kim TW, Lee HS, Kang SG (2015) A novel CO-responsive transcriptional regulator and enhanced H_2 production by an engineered *Thermococcus onnurineus* NA1 strain. Appl Environ Microbiol 81:1708–1714
128. Shen N, Dai K, Xia X, Jianxiong R, Zhang F (2018) Conversion of syngas (CO and H_2) to biochemicals by mixed culture fermentation in mesophilic and thermophilic hollow- fiber membrane biofilm reactors. J Clean Prod 202:536–542
129. Shen Y, Brown R, Wen Z (2014) Syngas fermentation of *Clostridium carboxidivoran* P7 in a hollow fiber membrane biofilm reactor: evaluating the mass transfer coefficient and ethanol production performance. Biochem Eng J 85:21–29
130. Kim Y, Lee H (2016) Use of magnetic nanoparticles to enhance bioethanol production in syngas fermentation. Bioresour Technol 204:139–144
131. Zhu H, Shanks BH, Heindel TJ (2008) Enhancing CO-water mass transfer by functionalized MCM41 nanoparticles. Ind Eng Chem Res 47:7881–7887
132. Fang X, Wang Y, Wang Z, Jiang Z, Dong M (2019) Microorganism assisted synthesized nanoparticles for catalytic applications. Energies 12:1–21
133. Hulkoti NI, Taranath TC (2014) Biosynthesis of nanoparticles using microbes—a review. Colloids Surf B Biointerf 121:474–483
134. Pereira L, Mehboob F, Stams AJM, Mota MM, Rijnaarts HHM, Alves MM (2015) Metallic nanoparticles: microbial synthesis and unique properties for biotechnological applications, bioavailability and biotransformation. Crit Rev Biotechnol 35:114–128

Organometallic Chemistry Control of Hydrogenases

Marcetta Y. Darensbourg, Erica Lyon Oduaran, Shengda Ding, Allen M. Lunsford, K. Dilshan Kariyawasam Pathirana, Pokhraj Ghosh, and Xuemei Yang

Abstract

This chapter provides an abbreviated overview of the discovery, exploration, and current knowledge of hydrogenase enzymes with particular regard to the mechanisms of electrocatalytic proton reduction in both the natural enzymes and synthetic analogues of the active sites. The timeline of key breakthroughs for defining the enzymes as well as in hydrogenase-inspired biomimetic research serves as a basis for the discussion.

Keywords

Hydrogenase enzymes · Microbial metabolism · Hydrogen evolution reaction · Active site structures · Mechanism · Models · Pendant base · Cofactor · Nitrogenase · Electrocatalysis

1 Prologue

With regard to the purpose of this collection, "Enzymes for Solving Humankind's Problems", from observations by careful microbiologists at the time of their discovery the Hydrogenases were known to be integral units in a microbial factory that was remediating a major pollution problem. Their biochemical and chemical

M. Y. Darensbourg (✉) · S. Ding · A. M. Lunsford · K. D. Kariyawasam Pathirana · P. Ghosh · X. Yang
Department of Chemistry, Texas A&M University, College Station, TX, USA
e-mail: marcetta@chem.tamu.edu

E. L. Oduaran
Department of Chemistry, Roger Williams University, Bristol, RI, USA

J. J. G. Moura et al. (eds.), *Enzymes for Solving Humankind's Problems*,
https://doi.org/10.1007/978-3-030-58315-6_10

characteristics have inspired scientists from that time forward, most recently for the possibility that their enzyme active sites might serve as potential templates for sustainable molecular catalysts in electrolyzers (the water splitting reaction making use of renewable energy sources of electrons and storing them in chemical bonds of H_2) and fuel cells (hydrogen oxidation for on-demand electrons). This work has continued for nearly a century and continues at ever more fundamental levels.

An occasional pause in efforts focused on discovery for reflection on the history of a scientific pursuit that has occupied the attention of a broad range of experimentalists and theoreticians is a worthwhile exercise. Such efforts are particularly engaging, and useful, for metalloenzymes where characterization of the relationship of biological function to structure requires a small army of microbiologists, enzymologists, spectroscopists, crystallographers, and both synthetic and computational chemists. In this particular case, a new cadre of chemists was called upon to account for the decidedly organometallic-like components and function of the hydrogenase active sites. The time-line for hydrogenase discoveries given in Fig. 1 is necessarily incomplete and apologies for omissions are sincerely offered. It reflects the bias of the synthetic chemist who is lead author on this chapter, and it is intended to as efficiently as possible provide the background for the inspiration from hydrogenases in twenty-first century goals for sustainable catalysts from solar energy. It also inscribes an amazing span of scientific eras in biological techniques, most of which are beyond the knowledge of the author. Appreciation abounds for those who truly understand the origins of the microbes that harbor such fragments of organometallic chemistry, microbes that Paulette Vignais and coworkers [1–3], patiently and extensively catalogued and organized for our referral in decades to come. Our focus in this chapter is on the organometallic concepts that define mechanisms in hydrogenases.

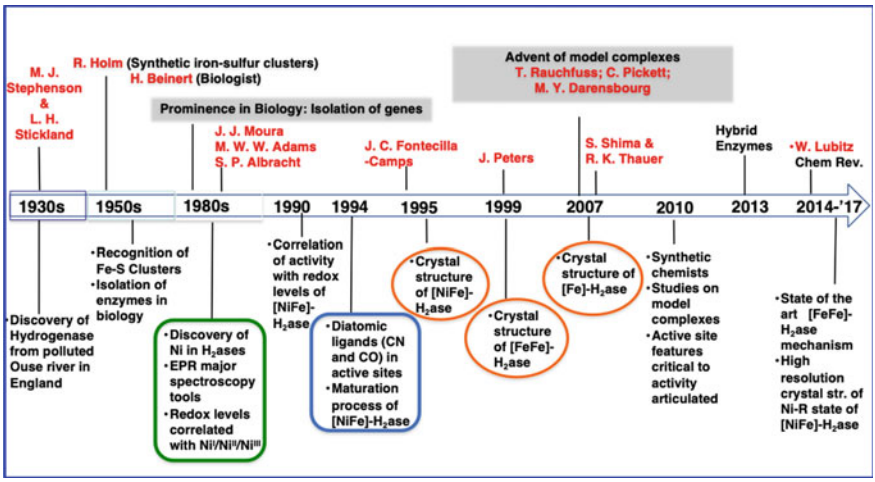

Fig. 1 Timeline for science of hydrogenase development

2 Introduction

The timeline (Fig. 1) for development and understanding of hydrogenase enzymes covers remarkable progress in the scientific interfaces of micro- and molecular biology. Beginning nearly a century ago, before isolation of single cells was common, as well as isolation of enzymes from them, the science of H_2ase's has advanced to the current point where structures of the crystallized giant biomolecules can be interrogated atom by atom in order to guide understanding of structure and function. Simultaneous advances in fundamental chemistry [4], especially the synthesis and isolation of self-assembled iron–sulfur clusters connected their natural inclusion and evolution as electron storage units and electron transport chains.

Special notice must be given to the Cambridge Laboratories and the research of Stephenson [5, 6], which established fundamental properties of hydrogenases derived from methanogens nearly a century ago. A historical review of the times and research of Stephenson is fascinating [7], demonstrating as it does scientific sleuthing on a practical problem of organic waste degradation and methane production by unidentified microbes in the river Ouse. Despite interruptions from service in World Wars, her persistence and devotion to bacterial metabolism, ultimately provided pivotal clues to the properties of the bidirectional hydrogenase enzymes, and their use in natural methane synthesis by archaea.

According to M. J. Stephenson and her coworker, L. H. Stickland, the microbes that thrived on the sugar beet waste did not produce alcohol, unlike yeasts, but lived via an anerobic metabolic pathway that made gases—hydrogen, carbon dioxide, and the "swamp gas", methane [4]. She found that their microbial cultures could chemically reduce methylene blue, in a Thunberg tube, in the presence of hydrogen but not nitrogen as an alternative. Thus, they established that the microbes contained an enzyme which was widespread, that could activate H_2, justifying their appellation of 'hydrogenase' [6].

In 1934, Green and Stickland demonstrated the reversibility of the reaction carried out by hydrogenases [8]. The equilibrium point for the H_2-induced reduction of methyl viologen was the same whether colloidal palladium or a bacterial suspension of hydrogenase was used as the catalyst [8]. They quantified their results over a wide range of H_2 partial pressures and H^+ ion concentrations and found that the calculated electrochemical potential was identical to that of a standard hydrogen electrode [8]. Following up on an earlier report [10], Stephenson and Stickland quantified the bacterial production of hydrogen to formate as 1:1 and formulated the reaction pathway seen in Fig. 2 [8].

Such results forecast the interest to come of possible technological development of the enzymes themselves, and the dream of synthetic chemists to develop molecular catalysts containing cheap first row transition metals as mimetics of hydrogenase active sites [9].

Such was the beginning of the hydrogenase story; indeed it was only a part of M. J. Stephenson's public lecture "How microbes live or some aspects of bacterial physiology" and her highly regarded publications and treatise, "*Bacterial*

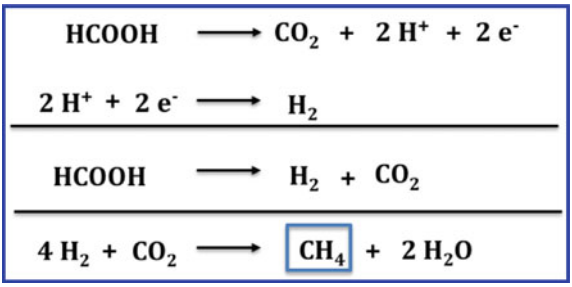

Fig. 2 Some reactions occurring in the methanogenic microbes. Although formate decomposes to H_2 and CO_2, it is not an intermediate in the methane production [8–10]

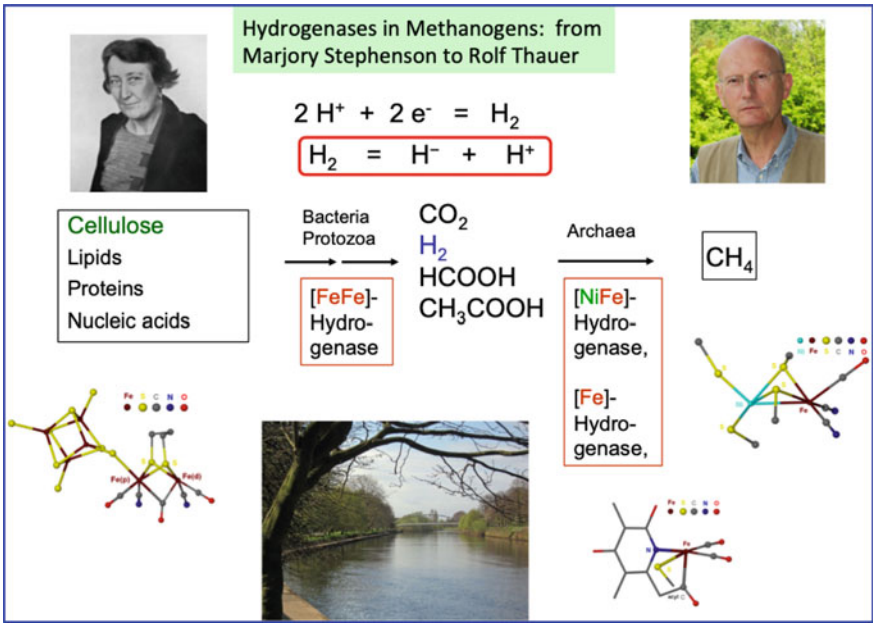

Fig. 3 Overview of the microbial cohort responsible for methane production from organic waste of sugar beet factory in the dark silt of the River Ouse, Cambridge, 1920/1930s (Figure gifted from Professor Thauer and modified to include stick structures of enzyme active sites.)

Metabolism" [11]. Before her death in 1948 Marjory Stephenson was elected Fellow of the Royal Society; a Prize for Microbiology in her name was established in 1955.

As the 50th recipient of the Stephenson prize in 1998, Professor Rolf Thauer of the Max Planck Institute for Terrestrial Microbiology in Marburg presented an updated understanding of the role of the different hydrogenases in the sequence of reactions explored by Stephenson and Stickland [12]. Kindly shared by Professor Thauer, the chemical parts of the graphic in Fig. 2 show that the [FeFe]-H_2ase is employed for the production of H_2 as the organic refuse is digested, while the [NiFe]-H_2ase is more suited to take up H_2, using it as an electron/energy bearing substrate in the subsequent reduction of CO_2 and the methane-producing reaction. Note that a poor cousin of the [NiFe]-H_2ase containing a single iron is also listed in the latter step. It will be described in a separate dedicated section.

The organisms responsible for this remarkable reaction are archaea; other anerobic processes requiring hydrogenases, such as sulfate, ferric and nitrate reducers, are found in myriad bacteria or protozoa [13, 14]. With O_2 as electron acceptor, Knallgas bacteria are, obviously, aerobes and much study has addressed the capability of these organisms to orchestrate hydrogen chemistry under aerobic conditions [15].

Some historical events critical to establishing the basis of organometallic chemistry in these enzymes follow. Electron paramagnetic spectroscopic studies in the 1980s detected various oxidation states of nickel that were used in attempts to understand the electrochemical control of an intricate mix of ready (rapidly reactivated) and unready (slow to reactivate) states of the hydrogenase known to contain both nickel and iron, [NiFe]-H_2ase [16, 17]. A decade later, a team of spectroscopists discovered that infrared spectroscopy could also be a diagnostic probe of redox levels, unexpectedly in the diatomic ligand region [18]. The ν(C≡X) three band IR pattern of the Ni-A unready state is almost identical to that of a classic piano-stool complex, $(\eta^5\text{-}C_5H_5)Fe(CO)(CN)_2^-$, Fig. 4 [19]. Used initially as a benchmark in vibrational spectroscopy, and manipulated by derivatization at the cyclopentadienyl ring and H-bonding at cyanide [20], this small molecular anion with its accessible spectroscopic handles encouraged synthetic chemists from the organometallic chemistry realm to apply their expertise and imagination towards biomimetic chemistry. Most recently it finds use as the iron unit in bimetallic constructions of import to synthetic analogues of the [NiFe]-H_2ase active site that are potential electrocatalysts for proton reduction or the Hydrogen Evolution Reaction (HER); or, alternatively, the H_2 reduction reaction, vide infra [21–23].

Certainly the decade spanning the twentieth and twenty-first century was the most influential for engaging synthetic chemists in attempts to model the active sites of enzymes that likely have metal hydrides as intermediates in their catalytic cycles. Figure 5 gives examples of various bacterial or archaea sources from which hydrogenases have been isolated, and with structures focusing on their active sites [24–31]. Many excellent reviews have focused on these structures [32–35]. We will explore them only as they relate to the mechanism of HER or H_2 oxidation.

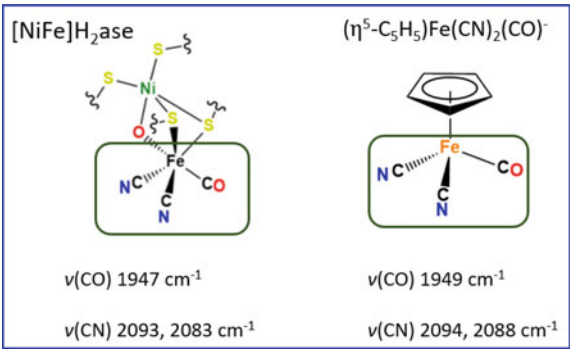

Fig. 4 Molecular structures from XRD of $(\eta^5\text{-}C_5H_5)$ $Fe(CO)(CN)_2^-$ in its protonated form [19]. The ν(CX) bands are almost identical to that of Ni-A [18], in which two cysteinyl-S from bridging thiolates and one bridging OH ligand mimic the $\eta^5\text{-}C_5H_5$ 6-electron donor

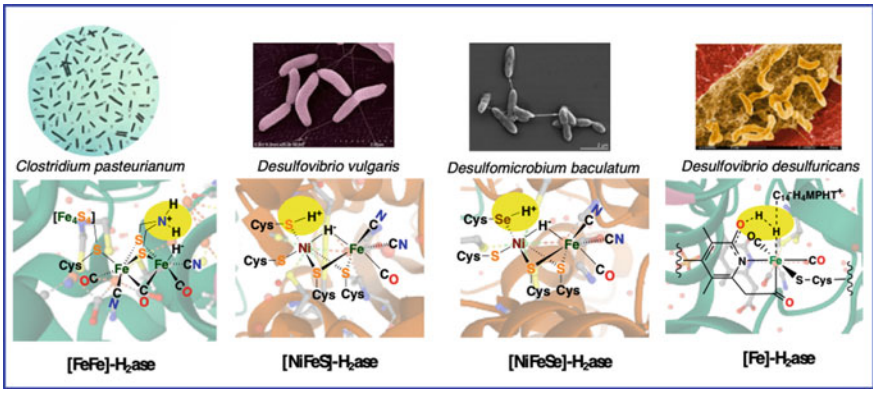

Fig. 5 The four known hydrogenase active sites rendered as XRD [27] or presumed structures in the act of H_2 heterolysis or heterogenesis. Selected microbes are taken from multiple possibilities [1–3] (Images used in figure are permitted from https://phil.cdc.gov/details.aspx?pid=2107; https://commons.wikimedia.org/wiki/File:Desulfovibrio_desulfuricans.jpg; https://link.springer.com/article/10.4056/sigs.13134/figures/2; https://www.flickr.com/photos/pnnl/3659555383 (Courtesy of Pacific Northwest National Laboratory))

3 Active Site Structures and Mechanism of Bimetallic Hydrogenases

Rarely have the structures of any biomolecular catalyst so obviously indicated design for their intended function as the hydrogenases. Certainly the entire proteins, their secondary and tertiary structures, are required for regulating proton and

electron access to the active sites, and account for the remarkable activity (with turnover frequencies as much as 9000 s^{-1}). Nevertheless the confluence of understanding of organometallic structure and bonding in the first coordination spheres of Ni and Fe, and the structural elements themselves, have propelled this area forward. Yet another factor, the promise of delivering molecular catalysts prepared from abundant, cheap metals (rather than Platinum) for conversion of sustainable energy sources (such as solar) to H_2 for energy storage [36–38] has provided a funding basis from national research institutes (Fig. 6).

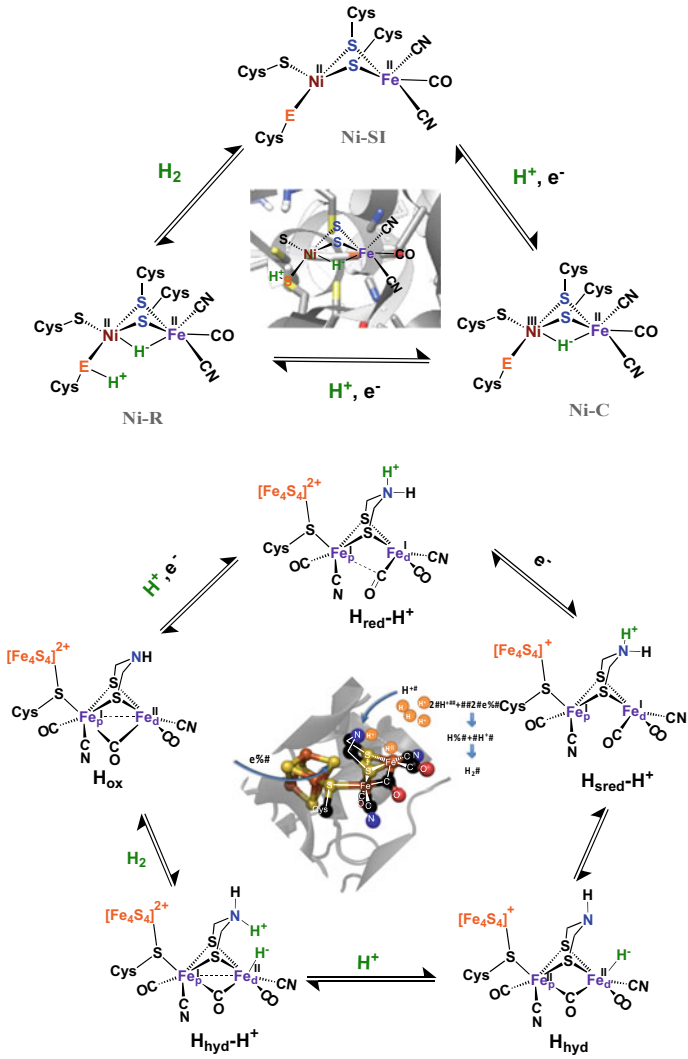

Fig. 6 Consensus mechanistic cycles of [NiFeE]- and [FeFe]-H_2ase (E = S or Se) [32, 46] The stick structures are drawn to match the XRD active site structures from single crystals that are placed in the center of each cycle

As indicated in Fig. 5 the [NiFe]-H_2ase family has two variants; the much more abundant, all cysteinyl form is better referred to as [NiFeS]-H_2ase while the selenium variant is known as [NiFeSe]-H_2ase. The impact of selenium on the activity of [NiFe]-H_2ase is to make it better, both in rates and in oxygen tolerance [39–41]. However the irregular biodistribution and scarcity of selenium, and the cost of biosynthetic pathways to the installation of Selenocysteine in the specific point required, leads to much smaller abundance of [NiFeSe]-H_2ase. For biology, it is something to learn from; for synthetic analogues as more robust artificial electrocatalysts, it should be considered to be a promising target [42, 43].

The currently accepted mechanisms for the two major hydrogenases are described in Fig. 6. While these biocatalysts evolved via separate phylogenetic paths, the convergent features required for proton/electron uptake, and H_2 formation via an H^+/H^- coupling process (or heterolytic H_2 cleavage) are readily seen [44–46]. Each are bimetallic with thiolate sulfur bridges between Ni and Fe or between the two irons in [FeFe]-H_2ase. Such thiolate sulfur bridges place the metals within bonding or semi-bonding distances so as to suggest the possibility of M-M bonding and electron delocalization. Both [NiFe]- and [FeFe]-H_2ase contain CO and CN^- ligands for maintaining low-valence, electron-rich iron via π-delocalization; the cyanide, both a good donor and π-acceptor ligand, additionally provides H-bonding connections to the protein. Both H_2ase active sites contain an open site on iron and a well-positioned "pendant" base for proton relay in the last step of proton delivery. For the [NiFe]-H_2ase duo, the cysteinyl sulfur is shown in Ni-R by crystallography to bind a proton in proximity to the hydride that is an asymmetric NiFe bridge, and largely on Ni [29]. Giving credence to the significance of the thiolate sulfur as a proton shuttle/pendant base indicated in Fig. 6, Nature positions selenium in the Se analogue in precisely that spot (Fig. 5) [40, 41] and accounts for the superior activity [NiFeSe]-H_2ase.

The pendant base in the [FeFe]-H_2ase is obviously the amine in the unique azadithiolate unit that creates two metallocyclohexane-type rings in the HN$(CH_2)_2S_2$Fe arrangement. Its efficacious design has been proven in hybrid enzyme studies where the NH has been replaced by O or CH_2 in synthetic diiron units [47–49]. Only the amine base works, achieving wild-type activity.

4 The Mono-iron Hydrogenase: From the Historical Conundrum of "Metal-Free" Hydrogenase

4.1 A Bit of History

The third hydrogenase class, the [Fe]-H_2ase, was recognized from its discovery, in 1992, to be distinctly different from both the [NiFe]- and [FeFe]-H_2ases [50]. Isolated from methanogenic archaea grown under nickel limitation in order to suppress the expression of the [NiFe]-H_2ase, the enzyme clearly did not contain any iron-sulfur clusters [50–52]. While preparations were found to contain up to 1 mol

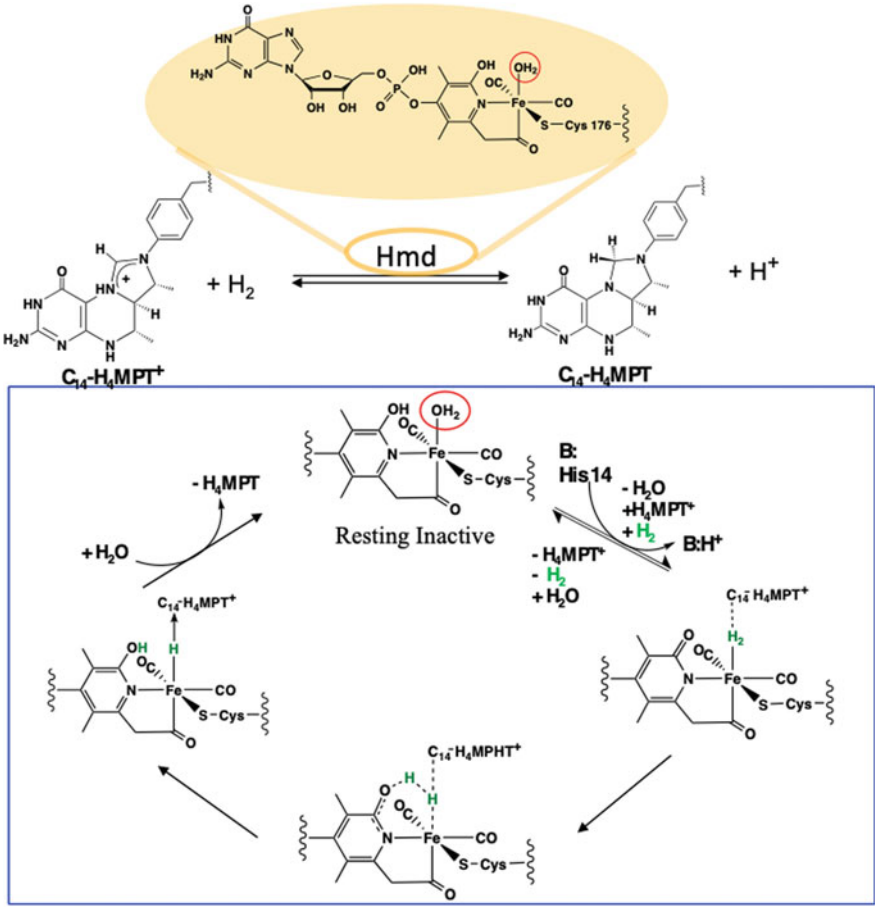

Fig. 7 In the oval are the cofactors of [Fe]-H_2ase, collectively Hmd, the catalyst for hydrogen splitting and hydride addition to the substrate, C_{14}-H_4MPT^+, yielding reduced product C_{14}-H_4MPT

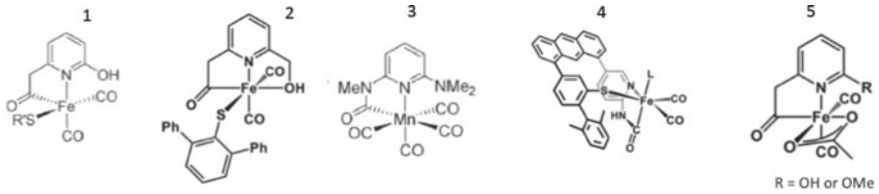

Fig. 8 Structure (1) truncated version of [Fe]-H_2ase active site; [65]. (2) An iron model faithful to the first coordination sphere of the active site; [77]. (3) An acyl-manganese analogue inspired by the [Fe]-H_2ase active site [78]. (4) Rose's anthracene platform [79]. (5) Hu and Shima's Fe-model used in hybrid enzyme preparations [80]

of iron per 40 kDa subunit, the iron was initially thought to be a contaminant [50, 53]. The enzyme is not redox active, as it does not oxidize H_2 or reduce protons; rather, this third hydrogenase heterolytically cleaves H_2 using its substrate methenyl-tetrahydromethanopterin as a stereo-selective hydride acceptor [50, 54–58]. For this reason, the enzyme was called the H_2-forming methylenetetrahydromethanopterin dehydrogenase, Hmd; it is better considered as a hydrogenation agent or catalyst. Methanogen expert Rolf Thauer and colleague Seigo Shima at the MPI Marburg are chiefly responsible for unraveling the complexities of this perplexing enzyme; however a community of spectroscopists such as Simon P. J. Albracht (Amsterdam), Albrecht Berkessel (Köln), Eckhard Bill (Mülheim), Ulrich Ermler (Frankfurt), Victor Fernández (Madrid), Christian Griesinger (Göttingen), and Wolfram Meyer-Klaucke (Hamburg) contributed much to the understanding [54, 56–72].

In 2000, recombinant over-expression of the enzyme in *Escherichia coli* led to the discovery of a cofactor that is necessary for its catalytic activity [73]. This cofactor, which could be extracted from the holoenzyme, readily recombines with apoenzyme to restore the enzyme's activity. Still, there was no indication at that time that the enzyme required a transition metal for its activity. For example, enzyme kinetics suggested that a ternary mechanism is employed for H_2 splitting, as opposed to a binary mechanism that would be indicative of the involvement of transition metals [53, 74]. Furthermore, the nearly colorless enzyme had activity that was not affected by the presence of 50% CO or acetylene in the gas phase [50].

A major clue to solve the conundrum of whether there was a metal in this hydrogenase was the finding that both the enzyme and the cofactor isolated from it were sensitive to light. Ultraviolet-A/blue-light inactivated and bleached the enzyme, accompanied by release of up to one mole of iron per subunit [75]. Furthermore, the enzyme was stabilized by the presence of CO in the gas phase. With 100% CO in the gas phase, the enzyme was reversibly inhibited by 50%. The final acceptance that CO was present in the active site, as light-sensitive, labile ligands to iron, resolved conflicts in the required vs. inhibitory CO at the active site [59]. At this point it was clear that the common name for Hmd, 'metal-free hydrogenase', was no longer accurate [75]. For this reason, Hmd is now referred to as the iron-sulfur-cluster-free hydrogenase or simply [Fe]-H_2ase, since it contains a singular iron center in its active site.

4.2 Determination of Active Site/Cofactor Structure

Removal of iron from the isolated cofactor, by light or heat inactivation, revealed the presence of a unique pyridone, (6-carboxymethyl-3,5-dimethyl-2-pyridone-4-yl)-(5′-guanosyl)phosphate [66]. As shown in Fig. 7 X-ray crystallography eventually showed this pyridone is coordinated to the iron through N as well as an Fe-acyl group involving an unusually short Fe–C bond [65, 68, 69]. It demonstrates yet another type of metal–carbon bond in biology. Albeit much more elaborate in its composition, the pyridone illustrates a non-protein-bound cofactor that orients its

OH to serve as a pendant base for heterolytic splitting of H_2, similarly to the azadithiolate in the [FeFe]-H_2ase. As with the diiron hydrogenase, a single cysteine is the sole covalent binding unit of the iron center to the protein, although van der Waals interactions to the overall cofactor are extensive. The current consensus mechanism is given in Fig. 7 [65, 81–85].

Further details from x-ray crystallography addressed the active site/substrate interaction, finding that methenyl-tetrahydromethanopterin binds in a π-fashion and leaves the active site geometry essentially unchanged [65]. The closest approach of the substrate to the iron is the hydride acceptor site, the methenyl carbon C-14, at 3.73 A. When bound in the active site, the aromatic heterocycle of the substrate is no longer planar, having a twist of 30° from aromaticity, presumably via hydrophobic interactions that activate the carbon for accepting the hydride.

4.3 Active Site Binding and Spectral Responses

Whereas protein crystallography satisfactorily solved most questions of the structure of the static [Fe]-H_2ase enzyme, the plethora of characterizations, spectroscopies observing transients on a fast time scale, and computations gave the needed fundamental support for the steps in H_2-uptake and splitting process given in the current state of understanding in Fig. 7 [65, 81–85].

The central metal complex gives tempting synthetic targets to synthetic chemists, however their/our plan to replace the 4 billion years of evolution that gives ideal electronic conditions for low barrier mechanistic pathways, usually meets with failure. Nevertheless, the assumed mechanistic pathway, made plausible or fleshed out by spectroscopic clues as to transient intermediates, can give hope that replacement of Nature's design of outer-sphere interactions with unusual synthetic components might illicit the desired catalytic properties. A discussion of some spectral properties follows.

Consistent with the snapshot from protein crystallography, the two CO molecules bound to the iron center display nearly identical intensities of the symmetric and asymmetric infrared bands indicating that the ligands are adjacent to one another, coordinated at nearly 90° [59]. The infrared bands are found to reversibly shift to lower frequencies when the pH was lowered, suggesting that an acidic group, with a pKa near 5, is in close proximity to the iron center. Furthermore, extrinsic CO was found to bind reversibly to iron, in a mirror plane bisecting the enzyme's intrinsically bound CO groups—i.e., the open site on iron. Similar to both the [NiFe]- and [FeFe]-hydrogenases, the intrinsically bound CO's do not exchange with extrinsic CO. Cyanide was found to reversibly bind to the active site and its binding is competitive with the extrinsic CO.

Binding of oxidized substrate, methenyl-tetrahydromethanopterin, CH = H_4MPT^+, or reduced substrate, methylene-tetrahydromethanopterin, CH_2 = H_4MPT, led to slightly higher infrared stretching frequencies for the intrinsic CO

ligands [59]. Most notable was the sharpening of the absorption bands, especially upon the binding of methylene-tetrahydromethanopterin, indicating a more rigid environment as a result of substrate binding. These changes in the shape and frequencies of the absorption bands were greater in the presence of H_2 when compared to Ar. These findings indicated that both the substrate and H_2 bind near to the iron center.

The mixture of hard and soft ligand donors to iron is likely the reason for alternate interpretations or conclusions from Mössbauer studies vs. X-ray absorption spectroscopy as to the redox states of iron. The former indicated that the active site is a diamagnetic mononuclear iron center, either low-spin Fe^{II} or low-spin Fe^0, with an isomer shift most consistent with Fe^0 [64]. In contrast the similarity of the K-edge and XANES to a low spin, octahedrally coordinated Fe^{II} complex, which contained two CO, suggested that the iron center in [Fe]-H_2ase is low-spin Fe^{II} [76]. While mixed hard/soft ligand environments are challenging for synthetic chemists, they are likely required for goals of eliciting noble metal-like catalysis from first row transition metals.

4.4 From Active Site Structure to Activity

The determination of the [Fe]-H_2ase active site structure again opened the door for synthetic chemists to attempt to mimic nature's design for application of heterolytic cleavage of H_2. It led to examples of rich heteroleptic environments in Fe^{II} complexes, typically based on pyridines substituted in the ortho position. The extensive review from Rose is recommended for description of the evolution of model complexes, demonstrating the stability of the iron(II) dicarbonyl moiety by strongly coordinated anionic ligands, including an acyl, a thiolate, and an OH group [82]. A report from Hu and Shima showed that complex 5 in Fig. 8 can be used in hybrid enzyme preparations [80]. That is, they found that reconstitution of the inactive apoenzyme with this complex led to a return of enzymatic activity. While reclaimed activity is not as impressive as was seen with the semi-synthetic [FeFe]-H_2ase [47–49] the lessons learned were that activity was reversible and dependent on the presence of the pyridone/pyridinol, i.e., the methylether version was inactive, thus confirming the pendant base role of the extraordinary cofactor [80].

5 The "Hydrogenase" that Comes from Nitrogenase

Interestingly, while H_2 is an intended product from some enzymes, it is a byproduct from other reactions, a good example of which is the nitrogen fixation reaction by Nitrogenase. To some degree, the "Nitrogenase" constitutes another type of Hydrogenase. In the absence of N_2, nitrogenases readily produce H_2; in its presence, at least one H_2 molecule is produced in each of the nitrogenases. The structure

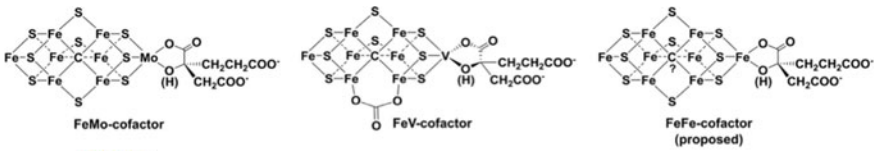

FeMo-co

$$N_2 + 16\ MgATP^{2-} + 8\ e^- + 8\ H^+ \longrightarrow 2\ NH_3 + 16\ MgADP^- + 16\ H_2PO_4^- + H_2$$

FeV-co

$$N_2 + 24\ MgATP^{2-} + 12\ e^- + 12\ H^+ \longrightarrow 2\ NH_3 + 24\ MgADP^- + 24\ H_2PO_4^- + 3H_2$$

FeFe-co

$$N_2 + 48\ MgATP^{2-} + 24\ e^- + 24\ H^+ \longrightarrow 2\ NH_3 + 48\ MgADP^- + 48\ H_2PO_4^- + 9H_2$$

Fig. 9 The active sites of three types of nitrogenases and the reactions that they catalyze. The structure of the FeMo-cofactor is known; the vanadium analogue is known to be similar and the iron analogue is presumed to be similar, but the structure is yet to be determined [86–88]

of the catalytic active sites of the three classes of nitrogenases and related chemical equations are found in Fig. 9 [86–88]. Its complexity has thus far defied precise mechanistic understanding at the individual atom level. However it is now understood that H_2 is an obligatory "byproduct"; its production is essential for the N_2 fixation [89, 90]. In the FeMo-co, the binding and activation of N_2 is reported to require the reductive elimination of H_2 [91]. Hoffman, et al., reported the push–pull model that demonstrates how reductive elimination (*re*) of H_2 might assist in N_2 activation, Fig. 10 [91]. Their hypothesis is that there is coupling of two H atoms, H_2, from two hydrides, $2H^-$, following the sequential uptake of $4H^+$ and $4e^-$. Such a maneuver generates electron-rich Fe, in a cluster configuration that is prime for N_2 binding and provides a "push" force for, while the H^+ bonding to sulfur provides a "pull" force, resulting in N_2 polarization and activation. This type (*re*) of H_2 production is also a possible mechanism for models of hydrogenase active sites, the $[M(N_2S_2)\cdot Fe(NO)_2]^+[Fe–Fe]^+$ (M = Fe(NO)) complexes under over-reduced conditions, vide infra [92].

Although there is no specific model complex for Nitrogenase's active site that only aims for H_2 production, all of the biomimetics for Nitrogenases produce H_2 in the presence of protons and electrons, the HER, and compete with N_2 for the Nitrogen reduction reaction (N_2RR) [93]. Different from the enzymes, the H_2 production from the biomimetics is not required for N_2 fixation; indeed, it is usually a competitively catalyzed reaction [94]. Nevertheless, in the absence of added N_2, these synthetic Nitrogenase complexes are transformed to Hydrogenase biomimetics and only produce H_2 under electrochemical conditions and added H^+.

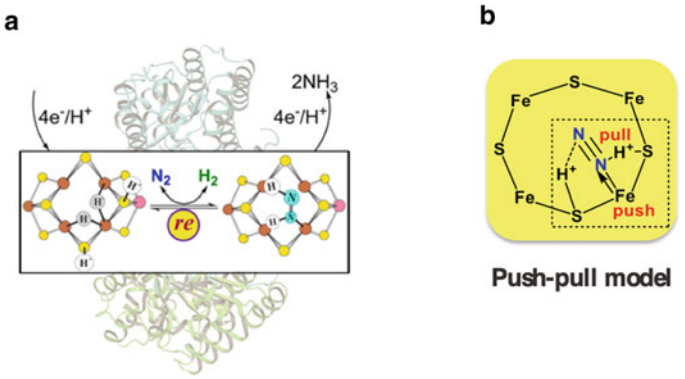

Fig. 10 **a** the reductive elimination (*re*) of H_2 during the N_2 fixation and **b** the proposed "push–pull" model that illustrates the proposal that *re* is necessary for N_2 binding and activation [89]. Graphic **a** is reproduced with permission from Ref. [90]

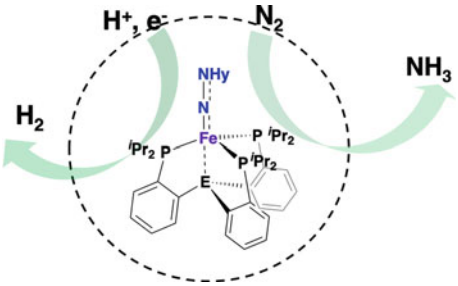

Fig. 11 HER versus N_2RR in model complexes (E = B, C or Si) for the active sites of Nitrogenase [93]

6 Features of Active Sites of [FeFe]- and [NiFe]-H_2ases Built into Synthetic Analogues for Hydrogen Production or Activation

While reductive elimination of two H• atoms forming H_2 has its overall rewards in the Nitrogenase cycle, proton/hydride coupling/decoupling of H_2 is less energy intensive by *ca.* 30 kcal/mol [12]. As illustrated in Fig. 6 the assistance of a strategically positioned base is key to lowering the barrier to heterolytic cleavage and the obvious base in the [FeFe]-H_2ase active site is the secondary amine in the bridgehead of the azadithiolate linker between the two irons [94]. This pendant base within a 6-membered ring reminded DuBois and colleagues of tetradentate bis-phosphine ligands (P_2N_2 ligands), inspiring the development of a family of Ni

$(P_2N_2)_2$ electro-catalysts that reproduce features displayed in the [FeFe]-H_2ase active site, **2** in Fig. 12 [95]. The conformation imposed by the NiP_2C_2N ring that mimics the FeS_2C_2N unit in [FeFe]-H_2ase is ideal for proton relay in the final step of H^+/H^- coupling or decoupling, as suggested in the third structure of Figs. 12 and 13, as an expected transition state [96]. A stable form of this $H^{\delta+}/H^{\delta-}$ structure was also reported from the PNNL group, using the versatile $(\eta^5\text{-}C_5H_5)Fe$ platform to provide the setting for heterolytic H_2 binding [96]. It should be noted that the Mary and Dan Dubois catalyst, Complex 2 and analogues, and modified versions explored in detail by Bullock, Helm etc. [97, 98] are not structural mimics of either the [FeFe]- or the [NiFe]-H_2ase, but rather use features of both in a mononuclear complex and the knowledge of coordination geometry preferences of reduced nickel. That is, the flexibility of the P_4 binding environment can switch between square planar and tetrahedral, and readily stabilize a Ni^0 that might connect structures 2 and 3. Such molecular gyrations would be conducive to the oxidative addition of a proton should the nickel indeed exist as Ni^0, generating a Ni^{II}-H. It has been elaborated to explore 2nd and 3rd coordination sphere effects that impact the efficacy of the catalyst [99, 100].

An obvious and readily available precursor to the [FeFe]-H_2ase active site, $(\mu\text{-}S(CH_2)_3S)[Fe(CO)_3]_2$ or $(\mu\text{-pdt})[Fe(CO)_3]_2$, Fig. 13, has performed outstandingly for the interrogation of fundamental chemistry related to the active site functions such as CO-ligand exchange, derivatization at the bridgehead in the S to S linker, fluxionality and stereospecific site exchange reactivity [101]. It connected computational studies with the effect of redox level on stereochemistry that would lead

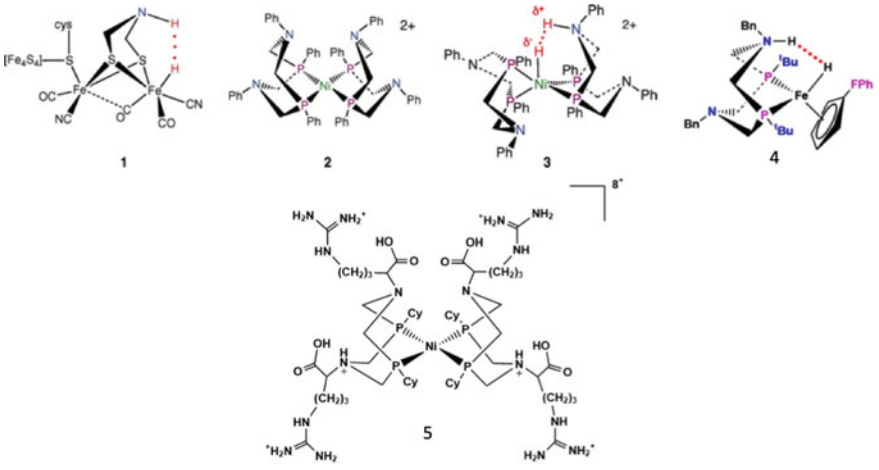

Fig. 12 The heterolytic H_2 formation or splitting in the [FeFe]-H_2ase that inspired the pendant base P_2N_2 ligand complexes of nickel from the Pacific Northwest National Laboratory team. Structure **4** is from a neutron diffraction analysis of an asymmetrical trapped and polarized H_2 [96]. Structure **5** is a modification of complex **2** with peptidic appendages that afford insight into 2nd and 3rd coordination sphere effects particularly on proton delivery [99, 100]

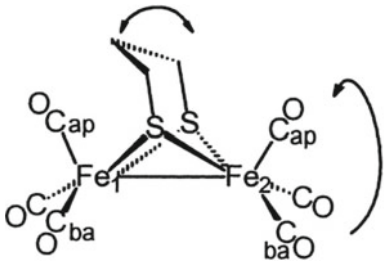

Fig. 13 The simple (μ-pdt)-$[Fe(CO)_3]_2$ complex that has served as synthon and inspiration for hundreds of diiron derivatives as synthetic analogues of the [FeFe]-H_2ase active site. Its fluxional characteristics (stereochemical non-rigidity) in the FeS_2C_3 ring and the CO ligands are indicated [101]

to isolation of "rotated structures" [102] as a transition state structure in the neutral diiron complex became the stable form in the one-electron oxidized structure that had the diminished Fe–Fe bond order. It showed effects of steric encumbrance at the bridgehead of the S to S linker [103]. It formed the basis of hybrid enzymes prepared from the dicyano aza-dithiolate, (μ-adt)$[Fe(CN)(CO)_2]_2^{2-}$ that illustrated artificial maturation of the [FeFe]-H2ase [47, 49].

Despite its lack of several critical features, e.g., the CN^- ligands, the N-bridgehead as pendant base, or a stable mixed-valent "rotated" structure, the classic (μ-pdt)$[Fe(CO)_3]_2$ has even been shown to be an electrocatalyst for proton reduction [104]. An early computational mechanism for the uptake of electrons and protons in the catalytic cycle of the HER catalyzed by (μ-pdt)$[Fe(CO)_3]_2$ was the harbinger of a better electrocatalyst based on arene-dithiolates from the Arizona laboratory of Lichtenberger, Glass, et al., Fig. 14 [105]. A shift of the μ^2-bridging dithiolate into a mono-thiolate bridge opens up the dimeric iron to provide considerable asymmetry and the potential for proton landing into the Fe–Fe bond density. It simultaneously creates a base site on the sulfur in proximity to the hydride. Addition of the second proton to the doubly reduced species likely occurs on the mono-dentate thiolate. Even better performances of this system were seen with modifications of the arene that permitted its incorporation into a water-soluble polymer [106]. In that case, H_2 production occurs in neutral water with a catalytic rate of $2.5 \times 10^5\ s^{-1}$ and a turnover number on the order of 40,000 under both anaerobic and aerobic conditions with loadings as low as 2 ppm [106].

A phosphine-substituted version of (μ-pdt)$[Fe(CO)_3]_2$, developed in the Rauchfuss laboratory, offers other features, finding a stable rotated structure that provides an open site on iron, it permits H^+/H^- coupling (in the computational mechanism), and it has as well the efficient amine base proton relay [107, 108]. Here we see the agility of the diphosphine ligand that was key to the success of the Dubois' catalyst in stabilizing the lower oxidation state and altered coordination geometry of reduced nickel. In the diiron case, there is further stabilization offered by the bridging CO and the "come and go" Fe–Fe bonding interaction assists in the

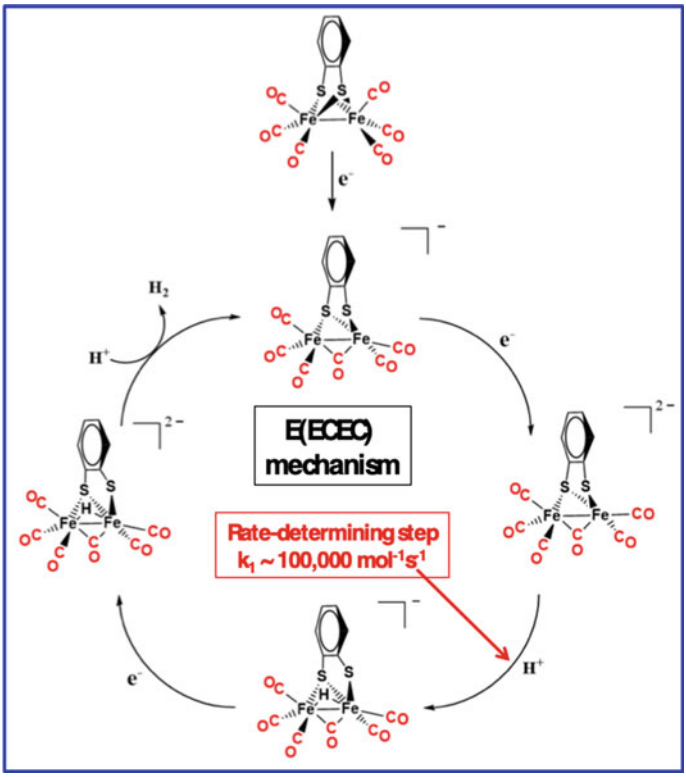

Fig. 14 Calculated electrochemical mechanism for the benzene-dithiolate diiron hexacarbonyl as proton reduction catalyst

two electron uptake prior to proton addition at iron and conversion to an iron-hydride. Such a result as described in Fig. 15 emphasizes the imaginative synthetic vistas opened up in pursuit of molecular H^+ reduction electrocatalysts.

Hemi-lability and Redox Activity in Heterobimetallic Complexes for HER Electrocatalysis. While it is accepted that the combination of protein features with organometallic active sites is the only way to even come close to the extraordinary activity of the enzymes, the basic principles of these active sites may be used to advantage in new creations and new concepts. The $(\eta^5\text{-}C_5H_5)Fe(CO)(CN)_2^-$, so useful for mimicking the diatomic ligands in the three legs of the piano-stool, has been extensively used when turned on its head, using the 6-electron donor (η^5-$C_5H_5^-$) as surrogate for the three diatomic ligands of the [NiFe]H_2ase, permitting the synthesis of bridging dithiolate heterobimetallics such as the cationic NiFe complex shown in Fig. 16 and many analogous complexes [21–23]. These have been collected and displayed in various publications, and we will describe only those that are from our work here [21, 92, 109, 110].

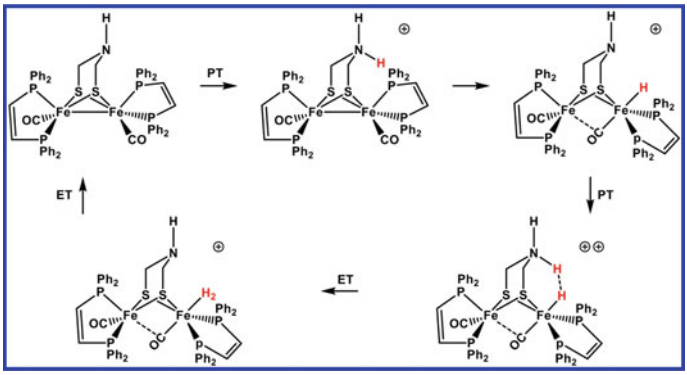

Fig. 15 Calculated mechanism for proton reduction to H_2 in the Rauchfuss azadithiolate, diiron dppv complex [107, 108]

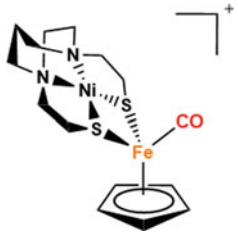

Fig. 16 Alternate view of the NiN_2S_2-Fe(CO)Cp structure. The 6-electron $(\eta^5\text{-}C_5H_5)^-$ donor is a surrogate for 2 CN^- and one CO ligand of the [NiFe]-H_2ase active site, Fig. 3

The matrix shown in Fig. 17 of electrocatalysts for the HER reaction was originally conceived for synthetic analogues of the [NiFe]-H_2ase active site containing features that might be compared in a structure/function relationship. Each of the complexes show electrocatalytic responses to added electrons and protons in electrocatalysis and controlled potential solution studies.

The mechanisms differ in the position of those electrochemical responses and to the strength of the acid, according to the availability of the electron buffering NO, i.e., the presence of a redox active ligand. As shown in Fig. 17, the NiFe and FeFe complexes are characterized as Hard and Soft, an analogy to acid/base designations, however here Hard/Soft refers to the absence or presence of electron-delocalizing NO ligands either on the metallodithiolate donor ligand or the iron acceptor. For example, the $[Fe(NO)]N_2S_2$ metallodithiolate ligand is classified as a "soft" donor relative to NiN_2S_2, a hard donor reflecting the electron densities on the donor thiolate sulfurs. Similarly the $Fe(NO)_2$ unit is a "soft" acceptor, while the $(\eta^5\text{-}C_5H_5)$ Fe unit is "hard". For the metallodithiolate donors, the reversible one-electron

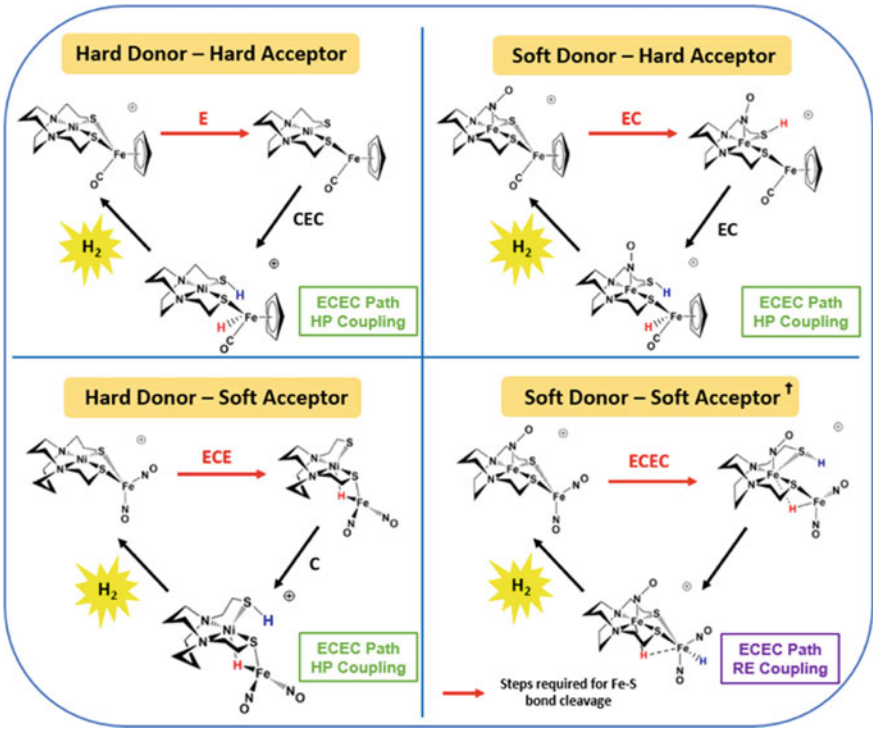

Fig. 17 Electrocatalytic H_2 evolution from M-MN_2S_2 heterobimetallic complexes that contain hard donor-hard acceptor (top left), soft donor-hard acceptor (top right), hard donor-soft acceptor (bottom left), soft donor-soft acceptor (bottom right) units. In the case of soft donor-soft acceptor, calculations have shown the possibility of converting the starting material to final intermediate after ECEC steps without cleaving the Fe–S bond [92]

reduction potentials are a numerical approach to quantifying the difference in donors: *ca.* −2.7 V for the NiN_2S_2 and −1.7 V for the $[Fe(NO)]N_2S_2$ relative to Fc/Fc^+ = 0.00 V.

These differences control the position of the first-added electron in the cyclic voltammograms of the NiFe complexes containing the "hard" acceptor as well as the proton/electron level that defines the ultimate coupling process. Figure 18 illustrates the hypotheses behind selection of sample structures to calculate according to landing sites for protons that remain protonic (blue sites) or hydridic (green, the hydrides on iron or nickel). The purple arrows represent points of bond breaking as electron density builds up on the iron acceptor. As mentioned above, cleavage of the iron-sulfur donor provides landing sites for proton uptake both at sulfur and at iron. DFT calculations correlate the pKa and $E_{1/2}$ of these processes, and relate to observed electrochemical events.

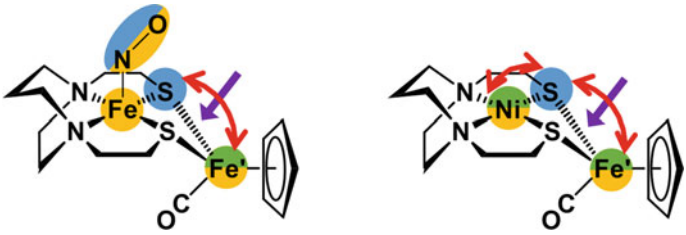

Fig. 18 Hypotheses for sequential electron and proton uptake in bimetallic complexes with a "soft" vs. "hard" metallodithiolate donor and a "hard" acceptor in each case. Yellow circles indicate possible sites to store the incoming electrons; while possible landing sites for protons are colored by the hydrogen's electronegativity after binding: blue (electropositive) and green (electronegative). The purple arrow represents Fe–S bond cleavage and the red arrow represents proton-hydride coupling routes. The computational results expressed in Fig. 17 are founded on the organometallic concepts of electron counting, delocalization, and structural preferences

The take-home message of Fig. 17 is that although there is no obvious pendant base in any of these complexes, the computational analysis that addressed addition of protons and electrons, found reaction pathways that recognized the cleavage of bridging thiolate and offers a reasonable path for H^+/H^- coupling. That is, if needed the bridging thiolates can turn themselves into a pendant base. Nevertheless, the electron delocalization on both sides of the $Fe_2(NO)_3$ derivative, is suggested to produce two iron hydrides without the need for the $SH^{\delta+} -^{\delta}HFe$ directing effect. In that case the hydrides are sufficiently close to couple as H atoms. An experimental confirmation or additional support of this theoretical calculation is at this time not available.

7 Concluding Remarks

From the dark recesses in pond and river silt where microbial pollution remediation occurred, into the light harvesting process that connects solar electrons and electrochemical cells, hydrogenases have proven to be of use in the solution of human-kinds problems either directly or through application of knowledge gleaned from studies of them. Certainly biology in all its forms has provided more exact conclusions; nevertheless hydrogenase-inspired chemistry research, in attempts to understand the intriguing active sites, has also made broad advances in many areas. An incomplete list from the last two decades follows:

- Synthesis of asymmetric/dissymmetric bimetallic binding sites;
- Spectroscopy to link fleeting signals to likely structures in mechanistic cycles;
- Interrogation of isolated enzymes by protein film voltammetry;
- Computations to reference spectroscopy in lead possibilities;
- Definition of roles of individual components in the active sites;

- Roles of chalcogens in the O_2/H^+ competition for biological reducing equivalents; and
- Development of "hybrid" enzymes, or loading of apo-enzymes with synthetic components for probing the peptide itself.

The major contribution from both chemistry and biology that will guide the future can be expressed in a single word: knowledge. There is no substitute for it.

Acknowledgements Most of the scientific contributions from the author and coworkers were produced with funds from the National Science Foundation, most recently grant number CHE-1665258 and the R. A. Welch Foundation, most recently, A-0924. Special appreciation is expressed to Professor M. B. Hall, a major contributor to the understanding of Hydrogenase mechanisms, and a long time collaborator of MYD.

References

1. Vignais PM, Billoud B (2007) Occurrence, classification, and biological function of hydrogenases: an overview. Chem Rev 107:4206–4272
2. Vignais PM, Billoud B, Meyer J (2001) Classification and phylogeny of hydrogenases. FEMS Microbiol Rev 25:455–501
3. Copeland A, Nolan M et al (2009) Complete genome sequence of desulfomicrobium baculatum type strain (X T). Stand Genom Sci 1:29–37
4. Bethel RD, Darensbourg MY (2015) The bioorganometallic Chemistry of hydrogenase. bioorganometallic Chemistry: applications in drug discovery, biocatalysis, and imaging, Jaouen G, Salmain M (eds). Wiley-VCH Verlag GmbH & Co, Weinheim, pp 241–272
5. Elsden SR (1981) Hydrogenase 1931–1981. Trends Biochem Sci 6:251–253
6. Stephenson MJ, Stickland LH (1931) Hydrogenases: a bacterial enzyme activating molecular hydrogen. Biochem J 25:205–214
7. Štrbáňová S (2016) Holding hands with bacteria: the life and work of Marjory Stephenson. Springer
8. Green DE, Stickland LH (1934) Studies on reversible dehydrogenase systems: The reversibility of the hydrogenase system of Bact. coli. Biochem J 28:898–900
9. Vincent KA, Cracknell JA, Lenz O et al (2005) Electrocatalytic hydrogen oxidation by an enzyme at high carbon monoxide or oxygen levels. PNAS 102:16951–16954
10. Pakes WCC, Jollyman WH (1901) The bacterial decomposition of formic acid into carbon dioxide and hydrogen. J Chem Soc Trans 79:386–391
11. Stephenson M (1949) Bacterial metabolism, 3rd edn. Longmans, Green and Co, London
12. Thauer RK (1998) Biochemistry of methanogenesis: a tribute to Marjory Stephenson. Microbiology 144:2377–2406
13. Vincent KA, Parkin A, Armstrong FA (2007) Investigating and exploiting the electrocatalytic properties of hydrogenases. Chem Rev 107:4366–4413
14. Conrad R (1996) Soil microorganisms as controllers of atmospheric trace gases (H_2, CO, CH_4, OCS, N_2O, and NO). Microbiol Rev 60:609–640
15. Goldet G, Wait AF, Cracknell JA et al (2008) Hydrogen production under aerobic conditions by membrane-bound hydrogenases from Ralstonia species. J Am Chem Soc 130:11106–11113
16. Moura JJG, Moura I, Huynh BH et al (1982) Unambiguous identification of the nickel EPR signal in 61Ni-enriched Desulfovibrio gigas hydrogenase. Biochem Biophys Res Commun 108:1388–1393

17. Teixeira M, Moura I, Xavier AV et al (1985) Electron paramagnetic resonance studies on the mechanism of activation and the catalytic cycle of the nickel-containing hydrogenase from Desulfovibrio gigas. J Biol Chem 260:8942–8950
18. Bagley KA, Duin EC, Roseboom W et al (1995) Infrared-detectable group senses changes in charge density on the nickel center in hydrogenase from Chromatium vinosum. Biochemistry 34:5527–5535
19. Darensbourg DJ, Reibenspies JH, Lai CH et al (1997) Analysis of an organometallic iron site model for the heterodimetallic unit of [NiFe] hydrogenase. J Am Chem Soc 119:7903–7904
20. Lai CH, Lee WZ, Miller ML et al (1998) Responses of the Fe $(CN)_2(CO)$ unit to electronic changes as related to its role in [NiFe] hydrogenase. J Am Chem Soc 120:10103–10114
21. Ding S, Ghosh P, Lunsford AM et al (2016) Hemilabile bridging thiolates as proton shuttles in bioinspired H_2 production electrocatalysts. J Am Chem Soc 138:12920–12927
22. Brazzolotto D, Gennari M, Queyriaux N et al (2016) Nickel-centred proton reduction catalysis in a model of [NiFe] hydrogenase. Nat Chem 8:1054–1060
23. Ogo S, Ichikawa K, Kishima T et al (2013) A functional [NiFe] hydrogenase mimic that catalyzes electron and hydride transfer from H_2. Science 339:682–684
24. Silakov A, Wenk B, Reijerse E, Lubitz W (2009) (14)N HYSCORE investigation of the H-cluster of [FeFe]-hydrogenase: evidence for a nitrogen in the dithiol bridge. Phys Chem Chem Phys 11:6592–6599
25. Winkler M, Senger M, Duan J et al (2017) Accumulating the hydride state in the catalytic cycle of [FeFe]-hydrogenases. Nat Commun 8:1–7
26. Nicolet Y, Lemon BJ, Fontecilla-Camps JC, Peters JW (2000) A novel FeS cluster in Fe-only hydrogenases. Trends Biochem Sci 25:138–143
27. Volbeda A, Charon MH, Piras C et al (1995) Crystal structure of the nickel–iron hydrogenase from Desulfovibrio gigas. Nature 373:580–587
28. Ogata H, Nishikawa K, Lubitz W (2015) Hydrogens detected by subatomic resolution protein crystallography in a [NiFe] hydrogenase. Nature 520:571–574
29. Garcin E, Vernede X, Hatchikian EC et al (1999) The crystal structure of a reduced [NiFeSe] hydrogenase provides an image of the activated catalytic center. Structure 7:557–566
30. Hiromoto T, Ataka K, Pilak O et al (2009) The crystal structure of C176A mutated [Fe]-hydrogenase suggests an acyl-iron ligation in the active site iron complex. FEBS Lett 58:585–590
31. Fontecilla-Camps JC, Volbeda A, Cavazza C, Nicolet Y (2007) Structure/function relationships of [NiFe]-and [FeFe]-hydrogenases. Chem Rev 107:4273–4303
32. Lubitz W, Ogata H, Rüdiger O, Reijerse E (2014) Hydrogenases. Chem Rev 114:4081–4148
33. Schilter D, Camara JM, Huynh MT et al (2016) Hydrogenase enzymes and their synthetic models: the role of metal hydrides. Chem Rev 116:8693–8749
34. Thauer RK (2011) Hydrogenases and the global H_2 cycle. Eur J Inorg Chem 2011:919–921
35. De Lacey AL, Fernandez VM, Rousset M, Cammack R (2007) Activation and inactivation of hydrogenase function and the catalytic cycle: spectroelectrochemical studies. Chem Rev 107:4304–4330
36. Cammack R, Frey M, Robson R (eds) (2001) Hydrogen as a fuel: learning from nature. CRC Press
37. Eberle U, Felderhoff M, Schueth F (2009) Chemical and physical solutions for hydrogen storage. Angew Chem Int Ed 48:6608–6630
38. Reece SY, Hamel JA, Sung K et al (2011) Wireless solar water splitting using silicon-based semiconductors and earth-abundant catalysts. Science 334:645–648
39. Reich HJ, Hondal RJ (2016) Why nature chose selenium. ACS Chem Biol 11:821–841
40. Baltazar CS, Marques MC, Soares CM et al (2011) Nickel–iron–selenium hydrogenases–an overview. Eur J Inorg Chem 2011:948–962
41. Wombwell C, Caputo CA, Reisner E (2015) [NiFeSe]-hydrogenase chemistry. Acc Chem Res 48:2858–2865

42. Yang X, Elrod LC, Reibenspies JH et al (2019) Oxygen uptake in complexes related to [NiFeS]-and [NiFeSe]-hydrogenase active sites. Chem Sci 10:1368–1373
43. Yang X, Elrod LC, Le T et al (2019) Controlling O_2 reactivity in synthetic analogues of [NiFeS]-and [NiFeSe]-hydrogenase active sites. J Am Chem Soc 141:15338–15347
44. Webster CE, Fan Y, Hall MB et al (2003) Experimental and computational evidence for a boron-assisted, σ-bond metathesis pathway for alkane borylation. J Am Chem Soc 125:858–859
45. Reijerse EJ, Pham CC, Pelmenschikov V et al (2017) Direct observation of an iron-bound terminal hydride in [FeFe]-hydrogenase by nuclear resonance vibrational spectroscopy. J Am Chem Soc 139:4306–4309
46. Siegbahn PE, Tye JW, Hall MB (2007) Computational studies of [NiFe] and [FeFe] hydrogenases. Chem Rev 107:4414–4435
47. Esselborn J, Muraki N, Klein K et al (2016) A structural view of synthetic cofactor integration into [FeFe]-hydrogenases. Chem Sci 7(2):959–968
48. Siebel JF, Adamska-Venkatesh A, Weber K et al (2015) Hybrid [FeFe]-hydrogenases with modified active sites show remarkable residual enzymatic activity. Biochemistry 54:1474–1483
49. Berggren G, Adamska A, Lambertz C et al (2013) Biomimetic assembly and activation of [FeFe]-hydrogenases. Nature 499:66
50. Zirngibl C, van Dongen W, Schwöre B et al (1992) H_2-forming methylenetetrahydromethanopterin dehydrogenase, a novel type of hydrogenase without iron-sulfur clusters in methanogenic archaea. Eur J Biochem 208:511–520
51. Afting C, Hochheimer A, Thauer RK (1998) Function of H_2-forming methylenetetrahydromethanopterin dehydrogenase from Methanobacterium thermoautotrophicum in coenzyme F_{420} reduction with H_2. Arch Microbiol 169:206–210
52. Afting C, Kremmer E, Brucker C et al (2000) Transcriptional regulation of the synthesis of H_2-forming methylenetetrahydromethanopterin dehydrogenase (Hmd) and of Hmd2 and Hmd3 in Methanothermobacter marburgensis. Arch Microbiol 174:225–232
53. Zirngibl C, Hedderich R, Thauer RK (1990) N^5, N^{10} -Methylenetetrahydromethanopterin dehydrogenase from *Methanobacterium* thermoautotrophicum has hydrogenase activity. FEBS Lett 261:112–116
54. Schleucher J, Griesinger C, Schwörer B, Thauer RK (1994) H_2-forming N^5, N^{10} -methylenetetrahydromethanopterin dehydrogenase from Methanobacterium thermoautotrophicum catalyzes a stereoselective hydride transfer as determined by two-dimensional NMR spectroscopy. Biochemistry 33:3986–3993
55. Klein AR, Hartmann GC, Thauer RK (1995) Hydrogen isotope effects in the reactions catalyzed by H_2-forming N^5, N^{10} -methylenetetrahydromethanopterin dehydrogenase from methanogenic Archaea. Eur J Biochem 233:372–376
56. Schleucher J, Schwörer B, Thauer RK, Griesinger C (1995) Elucidation of the stereochemical course of chemical reactions by magnetic labeling. J Am Chem Soc 117:2941–2942
57. Schwörer B, Fernandez VM, Zirngibl C et al (1993) H_2-forming N^5, N^{10} -methylenetetrahydromethanopterin dehydrogenase from Methanobacterium thermoautotrophicum. Studies of the catalytic mechanism of the H_2 formation with hydrogen isotopes. Eur J Biochem 212:255–261
58. Hartmann GC, Santamaria E, Fernández VM, Thauer RK (1996) Studies on the catalytic mechanism of H_2-forming methylenetetrahydromethanopterin dehydrogenase: para-ortho H_2 conversion rates in H_2O and D_2O. J Biol Inorg Chem 1:446–450
59. Lyon EJ, Shima S, Boecher R et al (2004) Carbon monoxide as an intrinsic ligand to iron in the active site of the iron-sulfur-cluster–free hydrogenase H_2-forming methylenetetrahydromethanopterin dehydrogenase as revealed by infrared spectroscopy. J Am Chem Soc 126:14239–14248
60. Berkessel A, Thauer RK (1995) On the mechanism of catalysis by a metal-free hydrogenase from methanogenic Archaea: enzymatic transformation of H_2 without a metal and its

analogy to the chemistry of alkanes in superacidic solution. Angew Chem Int Ed Engl 34:2247–2250
61. Teles JH, Brode S, Berkessel A (1998) Hydrogenation without a metal catalyst–an ab initio study on the mechanism of the metal-free hydrogenase from Methanobacterium thermoautotrophicum. J Am Chem Soc 120:1345–1346
62. Berkessel A (2001) Activation of dihydrogen without transition metals. Curr Opin Chem Biol 5:486–490
63. Berkessel A, Schubert TJ, Muller TN (2002) Hydrogenation without a transition-metal catalyst: on the mechanism of the base-catalyzed hydrogenation of ketones. J Am Chem Soc 124:8693–8698
64. Shima S, Lyon EJ, Thauer RK et al (2005) Mössbauer studies of the iron-sulfur-cluster-free hydrogenase: the electronic state of the mononuclear fe active site. J Am Chem Soc 127:10430–10435
65. Huang G, Wagner T, Wodrich MD et al (2019) The atomic-resolution crystal structure of activated [Fe]-hydrogenase. Nat Catal 2:537–543
66. Korbas M, Vogt S, Meyer-Klaucke W et al (2006) The iron-sulfur cluster-free hydrogenase (Hmd) is a metalloenzyme with a novel iron binding motif. J Biol Chem 281(41):30804–30813
67. Upadhyay V, Ceh K, Tumulka F et al (2016) Molecular characterization of Methanogenic N^5-Methyltetrahydromethanopterin: coenzyme M Methyltransferase. Biochim Biophys Acta Biomembr 1858:2140–2144
68. Shima S, Pilak O, Vogt S et al (2008) The crystal structure of [Fe]-hydrogenase reveals the geometry of the active site. Science 321:572–575
69. Hiromoto T, Ataka K, Pilak O, Vogt S et al (2009) The crystal structure of C176A mutated [Fe]-hydrogenase suggests an acyl-iron ligation in the active site iron complex. FEBS Lett 583:585–590
70. Hiromoto T, Warkentin E, Moll J et al (2009) The crystal structure of an [Fe]-hydrogenase-substrate complex reveals the framework for H_2 activation. Angew Chem Int Ed 48:6457–6460
71. Tamura H, Salomone-Stagni M, Fujishiro T et al (2013) Crystal structures of [Fe]-hydrogenase in complex with inhibitory isocyanides: implications for the H_2 activation site. Angew Chem Int Ed 52:9656–9659
72. Shima S, Lyon EJ, Sordel-Klippert M et al (2004) The cofactor of the iron-sulfur cluster free hydrogenase HMD: structure of the light-inactivation product. Angew Chem Int Ed 43:2547–2551
73. Buurman G, Shima S, Thauer RK (2000) The metal-free hydrogenase from methanogenic archaea: evidence for a bound cofactor. FEBS Lett 485:200–204
74. Ma K, Zirngibl C, Linder D et al (1991) N^5, ^{N1}0-Methylenetetrahydromethanopterin dehydrogenase ($_H$2-forming) from the extreme thermophile Methanopyrus kandleri. Arch Microbiol 156:43–48
75. Lyon EJ, Shima S, Buurman G et al (2004) UV—a/blue-light inactivation of the metal-free hydrogenase (HMD) from methanogenic archaea: the enzyme contains functional iron after all. Eur J Biochem 271:195–204
76. Salomone-Stagni M, Stellato F, Whaley CM et al (2010) The iron-site structure of [Fe]-hydrogenase and model systems: an X-ray absorption near edge spectroscopy study. Dalton Trans 39:3057–3064
77. Song LC, Zhu L, Hu FQ, Wang YX (2017) Studies on chemical reactivity and electrocatalysis of two acylmethyl(hydroxymethyl)pyridine ligand-containing [Fe]-hydrogenase models (2-$COCH_2$-6-$HOCH_2C_5H_3N$)$Fe(CO)_2L$ (L = η^1 -SCOMe, η^1 -2- SC_5H_4N). Inorg Chem 56:15216–15230
78. Pan HJ, Hu X (2020) Biomimetic hydrogenation catalyzed by a manganese model of [Fe]-hydrogenase. Angew Chem 132(12):4972–4976

79. Kerns SK, Magtaan AC, Vong P, Rose MJ (2018) Functional Hydride transfer by a thiolate-containing model of mono-iron hydrogenase featuring an Anthracene Scaffold. Angew Chem Int Ed 57:2855–2858
80. Shima S, Chen D, Xu T et al (2015) Reconstitution of [Fe]-hydrogenase using model complexes. Nat Chem 7:995–1002
81. Huang G, Wagner T, Ermler U, Shima S (2020) Methanogenesis involves direct hydride transfer from H_2 to an organic substrate. Nat Rev Chem 4:213–221
82. Rose MJ (2020) [Fe]-Hydrogenase (HMD): insights from enzyme structure, spectroscopy and synthetic models. In: Comprehensive coordination Chemistry III. Elsevier
83. Yang X, Hall MB (2009) Monoiron hydrogenase catalysis: hydrogen activation with the formation of a dihydrogen, Fe–H •••H–O, bond and methenyl-H_4MPT triggered hydride transfer. J Am Chem Soc 131:10901–10908
84. Finkelmann AR, Senn HM, Reiher M (2014) Hydrogen-activation mechanism of [Fe] hydrogenase revealed by multi-scale modeling. Chem Sci 5:4474–4482
85. Hedegård ED, Kongsted J, Ryde U (2015) Multiscale modeling of the active site of [Fe] hydrogenase: the H_2 binding site in open and closed protein conformations. Angew Chem Int Ed 54:6246–6250
86. Harris DF, Lukoyanov DA, Shaw S et al (2018) Mechanism of N_2 reduction catalyzed by Fe-nitrogenase involves reductive elimination of H_2. Biochemistry 57:701–771
87. Ribbe MW (Ed) (2011) Nitrogen fixation: methods and protocols. Springer
88. Sippel D, Einsle O (2017) The structure of vanadium nitrogenase reveals an unusual bridging ligand. Nat Chem Bio 13:956
89. Hoffman BM, Lukoyanov D, Yang ZY et al (2014) Mechanism of nitrogen fixation by nitrogenase: the next stage. Chem Rev 114:4041–4062
90. Lukoyanov D, Khadka N, Yang ZY et al (2016) Reductive elimination of H_2 activates nitrogenase to reduce the N-N triple bond: characterization of the E4(4H) Janus intermediate in wild-type enzyme. J Am Chem Soc 138:10674–10683
91. Hoffman BM, Lukoyanov D, Dean DR, Seefeldt LC (2013) Nitrogenase: a draft mechanism. Acc Chem Res 46:587–595
92. Ding S, Ghosh P, Darensbourg MY, Hall MB (2017) Interplay of hemilability and redox activity in models of hydrogenase active sites. PNAS 114:E9775–E9782
93. Matson BD, Peters JC (2018) Fe-mediated HER vs N_2RR: exploring factors that contribute to selectivity in $P_3^EFe(N_2)$ (E = B, Si, C) catalyst model systems. ACS Catal 8:1448–1455
94. Fan HJ, Hall MB (2001) A capable bridging ligand for Fe-only hydrogenase: density functional calculations of a low-energy route for heterolytic cleavage and formation of dihydrogen. J Am Chem Soc 123:3828–3829
95. Kilgore UJ, Roberts JA, Pool DH, et al (2011)$[Ni(P^{Ph}{}_2N^{C6H4X}{}_2)_2]^{2+}$ complexes as electrocatalysts for H_2 production: effect of substituents, acids, and water on catalytic rates. J Am Chem Soc 133:5861–5872
96. Helm ML, Stewart MP, Bullock RM et al (2011) A synthetic nickel electrocatalyst with a turnover frequency above 100,000 s^{-1} for H_2 production. Science 333(863–866):89
97. Liu T, DuBois DL, Bullock RM (2013) An iron complex with pendent amines as a molecular electrocatalyst for oxidation of hydrogen. Nat Chem 5:228
98. Liu T, Wang X, Hoffmann C et al (2014) Heterolytic cleavage of hydrogen by an iron hydrogenase model: an Fe–H⋯ H–N dihydrogen bond characterized by neutron diffraction. Angew Chem Int Ed 53:5300–5304
99. Dutta A, Roberts JA, Shaw WJ (2014) Arginine-containing ligands enhance H_2 oxidation catalyst performance. Angew Chem Int Ed 53:6487–6491
100. Ginovska-Pangovska B, Dutta A, Reback ML et al (2014) Beyond the active site: the impact of the outer coordination sphere on electrocatalysts for hydrogen production and oxidation. Acc Chem Res 47:2621–2630
101. Darensbourg MY, Lyon EJ, Zhao X, Georgakaki IP (2003) The organometallic active site of [Fe] hydrogenase: models and entatic states. PNAS 100:3683–3688

102. Hsieh CH, Erdem OF, Harman SD et al (2012) Structural and spectroscopic features of mixed valent $Fe^{II}Fe^{I}$ complexes and factors related to the rotated configuration of diiron hydrogenase. J Am Chem Soc 134:13089–13102
103. Singleton ML, Jenkins RM, Klemashevich CL, Darensbourg MY (2008) The effect of bridgehead steric bulk on the ground state and intramolecular exchange processes of $(\mu\text{-}SCH_2CR_2CH_2S)[Fe(CO)_3][Fe(CO)_2L]$ complexes. C R Chim 11:861–874
104. Chong D, Georgakaki IP, Mejia-Rodriguez R et al (2003) Electrocatalysis of hydrogen production by active site analogues of the iron hydrogenase enzyme: structure/function relationships. Dalton Trans 4158–4163
105. Felton GA, Vannucci AK, Chen J et al (2007) Hydrogen generation from weak acids: electrochemical and computational studies of a diiron hydrogenase mimic. J Am Chem Soc 129:12521–12530
106. Brezinski WP, Karayilan M, Clary KE et al (2018) [FeFe]-Hydrogenase mimetic metallopolymers with enhanced catalytic activity for hydrogen production in water. Angew Chem Int Ed 57:11898–11902
107. Olsen MT, Barton BE, Rauchfuss TB (2009) Hydrogen activation by biomimetic diiron dithiolates. Inorg Chem 48:7507–7509
108. Carroll ME, Barton BE, Rauchfuss TB, Carroll PJ (2012) Synthetic models for the active site of the [FeFe]-hydrogenase: catalytic proton reduction and the structure of the doubly protonated intermediate. J Am Chem Soc 134:18843–18852
109. Ghosh P, Ding S, Chupik RB et al (2017) A matrix of heterobimetallic complexes for interrogation of hydrogen evolution reaction electrocatalysts. Chem Sci 8:8291–8300
110. Ghosh P, Quiroz M, Wang N et al (2017) Complexes of $MN_2S_2{\cdot}Fe(\eta^5\text{-}C_5R_5)(CO)$ as platform for exploring cooperative heterobimetallic effects in HER electrocatalysis. Dalton Trans 46:5617–5624

Making Use of Biological Assets

Selective Enzymes at the Core of Advanced Electroanalytical Tools: The Bloom of Biosensors

Tiago Monteiro, Rosaceleste Zumpano, Célia M. Silveira, and M. Gabriela Almeida

Abstract

Enzymes are biological catalysts whose mission is to accelerate biochemical reactions in living organisms. Once extracted from cells they can be used in a broad range of applications for the benefit of humankind. One of the best examples is the so-called biosensor, i.e., a bioanalytical device where enzymes play a key role in the selective recognition of the analyte. Either as point-of-care tests, bench instruments, or continuous analysis systems, they have been useful in clinical diagnostics, environmental and food control, forensic sciences, and industrial processing, often replacing bulky and expensive equipment that require trained operators. Enzymes are by far the most commonly used biological elements in biosensors, being typically associated to electrochemical transducers, as in the case of the biggest commercial success, the blood glucose meter. In this context, redox enzymes are clearly dominant, since electrons exchange during the biochemical reaction facilitates their interaction with electrodes. However, hydrolases can also be used, provided that an electroactive species participates in the reaction. In this review, we address the topic of

T. Monteiro · C. M. Silveira · M. Gabriela Almeida (✉)
NOVA School of Science and Technology, UCIBIO, REQUIMTE, Campus de Caparica, Caparica, Portugal
e-mail: mg.almeida@fct.unl.pt

R. Zumpano
Department of Chemistry and Drug Technologies, Sapienza University of Rome, Rome, Italy

C. M. Silveira
Instituto de Tecnologia Química e Biológica António Xavier, Universidade NOVA de Lisboa, ITQB-NOVA, Oeiras, Portugal

M. Gabriela Almeida
Centro de Investigação Interdisciplinar Egas Moniz (CiiEM), Instituto Superior de Ciências Da Saúde Egas Moniz, Campus Universitário, Caparica, Portugal

J. J. G. Moura et al. (eds.), *Enzymes for Solving Humankind's Problems*,
https://doi.org/10.1007/978-3-030-58315-6_11

enzyme-based biosensors, with special emphasis on the electrochemical ones. The manuscript will cover four representative classes of enzymes, namely oxidases, dehydrogenases, reductases, and hydrolases.

Keywords

Enzymes · Oxidoreductases · Electrode · Electrochemical · Biosensors · Point-of-use tests

1 Introduction

Analytical chemistry plays a significant role in the control and monitoring of many anthropological activities, as different as health care, food control, agriculture and industrial processing, environmental, and security protection. Human progress constantly challenges analytical chemistry, thus promoting the continuous development of new methodologies, probes, and detection instruments for the quick, straightforward, and reliable examination of complex samples. Whenever possible, the analytical solutions should be portable and simple-to-use, enabling the shift from laboratory settings to on-site measurements. However, taking a sensitive and selective method to the field is a major challenge yet. One of the most exciting strategies relies on the integration of molecular recognition phenomena originated from biological systems, which are typically highly selective, sensitive, and fast, with a signal-transducing system that reflects the biorecognition event, and can be easily miniaturized, automated, and connected with a data transmission system. Such compact analytical devices are so-called biosensors. Briefly, a biosensor incorporates a biological sensing component—the biorecognition element—intimately associated with a physicochemical transducer. The output is a digital electronic signal that is proportional to the concentration of a target analyte or a related group of analytes [1, 2].

The history of biosensing devices started with the groundbreaking work of Leland C. Clark Jr., in 1962, describing an enzyme electrode for the first time. Building on the previously invented "Clark electrode" where O_2 is reduced at a platinum electrode, he demonstrated that the electrochemical detection of this species could be used to monitor the catalytic activity of O_2-consuming enzymes, like oxidases, upon immobilization on the electrode surface. Because the decrease in O_2 tension is stoichiometrically correlated with the consumption rate of the main enzyme substrate, this could serve as the basis for a broad range of bioanalytical applications. A glucose biosensor based on the entrapment of glucose oxidase was the first successful example, which was followed by a myriad of other enzyme electrochemical biosensors, either based on the assessment of the catalytic consumption of the co-substrate (O_2) or the formation of the also electroactive reaction product (H_2O_2), or even an artificial redox mediator. The first commercial glucose

analyzer, a benchtop instrument, was launched by Yellow Springs (Ohio, USA), between 1973 and 1975. In the late 80s and early 90s, several hand-held devices for glycemic control were successively commercialized, with a huge impact in the clinical diagnosis of diabetes mellitus. These point-of-care tests (POCT) are quick and easy to use, even by non-trained personal, enabling self-site monitoring of blood glucose levels [2, 3].

The concept of enzyme electrodes was further expanded to other biological materials, such as nucleic acids, antibodies, whole cells, and tissue slices. On the other hand, due to the rapid technological evolution that has taken place in the chemical sensors area, the concept of biosensing soon embraced a plethora of other transducing platforms, ranging from potentiometric and conductometric methods to optical, piezoelectric, thermometric, magnetic, and micromechanical techniques. The modern biosensing field has now reached a vast frontier of interdisciplinary R&D that combines biology, analytical chemistry, materials sciences, physics, electronics, and software programming, finding wide applications in biomedical research, food safety, process control, environmental monitoring, defense, and forensic analysis [1–3]. Nonetheless, the clinical diagnostics segment still dominates the market, where we can find the biggest opportunities, such as the glucose meters for diabetic patients. In 2019, the global biosensors market was valued at $21.2 billion, and is expected to grow in the next five years at a Compound Annual Growth Rate (CAGR) of 8.3% [4], fueled, in part, by the increasing demand for point-of-use testing in the medical diagnosis, and mandated control and monitoring in the industrial, and environmental sectors [1].

Electrochemical biosensors captured the largest market share, owing to their widespread applications, good analytical performance (wide linear response range, low detection limits, accuracy, reproducibility, long-term stability), independence from sample turbidity, low-cost, simplicity, robustness, portability, disposability, low power consumption, and compatibility with new microfabrication technologies [1, 5] and the fourth industrial revolution. This class of biosensors also dominates the R&D space, closely followed by optical biosensors. Enzyme electrochemical biosensors, in particular, keep a leading position. Among the over forty thousand documents published under the topic of “Biosensors” (data retrieved from the abstract & citation database Scopus, on 26th May 2020), about a third of all entries match the keywords “enzyme” and “electrode”. This is mainly due to the selectivity of detection usually conveyed by these biological catalysts, the easier access to different enzyme sources with broad catalytic activities, the facility in transducing the analyte recognition event, and the advances in protein engineering tools, which allow the customized modulation of the enzyme structural and activity features.

In this chapter, we aim at describing the main works concerning the development of enzyme biosensors, giving special emphasis to those based on electrochemical transducing systems. One should mention that all bioanalytical systems not including a physical transducer, i.e., where the output signal is not in the electric format (e.g., colorimetric test kits or lateral flow tests based on color visualization) were excluded from this review since they do not fall in the biosensors category. Among the different families of enzymes explored up to today, we will address the

oxidases (Sect. 2), dehydrogenases (Sect. 3), reductases (Sect. 4), and hydrolases (Sect. 5), each one representing a characteristic type of reaction for which specific transducing schemes have been developed. While hydrolases do not involve any exchange of electrons between reagents, the other three families belong to the oxidoreductases class. Oxidases and dehydrogenases, in particular, participate in substrate oxidation reactions, whereas reductases operate in the opposite direction (substrate reduction). In what concerns the transducing component, we will mainly focus on electrochemical dynamic techniques, which are based on current measurements at a "probe" (working electrode) as a function of a differential voltage that can either be time-dependent (voltammetric methods) or constant (amperometry). In the negative potential window (typically below −0.1 V vs. normal hydrogen electrode, NHE), dissolved O_2 can markedly interfere in the results, forcing solution deaeration before starting the assay. In order to avoid complex purging systems, several (bio)chemical O_2 scavenging systems have been used, including O_2 reducing enzymes, as described in Sect. 4.1.

2 Oxidases

2.1 Flavoenzymes

In this group of oxidases, the redox cofactor is a flavin (Table 1)—either flavin adenine dinucleotide (FAD) or flavin mononucleotide (FMN)—, which acts as the initial electron acceptor (Eq. 1) for the substrate's oxidation (e.g., glucose, lactate, alcohol). Afterward, the oxidized state of the cofactor is regenerated by reacting with O_2 (the final electron acceptor), leading to the formation of H_2O_2 (Eq. 2) [6–8]. Examples of such enzymes are glucose oxidase (GOx), alcohol oxidase (AOD), choline oxidase (ChOx), cholesterol oxidase (ChOD), glutamate oxidase (GluOx), lactate oxidase (LOx), and xanthine oxidase (XOD).

$$\text{Substrate} + \text{Enzyme}_{\text{FAD/FMN}} \rightarrow \text{Product} + \text{Enzyme}_{\text{FADH}_2/\text{FMNH}_2} \quad (1)$$

$$\text{Enzyme}_{\text{FADH}_2/\text{FMNH}_2} + \text{O}_2 \rightarrow \text{Enzyme}_{\text{FAD/FMN}} + \text{H}_2\text{O}_2 \quad (2)$$

GOx (Fig. 1a) is a FAD-dependent, homodimeric, glycosylated enzyme, with one tightly and non-covalently bound cofactor per monomer, which catalyzes the oxidation of β-D-glucose to D-1,5-gluconolactone, via a *ping-pong* mechanism [8, 9]. This oxidase belongs to the glucose-methanol-choline oxidoreductase superfamily (GMC), along with AOD, ChOx, and ChOD, with all members presenting common structural features, such as a highly conserved N-terminal FAD-binding domain and a less conserved C-terminal substrate-binding domain [10]. GOx has been isolated from several sources (e.g., red algae, bacteria, fungi), with the variant from *Aspergillus niger* being the most studied one [8, 9, 11]. This oxidase has been a very popular enzyme in several applications (e.g., clinical chemistry, energy, and

Table 1 Examples of oxidoreductase enzymes used in biosensors

Enzyme family	EC number	Enzyme	Cofactors	Source examples	Reduction potentials/ $E^{\circ\prime}$ vs. NHE	References
Oxidases	1.1.3.4	Glucose oxidase	FAD	*Aspergillus niger*	−99 mV (pH 7.6)	[62]
	1.17.3.2	Xanthine oxidase	Molybdenum (active site), [2Fe-2S], FAD	Bovine milk	−343 mV (Mo(VI/V)), −362 mV (Mo(V/IV))	[63]
	1.1.3.17	Choline oxidase	FAD	*Alcaligenes sp.*	−185 and −195 mV	[57]
	1.1.3.6	Cholesterol oxidase	FAD	*Streptomyces hygroscopicus*	−217 mV (pH 7.5)	[64]
	1.1.3.6	Cholesterol oxidase	FAD	*Brevibacterium sterolicum*	−101 mV (pH 7.5)	[64]
	1.1.3.2	Lactate oxidase	FMN	*Aerococcus viridans*	−128 mV	[65]
	1.10.3.2	Laccase	Type I and type II/III trinuclear copper	*Trametes versicolor*	520 mV (TI), 197 mV (TII), 360 mV (TIII), pH 5.8	[66]
	1.10.3.3	Ascorbate oxidase	Type I and type II/III trinuclear copper	*Cucurbita sp.*	420 mV (TI), 153 mV (TII), pH 6.8	[66]
	1.3.3.5	Bilirubin oxidase	Type I and type II/III trinuclear copper	*Myrothecium verrucaria*	546 mV (TI), 217 mV (TII), 385 mV (TIII), pH 5.8	[66]

(continued)

Table 1 (continued)

Enzyme family	EC number	Enzyme	Cofactors	Source examples	Reduction potentials/ $E^{\circ\prime}$ vs. NHE	References
Dehydrogenases	1.1.99.18	Cellobiose DH	FAD, heme *b*	*Pharenochaete chrysosporium*	100–160 mV (heme *b*)	[67]
	1.1.55	Alcohol DH	PQQ+ cyt *c*, heme *c* I, II_1, II_2, II_3	*Gluconobacter suboxydans*	−167 mV (PQQ), 101 mV (heme *c* I), 216 mV (heme *c* II_1), 370 mV (heme *c* II_2), 401 mV (heme *c* II_3)	[68]
	1.1.99.11	Fructose DH	PQQ+ cyt *c*, heme *c* I, II_1, II_2, II_3	*Gluconobacter sp.*	−183 mV (PQQ)	[69]
	1.1.5.2	Glucose DH	PQQ (active site)	*Escherichia coli*	156 mV (PQQ)	[70]
	1.1.2.B5	Pyranose DH	PQQ, heme *b*	*Coprinopsis cinerea*	130 mV (heme *b*)	[71]
	1.8.1.4	Diaphorase	FMN	*Bacillus stearothermophilus*	−325 mV (pH 8.5)	[72]
	1.8.2.1	Sulfite DH	Molybdenum, heme *c*	*Starkeya novella*	319 mV (Mo(VI/V)), −120 mV (Mo(V/IV)), 195 mV (heme *c*), pH 6[a]	[73]
	1.3.5.1	Succinate DH	[2Fe-2S], [4Fe-4S], [3Fe-4S], heme b_H, heme b_L, FAD	*Bacillus subtilis*	80 mV ([2Fe–S]), −240 mV ([4Fe–4S]), −25 mV ([3Fe–4S]), 65 mV (heme b_H), −95 mV (heme b_L)[a]	[74]
	1.5.8.2	Trimethylamine DH	FMN, [4Fe-4S]	bacterium W3A1	102 mV ([4Fe-4S]), 44 mV (FMN/FMN^-), 36 mV ($FMN^-/FMNH_2$)[a]	[75]
	1.4.9.1	Methylamine DH	PQQ	*Paracoccus denitrificans*	100 mV (PQQ)[a]	[76]

(continued)

Table 1 (continued)

Enzyme family	EC number	Enzyme	Cofactors	Source examples	Reduction potentials/ $E^{\circ\prime}$ vs. NHE	References
Reductases	1.7.1.1	Eukaryotic NaR	Molybdenum (active site), heme *b*, FAD	*Arabidopsis thaliana*	−300 to 15 mV range (all cofactors)	[77]
	1.7.5.1	Respiratory NaR	Molybdenum (active site), heme *b*, [4Fe-4S], [3Fe-4S]	*Escherichia coli*	200 mV (Mo(VI/V)) and 100 mV (Mo(V/IV))	[78]
	1.7.7.2	Dissimilatory NaR	Molybdenum (active site), heme *b*, [4Fe-4S]	*Rhodobacter sphaeroides*	550 mV (Mo(VI/V)) and −225 mV (Mo(V/IV))	[78]
	1.7.1.4	Assimilatory NaR	Molybdenum (active site), heme *b*, [4Fe-4S]	*Paracoccus denitrificans*	–	–
	1.7.7.1	Sirohemic NiR	siroheme (active site), [4Fe-4S]	*Spinacea oleracea*	−290 mV (active site)	[79]
	1.7.2.2	Cytochrome *c* NiR	penta-coordinated heme *c* (active site), hexa-coordinated heme *c*	*Desulfovibrio desulfuricans*	−80 mV (active site)	[80]
	1.7.2.1	Copper NiR	Type I and Type II (active site) copper	*Rhodobacter sphaeroides*	218 mV (active site, pH 6)	[81]
	1.7.2.1	Cytochrome cd_1 NiR	heme *c*, heme d_1 (active site)	*Marinobacter hydrocarbonoclasticus*	199 mV (active site, pH 7.6)	[82]
	1.7.2.5	NO reductase	heme b_3/non-heme FeB di-iron center	*Marinobacter hydrocarbonoclasticus*	−393 mV (active site)	[83]

(continued)

Table 1 (continued)

Enzyme family	EC number	Enzyme	Cofactors	Source examples	Reduction potentials/ $E^{\circ\prime}$ vs. NHE	References
			(active site), heme *b*, heme *c*			
	1.7.2.3	DMSO reductase	Molybdenum	*Rhodobacter sphaeroides*	144 mV (Mo(VI/V)) and 160 mV (Mo(V/IV))	[84]
	1.7.2.3	TMAO reductase	Molybdenum	*Escherichia coli*	∼−360 mV[b]	[85]
	1.97.1.1	Perchlorate reductase	Molybdenum (active site), [4Fe-4S], [3Fe-4S]	*Dechlorosoma sp.*	–	–
	1.8.1.7	Glutathione reductase	FAD (and a disulfide bond as the active site)	Wheat germ	−255 mV	[86]
	1.6.99.7	Nitroreductase	FMN	*Enterobacter cloacae*	−190 mV	[87]
	1.9.98.1	Cytochrome *c* reductase	heme *b*, heme c_1, [2Fe-2S] (Rieske)	Porcine heart	∼-200 mV (Fe(III/II))[b]	[88]

[a]Midpoint potentials. [b]Values were estimated from cyclic voltammetry data shown in the respective references. *cyt c* cytochrome *c*; *DH* dehydrogenase; *DMSO* dimethyl sulfoxide; *FAD* flavin adenine dinucleotide; *FMN* flavin mononucleotide; *NaR* nitrate reductase; *NiR* nitrite reductase; *NO* nitric oxide; *PQQ* pyrroloquinoline quinone; *TMSO* trimethylamine *N*-oxide

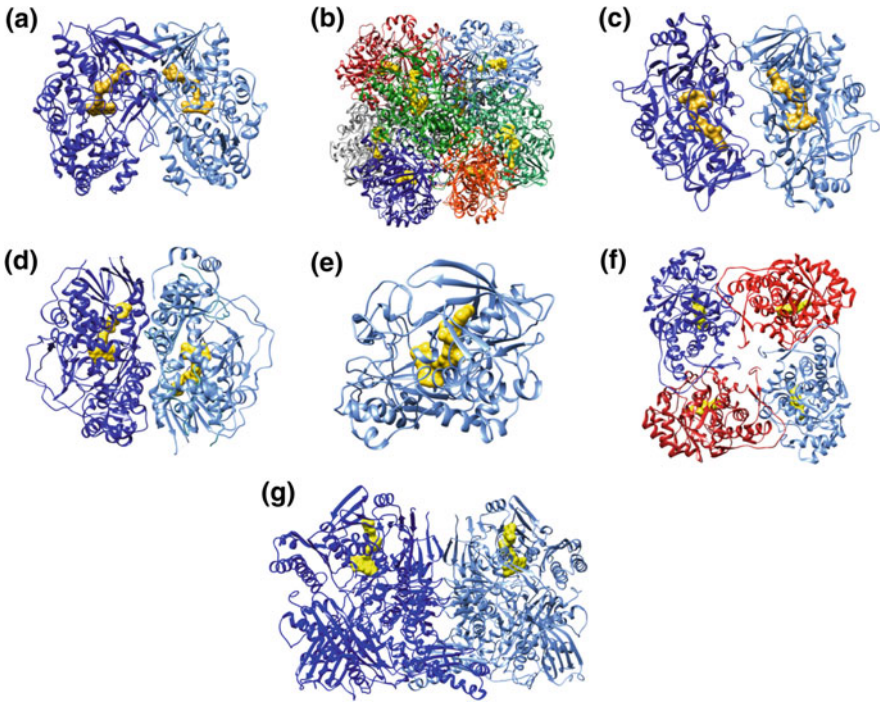

Fig. 1 Three-dimensional structures of flavoenzyme oxidases: **a** GOx from *Penicillium amagasakiense* (1GPE); **b** AOD from *Pichia Pastoris* (5HSA); **c** ChOx from *Arthobacter globiformis* (2JBV); **d** GluOx from *Streptomyces sp.* X-119-6 (2E1M); **e** ChOD from *Streptomyces sp.* (1B4V); **f** LOD from *Aerococcus viridians* (2J6X); **g** XOD from *Bos taurus* (1FIQ). Each monomer is represented in a different color. The FAD (**a**, **b**, **c**, **d**, **e**, **g**) and FMN (**f**) cofactors are represented in yellow. Structures were rendered using UCSF Chimera (version 1.13.1rc) and the respective entries (in brackets) from RCSB Protein Data Bank

food industries) due to its commercial availability, low-cost, stability, high activity, and substrate specificity [8, 12]. Also, the need for (bio)devices capable of monitoring glucose levels in patients suffering from diabetes mellitus has vastly contributed to the notoriety and widespread use of GOx in clinical bioelectrochemical applications [6, 13].

AOD (or methanol oxidase) catalyzes the oxidation of methanol (physiological substrate) and other short aliphatic alcohols, such as ethanol, propanol, and butanol, to the corresponding aldehyde [14–17]. This FAD-dependent enzyme is expressed in methylotrophic organisms that metabolize short primary alcohols as their main carbon and energy source, being identified in various yeast and filamentous fungi [15, 16]. The biologically active form of AOD (Fig. 1b) is generally that of a homo-octamer, with each monomer having a non-covalently bound FAD cofactor in the catalytic center [16, 17]. From an industrial application point-of-view, AOD possesses some interesting properties, such as the ability to selectively oxidize

several alcohols, being widely available from various aerobically grown sources, and not requiring the use of external cofactors for catalysis [15].

ChOx (Fig. 1c) is a homodimeric enzyme, like GOx, but the FAD cofactor is covalently bound to the respective monomer [18, 19]. ChOx catalyzes the four-electron oxidation of choline to glycine betaine, producing betaine aldehyde as an intermediate [18]. The enzyme has been applied in the development of biosensing devices for the indirect determination of acetylcholine, a major excitatory neurotransmitter implied in several neurological disorders [20]. Through the hydrolytic activity of acetylcholine esterase, the neurotransmitter is converted into choline, which can then be oxidized by ChOx with the concomitant production of electroactive H_2O_2 under aerobic conditions [20, 21]. The bacterial, dimeric, and FAD-dependent GluOx (Fig. 1d) has also been employed in the development of sensing devices for neurotransmitter detection, by catalyzing the oxidative deamination of glutamate to 2-ketoglutarate [22, 23]. The former is the principal excitatory neurotransmitter in the central nervous system, with excessive release into the cerebral extracellular space inducing neurotoxicity, and thus being implicated in several neurological disorders [23].

The monomeric ChOD catalyzes the oxidation and isomerization of cholesterol to cholest-4-en-3-one [24]. It is uniquely produced by several bacteria (e.g., *Arthobacter*, *Mycobacterium*, *Streptomyces*, *Rhodococcus*, *Brevibacterium*) that are capable of using cholesterol as a carbon and energy source [24–26]. The enzyme exists in two structurally diverse types that catalyze the same reactions: type I presents a non-covalently bound FAD cofactor and belongs to the GMC superfamily, found in *Streptomyces* (Fig. 1e) and *Rhodococcus*; type II contains a covalently bound FAD and is found in *Brevibacterium* and *Burkholderia* [26, 27]. Regarding clinical applications, ChOD has been used as an analytical probe in the determination of cholesterol in physiological samples (plasma, serum, gall stones, bile) [25, 28].

The multimeric LOx (Fig. 1f) catalyzes the conversion of α-hydroxy acids (e.g., lactate) to α-keto-acids (e.g., pyruvate), via a *ping-pong* mechanism [29]. The enzyme from the bacterial source *Aerococcus viridans* crystallizes as two tightly packed tetramers, with each one forming a biologically active unit [29, 30]. Each subunit contains one FMN cofactor deeply buried in the active site, as opposed to a FAD prosthetic group observed in other flavin-dependent oxidases [29, 30]. The substrate lactate is the key metabolite of the anaerobic glycolytic pathway, so its concentration in blood is an indirect biomarker of anaerobic glucose breakdown and cellular fatigue, being widely used in the clinical diagnostics for assessing patient health conditions and continuous surveillance in surgery, sports medicine, shock/trauma and food industry [31, 32]. Therefore, LOx has been applied in the development of lactate analytical devices, due to the combined simplicity of the enzymatic reaction and sensor design fabrication [32].

XOD differs from the aforementioned oxidases in respect to the cofactors present in the active site. The mammalian (human and bovine) enzyme is a homodimer Fig. 1g), with each monomer containing a molybdopterin cofactor, two spectroscopically distinct Fe–S clusters, and one FAD [33, 34]. The catalytic oxidation of

hypoxanthine to xanthine and then to uric acid occurs at the molybdenum center, with electrons being transferred intramolecularly via the Fe–S cluster to the FAD cofactor. The oxidized enzyme form is then regenerated when O_2 accepts electrons at the flavin center [34]. Another feature of this oxidase is that the mammalian sourced enzyme can exist in two reversible, interconvertible forms: xanthine dehydrogenase and XOD. The former prefers NAD^+ as the final electron acceptor, while XOD uses O_2 exclusively. The oxidation of specific sulfhydryl residues in the dehydrogenase form converts it reversibly into XOD, while the irreversible conversion is achieved via proteolysis [33, 35]. Key applications of XOD (and its dehydrogenase form) include metabolizing nitrogenous heterocyclic organic compounds (e.g., caffeine and hypoxanthine/xanthine), elimination of by-products in the synthesis of nucleoside analogs, clinical detection of xanthine/hypoxanthine content in physiological fluids, and biological remediation [36].

Flavin-dependent oxidases have been widely used in the construction of amperometric/voltammetric biosensors, being intimately related to the emergence of the field. As mentioned in Sect. 1, Leland C. Clark Jr developed the first biosensor ever proposed, a glucose biosensor based on GOx [37]. The enzyme was entrapped between semipermeable membranes fixed on the surface of an O_2 electrode. By coupling the catalytic oxidation of glucose with the localized depletion of O_2 levels, the indirect measurement of glucose concentration was achieved through a bioelectrochemical strategy. This analytical tool was the steppingstone for a myriad of biosensing devices that would soon follow [2, 38, 39]. In the late 80s and early 90s, a number of hand-held devices for glucose self-monitoring were made available to the public, which had an enormous impact on a clinical diagnosis of diabetes mellitus [2, 13, 39]. In present days, apart from glucose monitoring, which dominates the biosensor's market [3, 40], other clinically and industrially relevant analytes, such as lactate, cholesterol, and ethanol, drive the research focus towards novel, wearable, noninvasive, and/or smart tools based on flavin-dependent oxidases [41–45]. Table 2 summarizes some examples of amperometric/voltammetric bioanalytical tools designed for the detection of the mentioned analytes featuring such oxidases. For more detailed reviews, the reader is directed to references [14, 21, 23, 28, 46–48].

The analyte's detection by following the current associated with either the decrease in O_2 tension or the formation of H_2O_2 is a common protocol in amperometric/voltammetric sensors based on oxidases [13, 14, 21, 46, 49]. Such devices are classified as being first *generation biosensors*, where the communication between the redox enzyme and the electrode is done via a freely-diffusing, redox-active co-substrate (O_2 in this case) or co-product (H_2O_2) [2, 13, 50] (Fig. 2). However, this approach presents some disadvantages. The dependence on O_2 as the detection principle can lead to incorrect measurements since its concentration varies between samples. Given its restricted solubility in biological fluids, O_2 concentration may also be insufficient to guarantee the full oxidation of the analyte, requiring a sample dilution step in the detection protocol [2, 13, 51]. Finally, the oxidation of H_2O_2 requires quite positive overpotentials, which makes the analytical procedure prone to electrochemical interference from other redox-active species commonly

Table 2 Flavoprotein-based amperometric/voltammetric biosensors

Enz./Analyte	Device	Detection	Linear Range	Detection Limit	Sample	References
GOx						
Glucose	GOx/Carbon ink WE & Ag/AgCl RE integrated on dental floss	H_2O_2 oxidation	48 μM–12.5 mM	ND	Buffer	[45]
Glucose	GOx/AuNP/graphite electrode	PMS mediated	Up to 10 mM	100 μM	Buffer	[89]
Glucose	PPD/GOx-GA/platinum microelectrode array	H_2O_2 oxidation	Up to 4 mM	10 μM	Buffer, CES	[90]
Glucose	GOx/PtNP/PANI/microneedle array	H_2O_2 oxidation	2–12 mM	260 μM	Buffer, serum	[91]
AOD						
Ethanol	Wearable AOD/PB conductive carbon SPE	PB mediated	Up to 36 mM	ND	Buffer, sweat	[92]
Ethanol	Alginate-AOD-HRP/platinum electrode	TMB mediated	Up to 22 mM	800 μM	Buffer, blood	[93]
Ethanol	AOD/CNT WE and Ag/AgCl RE printed over cork	H_2O_2 oxidation	100 μM–1.7 mM	40 μM	Buffer	[44]
Ethanol	AOD/PB electrode cartridge integrated with a wristband	PB mediated	Up to 50 mM	ND	Buffer, sweat	[94]
LOx						
Lactate	LOx/PtNP-CNF-PDDA/carbon SPE	H_2O_2 oxidation	25 μM–1.5 mM	11.1 μM	Buffer, sweat	[31]
Lactate	LOx-PPD/PB carbon ink SPE integrated on a mouthguard	PB mediated	100 μM –1 mM 100 μM –500 μM	50 μM 10 μM	Buffer, saliva	[95]
Lactate	LOx/rGO-CNT-AuNP/platinum electrode	H_2O_2 oxidation	50 μM–100 mM	2.3 μM	Blood, milk	[96]
XOD						
Xanthine	XOD/MWCNT/glassy carbon electrode	DET	0.2–10 μM	0.1 μM	Buffer	[59]
Xanthine	XOD-AuNP/Chitosan-pyrrole/glassy carbon electrode	H_2O_2 oxidation	1–200 μM	0.25 μM	Meats	[97]

(continued)

Table 2 (continued)

Enz./Analyte	Device	Detection	Linear Range	Detection Limit	Sample	References
Hypoxanthine	(XOD-PDDA-MWCNT-Graphene)$_3$/carbon SPE	Uric acid oxidation	5–50 μM	4.4 μM	Serum	[98]
ChOD						
Cholesterol	PEI/(ChOx/PEI-rGO)$_3$/glassy carbon electrode	O_2 depletion	100 nM–9 mM	21 nM	Buffer, serum	[99]
Cholesterol	ChOD/PtNP/PANI/microneedle array	H_2O_2 oxidation	1–12 mM	440 μM	Buffer, serum	[91]
Cholesterol	ChOD/nickel oxide-platinum electrode with microfluidic channels	Ferricyanide mediated	120 μM–10 mM	100 μM	Buffer, serum	[100]
ChOx						
Choline	PEI$_{2\ \%}$/GA$_{0.5\ \%}$/BSA/ChOx/-MMA/CellAce/MMA/PPD/Pt electrode	H_2O_2 oxidation	Up to 100 μM	ND	Buffer, striatum (rat)	[20]
Choline	(PDDA/ChOx)$_3$/(PDDA/PAS)$_2$/MnO_2/SPE	H_2O_2 oxidation	0.3–100 μM	150 nM	Buffer	[101]
Choline	ChOx/RTIL/SWCNT/glassy carbon electrode ChOx/RTIL/MWCNT/glassy carbon electrode	DET DET	10–700 μM 100–800 μM	10 μM 100 μM	Buffer Buffer	[57]
GluOx						
Glutamate	GluOx/PtNP/gold nanoelectrode array	H_2O_2 oxidation	Up to 8 mM	14 μM	Buffer	[102]
Glutamate	BSA/AOx/GluOx/PPD/Pt electrode	H_2O_2 oxidation	5–150 μM	44 nM	Subthalamic nucleus (rat)	[103]
Glutamate	GluOx-PVA-SbQ/Pd electrode	H_2O_2 oxidation	50 nM–100 μM	50 nM	Buffer	[104]

AOx ascorbate oxidase; *AuNP* gold nanoparticles; *BSA* bovine serum albumin; *CellAce* cellulose acetate; *CES* cerebral extracellular space; *CNF* carbon nanofibers; *CNT* carbon nanotubes; *DET* direct electron transfer; *GA* glutaraldehyde; *HRP* horseradish peroxidase; *MMA* methyl methacrylate; *MWCNT* multi-walled carbon nanotubes; *ND* not determined; *PANI* polyaniline; *PAS* polyanethol sulfonate; *PB* Prussian blue; *PDDA* poly(diallyldimethyl ammonium chloride); *PEI* polyethylene imine; *PMS* N-methylphenazonium methyl sulphate; *PPD* poly-(m-phenylenediamine); *PQQ* pyrroloquinoline quinone; *PtNP* platinum nanoparticles; *PVA-SbQ* polyvinyl alcohol, N-methyl-4(4'-formylstyryl)pyridinium methosulfate acetal; *RE* reference electrode; *rGO* reduced graphene oxide; *RTIL* room temperature ionic liquids; *SPE* screen-printed electrode; *SWCNT* single-walled carbon nanotubes; *TMB* tetramethylbenzidine; *TNT* titanate nanotubes; *WE* working electrode

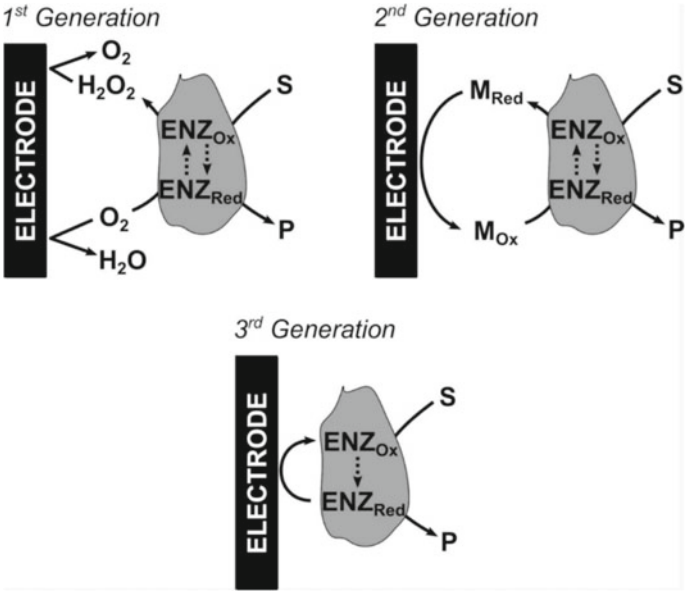

Fig. 2 Classification of enzyme-based amperometric/voltammetric biosensors according to the electron transfer (ET) mode between the bioreceptor (enzyme—ENZ) and the transducer (electrode). The given examples are for oxidases. 1st *generation* devices rely on monitoring natural diffusible mediators that take part in the reaction itself. 2nd *generation* devices rely on artificial redox mediators (M) for the electrochemical communication. In 3rd *generation*, the ET is made directly between the redox-active site of the enzyme and the surface of the electrode, without any intermediaries

present in physiological samples (e.g., ascorbic and uric acid) [2, 13, 52]. In order to decrease the necessary working potential, electron transfer (ET) mediators have been widely applied, where a redox molecule at a constant concentration serves as an electron shuttle (either free-diffusing or bound to an immobilization matrix) between the flavin cofactor and the surface of the electrode. O_2 is thus replaced by a non-physiological electron acceptor, which is recycled at the electrode, providing an amperometric signal; these devices are classified as second *generation biosensors*. [2, 13, 50, 53, 54]. The use of such redox mediators also poses technical difficulties regarding selectivity, since they are non-specific catalysts and can react with other electroactive species present in a sample. Also, toxicity issues arise, a common feature in the majority of artificial mediators [2, 6, 54].

As an alternative to the two previous generations, a third one exists where the electrochemical communication between the redox cofactor and the electrode occurs directly through an electron tunneling mechanism (third *generation biosensors*) [2, 50]. This strategy enables the development of reagent-free devices since it eliminates the use of extra reagents (the redox mediator) that are necessary for the analyte's detection, apart from the enzyme itself [2]. The direct ET has been

reported for GOx [55, 56], ChOx [57], ChOD [58], XOD [59] on modified electrodes. However, special care must be taken when considering the evaluation of such devices. For example, for GOx the idea of direct electron communication with the electrode has been recently revised by Wilson [60] and Bartlett [8], who concluded that there is no real evidence to sustain such claims in the majority of the literature. It was demonstrated that the commonly observed redox peaks around -400 mV (vs. Ag/AgCl reference) are mostly due to free, adsorbed flavin on carbon electrodes which are present either as an impurity from non-purified commercial enzyme preparations or as the result of cofactor dissociation due to protein denaturation [8]. The catalytic responses towards glucose and seen in the presence of O_2 are due to the consumption of the latter by adsorbed, enzymatically active, but electrochemically inactive enzyme at the electrode's surface, making these devices belong to the first rather than third generation [2, 8, 61].

2.2 Multicopper Oxidases

Multicopper oxidase enzymes are a diverse group that couple the one-electron oxidation of a variety of substrates with the four-electron reduction of O_2 to water, without the release of activated oxygen species [105]. This family of enzymes includes laccase, ascorbate oxidase, copper oxidases, ferroxidases, mammalian ceruloplasmin, and bilirubin oxidase [105, 106]. The catalytic site of multicopper oxidases is comprised of four copper atoms that are classified according to their spectroscopic and magnetic properties: type 1 "blue copper" (T1), type 2 "normal copper" (T2), and type 3 binuclear copper (T3) (Table 1) [105–107]. The mononuclear T1 accepts electrons from the reduced substrates and transfers them to the T2/T3 trinuclear cluster that binds and reduces O_2 (Fig. 3) [105–108].

Multicopper oxidases (Fig. 4) have been widely studied in the context of biofuel cell development, harnessing the potential of the (mediated and non-mediated)

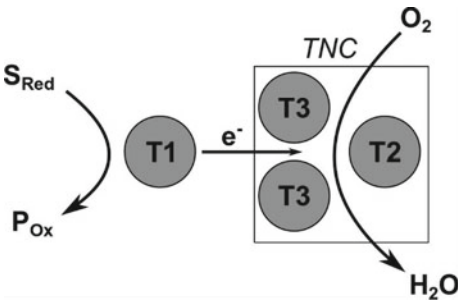

Fig. 3 General scheme of the catalytic mechanism of multicopper oxidases. The reduced substrate (S_{Red}) is oxidized (P_{Ox}) at the type 1 copper site (T1), which then transfers the received electrons to the trinuclear center (TNC), comprised of the type 2 (T2) and type 3 (T3) copper sites. O_2 binds at the TNC, where it is reduced to water, without any peroxide intermediaries being released. Adapted from [106]

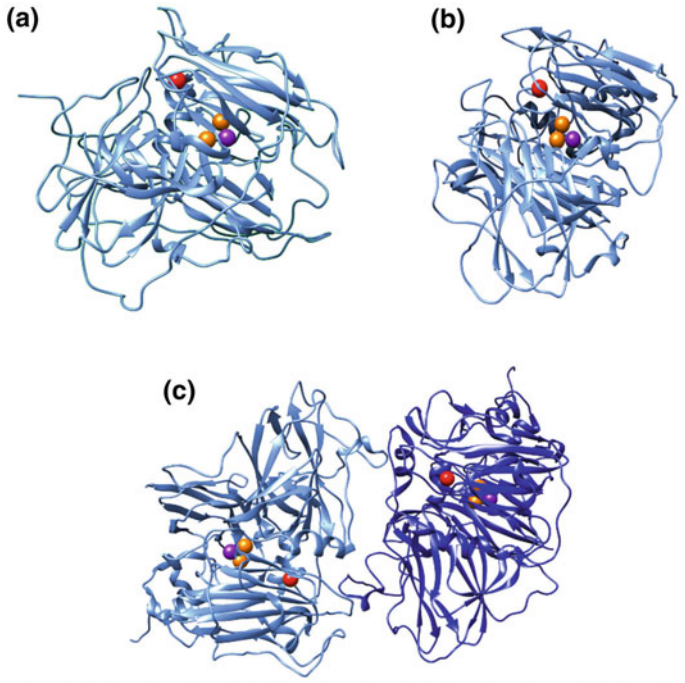

Fig. 4 Three-dimensional structures of multicopper oxidases: **a** BOD from Myrothecium verrucaria (3ABG); **b** laccase from *Trametes versicolor* (1KYA); **c** AOx from *Cucurbita pepo* (1AOZ). Copper centers T1, T2 and T3 are depicted in red, purple and orange, respectively. Structures were prepared using UCSF Chimera and the respective entries (in brackets) from RCSB Protein Data Bank

biochemical reduction of O_2 to generate electrical energy [109–113]. The direct ET between the enzyme and the electrode contributes significant design advantages in the construction of such devices, enabling them (theoretically) to be operated in a single compartment cell, without exogenous redox mediators, at a potential approaching the redox potential of the enzyme itself [66]. Biosensing electrodes have also been designed based on the catalytic activity of the multicopper enzymes, namely plant ascorbate oxidase (AOx) from *Cucurbita sp.* [114, 115] and bacterial bilirubin oxidase (BOD) from *Myrothecium verrucaria* [116, 117]; examples are presented in Table 3. Also, biosensors based on the plant or fungal laccases have been widely researched for the monitoring of phenolic compounds (e.g, phenol, catechol, dopamine) (extended reviews at references [118–120]). However, most of these devices are operated at more acidic conditions (pH 4–6) than the physiological pH and in the presence of very low concentrations of chlorine. This is due to the optimum pH for the catalytic activity being around pH 5, and to the low tolerance of the enzyme to high levels of halides [111, 121–123]. These two factors limit the direct application of laccase-based devices in environmental and clinical

Table 3 Electrochemical biosensing applications of bilirubin oxidase (BOD) and ascorbate oxidase (AO_x)

Enzyme	Analyte	Transducer	Detection	Sample	References
BOD	Bilirubin	SAM/$BOD_{multilayer}$ Au electrode	Fc–C mediated	Serum	[116]
	Bilirubin	O_2 electrode with BOD/BSA/glutaraldehyde membrane	O_2 depletion	Serum	[141]
	Bilirubin	MPTS sol-gel (containing BOD and AuNPs) Au electrode	Fc mediated	Serum	[142]
	DNAss	PAA-PVP-Os-DNA capture sequence modified SPE and DNA-bound BOD probe	O_2 catalytic reduction	Buffer	[122]
	Glucose	GOx/BOD-MWCNT Au electrode	O_2 catalytic reduction	Buffer	[117]
	O_2	BOD-MPA/NA-AuNP Au electrode	O_2 catalytic reduction	SLB	[123]
AOx	Ascorbate	O_2 electrode with AOx immobilized on Teflon membrane	O_2 depletion	Fruit juices	[126]
	Ascorbate	AOx micelle membrane AGC electrode	O_2 depletion	Fruit juices	[127]
	Ascorbate	AOx/eggshell membrane Au electrode	Ascorbate catalytic oxidation	Fruit juices, Serum	[128]
	Ascorbate	AOx/BOD-MWCNT Au electrode	O_2 catalytic reduction	Buffer	[117]
	Ascorbate	PEDOT-SWCNT/AOx/Nafion Pt electrode	Ascorbate catalytic oxidation	Buffer	[114]
	Ascorbate	Au-deposits graphite electrode	Ascorbate catalytic oxidation	Buffer	[115]
	Paraoxon	O_2 electrode with cucumber peel tissue sandwiched between Teflon/nylon membrane	O_2 depletion	Buffer	[130]

AGC aminated glassy carbon; *AuNP* gold nanoparticles; *BSA* bovine serum albumin; *DNAss* DNA short sequence; *GOx* glucose oxidase; *Fc* ferrocene; *Fc-C* ferrocene carboxylic acid; *MPA/NA* 3-mercaptopropionic acid/6-amino-2-naphtoic acid; *MPTS* (3-mercaptopropyl)-trimethoxysilane; *MWCNT* multi-walled carbon nanotubes; *PAA-PVP-Os* copolymer of polyacrylamide and poly (4-vinylpyridine) complexed with $[Os(2,2'\text{-bipyridine})_2Cl_2]^{2+/3+}$; *PEDOT* poly (3,4-ethylenedioxythiophene); *SAM* self-assembled monolayer; *SLB* serum-like buffe; *SWCNT* single-walled carbon nanotubes

samples, although efforts have been made to circumvent this by improving the immobilization of the enzyme, creating a more effective microenvironment [124].

The plant AOx is a homodimeric enzyme, with one catalytic site per monomer, which catalyzes the oxidation of ascorbate to dehydroascorbate via a disproportionation of the semidehydroascorbate radical [105, 107]. It has been obtained from several sources (plants, fungi, and eubacteria). The possibility of direct ET has been confirmed on gold (T1 center) and carbon-based electrodes (T1 and T2/T3 centers) [66, 115, 125]. The enzyme has been applied in the construction of biosensors for the detection of ascorbic acid [114, 117, 126–128] (ascorbate anion at physiological pH [129]), as well as organophosphorus pesticides monitoring [130]. Determination of ascorbic acid in the clinical and food industry is very important since its deficiency is known to cause several medical conditions (e.g., anemia, scurvy, muscle degeneration, atherosclerotic plaques, and capillary hemorrhaging, neurotic disturbances) [128], while in excess it can lead to gastric irritation, renal problems, inhibition of natural processes occurring in food, and can contribute to taste/aroma deterioration [131]. In these devices, the analyte is detected by monitoring the localized consumption of O_2 using a Clark electrode [126, 127, 130], or by observing the biocatalytic oxidation of ascorbate [114, 115, 128].

As for BOD, it is a monomeric enzyme that has been identified in various fungi and bacteria, and it catalyzes the oxidation of bilirubin to biliverdin, as well as other tetrapyrroles, phenols, and aryl diamines [105, 132–135]. The enzyme has the ability to produce mediated bioelectrocatalytic currents for the reduction of O_2 to water near-neutral pH [109–111, 136]. Although direct ET between the electrode and the T1 and T2/3 centers is possible [137–140], the use of mediators facilitates the electrochemical communication between the active site and the surface of the electrode [109–111, 136]. Owing to its high thermal stability, low sensitivity to chloride ions, and high activity at neutral pH 7, BOD is considered an excellent candidate for the elaboration of efficient biofuel cells and biosensors operating at physiological conditions [107, 135]. BOD has been applied to the development of electrochemical monitoring tools for a diverse group of analytes, such as glucose [117], DNA sequences [122], O_2 [123], and bilirubin [116, 141, 142]. The former is a bile pigment that results from the heme degradation of erythrocytes by reticuloendothelial cells and exists in the serum in free form, unconjugated (albumin-bound) and conjugated (with glucuronic acid), which is excreted in the bile [143, 144]. This form is a biomarker of liver function and is used in the diagnosis of jaundice and hyperbilirubinemia, while the unconjugated form is specifically used in newborns where the liver is not mature enough to convert the unconjugated bilirubin to conjugated bilirubin resulting in jaundice [143, 144].

Regarding the detection principle of the analyte, many BOD-based bioelectrode papers claim that it was performed indirectly by monitoring the increase in H_2O_2 concentration that resulted from the enzymatic reaction [135, 145, 146]. However, this goes against the established concept that BOD catalyzes the complete reduction of O_2 to water, without the release of intermediary reactive species [136, 147]. For this reason, such devices were not considered in this text. For the remaining works, the detection of the analyte has been carried out by monitoring the non-mediated

biocatalytic O_2 reduction [117, 122, 123], the mediated biocatalytic bilirubin oxidation [116, 142], and the localized consumption of O_2 [141].

3 Dehydrogenases

Dehydrogenases (DHs) form the largest group of enzymes currently known and are represented in all living tissues. They have in common the ability to oxidize a substrate (e.g., monosaccharides, aldehydes, alcohols, ketones) while transferring two hydrogen atoms to a suitable electron acceptor, without O_2 involvement [148]. In order to be functional, DHs require the presence of a cofactor (Fig. 5) that acts as an electron carrier. It can be covalently bound, as for example, FAD, FMN, pyrroloquinoline quinone (PQQ), and molybdopterin [149], but the great majority depends on the water-soluble nicotinamide adenine dinucleotide (phosphate) (NAD(P)$^+$) coenzyme, which is not covalently linked to the protein. Figure 6 shows the three-dimensional structures of several DHs examples, namely glucose dehydrogenase (PQQ-GDH), NADP-dependent alcohol dehydrogenase (ADH), cellobiose dehydrogenase (FAD-CDH), the molybdenum-heme sulfite containing dehydrogenase (SulDH), and mandelate dehydrogenase (FMN-MDH). The next sections will address the development of biosensors based on NAD(P)-dependent and non-dependent hydrogenases.

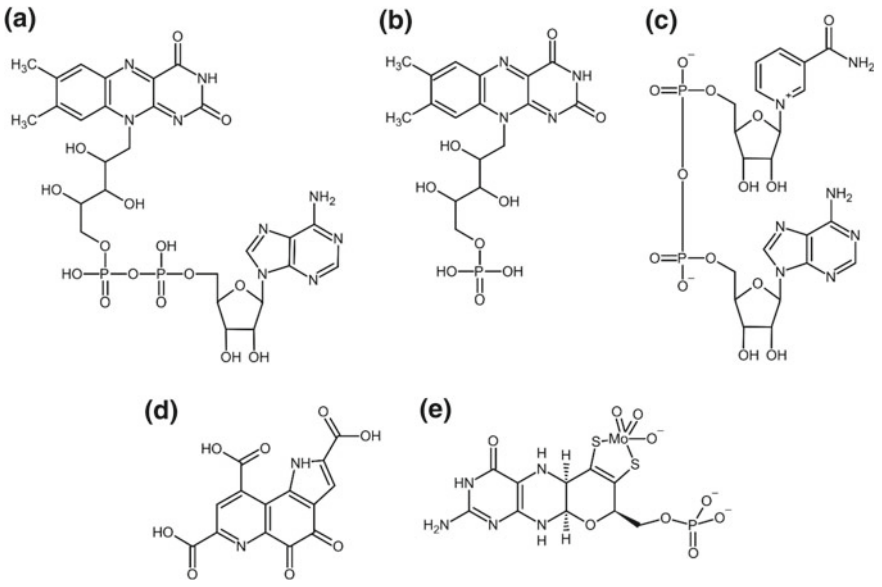

Fig. 5 Dehydrogenases' cofactors: **a** FAD, **b** FMN, **c** NAD$^+$, **d** PQQ **e** molybdenum center

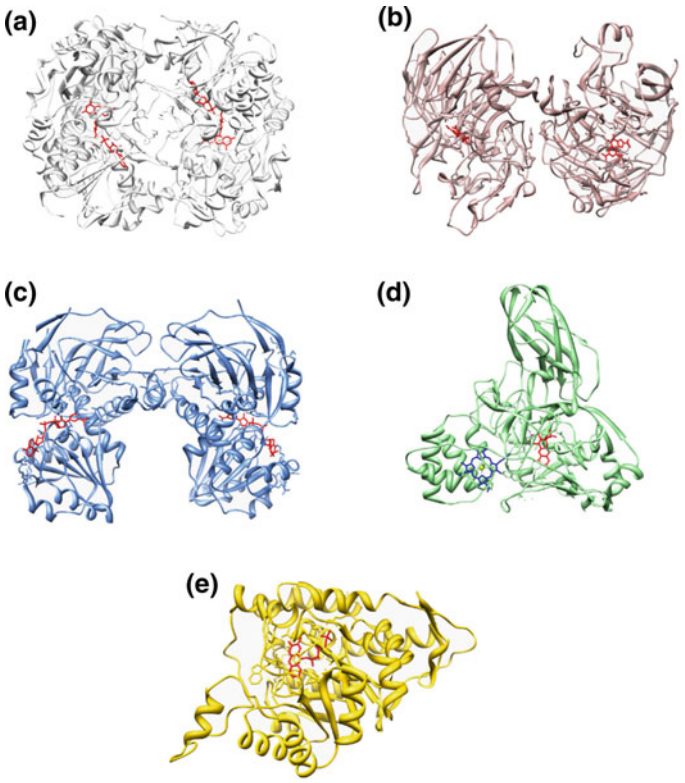

Fig. 6 Three-dimensional structures of dehydrogenase enzymes used in biosensors. **a** Flavin domain of cellobiose dehydrogenase (CDH) from *Phanerochaete chrysosporium* (1KDG); FAD cofactors are shown in red. **b** PQQ-dependent soluble glucose dehydrogenase (GDH) from *Acinetobacter calcoaceticus* (1C9U); PQQ cofactors are represented in red. **c** Alcohol dehydrogenase (ADH)—NADP complex from *Escherichia coli* (7BU3); NADP is depicted in red. **d** Molybdenum-dependent sulfite dehydrogenase (SulDH) from *Starkeya novella* (2BLF); molybdenum cofactor and heme c are shown in red and blue, respectively. **e** FMN-dependent (S)-mandelate dehydrogenase (MDH) from *Pseudomonas putida* (2A7P); FMN cofactor is represented in red. Structures were prepared using UCSF Chimera software and the respective entries from RCSB Protein Data Bank (codes in brackets)

Compared to oxidases, the O_2 independence of DHs brings a remarkable benefit to electrochemical biosensors. In the case of glucose biosensing, there was much hope that glucose dehydrogenase (GDH) would replace GOx, as has it happened indeed. Due to the vital importance of controlling blood glucose levels in diabetes patients, glucose meters account for the largest share of the global point-of-care diagnostic market [150]. Therefore, the development of new glucose biosensors involving GDH has been the object of great attention. As a result, modern blood glucose meters comprise electrochemical cells containing PQQ-GDH, NAD-GDH, FAD-GDH, and a redox mediator [151]. As mentioned above, the main advantage

of these GDHs is their insensitivity to O_2, whereas their main weakness is their lower substrate selectivity. The Abbott FreeStyle Optium and FreeStyle Optium Neo blood glucose meters, for example, employ the NAD^+-dependent GDH. Furthermore, by using the NAD^+-dependent β-hydroxybutyrate DH, they also test for β-ketone [152].

3.1 NAD(P)H Dependent Dehydrogenases

The prevalence of $NAD(P)^+$ DHs is easily explained by the fact that they are ubiquitous in nature making this cofactor a universal electron acceptor [148]. As a result, many of their substrates, including glucose, lactate, ethanol among others, are quite relevant from the analytical standpoint.

In general, the pair NAD^+/NADH is involved in catabolic pathways, whereas $NADP^+$/NADPH participates in anabolic reactions. Aside from the differences in their biological functions, both forms have similar thermodynamic properties ($E^{\circ\prime} = -0.315$ V vs. NHE, at pH 7) and reaction mechanisms [153]. Equations (3) and (4) show the typical catalytic mechanism associated with $NAD(P)^+$-linked dehydrogenases in a biological environment. The enzyme (E) removes two hydrogen atoms from its substrate (S). While one hydrogen is transferred as a hydride ion (H^-; the equivalent of a proton and two electrons) to NAD^+, the other is released as a proton (H^+), in a reversible process [148].

$$S + E + NAD(P)^+ \rightarrow S \cdot E \cdot NAD(P)^+ \rightarrow E + P + NAD(P)H + H^+ \quad (3)$$

$$NAD(P)H \rightarrow NAD(P)^+ + H^+ + 2e^- \quad (4)$$

Since the enzyme's substrate (analyte) is stoichiometrically equivalent to $NAD(P)^+$ (1:1), the electrochemical monitoring of the cofactor would allow the quantification of the former. In broad terms, this is the strategy underlying most of the DHs biosensors. However, the electroanalysis of the redox pairs NAD(P)H/$NAD(P)^+$ is highly challenging due to the marked lack of reversibility and the high overvoltages required to drive the electrochemical reaction. Unlike in nature, the electro-oxidation of NAD(P)H at bare electrodes, especially when made of carbonaceous or metallic materials, occurs through much complex high energy reaction routes, which require large overpotentials that typically go up to 1 V vs. saturated calomel electrode (SCE). This greatly increases the risks of interfering phenomena, including high background currents, electrode fouling due to the formation of stable adducts between surface species and radical intermediates as well as the adsorption of biologically inactive NAD dimers. The occurrence of unwanted reactions with other easily oxidizable compounds that are usually present in physiological samples such as, ascorbate, urate, and acetaminophen, can also interfere in the analysis [152, 154, 155].

On the other hand, owing to the low formal reduction potential of $NAD(P)^+$, its electrocatalytic reduction requires the application of a voltage within a very negative window (below −0.315 V vs. NHE), where dissolved O_2 also responds,

masking the truly analytic signals and making impractical the $NAD(P)^+$ reduction in biosensing applications without previous sample deaeration. Besides, the dimers' formation from reaction products also affects the electrochemical reaction. For these reasons, the design of amperometric biosensors based on NAD(P)H-dependent DHs have been mainly focused on the anodic oxidation of the cofactor's reduced form [153, 155].

To this end, several redox mediating strategies and electrode surface modifications have been successfully proposed, aiming at decreasing the overvoltage and promoting $NAD(P)^+$ regeneration (Fig. 7) by stabilizing the radical intermediates and avoiding coupled side reactions [154].

Notwithstanding, the presence of an additional redox species could bring other disadvantages such as unspecific chemical reactions and signal instability, so the selection of redox mediators is extremely important. The electronic mediator should have a redox potential as low as possible, exhibit fast reaction rates, be chemically stable at any redox state, and last, but not the least, be easy to immobilize, not compromising the biosensor's stability [2]. Back in 1978, Tse and Kuwana modified for the first time an electrode surface with a monolayer of primary amines substituted with functional groups such as 3,4-dihydroxybenzylamine, dopamine, or *o*-quinone derivatives, which worked as effective electron shuttle systems. In this case, the overpotential for the oxidation of NADH decreased to *ca.* 0.4 V *vs.* NHE [156]. Since then, numerous works reporting different strategies to modify the electrode surfaces with electron carriers were published. Among the mediators used, the most popular are quinones, phenoxazines, and phenothiazines [157] (the mediated electrochemical reactions of the $NADH/NAD^+$ couple were extensively reviewed by Gorton in reference [155]). Nonetheless, many other redox mediators for NADH oxidation were proposed over the years, including ferrocene, diimines, thionine oxometalates, polymetallophthalocyanines, ruthenium complexes, pyrroloquinoline quinone, fluorenones, and quinonoid redox dyes like indamines, and phenazines [152]. For their immobilization, a great variety of strategies have been adopted, such as direct adsorption on the electrode or on inorganic composite materials, entrapment in polymer matrices, generation of covalent bonds, incorporation in carbon/graphite pastes, electrochemical polymerization, etc. [158–160]. Actually, the list of examples is so vast that is impossible to cover the topic in just a

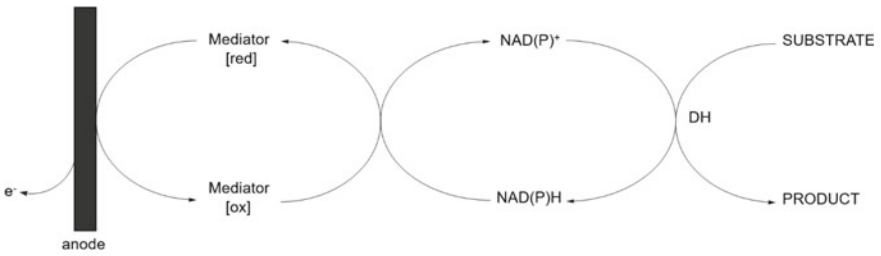

Fig. 7 Schematic representation of the mediated electrochemical oxidation of NADH

few paragraphs. A selection of works is thus presented in Table 4, highlighting some electrochemical biosensors based on NADH-dependent dehydrogenases for glucose, alcohol, lactate, and glutamate analysis, each one following a different approach for enzyme immobilization and to NADH monitoring. In what concerns electron carriers, alongside the frequently used Meldola Blue (8-dimethylamino-2,3-benzophenoxazin), examples of biosensors employing ferricyanide and FePhenTPy (5-[2,5-di(thiophen-2-yl)-1H-pyrrol-1-yl]-1,10-phenanthroline iron(III) chloride), are also provided. Strikingly, in some cases, no redox mediators were used at all. Instead, alternative approaches were lately used in order to facilitate the direct electrochemical oxidation of NADH. Tsai and coworkers, for instance, developed a multi-walled carbon nanotube (MWCNTs)-chitosan composite to entrap lactate dehydrogenase (LDH) onto a glassy carbon electrode. Owing to the inclusion of MWCNTs, the NADH electro-oxidation potential was considerably lower (+0.6 V vs. Ag/AgCl) [161]. Likewise, Tang et al. observed that the modification of MWCNTs with self-assembling glutamate dehydrogenase (GLDH) and poly(amidoamine) dendrimer-encapsulated Pt nanoparticles, not only increased the effective area of the electrode but also enhanced heterogeneous ET rates. In fact, the biosensor response to glutamate was investigated in the presence of NAD^+ at a low working potential of 0.2 V vs. Ag/AgCl, without electron carriers in solution [162]. On its turn, Jena et al. integrated lactate and ethanol DHs within a sol-gel-derived, 3D silicate network incorporating AuNPs. The specific features of the latter enabled the direct and efficient oxidation of NADH, with a remarkable decrease in overpotential of about 915 mV. While their nano-dimensions favored the kinetics of the electrochemical reaction, surface-bound hydrous oxides worked as efficient ET mediators [163]. In general, the modification of electrode surfaces with nanostructured carbon materials (e.g., carbon nanotubes, graphene oxides) and/or metallic nanoparticles enabled the development of new schemes for NAD(P)H electrochemical sensing, thereby avoiding the usage of electronic mediators [160, 164–166].

An alternative way to replace synthetic electronic carriers is the incorporation of an additional biocatalytic system constituted by an auxiliary enzyme that is able to regenerate NAD(P)H in the presence of its co-substrate. Common examples are formate/formate dehydrogenase, glucose/GDH, and isopropanol/alcohol dehydrogenase (ADH). Though, for biosensing applications, the enzymatic regeneration of NAD(P)H involving diaphorase and a redox mediator (Eqs. 5–7), such as reduced viologens, is often preferred [167]. These systems still require strong reductive mediators, and the use of a second enzyme and its substrate increases costs and diminishes the biosensor stability.

$$\mathrm{NADH} + \mathrm{Diaphorase_{Ox}} \leftrightarrow \mathrm{NAD^+} + \mathrm{Diaphorase_{Red}} \tag{5}$$

$$\mathrm{Diaphorase_{Red}} + \mathrm{Mediator_{Ox}} \rightarrow \mathrm{Diaphorase_{Ox}} + \mathrm{Mediator_{Red}} \tag{6}$$

$$\mathrm{Mediator_{Red}} \rightarrow \mathrm{Mediator_{Ox}} + \mathrm{e^-} \tag{7}$$

Table 4 Dehydrogenase-based biosensors construction and analytical characterization

Enzyme/Source	Transduction[a]	Analyte	Immobilization/electrode	Electron Transfer	Detection limit	Linear Range	Sample	References
NAD-ADH *S. cerevisiae*	Amperometric (−5 mV)	Ethanol	ADH in MPTS sol-gel (spontaneous adsorption on the electrode)/AuNPs self-assembled/Au	Mediated (NAD^+ via AuNPs)	20 μM	0.5–2.5 mM	Buffer	[163]
NAD-ADH *baker's yeast*	Amperometric (50 mV)	Ethanol	ADH + NAD^++SWCNT + MB + mineral oil/SWCNT paste	Mediated (NAD^+ via MB)	0.1 μM	0.1–4 μM	Buffer	[196]
NAD-ADH *S cerevisiae*	Amperometric (40 mV)	Ethanol	ADH + MB crosslinked on MWCNT via GA/MWCNT-MB	Mediated (NAD^+ via MB)	5 μM	50 μM–10 mM	Buffer	[197]
NAD-LDH *rabbit muscle*	Amperometric (600 mV)	Lactate	drop cast LDH + CH + MWCNT/GC	Mediated (NAD^+)	0.76 μM	5–120 μM	Buffer	[161]
NAD-GDH *Microorganism*	Amperometric (550 mV)	Glucose	drop cast FePhenTPy − RGO/drop cast GDH/Nafion protecting membrane/CarbonSPE	Mediated (NAD^+ via FePhenTPy)	12.02 ± 0.6 mg/dL	29–434 mg/dL	Blood	[198]
FAD-GDH *Aspergillus terreus*	Amperometric (500 mV)	Glucose	drop cast GDH/GC	Mediated ($[Fe(CN)_6]^{3-}$)	10 μM	5–30 mM	Buffer	[180]
NAD-GluDH *bovine liver*	Amperometric (200 mV)	Glutamate	drop cast $(GluDH/Pt\text{-}PAMAM)_n$/CNTs nanocomposites/GC	Mediated (NAD^+)	–	0.2–250 μM	Buffer	[162]
NAD-GluDH *beef liver*	Amperometric (100 mV)	Glutamate	drop cast MWCNT + CH + MB/drop cast GluDH + MB + CH + NAD^+/drop cast MWCNT + CH + MB/MB-Carbon SPE	Mediated (NAD^+ via MB)	3 μM	7.5–105 μM	Buffer	[199]
FAD-CDH *T. villosa*	Amperometric (100 mV)	Lactose	drop cast CDH/cross-linking via GA or PEGDGE/MWCNT/SPE	Direct ET	250 nM	500 nM–200 μM	Buffer	[200]

(continued)

Table 4 (continued)

Enzyme/Source	Transduction[a]	Analyte	Immobilization/electrode	Electron Transfer	Detection limit	Linear Range	Sample	References
FAD-CDH *Phanerochaete sordida*	Amperometric (250 mV)	Lactose	drop cast PEI-AuNPs/drop cast CDH/dialysis membrane/Au	Direct ET	330 nM	1–100 μM	Buffer	[201]
FAD-CDH ascomycete *Corynascus thermophilus*	Amperometric (250 mV)	Glucose	electrodeposition AuNPs/dip in 4-APh, 4-MBA/drop cast CDH + GA/GC	Direct ET	6.2 μM	20 μM–30 mM	Buffer	[170]
FAD-CDH ascomycete *Corynascus thermophilus*	Amperometric (100 mV)	Glucose	drop cast CDH/MWCNT-SPE	Direct ET	10 μM	25 μM–30 mM	Buffer	[202]
FAD-FDH *Gluconobacter japonicus*	Amperometric (250 mV)	Fructose	h-PG electrodeposition/dip in 4-MPh/drop cast FDH/Au	Direct ET	0.3 μM	50 μM–5 mM	Buffer	[203]
PQQ-FDH *Gluconobacter industrius*	Potentiostatic (400 mV)	Fructose	drop cast triton X-100/drop cast FDH/RGO	Direct ET	0.7 mM	0.7–8.8 mM	Buffer	[191]

[a]All potentials are quoted vs. Ag/AgCl reference electrodes. *4-APh* 4-aminothiophenol; *4-MBA* 4-mercaptobenzoic acid; *4-MPh* 4-mercaptophenol; *AuNPs* gold nanoparticles; *CH* chitosan; *ET* electron transfer; $[Fe(CN)_6]^{3-}$ Ferricyanide; *FePhenTPy* 5-[2,5-di (thiophen-2-yl)-1H-pyrrol-1-yl]-1,10-phenanthroline iron(III) chloride; *GA* Glutaraldehyde; *GC* glassy carbon; h-*PG* highly porous gold; *MB* Meldola Blue; *MPTS* (3 mercaptopropyl)trimethoxysilane; *MWCNT* multi-walled carbon nanotubes; NAD^+ nicotinamide adenine dinucleotide; *PEGDGE* poly(ethyleneglycol)diglycidyl ether; *PEI* polyethyleneimine; *Pt-PAMAM* poly(amidoamine dendrimer-encapsulated platinum nanoparticles; *RGO* reduced graphene oxide; *SPE* screen-printed electrode; *SWCNT* single-walled carbon nanotubes

In a recent work by Yuan and collaborators, a very promising method of NADH regeneration without redox mediators in solution was developed. Herein, NADH was bioelectrocatalytically regenerated by immobilizing diaphorase in a cobaltocene-modified poly(allylamine) redox polymer; faradaic efficiencies between 78 and 99% were achieved with high operational stability [168]. Electroactive polymers comprising redox moieties covalently bound to a polymeric backbone are proving to be viable alternatives to conventional redox mediators, due to an efficient ET through self-exchange based conduction.

Another possible solution for the electrochemical regeneration of $NAD(P)^+$ relies on the cofactor's photochemical restoration by introducing a photosensitizer in the matrix, such as *N*-methyl phenazonium methyl sulphate, porphyrins, Ru(II)-tris-bipyridine with viologens as electron acceptors [153]. For example, a photoelectrochemical NAD(P) regeneration system composed of $Ru(bipy)^{*+}$ as a photosensitizer and methyl viologen (MV^{2+}) as a primary electron acceptor (re-oxidized at the anode), was coupled to enzyme-catalyzed oxidations of alcohols [169]. Research on photochemical NAD(P) generation has been limited and its description is out of the scope of this chapter.

Despite the tremendous attention received by the scientific community over the last decades and a few commercial achievements, challenges persist in the implementation of NAD(P)-dependent hydrogenases in electrochemical biosensors. The need of adding the free-diffusing coenzyme, its complex electrochemistry, and the lack of long-term stability are the main setbacks [170]. Therefore, at some point, the trend shifted into the direction of other classes of dehydrogenases.

3.2 Other Dehydrogenases

In this section, we will address all other biosensors based on DHs that do not depend on the soluble coenzymes $NAD(P)H/NAD(P)^+$. Instead, these enzymes harbor a FAD, FMN, PQQ, or molybdenum cofactor group that can be strongly bound to the polypeptide chain, markedly improving the biosensors' stability. Another interesting feature of these cofactors is their formal reduction potentials (Table 1), which are less negative than that assigned to the $NAD(P)^+/NAD(P)H$ couple [149]. In particular, the flavin nucleotides, FMN and FAD, are two-electron, two-proton redox centers that act as carriers of reducing equivalents. In a biological context, the oxidized form can either accept one-electron (yielding the flavosemiquinone form) or two electrons (yielding $FADH_2$ or $FMNH_2$) by hydride transfer. Unlike $NAD(P)^+$, the reduction potential of flavin nucleotides depends on the protein environment, as local interactions with amino acid side chains can distort the electron orbitals in the flavin ring, affecting the stability of both oxidized and reduced forms [148]. Representative values for the $E^{\circ\prime}$ of protein-bound $FMN/FMNH_2$ and $FAD/FADH_2$ are −0.30 V and −0.12 V (vs. NHE), respectively [171]. PQQ is also reduced by two electrons but at a remarkably higher potential (+0.90 V). This cofactor is coordinately bound to the apoenzymes via Ca^2

$^{+}$ (or Mg^{2+}) ions [172]. From the functional standpoint, there are two types of PQQ-containing DHs: those that are bound to the bacterial membrane (PQQ-As) and those that are intracellular, and therefore water-soluble (PQQ-Bs). It has been shown that they are distinct enzymes, with different molecular weights, substrate specificity, optimal pH, and tolerance to heat. For example, the membrane-bound glucose PQQGDH-A shows high selectivity for glucose; though, it requires suitable detergents for solubilization [152, 153, 172]. In contrast, its water-soluble isoenzyme PQQGDH-B is not selective (catalyzes the oxidation of a variety of monosaccharides and disaccharides) and is thermally unstable. On the other hand, PQQGDH-B has a very high catalytic activity, which is over 25 times higher than GOx's activity [173]. Consequently, the interest in such active and O_2-independent enzymes for bioanalysis applications remained, and many studies based on protein engineering techniques were done with success, resulting in the improvement of water-soluble PQQGDH-B's thermal stability [174–176] and narrowing its substrate specificity [177–179].

In recent years, a new type of fungi-derived thermostable FAD-dependent glucose dehydrogenases (FADGDHs) has been receiving particular attention, both in the field of bioelectrochemistry and glucose biosensing. Tsujimura and Omura found, for instance, a novel FAD-GDH from *Aspergilus terreus*, showing a high thermostability, and specificity for glucose [180]. Since then, many other works were published in the field, as recently reviewed by Okuda-Shimazakia et al. [181]. The main advantages of these FADGDHs are the high turnover rates and improved substrate selectivity, good stability, and lower redox potentials [181].

Because flavin nucleotides and PQQ cofactors are embedded in the DHs polypeptide chain, redox mediators are usually required to achieve fast heterogeneous ET with electrodes (see Eqs. 8–10), resulting in second generation biosensors ([149, 172] and references therein). Different electronic mediators were tested but those based on ruthenium and osmium are the best [181].

$$\begin{aligned} S + E \cdot FAD(FMN/PQQ) &\rightarrow S \cdot E \cdot FAD(FMN/PQQ) \\ &\rightarrow P + E + FADH_2(FMNH_2/PQQH_2) \end{aligned} \tag{8}$$

$$\begin{aligned} FADH_2(FMNH_2/PQQH_2) + 2Mediator_{Ox} \\ \rightarrow FAD(FMN/PQQ) + 2Mediator_{Red} + 2H^+ \end{aligned} \tag{9}$$

$$2Mediator_{Red} \rightarrow 2Mediator_{Ox} + 2e^- \tag{10}$$

Several dehydrogenases harboring FAD, FMN, PQQ, and molybdenum cofactors can contain additional heme prosthetic groups; in some cases, they present Fe-S clusters as well. They are referred to as flavo-hemoproteins, quinohemoproteins, and molybdopterin hemoproteins, respectively. In these enzymes, reducing equivalents are sequentially transferred from substrates to FAD/FMN/PQQ/molybdenum cofactors, and then to the heme group, which finally delivers electrons to natural electron acceptors [149, 172]. Likewise, in some biosensing devices, these DHs are

connected to the electrode via the heme group, which works as an internal ET mediator, paving the way to a direct electrochemical response [173, 182]. In fact, a considerable number of multi-cofactor DHs have been successfully employed in third generation biosensors, thereby improving the selectivity and stability of analysis while avoiding interfering reactions. Ikeda and coworkers were the first to prove the concept, either using a flavohemo enzyme, such as *D*-gluconate DH (GADH) [183], or quinohemoproteins like fructose DH (FDH) [184] and ADH [185, 186]. These bacterial membrane-bound oxidoreductases were simply adsorbed on carbon paste [183, 185] or metal electrodes [185], and produced anodic currents in the presence of their substrates. Neither mediators nor promoters were necessary, demonstrating a facile heterogeneous ET. The heme domains were properly oriented towards the electrode surface while the catalytic sites were facing the solution side. Nevertheless, it was later shown that experimental variables such as pH, ionic strength, the composition in metal cations and the electrode material were crucial to achieving a favorable protein orientation towards the transducer surface and electronic communication between the heme domain and the electrode as well as a smooth internal ET from the catalytic site to the heme center. In this context, two interesting examples are the flavocytochrome cellobiose dehydrogenases (CDH) and FDH. CDHs, in particular, are extracellular enzymes expressed by several fungi involved in wood degradation and have found wide applications in food technology, biomedicine, for which several lactose and glucose biosensors were developed (Table 4). The FAD moiety is connected through a flexible linker to the smaller cytochrome domain, which houses a *b*-type heme. As shown in Fig. 8, the flavin domain carries out the oxidation of sugars such as di- and

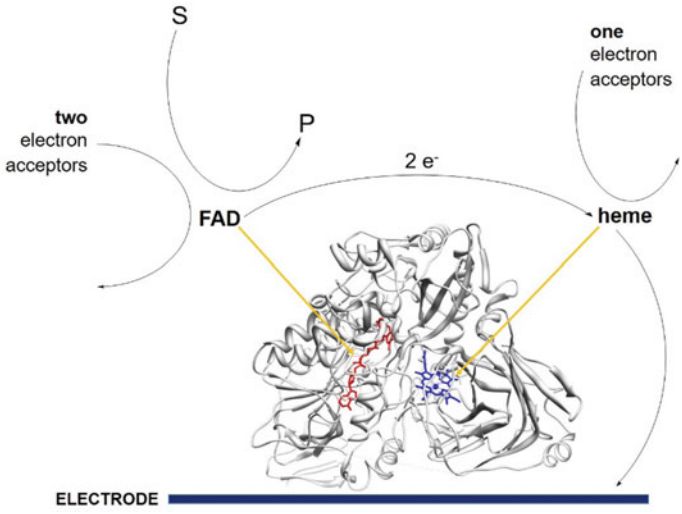

Fig. 8 Schematic representation of different possible ET pathways in CDHs

oligosaccharides (e.g, cellobiose, lactose, and cellodextrins) to the corresponding lactones and the two electrons extracted can be transferred directly to several two-electron acceptors (e.g., quinones or dichloroindophenol) or, alternatively, to one-electron acceptors while the second electron is firstly shuttled to the heme iron through internal ET, and then to one-electron acceptors (e.g., cytochrome *c* and ferricyanide) or solid electrodes (e.g., graphite, gold), thus allowing a direct electrochemical response. As mentioned above, for this to happen, the protein should be correctly oriented on the electrode surface but the simple deposition of CDHs directly on graphite or gold surfaces leads to a random orientation, hindering an efficient unmediated ET [149, 187].

Therefore, the electrode modification strategy has played a fundamental role in the construction of CDHs based third generation biosensors. Gorton's research group has done extensive work in this field [170, 182]. In one of their first studies [188], it was proved that gold electrodes modified with self-assembled monolayers promote the correct protein orientation, so one could observe both the direct ET with the heme cofactor and a good catalytic response in the presence of cellobiose. The latter was dependent on pH, showing a close agreement with the fact that internal ET between the two cofactors is switched off at high pH values [189, 190]. Similar catalytic behavior was found in many other heme-containing PQQ-dehydrogenases where the substrate oxidation takes place at PQQ site and electrons are subsequently transferred to the electrode via the heme domain. This is the case of FDH, which has been largely used in the development of several third generation fructose biosensors (see examples in Table 4), though in a less extensive way than CDH, most likely due to the little relevance of fructose analysis [149, 191, 192]. Other examples are alcohol dehydrogenase [186, 193], pyruvate dehydrogenase [194] or lactate dehydrogenase [195].

4 Reductases

This section is focused on biosensors based on reductase enzymes. The emphasis was put on enzymes alone, therefore, the reductase activities of ET proteins, such as chromate reduction by cytochrome c_3 [204], or of O_2 binding proteins, e.g., nitrite reduction by hemoglobin and myoglobin [205], are not discussed.

A small but diverse group of reductase enzymes has been explored, most of which are metalloproteins containing iron or molybdenum in their active sites (Table 1). The majority of works concerns nitrogen oxide reductases, namely nitrate and nitrite reductases (NaRs and NiRs, respectively), or glutathione reductase [206–209]. The remaining cases include three molybdenum dependent enzymes (dimethyl sulfoxide (DMSO) reductase, trimethylamine *N*-oxide (TMAO) reductase (TorA) and perchlorate reductase), nitroreductase (NR), and cytochrome *c* reductase (C*c*R), for which very few biosensor proposals have been described. Herein, representative biosensing applications of these enzymes are discussed alongside with transduction methods, immobilization strategies, and target samples.

Selected examples of reductase-based biosensors are also summarized in Table 5, including a description of their analytical performance. Owing to the nature of the catalytic reactions, the majority of devices rely on amperometric/voltammetric transducers; nonetheless, other detection modes have also been employed, such as potentiometric, impedimetric, conductometric, optical/spectrophotometric, and colorimetric biosensors [206, 209].

A common feature to almost all reports of reductase-based amperometric/voltammetric biosensors is the need to work in O_2 free conditions. In fact, with a few exceptions, the described sensing platforms operate in N_2 or argon purged solutions. Therefore, we start this section with some considerations on the importance of O_2 removal in biosensing with reductases.

4.1 The O_2 Scavenging Challenge

Perhaps the biggest problems for the commercialization of reductase-based biosensors are the maintenance of assay reducing conditions and the low potentials required for the catalytic reactions (Table 5). Interference from O_2, in particular, is a major challenge as it may react with the enzyme, analyte, or electron donor (e.g., mediators, reducing agents) involved in the biosensing reaction. Furthermore, in the case of amperometric/voltammetric biosensors, O_2 reduction to water or H_2O_2 at the electrode surface generates i) high cathodic background current (below ~ -0.1 V vs. NHE, Fig. 9) at the potentials typically used for analyte detection (Table 5) and ii) reactive oxygen species that can damage the enzymes. Consequently, in the majority of works, the solutions (and samples) are purged with inert gases (argon or N_2) to remove dissolved O_2, a method that is not compatible with on-site monitoring or POCT applications. Alternative strategies to overcome this problem have been explored with some success. The subject was reviewed by Plumeré [220]. The approaches span from i) the addition of chemical or enzymatic O_2 scavengers to the assay solution to remove dissolved O_2, such as sodium sulfite or GOx/catalase (Cat) system, ii) to the shifting of the measurement potential to more positive values, by using redox mediators or iii) by monitoring the reductase's activity through a coupled oxidase enzyme sharing a common co-substrate [220, 221]. The GOx/Cat O_2 scavenger system, in particular, has been proven very efficient in reductase biosensor applications [85, 222–224]. It is based on the concerted catalytic reactions of the two enzymes: glucose oxidation and concomitant O_2 reduction by GOx generates H_2O_2 that is dismutated by Cat into water and O_2. In the net catalytic reaction, two glucose molecules are used for the reduction of one O_2 molecule, which leads to a rapid decrease of O_2 concentration in solution [220]. This system was successfully implemented in a recently reported NiR biosensor. GOx and Cat were co-adsorbed with the nitrite reductase in disposable carbon screen-printed electrodes (CSPEs). The work revealed the good performance of this O_2 scavenger system in the immobilized state and consequently its potential for application in disposable biosensors free from O_2 interference [224].

Table 5 Reductase-based biosensors construction and analytical characterization

Enzyme Source	Transduction[a]	Analyte	Immobilization/electrode	Electron transfer	Detection limit	Linear range	Sample	References
eNaR *A. niger*	Potentiometric	Nitrate	NaR + PPy + Azure A electropolymerization/Pt	–	10 μM	50 μM–5 mM	Buffer	[210]
eNaR *A. niger*	Conductometric	Nitrate	drop cast NaR + BSA + glutaraldehyde + Nafion + MV/Au	–	5 μM	20–250 μM	Waters	[211]
eNaR *A. niger*	Amperometric (−0.25 V)	Nitrate	NaR + PPy + Azure A electropolymerization/Pt	Mediated (Azure A)	0.5 μM	20–500 μM	Buffer	[212]
cd_1NiR *M. hydrocarbonoclasticus*	Amperometric (0 V)	Nitrite	drop cast PVA + cd_1NiR + cyt c_{552} followed by photopolymerization/CSPE	Mediated (cyt c_{552})	0.075 μM	10–200 μM	Buffer	[213]
*cc*NiR *D. desulfuricans*	Voltammetric (CV, −0.8 V)	Nitrite	drop cast SWCNTs/drop cast *cc*NiR/PG	Direct ET	2.1 μM	up to 150 μM	Buffer	[214]
NO reductase *M. hydrocarbonoclasticus*	Voltammetric (SWV, −0.68 V)	NO	drop cast NOR + MWCNT + $BMIMBF_4$ ionic liquid/PG	Direct ET	0.07 μM	0.23–4.76 μM	Buffer	[215]
DMSO reductase *R. sphaeroides*	Amperometric (−0.75 V)	DMSO	drop cast Nafion + MV/DMSO reductase + dialysis membrane/GC	Mediated (MV)	–	up to 600 μM	Buffer	[216]
TMAO reductase *E. coli*	Amperometric (−0.8 V)	TMAO	drop cast TMAO reductase chimera + dialysis membrane/G	Mediated (MV in solution)	2.96 nM	2–110 μM	Human serum	[85]
Perchlorate reductase *Dechlorosoma* sp.	Amperometric (−0.8 V)	ClO_4^-	drop cast Nafion/drop cast perchlorate reductase + MV + dialysis membrane/GC	Mediated (MV)	–	25–100 μg L^{-1}	Buffer	[217]
GSH reductase wheat germ	Amperometric (−0.7 V)	GSSG	GNP electrodeposition/polyTTBA electropolymerization/drop cast GSH reductase + NADPH/GC	Mediated (NADPH)	12.5 nM	100–2.5 mM	Plasma	[207]

(continued)

Table 5 (continued)

Enzyme Source	Transduction[a]	Analyte	Immobilization/electrode	Electron transfer	Detection limit	Linear range	Sample	References
Nitroreductase *E. cloacae*	Voltammetric (CV, −0.35 V)	TNT	PPB electropolymerization/NR-MBP adsorption/GC	Mediated (PPB)	2 μM	up to 40 μM	Buffer	[218]
Cytochrome *c* reductase porcine heart	Voltammetric (CV, −0.45 V)	Cyt *c*	PPy electrodeposition/drop cast Nafion + ethanol + CNTs/CcR + glutaraldehyde cross-linking/CSPE	Direct ET	10 nM	10 nM–500 μM	Cardiomyocytes	[219]

[a]All potentials are quoted vs. Ag/AgCl reference electrodes. *BMIMBF4* 1-n-butyl-3-methylimidazolium tetrafluoroborate, *BSA* bovine serum albumin, *CcR* cytochrome *c* reductase, *CSPE* carbon screen-printed electrode, *CV* cyclic voltammetry, *Cyt* cytochrome; *DMSO* dimethyl sulfoxide, *ET* electron transfer, *G* graphite, *GC* glassy carbon, *GNP* gold nanoparticles, *GSH* glutathione, *GSSG* glutathione disulfide, *MV* methyl viologen, *MWCNT* multi-walled carbon nanotubes, *NaR* nitrate reductase, *NiR* nitrite reductase, *NOR* nitric oxide reductase, *NR-MBP* nitroreductase-maltose binding protein, *PG* pyrolytic graphite, *polyTTBA* poly[2,2′:5,2″-terthiophene-30-(p-benzoic acid)], *PPB* N-(3-pyrrol-1-ylpropyl)-4,4’-bipyridine, *PPy* polypyrrole, *PVA* poly(vinyl alcohol), *SWCNT* singled-walled carbon nanotubes, *SWV* square wave voltammetry, *TMAO* trimethylamine *N*-oxide, *TNT* trinitrotoluene

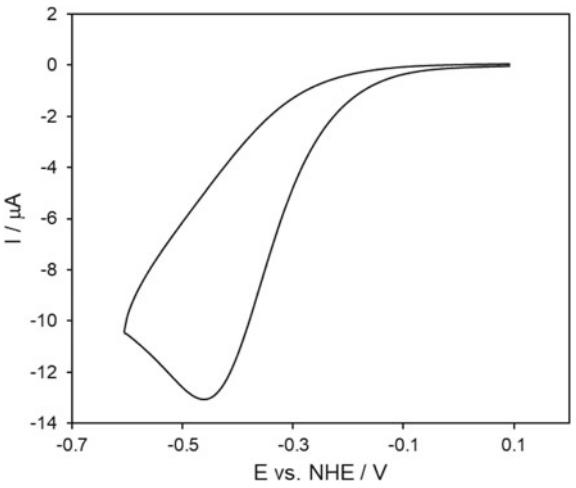

Fig. 9 O_2 reduction at a bare pyrolytic graphite electrode. Cyclic voltammogram was measured in aerated phosphate buffer (50 mM, pH 7.0) at a scan rate of 50 mV s^{-1}

4.2 Nitrogen Oxide Reductases

Among reported reductase-based biosensors, nitrate and nitrite reductases are the most widely explored enzymes. This is likely due to a combination of factors, including relatively easy purification processes, commercial availability of NaRs from different organisms, high catalytic activities, and/or facile ET with conductive supports. Importantly, NaRs and NiRs catalyze reactions of high environmental importance, as they take part of the denitrification pathway (bacterial driven multi-step reduction of nitrate to N_2), one of the main branches of the global nitrogen cycle [225]. The impact of high concentrations of the enzymes' substrates, nitrate and nitrite, in the environment, as well as, the potentially toxic effects in human health have prompted the World Health Organization and other regulation agencies to establish maximum levels, e.g., in drinking waters and meat products [206, 209]. The importance of nitrate and nitrite as biomarkers of human health and disease is another driving force for the development of new biosensing tools. These ions are involved in several physiological processes, either directly, in the case of nitrite, or through the connection to NO metabolism, which is an important mediator of cell signal transduction with critical roles in diverse physiological functions and in the pathophysiology of many human diseases [226, 227].

Several nitrate reductase biosensors have been proposed in the past three decades. NaRs are molybdenum dependent enzymes found in bacteria, algae, fungi, and plants. They constitute a heterogeneous group owing to their involvement in different biochemical pathways. NaRs have multiple redox centers and differ in terms of active site constitution, subunit structure, cellular localizations, and functions. Accordingly, they can be divided into four basic types: eukaryotic (eNaRs) and prokaryotic assimilatory (Nas), dissimilatory (Nap), and respiratory (Nar) nitrate reductases. Nitrate reduction to nitrite occurs at the molybdenum active site, which is coordinated by one or two pyranopterin cofactor molecules in

eukaryotic and prokaryotic NaRs, respectively. In addition, they contain other redox centers that are involved in electron flow to the catalytic site, namely heme *b*, flavins, and Fe-S clusters (Table 1 and Fig. 10a) [228, 229]. Although NaRs from all types have been employed in nitrate biosensors, the most commonly used are the commercially available NaRs from *Aspergillus niger* (fungal) and *E. coli* (Nar).

The majority of NaR biosensors are based on amperometric/voltammetric transducers [209]. Less explored approaches include colorimetric, potentiometric, and conductometric detection of the catalytic reaction [210, 211, 230–233]. As mentioned earlier, this work focuses on electrochemical biosensors.

In what concerns NaR amperometric/voltammetric biosensors, very few studies have explored direct ET for signal transduction [77, 234]. The majority of works employ redox mediators to facilitate the electrical communication between NaR and the electrode transducer. NAD(P)H and viologen derivatives are the most used compounds, but several other electron carrier molecules have been employed, such as azure A, safranins, hydroquinones, as well as, a heme-protein ET mediator, microperoxidase-11 [209, 235, 236]. The reaction scheme for mediated NaR (and other reductases) biosensors is depicted in Fig. 11a. In general, the redox mediators are co-immobilized with NaR on the surface of the electrode, although in some cases they are added to the assay solution. The immobilization methods used include adsorption, cross-linking, entrapment, electropolymerization, and covalent binding [208, 209]. As for the types of immobilization materials, they range from conducting and non-conduction polymers (e.g., polypyrrole [PPy] and Nafion) [212, 237] to self-assembled monolayers and nanomaterials (e.g., carbon nanotubes [CNTs] and poly(3,4-ethylenedioxythiophene) [PEDOT] nanowires) [238, 239]. Apart from the detection modes, potentiometric and conductometric NaR biosensors follow very similar construction modes to the amperometric/voltammetric counterparts. The enzymes are immobilized in polymeric matrices, such as Nafion and PPy, and redox mediators (Azure A, NADH, methyl viologen [MV]) are used to convert the enzyme to its reduced active state [210, 211, 232].

Fig. 10 Three-dimensional structures of reductase enzymes used in biosensors. **a** Catalytic ▶ subunit of periplasmic nitrate reductase (Nap) from *E. coli* (2NYA); molybdenum cofactor active site is depicted in green and Fe-S cluster in yellow. **b** Catalytic subunit of cytochrome *c* nitrite reductase (cc*NiR*) from *D. desulfuricans* (1OAH); heme groups are shown in dark red. **c** Nitric oxide reductase (NOR) from *Pseudomonas aeruginosa* (3O0R); non-heme iron (FeB) is represented in blue and heme groups are depicted in orange. **d** DMSO reductase from *R. sphaeroides* (1EU1); molybdenum cofactor active site is shown in green. **e** TMAO reductase from *Shewanella massilia* (1TMO); molybdenum cofactor active site is depicted in cyan; **f** Perchlorate reductase from *Azospira oryzae* PS (5CH7); molybdenum cofactor active site and Fe-S clusters are represented in green and in yellow, respectively. **g** GSH reductase from *Saccharomyces cerevisiae* (2HQM); Cys residues forming the disulfide bond at the catalytic site are represented in yellow and FAD cofactors are shown in orange. **h** Nitroreductase from *Enterobacter cloacae* (1NEC); FMN cofactors are shown in yellow. **i** Cytochrome *c* reductase (C*c*R) from *Bos taurus* (1BGY); hemes are depicted in red and Rieske cluster in green. Structures were prepared using UCSF Chimera software and the respective entries from RCSB Protein Data Bank (codes in brackets)

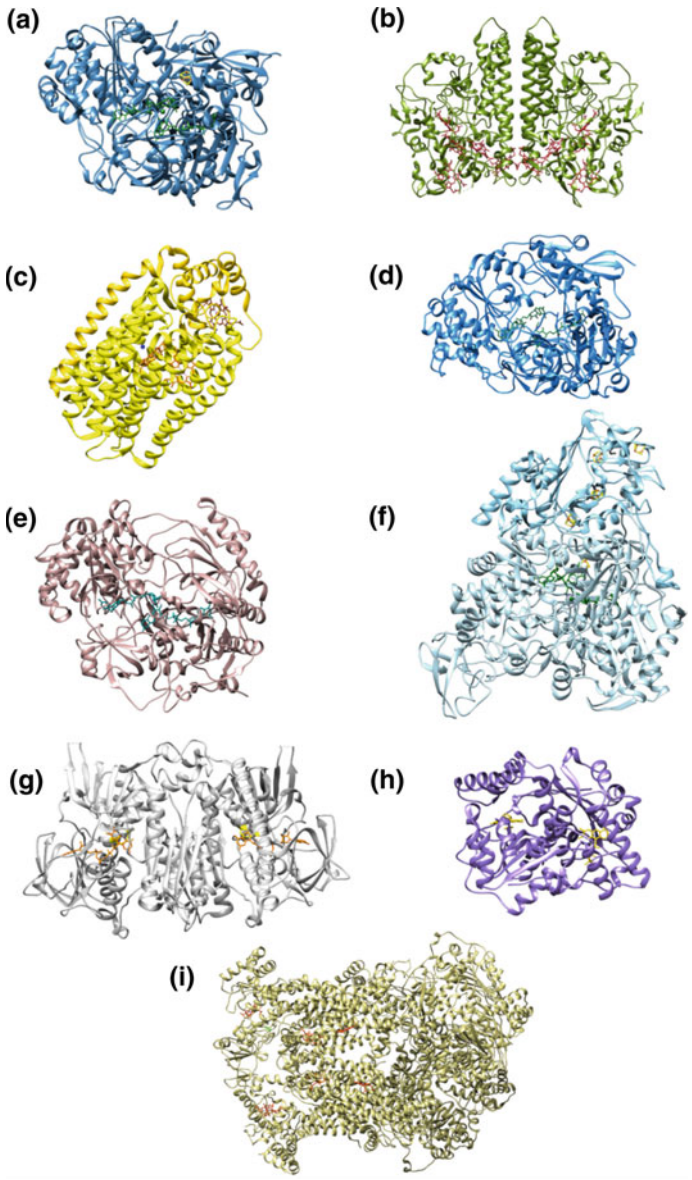

Although to a smaller extent than NaRs, nitrite reductases have also been explored for the construction of biosensing devices. NiRs are structurally diverse enzymes that contain heme, copper, and Fe-S prosthetic groups [240, 241]. They are organized into two groups: ammonia-forming (Eq. 11) and nitric oxide-forming (Eq. 12) NiRs. Each group is further divided into two classes, according to the

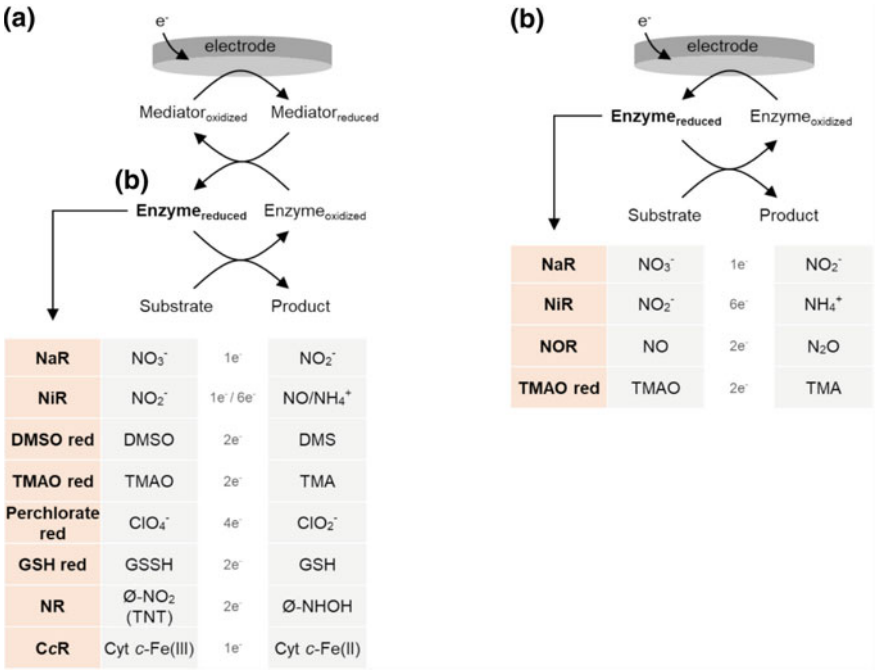

NaR	NO_3^-	1e⁻	NO_2^-
NiR	NO_2^-	1e⁻ / 6e⁻	NO/NH_4^+
DMSO red	DMSO	2e⁻	DMS
TMAO red	TMAO	2e⁻	TMA
Perchlorate red	ClO_4^-	4e⁻	ClO_2^-
GSH red	GSSH	2e⁻	GSH
NR	Ø-NO_2 (TNT)	2e⁻	Ø-NHOH
CcR	Cyt *c*-Fe(III)	1e⁻	Cyt *c*-Fe(II)

NaR	NO_3^-	1e⁻	NO_2^-
NiR	NO_2^-	6e⁻	NH_4^+
NOR	NO	2e⁻	N_2O
TMAO red	TMAO	2e⁻	TMA

Fig. 11 Schematic representations of the working principles of reductase-based amperometric/voltammetric biosensors. **a** mediated (second generation) and **b** direct electron transfer (third generation) based biosensors

redox cofactors (Table 1). Notably, all four NiR classes have been employed in nitrite biosensing. Cytochrome *c* (c*c*) NiRs, the most explored class, are oligomers containing multiple heme *c* groups, including a five-coordinated active site for nitrite binding (Fig. 10b) [80]. The sirohemic NiRs, the second class of ammonia-forming enzymes, harbor a siroheme active site connected by a bridging sulfur cysteine to a [4Fe–4S] cluster involved in ET [79]. The nitric oxide-forming enzyme class encompasses CuNiRs, which contain type-I copper centers, involved in ET, and type-II copper centers, as the active site and cytochrome cd_1NiRs, with heme *c* and heme d_1 groups as the electron acceptor and the substrate-binding sites, respectively [240, 241].

$$NO_2^- + 8H^+ + 6e^- \rightarrow NH_4^+ + 2H_2O \quad (11)$$

$$NO_2^- + 2H^+ + e^- \rightarrow NO + H_2O \quad (12)$$

Similarly to NaR, the majority of NiR-based biosensors rely on amperometric/voltammetric transducers, still, optical and conductometric biosensors have also been reported [206]. MV and viologen containing conducting polymers are the

most commonly used ET mediators in second generation NiR-based biosensors [206]. Aside from these chemical species, physiological redox mediators have also been employed, namely pseudoazurine coupled with the CuNiR from *Alcaligenes faecalis* S-6 and cytochrome c_{552} from *Marinobacter hydrocarbonoclausticus,* co-immobilized with the cd_1NiR from the same organism (Table 5) [213, 242]. The interaction between the NiRs and their natural ET partner proteins is thought to be advantageous relative to biosensors based on artificial mediators, given that it reproduces the ET processes occurring in vivo and improves detection selectivity [243].

The ability of c*c*NiRs to directly exchange electrons with carbon electrodes has been exploited for the construction of non-mediated, third generation, nitrite biosensors [214, 223, 224, 244]. In these devices, the electrocatalytic currents arise from the direct regeneration of enzyme cofactors at the electrode surface, following substrate reduction, as shown in Fig. 11b. Since they are operated at potentials directly related to the reduction potential of the enzyme, the selectivity is expected to increase, and the interfering reactions minimized. The use of carbon nanomaterials for electrode modification was shown to improve the wiring of the enzyme and to contribute to greatly enhanced enzyme catalysis [214, 245]. In effect, the highest current density response to nitrite so far has been obtained with a bioelectrode based on *Desulfovibrio desulfuricans* c*c*NiR adsorbed on multilayered single-walled CNTs (SWCNTs) deposits (sensitivity 2.4 $A \cdot M^{-1} \cdot cm^{-2}$) [214].

Nitric oxide reductases (NORs) are involved in the third step of bacterial denitrification pathway, being responsible for the conversion of NO to nitrous oxide [240, 241]. Recently the direct electrochemical response of *M. hydrocarbonoclasticus* NOR and the electrocatalytic activity towards NO have been studied at carbon electrode interfaces [83, 215, 246]. The heterodimeric enzyme belongs to the cNOR family of nitric oxide reductases and contains heme *c* and heme *b* ET groups, and a catalytic di-iron center formed by a heme b_3 and a non-heme Fe_B, bridged by a μ-oxo/hydroxo group (Fig. 10c) [240, 241]. Direct ET of NOR was observed upon adsorption to bare [215] and CNT composite modified pyrolytic graphite (PG) electrodes [83, 246]. The resulting bioelectrodes were employed as third generation biosensors for quantification of NO (Fig. 11b). The nanocomposite-based electrodes provided much higher sensitivities in comparison to the bare PG. The authors showed that the SWCNTs-lipid bilayer films and MWCNTs-ionic liquid composites constitute suitable microenvironments for the immobilization of the membrane protein, and for the preservation and enhancement of its activity [83, 246].

4.3 Other Reductase Enzymes

Aside NaRs, three other molybdenum dependent reductase enzymes have been used in amperometric biosensors, namely the DMSO reductase from *Rhodobacter sphaeroides*, the trimethylamine *N*-oxide (TMAO) reductase (TorA) from *E. coli,* and the perchlorate reductase from *Dechlorosoma* sp. Like the prokaryotic NaRs,

the molybdenum center in these enzymes is coordinated by two pyranopterin molecules; the first two enzymes have monomeric structures [228, 247, 248], while perchlorate reductase is a heterodimeric protein and contains Fe-S clusters (four [4Fe-4S] and one [3Fe-4S]) in addition to the molybdenum cofactor (Table 1 and Fig. 10d–f) [249].

DMSO reductase catalyzes the reduction of DMSO to dimethyl sulfide (DMS). As a common organic solvent used in numerous industrial and laboratory applications, DMSO can be found in wastewaters; besides, it is also naturally occurring in beverages and foodstuff. Given its unpleasant smell in high concentrations, DMSO detection is important in beverage quality control, as well as, in wastewater monitoring [216]. As for perchlorate reductase, the enzyme is involved in the first two steps of perchlorate breakdown to chloride and O_2 (ClO_4^-→-ClO_3^-→ClO_2^-→Cl^-+O_2) [249]. The contamination of groundwaters with perchlorate (that can derive from solid rocket propellant manufacturing for example) can have significant adverse defects in animal development and human health [217]. Finally, TorA is involved in the two-electron reduction of TMAO to trimethylamine (TMA) [247]. Because of its potential as a disease biomarker, TMAO quantification is relevant for clinical diagnosis [85]. Biosensors based on these three enzymes follow similar approaches. In the reported devices MV is used for mediated signal transduction and immobilization on electrode surfaces relies on non-conduction materials, such as Nafion and dialysis membranes [85, 216, 217, 222, 250]. The TorA biosensor also displayed direct electrocatalytic currents for TMAO reduction (Fig. 11b), however, the activity was about 80 times higher in the presence of the redox mediator [85]. Different methods have been employed to avoid O_2 background currents when operating these biosensors: addition of the GOx/Cat O_2 removal system in the case of DMSO and TMAO biosensors [85, 250] and of cysteine hydrochloride with the perchlorate reductase-based device [217].

The glutathione/glutathione disulfide ratio (GSH/GSSG) is an important indicator of cellular oxidative stress. The accumulation of the oxidized compound, GSSG, has been associated with several pathological conditions (e.g., diabetes and Alzheimer's disease), making it an important target in the clinical analysis [251]. In vivo, the enzyme glutathione reductase and NADPH are responsible for maintaining cellular GSH/GSSH equilibrium. Each monomer of the homodimer enzyme contains a FAD cofactor, while the active site consists of a disulfide bond formed by two cysteine residues (Fig. 10g) [252]. Several glutathione reductase-based amperometric biosensors have been reported in the past three decades. The electrocatalytic detection of GSSG by the immobilized enzyme is typically mediated by viologen redox mediators or NADPH. Glutathione reductase was shown to retain its activity while immobilized on thiolated self-assembled monolayers, electropolymerized PPy films, or chitosan membranes [251, 253, 254]. More recently, nanostructured interfaces based on MWCNTs and gold nanoparticles (GNPs) have allowed lowering the detections limits and increasing biosensor's lifetimes [207, 255]. The devices have been used for the analysis of blood and plasma samples, as well as, in vivo measurements in rat livers [207, 251].

Detection of nitroaromatic compounds is important for environmental monitoring given their widespread use in agro and warfare chemicals. The nitroreductase (NR) from *Enterobacter cloacae* catalyzes two-electron reductions of a variety of nitroaromatic compounds, including trinitrotoluene (TNT). The enzyme contains an FMN cofactor that binds in deep pockets located at the interface of its homodimeric structure (Fig. 10h) [87]. Naal et al. described a mediated voltammetric biosensor for TNT based on this NR fused to a maltose-binding protein (MBP) [218]. The fusion protein was immobilized on *N*-(3-pyrrol-1-ylpropyl)-4,4′-bipyridine modified electrodes through the MBP domain, which is thought to establish strong electrostatic interactions with the conducting polymer film and to contribute to the maintenance of the immobilized enzyme's activity [218].

Cytochrome *c* reductase, C*c*R (bc_1 complex), is an oligomeric membrane protein complex that catalyzes the oxidation of ubihydroquinone and the reduction of cytochrome *c* in photosynthetic and respiratory chains. The catalytic core of the enzyme is composed of three subunits, which carry a heme *b*, a heme c_1, and a [2Fe-2S] cluster (Rieske type) (Fig. 10i) [256]. Recently, C*c*R has been employed in biosensors for the detection of cytochrome *c* [88, 219] and nitrite [257]. Nanostructured electrodes based on CNTs and GNPs incorporated in PPy films were shown to improve ET to the deeply embedded enzyme cofactors [88]. Still, hydroquinone has been used as a redox mediator. The biosensors have been used for quantification of cytochrome *c* in apoptotic cardiomyocytes and cytosolic fractions of human lung carcinoma cells (Table 5) [88, 219] and nitrite in hypoxic H9c2 cardiac cells [257].

5 Hydrolases

The majority of amperometric/voltammetric devices featuring hydrolases (Fig. 12) as the biorecognition element are targeted towards organophosphate compounds monitoring [258]. These compounds (also known as phosphotriesters) are a class of highly neurotoxic synthetic compounds that are widely used as agricultural insecticides, petroleum additives, plasticizers, refrigerants, dyes, and chemical warfare agents. In vivo, these compounds inhibit irreversibly acetylcholinesterase, which hydrolyzes the neurotransmitter acetylcholine into choline and acetic acid at the cholinergic synapses and neuromuscular junctions, thus serving as a regulator of neurotransmission [259, 260].

The detection principle of hydrolase-based amperometric/voltammetric biosensors relies on the catalytic activity of the enzyme to produce an electroactive product that is detectable on the electrode's surface (much like H_2O_2 in oxidase-based devices, Fig. 2). The analyte itself could be the enzyme's substrate; alternatively, it could inhibit the bioreceptor, in which case detection is based on the level of activity inhibition [261, 262].

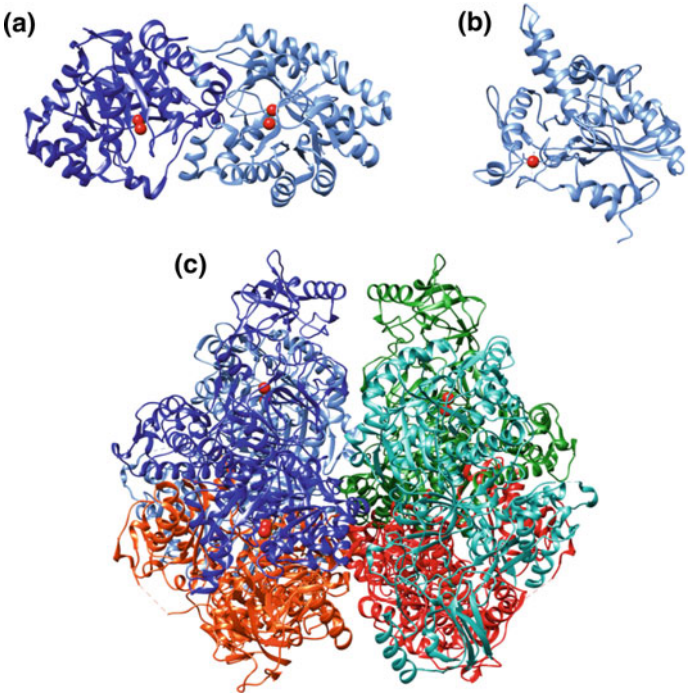

Fig. 12 Three-dimensional structures of hydrolytic enzymes with biosensing application: **a** OPH from *Geobacillus strearothermophillus* (3F4C); **b** lipase from *Burkholderia cepacia* (1OIL); **c** urease from *Canavalia formis* (3LA4). Red spheres represent the respective **a** cobalt, **b** calcium and **c** nickel divalent cations. Structures were rendered using UCSF Chimera and the respective entries (in brackets) from RCSB Protein Data Bank

For the direct detection of pesticides, bacterial organophosphorus hydrolase (OPH) has been vastly researched [262–266]. This enzyme is a phosphotriesterase with a broad substrate specificity that catalyzes the hydrolysis of P–O, P–S, P–F, and P–CN bonds in organophosphate pesticides, producing *p*-nitrophenol [262, 267, 268]. This hydrolysis product is redox-active and its oxidation above 700 mV (vs. Ag/AgCl reference system) is used for the amperometric/voltammetric detection of the precursor analyte [263, 264, 266]. Also, since two protons are released per parent molecule during hydrolysis, pH electrodes can be used to measure the localized decrease in pH as a function of the analyte concentration (potentiometric devices) [261, 263].

Mammalian paraoxonase 1 is another interesting candidate for the development of hydrolytic biosensors for organophosphorus compounds monitoring. This enzyme belongs to a family of highly conserved enzymes in mammals and that is comprised of three isoforms: PON1, PON2, and PON3. The nomenclature is a purely historical one since this family has one of the broadest specificities known

[269–271]. The early in vitro studies on PON1, where it was shown that it was able to hydrolyze paraoxon, were on the basis that led to the adoption of the name [271–273]. Thorough studies on the hydrolysis of over 50 substrates have concluded that the native activity of PON1 was that of a lactonase, with promiscuous phosphotriesterase and paraoxonase activities [270, 274]. Regarding its use in the construction of biosensing devices, while having in mind the wide variety of substrates that are reported to be metabolized by this hydrolase and their analytical interest, its application as a biorecognition element is rather non-existent in the literature. In fact, only two devices have been reported recently featuring the enzyme in such a role [275, 276]. Both analytical tools were targeted towards paraoxon and diazon detection, using either an optical or electrochemical transduction method, respectively.

As an alternative to OPH, lipases (triacylglycerol ester hydrolases) can be employed as the catalytic biorecognition element. These enzymes catalyze the hydrolysis and synthesis of long-chain acylglycerols and many other esters [277, 278]. Unlike OPH, lipases are commercially available at a more affordable price, making them an attractive alternative [277]. Lipases can also be used as an alternative to cholinesterases (ChE), which are the most common hydrolases used in inhibition-based organophosphate determination [268]. This was demonstrated in the amperometric determination of chlorfenvinphos and malathion using the decrease in lipase's activity towards *p*-nitrophenyl acetate as a function of the pesticides' concentration [279]. ChE-based devices are designed using a mono-, bi- and tri-enzymatic detection system. In the first, artificial substrates such as acetylthiocholine or butyrylthiocholine are used, and the hydrolysis product thiocholine is detected via oxidation [280, 281]. In the bi-enzymatic system, ChE is coupled to the flavoenzyme ChOx. The hydrolysis product choline is oxidized by ChOx and detection is made either through O_2 depletion or H_2O_2 oxidation monitoring [101, 282]. Lastly, the tri-enzymatic approach adds peroxidase to the previous, and detection is made by the catalytic reduction of H_2O_2 [283].

Apart from organophosphorus compounds monitoring, hydrolase-based amperometric/voltammetric biosensors have also been developed for clinical diagnostic application and metals detection. For example, urease which catalyzes the hydrolysis of urea to ammonia has been used as the key element in amperometric/voltammetric devices for urea [284–288], lead [289], and mercury [289–291] determination. The enzyme is commonly immobilized in a conducting polymer matrix (polypyrrole or polyaniline) that serves a dual purpose. First, it provides a good microenvironment for enzyme immobilization; secondly, its interaction with the produced ammonia makes it possible to detect the urea hydrolysis reaction using amperometric/voltammetric methods [285, 287, 292]. Another example of hydrolase-based clinical tools is that of multienzyme biodevices for triglycerides determination, in which lipase is the key biorecognition element. Together with glycerol kinase and glycerol-3-phosphate oxidase, lipase catalyzes the hydrolysis of triglycerides to fatty acids and glycerol, followed by oxidation of the later, producing H_2O_2 and locally consuming O_2 [293–296]. Alternatively, lipase can be combined with glycerol dehydrogenase, which oxidizes

glycerol in the presence of the redox cofactor NADH. Its electrochemical response can then be assessed through the use of a redox mediator [297, 298].

Hydrolases can also be used as part of target probes in affinity biosensors. When the probe binds to its specific target (the analyte in question), the hydrolytic reaction generates an electroactive product that is detected at the electrode's surface. The alkaline phosphatase has been applied in the construction of such devices for the detection of tumor and influenza virus biomarkers [299, 300]. The detection principle is based on the hydrolysis of amino- or nitrophenyl phosphates, which results in an oxidizable product that is detected at the electrode.

6 Summary and Outlook

From the early work of Clark and Lyons with glucose oxidase, biosensing with selective enzymes has become an extensive research field. Attractive features of these biocatalysts, such as high selectivity, sensitivity, and fast reaction rates, have maintained them as highly sought after bioreceptors for biosensor construction. The combination with electrochemical transducers has been widely explored due to added advantages, such as simplicity, relative low costs, high sensitivity, and the potential to create miniaturized, portable devices.

Glucose detection, which is mostly based on glucose oxidases and dehydrogenases, continues to dominate the biosensor's market and remains one of the largest areas in biosensor research. Nonetheless, the demand for improved analytical tools for a variety of target substrates increases continuously and stimulates the exploitation of a plethora of new enzymes. Accordingly, electrochemical enzyme-based biosensors have been proposed for the detection of several important analytes, such as cholesterol, neurotransmitters, or phenolic compounds using a variety of oxidase enzymes; nitrate, nitrite, or nitric oxide with selective reductases; and organophosphate compounds, urea or influenza virus biomarkers by employing different hydrolases.

The enzyme biosensor field shows no signs of slowing down. Still, a number of issues need to be addressed before new bioelectrocatalytic systems can make an impact on real-life applications. Further optimization of biosensor architectures is required to ensure efficient enzyme integration with electrode interfaces, facilitating ET, and improving device stability and reproducibility. Significant progress has been made through the years and will undoubtedly continue, owing to advances in material sciences, polymer chemistry, and electronics technology, as well as, the increased understanding of enzyme properties and the parameters that control their activity on electrode surfaces. Through combined research efforts, the advantages of these unique biocatalysts have and are expected to carry on supplying solutions to analytical challenges ranging from biomedical analysis to environmental pollution, food safety, or industrial bioprocess monitoring.

Acknowledgements Authors are grateful to the Applied Molecular Biosciences Unit-UCIBIO, which is financed by national funds from FCT/MCTES (UID/Multi/04378/2013) and co-financed by the ERDF under the PT2020 Partnership Agreement (POCI-01-0145-FEDER-007728). CMS acknowledges the support from Project LISBOA-01-0145-FEDER-007660 (Microbiologia Molecular, Estrutural e Celular) funded by FEDER funds through COMPETE 2020-Programa Operacional Competitividade e Internacionalização (POCI) and from FCT- Fundação para a Ciência e a Tecnologia (PTDC/BIA-BFS/31026/2017). TM thanks the financial support from Fundação para a Ciência e Tecnologia (Fellowship PD/BD/109687/2015).

References

1. Forster RJ (2017) Editorial: sensors and biosensors. Curr Opin Electrochem 3:1–3. https://doi.org/10.1016/j.coelec.2017.10.002
2. Monteiro T, Almeida MG (2019) Electrochemical enzyme biosensors revisited: old solutions for new problems. Crit Rev Anal Chem 49:44–66. https://doi.org/10.1080/10408347.2018.1461552
3. Turner APF (2013) Biosensors: sense and sensibility. Chem Soc Rev 42:3184–3196. https://doi.org/10.1039/c3cs35528d
4. Markets and Markets (2019) Biosensors market by type (sensor patch and embedded device), product (wearable and nonwearable), technology (electrochemical and optical), application (POC, home diagnostics, research lab, food & beverages), and geography—Global Forecast to 2024. In: https://www.marketsandmarkets.com/Market-Reports/biosensors-market-798.html. Accessed Mar 2020
5. Grand View Research (2020) Biosensors market size, share & trends analysis report by application (Agriculture, medical) by technology (thermal, electrochemical, optical), by end use (PoC testing, food industry), and segment forecasts, 2019–2026. In: https://www.grandviewresearch.com/industry-analysis/biosensors-market. Accessed Mar 2020
6. Yoo E-H, Lee S-Y (2010) Glucose biosensors: an overview of use in clinical practice. Sensors 10:4558–4576. https://doi.org/10.3390/s100504558
7. Fagan RL, Palfey BA (2010) Flavin-dependent enzymes. In: Liu H-W, Mander L (eds) Comprehensive natural products II. Elsevier Science, pp 37–113
8. Bartlett PN, Al-Lolage FA (2017) There is no evidence to support literature claims of direct electron transfer (DET) for native glucose oxidase (GO_x) at carbon nanotubes or graphene. J Electroanal Chem 819:26–37. https://doi.org/10.1016/j.jelechem.2017.06.021
9. Wohlfahrt G, Witt S, Hendle J et al (1999) 1.8 and 1.9 Å resolution structures of the *Penicillium amagasakiense* and *Aspergillus niger* glucose oxidases as a basis for modelling substrate complexes. Acta Crystallogr Sect D: Biol Crystallogr 55:969–977. https://doi.org/10.1107/S0907444999003431
10. Dijkman WP, de Gonzalo G, Mattevi A, Fraaije MW (2013) Flavoprotein oxidases: classification and applications. Appl Microbiol Biotechnol 97:5177–5188. https://doi.org/10.1007/s00253-013-4925-7
11. Wilson R, Turner APF (1992) Glucose oxidase: an ideal enzyme. Biosens Bioelectron 7:165–185. https://doi.org/10.1016/0956-5663(92)87013-F
12. Bankar SB, Bule MV, Singhal RS, Ananthanarayan L (2009) Glucose oxidase—an overview. Biotechnol Adv 27:489–501. https://doi.org/10.1016/j.biotechadv.2009.04.003
13. Wang J (2008) Electrochemical glucose biosensors. Chem Rev 108:814–825. https://doi.org/10.1021/cr068123a
14. Azevedo AM, Prazeres DMF, Cabral JMS, Fonseca LP (2005) Ethanol biosensors based on alcohol oxidase. Biosens Bioelectron 21:235–247. https://doi.org/10.1016/j.bios.2004.09.030

15. Goswami P, Chinnadayyala SSR, Chakraborty M et al (2013) An overview on alcohol oxidases and their potential applications. Appl Microbiol Biotechnol 97:4259–4275. https://doi.org/10.1007/s00253-013-4842-9
16. Koch C, Neumann P, Valerius O et al (2016) Crystal structure of alcohol oxidase from Pichia pastoris. PLoS ONE 11:e0149846. https://doi.org/10.1371/journal.pone.0149846
17. Nguyen Q-T, Romero E, Dijkman WP et al (2018) Structure-based engineering of phanerochaete chrysosporium alcohol oxidase for enhanced oxidative power toward glycerol. Biochemistry 57:6209–6218. https://doi.org/10.1021/acs.biochem.8b00918
18. Ghanem M, Fan Francis K, Gadda G (2003) Spectroscopic and kinetic properties of recombinant choline oxidase from Arthrobacter globiformis. Biochemistry 42:15179–15188. https://doi.org/10.1021/bi035435o
19. Quaye O, Lountos GT, Fan et al (2008) Role of Glu312 in binding and positioning of the substrate for the hydride transfer reaction in choline oxidase. Biochemistry 47:243–256. https://doi.org/10.1021/bi7017943
20. Baker KL, Bolger FB, Lowry JP (2017) Development of a microelectrochemical biosensor for the real-time detection of choline. Sensors Actuators B Chem 243:412–420. https://doi.org/10.1016/j.snb.2016.11.110
21. Rahimi P, Joseph Y (2019) Enzyme-based biosensors for choline analysis: A review. TrAC Trends Anal Chem 110:367–374. https://doi.org/10.1016/j.trac.2018.11.035
22. Arima J, Sasaki C, Sakaguchi C et al (2009) Structural characterization of l-glutamate oxidase from Streptomyces sp. X-119-6. FEBS J 276:3894–3903. https://doi.org/10.1111/j.1742-4658.2009.07103.x
23. Hughes G, Pemberton RM, Fielden PR, Hart JP (2016) The design, development and application of electrochemical glutamate biosensors. TrAC Trends Anal Chem 79:106–113. https://doi.org/10.1016/j.trac.2015.10.020
24. Yue QK, Kass IJ, Sampson NS, Vrielink A (1999) CCrystal structure determination of cholesterol oxidase from streptomyces and structural characterization of key active site mutants. Biochemistry 38:4277–4286. https://doi.org/10.1021/bi982497j
25. MacLachlan J, Wotherspoon ATL, Ansell RO, Brooks CJW (2000) Cholesterol oxidase: sources, physical properties and analytical applications. J Steroid Biochem Mol Biol 72:169–195. https://doi.org/10.1016/S0960-0760(00)00044-3
26. Lyubimov AY, Heard K, Tang H et al (2007) Distortion of flavin geometry is linked to ligand binding in cholesterol oxidase. Protein Sci 16:2647–2656. https://doi.org/10.1110/ps.073168207
27. Vrielink A, Ghisla S (2009) Cholesterol oxidase: biochemistry and structural features. FEBS J 276:6826–6843. https://doi.org/10.1111/j.1742-4658.2009.07377.x
28. Narwal V, Deswal R, Batra B et al (2019) Cholesterol biosensors: a review. Steroids 143:6–17. https://doi.org/10.1016/j.steroids.2018.12.003
29. Leiros I, Wang E, Rasmussen T et al (2006) The 2.1 Å structure of Aerococcus viridans L-lactate oxidase (LOX). Acta Crystallogr, Sect F: Struct Biol Cryst Commun 62:1185–1190. https://doi.org/10.1107/S1744309106044678
30. Li SJ, Umena Y, Yorita K et al (2007) Crystallographic study on the interaction of l-lactate oxidase with pyruvate at 1.9 Å resolution. Biochem Biophys Res Commun 358:1002–1007. https://doi.org/10.1016/j.bbrc.2007.05.021
31. Lamas-Ardisana PJ, Loaiza OA, Añorga L et al (2014) Disposable amperometric biosensor based on lactate oxidase immobilised on platinum nanoparticle-decorated carbon nanofiber and poly(diallyldimethylammonium chloride) films. Biosens Bioelectron 56:345–351. https://doi.org/10.1016/j.bios.2014.01.047
32. Rathee K, Dhull V, Dhull R, Singh S (2016) Biosensors based on electrochemical lactate detection: a comprehensive review. Biochem Biophys Reports 5:35–54. https://doi.org/10.1016/j.bbrep.2015.11.010

33. Enroth C, Eger BT, Okamoto K et al (2000) Crystal structures of bovine milk xanthine dehydrogenase and xanthine oxidase: structure-based mechanism of conversion. Proc Natl Acad Sci 97:10723–10728. https://doi.org/10.1073/pnas.97.20.10723
34. Pauff JM, Zhang J, Bell CE, Hille R (2008) Substrate orientation in xanthine oxidase. J Biol Chem 283:4818–4824. https://doi.org/10.1074/jbc.M707918200
35. Hille R, Nishino T (1995) Xanthine oxidase and xanthine dehydrogenase. FASEB J 9:995–1003. https://doi.org/10.1096/fasebj.9.11.7649415
36. Wang C-H, Zhang C, Xing X-H (2016) Xanthine dehydrogenase: an old enzyme with new knowledge and prospects. Bioengineered 7:395–405. https://doi.org/10.1080/21655979.2016.1206168
37. Clark LC, Lyons C (1962) Electrode Systems for continous mmonitoring in cardiovascular surgery. Ann N Y Acad Sci 102:29–45. https://doi.org/10.1111/j.1749-6632.1962.tb13623.x
38. D'Orazio P (2003) Biosensors in clinical chemistry. Clin Chim Acta 334:41–69. https://doi.org/10.1016/S0009-8981(03)00241-9
39. Newman JD, Turner APF (2005) Home blood glucose biosensors: a commercial perspective. Biosens Bioelectron 20:2435–2453. https://doi.org/10.1016/j.bios.2004.11.012
40. da Silva Pereira, Neves MM, González-García MB, Hernández-Santos D, Fanjul-Bolado P (2018) Future trends in the market for electrochemical biosensing. Curr Opin Electrochem 10:107–111. https://doi.org/10.1016/j.coelec.2018.05.002
41. Zhao C, Thuo MM, Liu X (2013) A microfluidic paper-based electrochemical biosensor array for multiplexed detection of metabolic biomarkers. Sci Technol Adv Mater 14:054402. https://doi.org/10.1088/1468-6996/14/5/054402
42. Desmet C, Marquette CA, Blum LJ, Doumèche B (2016) Paper electrodes for bioelectrochemistry: biosensors and biofuel cells. Biosens Bioelectron 76:145–163. https://doi.org/10.1016/j.bios.2015.06.052
43. Salim A, Lim S (2019) Recent advances in noninvasive flexible and wearable wireless biosensors. Biosens Bioelectron 141:111422. https://doi.org/10.1016/j.bios.2019.111422
44. Yu H, Luo X, Shi W et al (2019) A cork-based smart biosensing system for ethanol. IEEE Sens J 19:2313–2319. https://doi.org/10.1109/JSEN.2018.2885000
45. Sha P, Luo X, Shi W et al (2019) A smart dental floss for biosensing of glucose. Electroanalysis 31:791–796. https://doi.org/10.1002/elan.201800885
46. Pundir CS, Devi R (2014) Biosensing methods for xanthine determination: a review. Enzyme Microb Technol 57:55–62. https://doi.org/10.1016/j.enzmictec.2013.12.006
47. Alam F, RoyChoudhury S, Jalal AH et al (2018) Lactate biosensing: the emerging point-of-care and personal health monitoring. Biosens Bioelectron 117:818–829. https://doi.org/10.1016/j.bios.2018.06.054
48. Sabu C, Henna TK, Raphey VR et al (2019) Advanced biosensors for glucose and insulin. Biosens Bioelectron 141:111201. https://doi.org/10.1016/j.bios.2019.03.034
49. Johansson K, Jönsson-Pettersson G, Gorton L et al (1993) A reagentless amperometric biosensor for alcohol detection in column liquid chromatography based on co-immobilized peroxidase and alcohol oxidase in carbon paste. J Biotechnol 31:301–316. https://doi.org/10.1016/0168-1656(93)90076-Y
50. Habermüller K, Mosbach M, Schuhmann W (2000) Electron-transfer mechanisms in amperometric biosensors. Fresenius J Anal Chem 366:560–568. https://doi.org/10.1007/s002160051551
51. Green MJ, Hill HAO (1986) Amperometric enzyme electrodes. J Chem Soc Faraday Trans 1 Phys Chem Condens Phases 82:1237. https://doi.org/10.1039/f19868201237
52. Wilson GS, Gifford R (2005) Biosensors for real-time in vivo measurements. Biosens Bioelectron 20:2388–2403. https://doi.org/10.1016/j.bios.2004.12.003
53. Borgmann S, Hartwich G, Schulte A, Schuhmann W (2005) Amperometric Enzyme Sensors based on Direct and Mediated Electron Transfer. In: Paleček E, Scheller F, Wang J (eds) Electrochemistry of nucleic acids and proteins Arthrobacter globiformis towards electrochemical sensors for genomics and proteomics. Elsevier Science, pp 599–655

54. Scheller FW, Lisdat F, Wollenberger U (2005) Application of electrically contacted enzymes for biosensors. In: Willner I, Katz E (eds) Bioelectronics. Wiley-VCH Verlag GmbH & Co, KGaA, Weinheim, FRG, pp 99–126
55. Jiang L, McNeil CJ, Cooper JM (1995) Direct electron transfer reactions of glucose oxidase immobilised at a self-assembled monolayer. J Chem Soc, Chem Commun 12:1293–1295. https://doi.org/10.1039/c39950001293
56. Courjean O, Gao F, Mano N (2009) Deglycosylation of glucose oxidase for direct and efficient glucose electrooxidation on a glassy carbon electrode. Angew Chemie - Int Ed 48:5897–5899. https://doi.org/10.1002/anie.200902191
57. Sajjadi S, Ghourchian H, Rahimi P (2011) Different behaviors of single and multi wall carbon nanotubes for studying electrochemistry and electrocatalysis of choline oxidase. Electrochim Acta 56:9542–9548. https://doi.org/10.1016/j.electacta.2011.04.039
58. Wu S, Chen J, Liu D et al (2016) A biocompatible cerasome based platform for direct electrochemistry of cholesterol oxidase and cholesterol sensing. RSC Adv 6:70781–70790. https://doi.org/10.1039/C6RA06368C
59. Gao Y, Shen C, Di J, Tu Y (2009) Fabrication of amperometric xanthine biosensors based on direct chemistry of xanthine oxidase. Mater Sci Eng, C 29:2213–2216. https://doi.org/10.1016/j.msec.2009.05.004
60. Wilson GS (2016) Native glucose oxidase does not undergo direct electron transfer. Biosens Bioelectron 82:7–8. https://doi.org/10.1016/j.bios.2016.04.083
61. Milton RD, Minteer SD (2017) Direct enzymatic bioelectrocatalysis: differentiating between myth and reality. J R Soc Interface 14:20170253. https://doi.org/10.1098/rsif.2017.0253
62. Vogt S, Schneider M, Schäfer-Eberwein H, Nöll G (2014) Determination of the pH dependent redox potential of glucose oxidase by spectroelectrochemistry. Anal Chem 86:7530–7535. https://doi.org/10.1021/ac501289x
63. Abbasi S, Gharaghani S, Benvidi A et al (2018) An in-depth view of potential dual effect of thymol in inhibiting xanthine oxidase activity: Electrochemical measurements in combination with four way PARAFAC analysis and molecular docking insights. Int J Biol Macromol 119:1298–1310. https://doi.org/10.1016/j.ijbiomac.2018.08.018
64. Gadda G, Wels G, Pollegioni L et al (1997) Characterization of cholesterol oxidase from Streptomyces hygroscopicus and Brevibacterium sterolicum. Eur J Biochem 250:369–376. https://doi.org/10.1111/j.1432-1033.1997.0369a.x
65. Yorita K, Matsuoka T, Misaki H, Massey V (2000) Interaction of two arginine residues in lactate oxidase with the enzyme flavin: conversion of FMN to 8-formyl-FMN. Proc Natl Acad Sci 97:13039–13044. https://doi.org/10.1073/pnas.250472297
66. Ivnitski DM, Khripin C, Luckarift HR et al (2010) Surface characterization and direct bioelectrocatalysis of multicopper oxidases. Electrochim Acta 55:7385–7393. https://doi.org/10.1016/j.electacta.2010.07.026
67. Ludwig R, Ortiz R, Schulz C et al (2013) Cellobiose dehydrogenase modified electrodes: advances by materials science and biochemical engineering. Anal Bioanal Chem 405:3637–3658. https://doi.org/10.1007/s00216-012-6627-x
68. Torimura M, Kano K, Ikeda T, Ueda T (1997) Spectroelectrochemical characterization of quinohemoprotein alcohol dehydrogenase from gluconobacter suboxydans. Chem Lett 26:525–526. https://doi.org/10.1246/cl.1997.525
69. Tkac J, Svitel J, Vostiar I, et al (2009) Membrane-bound dehydrogenases from Gluconobacter sp.: Interfacial electrochemistry and direct bioelectrocatalysis. Bioelectrochemistry 76:53–62. https://doi.org/10.1016/j.bioelechem.2009.02.013
70. Tanne C, Göbel G, Lisdat F (2010) Development of a (PQQ)-GDH-anode based on MWCNT-modified gold and its application in a glucose/O_2-biofuel cell. Biosens Bioelectron 26:530–535. https://doi.org/10.1016/j.bios.2010.07.052
71. Takeda K, Matsumura H, Ishida T et al (2015) Characterization of a novel PQQ-dependent quinohemoprotein pyranose dehydrogenase from Coprinopsis cinerea classified into

auxiliary activities family 12 in carbohydrate-active enzymes. PLoS ONE 10:e0115722. https://doi.org/10.1371/journal.pone.0115722
72. Larsson T, Lindgren A, Ruzgas T (2001) Spectroelectrochemical study of cellobiose dehydrogenase and diaphorase in a thiol-modified gold capillary in the absence of mediators. Bioelectrochemistry 53:243–249. https://doi.org/10.1016/S0302-4598(01)00099-X
73. Aguey-Zinsou KF, Bernhardt PV, Kappler U, McEwan AG (2003) Direct electrochemistry of a bacterial sulfite dehydrogenase. J Am Chem Soc 125:530–535. https://doi.org/10.1021/ja028293e
74. Christenson A, Gustavsson T, Gorton L, Hägerhäll C (2008) Direct and mediated electron transfer between intact succinate:quinone oxidoreductase from Bacillus subtilis and a surface modified gold electrode reveals redox state-dependent conformational changes. Biochim Biophys Acta Bioenerg 1777:1203–1210.https://doi.org/10.1016/j.bbabio.2008.05.450
75. Barber MJ, Pollock V, Spence JT (1988) Microcoulometric analysis of trimethylamine dehydrogenase. Biochem J 256:657–659. https://doi.org/10.1042/bj2560657
76. Husain M, Davidson VL, Gray KA, Knaff DB (1987) Redox properties of the quinoprotein methylamine dehydrogenase from paracoccus denitrificans. Biochemistry 26:4139–4143. https://doi.org/10.1021/bi00387a059
77. Kalimuthu P, Fischer-Schrader K, Schwarz G, Bernhardt PV (2013) Mediated Electrochemistry of Nitrate Reductase from Arabidopsis thaliana. J Phys Chem B 117:7569–7577. https://doi.org/10.1021/jp404076w
78. Coelho C, Marangon J, Rodrigues D et al (2013) Induced peroxidase activity of haem containing nitrate reductases revealed by protein film electrochemistry. J Electroanal Chem 693:105–113. https://doi.org/10.1016/j.jelechem.2013.01.030
79. Swamy U, Wang M, Tripathy JN et al (2005) Structure of Spinach Nitrite Reductase: Implications for Multi-electron Reactions by the Iron − Sulfur: Siroheme Cofactor †, ‡. Biochemistry 44:16054–16063. https://doi.org/10.1021/bi050981y
80. Cunha CA, Macieira S, Dias JM et al (2003) Cytochrome c nitrite reductase from Desulfovibrio desulfuricans ATCC 27774. The relevance of the two calcium sites in the structure of the catalytic subunit (NrfA). J Biol Chem 278:17455–17465. https://doi.org/10.1074/jbc.M211777200
81. Jacobson F, Pistorius A, Farkas D et al (2007) pH Dependence of Copper Geometry, Reduction Potential, and Nitrite Affinity in Nitrite Reductase. J Biol Chem 282:6347–6355. https://doi.org/10.1074/jbc.M605746200
82. Besson S, Carneiro C, Moura JJG et al (1995) A Cytochrome cd1-type Nitrite Reductase Isolated from the Marine Denitrifier Pseudomonas nautica 617: Purification and Characterization. Anaerobe 1:219–226. https://doi.org/10.1006/anae.1995.1021
83. Gomes FO, Maia LB, Delerue-Matos C et al (2019) Third-generation electrochemical biosensor based on nitric oxide reductase immobilized in a multiwalled carbon nanotubes/1-n-butyl-3-methylimidazolium tetrafluoroborate nanocomposite for nitric oxide detection. Sensors Actuators B Chem 285:445–452. https://doi.org/10.1016/j.snb.2019.01.074
84. Bastian NR, Kay CJ, Barber MJ, Rajagopalan KV (1991) Spectroscopic studies of the molybdenum-containing dimethyl sulfoxide reductase from Rhodobacter sphaeroides f. sp. denitrificans. J Biol Chem 266:45–51
85. Mitrova B, Waffo AFT, Kaufmann P et al (2019) Trimethylamine N -Oxide Electrochemical Biosensor with a Chimeric Enzyme. ChemElectroChem 6:1732–1737. https://doi.org/10.1002/celc.201801422
86. Rakauskiene GA, Čenas NK, Kulys JJ (1989) A ‘branched’ mechanism of the reverse reaction of yeast glutathione reductase An estimation of the enzyme standard potential values from the steady-state kinetics data. FEBS Lett 243:33–36. https://doi.org/10.1016/0014-5793(89)81212-8
87. Haynes CA, Koder RL, Miller A-F, Rodgers DW (2002) Structures of Nitroreductase in Three States. J Biol Chem 277:11513–11520. https://doi.org/10.1074/jbc.M111334200

88. Pandiaraj M, Madasamy T, Gollavilli PN et al (2013) Nanomaterial-based electrochemical biosensors for cytochrome c using cytochrome c reductase. Bioelectrochemistry 91:1–7. https://doi.org/10.1016/j.bioelechem.2012.09.004
89. German N, Ramanaviciene A, Voronovic J, Ramanavicius A (2010) Glucose biosensor based on graphite electrodes modified with glucose oxidase and colloidal gold nanoparticles. Microchim Acta 168:221–229. https://doi.org/10.1007/s00604-009-0270-z
90. Lourenço CF, Ledo A, Laranjinha J et al (2016) Microelectrode array biosensor for high-resolution measurements of extracellular glucose in the brain. Sensors Actuators B Chem 237:298–307. https://doi.org/10.1016/j.snb.2016.06.083
91. Gao J, Huang W, Chen Z et al (2019) Simultaneous detection of glucose, uric acid and cholesterol using flexible microneedle electrode array-based biosensor and multi-channel portable electrochemical analyzer. Sensors Actuators B Chem 287:102–110. https://doi.org/10.1016/j.snb.2019.02.020
92. Kim J, Jeerapan I, Imani S et al (2016) Noninvasive Alcohol Monitoring Using a Wearable Tattoo-Based Iontophoretic-Biosensing System. ACS Sensors 1:1011–1019. https://doi.org/10.1021/acssensors.6b00356
93. Aymerich J, Márquez A, Terés L et al (2018) Cost-effective smartphone-based reconfigurable electrochemical instrument for alcohol determination in whole blood samples. Biosens Bioelectron 117:736–742. https://doi.org/10.1016/j.bios.2018.06.044
94. Lansdorp B, Ramsay W, Hamid R, Strenk E (2019) Wearable Enzymatic Alcohol Biosensor. Sensors 19:2380. https://doi.org/10.3390/s19102380
95. Kim J, Valdés-Ramírez G, Bandodkar AJ et al (2014) Non-invasive mouthguard biosensor for continuous salivary monitoring of metabolites. Analyst 139:1632–1636. https://doi.org/10.1039/C3AN02359A
96. Hashemzadeh S, Omidi Y, Rafii-Tabar H (2019) Amperometric lactate nanobiosensor based on reduced graphene oxide, carbon nanotube and gold nanoparticle nanocomposite. Microchim Acta 186:680. https://doi.org/10.1007/s00604-019-3791-0
97. Dervisevic M, Dervisevic E, Çevik E, Şenel M (2017) Novel electrochemical xanthine biosensor based on chitosan–polypyrrole–gold nanoparticles hybrid bio-nanocomposite platform. J Food Drug Anal 25:510–519. https://doi.org/10.1016/j.jfda.2016.12.005
98. Si Y, Park JW, Jung S et al (2018) Layer-by-layer electrochemical biosensors configuring xanthine oxidase and carbon nanotubes/graphene complexes for hypoxanthine and uric acid in human serum solutions. Biosens Bioelectron 121:265–271. https://doi.org/10.1016/j.bios.2018.08.074
99. Wu S, Hao J, Yang S et al (2019) Layer-by-layer self-assembly film of PEI-reduced graphene oxide composites and cholesterol oxidase for ultrasensitive cholesterol biosensing. Sensors Actuators B Chem 298:126856. https://doi.org/10.1016/j.snb.2019.126856
100. Kaur G, Tomar M, Gupta V (2018) Development of a microfluidic electrochemical biosensor: Prospect for point-of-care cholesterol monitoring. Sensors Actuators B Chem 261:460–466. https://doi.org/10.1016/j.snb.2018.01.144
101. Dontsova EA, Zeifman YS, Budashov IA et al (2011) Screen-printed carbon electrode for choline based on MnO2 nanoparticles and choline oxidase/polyelectrolyte layers. Sensors Actuators B Chem 159:261–270. https://doi.org/10.1016/j.snb.2011.07.001
102. Jamal M, Xu J, Razeeb KM (2010) Disposable biosensor based on immobilisation of glutamate oxidase on Pt nanoparticles modified Au nanowire array electrode. Biosens Bioelectron 26:1420–1424. https://doi.org/10.1016/j.bios.2010.07.071
103. Ganesana M, Trikantzopoulos E, Maniar Y et al (2019) Development of a novel micro biosensor for in vivo monitoring of glutamate release in the brain. Biosens Bioelectron 130:103–109. https://doi.org/10.1016/j.bios.2019.01.049
104. Chang K-S, Chang C-K, Chou S-F et al (2007) Characterization of a planar l-glutamate amperometric biosensor immobilized with a photo-crosslinkable polymer membrane. Sensors Actuators B Chem 122:195–203. https://doi.org/10.1016/j.snb.2006.05.022

105. Solomon EI, Sundaram UM, Machonkin TE (1996) Multicopper Oxidases and Oxygenases. Chem Rev 96:2563–2606. https://doi.org/10.1021/cr950046o
106. Komori H, Higuchi Y (2015) Structural insights into the O 2 reduction mechanism of multicopper oxidase. J Biochem 158:293–298. https://doi.org/10.1093/jb/mvv079
107. Shleev S, Tkac J, Christenson A et al (2005) Direct electron transfer between copper-containing proteins and electrodes. Biosens Bioelectron 20:2517–2554. https://doi.org/10.1016/j.bios.2004.10.003
108. De Poulpiquet A, Kjaergaard CH, Rouhana J et al (2017) Mechanism of Chloride Inhibition of Bilirubin Oxidases and Its Dependence on Potential and pH. ACS Catal 7:3916–3923. https://doi.org/10.1021/acscatal.7b01286
109. Tsujimura S, Tatsumi H, Ogawa J et al (2001) Bioelectrocatalytic reduction of dioxygen to water at neutral pH using bilirubin oxidase as an enzyme and 2,2′-azinobis (3-ethylbenzothiazolin-6-sulfonate) as an electron transfer mediator. J Electroanal Chem 496:69–75. https://doi.org/10.1016/S0022-0728(00)00239-4
110. Nakagawa T, Tsujimura S, Kano K, Ikeda T (2003) Bilirubin Oxidase and [Fe(CN) 6] 3 −/4 − Modified Electrode Allowing Diffusion-controlled Reduction of O 2 to Water at pH 7.0. Chem Lett 32:54–55. https://doi.org/10.1246/cl.2003.54
111. Tsujimura S, Kawaharada M, Nakagawa T et al (2003) Mediated bioelectrocatalytic O2 reduction to water at highly positive electrode potentials near neutral pH. Electrochem Commun 5:138–141. https://doi.org/10.1016/S1388-2481(03)00003-1
112. Durand F, Kjaergaard CH, Suraniti E et al (2012) Bilirubin oxidase from Bacillus pumilus: A promising enzyme for the elaboration of efficient cathodes in biofuel cells. Biosens Bioelectron 35:140–146. https://doi.org/10.1016/j.bios.2012.02.033
113. Torrinha Á, Montenegro MCBSM, Araújo AN (2019) Conjugation of glucose oxidase and bilirubin oxidase bioelectrodes as biofuel cell in a finger-powered microfluidic platform. Electrochim Acta 318:922–930. https://doi.org/10.1016/j.electacta.2019.06.140
114. Liu M, Wen Y, Li D et al (2011) A stable sandwich-type amperometric biosensor based on poly(3,4-ethylenedioxythiophene)–single walled carbon nanotubes/ascorbate oxidase/nafion films for detection of L-ascorbic acid. Sensors Actuators B Chem 159:277–285. https://doi.org/10.1016/j.snb.2011.07.005
115. Dodevska T, Horozova E, Dimcheva N (2013) Electrochemical behavior of ascorbate oxidase immobilized on graphite electrode modified with Au-nanoparticles. Mater Sci Eng, B 178:1497–1502. https://doi.org/10.1016/j.mseb.2013.08.012
116. Shoham B, Migron Y, Riklin A et al (1995) A bilirubin biosensor based on a multilayer network enzyme electrode. Biosens Bioelectron 10:341–352. https://doi.org/10.1016/0956-5663(95)96852-P
117. Göbel G, Dietz T, Lisdat F (2010) Bienzyme Sensor Based on an Oxygen Reducing Bilirubin Oxidase Electrode. Electroanalysis 22:1581–1585. https://doi.org/10.1002/elan.200900540
118. Rodríguez-Delgado MM, Alemán-Nava GS, Rodríguez-Delgado JM et al (2015) Laccase-based biosensors for detection of phenolic compounds. TrAC Trends Anal Chem 74:21–45. https://doi.org/10.1016/j.trac.2015.05.008
119. Zhang Y, Lv Z, Zhou J et al (2018) Application of eukaryotic and prokaryotic laccases in biosensor and biofuel cells: recent advances and electrochemical aspects. Appl Microbiol Biotechnol 102:10409–10423. https://doi.org/10.1007/s00253-018-9421-7
120. Castrovilli MC, Bolognesi P, Chiarinelli J et al (2019) The convergence of forefront technologies in the design of laccase-based biosensors – An update. TrAC Trends Anal Chem 119:115615. https://doi.org/10.1016/j.trac.2019.07.026
121. Xu F (1997) Effects of Redox Potential and Hydroxide Inhibition on the pH Activity Profile of Fungal Laccases. J Biol Chem 272:924–928. https://doi.org/10.1074/jbc.272.2.924
122. Kim H-H, Zhang Y, Heller A (2004) Bilirubin Oxidase Label for an Enzyme-Linked Affinity Assay with O 2 as Substrate in a Neutral pH NaCl Solution. Anal Chem 76:2411–2414. https://doi.org/10.1021/ac035487j

123. Pita M, Gutierrez-Sanchez C, Toscano MD et al (2013) Oxygen biosensor based on bilirubin oxidase immobilized on a nanostructured gold electrode. Bioelectrochemistry 94:69–74. https://doi.org/10.1016/j.bioelechem.2013.07.001
124. Skoronski E, Souza DH, Ely C et al (2017) Immobilization of laccase from Aspergillus oryzae on graphene nanosheets. Int J Biol Macromol 99:121–127. https://doi.org/10.1016/j.ijbiomac.2017.02.076
125. Santucci R, Ferri T, Morpurgo L et al (1998) Unmediated heterogeneous electron transfer reaction of ascorbate oxidase and laccase at a gold electrode. Biochem J 332:611–615. https://doi.org/10.1042/bj3320611
126. Akyilmaz E, Dinçkaya E (1999) A new enzyme electrode based on ascorbate oxidase immobilized in gelatin for specific determination of l-ascorbic acid. Talanta 50:87–93. https://doi.org/10.1016/S0039-9140(99)00107-1
127. Wang X, Watanabe H, Uchiyama S (2008) Amperometric l-ascorbic acid biosensors equipped with enzyme micelle membrane. Talanta 74:1681–1685. https://doi.org/10.1016/j.talanta.2007.09.008
128. Chauhan N, Dahiya T, Priyanka Pundir CS (2010) Fabrication of an amperometric ascorbate biosensor using egg shell membrane bound Lagenaria siceraria fruit ascorbate oxidase. J Mol Catal B Enzym 67:66–71. https://doi.org/10.1016/j.molcatb.2010.07.007
129. Zhang M, Liu K, Xiang L et al (2007) Carbon Nanotube-Modified Carbon Fiber Microelectrodes for In Vivo Voltammetric Measurement of Ascorbic Acid in Rat Brain. Anal Chem 79:6559–6565. https://doi.org/10.1021/ac0705871
130. Rekha K, Gouda MD, Thakur MS, Karanth NG (2000) Ascorbate oxidase based amperometric biosensor for organophosphorous pesticide monitoring. Biosens Bioelectron 15:499–502. https://doi.org/10.1016/S0956-5663(00)00077-4
131. Pisoschi AM, Pop A, Serban AI, Fafaneata C (2014) Electrochemical methods for ascorbic acid determination. Electrochim Acta 121:443–460. https://doi.org/10.1016/j.electacta.2013.12.127
132. Tanaka N, Murao S (1983) Difference between Various Copper-containing Enzymes (Polyporus Laccase, Mushroom Tyrosinase and Cucumber Ascorbate Oxidase) and Bilirubin Oxidase. Agric Biol Chem 47:1627–1628. https://doi.org/10.1271/bbb1961.47.1627
133. Mizutani K, Toyoda M, Sagara K et al (2010) X-ray analysis of bilirubin oxidase from Myrothecium verrucaria at 2.3 Å resolution using a twinned crystal. Acta Crystallogr, Sect F: Struct Biol Cryst Commun 66:765–770. https://doi.org/10.1107/S1744309110018828
134. Mano N (2012) Features and applications of bilirubin oxidases. Appl Microbiol Biotechnol 96:301–307. https://doi.org/10.1007/s00253-012-4312-9
135. Mano N, Edembe L (2013) Bilirubin oxidases in bioelectrochemistry: Features and recent findings. Biosens Bioelectron 50:478–485. https://doi.org/10.1016/j.bios.2013.07.014
136. Tonda-Mikiela P, Habrioux A, Boland S et al (2011) Oxygen Electroreduction Catalyzed by Bilirubin Oxidase Does Not Release Hydrogen Peroxide. Electrocatalysis 2:268–272. https://doi.org/10.1007/s12678-011-0062-1
137. Tsujimura S, Kano K, Ikeda T (2005) Bilirubin oxidase in multiple layers catalyzes four-electron reduction of dioxygen to water without redox mediators. J Electroanal Chem 576:113–120. https://doi.org/10.1016/j.jelechem.2004.09.031
138. Shleev S, El Kasmi A, Ruzgas T, Gorton L (2004) Direct heterogeneous electron transfer reactions of bilirubin oxidase at a spectrographic graphite electrode. Electrochem Commun 6:934–939. https://doi.org/10.1016/j.elecom.2004.07.008
139. Brocato S, Lau C, Atanassov P (2012) Mechanistic study of direct electron transfer in bilirubin oxidase. Electrochim Acta 61:44–49. https://doi.org/10.1016/j.electacta.2011.11.074
140. Li D an, Okajima T, Mao L, Ohsaka T (2014) Bioelectrocatalytic oxygen reduction reaction by bilirubin oxidase adsorbed on glassy carbon and edge-plane pyrolytic graphite electrodes: Effect of redox mediators. Int J Electrochem Sci 9:1390–1398

141. Klemm J, Prodromidis MI, Karayannis MI (2000) An Enzymic Method for the Determination of Bilirubin Using an Oxygen Electrode. Electroanalysis 12:292–295. https://doi.org/10.1002/(SICI)1521-4109(20000301)12:4%3c292:AID-ELAN292%3e3.0.CO;2-3
142. Kannan P, Chen H, Lee VT-W, Kim D-H (2011) Highly sensitive amperometric detection of bilirubin using enzyme and gold nanoparticles on sol–gel film modified electrode. Talanta 86:400–407. https://doi.org/10.1016/j.talanta.2011.09.034
143. Durand F, Gounel S, Kjaergaard CH et al (2012) Bilirubin oxidase from Magnaporthe oryzae: an attractive new enzyme for biotechnological applications. Appl Microbiol Biotechnol 96:1489–1498. https://doi.org/10.1007/s00253-012-3926-2
144. Perlman JM, Volpe JJ (2018) Bilirubin. In: Volpe's Neurology of the Newborn, Sixth Edit. Elsevier, pp 730–762.e4
145. Hooda V, Gahlaut A, Gothwal A, Hooda V (2017) Bilirubin enzyme biosensor: potentiality and recent advances towards clinical bioanalysis. Biotechnol Lett 39:1453–1462. https://doi.org/10.1007/s10529-017-2396-0
146. Ngashangva L, Bachu V, Goswami P (2019) Development of new methods for determination of bilirubin. J Pharm Biomed Anal 162:272–285. https://doi.org/10.1016/j.jpba.2018.09.034
147. Mano N, Fernandez JL, Kim Y et al (2003) Oxygen Is Electroreduced to Water on a "Wired" Enzyme Electrode at a Lesser Overpotential than on Platinum. J Am Chem Soc 125:15290–15291. https://doi.org/10.1021/ja038285d
148. Nelson DL, Cox MM (2000) Lehninger Principles of Biochemistry, 6th edn. Worth Publishers, New York
149. Bollella P, Gorton L, Antiochia R (2018) Direct Electron Transfer of Dehydrogenases for Development of 3rd Generation Biosensors and Enzymatic Fuel Cells. Sensors 18:1319. https://doi.org/10.3390/s18051319
150. No Title. https://www.fortunebusinessinsights.com/
151. Heller A, Feldman B (2008) Electrochemical Glucose Sensors and Their Applications in Diabetes Management. Chem Rev 108:2482–2505. https://doi.org/10.1021/cr068069y
152. Cardosi M, Liu Z (2012) amperometric glucose sensors for whole blood measurement based on dehydrogenase enzymes. In: Dehydrogenases. InTech, pp 116–124
153. Bartlett PN (2008) Bioelectrochemistry: Fundamentals. Experimental Techniques and Applications. John Wiley & Sons Ltd, Chichester, UK
154. Katakis I, Domínguez E (1997) Catalytic Electrooxidation of NADH for Dehydrogenase Amperometric Biosensors. Mikrochim Acta 126:11–32
155. Gorton L, Csöregi E, Domínguez E et al (1991) Selective detection in flow analysis based on the combination of immobilized enzymes and chemically modified electrodes. Anal Chim Acta 250:203–248. https://doi.org/10.1016/0003-2670(91)85072-Z
156. Tse DC-S, Kuwana T (1978) Electrocatalysis of dihydronicotinamide adenosine diphosphate with quinones and modified quinone electrodes. Anal Chem 50:1315–1318. https://doi.org/10.1021/ac50031a030
157. Munteanu F, Mano N, Kuhn A, Gorton L (2004) NADH electrooxidation using carbon paste electrodes modified with nitro-fluorenone derivatives immobilized on zirconium phosphate. J Electroanal Chem 564:167–178. https://doi.org/10.1016/j.jelechem.2003.10.034
158. Vasilescu A, Andreescu S, Bala C et al (2003) Screen-printed electrodes with electropolymerized Meldola Blue as versatile detectors in biosensors. Biosens Bioelectron 18:781–790. https://doi.org/10.1016/S0956-5663(03)00044-7
159. Jiang X, Zhu L, Yang D et al (2009) Amperometric Ethanol Biosensor Based on Integration of Alcohol Dehydrogenase with Meldola's Blue/Ordered Mesoporous Carbon Electrode. Electroanalysis 21:1617–1623. https://doi.org/10.1002/elan.200804586
160. Radoi A, Compagnone D (2009) Recent advances in NADH electrochemical sensing design. Bioelectrochemistry 76:126–134. https://doi.org/10.1016/j.bioelechem.2009.06.008

161. Tsai Y-C, Chen S-Y, Liaw H-W (2007) Immobilization of lactate dehydrogenase within multiwalled carbon nanotube-chitosan nanocomposite for application to lactate biosensors. Sensors Actuators B Chem 125:474–481. https://doi.org/10.1016/j.snb.2007.02.052
162. Tang L, Zhu Y, Xu L et al (2007) Amperometric glutamate biosensor based on self-assembling glutamate dehydrogenase and dendrimer-encapsulated platinum nanoparticles onto carbon nanotubes. Talanta 73:438–443. https://doi.org/10.1016/j.talanta.2007.04.008
163. Jena BK, Raj CR (2006) Electrochemical Biosensor Based on Integrated Assembly of Dehydrogenase Enzymes and Gold Nanoparticles. Anal Chem 78:6332–6339. https://doi.org/10.1021/ac052143f
164. Wooten M, Gorski W (2010) Facilitation of NADH Electro-oxidation at Treated Carbon Nanotubes. Anal Chem 82:1299–1304. https://doi.org/10.1021/ac902301b
165. Zhou H, Zhang Z, Yu P et al (2010) Noncovalent Attachment of NAD + Cofactor onto Carbon Nanotubes for Preparation of Integrated Dehydrogenase-Based Electrochemical Biosensors. Langmuir 26:6028–6032. https://doi.org/10.1021/la903799n
166. Azzouzi S, Rotariu L, Benito AM et al (2015) A novel amperometric biosensor based on gold nanoparticles anchored on reduced graphene oxide for sensitive detection of l-lactate tumor biomarker. Biosens Bioelectron 69:280–286. https://doi.org/10.1016/j.bios.2015.03.012
167. Wong CH, Whitesides GM (1994) Enzymes in synthetic organic chemistry, tetrahedron organic chemistry series
168. Yuan M, Kummer MJ, Milton RD et al (2019) Efficient NADH Regeneration by a Redox Polymer-Immobilized Enzymatic System. ACS Catal 9:5486–5495. https://doi.org/10.1021/acscatal.9b00513
169. Ruppert R, Steckhan E (1989) Efficient photoelectrochemical in-situ regeneration of NAD (P) + coupled to enzymatic oxidation of alcohols. J Chem Soc Perkin Trans 2:811. https://doi.org/10.1039/p29890000811
170. Bollella P, Gorton L, Ludwig R, Antiochia R (2017) A Third Generation Glucose Biosensor Based on Cellobiose Dehydrogenase Immobilized on a Glassy Carbon Electrode Decorated with Electrodeposited Gold Nanoparticles: Characterization and Application in Human Saliva. Sensors (Basel) 17:2033–2036. https://doi.org/10.3390/s17081912
171. Puri D (2006) Textbook of Medical Biochemistry, 2nd edn. Reed Elsevier India, New Delhi
172. Laurinavicius V, Razumiene J, Ramanavicius A, Ryabov AD (2004) Wiring of PQQ–dehydrogenases. Biosens Bioelectron 20:1217–1222. https://doi.org/10.1016/j.bios.2004.05.012
173. Ferri S, Kojima K, Sode K (2011) Review of Glucose Oxidases and Glucose Dehydrogenases: A Bird's Eye View of Glucose Sensing Enzymes. J Diabetes Sci Technol 5:1068–1076. https://doi.org/10.1177/193229681100500507
174. Sode K, Ootera T, Shirahane M et al (2000) Increasing the thermal stability of the water-soluble pyrroloquinoline quinone glucose dehydrogenase by single amino acid replacement. Enzyme Microb Technol 26:491–496. https://doi.org/10.1016/S0141-0229(99)00196-9
175. Igarashi S, Sode K (2003) Stabilization of Quaternary Structure of Water-Soluble Quinoprotein Glucose Dehydrogenase. Mol Biotechnol 24:97–104. https://doi.org/10.1385/MB:24:2:97
176. Tanaka S, Igarashi S, Ferri S, Sode K (2005) Increasing stability of water-soluble PQQ glucose dehydrogenase by increasing hydrophobic interaction at dimeric interface. BMC Biochem 6:1. https://doi.org/10.1186/1471-2091-6-1
177. Sode K, Igarashi S, Morimoto A, Yoshida H (2002) Construction of Engineered Water-soluble PQQ Glucose Dehydrogenase with Improved Substrate Specificity. Biocatal Biotransformation 20:405–412. https://doi.org/10.1080/1024242021000058694
178. Igarashi S, Hirokawa T, Sode K (2004) Engineering PQQ glucose dehydrogenase with improved substrate specificity. Biomol Eng 21:81–89. https://doi.org/10.1016/j.bioeng.2003.12.001

179. Hamamatsu N, Suzumura A, Nomiya Y et al (2006) Modified substrate specificity of pyrroloquinoline quinone glucose dehydrogenase by biased mutation assembling with optimized amino acid substitution. Appl Microbiol Biotechnol 73:607–617. https://doi.org/10.1007/s00253-006-0521-4
180. Tsujimura S, Kojima S, Kano K et al (2006) Novel FAD-dependent glucose dehydrogenase for a dioxygen-insensitive glucose biosensor. Biosci Biotechnol Biochem 70:654–659. https://doi.org/10.1271/bbb.70.654
181. Okuda-Shimazaki J, Yoshida H, Sode K (2020) FAD dependent glucose dehydrogenases – Discovery and engineering of representative glucose sensing enzymes -. Bioelectrochemistry 132:107414. https://doi.org/10.1016/j.bioelechem.2019.107414
182. Ludwig R, Harreither W, Tasca F, Gorton L (2010) Cellobiose Dehydrogenase: A Versatile Catalyst for Electrochemical Applications. ChemPhysChem 11:2674–2697. https://doi.org/10.1002/cphc.201000216
183. Ikeda T, Fushimi F, Miki K, Senda M (1988) Direct Bioelectrocatalysis at Electrodes Modified with D-Gluconate Dehydrogenase. Agric Biol Chem 52:2655–2658. https://doi.org/10.1080/00021369.1988.10869104
184. Ikeda T, Matsushita F, Senda M (1991) Amperometric fructose sensor based on direct bioelectrocatalysis. Biosens Bioelectron 6:299–304. https://doi.org/10.1016/0956-5663(91)85015-O
185. Ikeda T, Miyaoka S, Matsushita F et al (1992) Direct Bioelectrocatalysis at Metal and Carbon Electrodes Modified with Adsorbed D-Gluconate Dehydrogenase or Adsorbed Alcohol Dehydrogenase from Bacterial Membranes. Chem Lett 21:847–850. https://doi.org/10.1246/cl.1992.847
186. Ikeda T, Kobayashi D, Matsushita F et al (1993) Bioelectrocatalysis at electrodes coated with alcohol dehydrogenase, a quinohemoprotein with heme c serving as a built-in mediator. J Electroanal Chem 361:221–228. https://doi.org/10.1016/0022-0728(93)87058-4
187. Gorton L, Lindgren A, Larsson T et al (1999) Direct electron transfer between heme-containing enzymes and electrodes as basis for third generation biosensors. Anal Chim Acta 400:91–108. https://doi.org/10.1016/S0003-2670(99)00610-8
188. Lindgren A, Larsson T, Ruzgas T, Gorton L (2000) Direct electron transfer between the heme of cellobiose dehydrogenase and thiol modified gold electrodes. J Electroanal Chem 494:105–113. https://doi.org/10.1016/S0022-0728(00)00326-0
189. Samejima M, Phillips RS, Eriksson K-EL (1992) Cellobiose oxidase from Phanerochaete chrysosporium Stopped-flow spectrophotometric analysis of pH-dependent reduction. FEBS Lett 306:165–168. https://doi.org/10.1016/0014-5793(92)80991-O
190. Hyde SM, Wood PM (1996) Kinetic and antigenic similarities for cellobiose dehydrogenase from the brown rot fungus Coniophora puteana and the white rot fungus Phanerochaete chrysosporium. FEMS Microbiol Lett 145:439–444. https://doi.org/10.1016/S0378-1097(96)00448-X
191. Šakinytė I, Barkauskas J, Gaidukevič J, Razumienė J (2015) Thermally reduced graphene oxide: The study and use for reagentless amperometric d-fructose biosensors. Talanta 144:1096–1103. https://doi.org/10.1016/j.talanta.2015.07.072
192. Tsujimura S, Nishina A, Kamitaka Y, Kano K (2009) Coulometric d-Fructose Biosensor Based on Direct Electron Transfer Using d-Fructose Dehydrogenase. Anal Chem 81:9383–9387. https://doi.org/10.1021/ac901771t
193. Ramanavicius A, Habermüller K, Csöregi E et al (1999) Polypyrrole-Entrapped Quinohemoprotein Alcohol Dehydrogenase. Evidence for Direct Electron Transfer via Conducting-Polymer Chains. Anal Chem 71:3581–3586. https://doi.org/10.1021/ac981201c
194. Treu BL, Sokic-Lazic D, Minteer S (2010) Bioelectrocatalysis of pyruvate with PQQ-dependent pyruvate dehydrogenase. pp 1–11

195. Treu BL, Minteer SD (2008) Isolation and purification of PQQ-dependent lactate dehydrogenase from Gluconobacter and use for direct electron transfer at carbon and gold electrodes. Bioelectrochemistry 74:73–77. https://doi.org/10.1016/j.bioelechem.2008.07.005
196. Antiochia R, Lavagnini I (2006) Alcohol Biosensor Based on the Immobilization of Meldola Blue and Alcohol Dehydrogenase into a Carbon Nanotube Paste Electrode. Anal Lett 39:1643–1655. https://doi.org/10.1080/00032710600713537
197. Santos AS, Pereira AC, Durán N, Kubota LT (2006) Amperometric biosensor for ethanol based on co-immobilization of alcohol dehydrogenase and Meldola's Blue on multi-wall carbon nanotube. Electrochim Acta 52:215–220. https://doi.org/10.1016/j.electacta.2006.04.060
198. Kim D-M, Kim M, Reddy SS et al (2013) Electron-Transfer Mediator for a NAD-Glucose Dehydrogenase-Based Glucose Sensor. Anal Chem 85:11643–11649. https://doi.org/10.1021/ac403217t
199. Hughes G, Pemberton RM, Fielden PR, Hart JP (2015) Development of a novel reagentless, screen-printed amperometric biosensor based on glutamate dehydrogenase and NAD + , integrated with multi-walled carbon nanotubes for the determination of glutamate in food and clinical applications. Sensors Actuators B Chem 216:614–621. https://doi.org/10.1016/j.snb.2015.04.066
200. Safina G, Ludwig R, Gorton L (2010) A simple and sensitive method for lactose detection based on direct electron transfer between immobilised cellobiose dehydrogenase and screen-printed carbon electrodes. Electrochim Acta 55:7690–7695. https://doi.org/10.1016/j.electacta.2009.10.052
201. Tavahodi M, Ortiz R, Schulz C et al (2017) Direct Electron Transfer of Cellobiose Dehydrogenase on Positively Charged Polyethyleneimine Gold Nanoparticles. ChemPlusChem 82:546–552. https://doi.org/10.1002/cplu.201600453
202. Zafar MN, Safina G, Ludwig R, Gorton L (2012) Characteristics of third-generation glucose biosensors based on Corynascus thermophilus cellobiose dehydrogenase immobilized on commercially available screen-printed electrodes working under physiological conditions. Anal Biochem 425:36–42. https://doi.org/10.1016/j.ab.2012.02.026
203. Bollella P, Hibino Y, Kano K et al (2018) Highly Sensitive Membraneless Fructose Biosensor Based on Fructose Dehydrogenase Immobilized onto Aryl Thiol Modified Highly Porous Gold Electrode: Characterization and Application in Food Samples. Anal Chem 90:12131–12136. https://doi.org/10.1021/acs.analchem.8b03093
204. Michel C, Battaglia-Brunet F, Minh CT et al (2003) Amperometric cytochrome c3-based biosensor for chromate determination. Biosens Bioelectron 19:345–352. https://doi.org/10.1016/S0956-5663(03)00191-X
205. Lin R, Bayachou M, Greaves J, Farmer PJ (1997) Nitrite Reduction by Myoglobin in Surfactant Films. J Am Chem Soc 119:12689–12690. https://doi.org/10.1021/ja972529a
206. Almeida MG, Serra A, Silveira CM, Moura JJG (2010) Nitrite Biosensing via Selective Enzymes—A Long but Promising Route. Sensors 10:11530–11555. https://doi.org/10.3390/s101211530
207. Noh H-B, Chandra P, Moon JO, Shim Y-B (2012) In vivo detection of glutathione disulfide and oxidative stress monitoring using a biosensor. Biomaterials 33:2600–2607. https://doi.org/10.1016/j.biomaterials.2011.12.026
208. Hooda V, Sachdeva V, Chauhan N (2016) Nitrate quantification: recent insights into enzyme-based methods. Rev Anal Chem 35:99. https://doi.org/10.1515/revac-2016-0002
209. Sohail M, Adeloju SB (2016) Nitrate biosensors and biological methods for nitrate determination. Talanta 153:83–98. https://doi.org/10.1016/j.talanta.2016.03.002
210. Sohail M, Adeloju SB (2009) Fabrication of Redox-Mediator Supported Potentiometric Nitrate Biosensor with Nitrate Reductase. Electroanalysis 21:1411–1418. https://doi.org/10.1002/elan.200804542

211. Wang X, Dzyadevych SV, Chovelon J-M et al (2006) Development of a conductometric nitrate biosensor based on Methyl viologen/Nafion® composite film. Electrochem Commun 8:201–205. https://doi.org/10.1016/j.elecom.2005.11.006
212. Adeloju SB, Sohail M (2011) Azure A Mediated Polypyrrole-Based Amperometric Nitrate Biosensor. Electroanalysis 23:987–996. https://doi.org/10.1002/elan.201000386
213. Serra AS, Jorge SR, Silveira CM et al (2011) Cooperative use of cytochrome cd1 nitrite reductase and its redox partner cytochrome c552 to improve the selectivity of nitrite biosensing. Anal Chim Acta 693:41–46. https://doi.org/10.1016/j.aca.2011.03.029
214. Silveira CM, Baur J, Holzinger M et al (2010) Enhanced Direct Electron Transfer of a Multihemic Nitrite Reductase on Single-walled Carbon Nanotube Modified Electrodes. Electroanalysis 22:2973–2978. https://doi.org/10.1002/elan.201000363
215. Gomes FO, Maia LB, Cordas C et al (2019) Electroanalytical characterization of the direct Marinobacter hydrocarbonoclasticus nitric oxide reductase-catalysed nitric oxide and dioxygen reduction. Bioelectrochemistry 125:8–14. https://doi.org/10.1016/j.bioelechem.2018.08.005
216. Cheng H, Abo M, Okubo A (2003) Development of dimethyl sulfoxide biosensor using a mediator immobilized enzyme electrode. Analyst 128:724. https://doi.org/10.1039/b212917e
217. Okeke BC, Ma G, Cheng Q et al (2007) Development of a perchlorate reductase-based biosensor for real time analysis of perchlorate in water. J Microbiol Methods 68:69–75. https://doi.org/10.1016/j.mimet.2006.06.007
218. Naal Z, Park J-H, Bernhard S et al (2002) Amperometric TNT Biosensor Based on the Oriented Immobilization of a Nitroreductase Maltose Binding Protein Fusion. Anal Chem 74:140–148. https://doi.org/10.1021/ac010596o
219. Pandiaraj M, Benjamin AR, Madasamy T et al (2014) A cost-effective volume miniaturized and microcontroller based cytochrome c assay. Sensors Actuators A Phys 220:290–297. https://doi.org/10.1016/j.sna.2014.10.018
220. Plumeré N (2013) Interferences from oxygen reduction reactions in bioelectroanalytical measurements: the case study of nitrate and nitrite biosensors. Anal Bioanal Chem 405:3731–3738. https://doi.org/10.1007/s00216-013-6827-z
221. Cui Y, Barford JP, Renneberg R (2006) Development of a bienzyme system for the electrochemical determination of nitrate in ambient air. Anal Bioanal Chem 386:1567–1570. https://doi.org/10.1007/s00216-006-0673-1
222. Abo M, Ogasawara Y, Tanaka Y et al (2003) Amperometric dimethyl sulfoxide sensor using dimethyl sulfoxide reductase from Rhodobacter sphaeroides. Biosens Bioelectron 18:735–739. https://doi.org/10.1016/S0956-5663(03)00043-5
223. Monteiro T, Rodrigues PR, Gonçalves AL et al (2015) Construction of effective disposable biosensors for point of care testing of nitrite. Talanta 142:246–251. https://doi.org/10.1016/j.talanta.2015.04.057
224. Monteiro T, Gomes S, Jubete E et al (2019) A quasi-reagentless point-of-care test for nitrite and unaffected by oxygen and cyanide. Sci Rep 9:2622. https://doi.org/10.1038/s41598-019-39209-y
225. Fowler D, Coyle M, Skiba U et al (2013) The global nitrogen cycle in the twenty-first century. Philos Trans R Soc B Biol Sci 368:20130164. https://doi.org/10.1098/rstb.2013.0164
226. Dejam A, Hunter CJ, Schechter AN, Gladwin MT (2004) Emerging role of nitrite in human biology. Blood Cells Mol Dis 32:423–429. https://doi.org/10.1016/j.bcmd.2004.02.002
227. Tuteja N, Chandra M, Tuteja R, Misra MK (2004) Nitric Oxide as a Unique Bioactive Signaling Messenger in Physiology and Pathophysiology. J Biomed Biotechnol 2004:227–237. https://doi.org/10.1155/S1110724304402034
228. Hille R, Hall J, Basu P (2014) The Mononuclear Molybdenum Enzymes. Chem Rev 114:3963–4038. https://doi.org/10.1021/cr400443z

229. Maia LB, Moura I, Moura JJG (2016) Chapter 1. molybdenum and tungsten-containing enzymes: an overview. in: molybdenum and tungsten enzymes: biochemistry. Royal Soc Chem pp 1–80
230. Jalalvand AR, Mahmoudi M, Goicoechea HC (2018) Developing a novel paper-based enzymatic biosensor assisted by digital image processing and first-order multivariate calibration for rapid determination of nitrate in food samples. RSC Adv 8:23411–23420. https://doi.org/10.1039/C8RA02792G
231. Sachdeva V, Hooda V (2014) A new immobilization and sensing platform for nitrate quantification. Talanta 124:52–59. https://doi.org/10.1016/j.talanta.2014.02.014
232. Sohail M, Adeloju SB (2008) Electroimmobilization of nitrate reductase and nicotinamide adenine dinucleotide into polypyrrole films for potentiometric detection of nitrate. Sensors Actuators B Chem 133:333–339. https://doi.org/10.1016/j.snb.2008.02.032
233. Xuejiang W, Dzyadevych S, Chovelon J et al (2006) Conductometric nitrate biosensor based on methyl viologen/Nafion®/nitrate reductase interdigitated electrodes. Talanta 69:450–455. https://doi.org/10.1016/j.talanta.2005.10.014
234. Zhang K, Zhou H, Hu P, Lu Q (2019) The direct electrochemistry and bioelectrocatalysis of nitrate reductase at a gold nanoparticles/aminated graphene sheets modified glassy carbon electrode. RSC Adv 9:37207–37213. https://doi.org/10.1039/C9RA07082F
235. Patolsky F, Katz E, Heleg-Shabtai V, Willner I (1998) A Crosslinked Microperoxidase-11 and Nitrate Reductase Monolayer on a Gold Electrode: An Integrated Electrically Contacted Electrode for the Bioelectrocatalyzed Reduction of NO3−. Chem - A Eur J 4:1068–1073. https://doi.org/10.1002/(SICI)1521-3765(19980615)4:6%3c1068:AID-CHEM1068%3e3.0.CO;2-Q
236. Kirstein D, Kirstein L, Scheller F et al (1999) Amperometric nitrate biosensors on the basis of Pseudomonas stutzeri nitrate reductase. J Electroanal Chem 474:43–51. https://doi.org/10.1016/S0022-0728(99)00302-2
237. Quan D, Shim JH, Kim JD et al (2005) Electrochemical Determination of Nitrate with Nitrate Reductase-Immobilized Electrodes under Ambient Air. Anal Chem 77:4467–4473. https://doi.org/10.1021/ac050198b
238. Can F, Korkut Ozoner S, Ergenekon P, Erhan E (2012) Amperometric nitrate biosensor based on Carbon nanotube/Polypyrrole/Nitrate reductase biofilm electrode. Mater Sci Eng, C 32:18–23. https://doi.org/10.1016/j.msec.2011.09.004
239. Gokhale AA, Lu J, Weerasiri RR et al (2015) Amperometric Detection and Quantification of Nitrate Ions Using a Highly Sensitive Nanostructured Membrane Electrocodeposited Biosensor Array. Electroanalysis 27:1127–1137. https://doi.org/10.1002/elan.201400547
240. Moura I, Moura JJG (2001) Structural aspects of denitrifying enzymes. Curr Opin Chem Biol 5:168–175. https://doi.org/10.1016/S1367-5931(00)00187-3
241. Einsle O, Kroneck PMH (2004) Structural basis of denitrification. Biol Chem 385:875–883. https://doi.org/10.1515/BC.2004.115
242. Astier Y, Canters GW, Davis JJ et al (2005) Sensing Nitrite through a Pseudoazurin-Nitrite Reductase Electron Transfer Relay. ChemPhysChem 6:1114–1120. https://doi.org/10.1002/cphc.200400384
243. Silveira CM, Almeida MG (2013) Small electron-transfer proteins as mediators in enzymatic electrochemical biosensors. Anal Bioanal Chem 405:3619–3635. https://doi.org/10.1007/s00216-013-6786-4
244. Silveira CM, Gomes SP, Araújo AN et al (2010) An efficient non-mediated amperometric biosensor for nitrite determination. Biosens Bioelectron 25:2026–2032. https://doi.org/10.1016/j.bios.2010.01.031
245. Silveira CM, Pimpão M, Pedroso HA et al (2013) Probing the surface chemistry of different oxidized MWCNT for the improved electrical wiring of cytochrome c nitrite reductase. Electrochem Commun 35:17–21. https://doi.org/10.1016/j.elecom.2013.07.027
246. Gomes FO, Maia LB, Loureiro JA et al (2019) Biosensor for direct bioelectrocatalysis detection of nitric oxide using nitric oxide reductase incorporated in carboxylated

single-walled carbon nanotubes/lipidic 3 bilayer nanocomposite. Bioelectrochemistry 127:76–86. https://doi.org/10.1016/j.bioelechem.2019.01.010
247. Kaufmann P, Duffus BR, Mitrova B et al (2018) Modulating the Molybdenum Coordination Sphere of Escherichia coli Trimethylamine N -Oxide Reductase. Biochemistry 57:1130–1143. https://doi.org/10.1021/acs.biochem.7b01108
248. Schindelin H, Kisker C, Hilton J, et al (1996) Crystal Structure of DMSO Reductase: Redox-Linked Changes in Molybdopterin Coordination. Science (80-) 272:1615–1621. https://doi.org/10.1126/science.272.5268.1615
249. Youngblut MD, Tsai C-L, Clark IC et al (2016) Perchlorate Reductase Is Distinguished by Active Site Aromatic Gate Residues. J Biol Chem 291:9190–9202. https://doi.org/10.1074/jbc.M116.714618
250. Yonehara H, Fujii S, Sato K et al (2007) Construction of a Dimethyl Sulfoxide Sensor Based on Dimethyl Sulfoxide Reductase Immobilized on a Au Film Electrode. Anal Sci 23:55–58. https://doi.org/10.2116/analsci.23.55
251. Timur S, Odaci D, Dincer A et al (2008) Biosensing approach for glutathione detection using glutathione reductase and sulfhydryl oxidase bienzymatic system. Talanta 74:1492–1497. https://doi.org/10.1016/j.talanta.2007.09.026
252. Yu J, Zhou C-Z (2007) Crystal structure of glutathione reductase Glr1 from the yeast Saccharomyces cerevisiae. Proteins Struct Funct Bioinforma 68:972–979. https://doi.org/10.1002/prot.21354
253. Willner I, Katz E, Riklin A, Kasher R (1992) Mediated electron transfer in gluthathione reductase organized in self-assembled monolayers on gold electrodes. J Am Chem Soc 114:10965–10966. https://doi.org/10.1021/ja00053a045
254. Carano M, Cosnier S, Kordatos K et al (2002) A glutathione amperometric biosensor based on an amphiphilic fullerene redox mediator immobilised within an amphiphilic polypyrrole film. J Mater Chem 12:1996–2000. https://doi.org/10.1039/b201469f
255. Corrêa CC, Santhiago M, Formiga ALB, Kubota LT (2013) In situ activated nanostructured platform for oxidized glutathione biosensing. Electrochim Acta 90:309–316. https://doi.org/10.1016/j.electacta.2012.12.046
256. Crofts AR (2004) The Cytochrome bc 1 Complex: Function in the Context of Structure. Annu Rev Physiol 66:689–733. https://doi.org/10.1146/annurev.physiol.66.032102.150251
257. Santharaman P, Venkatesh KA, Vairamani K et al (2017) ARM-microcontroller based portable nitrite electrochemical analyzer using cytochrome c reductase biofunctionalized onto screen printed carbon electrode. Biosens Bioelectron 90:410–417. https://doi.org/10.1016/j.bios.2016.10.039
258. Navaee A, Salimi A (2019) Enzyme-based electrochemical biosensors. In: Electrochemical Biosensors. Elsevier, pp 167–211
259. Colovic MB, Krstic DZ, Lazarevic-Pasti TD et al (2013) Acetylcholinesterase Inhibitors: Pharmacology and Toxicology. Curr Neuropharmacol 11:315–335. https://doi.org/10.2174/1570159X11311030006
260. Latip W, Knight VF, Abdul Halim N et al (2019) Microbial Phosphotriesterase: Structure, Function, and Biotechnological Applications. Catalysts 9:671. https://doi.org/10.3390/catal9080671
261. Trojanowicz M (2002) Determination of Pesticides Using Electrochemical Enzymatic Biosensors. Electroanalysis 14:1311–1328. https://doi.org/10.1002/1521-4109(200211)14:19/20%3c1311:AID-ELAN1311%3e3.0.CO;2-7
262. Pundir CS, Malik A, Preety (2019) Bio-sensing of organophosphorus pesticides: a review. Biosens Bioelectron 140:111348. https://doi.org/10.1016/j.bios.2019.111348
263. Schöning MJ, Krause R, Block K et al (2003) A dual amperometric/potentiometric FIA-based biosensor for the distinctive detection of organophosphorus pesticides. Sensors Actuators B Chem 95:291–296. https://doi.org/10.1016/S0925-4005(03)00426-X

264. Lee JH, Park JY, Min K et al (2010) A novel organophosphorus hydrolase-based biosensor using mesoporous carbons and carbon black for the detection of organophosphate nerve agents. Biosens Bioelectron 25:1566–1570. https://doi.org/10.1016/j.bios.2009.10.013
265. Sahin A, Dooley K, Cropek DM et al (2011) A dual enzyme electrochemical assay for the detection of organophosphorus compounds using organophosphorus hydrolase and horseradish peroxidase. Sensors Actuators B Chem 158:353–360. https://doi.org/10.1016/j.snb.2011.06.034
266. Mishra RK, Hubble LJ, Martín A et al (2017) Wearable Flexible and Stretchable Glove Biosensor for On-Site Detection of Organophosphorus Chemical Threats. ACS Sensors 2:553–561. https://doi.org/10.1021/acssensors.7b00051
267. Gahlaut A (2012) Electrochemical Biosensors for Determination of Organophosphorus Compounds: Review. Open J Appl Biosens 1:1–8. https://doi.org/10.4236/ojab.2012.11001
268. Kaur N, Prabhakar N (2017) Current scenario in organophosphates detection using electrochemical biosensors. TrAC Trends Anal Chem 92:62–85. https://doi.org/10.1016/j.trac.2017.04.012
269. Harel M, Aharoni A, Gaidukov L et al (2004) Structure and evolution of the serum paraoxonase family of detoxifying and anti-atherosclerotic enzymes. Nat Struct Mol Biol 11:412–419. https://doi.org/10.1038/nsmb767
270. Draganov DI, Teiber JF, Speelman A et al (2005) Human paraoxonases (PON1, PON2, and PON3) are lactonases with overlapping and distinct substrate specificities. J Lipid Res 46:1239–1247. https://doi.org/10.1194/jlr.M400511-JLR200
271. Ceron JJ, Tecles F, Tvarijonaviciute A (2014) Serum paraoxonase 1 (PON1) measurement: an update. BMC Vet Res 10:1–11. https://doi.org/10.1186/1746-6148-10-74
272. Mackness M, Mackness B (2015) Human paraoxonase-1 (PON1): Gene structure and expression, promiscuous activities and multiple physiological roles. Gene 567:12–21. https://doi.org/10.1016/j.gene.2015.04.088
273. Furlong CE, Marsillach J, Jarvik GP, Costa LG (2016) Paraoxonases-1, -2 and -3: What are their functions? Chem Biol Interact 259:51–62. https://doi.org/10.1016/j.cbi.2016.05.036
274. Khersonsky O, Tawfik DS (2005) Structure-Reactivity Studies of Serum Paraoxonase PON1 Suggest that Its Native Activity Is Lactonase. Biochemistry 44:6371–6382. https://doi.org/10.1021/bi047440d
275. Chen C, Yang K (2013) A liquid crystal biosensor for detecting organophosphates through the localized pH changes induced by their hydrolytic products. Sensors Actuators B Chem 181:368–374. https://doi.org/10.1016/j.snb.2013.01.036
276. Wang J, Yokokawa M, Satake T, Suzuki H (2015) A micro IrO potentiometric sensor for direct determination of organophosphate pesticides. Sensors Actuators B Chem 220:859–863. https://doi.org/10.1016/j.snb.2015.05.115
277. Ma B, Cheong L, Weng X et al (2018) Lipase@ZIF-8 nanoparticles-based biosensor for direct and sensitive detection of methyl parathion. Electrochim Acta 283:509–516. https://doi.org/10.1016/j.electacta.2018.06.176
278. Wang Z, Ma B, Shen C, Cheong L-Z (2019) Direct, selective and ultrasensitive electrochemical biosensing of methyl parathion in vegetables using Burkholderia cepacia lipase@MOF nanofibers-based biosensor. Talanta 197:356–362. https://doi.org/10.1016/j.talanta.2019.01.052
279. Gangadhara Reddy K, Madhavi G, Kumara Swamy BE (2014) Mobilized lipase enzymatic biosensor for the determination of Chlorfenvinphos and Malathion in contaminated water samples: A voltammetric study. J Mol Liq 198:181–186. https://doi.org/10.1016/j.molliq.2014.06.019
280. Arduini F, Guidone S, Amine A et al (2013) Acetylcholinesterase biosensor based on self-assembled monolayer-modified gold-screen printed electrodes for organophosphorus insecticide detection. Sensors Actuators B Chem 179:201–208. https://doi.org/10.1016/j.snb.2012.10.016

281. Cinti S, Minotti C, Moscone D et al (2017) Fully integrated ready-to-use paper-based electrochemical biosensor to detect nerve agents. Biosens Bioelectron 93:46–51. https://doi.org/10.1016/j.bios.2016.10.091
282. Kok FN, Hasirci V (2004) Determination of binary pesticide mixtures by an acetylcholinesterase–choline oxidase biosensor. Biosens Bioelectron 19:661–665. https://doi.org/10.1016/j.bios.2003.07.002
283. Espinosa M, Atanasov P, Wilkins E (1999) Development of a disposable organophosphate biosensor. Electroanalysis 11:1055–1062. https://doi.org/10.1002/(SICI)1521-4109(199910)11:14%3c1055:AID-ELAN1055%3e3.0.CO;2-E
284. Adeloju SB, Shaw SJ, Wallace GG (1997) Pulsed-amperometric detection of urea in blood samples on a conducting polypyrrole-urease biosensor. Anal Chim Acta 341:155–160. https://doi.org/10.1016/S0003-2670(96)00502-8
285. Luo Y-C, Do J-S (2004) Urea biosensor based on PANi(urease)-Nafion®/Au composite electrode. Biosens Bioelectron 20:15–23. https://doi.org/10.1016/j.bios.2003.11.028
286. Bozgeyik İ, Şenel M, Çevik E, Abasıyanık MF (2011) A novel thin film amperometric urea biosensor based on urease-immobilized on poly(N-glycidylpyrrole-co-pyrrole). Curr Appl Phys 11:1083–1088. https://doi.org/10.1016/j.cap.2011.01.041
287. Soares JC, Brisolari A, Rodrigues VDC et al (2012) Amperometric urea biosensors based on the entrapment of urease in polypyrrole films. React Funct Polym 72:148–152. https://doi.org/10.1016/j.reactfunctpolym.2011.12.002
288. Emami Meibodi AS, Haghjoo S (2014) Amperometric urea biosensor based on covalently immobilized urease on an electrochemically polymerized film of polyaniline containing MWCNTs. Synth Met 194:1–6. https://doi.org/10.1016/j.synthmet.2014.04.009
289. Do J-S, Lin K-H (2016) Kinetics of urease inhibition-based amperometric biosensors for mercury and lead ions detection. J Taiwan Inst Chem Eng 63:25–32. https://doi.org/10.1016/j.jtice.2016.03.011
290. Rodriguez BB, Bolbot JA, Tothill IE (2004) Development of urease and glutamic dehydrogenase amperometric assay for heavy metals screening in polluted samples. Biosens Bioelectron 19:1157–1167. https://doi.org/10.1016/j.bios.2003.11.002
291. Domínguez-Renedo O, Alonso-Lomillo MA, Ferreira-Gonçalves L, Arcos-Martínez MJ (2009) Development of urease based amperometric biosensors for the inhibitive determination of Hg (II). Talanta 79:1306–1310. https://doi.org/10.1016/j.talanta.2009.05.043
292. Scott D, Cooney MJ, Liaw BY (2008) Sustainable current generation from the ammonia–polypyrrole interaction. J Mater Chem 18:3216. https://doi.org/10.1039/b800894a
293. Phongphut A, Sriprachuabwong C, Wisitsoraat A et al (2013) A disposable amperometric biosensor based on inkjet-printed Au/PEDOT-PSS nanocomposite for triglyceride determination. Sensors Actuators B Chem 178:501–507. https://doi.org/10.1016/j.snb.2013.01.012
294. Yücel A, Özcan HM, Sağıroğlu A (2016) A new multienzyme-type biosensor for triglyceride determination. Prep Biochem Biotechnol 46:78–84. https://doi.org/10.1080/10826068.2014.985833
295. Narwal V, Pundir CS (2017) An improved amperometric triglyceride biosensor based on co-immobilization of nanoparticles of lipase, glycerol kinase and glycerol 3-phosphate oxidase onto pencil graphite electrode. Enzyme Microb Technol 100:11–16. https://doi.org/10.1016/j.enzmictec.2017.01.009
296. Pundir CS, Aggarwal V (2017) Amperometric triglyceride bionanosensor based on nanoparticles of lipase, glycerol kinase, glycerol-3-phosphate oxidase. Anal Biochem 517:56–63. https://doi.org/10.1016/j.ab.2016.11.013
297. Laurinavicius V, Kurtinaitiene B, Gureviciene V et al (1996) Amperometric glyceride biosensor. Anal Chim Acta 330:159–166. https://doi.org/10.1016/0003-2670(96)00114-6
298. Solanki S, Pandey CM, Soni A et al (2016) An amperometric bienzymatic biosensor for the triglyceride tributyrin using an indium tin oxide electrode coated with electrophoretically deposited chitosan-wrapped nanozirconia. Microchim Acta 183:167–176. https://doi.org/10.1007/s00604-015-1618-1

299. Diba FS, Kim S, Lee HJ (2015) Amperometric bioaffinity sensing platform for avian influenza virus proteins with aptamer modified gold nanoparticles on carbon chips. Biosens Bioelectron 72:355–361. https://doi.org/10.1016/j.bios.2015.05.020
300. Čadková M, Dvořáková V, Metelka R et al (2015) Alkaline phosphatase labeled antibody-based electrochemical biosensor for sensitive HE4 tumor marker detection. Electrochem Commun 59:1–4. https://doi.org/10.1016/j.elecom.2015.06.014

Current Applications of Artificial Metalloenzymes and Future Developments

Jean-Pierre Mahy, Frédéric Avenier, Wadih Ghattas, Rémy Ricoux, and Michèle Salmain

Abstract

In between traditional homogeneous metal catalysts and enzyme catalysts, a new class of hybrid catalysts named artificial metalloenzymes resulting from the controlled embedding of transition metal species (ions, synthetic inorganic or organometallic complexes) within natural, genetically-engineered or even *de novo* protein scaffolds currently undergoes a tremendous development at the academic level. This family of hybrid assemblies ideally combines the features of their individual components, allowing a wide range of chemical reactions, including new-to-nature reactions, to be catalyzed under mild, eco-compatible conditions with high chemo- and/or stereoselectivity. This chapter intends to summarize the most remarkable achievements in artificial metalloenzyme design and properties with emphasis put on industrially relevant chemical reactions, including oxidations, imine reductions, C–C and C–N bonds formation. It also gives an up-to-date survey on the most advanced applications of artificial metalloenzymes in cascade reactions and in vivo catalysis.

Keywords

Oxidation · Reduction · Polymerization · Metathesis · Cascade reactions · In vivo catalysis · Uncaging · Carbene insertion · Directed evolution

J.-P. Mahy · F. Avenier · W. Ghattas · R. Ricoux
Institut de Chimie Moléculaire et des Matériaux d'Orsay (ICMMO), UMR 8182, CNRS, Université Paris Sud, Université Paris-Saclay, Orsay, France

M. Salmain (✉)
Sorbonne Université, CNRS, Institut Parisien de Chimie Moléculaire (IPCM), Paris, France
e-mail: michele.salmain@sorbonne-universite.fr

J. J. G. Moura et al. (eds.), *Enzymes for Solving Humankind's Problems*,
https://doi.org/10.1007/978-3-030-58315-6_12

Abbreviations list

ADH	alcohol dehydrogenase;
ArM	artificial metalloenzyme;
ATH	asymmetric transfer hydrogenation;
ATHase	artificial transfer hydrogenase;
Az	azurin;
BSA	bovine serum albumin;
Cod	cyclooctadiene;
CODH	carbon monoxide dehydrogenase;
Cyt	cytochrome;
DAAO	D-aminoacid oxidase;
DF	Due Ferri;
EDA	ethyl diazoacetate;
Ee	enantiomeric excess;
FhuA	ferric hydroxamate uptake protein component A;
Fr	ferritin;
hCA II	human carbonic anhydrase isoform II;
HRP	horseradish peroxidase;
HSA	human serum albumin;
LAAO	L-aminoacid oxidase;
LmrR	lactococcal multidrug-resistant regulator;
MAO	monoaminoxidase;
Mb	myoglobin;
MP8	microperoxidase 8;
Nbd	norbornadiene;
NB	nitrobindin;
OmpA	outer membrane protein A;
PA	phenylacetylene;
Phen	1,10-phenanthroline;
PPIX	protoporphyrin IX;
ROMP	ring-opening metathesis polymerization;
SAV	streptavidin;
scdSAV	single chain dimeric SAV;
TEV	tobacco etching virus;
TOF	turnover frequency;
TON	turnover number;
WT	wild-type;
Xln	xylanase

1 Introduction

In the present context of worldwide consciousness regarding the necessity to preserve our habitat, it is now obvious that any human activity has to take into consideration its impact on the environment. This is particularly true for the chemical industry, which is at the origin of most manufactured products, and therefore withstands a huge part of the responsibility for tomorrow's wellness of the planet. After about two centuries of prosperity and wild enterprise, the chemical industry is now facing the daunting challenge to rethink most of its well-proven processes and promote the development of environmentally friendly new ones meeting standards for sustainable growth. While chemists still struggle to meet these standards, nature has already solved the problem by evolving natural enzymes, including metalloenzymes, which are capable of performing efficient catalytic processes using harmless reactants under mild conditions. Such biocatalysts can indeed perform selective reactions in aqueous medium at ambient temperature and under atmospheric pressure. Yet, the use of natural enzymes in biocatalytic processes shows some limitations such as thermal instability, substrate specificity, or restriction to natural reactions. Evolving these natural enzymes by replacing the original cofactor with a synthetic catalyst or simply inserting an artificial metal complex into a protein scaffold by covalent or supramolecular ("Trojan Horse") anchoring affords a new class of catalysts that ideally combine the robustness and wide range of reactions achieved by chemical catalysts with the ability of enzymes to work under mild conditions, in aqueous medium, and with high selectivity. Insertion of a synthetic metal complex into a protein gives rise to so-called artificial metalloenzymes (ArMs) that eventually catalyze both natural and non-natural reactions under eco-compatible conditions. The selectivity, the efficiency, and the stability of these ArMs can then be optimized by chemical engineering of the metal complex and/or biochemical engineering of the protein scaffold, notably using the powerful technique of directed evolution. The present chapter gives an overview of the wide range of reactions catalyzed by ArMs but also goes beyond by describing how ArMs can be involved in cascade reaction processes, as well as in in vivo catalysis for both natural and abiotic reactions.

2 Biotechnological Applications of Artificial Metalloenzymes

Biotechnological applications of ArMs are potentially endless since the obvious long-term objective is to replace all the contemporary polluting and energy-consuming chemical processes by environmentally friendly new ones. This sub-chapter surveys the variety of reactions that have successfully been catalyzed by ArMs so far at the laboratory level, covering both the fields of oxidation and reduction reactions as well as polymerization reactions.

2.1 Oxidations

Nowadays, most of the industrial stoichiometric oxidations of hydrocarbons involve harsh conditions using strong polluting oxidants, under high pressure and temperature conditions, and occur with low selectivity. There is thus a crucial need to develop new catalysts that would allow oxidations to take place under mild eco-compatible conditions, in water as a solvent, and with high selectivity. Nature has elegantly solved this problem by using the very sophisticated biocatalysts that are metalloenzymes, including heme and non-heme iron enzymes, that can catalyze the highly selective oxidation of chemicals at room temperature and under atmospheric pressure [1, 2]. These enzymes can activate molecular dioxygen at their active site transition metal center, most frequently an iron(III) ion. Mimicking metalloenzymes thus appears to be a logical strategy for developing new catalysts that would catalyze oxidation reactions with excellent selectivity and a high turnover number (TON) under mild conditions. Researchers have long been preparing synthetic models in which a metal ion is inserted into a ligand mimicking the first coordination sphere of this metal ion in the native enzyme [3]. This strategy was particularly successful, for example, to prepare metalloporphyrins, including Fe, Mn, Cr, Co, V … metal ions in their center, that have been used as very efficient catalysts for the oxidation of organic compounds by various organic and inorganic oxidants such as PhI = O, H_2O_2, $KHSO_5$, $NaIO_4$… with efficiencies rivaling those of enzymes themselves [4–7]. However, several problems still remained to be solved as most of the metal catalysts were only soluble in organic solvents and the stereoselectivity of the reactions catalyzed was generally low. Taking advantage of the chiral environment of proteins and their solubility in water, researchers have prepared ArMs by incorporating metal ions or synthetic metal complexes into proteins following the strategies detailed in the introduction of this chapter [8, 9]. This allowed them to obtain new water-soluble metal-based hybrid biocatalysts that catalyzed various oxidation reactions. Among those, ArMs possessing a peroxidase activity have already been extensively reviewed [10–13]. The present paragraph will then focus on ArMs designed to catalyze the selective oxidation of substrates of synthetic interest, starting from the most easily oxidizable ones including alcohols, amines, and sulfides to the most difficult to oxidize substrates such as aromatics, alkenes, and alkanes.

2.1.1 Alcohol Oxidation

In 2004, Kaplan and De Grado first reported the *de novo* design of diiron protein with four helical bundles displaying phenol oxidase activity [14]. For this, they started from the Due Ferri (DF) family of *de novo*-designed diiron proteins in which the combination of two Fe(II) ions within a single site, allowed to perform two-electron chemistry with O_2, thereby avoiding the formation of oxygen radicals. Indeed, the diiron center reacts quickly with O_2, with the concomitant formation of di-Fe(III) species where the two iron(III) ions are bound by an oxo bridge and the reduction of molecular oxygen. They focused on DFtet, a four-chain heterotetrameric helical bundle whose structure, sequence, and catalytic properties were

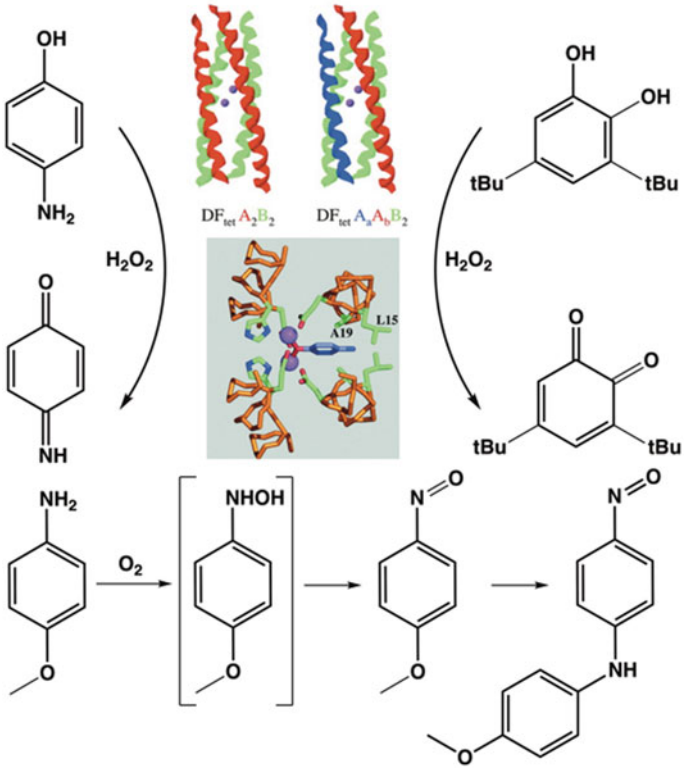

Fig. 1 Reactions catalyzed by *de novo*-designed di iron protein with four helical bundles from the Due Ferri (DF) family: oxidation of 4-aminophenol into the corresponding quinone-mono-imine [15], oxidation of a larger catechol derivative, 3,5-di-tert-butyl-catechol (3,5-DTBC) [16], N-hydroxylation of arylamines [17, 18]

originally designed by a computational method that not only considered the stabilization of the desired fold, but also the destabilization of likely alternatives [15]. Combinations of different monomer units and the introduction of mutations at the active site led to highly active variants, the best ArM (G4-DFtet) catalyzing the two-electron oxidation of 4-aminophenol into the corresponding quinone-mono-imine compound with high efficiency (Fig. 1) (k_{cat}/K_M = 1500 M^{-1} min^{-1}).

In 2009, Lombardi et al. also designed an artificial oxidase using a scaffold from the same Due Ferri family (DF1) inspired by highly complex natural di-metal proteins. DF1 is a dimeric protein in which each monomer consists of a helix-loop-helix structure [16]. The metal-binding site consists of four glutamate and two histidine residues as first-shell ligands, which are positioned in the core of the protein by hydrogen bonding interactions with two aspartate, tyrosine, and lysine residues. The authors were able to introduce beneficial mutations at the metal cofactor and phenol binding sites, which led to destabilization of the protein fold of

the analog G4-DFtet. This problem was solved by optimizing the sequence of a loop far from the active site [16]. The finally designed ArM catalyzed the O_2-dependent oxidation of a larger catechol derivative, 3,5-di-tert-butyl-catechol (3,5-DTBC), to the corresponding quinone (3,5-DTBQ) (Fig. 1), with a catalytic efficiency (k_{cat}/K_M = 6315 M^{-1} min^{-1}) about 4.6 times higher than that observed for a smaller substrate, 4-aminophenol (4-AP) (k_{cat}/K_M = 1380 M^{-1} min^{-1}).

Finally, the group of T. R. Ward developed ArMs that were active for the oxidation of secondary alcohols (phenethyl alcohol, benzyl alcohol, and cyclohexanol) in water using ^{t}BuOOH as oxidizing agent. They used the above mentioned "Trojan Horse" strategy based on the non-covalent incorporation of biotinylated d_6 piano stool ruthenium complexes into (strept)avidin. The best of them catalyzed the oxidation of dry phenethyl alcohol with a yield greater than 90% [19] in 90 h at room temperature.

2.1.2 Amine Oxidation

DeGrado et al. also used their metalloproteins, that were originally designed for the oxidation of hydroquinones, in order to catalyze the selective *N*-hydroxylation of arylamines [17]. For this purpose, on the one hand, they reshaped the access to the substrate cavity by incorporating three mutations at different levels of the protein and, on the other hand, they introduced an additional iron-binding histidine into the active site in order to mimic the active site of the natural di-oxoxine *p*-aminobenzoate *N*-oxygenase which is the only structurally characterized *N*-oxygenase known to contain a diiron catalytic center [20]. The resulting biohybrid proved to efficiently convert p-anisidine to the corresponding hydroxylamine (Fig. 1). In 2015, spectroscopic studies demonstrated that the 4-aminophenol substrate directly binds to the bi-ferrous site in the active site of the proteins. The actual active species of the Due Ferri scaffolds were thus identified and mechanisms explaining their different reactivities were suggested [18].

2.1.3 Sulfide Oxidation

The oxidation of sulfides by various oxidants catalyzed by ArMs, elaborated by all of the strategies described in the introduction of this chapter, has been by far the most widely investigated. One of the first reports was published by Sheldon et al. who constructed an ArM for the catalysis of sulfide oxidation using phytase as a protein scaffold (Fig. 2) [21]. Vanadium chloroperoxidases are non-heminic metalloenzymes that are more resistant to oxidative degradation than their heminic analogs [22]. Unfortunately, these enzymes can only accommodate small substrates in their relatively small active site, which impedes their potential use in asymmetric synthesis. Since this active site shows very high similarities with that of metal-free phytases, Sheldon et al. thought about building an ArM by inserting vanadate into phytase. The new artificial metalloprotein showed a catalytic activity similar to that of natural vanadium chloroperoxidase and catalyzed the quantitative sulfoxidation of thioanisole by H_2O_2, with up to 66% *ee* [23]. Further experiments were performed to improve the system, both by varying the nature of the host protein (acid–phosphatase, phospholipase, sulfatase, apo-ferritin, BSA) and of the metal moiety

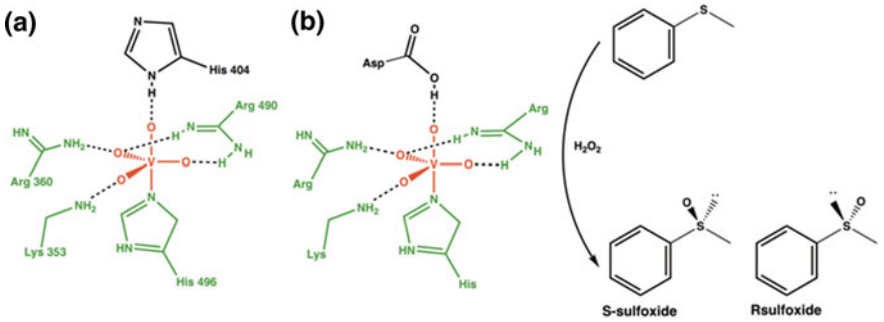

Fig. 2 New artificial metalloenzyme constructed by insertion of vanadate into phytase catalyzing the quantitative and stereoselective sulfoxidation of thioanisole by H_2O_2 [21]

(Mo, Re, W, Se, Os). One of the best results was obtained by Ward et al. with vanadate-loaded streptavidin (SAV), that catalyzed the enantioselective thioether sulfoxidation by ^{t}BuOOH with up to 93% *ee* in favor of the (*R*)-product and 96% conversion [24].

Several artificial metalloenzymes, generated using the "Trojan Horse" strategy, were also reported to catalyze chemoselective sulfide oxidations. Not surprisingly, in 2009, the group of Ward incorporated achiral biotinylated manganese-salen complexes into WT-SAV and five mutants to obtain ArMs that were tested as enantioselective sulfoxidation catalysts. The resulting enzymes showed moderate conversions (up to 56%) and low enantioselectivities (up to 13%) for the sulfoxidation of thioanisole using hydrogen peroxide as an oxidant in water (Fig. 3) [25]. Later, following the same strategy, Mahy et al. have exploited the neocarzinostatin (NCS) variant NCS-3.24, which displays an affinity for testosterone to prepare a novel ArM. A water-soluble anionic iron-porphyrin–testosterone conjugate was synthesized and subsequently associated with the NCS-3.24 variant (Fig. 3) [26]. The obtained Fe(III)-porphyrin–testosterone-NCS-3.24 artificial metalloenzyme was able to catalyze the chemo- and enantio-selective (*ee* = 13%) sulfoxidation of thioanisole by H_2O_2. Molecular modeling studies revealed synergy between the binding of the steroid moiety and that of the porphyrin macrocycle into the protein binding site, thus explaining both the observed better affinity for the conjugate (K_D = 1.6 μM) and the selectivity.

"The Host-Guest" strategy that appears to be the simplest one to incorporate metal cofactors into the cavity of proteins, has of course been the most often used to generate ArMs for sulfide oxidation catalysis. First of all, Human serum albumin (HSA) that is known to bind heme within a narrow cavity with a strong affinity ($K_a = 1.1 \times 10^8$ M^{-1}) was widely used not only for the generation of new efficient O_2 binding artificial hemoproteins but also for preparing ArMs [27–29]. Gross et al. inserted bis-sulfonated Ga- and Mn-corrole into HSA [30] as well as iron and manganese complexes of the same corrole into human, bovine (BSA), porcine (PSA), rabbit (RSA), and sheep (SSA) serum albumins to build new ArMs. These

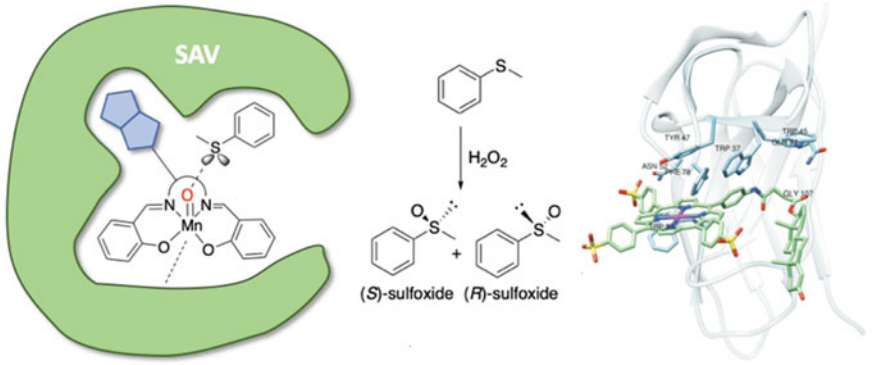

Fig. 3 Stereoselective and chemoselective oxidation of thioanisole by H_2O_2 catalyzed by ArMs constructed following the "Trojan Horse" strategy: insertion of a manganese-salen-biotin conjugate into SAV [25] and of an iron-porphyrin-testosterone conjugate into neocarzinostatin [26]

constructs were found to catalyze the sulfoxidation of thioanisole derivatives by hydrogen peroxide with conversions up to 98% and up to 74% *ee* [31]. Generally, better activities, selectivities as well as stabilities were obtained with albumin-Mn-corrole complexes with respect to their iron counterparts. More recently, the BSA-Mn-corrole artificial metalloenzyme was revealed to catalyze light-induced enantioselective oxidation of thioanisole into sulfoxide with 20% *ee* using water as the oxygen atom source in the presence of a ruthenium complex as photosensitizer (Fig. 4) [32].

The non-covalent association of metal-salen or -salophen complexes with serum albumins to produce ArMs was also reported. First, a series of ArMs were prepared by incorporation of Mn-salen into HSA. The HSA-Mn-salen artificial metalloenzymes catalyzed the chemoselective oxidation of thioanisole by NaOCl with 90–

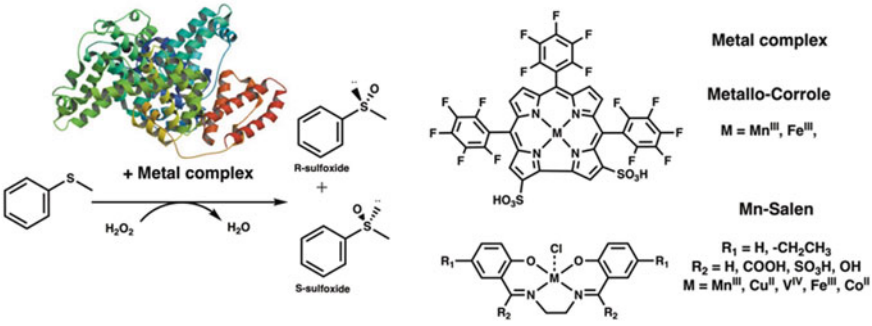

Fig. 4 Metallocorroles [30–32] and Mn-salen complexes [33] inserted non-covalently in serum albumins to afford artificial metalloenzymes that catalyze the stereoselective and chemoselective oxidation of thioanisole by H_2O_2

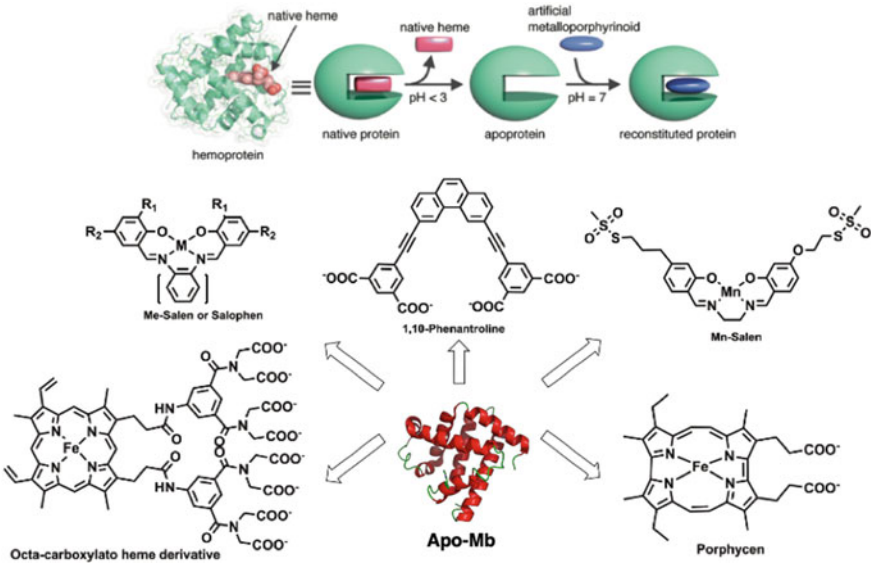

Fig. 5 Preparation of apo-myoglobin [36] and metal complexes of salen and salophen ligands [37–41] inserted non-covalently in apo-Mb to get artificial metalloenzymes that catalyze the stereoselective and chemoselective oxidation of thioanisole as well as iron complexes of heme derivatives bearing eight anionic carboxylate moieties and of porphycens that catalyze the hydroxylation of ethylbenzene into 1-phenylethanol by H_2O_2 [36, 42]

100% conversion and the almost exclusive formation of methylphenylsulfoxide whereas the Mn-salen complexes alone led to an about 60% conversion with the almost exclusive formation of methylphenylsulfone (Fig. 4) [33]. Another ArM was obtained by incorporation of a cobalt(II) Schiff base complex {CoL, H_2L = 2,2′-[(1,2-ethanediyl)bis(nitrilopropylidyne)]bisphenol} in BSA and its catalytic activity in the enantioselective oxidation of a variety of sulfides by H_2O_2 was studied as a function of pH, temperature, and concentration of catalyst and oxidant. Under optimal conditions, the BSA–CoL hybrid biocatalyst appeared as efficient for the enantioselective oxidation of a series of sulfides into the corresponding sulfoxides and reached excellent conversions (up to 100%), chemoselectivity (up to 100%), and good enantiomeric excesses (up to 87% *ee*) [34].

More recently, the oxygen-binding hemoprotein, myoglobin (Mb), has also been used by several teams to build up artificial metalloenzymes. The general strategy used is based on the replacement of its iron-heme prosthetic group by other heme or non-heme metal complexes. Indeed, this heme is linked inside the hydrophobic 10 Å diameter cavity of the protein by non-covalent interactions, including hydrophobic interactions, electrostatic interactions via its two carboxylate moieties, and coordination of its iron by the imidazole of H93 [35]. The prosthetic group of Mb can be easily removed without impairing its folding to yield apo-Mb, which shows a free cavity able to accommodate another metal cofactor (Fig. 5) [36].

Watanabe and coll. Used this strategy to prepare new ArMs. In particular, they first inserted synthetic chromium salophens into apo-Mb and mutants. The artificial metalloenzyme obtained from the H64D/A71G double mutant catalyzed the stereoselective sulfoxidation of thioanisole, with rather low turnover frequencies (TOF $\leq$ 0.13 min^{-1}) and enantiomeric excesses (*ee* $\leq$ 30% in favor of the (*S*)-product) [37]. The 3D structures of two apo-Mb A71G mutant-Mn- and Cr-salophen complexes revealed that the accessibility to the active site was sterically hindered by the bulky phenylenediamine moiety of the salophen cofactors. They then used metal-salen cofactors instead, which had a rather low effect on the efficiency of the chromium cofactors (TOF = 0.21 min^{-1}) but induced a noticeable increase in the efficiency of the manganese cofactor (TOF = 2.7 min^{-1}). In addition, insertion of the later cofactor in the H64D/A71G double mutant led to a slightly increased enantiomeric excess (30% *ee* in favor of the (*S*)-product) whereas its insertion in the A71G single mutant led to an enantiomeric excess very similar to that obtained with the WT protein (27% *ee* in favor of the (*R*)-product) [38].

Several other teams further inserted various Fe-tetrapyrrolic compounds into apo-Mb to produce new biohybrids that catalyzed the oxidation of thioanisole by H_2O_2 and led to up to 38% *ee* in favor of the (*S*)-sulfoxide. The enantiomeric excess could be increased either by covalent anchoring of metal complexes into apo-Mb and mutants [39–41] or by changing the metal such as, for example, replacing iron by manganese [41]. Accordingly, Lu et al. showed that a dual-point attachment of manganese-salen complex to a double mutant of apo-Mb (apo-Mb Y103C/L72C) led to an improved selectivity (51% *ee*) in thioanisole sulfoxidation relative to the analogous single-point mutant (Y103C, 12% *ee*) (Fig. 5) [40, 41].

Xylanase A from *Streptomyces lividans* (Xln10A), a thermostable β-1,4-endoxylanase glycoside hydrolase that hydrolyzes β-1,4 bonds in the main chain of xylan [43], was also used to build up new artificial hemoproteins using the host-guest strategy. This choice was guided by an early report from Nakamura and Tsushida et al. that showed that xylanase possessed a wide enough active site to accommodate an Fe(II)-α4-tetra-o-pivalamidophenylporphyrin. The resulting heat-resistant hemoproteins were found to bind and release O_2 in aqueous medium [44]. Metal complexes of synthetic tetraaryl porphyrins bearing negatively charged substituents, such as Iron(III)tetra(4-carboxyphenyl)porphyrin (Fe(TpCPP)) and iron(III)-*meso*-tetra(4-sulfonatophenyl)porphyrin (Fe(TpSPP)), were then inserted into Xln10A to lead to new artificial hemoproteins that showed peroxidase activity [12]. The catalytic activity of these Fe(TpCPP)-Xln10A and Fe(TpSPP)-Xln10A biohybrids for the oxidation of thioanisole by H_2O_2 (Fig. 6) was then investigated and compared to that of Fe(TpCPP) and Fe(TpSPP) alone. These two Fe-porphyrin complexes led, respectively to 45 and 33% yields in sulfoxide and to respective TOFs of 0.56 and 0.41 min^{-1}, but no enantiomeric excess could be detected. Use of the Fe(TpCPP)- and Fe(TpSPP)-Xln10A biohybrids as catalysts led to a decrease in the yields (about 24%) and turnover frequencies (about 0.30 min^{-1}), but enantiomeric excesses of up to 36% and 24% in favor of the (*S*)-sulfoxide could respectively be observed. It is noteworthy that better yield and turnover frequencies (85% and 1.09 min^{-1}) as well as a better enantiomeric excess in favor of the (*S*)-

sulfoxide (*ee* = 40%) could be obtained in the presence of 100 equivalents of imidazole as a co-catalyst [11, 45].

The host-guest strategy was also applied by Ménage et al. who used NikA as a guest protein, a periplasmic nickel-binding protein involved in the transport of nickel in *E. coli* and other related Gram-negative bacteria. It was shown by X-ray diffraction studies that NikA required in vivo butane-1,2,4-tricarboxylate (BTC) as a specific metal-binding ligand [47]. Structural characterization of a putative endogenous metal chelator in the Periplasmic Nickel Transporter NikA showed that it was also able to bind Fe(EDTA)(H_2O) [48]. Ménage et al. then took advantage of this property and inserted into NikA EDTA-like inorganic metal complexes of the N_2Py_2 type that mimic the metal environment of iron oxygenases. After the crystal structure of one of the NikA–Fe–N_2Py_2 complexes have been solved at 1.7 Å resolution, they followed an original approach based on molecular docking calculations to screen sulfide substrates, of the C_6H_5–S–CH_2–X type, for catalytic oxidation by the series of iron complex NikA hybrids. A set of 374 potential sulfide substrates was identified, among which six potential substrates had a common R_1–S–CH_2–CONH–R_2 motif. Interestingly, the skeleton of the defined substrate is comparable to the one of omeprazole or modafinil, which are major drugs from the pharmaceutical industry. The catalytic oxidation of those six substrates was performed in the presence of each hybrid, and the best catalytic results were obtained for the oxidation of 4-CH_3–Ph–S–CH_2–CONH–Ph by NaOCl, in the presence of one NikA–Fe–N_2Py_2 catalyst, that led to the chemoselective formation of sulfoxide in 78% yield, with a TON of 199 but a weak enantiomeric excess (5%). This study constituted a nice proof-of-concept for the design of a substrate family, that allowed Ménage et al. to define a new kind of artificial oxygenase for the catalysis of sulfoxidation reactions of pharmaceutical interest (Fig. 7) [49].

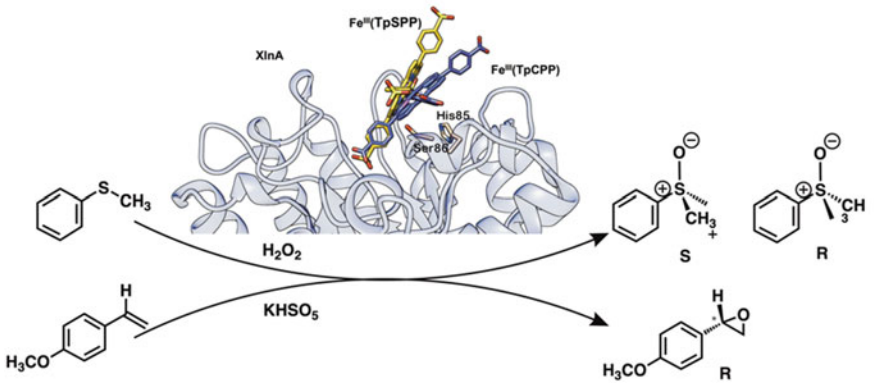

Fig. 6 Stereoselective and chemoselective oxidation of thioanisole by H_2O_2 [11, 45] and of 4-methoxystyrene by $KHSO_5$ [46] catalyzed by Fe-tetrarylporphyrin-xylanase A ArM

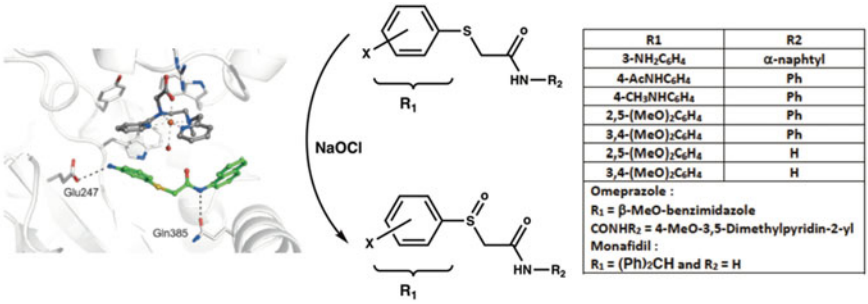

R1	R2
3-$NH_2C_6H_4$	α-naphtyl
4-$AcNHC_6H_4$	Ph
4-$CH_3NHC_6H_4$	Ph
2,5-$(MeO)_2C_6H_4$	Ph
3,4-$(MeO)_2C_6H_4$	Ph
2,5-$(MeO)_2C_6H_4$	H
3,4-$(MeO)_2C_6H_4$	H

Omeprazole :
R_1 = β-MeO-benzimidazole
$CONHR_2$ = 4-MeO-3,5-Dimethylpyridin-2-yl
Monafidil :
$R_1 = (Ph)_2CH$ and R_2 = H

Fig. 7 Design of a new kind of artificial oxygenase for the synthesis of sulfoxides of pharmaceutical interest: molecular docking of sulfides with a R_1–S–CH_2–CONH–R_2 formula allowed to determine the best 4-CH_3–Ph–S–CH_2–CONH–Ph to be chemo-selectively oxidized by the NikA–Fe–N_2Py_2/H_2O_2 system [49]

Finally, Mahy et al. covalently and selectively grafted a non-heme Fe(II) polyazadentate complex to the accessible cysteine 121 of bovine *β*-lactoglobulin. The biohybrid catalyzed the chemoselective oxidation of thioanisole by H_2O_2 into phenylmethylsulfoxide with an *ee* of 20%. Mechanistic studies showed that the reaction proceeded via a high spin ($S = 5/2$) $Fe^{III}(\eta^2\text{-}O_2)$ intermediate that was proposed to be responsible for the catalytic sulfoxidation [50].

2.1.4 Catechol Oxidation

Itoh and collaborators converted a bacterial hydrolytic di-zinc β-lactamase, into a redox-active di-copper oxidase. For this, they used a mutational method based on a rational computer-assisted recasting of the metal-binding site. This analysis suggested generating a triple D88G/S185H/P224G mutant of this protein, which made it possible to convert its active site into a type III dicopper reactive center. The new metalloprotein showed spectroscopic characteristics similar to those of type III copper proteins and showed high catalytic activity with an increase of two orders of magnitude in the k_{cat}/K_M value in the oxidation of catechols under aerobic conditions [51].

2.1.5 C–H Oxidation

Very few artificial metalloenzymes have been reported so far for the catalysis of alkane hydroxylation. However, Ricoux et al. produced monoclonal antibodies raised against microperoxidase 8 (MP8), that possesses an iron(III)-heme c cofactor. The association of these antibodies with MP8 gave an antibody-MP8 complex that was capable of effectively catalyzing the regioselective nitration of phenol to 2- and 4-nitrophenol by NO_2^- in the presence of H_2O_2 [52]. Inhibition by cyanide and radical scavengers suggested a peroxidase-like mechanism mediated by MP8, involving the formation of high-valent iron oxo species. The successive one-electron reduction of these intermediates by NO_2^- and phenol, respectively, led

to the production of nitro and phenoxy radicals, which then reacted together to give 2- and 4-nitrophenols. In this catalytic antibody, the protein thus appeared to have two main roles, it protected MP8 against oxidative degradation and induced a regioselectivity of the reaction towards the formation of 2-nitrophenol as a major product [52].

The only report to date on oxygen atom insertion into a C–H bond catalyzed by ArMs was from the group of Hayashi and Hisaeda. They prepared apo-Mb and mutants and then inserted heme derivatives bearing up to eight anionic carboxylate moieties into the heme-binding pocket (Fig. 5). The resulting ArMs not only showed peroxidase activity but also catalyzed the oxidation of catechol with rates up to 11-fold higher than native Mb, as well as the regioselective hydroxylation of ethylbenzene to 1-phenylethanol by H_2O_2, when Mb was reconstituted with a manganese-porphycene cofactor (Fig. 5) [36, 42].

2.1.6 Epoxidation

Here also, only a few examples of artificial metalloenzymes catalyzing alkene epoxidation have been reported so far. In the first papers simultaneously reported by Soumillion and Kazlauskas et al. the native Zn(II) ion of isoform II of human carbonic anhydrase (hCAII) was replaced by several metal cations including Co(II), Cu(II), Ni(II), Mn(II) and Rh(I). The X-ray crystal structures of hCAII substituted with these metal cations revealed that the primary coordination sphere of each of these was uniquely perturbed relative to the native Zn(II), although the overall metal-binding motif constituted by three histidine residues remained intact [53]. In the particular case when the Zn(II) ion was replaced by Mn(II), the new hCAII-Mn (II) metalloenzyme was found to catalyze the enantioselective alkene epoxidation with up to 66.5% *ee* and 12.5% conversion [54, 55]. To broaden the range of catalysts capable of catalyzing the epoxidation reaction, Reetz et al. have decided to covalently modify papain with a manganese-salen complex, using Michael addition of the thiolate function of cysteine 25 from papain to a maleimide substituent carried by the salen ligand. The artificial enzymes appeared to catalyze epoxidation reaction with enantiomeric excesses of about 10% [56, 57].

Finally, the catalytic activity of Xln A-based artificial hemoproteins was also investigated for the selective oxidation of alkenes. Mn(III)(TpCPP) was non-covalently inserted into Xln10A and the oxidation of various styrene derivatives by various oxidants such as hydroperoxides (H_2O_2 and ^tBuOOH), sodium hypochlorite (NaOCl), sodium periodate ($NaIO_4$), and oxone® ($KHSO_5$) was tested in the presence of the Mn(III)(TpCPP)-Xln10A biocatalyst. Positive results were only observed with $KHSO_5$ as oxidant, together with the highest catalytic activity reported so far for the oxidation of styrene catalyzed by artificial metalloproteins. However, a rather low chemo- and enantio-selectivities ($3\% < ee < 25\%$ in favor of the (*S*)-product) were observed for the epoxidation of styrene and poorly activated styrenes derivatives. On the contrary, high reverse enantioselectivity (80% in favor of the (*R*)-isomer) was observed for the epoxidation of *para*-methoxystyrene by $KHSO_5$ (Fig. 6), which constitutes the highest enantioselectivity ever reported to date for an epoxidation reaction catalyzed by an ArM [46].

2.1.7 Dihydroxylation

Dihydroxylation of double bonds is another oxidation reaction of synthetic interest, that is generally carried out in organic solvents using most often a high-oxidation-state transition metal such as osmium tetroxide as an oxidant [58]. In a biological medium, this reaction either requires a two-step process involving the first epoxidation by a monooxygenase followed by hydrolysis of the epoxide by an epoxide hydrolase or a one-step dihydroxylation, like for example Rieske dioxygenases that use O_2 as an oxidant in a complex process that also involves electron transfer from a biological reductant (generally NADH) mediated by a reductase, a ferredoxin containing [2Fe–2S] Rieske cluster [59]. There is thus a double interest to find artificial metalloenzymes that would perform such a reaction in one step under eco-compatible conditions.

The first team that tackled this challenge in 1983, was that of Okano et al., who used serum albumins derived ArMs for this purpose. They inserted osmium tetroxide into BSA and the formed ArM catalyzed the stereoselective *cis*-bis-hydroxylation of up to 40 equivalents of α-methylstyrene by ^{t}BuOOH with 68% *ee* in favor of the (*S*)-diol [60]. Later, Ward and coll. also prepared an osmium tetroxide-loaded SAV that catalyzed enantioselective olefin *cis*-dihydroxylation with up to 97% *ee* in favor of the (*R*)-product at ~20 TON in the presence of potassium ferricyanide [61].

Finally, Ménage et al. also took advantage of their NikAFeN_2Py_2 artificial metalloenzyme, and, by combining model chemistry and protein X-ray crystallography, they were able to study the intramolecular dihydroxylation of one of the *N*-benzyl substituents of the [*N*-benzyl-*N*′-(2-hydroxybenzyl)-*N*,*N*′-ethylenediaminediacetic acid] ligand. Indeed, the bound complex was able to activate dioxygen in the presence of a reductant (Dithiothreitol, DTT), leading to the formation of catechol as the sole product. The X-ray diffraction structure determination of four of the catalytic cycle intermediates and the end product showed that the hydroxylation reaction implicated an iron peroxo, which was also observed in natural iron monooxygenases (Fig. 8) [62].

2.2 Reductions

2.2.1 Hydrogen Production

With the inevitable future shortage of fossil fuels, it becomes crucial to develop alternative energy sources and hydrogen appears to possess almost ideal features to fulfill this challenge. Moreover, hydrogen is a clean and renewable energy source. Hydrogen is still essentially produced by steam reforming of methane but other fossil fuel independent processes are actively investigated such as water splitting.

In nature hydrogen metabolism is ensured by enzymes called hydrogenases that catalyze the interconversion between protons and dihydrogen. Hydrogenases are metalloenzymes containing iron and/or nickel in their active site. One of the best-studied hydrogenases is the [FeFe]-hydrogenase. Its active site (the H-cluster) contains a diiron cluster connected to a [4Fe4S] cluster via a cysteine bridge

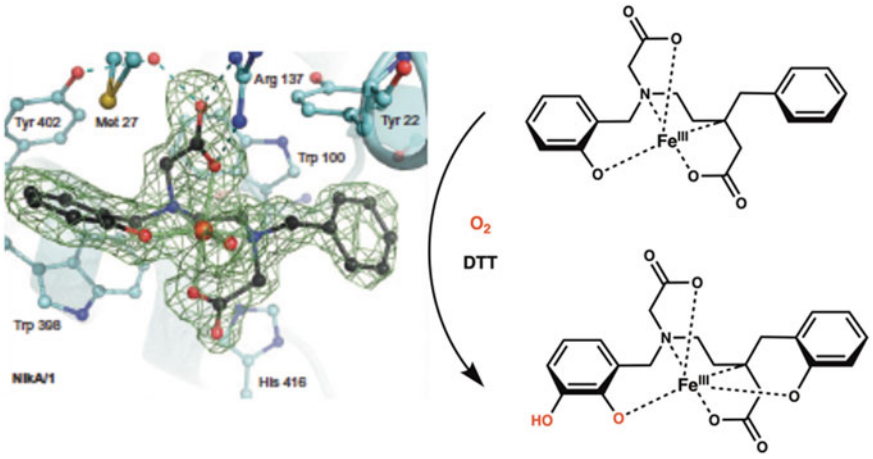

Fig. 8 Intramolecular dihydroxylation of one of the *N*-benzyl substituents of the [*N*-benzyl-*N*′-(2-hydroxybenzyl)-*N,N*′-ethylenediaminediacetic acid] ligand in the reaction of the $NikAFeN_2Py_2$ complex with O_2 in the presence of DTT as a reductant

(Fig. 9). The latter cluster serves as an electron reservoir during the catalytic cycle while the former cluster is responsible for proton activation and reduction.

Many efforts have been devoted to the design of low molecular weight mimics of hydrogenases active site (see Chap. 3). However, these molecules hardly mimic the second coordination sphere of the metal center, and even less the outer sphere provided by the protein environment. Embedding active site models of hydrogenase in protein scaffolds may lead to more efficient catalysts, shielding the metal center against degradation and enabling electron/proton tunneling to the active site [63].

The first strategy to design a functional artificial hydrogenase consisted of incorporating a simplified diiron carbonyl dithiolate cluster into an appropriate protein scaffold to mimic [FeFe]–hydrogenase. In the seminal work published by Hayashi and coworkers, apo-cytochrome c (Cyt c) was chosen as a protein scaffold [64]. When devoid of its natural prosthetic group, heme c, Cyt c displays a CXXC motif that can mimic the bridging dithiolate ligand of the diiron subcluster (Fig. 10).

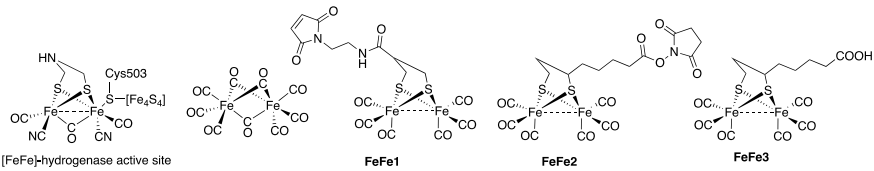

Fig. 9 Structure of the active site of [FeFe]-hydrogenase; structures of iron cluster precursors used to build up iron-based artificial hydrogenases

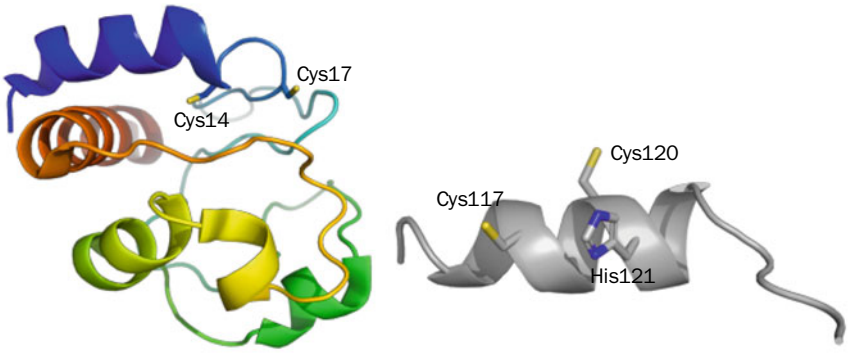

Fig. 10 Apo-proteins displaying a CXXC motif for bridging a diiron hexacarbonyl cluster. Left: apo-cytochrome c; right: C-terminal peptide fragment of cytochrome c556

Indeed, the reaction of $Fe_2(CO)_9$ with apo-Cyt c afforded a metalloprotein where the diiron hexacarbonyl cluster is bridged by two sulfur atoms provided by the cysteine side chains. The hydrogenase activity of the biohybrid was tested under photochemical conditions using ascorbate as a sacrificial electron donor and $[Ru(bpy)_3]^{2+}$ as photosensitizer (Fig. 11). A TON of 80 was measured after 2 h at pH 4.7.

Along the same line, the same team reported the use of a hexadecapeptide located at the C-terminus of cytochrome c_{556} presenting a CXXC motif assorted by a neighboring histidine that was used to coordinate a ruthenium-based photosensitizer (Fig. 10) [65]. Photocatalytic reduction of H^+ was effective at pH 8.5 with a TON of 9 after 2 h.

The Q96C mutant of heme-free nitrobindin (NB) was also employed as protein scaffold to covalently anchor the model **FeFe1** of the $[Fe_2]$-subsite of [FeFe]-hydrogenase via reaction between its maleimide group and the thiol of C96 [66]. Photocatalytic reduction of H^+ was effective at pH 4.0 with a TON of 130 after 6 h.

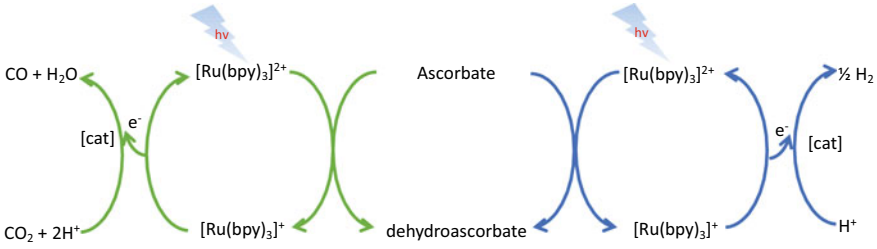

Fig. 11 Photocatalytic reduction of H^+ or CO_2 using $[Ru(bpy)_3]^{2+}$ as photosensitizer and ascorbate as sacrificial electron donor

Apo-ferritin (Fr) was also used to host diiron hexacarbonyl dithiolate clusters inside its cavity that naturally presents numerous metal-binding sites [67]. Loading of **FeFe2** within the cavity of apo-Fr was readily achieved at neutral pH without alteration of its structure. Light-driven reduction of H^+ afforded H_2 with a TON of 31 after 3 h at pH 5 to be compared with free **FeFe2** that gave a TON of 3.6 in the same conditions. It was shown that, since the photosensitizer remained outside the cavity, electron tunneling through the Fr shell necessarily followed a multistep pathway.

The N-hydroxysuccinimide ester derivative of **FeFe3** was conjugated to calf thymus histone H1 whose C-terminal domain contains numerous lysine residues and is intrinsically disordered [68]. Conjugation induced a significant conformational change with formation of α-helices. A change in the size and density of the nanoparticles was also observed. This biohybrid was able to catalyze the light-driven production of H_2 with a TON of 359 after 6 h at pH 5.0 to be compared with a TON of 54 for the precursor.

Nevertheless, all the artificial hydrogenases containing a diiron hexacarbonyl dithiolate active site suffer from progressive degradation upon illumination even if the protein scaffold provides some kind of protection resulting in increased catalyst lifetime. This is why Ghirlanda's team proposed to exploit the hydrogen reduction ability of cobalt protoporphyrin IX (CoPPIX, Fig. 12) to build up artificial hydrogenases. Considering the high similitude between heme b (=Fe-protoporphyrin IX) and CoPPIX, Ghirlanda and coworkers selected two hemoproteins, namely Mb [69] and cytochrome b_{562} (Cyt b_{562}) [70] to build up Co-based artificial hydrogenases.

In Mb, the iron of heme b is pentacoordinated, with H93 occupying one of the axial positions (Fig. 12). In Cyt b_{562}, the iron ion is hexacoordinated, the two axial positions being occupied by H102 and M7 (Fig. 12). Mb-CoPPIX catalyzed the light-driven production of H_2 with a TON of 243 after 12 h at pH 6.5 and 518 at pH 7.0, which is 3 times higher than that CoPPIX alone. The double mutant H64A/H97A was even more active with a TON of 512 at pH 6.5. Embedding of CoPPIX into WT apo-Cyt b_{562} did not increase the catalytic performance of the

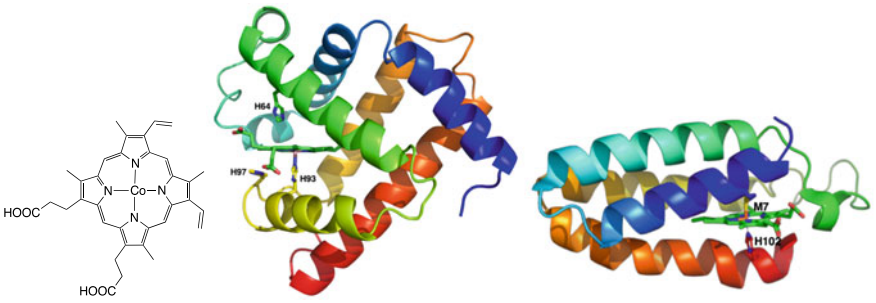

Fig. 12 Left: Structure of Co-PPIX; middle: X-ray structure of Cyt C-CoPPIX; right: X-ray structure of Cyt b_{562}

metal complex in light-driven H_2 production (TON = 120 after 8 h at pH 7). However, mutation of the coordinating M7 by alanine or aspartate led to more efficient hybrid catalysts with TONs of 310 and 270, respectively. Photocatalytic production of H_2 was also effective under aerobic conditions, which opens attractive avenues in the future development of environmentally benign artificial hydrogenases.

2.2.2 Carbon Dioxide Hydrogenation and Reduction

Carbon dioxide emissions owing to fossil fuel consumption are a real environmental threat because of the associated greenhouse effect. On the other hand, conversion of CO_2 into added-value chemicals such as CO or HCOOH may contribute to counteract this threat [71].

CO_2 Reduction

In nature, the interconversion between CO_2 and CO is catalyzed by [NiFe] carbon monoxide dehydrogenase (CODH) via a two-electron, proton-coupled process [72]. An ArM catalyzing the selective two-electron CO_2 reduction to CO in water was assembled by dative anchoring of $[Ni(cyclam)]^{2+}$ to the single histidine residue at position 83 of WT azurin (WT-CuAz) or to the double mutant H83Q/Q107H (Fig. 13) [73].

Electrocatalytic reduction of CO_2 was observed at a slightly more positive potential for H83Q/Q107H CuAz-[Ni(cyclam)] compared to free $[Ni(cyclam)]^{2+}$. Moreover, the redox-active copper ion in the ArM appeared to serve as electron relay/storage during catalysis. Photocatalytic reduction of CO_2 catalyzed by CuAz-[Ni(cyclam)] was also achieved in solution in the presence of $[Ru(bpy)_3]^{2+}$ as photoinitiator and ascorbate as sacrificial electron donor (Fig. 11). Most interestingly, ArMs were much more selective for CO_2 reduction *vs.* H^+ reduction as the

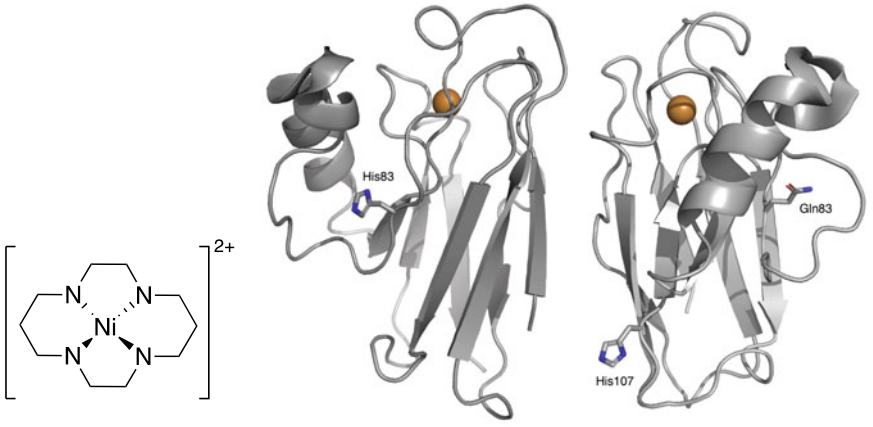

Fig. 13 Structure of $[Ni(cyclam)]^{2+}$; X-ray structures of WT-CuAz and H83Q/Q107H mutant

produced CO/H_2 molar ratios were significantly larger than those obtained with the free nickel complex. Also, the ArM built up from WT Az was more selective than the double mutant, likely owing to the partially buried position of H83.

A light-driven ArM to catalyze CO_2 reduction was further built up by simultaneous anchoring of $[Ru(bpy)_3]^{2+}$ and $[Ni(cyclam)]^{2+}$ to Az [74]. The former one was covalently attached by reaction of the epoxide derivative (Fig. 14) to Az variants carrying a surface-exposed cysteine at three different positions to study the dependence of the distance between Ru and Ni on the photocatalytic activity. The most active ArM was built up from the S78C Az mutant (Fig. 14) that exclusively reduced CO_2 and not H^+ under photoirradiation. The mechanism of reduction was elucidated thanks to photophysical studies.

CO_2 Hydrogenation

Formate dehydrogenases (FDHs) catalyze the reduction of CO_2 to formate and the reverse oxidation of formic acid to CO_2. The mechanism of NADH-dependent FDHs involves hydride transfer from NADH to CO_2 [75]. An ArM catalyzing the hydrogenation of CO_2 to formic acid was built up by covalent anchoring of the bis(diphosphine)Rh(I) complex to lactococcal multidrug-resistant regulator (LmrR, Fig. 15) [76].

This protein scaffold has a homodimeric structure creating a cavity to host the metal center. A cysteine residue was engineered at position 89 of LmrR. This position was chosen so that, in the dimer, the cysteines were located at a distance compatible with the double anchoring of the rhodium complex by reaction of its two maleimides. Indeed, under appropriate reactional conditions, a protein conjugate with a 2:1 monomer:rhodium ratio was formed with the complex almost fully occupying the cavity of LmrR (Fig. 15). While the bis(diphosphine)Rh(I) complex was unable to catalyze the hydrogenation of CO_2 on its own, LmrR-[Rh] catalyzed the formation of formic acid upon exposure to stoichiometric mixtures of CO_2 and H_2 in bicarbonate solution. A catalytic cycle involving the successive formation of Rh(III)-dihydride and Rh(I)-monohydride intermediates was proposed. The

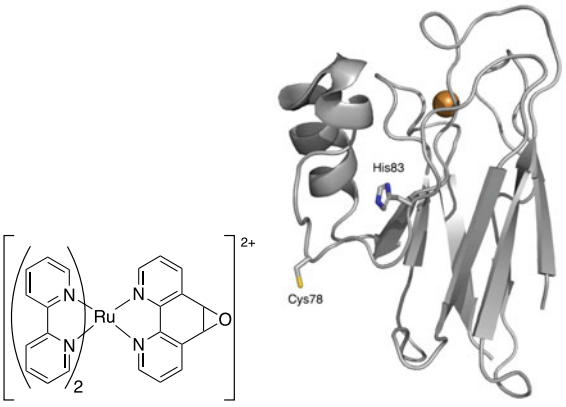

Fig. 14 Photosensitizer precursor and X-ray structure of S78C CuAz

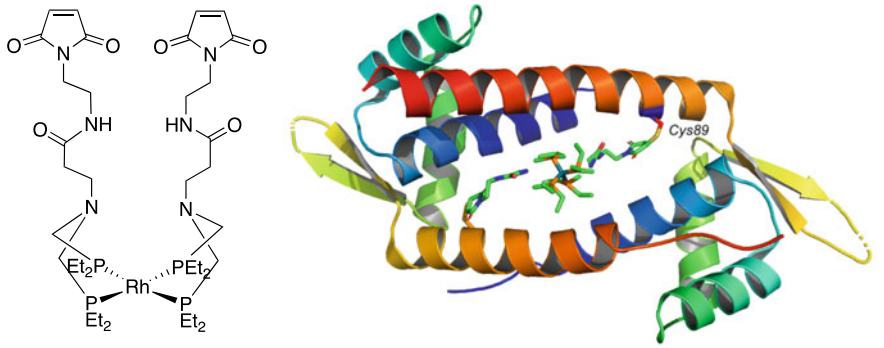

Fig. 15 Left: structure of bis(diphosphine)Rh(I) complex; Right: X-ray crystal structure of LmrR-[Rh] showing covalent linkage between C89 of one of the monomers and one of the maleimide groups of the complex (disorder is observed for the other linkage)

difference of catalytic activity between the free complex and LmrR-[Rh] was tentatively explained by the assumption that only LmrR-[Rh] was able to transfer a hydride to CO_2 likely due to favorable second and outer-sphere interactions with the substrate.

2.2.3 Enantioselective Cyclic Imine Reduction

Enantiopure amines are key compounds, found in numerous pharmaceuticals and agrochemicals to name a few applications. A strategy to access these compounds relies on enantioselective reduction of imines catalyzed by imine reductases [77]. However, natural imine reductases are still scarce, leaving room for the development of artificial imine reductases.

Nearly all the examples reported in the literature so far deal with the production of salsolidine by asymmetric transfer hydrogenation (ATH) of its imine precursor (Scheme 1). Salsolidine is a tetrahydroisoquinoline alkaloid produced by plants of the genus *Salsola*. The (*R*)-enantiomer of salsolidine has been found as a potent inhibitor of monoamine oxidase A [78]. Plant extracts were also shown to display significant choline esterase inhibition [79].

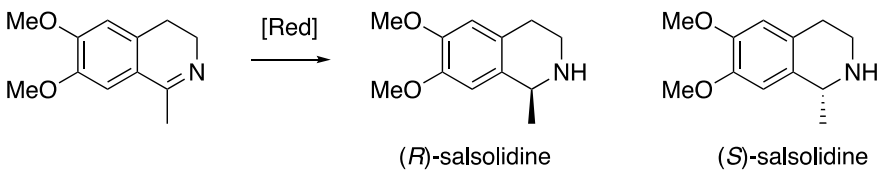

Scheme 1 Transfer hydrogenation of salsolidine precursor

Streptavidin as Protein Scaffold

The first ArM catalyzing the ATH of the salsolidine precursor was designed from the biotin – SAV system [80]. The biotin derivative **BTN-[Ir]** (Fig. 16) carrying half-sandwich iridium(III) complex comprising a chelating beta-amino sulfonamide ligand was synthesized and assembled by supramolecular anchoring to WT-SAV. WT-SAV ⊂ **BTN-[Ir]** catalyzed the quantitative conversion to salsolidine with an enantiomeric excess of 57% for the (*R*)-isomer using formate as hydrogen donor. Subsequently, an array of mutants was prepared by saturation mutagenesis at position S112. The crystal structure of the S112A-SAV ⊂ **BTN-[Ir]** biohybrid showed that the biotin derivative occupied the biotin-binding site and that A112 was located at a short distance from the metal center (Fig. 16). Moreover, the absolute configuration of iridium in the biohybrid was shown to be S. The *ee* reached 96% for the (*R*)-isomer with the S112A mutant while the enantioselectivity was nearly fully reversed with the S112K-SAV mutant (*ee* = 78% for the (*S*)-isomer). Furthermore, it was found that K121 from an adjacent monomer might act as an external proton donor during the catalytic cycle.

Computational and saturation kinetics studies were further performed to understand the opposite enantioselectivities afforded by both mutants [81]. It appeared that the final absolute configuration of the salsolidine product was dictated by the configuration of the metal center which was initially imposed by the protein environment.

Still, the ArM resulting from supramolecular anchoring of **BTN-[Ir]** to WT-SAV catalyzed the ATH at a much slower rate than the free complex [82]. To circumvent this issue, aminoacids K121, R84, and D67 located at the vicinity of the metal center were systematically mutated. The best mutant in terms of k_{cat} and K_m measured on 1-methyl-3,4-dihydroisoquinoline was R84A/S112A/K121A where the positively charged K and R aminoacids were replaced by the small and neutral alanine.

Other artificial imine reductases were built up by combining supramolecular and dative anchoring of half-sandwich rhodium(III) or iridium(III) to SAV [83]. This time, the biotin entity was linked to the ancillary cyclopentadienyl ligand rather than to the N^N chelating ligand (Fig. 17). A histidine was introduced at positions S112 or K121 of SAV to provide a coordination site for rhodium or iridium once in

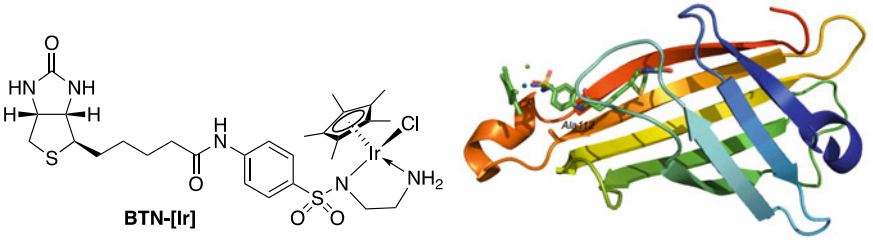

Fig. 16 Left: structure of **BTN-[Ir]**; right: X-ray structure of S112A-SAV ⊂ **BTN-[Ir]**

the binding pocket of the protein host and to activate it. The X-ray structure of the resulting ArMs showed that the rhodium ion was indeed coordinated to the imidazole of H112 of the same monomer while it was coordinated to the imidazole side chain of a neighboring monomer in K121H-SAV (Fig. 17).

Embedding the rhodium and iridium complexes into WT-SAV, S112H-SAV and K121H-SAV afforded artificial imine reductases whose efficacy in the ATH of the salsolidine precursor differed markedly from the complexes alone. The most enantioselective ArM resulted from the embedding of the rhodium cofactor into K121H-SAV yielding mainly (*R*)-salsolidine with 79% *ee*. Interestingly, inversion of selectivity was again observed with S112H-SAV since (*S*)-salsolidine was preferentially produced with an *ee* of 55%.

Directed evolution was applied to the ArM resulting from the supramolecular anchoring of the iridium complex **BTN-[Ir]** to SAV [84]. Aminoacids located at close range to the metal cofactor were subjected to iterative saturation mutagenesis. Catalysis tests were directly run on cell-free extracts supplemented with a diamide to prevent catalyst poisoning by glutathione [85]. This strategy allowed to identify a

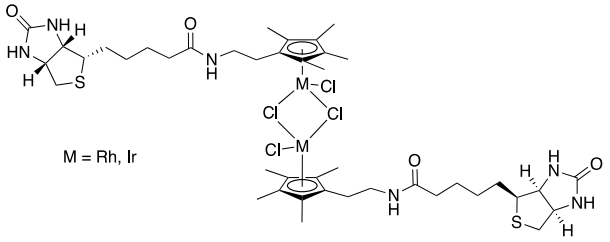

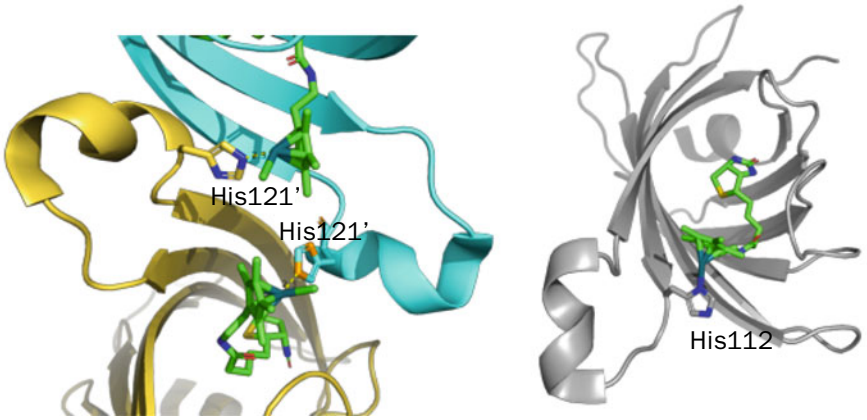

Fig. 17 Up: iridium precursor for double anchoring to SAV. Down: left: X-ray structure of K121H-SAV ⊂ [Rh] (Two symmetry-related monomers); right: X-ray structure of S112H-SAV ⊂ [Rh]

mutant affording an *ee* of 50% for (*S*)-salsolidine with 75% conversion. Another mutant displayed an 8-fold increase in k_{cat} compared to the cofactor alone.

Recently, to overcome the previously noticed dependence of SAV-to-Ir ratio on the enantioselectivity owing to the tetrameric nature of SAV, a single chain dimeric streptavidin (scdSAV) was engineered followed by genetic optimization of positions 112 and 121 [86]. Two monovalent scdSAVs (scdSAVmv1 and scdSAVmv2) were also produced to study the influence of the second cofactor on the catalytic properties of the ArM. X-ray structural analysis showed that the iridium cofactor adopts two different conformations in scdSAV, one being more solvent-exposed than the other. Conversely, the Ir cofactor adopts only one conformation once bound to its binding pocket. Under optimized conditions, an ArM affording a high TON and high *ee* were identified. Most importantly, ATH experiment could be extended to the preparative scale without detrimental effects on the conversion and *ee*. This breakthrough lets us anticipate biotechnological developments of artificial imine hydrogenases in the near future.

Carbonic Anhydrase as Protein Scaffold

The half-sandwich iridium complex **CA-[Ir]** bearing an arylsulfonamide entity (Fig. 18) was synthesized and assembled to hCAII [87]. Binding of the metal cofactor by coordination to the catalytic zinc ion was assessed by X-ray structural analysis (Fig. 18) that also highlighted the low occupation of the metal cofactor in the binding site. WT-hCAII ⊂ **CA-[Ir]** catalyzed the transfer hydrogenation of the salsolidine precursor with 82% conversion (TON = 9) and 70% *ee* in (*S*)-salsolidine. The catalytic performances of the ArM were further improved by mutating positions 91 and 170 to alanines.

Rosetta protein design software was further applied to increase the affinity of the iridium cofactor for CA II and in turn to increase the catalytic performances of the ArM [88]. Up to eight combinations of mutations were produced and assembled to **CA-[Ir]**. The best mutant afforded (*S*)-salsolidine with 94% *ee* and a TON of 98. Slight improvement of the selectivity was observed by replacing one of the methyl substituents of the cyclopentadienyl ligand by a bulkier propyl group.

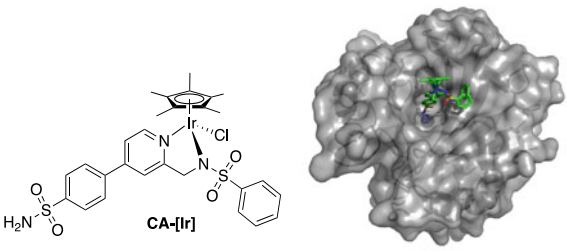

Fig. 18 Left: structure of the iridium catalyst to be anchored to hCA II; right: X-ray structure of WT-hCAII ⊂ **CA-[Ir]**

2.3 Artificial Metalloenzymes for Polymerization Catalysis

2.3.1 Polymerization of Phenylacetylene

Polyacetylenes are a group of conjugated polymers with unique electrical, (non-linear) optical, optoelectronic, magnetic, chiroptical, (enantio)permselective, and photolithographic properties. Prior to the design of ArMs catalyzing the polymerization of phenylacetylene (PA), it had been shown that PA could be polymerized in water in the presence of various rhodium complexes, for instance $[Rh(L)Cl]_2$ (with L = nbd; cod) and that the resulting polymers displayed up to 100% *cis* configuration depending on the rhodium catalyst [89].

The first ArM to catalyze a polymerization reaction was built up by dative anchoring of Rh(nbd) entities to horse apo-Fr as protein scaffold [90]. Apo-ferritin is a multimeric protein made of 24 identical subunits forming spherical nanoparticles of 8 nm inner diameter. Metallation of apo-Fr by $[Rh(nbd)Cl]_2$ (Fig. 19) afforded the metalloprotein Fr-$[Rh]_n$ containing 57.5 ± 3.5 Rh per Fr in average. The 3D structure of Fr-$[Rh]_n$ was solved by X-ray crystallography. Each subunit was shown to contain three Rh ions, two of them being coordinated by the imidazole of His residues while the last one was coordinated by C48 and E45 residues. Furthermore, a change of hapticity from η^4 to η^2 was observed for the nbd ligand since the other double bond underwent nucleophilic addition of the thiol function of Cys (Fig. 20). All the rhodium ions were located inside the cavity of Fr.

Polymerization of PA occurred in the cavity of Fr-$[Rh]_n$. Subsequent extraction from the cage afforded a polymer with a *cis*-transoidal configuration (Scheme 2) as determined by NMR, an M_n of $(13.1 \pm 1.5) \times 10^3$ (i.e. 130 monomers per polymer chain in average) and dispersity of 2.6 ± 0.3. The average size of the polymer as well as the dispersity appear to be governed by the size of the Fr cavity while its *cis* configuration is identical to that obtained with the rhodium precursor.

Insight into the actual active site of Fr-$[Rh]_n$ and the mechanism of polymerization was provided by computational studies using QM/MM approach [91]. The rhodium ion coordinated to H49 was suggested to extrude from its binding site upon insertion of PA to move to site D comprising an ensemble of three hydrophobic residues where propagation occurred (Fig. 20).

Later on, a new biohybrid construct was designed to catalyze the polymerization of PA. This time, heme-free NB was selected as a protein scaffold owing to its β-barrel structure made of 10 twisted β-strands creating a well-defined rigid cavity

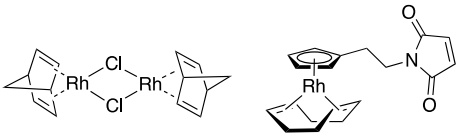

Fig. 19 Rhodium precursors used to build up artificial enzymes catalyzing the polymerization of PA

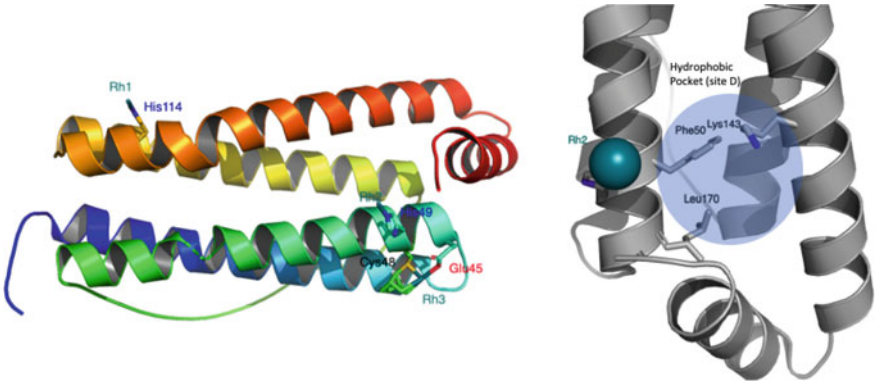

Fig. 20 Left: X-ray structure of a Fr-$[Rh]_n$ subunit showing the three coordination sites of rhodium; right: Hypothetical active site of Fr-[Rh]n

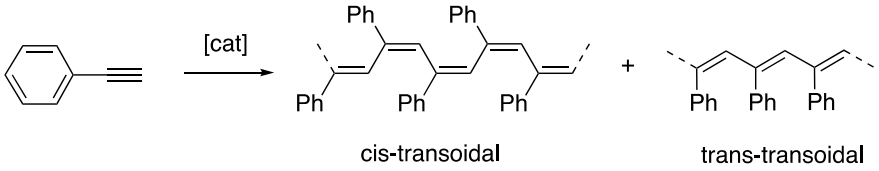

Scheme 2 Polymerization of phenylacetylene

for hosting the metal-binding site and the substrate [92]. The half-sandwich Rh(cod) complex carrying a maleimide group (Fig. 19) was synthesized and conjugated to the Q96C mutant of NB. The anchoring point was chosen so as to be located at the entrance of the cavity. Polymerization of PA proceeded under mild conditions to afford a polymer with an M_n of 42.6×10^3 and dispersity of 2.6. The most interesting finding was the stereochemistry of the generated polymer since the *trans:cis* ratio equaled 53:47, to be compared to the precursor complex that gave almost exclusively the cis configuration as previously reported for other Rh(I) catalysts [89]. The *trans:cis* ratio even increased to 30:70 when the reaction was performed at 2 °C. NB was further engineered to enlarge the cavity by mutating positions distant by 6 Å from the Rh center. Mutant NB4 (H76L/Q96C/H158L) afforded the highest *trans:cis* ratio (82:12). X-ray crystallography of NB4-[Rh] assorted by molecular dynamics simulation suggested that the metal center in NB4-[Rh] displays a defined orientation probably explaining the high stereoselectivity of the reaction (Fig. 21).

Another ArM was built up by covalent anchoring of the same rhodium(cod) complex to an engineered form of Fhu A [93]. [Note: Description of FhuA and its engineered form ΔCVF^{TEV} will be given below]. The amphipathic solvent MPD was shown to efficiently stabilize the resulting biohybrid in its fully folded form.

FhuA-[Rh] was able to catalyze the polymerization of PA in 52% yield to afford a polymer with an M_n of 5,500 and dispersity of 2.9. Most interestingly, the *trans:cis* ratio equaled 75:25, meaning that embedding of the rhodium complex within the protein environment provided by FhuA reversed the stereoselectivity of the reaction.

2.3.2 Ring-Opening Metathesis Polymerization (ROMP) of Olefins

The first biohybrid to catalyze a ROMP reaction was introduced by Schwaneberg and Okuda in 2013 [94]. The synthesis of this ArM is based on the covalent anchoring of a Hoveyda-Grubbs metathesis catalyst [95, 96] to a variant of the *E. coli* transmembrane protein FhuA (ferric hydroxamate uptake protein component A). This protein conveniently displays a β-barrel folding made of 22 anti-parallel β-sheets creating a wide cavity suitable for hosting the metal catalyst and the substrate. Prior to ArM assembling, FhuA was engineered to create an anchoring point for the metal complex via a cysteine at position 545 and optimize its accessibility; TEV cleavage sites were also introduced in two loops to facilitate mass analysis of the ArM. The ruthenium benzylidene complex **HG3** (Fig. 22) designed from a previously published water-soluble Grubbs catalyst [96] was conjugated to FhuA in its unfolded form by Michael addition of the single cysteine to the maleimide group of **HG3**. Refolding of FhuA-**HG3** was then achieved by dialysis in the presence of polyethylene – polyethyleneglycol (PE-PEG).

The catalytic activity of the ArM was tested in the ROMP reaction of a water-soluble 7-oxanorbornene derivative (Scheme 3). The partially folded ArM FhuA-**HG3** afforded a polymer with 77% yield and a *cis:trans* ratio of 60:40 while the fully folded FhuA-**HG3** gave rise to a lower conversion (37%).

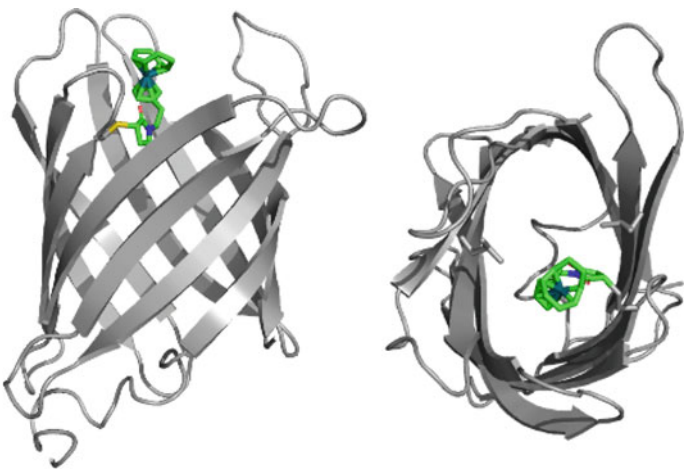

Fig. 21 X-ray structure of NB4-[Rh]

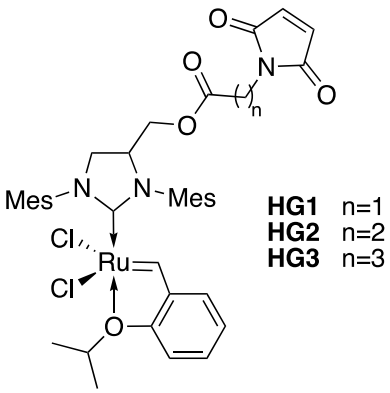

Fig. 22 ROMP catalyst precursors

The same team next investigated the influence of the linker arm length on the activity of ArMs derived from FhuA [97]. They synthesized complexes **HG1** and **HG2** and assembled them to FhuA. Under conditions where the biohybrid is folded, the highest conversion was obtained with FhuA-**HG1**. Conjugation of the same series of ruthenium benzylidene complexes **HG1-3** to NB variants carrying a single cysteine was further investigated [98]. Only **HG3** was successfully conjugated to NB4 most probably owing to steric constraints. This prompted the research team to engineer a new NB variant (L75A/H76L/Q96C/M184L/H158L; NB11) displaying a larger cavity. Indeed, all three complexes afforded the expected conjugates with high yield this time. The best combination in terms of catalytic activity in ROMP was provided by NB11-**HG3** at pH 6 with a conversion of 78% and of TON of 9900. The resulting polymer had an M_n of $180x10^3$ and a narrow dispersity of 1.05.

A new NB variant called NB4exp was recently engineered in an attempt to increase the size of the protein cavity [99]. Two additional β-strands were incorporated to form an extended β-barrel structure with a calculated cavity size of 1389 $Å^3$. Complexes **HG1-3** were successfully coupled to NB4exp and their activity tested in the ROMP of the 7-oxanorbornene derivative. The best catalyst appeared to be NB4exp-**HG2** that afforded a polymer with an M_n of 750×10^3, a dispersity of 1.21, and a conversion of 81%. Interestingly NB4exp-**HG2** outperformed the water-soluble metathesis catalyst Aquamet in terms of initial rate of reaction and conversion.

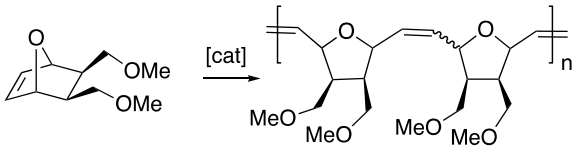

Scheme 3 Ring-opening metathesis polymerization (ROMP) of 7-oxanorbornene derivative

3 Advanced Developments of Artificial Metalloenzymes

3.1 Cascade Reactions

Enzymes function in vivo in the presence of other biomacromolecules including other enzymes and small molecules other than their substrates. In vitro, combinations of enzymes are routinely employed, to catalyze cascades of reactions, including at the industrial scale [100, 101]. The combination of transition metal catalysts with enzymes has however often led to mutual inhibition [102–105]. To overcome this issue, scientists rely mainly on compartmentalization strategies [106, 107] but ArMs offer another strategy as they may operate in harmony with other enzymes to achieve a synthetic goal. After all, the protein shell constitutes a protective environment for the metal of the active site of an ArM.

3.1.1 Cascade Reactions Employing Artificial Transfer Hydrogenase

By incorporating a d^6-piano stool iridium complex bound to biotin within SAV, Hollmann et al. [108] generated an artificial transfer hydrogenase (ATHase) that catalyzed the racemic reduction of imines by formate. They subsequently combined this ATHase with the natural monoaminooxidase-N-9 (MAO-N-9) that uses dioxygen to selectively oxidize the (*S*)-stereoisomer of a variety of amine substrates and provide the corresponding imines along with hydrogen peroxide. While the ATHase reduced imines into racemic (*RS*)-amine, only the (*S*)-isomer was reoxidized by MAO-N-9 into imine leading to the accumulation of the (*R*)-amine isomer. The reaction did not proceed unless either catalase or peroxidase was also added to the combination as hydrogen peroxide produced by MAO-N-9 was found to be detrimental to the ATHase activity. The combination of the three enzymes was efficient in the dynamic kinetic resolution of various chiral amines. It is noteworthy that inactivation was observed when the free iridium complex was used instead of the ATHase emphasizing the protective role of the protein shell and thus of artificial enzymes. HRP was also used as a catalase alternative that consumed hydrogen peroxide to bleach scopoletin and thus allowed to follow the ATHase activity (Scheme 4, left). In a similar approach, Ward et al. prepared another ATHase that was able to reduce imines using NADPH instead of formate as it relied on 4,7-dihydroxy-1,10-phenanthroline d^6-piano stool iridium complex. Glucose dehydrogenase (GDH) uses glucose to reduce $NADP^+$ to NADPH and the combination of the ATHase/MAO/catalase and GDH proved to be efficient in the dynamic kinetic resolution of various amines using simply glucose and dioxygen in the presence of catalytic amount of NADPH (Scheme 4, left) [109]. Finally, MAO could also be replaced by $_L$-amino acid oxidase (LAAO) and $_D$-amino acid oxidase (DAAO) that resulted in the accumulation of $_L$-pipecolic acid starting from $_L$-lysine (Scheme 4, right).

Additionally, the ATHase was used in combination with ene reductase-catalyzed asymmetric reduction of α,β-unsaturated compounds. NADH mimics (mNADHs)

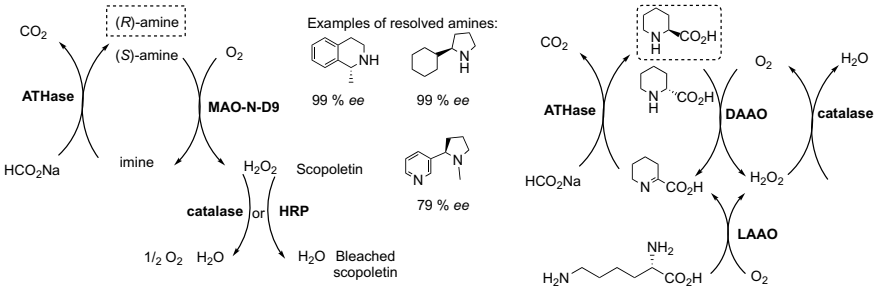

Scheme 4 Left, the artificial metalloenzyme ATHase and the natural MAO catalyzing a cascade of two reactions leading to the production of (*R*)-amines, starting from either racemic amines or imines and using oxygen and formate. Either catalase or HRP could be used to catalyze H_2O_2 to H_2O dismutation thus protecting the ATHase but the later could additionally bleach scopoletin enabling kinetic monitoring of ATHase activity. Right, ATHase in a cascade of reaction with LAAO and DAAO to form L-pipecolic acid

have been shown to accelerate the ene reductase-catalyzed reaction but existing regeneration methods of NADPH fail for mNADHs. Nonetheless, the ATHase regenerated mNADH by using formate therefore only catalytic amount of mNADH was needed for ene reductase to catalyze the reduction with TON reaching 2000 (Scheme 5).

3.1.2 Cascade Reactions Employing Other Artificial Reductases

An artificial reductase using formate to regenerate NADPH from $NADP^+$ was prepared by covalently grafting a Cp*Rh(III) 1,10-phenathroline or 1,1'-bipyridine complex (Cp* = pentamethylcyclopentadienyl) in the active site of alcohol dehydrogenase (ADH) [110]. The natural ADH uses NADPH to reduce ketones into alcohol. The combination of ADH with the artificial reductase enabled the recycling of NADPH by formate thus requiring only a catalytic amount of NADPH (Scheme 6).

3.2 In Vivo Catalysis

The main problem faced by in vivo catalysis by transition metal complexes is the potential deactivation of the catalyst in the living cell medium, which is quite different from simple in vitro aqueous media. Living cells are indeed complex entities containing very large amounts of potential inhibitors for unprotected catalysts such as glutathione that has clearly been identified as a major inhibitor for precious metal catalysts in aqueous media [85]. One way to protect catalysts for in vivo applications is their incorporation into a protein scaffold. This does not only protect the catalysts from the living cell environment but also helps their solubilization in aqueous media.

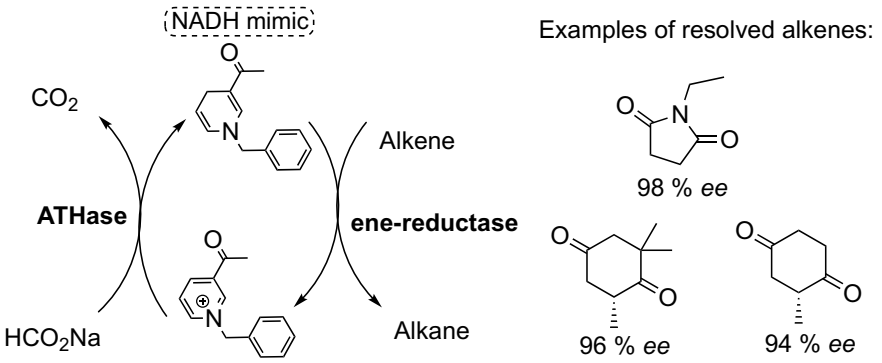

Scheme 5 Artificial ATHase for recycling NADH from formate, which was used in cascade with ene reductase to reduce various alkenes

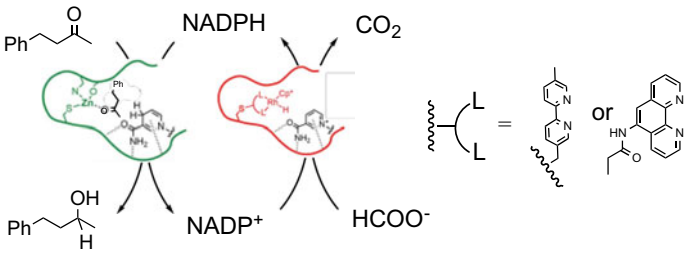

Scheme 6 Artificial reductase (in red) and natural alcohol dehydrogenase (in green) catalyzing a cascade of two reactions leading to the production of alcohol from ketone and formate using catalytic amounts of NADPH

3.2.1 Olefin Metathesis

With this issue in mind, Ward and coworkers developed the *in cellulo* production of SAV and its exportation to the periplasm of bacteria thanks to its fusion with the OmpA signal peptide. The choice of the periplasm as a compartment was mainly to take advantage of its low content in glutathione compared to that of the cytoplasm. Once in this compartment, SAV was also easily accessible to exogeneous molecules such as a synthetic biotinylated Hoveyda-Grubbs ruthenium complex to form the artificial metathase directly in the bacterial periplasm. The artificial metathase was shown to catalyze ring-closing metathesis. This was demonstrated in vivo by the transformation of a non-fluorescent substrate into the fluorescent umbelliferone **2** (Fig. 23). The scope of the reaction was then extended to the water-soluble benchmark substrate **3** which provided a poor yield. Interestingly, the authors took advantage of this low activity to perform directed evolution of the artificial metalloenzyme *in cellulo* and managed to get a 5-fold yield improvement from a quintuple mutant (Fig. 23) [111].

In vivo artificial metathases can also find potential agronomic and therapeutic applications. A fluorescent 7-diethylaminocoumarin (DEAC) and a *N*-[4-(4-dimethylamino)phenylazo]benzoate (DABCYL) based quencher were grafted to an Hoveyda-Grubbs ruthenium complex and incorporated in the hydrophobic pocket of HSA to afford an ArM-based ethylene biosensor [112]. Ethylene competitively displaced the DABCYL entity from coordination to ruthenium thus restoring the fluorescence of DEAC (Fig. 24, left). The reaction occurred in fruit flesh as demonstrated by the imaging of a thin slice of kiwifruit incubated with the artificial enzyme. In this case, although the macroscopic analysis does not demonstrate the activity within living cells, it clearly shows that the artificial metalloenzyme is active within the tissue of a living organism and could be used to quantify ethylene which is directly linked to ripening of fruits (Fig. 24, right).

In a similar strategy, a fluorescent Hoveyda-Grubbs ruthenium complex was incorporated in the hydrophobic pocket of HSA functionalized with N-glycan targeting moieties for selective accumulation in cancer cells. The resulting artificial methatase was then used to catalyze the in vivo activation of cytotoxic umbelliprenin by ring-closing metathesis. Results indicated that the enzyme accumulated in different cancer cell lines (SW620, HeLa, A549) leading to cell death [113].

3.2.2 Polymerization of Phenylacetylene

As described earlier, rhodium-based ArMs were developed for the catalysis of the polymerization of PA. Grimm et al. have transposed this reaction into whole-cell catalytic systems [114]. The authors constructed a variant of NB fused with an autotransporter of esterase (EstA). Expression in *E. Coli* resulted in displaying NB

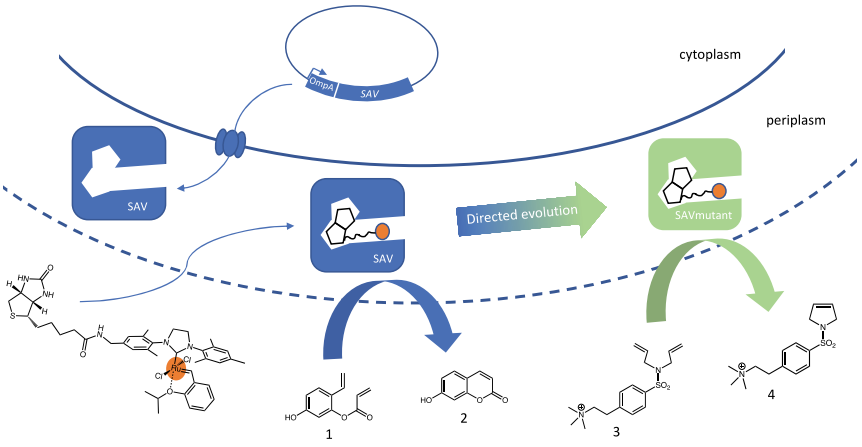

Fig. 23 Expression of SAV in the periplasm of *E. coli* by relying on the OmpA signal peptide and formation an artificial metathase upon the incorporation of a biotinylated ruthenium complex. Metathase activity detected via the formation of fluorescent umbelliferone **2** and directed evolution facilitated the reaction with benchmark substrate **3** [111]

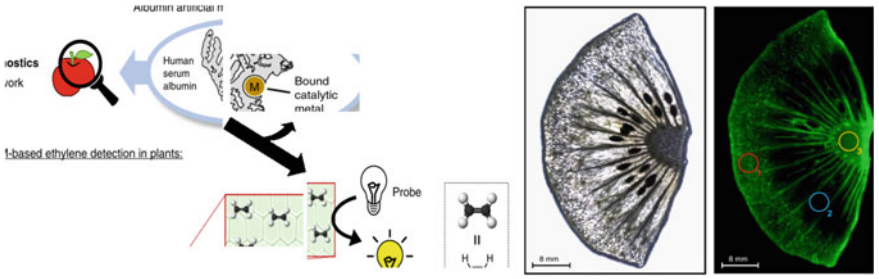

Fig. 24 Left, reaction of ethylene, and the artificial methatase. Right, fluorescence imaging of a kiwifruit slice incubated with the metalloenzyme reflecting ethylene distribution within the slice [112]

on the outer membrane of the bacterial cells. The covalent anchoring of the half-sandwich Rh(cod) (Fig. 19) to NB4 at the surface of the cells formed an artificial enzyme. The generated biohybrid bugs were evaluated for the catalysis of the polymerization of PA. This cellular system provided poly(phenylacetylene) with 80% of *trans* content and with 39×10^6 TON per cell.

3.2.3 Deallylation

Bioorthogonal uncaging of amines by cleavage of allyl carbamate protecting group catalyzed by organometallic ruthenium complexes has been shown to function under biologically relevant conditions and even inside living cells. Several organometallic ruthenium complexes were assayed and $[(Cp)(Me_2NQ)(allyl)Ru]PF_6$ ($Cp = \eta^5$-cyclopentadienyl, Me_2NQ = 4-(*N*,*N*-dimethylamino)-2-quinolinecarboxyl) showed the highest TON in the deprotection of *N*-(allyloxycarbonyl)aminocoumarin of bis[*N*-(allyloxycarbonyl)]rhodamine 110 and of *N*-(allyloxycarbonyl)doxorubicin (Scheme 7) [115].

The ruthenium complex was thereafter covalently bound to biotin and assembled to SAV to form an artificial allylic deallylase. Cell-penetrating benzopentasulfides (B5S) were bound to biotin and the four streptavidin binding pockets of the artificial enzyme were shared between biotin bound ruthenium complex and biotin bound B5S. Such artificial enzymes could accumulate in the cytoplasm of HeLa Kyoto cells, wherein they catalyzed the uncaging of rhodamine 110 from bis[*N*-(allyloxycarbonyl)]rhodamine 110. In another approach that allowed the artificial enzyme to cross the cellular membrane, B5S were covalently bound to streptavidin leaving its four binding pockets available for biotin bound ruthenium complex. The artificial enzyme also accumulated in the cytoplasm and it could be fully exploited as its four binding pockets were available for catalysis [116].

Bacterial cells were also used as a platform for allylic deallylase activity. SAV was expressed at the surface of cells as described earlier relying on OmpA then incubated with the biotin bound ruthenium complex to form the artificial allylic deallylase. Directed evolution was used to further improve the activity in the

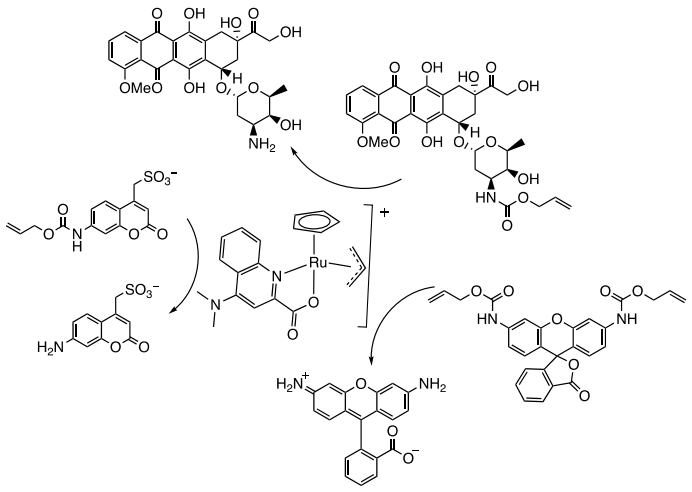

Scheme 7 Catalysis of the uncaging of a coumarin derivative, a rhodamine derivative and of doxorubicin by the ruthenium complex employed as a cofactor at the active site of allylic deallylase

uncaging of aminocoumarin, which was measured in 96-well plates and the most efficient mutants were identified as double mutants S112Y–K121S and S112M–K121A [117]. In addition to bacterial cells and human cells, algae cells, i.e. *Chlamydomonas reinhardtii* cells, were also exploited. The *N*-hydroxysuccinimide ester derivative of biotin was reacted with available amines and thiols at the cell membrane resulting in algae cells displaying biotin entities at their surface. These cells were incubated with SAV, which could then bind one of the displayed biotins at one of its four binding pockets. The remaining three binding pockets were then used to bind the biotin bound ruthenium complex. The formed artificial allylic deallylase displayed at the surface of algae cells was used for in vivo catalysis (Fig. 25) [118].

3.2.4 Enantioselective Cyclic Imine Reduction

The same SAV construction described in 2.1 together with **BTN-[Ir]** (Fig. 16) was employed to assemble an ATHase catalyzing the reduction of cyclic imines in *E. coli*. Although the addition of the FPD motif increased the TON by 5-fold for WT-SAV, it was at the expense of the enantioselectivity. Further genetic optimization of the protein scaffold allowed to reach an *ee* of 59% with a TON of 289 [119].

3.2.5 C–N and C–C Bond Formation

C–N and C–C bond formations are among the most important processes in organic synthesis. These reactions are considered abiological despite a specific cytochrome P450 enzyme (Bez E) that was reported to catalyze the intramolecular transfer of

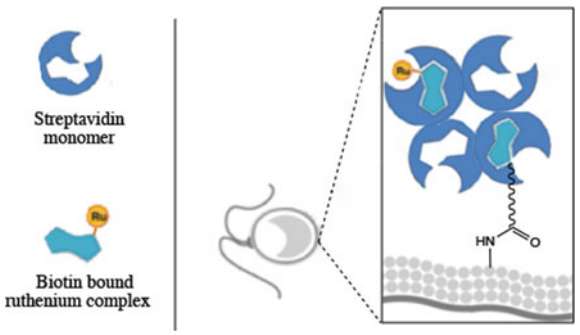

Fig. 25 Artificial allylic deallylase displayed at the surface of *C. reinhardtii*

natural nitrene to a C=C bond leading to an aziridine intermediate in the biosynthesis of benzastatin [120]. Inspired by Bez E, efforts were dedicated to the development of artificial enzymes capable of catalyzing nitrene and carbene transfer reactions in water and particularly in vivo.

Nitrene transfer reactions were initiated with iron porphyrins and then Cyt P450 by Breslow and Gellman [121–123] and Mansuy [124] in the early 1980s. 25 years later, Fasan and coworkers showed that cytochrome $P450_{BM3}$ and some of its variants were able to catalyze intramolecular C–H amination [125, 126]. Hartwig and coworkers replaced the iron of the heme of a Cyt P450 from a thermophilic organism, CYP119, by iridium and obtained the most active and the most chemoselective artificial enzyme for intramolecular C–H aminations, which they further improved the yield and selectivity by mutation [127]. 2018 Nobel Prize laureate F. Arnold [128] and coworkers showed that Cyt P450 engineered into a cytochrome P411 that contained a serine axial ligand to the heme iron in place of the WT cysteine ligand was able to catalyze, in the presence of NADPH as reductant, the intermolecular transfer of nitrene moieties into benzylic C–H bonds under anaerobic conditions (Scheme 8) [129]. Application of directed evolution to the protein afforded mutant $P411_{CHA}$ that catalyzed the benzylic tosylamidation of 4-ethylanisole by tosyl azide (TsN_3) to form the benzylic N-tosylamide with up to 1,300 turnovers, 66% yield, and excellent enantioselectivity (99% *ee*) even at the preparative scale and in vivo in whole *E. coli* cells. Further investigations in whole *E. coli* cells led to other variants that catalyzed the to sylamidation of indoles, such as 1-methylindole [130]. The most efficient variant, namely P411-IA, provided the desired indole amidation products with up to 8400 turnovers and 90% yield, with a chemoselectivity of 110:12:1 in favor of nitrene transfer over reduction or triazole formation. Finally, the variant of P411BM3-CIS-T438S having a single active site mutation, I263F, was the most active in the aziridination of a series of styrene derivatives, including less electron-rich substrates with up to 600 TTN, 70% yield, and 99% *ee* (Scheme 8) [131].

Roelfes and coworkers prepared an ArM by incorporation of heme into LmrR and showed that this enzyme as well as its mutants were able to catalyze carbene transfer reactions by ethyl diazoacetate **2** (EDA) into the double bond of styrene derivatives [132–134]. Ward and coworkers brought this activity to whole cells by

incorporation of a biotinylated dirhodium complex within engineered streptavidin variants and using EDA as a transfer agent, the resulting biohybrids were found to catalyze the carbene insertion into styrene, leading to the corresponding cyclopropane as well as the insertion of the carbene moiety of trifluoroethylphenyl diazoacetate into allylic C–H bonds of cyclohexadiene. Chemical and genetic optimizations allowed to modulate the catalytic activity of the ArMs which could be expressed in the periplasm of *E. Coli* cells. The most efficient artificial enzyme in vivo was obtained by assembling the dirhodium complex with the SAV K121C mutant expressed in the periplasm of *E. coli* and catalyzed the cyclopropanation of styrene with up to 20 turnovers (Fig. 26) [135].

The directed evolution of Cyt $P450_{BM3}$ was also employed by several groups including Arnold's who was the first to enhance the activity and the selectivity of cytochrome $P450_{BM3}$ for the catalysis of cyclopropanation reactions [136]. Directed evolution was also applied to Mb by Fasan et al. to produce artificial hemoproteins that could catalyze cyclopropanation reactions. The H64V-V68A double mutant catalyzed the benchmark reaction with 99% yield and 99.9% *ee*. Additionally, this mutant was found to catalyze the functionalization of the C–H of indoles by EDA, with 85% conversion and a TON of 106 [137]. It is noteworthy that this reaction could even be performed in whole cells, with 99% conversion and a TON of 82 [138, 139]. Brustad and coworkers used orthogonal expression techniques of hemoproteins to introduce mutations in the heme-binding pocket to allow the direct "in cellulo" incorporation of metal complexes of Deuteroporphyrin IX as cofactors into the apoprotein. Incorporation of Fe(Me)-Deuteroporphyrin IX and Ir(Me)-Deuteroporphyrin IX in the WIVS-FM*T268A variant, derived Cyt $P450_{BM3,}$ led to artificial hemoproteins that catalyzed the cyclopropanation of styrene by EDA [140,

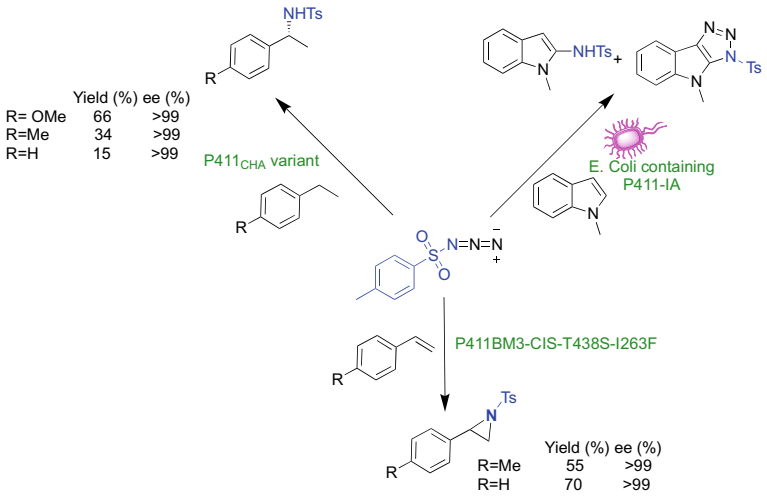

Scheme 8 Intermolecular nitrene transfer reactions catalyzed by cytochrome P411 variants

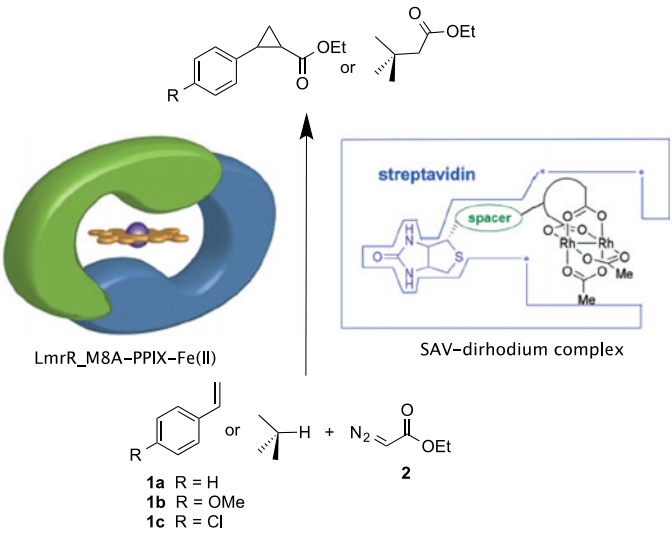

Fig. 26 Carbene transfer reactions catalyzed by ArMs derived from LmrR or SAV

141]. Hayashi and coworkers found out that Mb reconstituted (rMb) with iron(II)-porphycene was able to catalyze the cyclopropanation of styrene by EDA, and was 26-fold more efficient than native Mb [142, 143]. Substituting the native Fe ion of Mb by either Co, Cu, Mn, Ru, Rh, Pd, Ag, or Ir allowed Hartwig and coworkers to generate new hemoproteins that catalyzed the intramolecular carbene insertion of a diazoester into a C–H bond to form a dihydrobenzofuran product as well as the enantio- and diastereoselective cyclopropanation of unactivated olefins [144]. CYP119 mutants containing iridium methyl unit were found able to catalyze intramolecular carbene insertion [145, 146] and directed evolution, focusing on amino acids close to the active site, allowed to select four mutants, C317G, T213G, L69V, V254L, that were able to catalyze the reaction with 94% *ee* and a TOF of 43 min^{-1} at best. Arnold and coworkers showed that engineered cytochrome P450s, catalyzed the insertion of fluoroalkyl carbene intermediates into α-amino $C(sp^3)$–H bonds [147] and the reaction be performed on a preparative scale, but in vivo catalysis was not documented.

3.2.6 Diels–Alder Reaction

Because natural Diels–Alderases are rare and the Diels–Alder cycloaddition reaction is of major importance for chemical syntheses, many research teams have been tackling the elaboration of new artificial metalloenzymes that would catalyze the Diels–Alder reaction under ecofriendly conditions. Cu^{II} was shown to be the most efficient water-compatible transition metal for the Lewis acid catalysis of this cycloaddition [148–150] and therefore most artificial metallo-Diels-Alderases have

been prepared by incorporating Cu^{II} complexes into biomacromolecules covalently or non-covalently.

Reetz and coworkers inserted Cu^{II}–phtalocyanine into serum albumins including BSA and HSA [151, 152]. Palomo et al. generated an heterogeneous artificial Diels–Alderase by assembling Cu^{II}-phenanthroline-lipase at the surface of Sepabeads™ [153, 154]. Cu^{II}-1,10-phenanthroline was also coupled to a testosterone anchor and inserted into the neo-carzinostatin variant NCS-3.24, thanks to its affinity for the testosterone moiety [155]. (η^6-arene)-Ru^{II} complexes were covalently anchored into papain [156] whereas Cu^{II}-phenanthroline and terpyridine complexes were covalently anchored into F119C and Y26C mutants of dimeric double chain (A_3) [157] and dimeric single chain (A3_A3') [158] synthetic alpha-repeat proteins. Cu^{II}-pyrenyl and -terpyridine complexes were also anchored, respectively, into Nb and FhuA [159]. Deuss et al. also covalently bound Cu^{II}-phenanthroline (Phen) and -dipicolylamine complexes in two sterol carrier protein type 2 like domain (SCP-2L) mutants [160]. Finally, the Cu^{II}-1,10-phenanthroline complex was also bound to the LmrR M89C mutant [161]. All of the prepared ArMs catalyzed the Diels–Alder cycloaddition using benchmark substrates 2-azachalcone and cyclopentadiene, providing up to four isomer products. Yields ranging between 11 and 98% could be obtained, whereas the *endo* isomer was always the major isomer with *endo/exo* ratios ranging from 66/34 to 96/4. The enantiomeric excesses varied greatly with values between 0 and 97%. The most efficient of these enzymes were the Cu^{II}-Phen-SB-Lys-GTL*/196 catalyst [154] and the Cu^{II}-Phen-LmrR-M89C [161] that provided 98 and 93% yield and 97% *ee* with an *endo/exo* ratio of about 95:5, respectively. Directed evolution was used by Reetz et al. to design a Cu(II)-specific binding site in the thermostable protein tHisF. The introduction of a His-His-Asp coordinating triad for the Cu^{II} ion into this F affording a copper enzyme catalyzing the Diels–Alder reaction of the benchmark substrates with 73% yield, 93/7 *endo/exo* ratio and 46% *ee* [152], [162]. The substitution of the native Fe(II) of the His-His-Asp coordinating triad of 1-aminocyclopropane carboxylic acid oxidase by Cu^{II} afforded the most efficient artificial Diels–Alderase ever reported with a quantitative yield and >99 % *ee* [163].

Finally, Ghattas et al. used the A_{2A} adenosine receptor embedded in the cytoplasmic membrane of living human cells as a platform to build artificial metallo-Diels Alderases. The metalloenzymes were assembled by inserting in the WT receptor conjugates of a strong antagonist covalently bound to Cu(II) catalysts. The resulting cells enantio selectively catalyzed the abiotic Diels–Alder cycloaddition reaction with up to 42% yield, an 82/18 *endo/exo* ratio, and 14% *ee* (Fig. 27) [164]. The prospects of this strategy lie in the in vivo preparation of organ-confined receptor-based artificial metalloenzymes for the catalysis of reactions exogenous to the human metabolism. This strategy could be used for the targeted synthesis of either drugs or deficient metabolites and for the activation of prodrugs, leading to therapeutic tools with unforeseen applications.

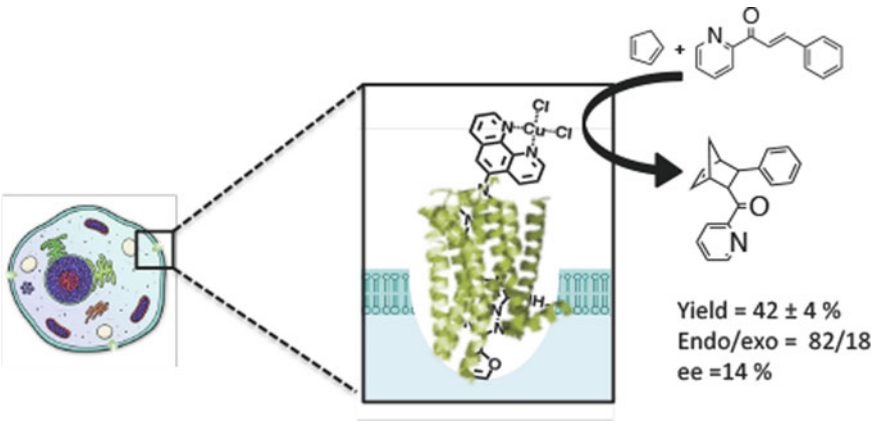

Fig. 27 Diels-Alder cycloaddition catalyzed by an artificial metalloenzyme assembled at the surface of a living HEK cell via the insertion of a Cu^{II}-phenanthroline-A_{2A} agonist conjugate in the A_{2A} adenosine receptor

4 Conclusions

To sum up, ArMs are powerful biohybrids capable of catalyzing a wide range of reactions under eco-compatible conditions. The construction of such catalysts is typically designed through different strategies including the host/guest interaction, the "Trojan horse" strategy, the covalent binding of the metallic complex into the protein scaffold, or *de novo* design of metal-binding peptides. In terms of oxidation reactions, sulfide oxidation has been the most studied reaction and one of the best results was obtained by Ward et al. with vanadate-loaded streptavidin, which catalyzed the enantioselective thioether sulfoxidation with up to 93% *ee* and 96% conversion [24]. Other oxidation reactions were successfully catalyzed by ArMs, including alcohol oxidation, amine oxidation, catechol oxidation, epoxidation, and dihydroxylation. However, C–H activation remains one of the biggest challenges to tackle, with only one example of oxygen insertion into a C–H bond described so far [36, 42]. Concerning reduction reactions, a lot of efforts have been devoted to mimic the activity of [FeFe]-hydrogenases by taking advantage of the second coordination sphere surrounding handmade metallic complexes in ArMs. Yet, the stability of the systems still needs to be improved to reach the high activity required for future hydrogen production applications. Another active field for ArMs is the CO_2 reduction catalysis, but the most successful reduction reaction catalyzed by ArMs is the enantioselective reduction of cyclic imines catalyzed by Ir or Ru complexes incorporated in various protein scaffolds with up to 94% *ee* and a TON of 98. ArMs have also been designed for the catalysis of polymerization reactions such as phenylacetylene polymerization, as well as ring-opening Metathesis Polymerization which have both been performed with good conversion rates and high

TON. Apart from the simple applications described above, ArMs have also been used for the development of cascade reactions by association with natural enzymes for dynamic kinetic resolution of amines or for the stereoselective synthesis of L-pipecolic acid. Finally, the capacity of ArMs to catalyze abiotic reactions in biological medium opens new opportunities to improve the toolbox of bioorthogonal chemistry applications. This prompted the scientific community to develop catalytic hybrid systems operating in vivo and some exciting constructs have been obtained for olefin metathesis, polymerization of phenylacetylene, uncaging by deallylation, C–N and C–C bond formation, as well as Diels–Alder reactions. There is no doubt that artificial metalloenzymes have a bright future ahead as sustainable and environmentally friendly catalysts.

References

1. Degtyarenko K (2005) Metalloproteins. Encycl Genet Genom Prot Bioinf g306204. https://doi.org/10.1002/047001153X.g306204
2. Valdez CE, Smith QA, Nechay MR, Alexandrova AN (2014) Mysteries of metals in metalloenzymes. Acc Chem Res 47:3110–3117. https://doi.org/10.1021/ar500227u
3. Que L, Tolman WB (2008) Biologically inspired oxidation catalysis. Nature 455:333–340. https://doi.org/10.1038/nature07371
4. Liu J-Y, Li X-F, Li Y-Z, Chang W-B, Huang A-J (2002) Oxidation of styrene by various oxidants with different kinds of metalloporphyrins. J Mol Catal Chem 187:163–167. https://doi.org/10.1016/S1381-1169(02)00137-1
5. Meunier B (1992) Metalloporphyrins as versatile catalysts for oxidation reactions and oxidative DNA cleavage. Chem Rev 92:1411–1456. https://doi.org/10.1021/cr00014a008
6. de Araujo Tôrres MG, da Silva VS, Idemori YM, DeFreitas-Silva G (2017) Manganese porphyrins as efficient catalysts in solvent-free cyclohexane oxidation. Arab J Chem S1878535217302423. https://doi.org/10.1016/j.arabjc.2017.12.007
7. Barona-Castaño J, Carmona-Vargas C, Brocksom T, de Oliveira K (2016) Porphyrins as catalysts in scalable organic reactions. Molecules 21:310. https://doi.org/10.3390/molecules21030310
8. Schwizer F, Okamoto Y, Heinisch T, Gu Y, Pellizzoni MM, Lebrun V, Reuter R, Köhler V, Lewis JC, Ward TR (2018) Artificial metalloenzymes: reaction scope and optimization strategies. Chem Rev 118:142–231. https://doi.org/10.1021/acs.chemrev.7b00014
9. Mahy J-P, Ghattas W, Di Méo T, Ricoux R (2018) Artificial metalloenzymes (Chap. 3). In: Williams G, Hall M (eds) Catalysis Series. Royal Society of Chemistry, Cambridge, pp 53–87
10. Mahy J-P, Raffy Q, Allard M, Ricoux R (2009) Various strategies for obtaining artificial hemoproteins: From "hemoabzymes" to "hemozymes". Biochimie 91:1321–1323. https://doi.org/10.1016/j.biochi.2009.03.002
11. Mahy J-P, Maréchal J-D, Ricoux R (2014) Various strategies for obtaining oxidative artificial hemoproteins with a catalytic oxidative activity: from "Hemoabzymes" to "Hemozymes"? J Porphyr Phthalocyanines 18:1063–1092. https://doi.org/10.1142/S1088424614500813
12. Ricoux R, Dubuc R, Dupont C, Marechal J-D, Martin A, Sellier M, Mahy J-P (2008) Hemozymes peroxidase activity of artificial hemoproteins constructed from the *streptomyces lividans* Xylanase A and Iron(III)-carboxy-substituted porphyrins. Bioconjug Chem 19:899–910. https://doi.org/10.1021/bc700435a

13. Mahy J-P, Ricoux R (2016) Design, synthesis and reactivity for a new kind of eco-compatible hybrid biocatalyst : artificial hemoproteins. Handb Porphyr Sci Appl Chem Phys Mater Sci Eng Biol Med, 38 Green Chem
14. Kaplan J, DeGrado WF (2004) De novo design of catalytic proteins. Proc Natl Acad Sci 101:11566–11570. https://doi.org/10.1073/pnas.0404387101
15. Summa CM, Rosenblatt MM, Hong J-K, Lear JD, DeGrado WF (2002) Computational de novo design, and characterization of an A2B2 Diiron protein. J Mol Biol 321:923–938. https://doi.org/10.1016/S0022-2836(02)00589-2
16. Faiella M, Andreozzi C, de Rosales RTM, Pavone V, Maglio O, Nastri F, DeGrado WF, Lombardi A (2009) An artificial di-iron oxo-protein with phenol oxidase activity. Nat Chem Biol 5:882–884. https://doi.org/10.1038/nchembio.257
17. Reig AJ, Pires MM, Snyder RA, Wu Y, Jo H, Kulp DW, Butch SE, Calhoun JR, Szyperski T, Solomon EI, DeGrado WF (2012) Alteration of the oxygen-dependent reactivity of de novo Due Ferri proteins. Nat Chem 4:900–906. https://doi.org/10.1038/nchem.1454
18. Snyder RA, Butch AJ, Reig AJ, DeGrado WF, Solomon EI (2012) Molecular-level insight into the differential oxidase and oxygenase reactivities of De Novo Due Ferri proteins. J Am Chem Soc 137:9302–9314. https://doi.org/10.1021/jacs.5b03524
19. Thomas CM, Letondor C, Humbert N, Ward TR (2005) Aqueous oxidation of alcohols catalyzed by artificial metalloenzymes based on the biotin–avidin technology. J Organomet Chem 690:4488–4491. https://doi.org/10.1016/j.jorganchem.2005.02.001
20. Choi YS, Zhang H, Brunzelle JS, Nair SK, Zhao H (2008) In vitro reconstitution and crystal structure of p-aminobenzoate N-oxygenase (AurF) involved in aureothin biosynthesis. Proc Natl Acad Sci 105:6858–6863. https://doi.org/10.1073/pnas.0712073105
21. van de Velde F, Arends IWCE, Sheldon RA (2000) Vanadium-catalysed enantioselective sulfoxidations: rational design of biocatalytic and biomimetic systems. Top Catal 13:259–265. https://doi.org/10.1023/A:1009094619249
22. van de Velde F, Arends IWCE, Sheldon RA (2000) Biocatalytic and biomimetic oxidations with vanadium. J Inorg Biochem 80:81–89. https://doi.org/10.1016/S0162-0134(00)00043-X
23. van de Velde F, Könemann L (1998) Enantioselective sulfoxidation mediated by vanadium-incorporated phytase: a hydrolase acting as a peroxidase. Chem Commun 1891–1892. https://doi.org/10.1039/a804702b
24. Pordea A, Creus M, Panek J, Duboc C, Mathis D, Novic M, Ward TR (2008) Artificial metalloenzyme for enantioselective sulfoxidation based on vanadyl-loaded streptavidin. J Am Chem Soc 130:8085–8088. https://doi.org/10.1021/ja8017219
25. Pordea A, Mathis D, Ward TR (2009) Incorporation of biotinylated manganese-salen complexes into streptavidin: new artificial metalloenzymes for enantioselective sulfoxidation. J Organomet Chem 694:930–936. https://doi.org/10.1016/j.jorganchem.2008.11.023
26. Sansiaume-Dagousset E, Urvoas A, Chelly K, Ghattas W, Maréchal J-D, Mahy J-P, Ricoux R (2014) Neocarzinostatin-based hybrid biocatalysts for oxidation reactions. Dalton Trans 43:8344–8354. https://doi.org/10.1039/c4dt00151f
27. Nakagawa A, Komatsu T, Iizuka M, Tsuchida E (2008) O_2 binding to human serum albumin incorporating iron porphyrin with a covalently linked methyl- L -histidine isomer. Bioconjug Chem 19:581–584. https://doi.org/10.1021/bc700400n
28. Komatsu T, Nakagawa A, Qu X (2009) Structural and mutagenic approach to create human serum albumin-based oxygen carrier and photosensitizer. Drug Metab Pharmacokinet 24:287–299. https://doi.org/10.2133/dmpk.24.287
29. Zunszain PA, Ghuman J, Komatsu T, Tsuchida E, Curry S (2003) Crystal structural analysis of human serum albumin complexed with hemin and fatty acid. BMC Struct Biol 3:6. https://doi.org/10.1186/1472-6807-3-6
30. Mahammed A, Gray HB, Weaver JJ, Sorasaenee K, Gross Z (2004) Amphiphilic corroles bind tightly to human serum albumin. Bioconjug Chem 15:738–746. https://doi.org/10.1021/bc034179p

31. Mahammed A, Gross Z (2005) Albumin-conjugated corrole metal complexes: extremely simple yet very efficient biomimetic oxidation systems. J Am Chem Soc 127:2883–2887. https://doi.org/10.1021/ja045372c
32. Herrero C, Quaranta A, Ricoux R, Trehoux A, Mahammed A, Gross Z, Banse F, Mahy J-P (2016) Oxidation catalysis via visible-light water activation of a $[Ru(bpy)_3]^{2+}$ chromophore BSA–metallocorrole couple. Dalton Trans 45:706–710. https://doi.org/10.1039/C5DT04158A
33. Rousselot-Pailley P, Bochot C, Marchi-Delapierre C, Jorge-Robin A, Martin L, Fontecilla-Camps JC, Cavazza C, Ménage S (2009) The protein environment drives selectivity for sulfide oxidation by an artificial metalloenzyme. ChemBioChem 10:545–552. https://doi.org/10.1002/cbic.200800595
34. Tang J, Huang F, Wei Y, Bian H, Zhang W, Liang H (2016) Bovine serum albumin–cobalt (II) Schiff base complex hybrid: an efficient artificial metalloenzyme for enantioselective sulfoxidation using hydrogen peroxide. Dalton Trans 45:8061–8072. https://doi.org/10.1039/C5DT04507J
35. Hunter CL, Lloyd E, Eltis LD, Rafferty SP, Lee H, Smith M, Mauk AG (1997) Role of the heme propionates in the interaction of heme with apomyoglobin and apocytochrome b_5. Biochemistry 36:1010–1017. https://doi.org/10.1021/bi961385u
36. Hayashi T, Hisaeda Y (2002) New functionalization of myoglobin by chemical modification of heme-propionates. Acc Chem Res 35:35–43. https://doi.org/10.1021/ar000087t
37. Ueno T, Koshiyama T, Abe S, Yokoi N, Ohashi M, Nakajima H, Watanabe Y (2007) Design of artificial metalloenzymes using non-covalent insertion of a metal complex into a protein scaffold. J Organomet Chem 692:142–147. https://doi.org/10.1016/j.jorganchem.2006.08.043
38. Ueno T, Koshiyama T, Ohashi M, Kondo K, Kono M, Suzuki A, Yamane T, Watanabe Y (2005) Coordinated design of cofactor and active site structures in development of new protein catalysts. J Am Chem Soc 127:6556–6562. https://doi.org/10.1021/ja045995q
39. Ohashi M, Koshiyama T, Ueno T, Yanase M, Fujii H, Watanabe Y (2003) Preparation of artificial metalloenzymes by insertion of chromium(III) Schiff base complexes into apomyoglobin Mutants. Angew Chem Int Ed 42:1005–1008. https://doi.org/10.1002/anie.200390256
40. Carey JR, Ma SK, Pfister TD, Garner DK, Kim HK, Abramite JA, Wang Z, Guo Z, Lu Y (2004) A site-selective dual anchoring strategy for artificial metalloprotein design. J Am Chem Soc 126:10812–10813. https://doi.org/10.1021/ja046908x
41. Zhang J-L, Garner DK, Liang L, Chen Q, Lu Y (2008) Protein scaffold of a designed metalloenzyme enhances the chemoselectivity in sulfoxidation of thioanisole. Chem Commun 1665. https://doi.org/10.1039/b718915j
42. Hayashi T, Murata D, Makino M, Sugimoto H, Matsuo T, Sato H, Shiro Y, Hisaeda Y (2006) Crystal structure and peroxidase activity of myoglobin reconstituted with iron porphycene. Inorg Chem 45:10530–10536. https://doi.org/10.1021/ic061130x
43. Ducros V, Charnock SJ, Derewenda U, Derewenda ZS, Dauter Z, Dupont C, Shareck F, Morosoli R, Kluepfel D, Davies GJ (2000) Substrate specificity in glycoside hydrolase family 10: structural and kinetic analysis of the *Streptomyces Lividans* Xylanase 10A. J Biol Chem 275:23020–23026. https://doi.org/10.1074/jbc.275.30.23020
44. Komatsu T, Ishihara S, Tsuchida E, Nishide H, Morokuma C, Nakamura S (2005) Heat-resistant oxygen-carrying hemoproteins consist of recombinant xylanases and synthetic iron(II) porphyrin. Biomacromol 6:1489–1494. https://doi.org/10.1021/bm049255l
45. Ricoux R, Allard M, Dubuc R, Dupont C, Maréchal J-D, Mahy J-P (2009) Selective oxidation of aromatic sulfide catalyzed by an artificial metalloenzyme: new activity of hemozymes. Org Biomol Chem 7:3208–3211. https://doi.org/10.1039/b907534h
46. Allard M, Dupont C, Muñoz Robles V, Doucet N, Lledós A, Maréchal J-D, Urvoas A, Mahy J-P, Ricoux R (2012) Incorporation of manganese complexes into xylanase: new artificial metalloenzymes for enantioselective epoxidation. ChemBioChem 13:240–251. https://doi.org/10.1002/cbic.201100659

47. Cherrier MV, Cavazza C, Bochot C, Lemaire D, Fontecilla-Camps JC (2008) Structural characterization of a putative endogenous metal chelator in the periplasmic nickel transporter NikA. Biochemistry 47:9937–9943. https://doi.org/10.1021/bi801051y
48. Cherrier MV, Martin L, Cavazza C, Jacquamet L, Lemaire D, Gaillard J, Fontecilla-Camps JC (2005) Crystallographic and spectroscopic evidence for high affinity binding of FeEDTA $(H_2O)^-$ to the periplasmic nickel transporter NikA. J Am Chem Soc 127:10075–10082. https://doi.org/10.1021/ja0518530
49. Esmieu C, Cherrier MV, Amara P, Girgenti E, Marchi-Delapierre C, Oddon F, Iannello M, Jorge-Robin A, Cavazza C, Ménage S (2013) An artificial oxygenase built from scratch: substrate binding site identified using a docking approach. Angew Chem Int Ed 52:3922–3925. https://doi.org/10.1002/anie.201209021
50. Buron C, Sénéchal-David K, Ricoux R, Le Caër J-P, Guérineau V, Méjanelle P, Guillot R, Herrero C, Mahy J-P, Banse F (2015) An artificial enzyme made by covalent grafting of an Fe^{II} complex into β-lactoglobulin: molecular chemistry, oxidation catalysis, and reaction-intermediate monitoring in a protein. Chem Eur J 21:12188–12193. https://doi.org/10.1002/chem.201501755
51. Fujieda N, Hasegawa A, Ishihama K, Itoh S (2012) Artificial dicopper oxidase: rational reprogramming of bacterial metallo-β-lactamase into a catechol oxidase. Chem Asian J 7:1203–1207. https://doi.org/10.1002/asia.201101014
52. Ricoux R, Girgenti E, Sauriat-Dorizon H, Blanchard D, Mahy J-P (2002) Regioselective nitration of phenol induced by catalytic antibodies. J Protein Chem 21:473–477. https://doi.org/10.1023/A:1021351120772
53. Håkansson K, Wehnert A, Liljas A (1994) X-ray analysis of metal-substituted human carbonic anhydrase II derivatives. Acta Crystallogr D Biol Crystallogr 50:93–100. https://doi.org/10.1107/S0907444993008790
54. Okrasa K, Kazlauskas RJ (2006) Manganese-substituted carbonic anhydrase as a new peroxidase. Chem Eur J 12:1587–1596. https://doi.org/10.1002/chem.200501413
55. Fernández-Gacio A, Codina A, Fastrez J, Riant O, Soumillion P (2006) Transforming carbonic anhydrase into epoxide synthase by metal exchange. Chem Bio Chem 7:1013–1016. https://doi.org/10.1002/cbic.200600127
56. Reetz MT (2002) Directed evolution of selective enzymes and hybrid catalysts. Tetrahedron 58:6595–6602. https://doi.org/10.1016/S0040-4020(02)00668-3
57. Reetz MT, Rentzsch M, Pletsch A, Maywald M, Maiwald P, Peyralans JJ-P, Maichele A, Fu Y, Jiao N, Hollmann F, Mondière R, Taglieber A (2007) Directed evolution of enantioselective hybrid catalysts: a novel concept in asymmetric catalysis. Tetrahedron 63:6404–6414. https://doi.org/10.1016/j.tet.2007.03.177
58. Kolb HC, VanNieuwenhze MS, Sharpless KB (1994) Catalytic asymmetric dihydroxylation. Chem Rev 94:2483–2547. https://doi.org/10.1021/cr00032a009
59. Abu-Omar MM, Loaiza A, Hontzeas N (2005) Reaction mechanisms of mononuclear non-heme iron oxygenases. Chem Rev 105:2227–2252. https://doi.org/10.1021/cr040653o
60. Kokubo T, Sugimoto T, Uchida T, Tanimoto S, Okano M (1983) The bovine serum albumin–2-phenylpropane-1,2-diolatodioxo-osmium(VI) complex as an enantioselective catalyst for cis-hydroxylation of alkenes. J Chem Soc Chem Commun 769–770. https://doi.org/10.1039/C39830000769
61. Köhler V, Mao J, Heinisch T, Pordea A, Sardo A, Wilson YM, Knörr L, Creus M, Prost J-C, Schirmer T, Ward TR (2011) OsO4·Streptavidin: a tunable hybrid catalyst for the enantioselective cis-dihydroxylation of olefins. Angew Chem Int Ed 50:10863–10866. https://doi.org/10.1002/anie.201103632
62. Cavazza C, Bochot C, Rousselot-Pailley P, Carpentier P, Cherrier MV, Martin L, Marchi-Delapierre C, Fontecilla-Camps JC, Ménage S (2010) Crystallographic snapshots of the reaction of aromatic C–H with O_2 catalysed by a protein-bound iron complex. Nat Chem 2:1069–1076. https://doi.org/10.1038/nchem.841

63. Alcala-Torano R, Sommer DJ, Bahrami Dizicheh Z, Ghirlanda G (2016) Chapter seventeen—design strategies for redox active metalloenzymes: applications in hydrogen production. In: Pecoraro VL (ed) Methods in enzymology. Academic Press, pp 389–416
64. Sano Y, Onoda A, Hayashi T (2011) A hydrogenase model system based on the sequence of cytochrome c: photochemical hydrogen evolution in aqueous media. Chem Commun 47:8229. https://doi.org/10.1039/c1cc11157d
65. Sano Y, Onoda A, Hayashi T (2012) Photocatalytic hydrogen evolution by a diiron hydrogenase model based on a peptide fragment of cytochrome c556 with an attached diiron carbonyl cluster and an attached ruthenium photosensitizer. J Inorg Chem 108:159–162. https://doi.org/10.1016/j.jinorgbio.2011.07.010
66. Onoda A, Kihara Y, Fukumoto K, Sano Y, Hayashi T (2014) Photoinduced hydrogen evolution catalyzed by a synthetic diiron dithiolate complex embedded within a protein matrix. ACS Catal 4:2645–2648. https://doi.org/10.1021/cs500392e
67. Chen W, Li S, Li X, Zhang C, Hu X, Zhu F, Shen G, Feng F (2019) Iron sulfur clusters in protein nanocages for photocatalytic hydrogen generation in acidic aqueous solutions. Chem Sci 10:2179–2185. https://doi.org/10.1039/C8SC05293J
68. Hu X, Chen W, Li S, Sun J, Du K, Xia Q, Feng F (2019) Diiron dithiolate complex induced helical structure of histone and application in photochemical hydrogen generation. ACS Appl Mater Interfaces 11:19691–19699. https://doi.org/10.1021/acsami.9b01866
69. Sommer DJ, Vaughn MD, Ghirlanda G (2014) Protein secondary-shell interactions enhance the photoinduced hydrogen production of cobalt protoporphyrin IX. Chem Commun 50:15852–15855. https://doi.org/10.1039/C4CC06700B
70. Sommer DJ, Vaughn MD, Clark BC, Tomlin J, Roy A, Ghirlanda G (2016) Reengineering cyt b562 for hydrogen production: a facile route to artificial hydrogenases. Biochim Biophys Acta BBA—Bioenerg 1857:598–603. https://doi.org/10.1016/j.bbabio.2015.09.001
71. Artz J, Müller TE, Thenert K, Kleinekorte J, Meys R, Sternberg A, Bardow A, Leitner W (2018) Sustainable conversion of carbon dioxide: an integrated review of catalysis and life cycle assessment. Chem Rev 118:434–504. https://doi.org/10.1021/acs.chemrev.7b00435
72. Shi J, Jiang Y, Jiang Z, Wang X, Wang X, Zhang S, Han P, Yang C (2015) Enzymatic conversion of carbon dioxide. Chem Soc Rev 44:5981–6000. https://doi.org/10.1039/C5CS00182J
73. Schneider CR, Shafaat HS (2016) An internal electron reservoir enhances catalytic CO_2 reduction by a semisynthetic enzyme. Chem Commun 52:9889–9892. https://doi.org/10.1039/C6CC03901D
74. Schneider CR, Manesis AC, Stevenson MJ, Shafaat HS (2018) A photoactive semisynthetic metalloenzyme exhibits complete selectivity for CO_2 reduction in water. Chem Commun 54:4681–4684. https://doi.org/10.1039/C8CC01297K
75. Amao Y (2018) Formate dehydrogenase for CO_2 utilization and its application. J CO2 Util 26:623–641. https://doi.org/10.1016/j.jcou.2018.06.022
76. Laureanti JA, Buchko GW, Katipamula S, Su Q, Linehan JC, Zadvornyy OA, Peters JW, O'Hagan M (2019) Protein scaffold activates catalytic co_2 hydrogenation by a rhodium bis (diphosphine) complex. ACS Catal 9:620–625. https://doi.org/10.1021/acscatal.8b02615
77. Gamenara D, Domínguez de María P (2014) Enantioselective imine reduction catalyzed by imine reductases and artificial metalloenzymes. Org Biomol Chem 12:2989–2992. https://doi.org/10.1039/C3OB42205D
78. Bembenek ME, Abell CW, Chrisey LA, Rozwadowska MD, Gessner W, Brossi A (1990) Inhibition of monoamine oxidases A and B by simple isoquinoline alkaloids: racemic and optically active 1,2,3,4-tetrahydro-, 3,4-dihydro-, and fully aromatic isoquinolines. J Med Chem 33:147–152. https://doi.org/10.1021/jm00163a025
79. Tundis R, Menichini F, Conforti F, Loizzo MR, Bonesi M, Statti G, Menichini F (2009) A potential role of alkaloid extracts from Salsola species (Chenopodiaceae) in the treatment of Alzheimer's disease. J Enzyme Inhib Med Chem 24:818–824. https://doi.org/10.1080/14756360802399662

80. Duerrenberger M, Heinisch T, Wilson YM, Rossel T, Nogueira E, Knoerr L, Mutschler A, Kersten K, Zimbron MJ, Pierron J, Schirmer T, Ward TR (2011) Artificial transfer hydrogenases for the enantioselective reduction of cyclic imines. Angew Chem-Int Ed 50:3026–3029. https://doi.org/10.1002/anie.201007820
81. Muñoz Robles V, Dürrenberger M, Heinisch T, Lledós A, Schirmer T, Ward TR, Maréchal J-D (2014) Structural, kinetic, and docking studies of artificial imine reductases based on biotin-streptavidin technology: an induced lock-and-key hypothesis. J Am Chem Soc 136:15676–15683. https://doi.org/10.1021/ja508258t
82. Schwizer F, Koehler V, Duerrenberger M, Knoerr L, Ward TR (2013) Genetic optimization of the catalytic efficiency of artificial imine reductases based on biotin-streptavidin technology. ACS Catal 3:1752–1755. https://doi.org/10.1021/cs400428r
83. Zimbron JM, Heinisch T, Schmid M, Hamels D, Nogueira ES, Schirmer T, Ward TR (2013) A dual anchoring strategy for the localization and activation of artificial metalloenzymes based on the biotin-streptavidin technology. J Am Chem Soc 135:5384–5388. https://doi.org/10.1021/ja309974s
84. Hestericova M, Heinisch T, Alonso-Cotchico L, Marechal J-D, Vidossich P, Ward TR (2018) Directed evolution of an artificial imine reductase. Angew Chem-Int Ed 57:1863–1868. https://doi.org/10.1002/anie.201711016
85. Wilson YM, Duerrenberger M, Nogueira ES, Ward TR (2014) Neutralizing the detrimental effect of glutathione on precious metal catalysts. J Am Chem Soc 136:8928–8932. https://doi.org/10.1021/ja500613n
86. Wu S, Zhou Y, Rebelein JG, Kuhn M, Mallin H, Zhao J, Igareta NV, Ward TR (2019) Breaking symmetry: engineering single-chain dimeric streptavidin as host for artificial metalloenzymes. J Am Chem Soc 141:15869–15878. https://doi.org/10.1021/jacs.9b06923
87. Monnard FW, Nogueira ES, Heinisch T, Schirmer T, Ward TR (2013) Human carbonic anhydrase II as host protein for the creation of artificial metalloenzymes: the asymmetric transfer hydrogenation of imines. Chem Sci 4:3269–3274. https://doi.org/10.1039/c3sc51065d
88. Heinisch T, Pellizzoni M, Duerrenberger M, Tinberg CE, Koehler V, Klehr J, Haeussinger D, Baker D, Wardt TR (2015) Improving the catalytic performance of an artificial metalloenzyme by computational design. J Am Chem Soc 137:10414–10419. https://doi.org/10.1021/jacs.5b06622
89. Tang BZ, Poon WH, Leung SM, Leung WH, Peng H (1997) Synthesis of stereoregular poly (phenylacetylene)s by organorhodium complexes in aqueous media. Macromolecules 30:2209–2212. https://doi.org/10.1021/ma961573s
90. Abe S, Hirata K, Ueno T, Morino K, Shimizu N, Yamamoto M, Takata M, Yashima E, Watanabe Y (2009) Polymerization of phenylacetylene by rhodium complexes within a discrete space of apo-ferritin. J Am Chem Soc 131:6958–6960. https://doi.org/10.1021/ja901234j
91. Ke Z, Abe S, Ueno T, Morokuma K (2012) Catalytic mechanism in artificial metalloenzyme: QM/mm study of phenylacetylene polymerization by rhodium complex encapsulated in apo-ferritin. J Am Chem Soc 134:15418–15429. https://doi.org/10.1021/ja305453w
92. Onoda A, Fukumoto K, Arlt M, Bocola M, Schwaneberg U, Hayashi T (2012) A rhodium complex-linked beta-barrel protein as a hybrid biocatalyst for phenylacetylene polymerization. Chem Commun 48:9756–9758. https://doi.org/10.1039/c2cc35165j
93. Kinzel J, Sauer DF, Bocola M, Arlt M, Garakani TM, Thiel A, Beckerle K, Polen T, Okuda J, Schwaneberg U (2017) 2-Methyl-2,4-pentanediol (MPD) boosts as detergent-substitute the performance of ß-barrel hybrid catalyst for phenylacetylene polymerization. Beilstein J Org Chem 13:1498–1506. https://doi.org/10.3762/bjoc.13.148
94. Philippart F, Arlt M, Gotzen S, Tenne S-J, Bocola M, Chen H-H, Zhu L, Schwaneberg U, Okuda J (2013) A hybrid ring-opening metathesis polymerization catalyst based on an engineered variant of the β-barrel protein FhuA. Chem Eur J 19:13865–13871. https://doi.org/10.1002/chem.201301515

95. Garber SB, Kingsbury JS, Gray BL, Hoveyda AH (2000) Efficient and recyclable monomeric and dendritic Ru-based metathesis catalysts. J Am Chem Soc 122:8168–8179. https://doi.org/10.1021/ja001179g
96. Jordan JP, Grubbs RH (2007) Small-molecule N-heterocyclic-carbene-containing olefin-metathesis catalysts for use in water. Angew Chem Int Ed 46:5152–5155. https://doi.org/10.1002/anie.200701258
97. Sauer DF, Bocola M, Broglia C, Arlt M, Zhu L-L, Brocker M, Schwaneberg U, Okuda J (2015) Hybrid ruthenium ROMP catalysts based on an engineered variant of β-barrel protein FhuA ΔCVFtev: effect of spacer length. Chem Asian J 10:177–182. https://doi.org/10.1002/asia.201403005
98. Sauer DF, Himiyama T, Tachikawa K, Fukumoto K, Onoda A, Mizohata E, Inoue T, Bocola M, Schwaneberg U, Hayashi T, Okuda J (2015) A highly active biohybrid catalyst for olefin metathesis in water: impact of a hydrophobic cavity in a beta-barrel protein. ACS Catal 5:7519–7522. https://doi.org/10.1021/acscatal.5b01792
99. Grimm AR, Sauer DF, Davari MD, Zhu L, Bocola M, Kato S, Onoda A, Hayashi T, Okuda J, Schwaneberg U (2018) Cavity size engineering of a beta-barrel protein generates efficient biohybrid catalysts for olefin metathesis. ACS Catal 8:3358–3364. https://doi.org/10.1021/acscatal.7b03652
100. Ricca E, Brucher B, Schrittwieser JH (2011) Multi-enzymatic cascade reactions: overview and perspectives. Adv Synth Catal 353:2239–2262. https://doi.org/10.1002/adsc.201100256
101. O'Reilly E, Turner NJ (2015) Enzymatic cascades for the regio- and stereoselective synthesis of chiral amines. Perspect Sci 4:55–61. https://doi.org/10.1016/j.pisc.2014.12.009
102. Betanzos-Lara S, Liu Z, Habtemariam A, Pizarro AM, Qamar B, Sadler PJ (2012) Organometallic Ruthenium and Iridium transfer-hydrogenation catalysts using coenzyme NADH as a cofactor. Angew Chem Int Ed 51:3897–3900. https://doi.org/10.1002/anie.201108175
103. Wingstrand E, Laurell A, Fransson L, Hult K, Moberg C (2009) Minor enantiomer recycling: metal catalyst, organocatalyst and biocatalyst working in concert. Chem Eur J 15:12107–12113. https://doi.org/10.1002/chem.200901338
104. Simons C, Hanefeld U, Arends IWCE, Maschmeyer T, Sheldon RA (2006) Towards catalytic cascade reactions: asymmetric synthesis using combined chemo-enzymatic catalysts. Top Catal 40:35–44. https://doi.org/10.1007/s11244-006-0106-6
105. Wieczorek B, Träff A, Krumlinde P, Dijkstra HP, Egmond MR, van Koten G, Bäckvall J-E, Gebbink RJMK (2011) Covalent anchoring of a racemization catalyst to CALB-beads: towards dual immobilization of DKR catalysts. Tetrahedron Lett 52:1601–1604. https://doi.org/10.1016/j.tetlet.2011.01.106
106. Worsdorfer B, Woycechowsky KJ, Hilvert D (2011) Directed evolution of a protein container. Science 331:589–592. https://doi.org/10.1126/science.1199081
107. Engström K, Johnston EV, Verho O, Gustafson KPJ, Shakeri M, Tai C-W, Bäckvall J-E (2013) Co-immobilization of an enzyme and a metal into the compartments of mesoporous silica for cooperative tandem catalysis: an artificial metalloenzyme. Angew Chem Int Ed 52:14006–14010. https://doi.org/10.1002/anie.201306487
108. Köhler V, Wilson YM, Dürrenberger M, Ghislieri D, Churakova E, Quinto T, Knörr L, Häussinger D, Hollmann F, Turner NJ, Ward TR (2012) Synthetic cascades are enabled by combining biocatalysts with artificial metalloenzymes. Nat Chem 5:93–99. https://doi.org/10.1038/nchem.1498
109. Okamoto Y, Köhler V, Ward TR (2016) An NAD(P)H-dependent artificial transfer hydrogenase for multienzymatic cascades. J Am Chem Soc 138:5781–5784. https://doi.org/10.1021/jacs.6b02470
110. Morra S, Pordea A (2018) Biocatalyst–artificial metalloenzyme cascade based on alcohol dehydrogenase. Chem Sci 9:7447–7454. https://doi.org/10.1039/C8SC02371A

111. Jeschek M, Reuter R, Heinisch T, Trindler C, Klehr J, Panke S, Ward TR (2016) Directed evolution of artificial metalloenzymes for in vivo metathesis. Nature 537:661–665. https://doi.org/10.1038/nature19114
112. Vong K, Eda S, Kadota Y, Nasibullin I, Wakatake T, Yokoshima S, Shirasu K, Tanaka K (2019) An artificial metalloenzyme biosensor can detect ethylene gas in fruits and Arabidopsis leaves. Nat Commun 10:5746. https://doi.org/10.1038/s41467-019-13758-2
113. Eda S, Nasibullin I, Vong K, Kudo N, Yoshida M, Kurbangalieva A, Tanaka K (2019) Biocompatibility and therapeutic potential of glycosylated albumin artificial metalloenzymes. Nat Catal 2:780–792. https://doi.org/10.1038/s41929-019-0317-4
114. Grimm AR, Sauer DF, Polen T, Zhu L, Hayashi T, Okuda J, Schwaneberg U (2018) A whole cell E. coli display platform for artificial metalloenzymes: poly(phenylacetylene) production with a rhodium-nitrobindin metalloprotein. ACS Catal 8:2611–2614. https://doi.org/10.1021/acscatal.7b04369
115. Völker T, Dempwolff F, Graumann PL, Meggers E (2014) Progress towards bioorthogonal catalysis with organometallic compounds. Angew Chem Int Ed 53:10536–10540. https://doi.org/10.1002/anie.201404547
116. Cheng Y, Zong L, López-Andarias J, Bartolami E, Okamoto Y, Ward TR, Sakai N, Matile S (2019) Cell-penetrating dynamic-covalent benzopolysulfane networks. Angew Chem Int Ed 58:9522–9526. https://doi.org/10.1002/anie.201905003
117. Heinisch T, Schwizer F, Garabedian B, Csibra E, Jeschek M, Vallapurackal J, Pinheiro VB, Marlière P, Panke S, Ward TR (2018) *E. coli* surface display of streptavidin for directed evolution of an allylic deallylase. Chem Sci 9:5383–5388. https://doi.org/10.1039/C8SC00484F
118. Szponarski M, Schwizer F, Ward TR, Gademann K (2018) On-cell catalysis by surface engineering of live cells with an artificial metalloenzyme. Commun Chem 1:84. https://doi.org/10.1038/s42004-018-0087-y
119. Zhao J, Rebelein JG, Mallin H, Trindler C, Pellizzoni MM, Ward TR (2018) Genetic Engineering of an Artificial Metalloenzyme for Transfer Hydrogenation of a Self-Immolative Substrate in Escherichia coil's Periplasm. J Am Chem Soc 140:13171–13175. https://doi.org/10.1021/jacs.8b07189
120. Tsutsumi H, Katsuyama Y, Izumikawa M, Takagi M, Fujie M, Satoh N, Shin-ya K, Ohnishi Y (2018) Unprecedented cyclization catalyzed by a cytochrome P450 in benzastatin biosynthesis. J Am Chem Soc 140:6631–6639. https://doi.org/10.1021/jacs.8b02769
121. Breslow R, Gellman SH (1982) Tosylamidation of cyclohexane by a cytochrome P-450 model. J Chem Soc Chem Commun 1400–1401. https://doi.org/10.1039/c39820001400
122. Breslow R, Gellman SH (1983) Intramolecular nitrene carbon-hydrogen insertions mediated by transition-metal complexes as nitrogen analogs of cytochrome P-450 reactions. J Am Chem Soc 105:6728–6729. https://doi.org/10.1021/ja00360a039
123. Svastits EW, Dawson JH, Breslow R, Gellman SH (1985) Functionalized nitrogen atom transfer catalyzed by cytochrome P-450. J Am Chem Soc 107:6427–6428. https://doi.org/10.1021/ja00308a064
124. Mansuy D, Mahy J-P, Dureault A, Bedi G, Battioni P (1984) Iron- and manganese-porphyrin catalysed aziridination of alkenes by tosyl- and acyl-iminoiodobenzene. J Chem Soc Chem Commun 1161–1163. https://doi.org/10.1039/c39840001161
125. Singh R, Kolev JN, Sutera PA, Fasan R (2015) Enzymatic C(sp ^{3})-H amination: P450-catalyzed conversion of carbonazidates into oxazolidinones. ACS Catal 5:1685–1691. https://doi.org/10.1021/cs5018612
126. Singh R, Bordeaux M, Fasan R (2014) P450-catalyzed intramolecular sp 3 C–H amination with arylsulfonyl azide substrates. ACS Catal 4:546–552. https://doi.org/10.1021/cs400893n
127. Dydio P, Key HM, Hayashi H, Clark DS, Hartwig JF (2017) Chemoselective, enzymatic C–H bond amination catalyzed by a cytochrome P450 containing an Ir(Me)-PIX cofactor. J Am Chem Soc 139:1750–1753. https://doi.org/10.1021/jacs.6b11410

128. Arnold FH (2018) Directed evolution: bringing new chemistry to life. Angew Chem Int Ed 57:4143–4148. https://doi.org/10.1002/anie.201708408
129. Prier CK, Zhang RK, Buller AR, Brinkmann-Chen S, Arnold FH (2017) Enantioselective, intermolecular benzylic C–H amination catalysed by an engineered iron-haem enzyme. Nat Chem 9:629–634. https://doi.org/10.1038/nchem.2783
130. Brandenberg OF, Miller DC, Markel U, Ouald Chaib A, Arnold FH (2019) Engineering chemoselectivity in hemoprotein-catalyzed indole amidation. ACS Catal 9:8271–8275. https://doi.org/10.1021/acscatal.9b02508
131. Farwell CC, Zhang RK, McIntosh JA, Hyster TK, Arnold FH (2015) Enantioselective enzyme-catalyzed aziridination enabled by active-site evolution of a cytochrome P450. ACS Cent Sci 1:89–93. https://doi.org/10.1021/acscentsci.5b00056
132. Roelfes G (2019) LmrR: a privileged scaffold for artificial metalloenzymes. Acc Chem Res 52:545–556. https://doi.org/10.1021/acs.accounts.9b00004
133. Bos J, Browne WR, Driessen AJM, Roelfes G (2015) Supramolecular assembly of artificial metalloenzymes based on the dimeric protein lmrr as promiscuous scaffold. J Am Chem Soc 137:9796–9799. https://doi.org/10.1021/jacs.5b05790
134. Villarino L, Splan KE, Reddem E, Alonso-Cotchico L, Gutiérrez de Souza C, Lledós A, Maréchal J-D, Thunnissen A-MWH, Roelfes G (2018) An artificial heme enzyme for cyclopropanation reactions. Angew Chem Int Ed 57:7785–7789. https://doi.org/10.1002/anie.201802946
135. Zhao J, Bachmann DG, Lenz M, Gillingham DG, Ward TR (2018) An artificial metalloenzyme for carbene transfer based on a biotinylated dirhodium anchored within streptavidin. Catal Sci Technol 8:2294–2298. https://doi.org/10.1039/C8CY00646F
136. Coelho PS, Brustad EM, Kannan A, Arnold FH (2013) Olefin cyclopropanation via carbene transfer catalyzed by engineered cytochrome P450 enzymes. Science 339:307–310. https://doi.org/10.1126/science.1231434
137. Vargas DA, Tinoco A, Tyagi V, Fasan R (2018) Myoglobin-catalyzed C–H functionalization of unprotected indoles. Angew Chem Int Ed 57:9911–9915. https://doi.org/10.1002/anie.201804779
138. Tinoco A, Steck V, Tyagi V, Fasan R (2017) Highly diastereo- and enantioselective synthesis of trifluoromethyl-substituted cyclopropanes via myoglobin-catalyzed transfer of trifluoromethylcarbene. J Am Chem Soc 139:5293–5296. https://doi.org/10.1021/jacs.7b00768
139. Tinoco A, Wei Y, Bacik J-P, Carminati DM, Moore EJ, Ando N, Zhang Y, Fasan R (2019) Origin of high stereocontrol in olefin cyclopropanation catalyzed by an engineered carbene transferase. ACS Catal 9:1514–1524. https://doi.org/10.1021/acscatal.8b04073
140. Reynolds EW, McHenry MW, Cannac F, Gober JG, Snow CD, Brustad EM (2016) An evolved orthogonal enzyme/cofactor pair. J Am Chem Soc 138:12451–12458. https://doi.org/10.1021/jacs.6b05847
141. Reynolds EW, Schwochert TD, McHenry MW, Watters JW, Brustad EM (2017) Orthogonal expression of an artificial metalloenzyme for abiotic catalysis. ChemBioChem 18:2380–2384. https://doi.org/10.1002/cbic.201700397
142. Oohora K, Onoda A, Hayashi T (2019) Hemoproteins reconstituted with artificial metal complexes as biohybrid catalysts. Acc Chem Res 52:945–954. https://doi.org/10.1021/acs.accounts.8b00676
143. Oohora K, Meichin H, Zhao L, Wolf MW, Nakayama A, Hasegawa J, Lehnert N, Hayashi T (2017) Catalytic cyclopropanation by myoglobin reconstituted with iron porphycene: acceleration of catalysis due to rapid formation of the carbene species. J Am Chem Soc 139:17265–17268. https://doi.org/10.1021/jacs.7b10154
144. Key HM, Dydio P, Clark DS, Hartwig JF (2016) Abiological catalysis by artificial haem proteins containing noble metals in place of iron. Nature 534:534–537. https://doi.org/10.1038/nature17968

145. Dydio P, Key HM, Nazarenko A, Rha JY-E, Seyedkazemi V, Clark DS, Hartwig JF (2016) An artificial metalloenzyme with the kinetics of native enzymes. Science 354:102–106. https://doi.org/10.1126/science.aah4427
146. Natoli SN, Hartwig JF (2019) Noble–metal substitution in hemoproteins: an emerging strategy for abiological catalysis. Acc Chem Res 52:326–335. https://doi.org/10.1021/acs.accounts.8b00586
147. Zhang J, Huang X, Zhang RK, Arnold FH (2019) Enantiodivergent α-amino C–H fluoroalkylation catalyzed by engineered cytochrome P450s. J Am Chem Soc 141:9798–9802. https://doi.org/10.1021/jacs.9b04344
148. Otto S, Bertoncin F, Engberts JBFN (1996) Lewis Acid Catalysis of a Diels − Alder Reaction in Water. J Am Chem Soc 118:7702–7707. https://doi.org/10.1021/ja960318k
149. Otto S, Engberts JBFN (1999) A systematic study of ligand effects on a lewis-acid-catalyzed Diels–Alder reaction in water: water-enhanced enantioselectivity. J Am Chem Soc 121:6798–6806. https://doi.org/10.1021/ja984273u
150. Mubofu EB, Engberts JBFN (2004) Specific acid catalysis and Lewis acid catalysis of Diels–Alder reactions in aqueous media. J Phys Org Chem 17:180–186. https://doi.org/10.1002/poc.711
151. Reetz MT, Jiao N (2006) Copper-phthalocyanine conjugates of serum albumins as enantioselective catalysts in Diels–Alder reactions. Angew Chem Int Ed 45:2416–2419. https://doi.org/10.1002/anie.200504561
152. Reetz MT (2012) Artificial Metalloenzymes as Catalysts in Stereoselective Diels-Alder Reactions. Chem Rec 12:391–406. https://doi.org/10.1002/tcr.201100043
153. Roelfes G, Boersma AJ, Feringa BL (2006) Highly enantioselective DNA-based catalysis. Chem Commun 635–637. https://doi.org/10.1039/b516552k
154. Filice M, Romero O, Gutiérrez-Fernández J, de las Rivas B, Hermoso JA, Palomo JM (2015) Synthesis of a heterogeneous artificial metallolipase with chimeric catalytic activity. Chem Commun 51:9324–9327. https://doi.org/10.1039/C5CC02450A
155. Ghattas W, Cotchico-Alonso L, Maréchal J-D, Urvoas A, Rousseau M, Mahy J-P, Ricoux R (2016) Artificial metalloenzymes with the neocarzinostatin scaffold: toward a biocatalyst for the Diels-Alder reaction. ChemBioChem 17:433–440. https://doi.org/10.1002/cbic.201500445
156. Talbi B, Haquette P, Martel A, de Montigny F, Fosse C, Cordier S, Roisnel T, Jaouen G, Salmain M (2010) (η6-Arene) ruthenium(II) complexes and metallo-papain hybrid as Lewis acid catalysts of Diels-Alder reaction in water. Dalton Trans 39:5605–5607. https://doi.org/10.1039/c001630f
157. Di Meo T, Ghattas W, Herrero C, Velours C, Minard P, Mahy J-P J-P, Ricoux R, Urvoas A (2017) αRep A3: a versatile artificial scaffold for metalloenzyme design. Chem Eur J 23:10156–10166. https://doi.org/10.1002/chem.201701518
158. Di Meo T, Kariyawasam K, Ghattas W, Valerio-Lepiniec M, Sciortino G, Maréchal J-D, Minard P, Mahy J-P, Urvoas A, Ricoux R (2019) functionalized artificial bidomain proteins based on an α-solenoid protein repeat scaffold: a new class of artificial Diels-Alderases. ACS Omega 4:4437–4447. https://doi.org/10.1021/acsomega.8b03448
159. Himiyama T, Taniguchi N, Kato S, Onoda A, Hayashi T (2017) A pyrene-linked cavity within a β-barrel protein promotes an asymmetric Diels-Alder reaction. Angew Chem Int Ed 56:13618–13622. https://doi.org/10.1002/anie.201704524
160. Deuss PJ, Popa G, Slawin AMZ, Laan W, Kamer PCJ (2013) Artificial copper enzymes for asymmetric Diels-Alder reactions. Chem Cat Chem 5:1184–1191. https://doi.org/10.1002/cctc.201200671
161. Bos J, Fusetti F, Driessen AJM, Roelfes G (2012) Enantioselective artificial metalloenzymes by creation of a novel active site at the protein dimer interface. Angew Chem Int Ed 51:7472–7475. https://doi.org/10.1002/anie.201202070

162. Podtetenieff J, Taglieber A, Bill E, Reijerse EJ, Reetz MT (2010) An artificial metalloenzyme: creation of a designed copper binding site in a thermostable protein. Angew Chem Int Ed 49:5151–5155. https://doi.org/10.1002/anie.201002106
163. Ghattas W, Dubosclard V, Tachon S, Beaumet M, Guillot R, Réglier M, Simaan AJ, Mahy J-P (2019) Cu^{II} -Containing 1-aminocyclopropane carboxylic acid oxidase is an efficient stereospecific Diels–Alderase. Angew Chem Int Ed 58:14605–14609. https://doi.org/10.1002/anie.201909407
164. Ghattas W, Dubosclard V, Wick A, Bendelac A, Guillot R, Ricoux R, Mahy J-P (2018) Receptor-based artificial metalloenzymes on living human cells. J Am Chem Soc 140:8756–8762. https://doi.org/10.1021/jacs.8b04326

New Phototrophic Factories for Resource Recovery

Joana C. Fradinho, Virgínia C. F. Carvalho, and Maria A. M. Reis

Abstract

Human activities are threatening the environment. Pollutants are spread across the ecosystems damaging the biological diversity and human health. New sustainable practices must be brought forward and phototrophic organisms may contribute to overcome such complex challenge. Enclosed on these living organisms are a multitude of enzymes and metabolic pathways that act as a unit providing solutions to each environmental scenario. Phototrophic systems have been explored for their capability of recovering carbon, nitrogen, and phosphorous from the most diverse wastewater streams enabling water reutilization and the production of value-added products. And all simply using sunlight as their energy source. This chapter will provide an overview of the diversity of phototrophic organisms and elucidate on current phototrophic technologies that aim the prevention and mitigation of environmental pollution, acting on wastewater treatment and resource recovery. Two case studies will be detailed, one regarding phosphorous recovery with a photo-enhanced biological phosphorus removal system, and other regarding carbon recovery in the form of polyhydroxyalkanoates, a biodegradable polymer produced in purple phototrophic bacteria ponds. These innovative photosynthetic factories address society's request for sustainable practices where waste is no longer the end of a production line, but instead, a fundamental and integrated element of the circular economy.

J. C. Fradinho (✉) · V. C. F. Carvalho · M. A. M. Reis
REQUIMTE, UCIBIO, NOVA School of Science and Technology, Campus de Caparica, Caparica, Portugal
e-mail: j.fradinho@fct.unl.pt

J. J. G. Moura et al. (eds.), *Enzymes for Solving Humankind's Problems*,
https://doi.org/10.1007/978-3-030-58315-6_13

Keywords

Wastewater treatment · Resource recovery · Microalgae · Phosphate accumulating organisms (PAOs) · Phosphorous recovery · Anoxygenic phototrophic bacteria (APB) · Purple phototrophic bacteria (PPB) · Polyhydroxyalkanoates · Purple phototrophic bacteria ponds

1 Introduction

In the last decades, the world has been facing several environmental problems created by pollution, increasing urbanization and resources over-exploitation. Pollutants have spread throughout nature as mixtures of organic and inorganic compounds originated from industrial activity (e.g., petrochemical, dye, manufacturing, paper industry), agriculture and commuting (e.g., traffic emissions) [1]. Water and soils are under constant pressure from accumulation of recalcitrant compounds, and CO_2 concentrations in the atmosphere have reached alarming values, with more than a 30% rise in comparison to pre-industrial levels [2]. The existence of such high levels of hazard and polluting components in the environment is affecting human and animals' health, as well as damaging ecosystems and contributing to global warming and climate change [3, 4].

Since it is increasingly urgent to control pollution, prevent water streams contamination, and recover soil fertility, it is fundamental to develop efficient, clean, and environmentally sound technologies and adopt the use of sustainable alternatives to conventional everyday products. Although these practices may seem to conflict with economic development, research and industries are focusing on developing new, low-cost, and eco-friendly technologies that can couple environmental protection with economic growth. With both physical/chemical and biological approaches at hand, biological strategies have been the subject of great development, making use of living organisms (microorganisms and plants), that can be environmentally friendly and can efficiently promote the complete conversion of toxic molecules into safe end products [5]. Also, biological systems can be applied to processes for which efficient chemical solutions are yet to be developed. Such wide application of biological systems to different environmental scenarios is founded on the richness of metabolic pathways that are present in living organisms which makes them natural catalysts that can play an important role in solving most environmental issues [5–7]. Enzymes are the main effectors of the metabolic pathways being able to detoxify polluting substances and transform them into safer and innocuous products [1]. These biomolecules can perform very specific chemical transformations, making them attractive not only for environmental applications but also for industrial processes. Either intracellularly (inside of their originating cells) or extracellularly (in the presence or absence of their originating cells), free or immobilized, enzymes have been used as green alternatives to complex chemicals

for several scientific and industrial applications [1]. Moreover, by reducing the need for virgin raw materials and waste disposal, they have been the key for sustainable industrial development along the fields of raw material processing like leather, pulp, and paper production, up to more complex fields of detergent, textile, cosmetics, and pharmaceuticals production [8, 9]. For the particular case of enzyme utilization in environmental applications, this chapter will provide an overview of biological systems that make use of photosynthetic microorganisms and their unique enzyme-mediated metabolism for the treatment of wastewater, nutrient recovery, and wastes valorization. A special focus will be given to the case studies of the photo-enhanced biological phosphorus removal (photo–EBPR) and the phototrophic purple bacteria pond (PPBPond), which are, respectively, two innovative technologies for phosphorous recovery and polyhydroxyalkanoates production in illuminated open systems.

2 Diversity of Phototrophic Organisms: Overview

Phototrophy is a process that consists in converting light energy into a usable form of chemical energy and it can be used by a great diversity of organisms, both eukaryotic and prokaryotic. While all chlorophyll and/or bacteriochlorophyll containing phototrophs can synthetize ATP from light, one of the most differentiating features between them regards their electron source and capability of producing oxygen [10]. Microalgae and cyanobacteria are able to use water as the electron source and thus, are capable of performing an oxygenic photosynthesis (i.e., oxygen is produced) in a process that occurs in two distinct stages. The first stage includes light-dependent reactions and takes place in specialized structures (chloroplasts) where light energy is absorbed, driving the synthesis of ATP and NADPH in a process coupled to the formation of oxygen from water (Fig. 1).

Photosystem II (PS II) produces a very strong oxidant ($\sim$+1250 mV) that is capable of oxidizing water to molecular oxygen (+810 mV) [13]. Then, the electrons proceed via cytochrome *bf* complex to $NADP^+$ in photosystem I (PS I) producing the reductant NADPH [14]. During this linear electron transport, a proton-motive force is created and used for ATP production. The second stage of oxygenic photosynthesis includes the dark reactions (independent of light) where the produced ATP and NADPH are used for CO_2 fixation into carbohydrates through the Calvin–Benson–Bassham (CBB) cycle [11].

While microalgae and cyanobacteria contain two reaction centers (PS II and PS I) that operate in series, anoxygenic (non-oxygen evolving) phototrophic bacteria (APB) contain only one reaction center (Fig. 2).

The reaction center can either be of Type I where light drives the reduction of a ferredoxin protein or a Type II reaction center (RC II) where the electrons are donated to quinones [13]. Heliobacteria, Chlorobi, and Chloroacidobacteria employ Type I reaction centers, while Chloroflexi, Gemmatimonadetes, and phototrophic members of Proteobacteria employ Type II reaction centers [10, 14]. APB reaction

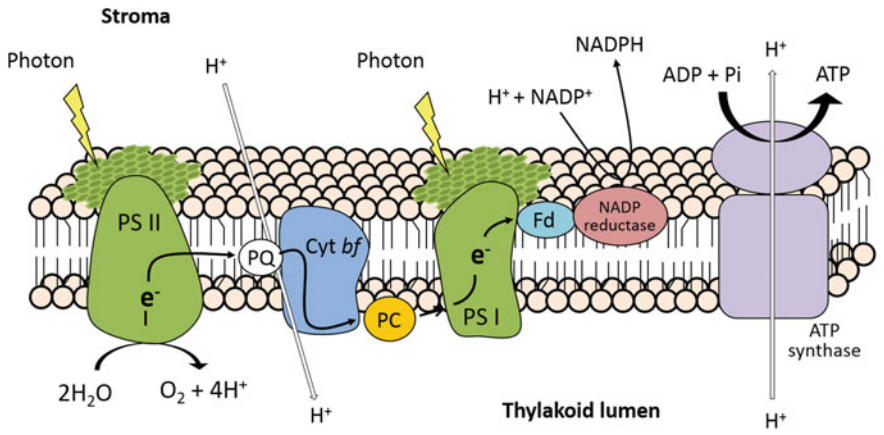

Fig. 1 Light reactions of photosynthesis occurring in the chloroplast of microalgae and cyanobacteria. Light energy absorbed at photosystem II (PS II) is used for water splitting, generating oxygen, protons, and electrons. These electrons flow through a series of proteins, and their energy is used to pump protons to the thylakoid lumen. In photosystem I (PS I), light energy is absorbed, increasing the energy state of the electrons which are then used to produce NADPH from $NADP^+$. The proton gradient created during the non-cyclic electron transport is used by ATP synthase to generate ATP. For further details, please refer to [11, 12]. PQ—Plastoquinones, Cyt *bf* —Cytochrome *bf* complex, PC—Plastocyanin, and Fd—Ferrodoxin.

centers have redox potentials that range from + 300 to + 500 mV, being capable of oxidizing only lower potential (<+100 mV) electron donors [13]. Water cannot be used as an electron donor and thus APB do not evolve oxygen. In the particular case of APB with a Type II RC (e.g., Chloroflexi and the purple phototrophic bacteria of the phylum Proteobacteria), a cyclic electron transport is operated to generate ATP and as such, no NADPH is directly synthesized (Fig. 2). Instead, a reverse electron transport is used to regenerate NAD(P)H through the oxidation of electron donors with higher redox potential than $NAD(P)H/NAD(P)^+$, like hydrogen, hydrogen sulfide, and organic molecules [10, 14]. The ATP and NAD(P)H generated from light-induced electron transport can then be used to assimilate carbon through diverse carbon metabolic pathways ranging from autotrophic CO_2 assimilation (e.g., CBB cycle, reverse Krebs cycle, and 3-hydroxy-propionate bicycle) to the heterotrophic uptake of external organic molecules [11].

- **Pigments**

  To increase the amount of light energy harvested by the cells, the reaction centers of microalgae/cyanobacteria and APB are assisted by light-harvesting antenna complexes that capture light and transfer the excitation energy to the photochemical reaction centers [15]. The major photoactive pigments that can be found in the antenna complexes are chlorophylls (Chls) or bacteriochlorophylls (BChls) and carotenoids, which ensure photosynthesis function over a wide range of incident light intensity from near-UV to visible and infrared [16].

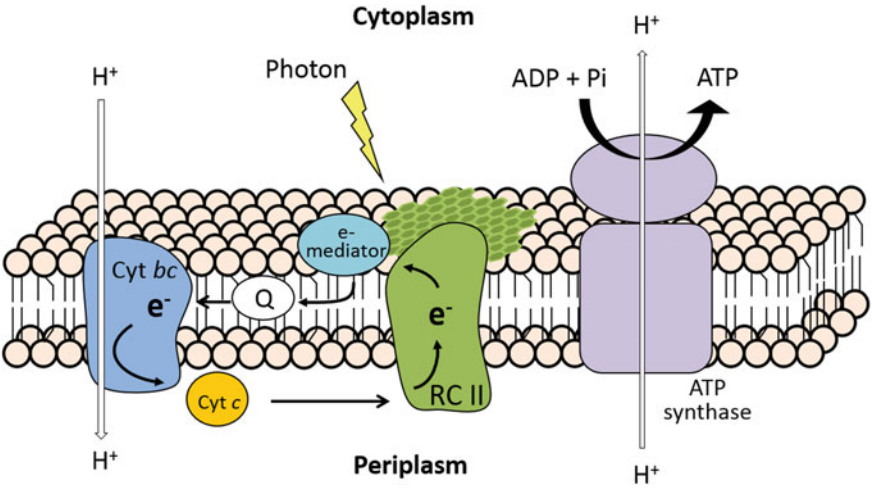

Fig. 2 Light reactions of phototrophy occurring in the chlorosomes of Chloroflexi and in membrane systems of purple Proteobacteria. In these organisms, phototrophy occurs in a cyclic electron flow pathway. Light energy absorbed at RC II increases the energy state of electrons which then flow through a series of proteins and their energy is used to pump protons to the periplasm. The electrons return to RC II, carried by the soluble cytochrome *c*. The proton gradient created during the cyclic electron flow is used by ATP synthase to generate ATP. For further details, please refer to [11, 12]. Q—Quinone, Cyt *bc*—Cytochrome *bc*—complex, Cyt *c*—Cytochrome *c*.

Chl *a* can be found in almost all microalgae and cyanobacteria, and it presents two intense absorption maxima at the edges of the visible spectrum (≈430 and ≈680 nm). This results in a green absorption gap of ≈250 nm that can be further reduced to the spectral region between 500 and 600 nm if the Chl *b* pigment is also expressed by the oxygenic organism (Chl *b* absorption maxima at λ_{max}≈460 and λ_{max} ≈650 nm) [17].

In APB, the major pigments are known as Bchls and thus far, six have been found in nature: Bchl *a*, *b*, *c*, *d*, *e* and *g*. Bchl *c*, *d*, and *e* have the particularity of being organized into large light-harvesting organelles known as chlorosomes that enable phototrophy in very low-light environments [10, 16]. The six pigments are distributed among the diverse APB, and while Heliobacter only contain Bchl *g*, purple phototrophic bacteria (PPB) of the phylum Proteobacteria contain BChls *a*, *b*, Chloroflexi contain BChls *a, c* or *d*, and Chlorobi contain BChls *a, c*, *d* or *e* [17]. Unlike Chls that only absorb in the visible range, the absorption maxima of Bchls occurs in the far-red light with BChls *c*, *d* and *e* showing absorptions in the range of 700–750 nm and BChls *a*, *b* and *g* absorbing even farther in the infrared light 800–1020 nm. The latest pigments also present a blue-shifted absorption maxima in the near-UV (< 400 nm). As such, organisms containing BChls *a*, *b* and *g* can extend the usable spectrum beyond both directions of the visible

range [16]. The possibility of APB to use alternative wavelength ranges can be an important feature when competing for light energy with the visible light absorbing microalgae and cyanobacteria.

Carotenoids are a group of pigments commonly present in microalgae/cyanobacteria and APB which have the important function of harvesting light (transference of resonant energy to Chls/Bchls) [18] and protecting the photosynthetic apparatus from light and oxygen damage. In general, most carotenoids have an absorption range around 400–550 nm, in the middle of the visible light spectrum [12].

- **Ecological distribution and applications**

The metabolic richness, heterogeneity, and ability of phototrophic organisms to tolerate extreme conditions allow them to adapt to a great diversity of environments. The type of phototrophic organisms that can be found in a specific area is greatly influenced by the environmental conditions like temperature, light intensity, salinity, pH, presence of oxygen, CO_2, sulfide, organic compounds, and nutrients [19, 20]. In particular, microgradients of light, sulfide, and oxygen strongly affect the organism's distribution along the photic zones. Phototrophs that harbor oxygen-sensitive enzymes, like the strict anaerobic Chlorobi, can be found in sulfidic environments, deeply in the water columns or mats. To overcome the lower light availability, they use specialized light-harvesting structures, the chlorosomes [10, 21]. As lithotrophs that can use H_2S as electron donor, most studies have reported the utilization of Chlorobi organisms (e.g., *Chlorobium limicola*) for sulfide removal and sulfur recovery from biogas and wastewater streams [22, 23].

In the case of aerobic APB and oxygen-tolerant PPB, these can be found at shallow depths of water bodies, sediments, moist soils, and paddy fields, in oxic—anoxic interfaces [24]. With their highly diverse and flexible metabolism, PPB are capable of growing under phototrophic conditions in the light and under chemotrophic conditions in the dark, either autotrophically (fixating CO_2) or heterotrophically, using oxygen or inorganic molecules as terminal electron acceptors in respiratory processes [24]. Though they have so many possible metabolic combinations, they still have a preferred mode of growth. Consequently, these organisms can be divided into two groups: the purple sulfur bacteria (γ-proteobacteria) and the purple non-sulfur bacteria, which are mostly α-proteobacteria, with the exception of one genus that is β-proteobacteria [12]. Purple sulfur bacteria (PSB) typically grow phototrophically under anoxic environments using hydrogen, sulfide, and sulfur as electron donors, producing sulfur granules that can be deposited internally or externally, depending on the organism family [25]. As for the purple non-sulfur bacteria (PNSB), these organisms also typically grow under light anoxic conditions, but they present a much more highly diverse and flexible metabolism in relation to PSB. In fact, their preferred mode of growth is photoorganoheterotrophy, meaning they use organic molecules both as electron donors and carbon source [24]. Nevertheless, many species can also use hydrogen and reduced sulfur compounds as photosynthetic electron donors. Besides phototrophy, some PNSB can grow equally

well in the dark, in aerobic conditions or anaerobically, using fermentative processes for energy production. In this latter case, reduced organic compounds are produced (e.g., succinate, lactate, acetate, propionate, formate) as well as CO_2 and H_2 [24, 26]. The versatility of PPB is reflected on the high number of applications that use them for wastewater treatment, and production of high value-added compounds (e.g., Polyhydroxyalkanoates) has detailed in further sections.

Finally, microalgae and cyanobacteria are oxygenic primary producers that generally dominate the top layers of stratified sediments [20]. In general, the preferred mode of growth of microalgae/cyanobacteria is photoautotrophy, but some species are also capable of photoheterotrophy, taking up simple organic molecules like glucose, acetate, glycerol, and ethanol as carbon source [27, 28]. This feature, combined with their oxygen producing ability, capacitates microalgae for wastewater treatment in bacterial–microalgae consortia [29, 30] and in particular, for phosphorous recovery in consortium with phosphate accumulating organisms (PAOs), as recently proposed in the photo-EBPR process [31, 32]. Additionally, microalgae and cyanobacteria have also been thoroughly studied along the years for their use as fertilizers, source of food and animal feed [29, 33], and capacity to produce biofuels and commercially attractive molecules, like antioxidants and carotenoids [34].

Overall, the clear distinction between the metabolism of microalgae/cyanobacteria and APB and their different ecological distributions, strongly impacts the metabolic capacity of these organisms and from a technical point of view, also their applications to different environmental situations. The high diversity of phototrophic organisms offers a multitude of metabolic solutions that can be assembled in photosynthetic factories for robust responses to each demanding scenario.

3 Wastewater Treatment and Resource Recovery

The worldwide increase of population and the lifestyle improvement is leading to an escalating generation of solid wastes and polluted liquid streams, namely wastewaters. To guarantee sanitation and avoid pollutant discharges in the environment, it is fundamental to implement wastewater collection and reliable treatment systems. The technologies used in wastewater treatment can be complex and expensive but along the years, new, low-cost, more environmentally responsible and suitable wastewater treatment technologies were continuously proposed to fit the requirements of environmental, economic, and social sustainability [35]. The sustainability of wastewater treatment has to be approached within the larger frame of water resource management, where water must be preserved and used more efficiently. Taking into account the current global water scarcity and the expensive operation and maintenance cost of wastewater treatment, it is crucial to move wastewater treatment from being primarily a

sanitation technology toward a bioproduct recovery industry and a recycled water supplier. This is a paradigm shift from the general conception of wastewater treatment, where carbon and reactive nitrogen are removed from water to the atmosphere as CO_2 and N_2, into the more recent concept of resource recovery [26, 36]. Biogas, biopolymers, irrigation water, and biofertilizers are examples of possible products that can be obtained from converting Waste Water Treatment Plants (WWTP) into the new "water factories" [37]. Nonetheless, the sustainability of wastewater treatment still continues to strongly depend on the adequate selection of a particular treatment methodology, determined through multicriteria decision-making techniques that take into consideration economic, socio-cultural, and environmental objectives as a whole [38]. With a multitude of different factors impacting on the technology selection, the implementation of phototrophic treatment processes has risen since it targets a decrease of capital, operational and maintenance costs, a simplification of the treatment process, a high removal efficiency of nutrients and organic pollutants, and associated high carbon and nutrient capture [27, 39, 40]. However, it is also clear that as a light dependent technology, local climate (sunlight availability) and land requirement (sufficient space to accommodate the facilities) will naturally impact the global application of the process. Nevertheless, the last decade has witnessed an increasing number of studies proposing phototrophic systems for wastewater treatment and resource recovery using microalgae–bacterial-based processes [29, 41, 42], or also, the more recently developed anoxygenic purple phototrophic bacteria (PPB)-based treatment [26, 43, 44]. These systems exhibit different treatment efficiencies and should be used according to the wastewater treatment requirement. All together, these new technologies either applied to domestic, industrial, or livestock wastewaters, from laboratory up to full-scale treatment, are contributing to define local and global water management strategies that assure proper sanitation to populations while preserving the environment.

3.1 Microalgae–Bacterial Processes

Wastewaters are polluted liquid streams which result from domestic, agricultural, and industrial activities. Its composition may contain variable concentrations of organics and nutrients, such as nitrogen and phosphorous, as well as pollutants like xenobiotics, heavy metals and microplastics [29, 42]. Conventional wastewater treatment usually employs aerobic activated sludge, which requires intensive aeration (accounts for $\sim$50% of the total energy consumption) and presents low-carbon capture efficiency with the organics being partially dissipated to the atmosphere as CO_2 [27, 44]. The combination of microalgae and heterotrophic bacteria in microalgae–bacterial processes is a cost effective and sustainable alternative that can overcome activated sludge constrains. Microalgae provide natural and free oxygenation to the heterotrophic bacteria which in turn produce CO_2 that is used for microalgae photosynthesis, leading to an

overall reduction of CO_2 emissions from organic matter oxidation [27]. In addition, microalgae can also directly uptake or transform water contaminants, efficiently removing large amounts of nitrogen and phosphorus and some organics, through chemoheterotrophic and/or mixotrophic assimilation [42, 45]. The biomass resultant from this synergistic process can be recovered and directed to different applications (e.g., biofuel production, fertilizers, and animal feed), depending on the source/type of treated wastewater and on national regulations for the reuse of the biomass [42].

The development of a microalgae–bacterial consortia can occur naturally through wastewater-borne microorganisms or can be artificially created through the inoculation of selected species to address particular wastewater treatment requirements [29]. Overall, the combination of microorganisms with different metabolic capacities results in robust biological systems that remove a multitude of different compounds with increased removal efficiencies while being able to respond to environmental and nutrient loads fluctuations [29, 42].

Wastewater treatment with microalgae–bacteria consortia can occur in facilities with different configurations, mostly using open systems, either employing suspended or immobilized methods. The operation of closed systems for large wastewater treatment is not a current practice due to the high investments and maintenance costs of photo-bioreactors [30, 42], while open systems are relatively cheap to build, can be easily scaled-up and operated. Among the open systems, the most used are the waste stabilization ponds (WSP) and open raceways ponds (ORP) [46]. WSP are indicated for wastewater treatment in small communities where land is inexpensive, offering effective treatment in terms of organic carbon and pathogen removal. Wastewater is treated in a combination of natural and physical processes without employing mixing or aeration systems which results in very low operation costs [47]. To compensate the slow removal of pollutants, WSP are typically operated with high hydraulic retention times (HRT) of 10–40 days [27]. ORP are alternative systems which are operated with shallow depths (0.15–0.3 m) and the culture is mixed and circulated around the raceway track by paddlewheels [30]. This increases removal efficiencies and as such, lower HRT can be applied (3–10 days) [27, 42]. Such ponds, commonly referred as high rate algae pond (HRAP), have been successfully implemented in several locations with demo-scale installations treating different types of wastewaters [48]. However, the short HRT of HRAP may occasionally limit the nitrogen removal from the wastewaters via nitrification/denitrification processes and the poor sedimentation capacity of the consortia can result in a total solid concentration in the effluent that does not fulfill the discharge limits into water bodies [45]. In this last case, promoting the selection of self-aggregating consortia or implementing immobilization methods that entrap the microorganisms in polymeric matrixes or support their attachment to surfaces, creating a biofilm, may be possible solutions [29, 42].

The relevance of microalgae–bacterial processes for wastewater treatment and resource recovery is reflected on the numerous technologies that are continuously proposed every year. The reduction of energy consumption and the decrease of CO_2 emissions while maintaining high removal efficiencies of pollutants are the most attractive features, but further technology development is required, especially targeting the reduction of land requirements and validating the proposed processes at larger scales for different types of wastewater.

3.2 Purple Phototrophic Bacteria Processes

Phototrophic wastewater treatment technologies have been proposed as means of decreasing operational costs (e.g., energy) and promoting higher carbon and nutrient recovery. As mentioned in Sect. 3.1, microalgae–bacteria consortia promote an overall reduction of CO_2 emissions that originate from organic matter oxidation due to CO_2 fixation by microalgae. However, reactive nitrogen species may still be lost to the atmosphere. Indeed, in aerobic environments, such as the ones found in conventional activated sludge and microalgae–bacterial systems, ammonia can be removed by aerobic nitrification, and if anoxia occurs, nitrites/nitrates can be further denitrified and removed from the liquid as gaseous nitrogen species, such as N_2O (greenhouse gas) and N_2 [36, 49]. Anoxygenic PPB-based processes were proposed for wastewater treatment in illuminated anaerobic environments to promote high removal and recovery of carbon, nitrogen, and phosphorous trough assimilative and accumulative processes [40, 43, 50]. These systems have seen an increased development in the last decade, exploring the unique features of PPB. PPB are well adapted for photoheterotrophy, being capable of direct treatment of high organic load wastewater [40]. The diversified metabolism of PPB, with some organisms like *Rhodobacter* spp. and *Rhodopseudomonas* spp. being reported as capable of degrading/remediating hazardous compounds, allows the employment of PPB systems for toxic wastewater treatment containing pharmaceuticals [51], emerging pollutants [52], heavy metals, oils or dyes [44, 53]. On the other hand, treatment of non-toxic wastewaters allows the extraction of high value-added compounds from the biomass, such as pigments, coenzyme Q-10, polyhydroxyalkanoates [40, 54, 55], or the whole biomass utilization as a protein rich food additive for animal feed [56]. As in other phototrophic technologies, the recovery of energy or high valuable compounds along with wastewater treatment is fundamental for the economic feasibility of PPB processes and their implementation at full scale. Currently, PPB technologies are still in an early stage of development with the first studies occurring in outdoor demo facilities [57]. New technology improvements are expected during the next years.

4 Nutrient Recovery: Phosphorous and Nitrogen

One of the several challenges faced during wastewater treatment is to comply with the discharge limits of phosphorus and nitrogen containing species, namely phosphate, ammonia, nitrites, and nitrates. If from one side discharging effluents with high amount of nitrogen and phosphorous to natural water courses will cause detrimental environmental problems, as eutrophication, from the other side, phosphorous sources are becoming depleted [58]. The increasing need of phosphorous fertilizers in agriculture to support the food demand of a growing population makes phosphorous a vital element and its recovery from waste streams, imperative [58, 59].

Nutrient removal and recovery from wastewater treatment can be achieved using combinations of physical, chemical, and/or biological processes, as extensively reviewed by [36, 60]. The process choice is naturally dependent on the characteristics of the wastewater, but typically, nutrient recovery is performed during secondary and tertiary treatment, with this latest stage, being used to polish nutrient concentrations down to the regulatory standards [61]. Chemical processes can occur through the addition of, e.g., iron to promote nitrates denitrification to ammonia, or magnesium, which co-precipitates with phosphates and ammonia producing struvite, a mineral fertilizer. It must be considered however the cost of the added chemicals and possible water contamination by side-reaction products or the chemical itself, if added in excess [60, 62]. Physical processes, such as adsorption or membrane filtration, do not require chemicals addition and a wide range of commercial products is available for effective nutrient recovery. However, rapid material saturation and degradation due to poor mechanical stability can lead to high investments and maintenance costs [60, 62].

Biological processes have long been studied and widely applied for wastewater treatment due to their simple and economical operation with efficient removal of biodegradable mater and nutrients [37, 60]. The biological nutrient removal occurs in a combination of dissipative and/or assimilative processes. In conventional biological treatment, ammonia removal is accomplished through assimilation into the biomass, and through dissipation in nitrification/denitrification processes (which occur in conventional activated sludge and microalgae-bacterial systems) or deammonification (in anammox systems) [30, 36]. In the dissipative cases, reactive nitrogen is removed from the liquid through conversion into gaseous nitrogen species, such as N_2O and N_2 [36]. Hence, the only recovered nitrogen is the fraction that becomes assimilated into the biomass, which can then be directed to further downstream applications [30, 36, 37, 61]. Increasing nitrogen recovery is one of the current challenges in WWTP, being required further technological developments to minimize nitrogen losses to the atmosphere.

In the case of phosphorous, its biological removal from wastewaters occurs mainly through assimilation into the biomass and internal accumulation as polyphosphate [58]. When polyphosphate (Poly-P) storage occurs without a previous phosphorous starvation, it is called as luxury uptake [47] and this feature is

transversal to eukaryotic and prokaryotic organisms, including phototrophs (e.g., microalgae, purple bacteria) and heterotrophs, like the well-studied polyphosphate accumulating organisms (PAO) [47, 58]. Enhanced biological phosphorus removal (EBPR) is the most common process used in conventional WWTP to remove and recover phosphorus from wastewaters. The process relies on PAOs that take up phosphate in excess of their requirements, under sequential anaerobic and aerobic periods [63]. In the anaerobic period, PAOs are able to hydrolyze intracellularly stored Poly-P and glycogen, producing energy and reducing power to take up volatile fatty acids from the wastewater and converting them into intracellular polyhydroxyalkanoates (PHAs). In the aerobic period, PAOs oxidize the PHA, obtaining energy for growth, and to take up phosphorous, replenishing glycogen and Poly-P pools. The amount of phosphorus taken up aerobically exceeds the phosphorus released anaerobically, resulting in a net P removal from wastewater that becomes concentrated in the sludge [64]. The sludge can then be digested and the phosphorus recovered through chemical precipitation as struvite [58]. As a process that requires intensive aeration during the aerobic phase, EBPR systems also face the same constrains of other aerated systems (e.g., aeration costs and carbon emissions). These can be overcome by combining PAOs with microalgae in the new Photo-EBPR technology.

4.1 Phosphate Recovery: The Case of Photo-EBPR

In recent years, an innovative technology that uses a PAO–microalgae consortium to recover phosphorus via a photosynthetic enhanced biological phosphorous removal system (photo-EBPR) was demonstrated by [31]. The photo-EBPR system was proposed with the objective of treating wastewaters with low COD/P ratios while eliminating the aeration requirements of EBPR systems. The photo-EBPR utilizes a consortium culture, composed of heterotrophic bacteria (PAOs) and photosynthetic organisms (e.g., microalgae and cyanobacteria) where the latest use light, consume CO_2, and produce the oxygen necessary for the system operation. Its configuration is based on sequential dark and light cycles (Fig. 3).

During the dark phase, where no oxygen production by photosynthetic organisms occurs, the system is anaerobic and PAOs take up VFAs and convert them into PHA, using the energy from poly-P and glycogen hydrolysis. In the light phase, photosynthetic organisms use the light to produce ATP while generating oxygen, which can be used by PAOs, to oxidize PHA and obtain ATP for P uptake [31]. The amount of P that is taken up in the light phase, both by PAOs and photosynthetic microorganisms, is higher than the P released in the dark phase, contributing to an effluent with low P concentrations. In the dark idle period, the biomass is settled, the supernatant is discharged, and anaerobic conditions are achieved, which is essential for the beginning of the next photo-EBPR cycle [31, 32]. Since the consortia self-aggregates in microalgae–PAOs biomass flocs, a good settling capacity is obtained and a clear supernatant is generated [65, 66]. The sludge produced during a photo-EBPR process can be directly used as fertilizer since

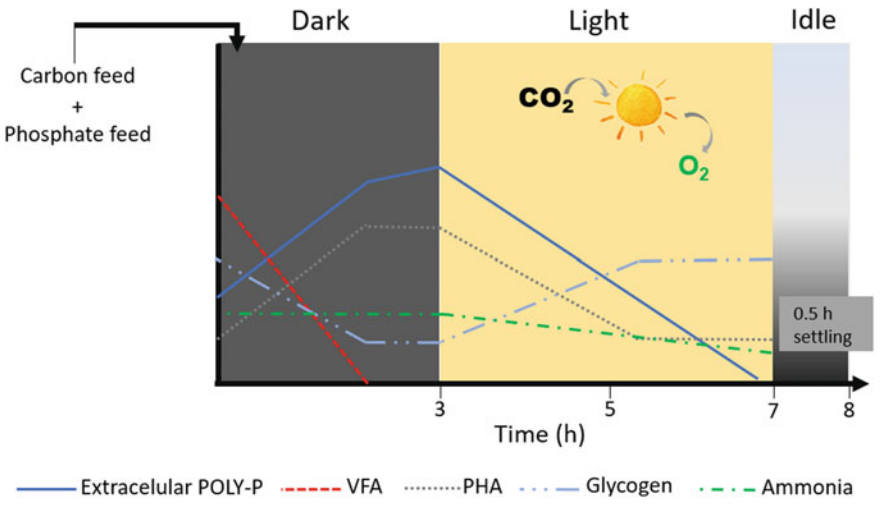

Fig. 3 Schematic representation of a typical photo-EBPR profile

microalgae biomass is a slow releaser of ammonia and phosphorus [67, 68]. Algal fertilizers have several advantages when compared to chemical fertilizers or other natural fertilizers like manure [68, 69]. The nitrogen present in microalgae biomass is less probable of being lost in run-off or leaching, since only ~5% of the microalgae nitrogen content is available as mineral N at the time of application, resulting in no volatilization of ammonia when dry microalgae biomass is disposed as fertilizer [69]. In terms of P release, the fact that the poly-P present in the biomass is slowly released in the soil, optimizes plants growth and reduces P soil run-off, in comparison to inorganic fertilizers [67]. The presence of eventual pathogens on the microalgae fertilizers can be controlled by the pH, temperature, and the UV exposure during the wastewater treatment [68].

The first studies on the development of the photo-EBPR technology were carried out at laboratory scale with the aim of understanding if a consortium of microalgae and PAOs could efficiently remove P, while solely assisted by photo-oxygenation, with no external aeration. The selection of a photo-EBPR system started by exposing a sludge previously enriched in the PAO *Accumulibacter phosphatis* to sequential dark/light cycles (as in Fig. 3), maintaining a short period of aeration during the light phase to guarantee the survival of PAOs until microalgae evolved and produced enough oxygen to sustain the system needs [31]. After understanding that the CO_2 released during the bacterial metabolism was not, *per si*, enough for microalgae to produce the needed oxygen, inorganic carbon started to be fed to the system which led to the fully development of the PAO-microalgae consortia (Fig. 4).

In the end of the photo-EBPR selection process, aeration could be completely removed from the light phase and microalgae were able not only to produce enough

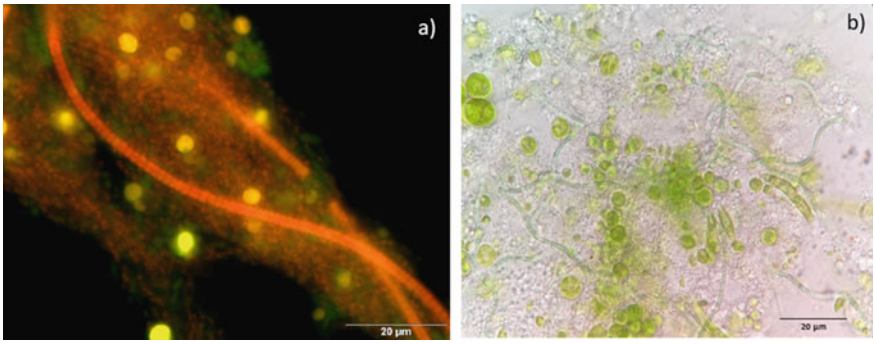

Fig. 4 Microscopic pictures of the PAO–microalgae consortium of photo-EBPR reactors illuminated with a light intensity of 328 W/m^2 and operated with no external aeration (the oxygenation of the system was provided only by photosynthetic organisms). **a** FISH image of photo-EBPR sludge with PAO mix probe (microorganisms in red color). Algae are in yellow due to their auto-fluorescence. **b** Bright field image showing photosynthetic microorganism (algae and cyanobacteria) in green and *Accumulibacter*-related PAOs microorganisms in light white/gray color. For further details, please refer to [31]

oxygen to allow phosphorus removal, but also contributed themselves for the phosphorus uptake [31]. This uptake occurred in amounts that were higher than the P needed for their growth, suggesting a possibly accumulation of phosphorus granules as internal reserves [31, 47, 58, 70]. The overall process results indicated that without any mechanical aeration, the photo-EBPR had a phosphorus removal capacity of 74%, with a P net removal of 34 mg P/L, when the reactor was fed with a COD/P ratio of 3.3/1 (mg COD/mg P) [31]. This ratio was much lower than the ratios found in domestic wastewaters, which normally range 30/1 [71], showing that the photo-EBPR is capable of treating effluents with low carbon concentrations and high P amount, which can occur in industrial and agricultural wastewaters [46]. In comparison with other conventional EBPR processes, the P net removal obtained by [31] was consistently higher: [72] in full-scale WWTPs with EBPR systems, indicating a net P removal of 10 mg P/L with a COD/P ratio of 10/1; [73] obtained a net P removal of 10 mg P/L with a COD/P ratio of 20/1 using real wastewaters in laboratory tests; [74] obtained 20 mg P/L of net P removal with a COD/P ratio of 10/1 using synthetic wastewaters in laboratory tests.

[32] also studied the possibility of selecting a photo-EBPR system starting from activated sludge and concluded that it was possible but required the double of the time to obtain a stable and efficient P removal culture. This extra time is necessary to simultaneously give conditions for algae growth and for the selection of PAOs with high P uptake capability, which require high oxygen availability. Although the culture selection process was slower in comparison with cultures already enriched

in PAOs, activated sludge is widely available and a photo-EBPR system can be readily implemented in WWTP that currently do not perform EBPR and where there is no direct access to a sludge enriched in PAOs [32].

Besides the phosphorous recovery, another feature that can be explored in photo-EBPR systems is their capacity for nitrogen removal. The operation with sludge retention times over 10 days and the cyclic variations of oxygen levels and light allows the development of a multitude of microorganisms with complementary metabolic pathways. Since the measured oxygen levels are always very low during the light phase [31, 32], and some PAOs are capable of using nitrates as electron acceptors in anoxic conditions (denitrifying PAOS—dPAOs) [75–77], it is expected that the photo-EBPR could be operated in sequential dark (anaerobic)—light (aerobic)—dark (anoxic) cycles. During the light aerobic phase, ammonia could be removed by the combination of assimilation processes and nitrification by aerobic autotrophic nitrifiers. During the dark anoxic phase, nitrates could be removed by dPAOs. Future research will ascertain on the photo-EBPR potential for the dual capacity removal of P and N.

Summing-up, the main advantage of the photo-EBPR, in relation to the conventional EBPR, is the independence from external aeration, since the oxygen needs are covered by microalgae that produce the O_2 used by PAOs, substantially reducing the process operation costs [31]. Furthermore, photo-EBPR systems require a lower amount of COD in the wastewater to remove phosphorous since the microalgae also contribute for P uptake while using CO_2 as carbon source. The high quantity of CO_2 that microalgae need to satisfy the O_2 requirements of aerobic bacteria [78] is a further feature of the photo-EBPR that contributes to CO_2 sequestration, reducing the concentration of greenhouse gases in the atmosphere [31]. Finally, the P-rich microalgae–bacterial sludge can be used as a slow-release fertilizer or directed for phosphorus recovery.

On the other hand, the photo-EBPR systems require land space and sunlight, being fit for implementation in areas with a good solar distribution along the year and warm temperatures [66]. Nevertheless, the system can be used in large city surroundings, as well as small towns and villages in rural areas where space is not a constraint for WWTPs and where wastewater is sometimes treated in WSP or ORP using algal–bacterial consortia. The photo-EBPR system can be an appropriate solution for these cases as it optimizes phosphorous removal in combination with low-cost operation (no aeration needed) and low maintenance requirements [32].

On a future note, the fact that current photo-EBPR systems show good P removal capacities (P net removal $\sim$34 mg P/L) for wastewaters with low COD/P ratios (phosphate concentration in the influent $\sim$60 mg P/L) [31, 32] indicates the possibility of full P removal when treating domestic wastewater, which typically present lower phosphate concentrations (<10–20 mg P/L). Furthermore, the presence of low oxygen levels during the cycles opens up the possibility of developing the photo-EBPR system for future simultaneous P and N removal.

5 Value-Added Products Recovery: Polyhydroxyalkanoates

Plastics are essential materials that in 2018 reached a demand of over 60 million tons in Europe [79]. Though a considerable amount of the plastics was used in long-life applications, 30 million ended up in the waste streams, with 25% being disposed in landfills [79]. Worldwide, it is estimated that a considerably higher percentage of plastics is discarded and directly disposed in nature. In this case, since conventional plastics cannot naturally feed back into the ecosystem through natural biogeochemical cycles, they will persist in the environment as invasive microplastics, interfering with our ecosystems and entering food-feed chains [80, 81]. This problematic is increasing the demand for bio-based and biodegradable plastics, and polyhydroxyalkanoates (PHAs) have been proposed as an alternative to petrochemical plastics. PHAs are microbially synthetized polyesters, internally accumulated as carbon and energy reserves, in the presence of excess carbon. They display thermoplastic properties similar to traditional plastics [82], yet, PHAs can be produced from renewable resources and because they are completely biodegradable upon disposal in the environment, they comprise all the ecological requirements for the production of sustainable biodegradable plastics.

PHAs are already available in the market, but their current industrial production is based on single strain processes that use expensive refined substrates, leading to high production costs and making PHA significantly more expensive than conventional plastics [83]. Efforts to create more economic PHA production strategies and increase its field of applicability have emerged in recent years for both single strain processes and mixed microbial cultures (MMC) [84]. In the case of MMC, low-cost PHA producing systems have been developed by operating non-sterile open systems that use complex, low-grade, inexpensive wastes as feedstock [85–87]. Unlike single strain systems that typically use carbohydrates as carbon source, volatile fatty acids (VFAs) (e.g., acetate, propionate and butyrate) are the best precursors for PHA production in MMCs, and they can be easily obtained by fermentation of waste streams [88]. But before the actual PHA production takes place, the MMC commonly undergoes a microbial selection in order to enrich the culture in PHA accumulating bacteria. The selection is carried out by subjecting the culture to transient feeding conditions in a strategy designated as feast and famine (FF). This consists in alternating periods with excess of external carbon (Feast), where organisms take up the carbon and accumulate it as PHA, with periods with no substrate addition (famine), where only the organisms that accumulated PHA will have carbon reserves and will thus be able to grow. Repeated FF cycles will favor the cell growth on storage products, thus creating a selection pressure for organisms with high PHA-storing capacity.

The PHA production systems with MMCs can then be described as a process that commonly comprises three steps (1) wastewater or agro-industrial waste acidogenic fermentation to VFAs, (2) selection of a PHA accumulating culture under

FF conditions, and (3) PHA accumulation in a batch reactor using sludge from the selected culture fed with the fermented effluent [88].

By applying this process to cultures fed with fermented agro-industrial wastes, high PHA accumulation values in the order of 75% using sugar cane molasses [89] and paper mill wastewater [90] have been achieved. Moreover, the accumulated PHAs were co-polymers composed of hydroxybutyrate (HB) and hydroxyvalerate (HV) monomers which confer better thermoplastic properties do the polymer [82]. Currently, many other fermented agro-industrial wastes have been successfully tested as potential feedstock for PHA production, like waste activated sludge [86], cheese whey [87], and waste mixtures as reviewed by [85]. While all of these studies were conducted with aerobic organisms, de fact is that a wider diversity of bacterial species can produce and accumulate PHA, including phototrophic bacteria, such as cyanobacteria and purple bacteria.

Cyanobacteria

PHA production in cyanobacteria has drawn great attention in recent years due to their ability to accumulate PHB under photoautothrophic conditions with just some requirements of simple inorganic nutrients (e.g., phosphate and nitrogen) and micronutrients [91]. PHB production is usually stimulated by applying a deficiency or limitation of nutrients, and thus far, several PHA accumulating cyanobacteria species have been identified (e.g., *Anabaena* spp., *Spirulina* spp., *Synechococcus* spp., *Synechocystis* spp., *Nostoc* spp., and *Aulosira* spp.) [91, 92]. Typically, their PHA content under autotrophy is low, around 2–20% of cell dry weight (cdw) [91, 92]. Higher PHA contents up to 70–80% cdw have been reported, but they were only achieved by multistage cultivation processes under heterotrophic conditions with additives supplementation such as glucose, acetate, and valerate [92]. Currently, metabolic engineering is being used to improve cyanobacteria PHA accumulation capacity, monomer diversity, and more importantly, productivity [91, 92] since the highest volumetric value reported thus far from CO_2 is in the order of 260 mg PHB $L^{-1}d^{-1}$ obtained with a genetically modified *Synechhocytis* spp.[93]. However, this is still a recent field of research and the CO_2 fixation capacity of cyanobacteria is an attractive characteristic with great potential for CO_2 recovery in the form of PHA during off-gas streams treatment.

Purple phototrophic bacteria

If cyanobacteria are suited for photoautotrophic PHA production, then purple bacteria are the choice for phototrophic PHA production from organic rich wastes. As mentioned in previous sections, PPB are highly versatile organisms which includes their capability to synthetize PHA, preferably from VFAs like acetate and propionate. High PHA accumulation capacities up to 80% cdw have been reported on VFAs, both for sulfur bacteria (e.g., *Thiosystis* spp., *Ectothiorhodospira* spp., *Chromatium* spp.) and non-sulfur purple bacteria (e.g., *Rhodobacter* spp., *Rhodopseudomonas* spp.) [94, 95]. It is important to stress that in PPB, PHA granules are internally stored not only as a carbon reserves but also, very importantly, as a sink for reduced power. Since PPB thrive in illuminated anaerobic environments, the cells' redox homeostasis is maintained through activation of

metabolic pathways that allow dissipation of electrons in response to the redox state of the consumed carbon and nitrogen sources [96]. In the particular case of using PPB for treating wastewaters or valorizing fermented agro-wastes, the uptake of reduced carbon sources (e.g., organic acids), present in the waste stream, requires electron dissipation which is possible through PHA accumulation, CO_2 fixation via CBB cycle or through N_2 fixation/H_2 production via nitrogenase enzyme [96, 97]. Since wastewaters and fermented streams usually contain NH_4^+, and this compound is a product of nitrogenase activity, nitrogenase synthesis is repressed and its activity is inhibited [97]. Thus, N_2 fixation/H_2 production is no longer a viable pathway for electron dissipation. Between CO_2 fixation and PHA accumulation, the first is an ATP demanding process, while the later, does not require ATP and cells can directly reoxidize reduced agents like NADH, by for example, reducing acetoacetyl-CoA molecules to 3-hydroxybutyryl-CoA, a precursor of PHB [82]. Both pathways can be used in parallel by the cells to dissipate electrons, but the more or less utilization of each one is dependent on the amount of ATP available, and on the type and redox state of the organic acids present in the feedstock. Cells are more likely to use the PHA synthesis pathway when they are fed with molecules that are easily converted to this polymer, like acetate and propionate [98], but will also resort to CO_2 fixation to dispose excess electrons if the organic acid is more reduced than the cell material (e.g., butyrate and valerate) [97]. These particularities of PHA accumulation in PPB are very important when designing strategies to promote PHA accumulation and choosing feedstocks, especially in mixed microbial cultures systems. The dual function of PHA that is stored as carbon and reducing power enables the implementation of selection strategies that specifically target each function, as detailed in Sect. 5.1.

5.1 Phototrophic Mixed Culture PHA Production: From Laboratory to Demo PPBPonds

As in other phototrophic processes, the main purpose of approaching mixed culture PHA production with phototrophic organisms is (i) to eliminate the high costs of intensive aeration observed in aerobic systems, aiming a more cost-effective PHA production and (ii) to promote a high carbon conversion efficiency to biomass and PHA, minimizing substrate losses as CO_2. While numerous studies on the PHA production capability of PPB as single strains have been reported (reviewed in [26, 95]), to the best of our knowledge, there are only a few studies on PHA production with phototrophic mixed cultures (PMC).

Studies with PMC started by targeting PPB capability of storing PHA as carbon reserves. By following the feast and famine (FF) strategy typically applied to aerobic mixed cultures, [99] proposed the combination of PPB with microalgae, in a consortia where microalgae would be the oxygen providers. Using a synthetic acetate feed and under continuous illumination (halogen lamp), sequential FF cycles led to the enrichment of a PMC (Fig. 5) where PPB stored PHB during the feast phase and consumed it during the famine phase, using the oxygen produced by microalgae [99].

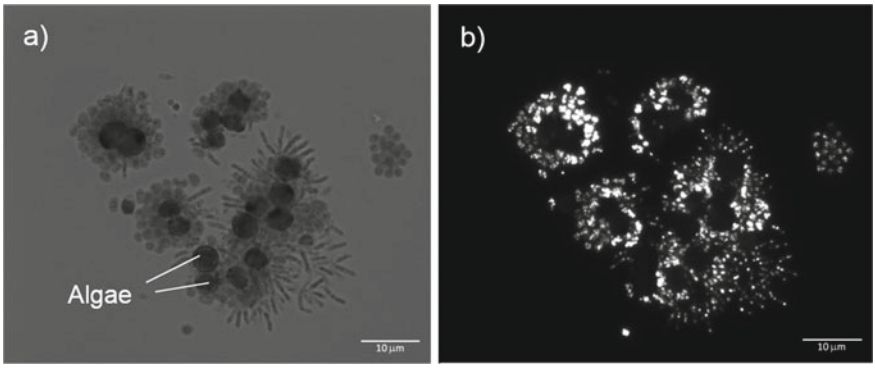

Fig. 5 Microscopic images of the PMC selected in a FF regime under acetate feeding and continuous halogen illumination. **a** Bright field showing the PPB and microalgae consortia. **b** Fluorescence image of Nile blue staining indicating PHA granules inside the bacteria. For further details, please refer to [99]

In accumulation tests, the culture attained 20% PHB content (gPHB/gVSS) with a polymer storage yield of 0.70 ± 0.04 Cmol PHB/Cmol Acet [99]. Subsequent studies showed that the acetate enriched PMC was also capable of consuming VFA mixtures (acetate, propionate, and butyrate), attaining similar PHA contents of 20%, but producing a PHA co-polymer of better quality with an HB:HV molar fraction of 84:16 [100].

Since this technology can only achieve economic feasibility if operated in outdoor conditions, the PMC capability of enduring transient illumination was tested, at laboratory scale, under FF dark/light conditions. This resulted in a decrease of microalgae levels, but that were still capable of sustaining the system oxygen needs. With the microalgae decrease, more light and carbon source became available for the PHA accumulating bacteria, leading to higher metabolic rates and to an increase of the PHA content up to 30% [101]. At this time, the PHB storage yield reached 0.90 ± 0.09 Cmol PHB/Cmol Substrate (acetate + internal glycogen) which resulted from the decrease of microalgae that could compete for the acetate and also, from the lower oxygen availability that enabled the higher carbon conversion efficiencies typically observed in PPB.

The studies with PMCs selected under the feast and famine strategy show that targeting PPB for their PHA storage capacity as carbon reserve enables effective culture selection. The results indicated that the PMC technology under dynamic feeding comprises the requirements for outdoor operation namely stability under dark/light conditions and capability of using VFA mixtures, typically found in fermented wastewaters, for PHA co-polymer production. Nevertheless, subsequent studies addressed the possibility of selecting PMCs by exploring PPB capability of storing PHA as electron sink. In this case, PMCs were selected under continuous illumination (halogen lamp), permanent presence of acetate (in a so-called permanent feast) and presence of ammonia to promote cell redox balance via PHB

accumulation [102]. In permanent feast conditions, microalgae were outcompeted and the culture become highly enriched in PPB. The culture favored carbon recovery as biomass in the selector reactor (0.64 Cmol *X*/Cmol S of growth yield) and thus, presented low PHB values (3–5% PHA). Yet, when exposed to higher light intensities in accumulator reactors (intensities achievable under natural sun-light illumination), the culture substantially increased its metabolic rates, doubling the carbon uptake rate and increasing 15 times the PHB storage rate, which resulted in a PHB content of 60%, the maximum ever recorded for a PMC. In this case, carbon recovery as PHB was favored with a storage yield of 0.67 Cmol PHB/Cmol Acetate. Globally, the carbon mass balance indicated an 80% carbon recovery as biomass and PHB. An interesting parallel finding was the high uptake rate of phosphate observed during the accumulation tests, with 95% of the removed phosphate being stored in the first hours of the tests, likely as polyphosphate [102]. These results indicate that selecting PMCs under the permanent presence of carbon and exposing them to high light availabilities enables a high carbon and phosphorous recovery, partly through assimilation into the cell biomass, but mostly through accumulation as internal PHB and polyphosphate polymers.

Under light optimized conditions in the accumulator reactors, it was possible to further increase PHA production rates up to 2.21 $\pm$ 0.07 Cmol PHB/Cmol *X* d [55]. This is less than a threefold difference in comparison to acetate-fed aerobic systems, which approaches the storage performances of phototrophic and aerobic systems. Also, high PHB storage yield on acetate was again registered (0.83 $\pm$ 0.07 Cmol PHB/Cmol Acetate) in contrast with the lower yields observed in aerobic systems (0.4–0.6 Cmol PHB/Cmol Acetate) [55]. When the PMC was fed with real fermented cheese whey containing lactate, ethanol, and VFAs (C2 to C5), the PPB culture showed its robustness, adapting well to the new feedstock and achieving 20% PHA content with 12% HV content. These values are even more relevant seeing that all the tests were conducted with light intensities that can be naturally obtained outdoors, indicating the possibility of system operation under direct sunlight illumination [55].

Taking all these results into consideration, both the selection of phototrophic mixed cultures through feast and famine conditions (targeting PHA storage as carbon reserve) or through the permanent presence of carbon (targeting PHA storage as electron sink) can be potential strategies for PHA production from VFA-rich streams under natural outdoor sunlight conditions. However, the establishment of PMC systems as sustainable PHA producing technologies requires the technology transfer from laboratory to demo-scale and technology validation with on-site studies. These studies have occurred under the framework of the European Project INCOVER [103] in collaboration with the company FCC AQUALIA, Spain. The technology initially developed in 6L laboratory reactors, simulating outdoor light and temperature conditions, was transferred to two demo-scale ponds of $\sim 10 m^3$ each (Fig. 6). These purple phototrophic bacteria ponds (PPBPonds) were illuminated by sunlight and fed with locally fermented domestic wastewater mixed with molasses for PHA production. Preliminary results indicated the culture capacity of producing up to 1.3 kg PHA $Pond^{-1}$ d^{-1} during spring time

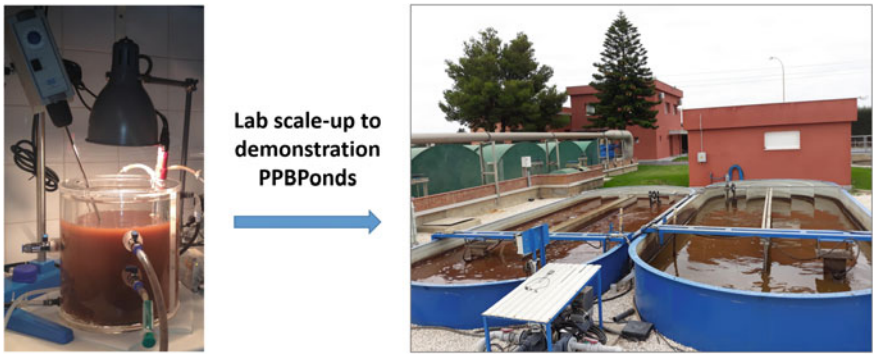

Fig. 6 Purple phototrophic bacteria ponds (PPBPonds) for demo-scale PHA production with PPB from fermented domestic wastewater (Chiclana de la Frontera WWTP, EU Horizon 2020 INCOVER project; for further details please refer to [103])

(unpublished results), prospecting higher productivities during summer periods. Future technology development is expected to bring forward PPBPonds as attractive systems for low-cost PHA production from waste streams with high carbon, nitrogen, and phosphorus recovery levels.

Acknowledgements The authors acknowledge FCC Aqualia for providing pictures of the INCOVER PPBPonds at Chiclana de la Frontera WWTP. The authors would also like to acknowledge the financial support from the Fundação para a Ciência e Tecnologia for the Grant PD/BD / 114574/2016 and the support by the Applied Molecular Biosciences Unit—UCIBIO which is financed by national funds from FCT (UIDB/04378/2020).

References

1. Rao MA, Scelza R, Scotti R et al (2010) Role of enzymes in the remediation of polluted environments. J Soil Sci Plant Nutr 10:333–353
2. IPCC 2018: Summary for Policymakers (2018) In: Masson-Delmotte V, Zhai P, Pörtner HO et al (eds) Global Warming of 1.5 °C. An IPCC Special Report on the impacts of global warming of 1.5 °C above pre-industrial levels and related global greenhouse gas emission pathways, in the context of strengthening the global response to the threat of climate change, sustainable development, and efforts to eradicate poverty. World Meteorological Organization, Geneva, Switzerland, 32 pp.
3. Agarwal N, Banternghansa C, Bui LTM (2010) Toxic exposure in America: estimating fetal and infant health outcomes from 14 years of TRI reporting. J Health Econ
4. Khan MA, Ghouri AM (2011) Environmental pollution: its effects on life and its remedies. Res World J Arts Sci Commer 2:276–285
5. Gianfreda L, Rao MA, Scelza R, De La Luz Mora M (2016) Role of enzymes in environment cleanup/remediation. In: Dhillon G, Kaur S (eds) Agro-industrial wastes as feedstock for enzyme production: apply and exploit the emerging and valuable use options of waste biomass. Academic Press.

6. Aitken MD (1993) Waste treatment applications of enzymes: opportunities and obstacles. Chem Eng J 52:49–58
7. Robinson PK (2015) Enzymes: principles and biotechnological applications. Essays Biochem 59:1–41
8. Li S, Yang X, Yang S et al (2012) Technology prospecting on enzymes: application, marketing and engineering. Comput Struct Biotechnol J 2:e201209017
9. Nielsen PH, Kuilderd H, Zhou W, Lu X (2009) Enzyme biotechnology for sustainable textiles. In: Blackburn RS (ed) Sustainable textile: life cycle and environment impact, Woodhead Publishing Limited & CRC Press, pp 113–138
10. Hamilton TL (2019) Free Radical Biology and Medicine The trouble with oxygen: the ecophysiology of extant phototrophs and implications for the evolution of oxygenic photosynthesis. Free Radic Biol Med 140:233–249
11. Cooper GM (2000) The cell: a molecular approach, 2nd edn. ASM Press, Washington DC
12. Prescott L, Harley JP, Klein DA (1999) Microbiology, 4th edn. The McGraw-Hill, Companies Inc, New York
13. Hemp J, Lücker S, Schott J et al (2016) Genomics of a phototrophic nitrite oxidizer: insights into the evolution of photosynthesis and nitrification. ISME J 10:2669–2678
14. Tang K-H, Tang YJ, Blankenship RE (2011) Carbon metabolic pathways in phototrophic bacteria and their broader evolutionary implications. Front Microbiol 2:165
15. Timpmann K, Chenchiliyan M, Jalviste E et al (2014) Efficiency of light harvesting in a photosynthetic bacterium adapted to different levels of light. Biochim Biophys Acta Bioenerg 1837:1835–1846
16. Frigaard N-U (2016) Biotechnology of anoxygenic phototrophic bacteria. In: Hatti-Kaul R, Mamo G, Mattiasson B (eds) Anaerobes in biotechnology. Advances in biochemical engineering/biotechnology, vol 156. Springer, Cham, pp 139–154.
17. Scheer H (2006) An overview of chlorophylls and bacteriochlorophylls: biochemistry, biophysics, functions and applications. In: Grimm B, Porra RJ, Rüdiger W, Scheer H (eds) Chlorophylls and bacteriochlorophylls. advances in photosynthesis and respiration, vol 25, Springer, Dordrecht.
18. Koyama Y, Kakitani Y (2006) Mechanisms of carotenoid-to-bacteriochlorophyll energy transfer in the light harvesting antenna complexes 1 and 2: dependence on the conjugation length of carotenoids. In: Grimm B, Porra RJ, Rüdiger W, Scheer H (eds) Chlorophylls and bacteriochlorophylls. Advances in photosynthesis and respiration, vol 25, Springer, Dordrecht.
19. Llorens-Marès T, Yooseph S, Goll J et al (2015) Connecting biodiversity and potential functional role in modern euxinic environments by microbial metagenomics. ISME J 9:1648–1661
20. Hubas C, Jesus B, Passarelli C, Jeanthon C (2011) Tools providing new insight into coastal anoxygenic purple bacterial mats: review and perspectives. Res Microbiol 162:858–868
21. Hügler M, Sievert SM (2011) Beyond the Calvin cycle: autotrophic carbon fixation in the ocean. Ann Rev Mar Sci 3:261–289
22. Hurse TJ, Kappler U, Keller J (2008) Using anoxygenic photosynthetic bacteria for the removal of sulfide from wastewater. In: Hell R, Dahl C, Knaff D, Leustek T (eds) Sulfur metabolism in phototrophic organisms. Advances in photosynthesis and respiration, vol 27. Springer, Dordrecht, pp 437–460.
23. Garcia GPP, Diniz RCO, Bicalho SK et al (2015) Biological sulphide removal from anaerobically treated domestic sewage: reactor performance and microbial community dynamics. Environ Technol (United Kingdom) 36:2177–2189
24. Imhoff JF (2006a) The Phototrophic Alpha-Proteobacteria. In: Dworkin M, Falkow S, Rosenberg E et al (eds) The prokaryotes. Springer, New York, pp 41–64
25. Imhoff J (2006b) The Chromatiaceae. In: Dworkin M, Falkow S, Rosenberg E et al (eds) The prokaryotes. Springer, New York, pp 846–873

26. Capson-Tojo G, Batstone DJ, Grassino M et al (2020) Purple phototrophic bacteria for resource recovery: challenges and opportunities. Biotechnol Adv 107567.
27. Muñoz R, Guieysse B (2006) Algal-bacterial processes for the treatment of hazardous contaminants: a review. Water Res 40:2799–2815
28. Perez-Garcia O, Escalante FME, de-Bashan LE, Bashan Y (2011) Heterotrophic cultures of microalgae: metabolism and potential products. Water Res 45:11–36
29. Gonçalves AL, Pires JCM, Simões M (2017) A review on the use of microalgal consortia for wastewater treatment. Algal Res 24:403–415
30. Gupta S, Pawar SB, Pandey RA (2019) Current practices and challenges in using microalgae for treatment of nutrient rich wastewater from agro-based industries. Sci Total Environ 687:1107–1126
31. Carvalho VCF, Freitas EB, Silva P et al (2018) The impact of operational strategies on the performance of a photo-EBPR system. Water Res 129:190–198
32. Carvalho VCF, Freitas EB, Fradinho JC et al (2019) The effect of seed sludge on the selection of a photo-EBPR system. N Biotechnol 49:112–119
33. Hayes M, Skomedal H, Skjånes K et al (2017) Microalgal proteins for feed, food and health. In: Gonzalez-Fernandez C, Muñoz R (eds) Microalgae-based biofuels and bioproducts. Woodhead Publishing, pp 347–368.
34. de Souza MP, Hoeltz M, Gressler PD et al (2019) Potential of microalgal bioproducts: general perspectives and main challenges. Waste Biomass Valoriz 10:2139–2156
35. Muga HE, Mihelcic JR (2008) Sustainability of wastewater treatment technologies. J Environ Manag 88(3):437–447
36. van der Hoek J, Duijff R, Reinstra O (2018) Nitrogen recovery from wastewater: possibilities, competition with other resources, and adaptation pathways. Sustainability 10:4605
37. Puyol D, Batstone DJ, Hülsen T et al (2017) Resource recovery from wastewater by biological technologies: opportunities, challenges, and prospects. Front Microbiol 7:1–23
38. Karimi AR, Mehrdadi N, Hashemian SJ et al (2011) Selection of wastewater treatment process based on the analytical hierarchy process and fuzzy analytical hierarchy process methods. Int J Environ Sci Technol 8:267–280
39. Hoffmann JP (1998) Wastewater treatment with suspended and nonsuspended algae. J Phycol 34:757–763
40. Lu H, Zhang G, Zheng Z et al (2019) Bio-conversion of photosynthetic bacteria from non-toxic wastewater to realize wastewater treatment and bioresource recovery: a review. Bioresour Technol 278:383–399
41. Wang Y, Ho SH, Cheng CL et al (2016) Perspectives on the feasibility of using microalgae for industrial wastewater treatment. Bioresour Technol 222:485–497
42. Wollmann F, Dietze S, Ackermann JU et al (2019) Microalgae wastewater treatment: biological and technological approaches. Eng Life Sci 19:860–871
43. Hülsen T, Batstone DJ, Keller J (2014) Phototrophic bacteria for nutrient recovery from domestic wastewater. Water Res 50:18–26
44. Chen J, Wei J, Ma C et al (2020) Photosynthetic bacteria-based technology is a potential alternative to meet sustainable wastewater treatment requirement? Environ Int 137:105417
45. Alcántara C, Domínguez JM, Garcia D et al (2015) Evaluation of wastewater treatment in a novel anoxic-aerobic algal-bacterial photobioreactor with biomass recycling through carbon and nitrogen mass balances. Bioresour Technol 191:173–186
46. Cai T, Park SY, Li Y (2013) Nutrient recovery from wastewater streams by microalgae: status and prospects. Renew Sustain Energy Rev 19:360–369
47. Powell N, Shilton A, Chisti Y, Pratt S (2009) Towards a luxury uptake process via microalgae—defining the polyphosphate dynamics. Water Res 43:4207–4213
48. de Godos I, Arbib Z, Lara E et al (2017) Wastewater treatment in algal systems. In: Lema J, Suarez S (eds) Innovative wastewater treatment and resource recovery technologies: impacts on energy, economy and environment, IWA Publishing.

49. Foladori P, Petrini S, Nessenzia M, Andreottola G (2018) Enhanced nitrogen removal and energy saving in a microalgal-bacterial consortium treating real municipal wastewater. Water Sci Technol 78:174–182
50. García D, de Godos I, Domínguez C et al (2019) A systematic comparison of the potential of microalgae-bacteria and purple phototrophic bacteria consortia for the treatment of piggery wastewater. Bioresour Technol 276:18–27
51. López-Serna R, García D, Bolado S et al (2019) Photobioreactors based on microalgae-bacteria and purple phototrophic bacteria consortia: a promising technology to reduce the load of veterinary drugs from piggery wastewater. Sci Total Environ 692:259–266
52. De las Heras I, Molina R, Segura Y et al (2020) Contamination of N-poor wastewater with emerging pollutants does not affect the performance of purple phototrophic bacteria and the subsequent resource recovery potential. J Hazard Mater 385:121617
53. Talaiekhozani A, Rezania S (2017) Application of photosynthetic bacteria for removal of heavy metals, macro-pollutants and dye from wastewater: a review. J Water Process Eng 19:312–321
54. Cao K, Zhi R, Zhang G (2020) Photosynthetic bacteria wastewater treatment with the production of value-added products: a review. Bioresour Technol 299:122648
55. Fradinho JC, Oehmen A, Reis MAM (2019) Improving polyhydroxyalkanoates production in phototrophic mixed cultures by optimizing accumulator reactor operating conditions. Int J Biol Macromol 126:1085–1092
56. Hülsen T, Hsieh K, Lu Y et al (2018) Simultaneous treatment and single cell protein production from agri-industrial wastewaters using purple phototrophic bacteria or microalgae—a comparison. Bioresour Technol 254:214–223
57. Puyol D, Monsalvo VM, Marin E et al (2020) Purple phototrophic bacteria as a platform to create the next generation of wastewater treatment plants: energy and resource recovery. In: Olivares JA, Puyol D, Melero JA, Dufour J (eds) Wastewater treatment residues as resources for biorefinery products and biofuels. Elsevier, pp 255–280.
58. Solovchenko A, Verschoor AM, Jablonowski ND, Nedbal L (2016) Phosphorus from wastewater to crops: an alternative path involving microalgae. Biotechnol Adv 34:550–564
59. van Dijk KC, Lesschen JP, Oenema O (2016) Phosphorus flows and balances of the European Union Member States. Sci Total Environ 542:1078–1093
60. Crini G, Lichtfouse E (2019) Advantages and disadvantages of techniques used for wastewater treatment. Environ Chem Lett 17:145–155
61. Acién Fernández FG, Gómez-Serrano C, Fernández-Sevilla JM (2018) Recovery of nutrients from wastewaters using microalgae. Front Sustain Food Syst 2:1–13
62. Bhatnagar A, Sillanpää M (2011) A review of emerging adsorbents for nitrate removal from water. Chem Eng J 168:493–504
63. Yuan Z, Pratt S, Batstone DJ (2012) Phosphorus recovery from wastewater through microbial processes. Curr Opin Biotechnol 23:878–883
64. Oehmen A, Zeng RJ, Keller J, Yuan Z (2007) Modeling the aerobic metabolism of polyphosphate-accumulating organisms enriched with propionate as a carbon source. Water Environ Res 79:2477–2486
65. González C, Marciniak J, Villaverde S et al (2008) Efficient nutrient removal from swine manure in a tubular biofilm photo-bioreactor using algae-bacteria consortia. Water Sci Technol 58:95–102
66. Su Y, Mennerich A, Urban B (2011) Municipal wastewater treatment and biomass accumulation with a wastewater-born and settleable algal-bacterial culture. Water Res 45:3351–3358
67. Mukherjee C, Chowdhury R, Ray K (2015) Phosphorus recycling from an unexplored source by polyphosphate accumulating microalgae and cyanobacteria-a step to phosphorus security in agriculture. Front Microbiol 6:1–7

68. Mulbry W, Westhead EK, Pizarro C, Sikora L (2005) Recycling of manure nutrients: use of algal biomass from dairy manure treatment as a slow release fertilizer. Bioresour Technol 96:451–458
69. Mulbry W, Kondrad S, Pizarro C (2006) Biofertilizers from algal treatment of dairy and swine manure effluents: characterization of algal biomass as a slow release fertilizer. J Veg Sci 12:107–125
70. Brown N, Shilton A (2014) Luxury uptake of phosphorus by microalgae in waste stabilisation ponds: current understanding and future direction. Rev Environ Sci Biotechnol 13:321–328
71. Henze M, van Loosdrecht MCM, Ekama GA, Brdjanovic D (2008) Biological wastewater treatment: principles. IWA Publishing, London, Modeling and Design
72. López-Vázquez CM, Hooijmans CM, Brdjanovic D et al (2008) Factors affecting the microbial populations at full-scale enhanced biological phosphorus removal (EBPR) wastewater treatment plants in The Netherlands. Water Res 42:2349–2360
73. Valverde-Pérez B, Wágner DS, Lóránt B et al (2016) Short-sludge age EBPR process—microbial and biochemical process characterisation during reactor start-up and operation. Water Res 104:320–329
74. Carvalheira M, Oehmen A, Carvalho G, Eusébio M, Reis MAM (2014) The impact of aeration on the competition between polyphosphate accumulating organisms and glycogen accumulating organisms. Water Res 66:296–307
75. Carvalho G, Lemos PC, Oehmen A, Reis MAM (2007) Denitrifying phosphorus removal: linking the process performance with the microbial community structure. 41:4383–4396
76. Lanham AB, Oehmen A, Carvalho G et al (2018) Denitrification activity of polyphosphate accumulating organisms (PAOs) in full-scale wastewater treatment plants. Water Sci Technol 78:2449–2458
77. Zeng RJ, Lemaire R, Yuan Z, Keller J (2003) Simultaneous nitrification, denitrification, and phosphorus removal in a lab-scale sequencing batch reactor. Biotechnol Bioeng 84:170–178
78. Boelee NC, Temmink H, Janssen M et al (2012) Scenario analysis of nutrient removal from municipal wastewater by microalgal biofilms. Water 4:460–473
79. Plastics Europe (2019) Plastics—the facts 2018. Association of Plastics Manufacters, Plastics Europe
80. Campanale C, Massarelli C, Savino I et al (2020) A detailed review study on potential effects of microplastics and additives of concern on human health. Int J Environ Res Public Health 17:1212
81. Toussaint B, Raffael B, Angers-Loustau A et al (2019) Review of micro and nanoplastic contamination in the food chain. Food Addit Contam Part a 36:639–673
82. Laycock B, Halley P, Pratt S et al (2013) The chemomechanical properties of microbial polyhydroxyalkanoates. Prog Polym Sci 38:536–583
83. Gahlawat G (2019) Production strategies for commercialization of PHA. In: Polyhydroxyalkanoates biopolymers. Springer Briefs in Molecular Science. Springer, Cham
84. Kourmentza C, Plácido J, Venetsaneas N et al (2017) Recent advances and challenges towards sustainable polyhydroxyalkanoate (PHA) production. Bioengineering 4:55
85. Fra-Vázquez A, Palmeiro-Sánchez T, del Río ÁV, Mosquera-Corral A (2020) Transformation of organic contamination from wastewater into bioplastics (polyhydroxyalkanoate) by microorganisms. In: Olivares JA, Puyo D, Melero JA, Dufou J (eds) Wastewater treatment residues as resources for biorefinery products and biofuels. Elsevier, pp 415–433.
86. Wang X, Bengtsson S, Oehmen A et al (2019) Application of dissolved oxygen (DO) level control for polyhydroxyalkanoate (PHA) accumulation with concurrent nitrification in surplus municipal activated sludge. New Biotechnol 50:37–43
87. Oliveira C, Silva C, Carvalho G, Reis MAM (2017) Strategies for efficiently selecting PHA producing mixed microbial cultures using complex feedstocks: feast and famine regime and uncoupled carbon and nitrogen availabilities. New Biotechnol 37:69–79

88. Reis M, Albuquerque M, Villano M, Majone M (2011) Mixed culture processes for polyhydroxyalkanoate production from agro-industrial surplus/wastes as feedstocks. In: Moo-Young M, Fava F, Agathos S (eds) Comprehensive biotechnology, Second Edi. Academic Press, Burlington, pp 669–683
89. Albuquerque MGE, Torres CAV, Reis MAM (2010) Polyhydroxyalkanoate (PHA) production by a mixed microbial culture using sugar molasses: effect of the influent substrate concentration on culture selection. Water Res 44:3419–3433
90. Jiang Y, Marang L, Tamis J et al (2012) Waste to resource: converting paper mill wastewater to bioplastic. Water Res 46:5517–5530
91. Balaji S, Gopi K, Muthuvelan B (2013) A review on production of poly β hydroxybutyrates from cyanobacteria for the production of bio plastics. Algal Res 2:278–285
92. Carpine R, Olivieri G, Hellingwerf KJ et al (2020) Industrial production of poly-β-hydroxybutyrate from CO_2: can cyanobacteria meet this challenge? Processes 8:1–23
93. Wang B, Xiong W, Yu J et al (2018) Unlocking the photobiological conversion of CO_2 to (*R*)-3-hydroxybutyrate in cyanobacteria. Green Chem 20:3772–3782
94. Liebergesell M, Hustede E, Timm A et al (1991) Formation of poly (3-hydroxyalkanoates) by phototrophic and chemolithotrophic bacteria. Arch Microbiol 155:415–421
95. Monroy I, Buitrón G (2020) Production of polyhydroxybutyrate by pure and mixed cultures of purple non-sulfur bacteria: a review. J Biotechnol 317:39–47
96. McKinlay JB, Harwood CS (2010) Carbon dioxide fixation as a central redox cofactor recycling mechanism in bacteria. Proc Natl Acad Sci U S a 107:11669–11675
97. Koku H, Eroğlu İ, Gunduz U et al (2002) Aspects of the metabolism of hydrogen production by Rhodobacter sphaeroides. Int J Hydrogen Energy 27:1315–1329
98. Wu SC, Liou SZ, Lee CM (2012) Correlation between bio-hydrogen production and polyhydroxybutyrate (PHB) synthesis by Rhodopseudomonas palustris WP3-5. Bioresour Technol 113:44–50
99. Fradinho JC, Domingos JMB, Carvalho G et al (2013) Polyhydroxyalkanoates production by a mixed photosynthetic consortium of bacteria and algae. Bioresour Technol 132:146–153
100. Fradinho JC, Oehmen A, Reis MAM (2014) Photosynthetic mixed culture polyhydroxyalkanoate (PHA) production from individual and mixed volatile fatty acids (VFAs): substrate preferences and co-substrate uptake. J Biotechnol 185:19–27
101. Fradinho J, Oehmen A, Reis M (2013) Effect of dark/light periods on the polyhydroxyalkanoate production of a photosynthetic mixed culture. Bioresour Technol 148:474–479
102. Fradinho JC, Reis MAM, Oehmen A (2016) Beyond feast and famine: selecting a PHA accumulating photosynthetic mixed culture in a permanent feast regime. Water Res 105:421–428
103. INCOVER, https://incover-project.eu/technologies. Accesssed 15 June 2020.

Recent Advances in Enzymatic Conversion of Lignin to Value Added Products

Giang-Son Nguyen, Anna Sofia Lewin, Francesca Di Bartolomeo, and Alexander Wentzel

Abstract

Lignin is the second most abundant biopolymer and the largest reservoir of bio-based aromatic building blocks on earth that could replace numerous products currently produced from fossil feedstock with more sustainable, bio-based alternatives. However, its large-scale exploitation for value creation beyond its current main use in energy applications is hampered by its natural inertness and structural complexity and the highly denatured state of the bulk of technical lignin available as a by-product of large-scale processing of lignocellulose in the pulp and paper industry. In this section, we outline current paths of lignin valorization for value creation with a focus on enzymatic processing. Microbial sources and the current status of knowledge of the most important classes of ligninolytic enzymes are presented, as are options for new enzyme discovery and possible approaches to solve some of the key challenges of efficient enzymatic depolymerization of lignin to derive compounds directly marketable as value-added chemicals or usable as a feedstock for further upgrading by microbial metabolism to bio-based fuels, chemicals, and materials.

Keywords

Lignin · Ligninolytic enzymes · Lignin depolymerization · Peroxidase · Laccase · Etherase · Enzyme discovery · Lignin valorization

G.-S. Nguyen · A. S. Lewin · F. Di Bartolomeo · A. Wentzel (✉)
Department of Biotechnology and Nanomedicine, SINTEF Industry, Trondheim, Norway
e-mail: alexander.wentzel@sintef.no

J. J. G. Moura et al. (eds.), *Enzymes for Solving Humankind's Problems*,
https://doi.org/10.1007/978-3-030-58315-6_14

1 Lignin—Structure and Functions, Sources and Uses

1.1 Occurrence of Lignin and Its Composition and Natural Roles

Lignin is, after cellulose, the second most abundant biopolymer on earth, comprising about 10–25% of the total biomass of plants and estimated to account for 30% of all non-fossil organic carbon on earth [1]. It is a highly branched polymer, consisting of aromatic subunits that are connected into a complex network that crosslinks cellulose and hemicellulose in the plant cell wall of softwood, hardwood, and other non-herbaceous plants (Fig. 1). As integral part of lignocellulose, lignin gives trees their rigidity and structure (e.g., [2, 3]), enabling them to grow to considerable heights and sizes.

Lignin is built from a combination of three aromatic phenylpropanoid units, i.e., guaiacyl (G), syringyl (S) and *p*-hydroxyphenyl (H) propanoid, derived from the monolignols coniferyl alcohol, sinapyl alcohol, and p-coumaryl alcohol, respectively, assembled via reactive radical intermediates under presumed involvement of enzymes such as laccases and peroxidases. The aromatic monomers are thereby linked by C–C or ether bonds into a complex 3D structure, a process often referred to as lignification [4, 5]. The ratio of the different monomers and the different connecting bonds vary greatly, depending on both plant type and structure within the plant. Hence there is no uniform 'lignin structure', but rather a spectrum of diverse variants [6–9]. Polymerized lignin is deposited in the plant cell wall where, besides structural function, it provides protection against invading pathogens [4]. In addition, its hydrophobicity facilitates the transport of water and nutrients through the plant's vascular system in both wood and bark.

1.2 Types and Sources of Lignin

The spectrum of lignins can be divided into (i) native lignin, referring to lignin within the lignocellulose structures of plants without any alterations, and (ii) technical/processed/ pretreated lignin, extracted from plant biomass or recovered from industrial processes [7, 9] (Fig. 1). Technical lignins are primarily derived from industrial pulping processes, including kraft, sulfite, and soda pulping. However, also Organosolv lignin and hydrolysis lignin are included under this category [4, 10]. Kraft lignin is a by-product of the kraft process, i.e., a traditional method used in pulp and paper production. Here, the woody biomass is treated with NaOH and Na_2S at high temperature (150–170 °C), resulting in breakage of the ether bonds and conversion of the complex rigid structures into smaller lignin fragments (alkali-soluble lignin). This process typically results in solubility of up to 90% of the lignin content. The liquidous mixture is then often referred to as 'black liquor', from which highly condensed lignin can be recovered by precipitation upon treatment with acid to a pH below 5.0 [7]. In contrast to the kraft process, sulfite

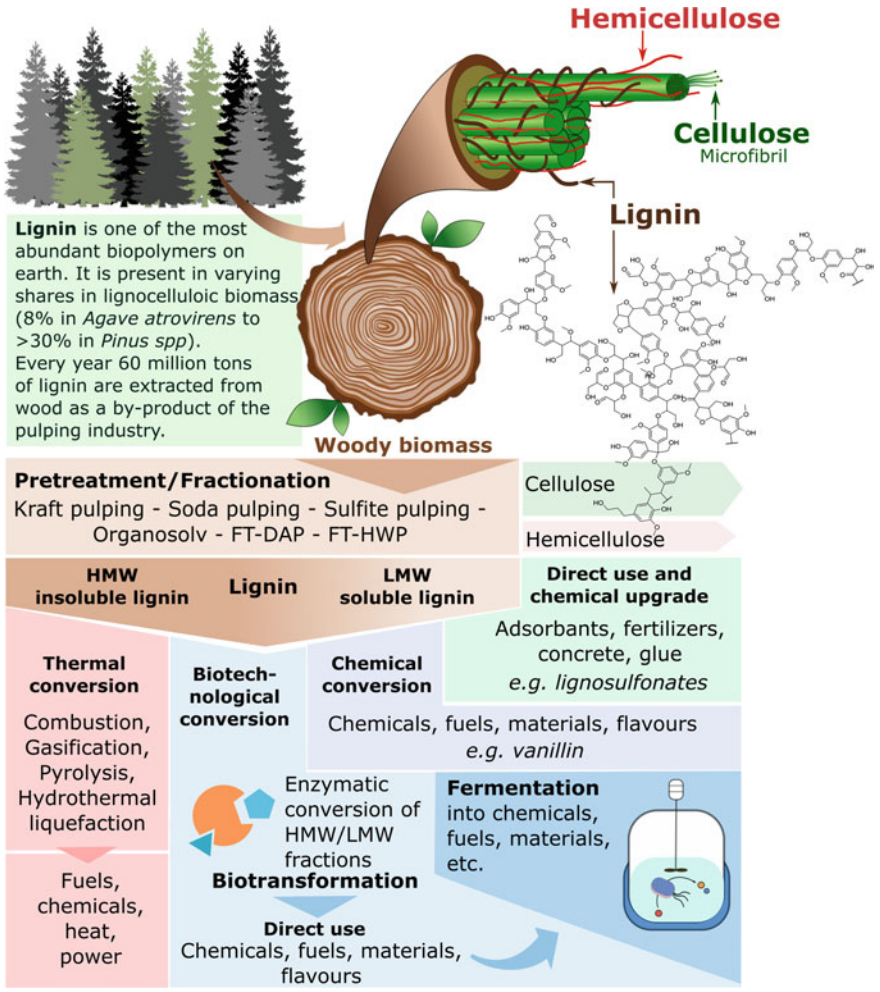

Fig. 1 Schematic overview of lignin occurrence in woody biomass, processing routes, and uses of lignin and lignin components in bio-based products. HMW/LMW—high/low molecular weight; FT-DAP—flow-through diluted acid pre-treatment; FT-HWP—flow-through diluted water pre-treatment

pulping is performed at a low pH (i.e., pH 1.5–5), using metal sulfites, generated by reaction of sulfur dioxide with alkali metal or alkaline earth hydroxides, and leading to acid-catalyzed cleavage of the ether bonds in lignin. This results in lignosulfonates that are soluble and therefore can be separated from the cellulose fibers and used in a range of different marketable products. Soda pulping involves cooking of lignocellulosic biomass with sodium hydroxide at similar temperatures and with similar effects on the lignin as kraft pulping. Also here, the fragmented, albeit sulfur-free lignin can be recovered from the spent liquid at low pH.

Organosolv lignin is a type of lignin recovered from biomass in the absence of sulfur through the treatment with organic solvent such as ethanol, methanol, acetic acid or ketone, at low pH [11]. The use of organic solvents for lignin extraction has the benefit of generating lignin with high purity and quality with minimal amounts of cellulose and the ether bonds largely intact. In addition, absence of sulfur compounds prevents the formation of organosulfur compounds, that in the case of lignins from kraft and sulfite pulping can inhibit subsequent (bio)catalytic processing [12]. The prevalence of native lignin and the absence of sulfur compounds renders this process advantageous for a greater biomass utilization towards high-value products. Usually, the cellulose and the hemicellulose fraction can be more efficiently employed in further processes, whilst the lignin is more accessible for enzymatic depolymerization into low molecular weight compounds for direct transformation into products or as a feedstock in fermentation (Fig. 1).

Hydrolysis lignin is a result of inefficient enzymatic processing of lignocellulose for bioethanol production and generally contains lignin, cellulose and oligosaccharides [7]. It often contains nitrogen but is free from sulfur and in principle represents native lignin. Fast pyrolysis [7, 9, 10] converts lignin (or lignocellulose) into bio-oil. Upon addition of water to bio-oil, a water-insoluble fraction is formed, called pyrolytic lignin, which in turn also can be recovered and further purified using organic solvents to remove ash and other inorganic compounds. In contrast to the other types of technical lignin, pyrolytic lignin is generated by repolymerization of lignin oligomers during the pyrolysis process.

1.3 Lignin Valorization and Added Value of Lignin Derived Products

Lignin is a polymer with high energy content due to its high C/O ratio and the largest reservoir of bio-based aromatic building blocks on earth. Despite of this, lignin is still an underutilized resource, mainly due to challenges in its valorization as value-added chemical linked to the poor qualities provided from the current bulk industrial processes that are targeting the cellulose portion of lignocellulose as the main product. Instead, lignin is typically used for heat and power generation [9, 13], although there exist options for the thermochemical conversion of lignin into syngas and bio-oil for deriving other products (Fig. 1). Controlled depolymerization of lignin is challenging due to its heterogeneity. In addition, the products from lignin depolymerization are highly diverse, which further complicates their processing and fractionation into homogenous products of marketable volumes. The most common chemical linkages between aromatic subunits in native lignin are β-O-4 ether linkages (representing almost 50% of all linkages), together with β-5, β-1, β-β, 5–5, and 4-O-5 bonds, which are all challenging to break through traditional processing since radicals are formed that lead to C–C bond formation and repolymerization [4]. In addition, in technical lignins recovered from pulping processes, most of the β-O-4 ether linkages are broken and fragments recombined with highly inert C–C bonds. Due to the high energy content of the polymer,

degradation of lignin into phenolic compounds or mono-lignins requires high energy input. This is one of the reasons why lignin is often regarded to have a higher value as a fuel compared to its exploitation as feedstock for other uses [4].

There are different methods for lignin isolation, aiming at opening and degrading the lignin structure well enough to solubilize the resulting fragments in the pulping media. Once solubilized, these fragments can be separated from the cellulose [4, 8]. However, the pulping process leaves behind a large fraction of highly condensed, low-quality and low-value lignin. Still from there, different technical and/or (thermo)chemical processes, i.e., pyrolysis, gasification, hydrothermal liquefaction, oxidation, and combustion convert lignin into products that can be directly employed as, or further upgraded into other chemicals [4, 6]. The output from these processes are bio-oil, char, syngas (CO, H_2) and other gases (CO_2, CH_4), where char is primarily used for power generation, whilst the produced gases can be channeled into both production of chemicals and fuels (Fig. 1). Besides, combustion produces heat that can be utilized for power production. Both pyrolysis and oxidation lead to production of liquid bio-oil including chemicals like phenols, aldehydes and aliphatics, that can be further processed in conventional oil refineries.

Besides its breakdown, the lignin macropolymer can be chemically modified and used in the synthesis of polyurethanes, polyesters, epoxide resins and phenolic resins [4]. Polyurethanes are generated by addition of, e.g., diisocyanates and polyols to the macropolymer backbone, forming polyurethane groups that provide the materials with different physical properties dependent on the lignin content used in the process. Polyesters from lignin are used as the starting material in, e.g., different kinds of plastics. Epoxy resins are built from monomers with minimum one epoxide group and are a type of thermoset polymer typically used in coatings, electronic materials, and adhesives. Phenolic resins are also thermosets with similar applications. These are, however, generated by acid- or base-catalyzed polymerization of phenols and aldehydes, whereas the phenolic content of lignin can be used as the phenol source in this process.

Some processed/technical lignins (such as the lignosulfonates from the sulfite pulping process) can be used directly in applications such as production of plasticizers in concrete, emulsifiers/emulsion stabilizers, surfactants for pesticides, drilling muds, resins, fertilizers, and glues [8], and most of the lignin in commercial application today is used in the form of lignosulfonates [14]. However, they can also be processed further, resulting in mono-lignins such as phenol, vanillin, guaiacol, ferulate, caffeate and *p*-coumarate, which in turn have other applications [10, 14] (Fig. 1). They can be used directly as chemicals or further converted by biotransformation and/or fermentation to produce a wide range of chemicals, fuels, materials, and flavors employing microbial cell factories [4, 8]. It is highly desirable to utilize the aromatic components of lignin for the production of aromatic solvents, such as benzene, toluene, and xylene, which are still primarily produced from petroleum [4, 15]. However, this would require the aromatic monomers to be deoxygenated and isolated from lignin. Chemical processes for that purpose exist but have not yet been successfully applied to utilize the bulk of the complex lignin

polymer system. Currently, chemical products derived from lignin are still partly oxygenated, such as phenol and vanillin.

The Norwegian company *Borregaard*, often referred to as the world's most advanced integrated biorefinery based on lignocellulose, has a *LignoTech* branch, focusing on the exploitation of lignin and lignosulfonates from softwood biomass (primarily spruce) through pulping, sulfonation, and chemical processing. *Borregaard* is a leader in the production of vanillin as artificial vanilla flavor, which is derivable through the oxidation of lignosulfonates from softwood trees. In addition, *Borregaard LignoTech* produces additives for a large number of industrial and commercial applications such as concrete mixtures, pesticide dispersants, textile dyes, oil well drilling chemicals, batteries and ceramic products, road binders, and feed pellet additives. In many applications, these products offer a direct replacement of petroleum-based compounds with a renewable bio-based alternative.

The degradation of lignin in nature is primarily performed by specialized fungi and bacteria [8, 16] that generate more simple aromatic breakdown products from the complex lignin structures, making these accessible for further processing by themselves and/or other microbes. Enzymes play a key role in that process as further presented and discussed in Sect. 2. These aromatic low molecular weight fragments are thereby channeled into the cellular central carbon metabolism, generating molecules like acetyl-CoA and pyruvate after cleavage of the aromatic ring structures [8, 17], as further described in Sect. 5. For bio-based industrial conversion of the polysaccharide content of lignocellulose, the feedstock conversion is generally preceded by a thermochemical pre-treatment step to open the complex structure of the macro-polymer and render it more accessible for enzymatic degradation [16]. Pre-treatments in use are, e.g., acid treatment, steam explosion, hot water treatment, and ammonia treatments (Fig. 1). The pre-treatment used also affects the structure and the properties of the derivable lignin fraction, and hence its suitability for different valorization strategies and end-products. This, as well as the formation of inhibitors like organic acids and furans like furfural and hydroxymethyl furfural (HMF) [18] also has consequences for the kind and the efficiency of enzymatic processing of lignin.

2 Biocatalytic Depolymerization of Lignin

In nature, lignin is degraded by fungi and bacteria using mixtures of enzymes from different classes, including oxidoreductases (peroxidases, laccases) and lyases (etherases). These enzymes appear to assist the host organisms to degrade wood materials (depolymerization) and gain access to smaller phenolic compounds that can be further metabolized (mineralization) [19–21]. According to the eLignin database [22], the majority of organisms that are able to degrade, or showing activity on, natural or technical lignin have been isolated from soil and forest/wood samples. This is a predictable outcome given the abundant processes of biomass degradation taking place in such habitats. Another natural origin of microbial

isolates is the digestive tracts of insects such as termites and beetles, which are dominated by symbiotic bacteria [23]. Besides these natural settings, artificial environments such as compost, waste water sludges, and effluents from pulp and paper manufacturers are also rich sources of lignin degrading microorganisms, and enzymes [22]. It has been suggested that biological lignin degradation processes are a result of a microbial community's undertaking rather than the effort of a single organism or enzyme. Based on our current understanding, the process starts with the depolymerization of macropolymer lignin with the help of fungal and/or bacterial oxidoreductases such as lignin peroxidases (LiPs), manganese peroxidases (MnPs), versatile peroxidases (VPs), dye-decolorizing peroxidases (DyPs), multicopper oxidase (MCOs), and/or laccase. The aromatic compounds that are derived from the depolymerization step, including syringyl- (S), guaiacyl- (G), *p*-hydroxyphenyl (H) units of varying combinations, are subsequently funneled into different aromatic catabolism pathways. This step is usually referred to as mineralization and is carried out mostly by bacteria [17, 19, 22, 24] (see also Sect. 5). The focus of this section is on currently known enzyme families involved in the depolymerization step.

Previous studies on lignin-degrading enzymes have been focusing on wood-degrading fungi such as white-rot fungi and brown-rot fungi, mainly from Basidiomycota and Ascomycota and with representatives such as *Phanerochaete chrysosporium*, *Trametes versicolor*, and *Phlebia radiata*. Wood-rotting fungi occupy diverse ecological habitats. White-rot fungi are more frequent on hardwood material, while brown-rot fungi are more common on softwood or partially decayed wood materials [8, 19, 22, 25]. Brown-rot fungi mainly act on the cellulose part of lignocellulosic biomass and only degrade lignin partially, resulting in oxidized lignin [17, 21]. On the other hand, white-rot fungi have been found to be able to degrade lignin completely [8, 22]. Consequently, white-rot fungi are the source of the majority of ligninolytic enzymes reported and described in the literature so far. Besides fungi, another eukaryote reported to act on lignin substrates such as (modified) wheat straw and the lignin fraction from beechwood is the yeast *Candida maltosa*, even though the involved enzymes and process have not been fully unraveled [22]. A detailed overview of the most relevant species from which relevant ligninolytic enzymes have been isolated and characterized is given by Janusz et al. [21].

Recently, more lignin-degrading enzymes originating from bacteria have been discovered and studied. Bacterial species identified to degrade lignin belong to different phyla such as Firmicutes (*Bacillus* sp., *Paenibacillus* sp.), Proteobacteria (*Pseudomonas* sp., *Acinetobacter* sp., *Klebsiella* sp.), and Actinobacteria (*Streptomyces* sp., *Rhodococcus* sp., *Amycolatopsis* sp., *Nocardia* sp.) [8, 21] (Table 1). Among these three phyla, species from Proteobacteria, including α-, γ-, and δ-Proteobacteria, have most often been reported in literature to harbour enzymes acting on lignin [21, 26]. However, many such discoveries have also been made from species of the phylum Actinobacteria [21, 27–30]. A few putative laccase genes have been identified in archaeal species such as *Haloferax* sp.[22, 26], even though little is known about the functionalities of these enzymes. Table 1

Table 1 Selection of known microorganisms producing lignin-degrading enzymes (adapted from [8, 21, 22, 74, 75]). LiP, lignin peroxidases; MnP, manganese peroxidases; VP, versatile peroxidases (VPs); DyP, dye-peroxidases; Lac, laccase; Eth, β-etherase

Organism			Enzymes
Fungi	Basidiomycota	*Auricularia auricular-judae*	DyP [76]
		Agaricus bisporus	MnP [77, 78]
		Agrocybe praecox	MnP [79]
		Bjerkandera adusta	Lac, LiP, MnP, VP, DyP [80–83]
		Bjerkandera fumosa	VP [84]
		Ceriporiopsis subvermispora	MnP, Lac [85–87]
		Collybia dryophila	MnP [79]
		Dichomitus squalens	Eth [72]
		Marasmius quercophilus	MnP, Lac [88, 89]
		Nematoloma frowardii	MnP, Lac, LiP [90, 91]
		Panaeolus sphinctrinus	MnP [86]
		Phanerochaete chrysosporium	LiP, MnP [35, 91, 92]
		Phallus impudicus	MnP [90]
		Phanerochaete sordida	MnP, Lac [93]
		Pleurotus sp. *Bhutan*	MnP, Lac [94]
		Phlebia radiata	LiP, Lac [95–97]
		Phlebia tremellosa	LiP, Lac [98]
		Pleurotus eryngii	VP, Lac [99]
		Pleurotus ostreatus	VP, Lac [100, 101]
		Stropharia coronilla	MnP [102, 103]
		Stropharia rugosoannulata	MnP [102, 103]
		Trametes versicolor	MnP, Lac [81, 104]
		Trametes hirsuta	Lac [81, 105]
	Ascomycota	*Aspergillus nidulans*	Lac [106]
		Botrytis cinerea	Lac [107]
		Chaetomium thermophilum	Lac [108]
		Melanocarpus albomyces	Lac [109]
		Neurospora crassa	Lac [110]
		Pyricularia grisea	Lac [111]

(continued)

Table 1 (continued)

Organism			Enzymes
Bacteria	Firmicutes	*Bacillus atrophaeus*	Lac [112, 113]
		Bacillus amyloliquefaciens	Lac [114]
		Bacillus licheniformis	Lac [115]
		Bacillus pumilus	Lac [116]
		Bacillus subtilis	Lac [117, 118]
		Geobacillus sp.	Lac [119]
	Actinobacteria	*Amycolatopsis* sp.	DyP [112]
		Rhodococcus jostii	DyP [120]
		Steptomyces coelicolor	DyP, Lac [58]
		Thermobifida fusca	DyP [50]
		Steptomyces griseus	Lac [121]
		Steptomyces ipomoea	Lac [122]
		Steptomyces lavendulae	Lac [123]
	α-proteobacteria	*Azospirillum lipoferum*	Lac [124, 125]
		Novosphingobium spp.	Eth [73]
		Sinorhizobium meliloti	Lac [126]
		Sphingomonas paucimobilis	Eth [127, 128]
	γ-proteobacteria	*Escherichia coli*	DyP, Lac [129, 130]
		Pseudomonas spp.	MnP, Dyp, Lac [131–133]
	Deinococcus-Thermus	*Thermus thermophilus*	Lac [134]
Archaea	Euryarchaeota	*Haloferax volcanii*	Lac [135]
		Pyrobaculum aerophilum	Lac [136]

summarizes key microbial clades and species described to date as a source of ligninolytic enzymes.

Efforts in categorizing and organizing information on enzymes involved in microbial lignin degradation has led to the establishment of several databases. Notable examples are: (i) eLignin Microbial Database [22], focusing on intracellular conversions; (ii) Laccase and Multicopper Oxidase Engineering Database (LccED) [31] focusing mainly on multicopper oxidases and (iii) RedoxiBase [32] containing comprehensive databases of different peroxidase and other oxidoreductase classes such as superoxide dismutases, blue copper proteins, glutathione reductases, etc. Recently, lignin-degrading enzymes are being discovered at an increasing rate, thanks to the growing number of published genomes and metagenomes, the rapid advancements in bioinformatics, and the availability of low-cost computing power. For relevant approaches deployed in new enzyme discovery it is referred to Sect. 3. The next sub-sections cover the main enzyme classes found to be active on lignin and involved in its depolymerization. For an overview, see Fig. 2.

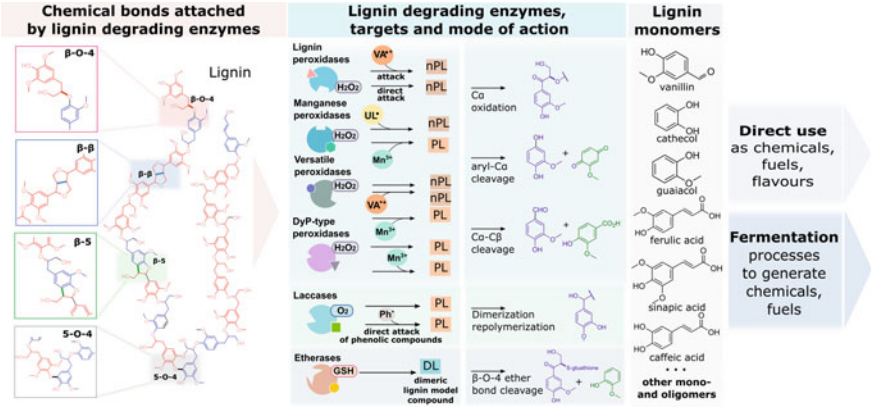

Fig. 2 Enzymatic conversion routes of lignin to value-added products. nPL—non-phenolic lignin; PL—phenolic lignin; VA—veratryl alcohol; UL—unsaturated lipids; Ph—phenolic compounds. For further details please refer to [19, 33]

2.1 Peroxidases

Peroxidases acting on lignin, including lignin peroxidases (LiPs), manganese peroxidases (MnPs), versatile peroxidases (VPs), and dye-peroxidases (DyPs), are the most studied enzymes involved in the process of lignin degradation. Lignin degrading peroxidases are mostly extracellular enzymes containing a heme prosthetic group in their active site (heme peroxidase superfamily) and require the supplement of hydrogen peroxide (H_2O_2) for their reactions (Fig. 3). These enzymes make use of small molecules like veratryl alcohol (VA), in case of LiPs, and unsaturated lipids (UL), in case of MnPs, as mediators for the depolymerization of lignin [19, 20]. While LiPs, MnPs, and VPs are grouped into Class II superfamily of heme peroxidases according to RedOxiBase [32], DyPs belong to a new family with no similarities in primary and tertiary structures with the formers [21, 34]. Additional enzymes, namely lignin-degrading auxiliary enzymes, such as glyoxal oxidase, aryl alcohol oxidase, or glucose dehydrogenase are necessary for degradation process through the oxidative generation of H_2O_2 [21, 35].

2.1.1 Lignin Peroxidases (LiPs) (EC 1.11.1.14)

LiPs have a higher redox potential than most other enzymes, such as horseradish peroxidase and laccases, and can oxidize non-phenolic aromatic substrates from lignin in many cases without the need for a mediator. The enzyme was first discovered in *P. chrysosporium* and later similar LiPs were found in other white-rot fungi, including *T. versicolor*, *P. radiata*, and *Bjerkandera* sp., as well as in Proteobacteria (*Acinetobacter* sp. and *Pseudomonas* sp.) and Actinobacteria (*Streptomyces* sp., *Norcadia* sp., *Rhodococcus* sp., etc.) [21, 24, 36, 37]. The catalytic cycle of LiP starts with the oxidation of the native ferric Fe(III) enzyme by H_2O_2 to

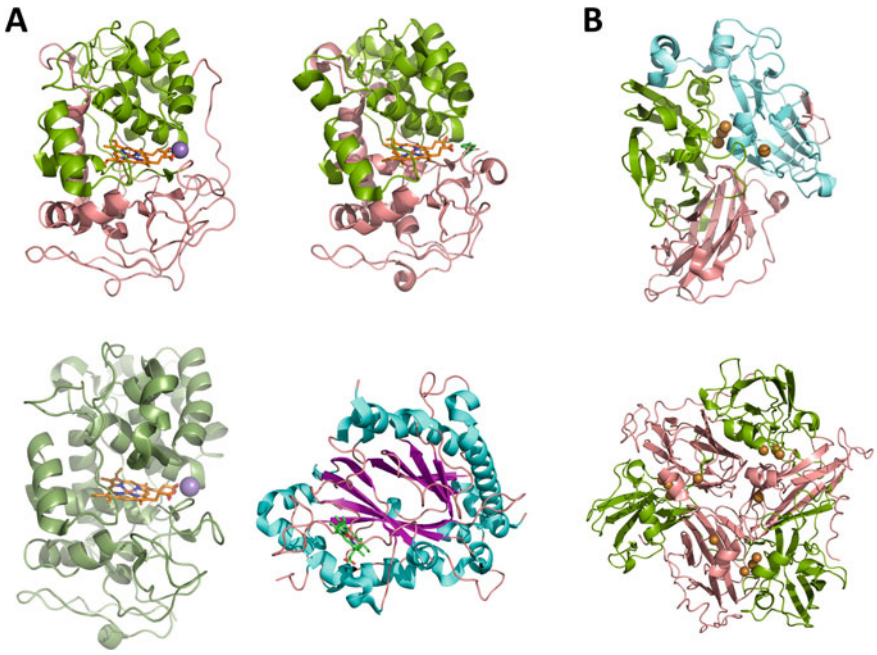

Fig. 3 Example structures of ligninolytic enzymes. **a** Peroxidases (from left to right, top to bottom): MnP from *Phanerochaete chrysosporium* (PDB ID: 1MNP), LiP from *Trametes cervina* (PDB ID: 3Q3U), VP from *Pleurotus eryngii* (PDB ID: 2BOQ), DyP from *Thermobifida fusca* YX (PDB ID: 5FW4); the heme group and the manganese ion of MnP and VP are indicated as ball and stick structures. **b** Multicopper oxidases/laccases (top to bottom): 1GYC—*Trametes versicolor* laccase, 3TAS—*Streptomyces coelicolor* small laccase SLAC; The copper ions of the active site are indicated as yellow balls

generate an oxo-ferryl intermediate [Fe(IV) = O^+] (compound I). In two consecutive steps of reduction of compound I, firstly compound II [Fe(IV) = O] is formed from compound I, receiving one electron from a reducing compound such as veratryl alcohol (VA). Then, compound II is reduced with another electron from the electron donor, regenerating the native enzyme and completing the catalytic cycle. The substrate scope of LiPs is broad, including phenolic aromatic compounds and non-phenolic lignin model compounds. VA, a non-phenolic compound, has been known to act as a redox mediator for LiPs due to its high redox potential and enables LiPs to act on substrates that normally cannot be oxidized by LiPs alone [36, 38].

Structurally, LiPs are two-domain globular glycoproteins consisting of eight main and some minor α-helices and β components. The heme complex group is interposed between a proximal and a distant domain. The structure is stabilized by four disulfide bonds, one Ca^{2+} binding site in each domain, and two glycosylation sites in the proximal domain [21, 24]. One residue on the surface of the LiP from

P. chrysosporium, W171, has been shown to have a major role in the catalysis of VA and other non-phenolic compounds through long-range electron transfer (LRET). The tryptophan residue is conserved in all LiPs, and exchanging the amino acid by site-directed mutagenesis (for example with a serine or phenylalanine), rendered the enzyme inactive [21, 36, 39]. Regarding recombinant production of LiPs, different LiP isoenzymes from *P. chrysosporium* have been expressed in different hosts such as *Escherichia coli* (with additional refolding and activation steps), *Saccharomyces cerevisiae* [40], and *Pichia methanolica* [24]. Using DNA shuffling, Ryu et al. [41 achieved variants of lignin peroxidase from *P. chrysosporium* with increased activity towards 2,4-dichlorophenol and an 89-fold increase in H_2O_2 stability. More recently, flow cytometry was applied to screen for a large mutant library (10^6) of *P. chrysosporium* lignin peroxidase H8 to obtain variants with higher tolerance to H_2O_2 [42]. One challenge of using LiPs for lignin depolymerization in vitro is the reverse reaction of (re-)polymerization happening at the same time. This could be overcome by methods for radical quenching and/or rapidly removing the low molecular weight phenolic products (see Sect. 4).

2.1.2 Manganese Peroxidases (MnPs) (EC 1.11.1.13)

MnP was originally discovered in the white-rot fungus *P. chrysosporium* and later also found in other Basidiomycota (*Panus tigrinus*, *Lenzites betulinus*, *Agaricus bisporus*, etc.), as well as in bacteria [21]. In the presence of H_2O_2, the enzyme oxidizes Mn^{2+} to Mn^{3+}, which then departs from the enzyme and is complexed by carboxylic acids (e.g., glycoxylate, malate, oxalate). The Mn^{3+} complexes behave like redox mediators and subsequently oxidize phenolic compounds from lignin [17, 21, 24]. Having lower redox potentials than LiPs [24] (see above), MnPs cannot oxidize non-phenolic compounds such as unsaturated fatty acids through the process called lipid peroxidation without mediators [20]. MnPs and LiPs share similarities in their tertiary structures as both are glycosylated two-domain globular proteins comprised of 11–12 α-helices with the heme group located in the middle and two Ca^{2+} binding sites [21, 24]. While the structures of LiPs are stabilized by four disulfide bridges, an additional disulfide bridge is found in MnPs in the C-terminal region [17, 20, 43].

Fungal MnPs such as the ones from *P. chrysosporium* have been successfully produced heterologously in *E. coli* and *Pichia pastoris* [24, 44]. Different attempts in protein engineering of MnPs have been carried out to improve thermostability by engineering a disulfide bond [45] or to increase the H_2O_2 stability by combinatorial mutagenesis [44].

2.1.3 Versatile Peroxidases (VPs) (EC 1.11.1.6)

A broad substrate scope, a high redox potential, and the combined molecular features of LiPs and MnPs have made the third family of ligninolytic heme peroxides gain the name versatile peroxidases (VP). So far, VPs have only been found in the species belonging to the genera *Pleurotus* and *Bjerkandera,* of which a VP from *Pleurotus eryngii* was the first VP enzyme described [21, 24, 36]. The catalytic

cycle of VPs is similar to that of LiPs. Due to having both, a manganese oxidation site like the one in MnPs and a surface catalytic tryptophan like in LiPs in their structures, VPs are able to oxidize not only lignin and compounds with high/medium redox potentials but also dyes such as Reactive Black 5 [21, 36, 46]. Studies on different LRET pathways of VP isoenzymes from *P. eryngii* have demonstrated the importance of the surface tryptophan residue, W164 in this case, for the ability of the enzyme to oxidize high redox aromatic substrates [47].

Heterologous production of VPs from *P. eryngii* has been successfully carried out in different types of hosts, including fungi (e.g., *P. chrysosporium* with the best yield around 300 mg/L, and *Pleurotus ostreatus*), filamentous fungi (*Emericella nidulans* and *Aspergillus niger*), yeasts (*S. cerevisiae*), and bacteria (*E. coli* BL21 (DE3), as thioredoxin fusion protein). Due to their substrate promiscuity, VPs are of high interest for industrial applications, leading to efforts in protein engineering to improve their stability and activity. To improve pH stability of the isoenzyme VPL2 from *P. eryngii*, a variant with the desired characteristic was obtained by site-directed mutagenesis guided by sequence alignment analysis and comparison of structures of the enzyme with the isoenzyme MnP4 from *P. ostreatus* [46]. A directed evolution strategy was employed to obtain variants of *P. eryngii* VP expressed in *S. cerevisiae* with higher tolerance against H_2O_2 and improved activity [21, 48].

2.1.4 Dye-Decolorizing Peroxidases (DyPs) (EC 1.11.1.19)

DyPs belong to a new heme peroxidase family that shares no similarity in sequence and structure with other families like LiPs, MnPs, and VPs. Though the first identified DyP is from the fungus *Bjerkandera adusta* and similar enzymes have later been found in other fungi such as *Irpex lacteus* and *Termitomyces albuminosus*, these enzymes are more commonly found in bacteria, notably in Proteobacteria (*Pseudomonas* spp.) and in Actinobacteria such as *Rhodococcus* spp. and *Thermobifida fusca* [21, 49]. Recently, the crystal structure of a DyP-type peroxidase from *Thermobifida fusca* (TfuDyP) was resolved. The enzyme itself showed activity against kraft lignin and a β-aryl ether lignin model compound [50]. Currently, DyPs are divided into four subfamilies in which type A enzymes are mostly extracellular bacterial enzymes having a Tat-dependent signal peptide. DyPs belonging to types B and C are putative cytoplasmic bacterial or fungal enzymes whose roles could be part of the intracellular metabolism, while type D DyPs are primarily from fungi [21, 49]. Recently, a new classification of DyPs has been suggested based on structural alignments that indicated only three classes, i.e., P (primitive)—former class B, I (intermediate)—former class A, and V (advanced)—former class C and D [34].

Owning their name to the ability of oxidizing various dyes, especially anthraquinone dyes, in addition to common peroxidase substrates at low pH, some DyPs apparently displayed ligninolytic activity towards lignin model compounds even though their role in the degradation of lignin in nature is still unclear [20, 49]. Some DyPs even exhibit promiscuous hydrolyzing or oxygenase activity [49]. The catalytic cycle of DyPs is not yet fully understood, but there is evidence of conserved

aspartate or arginine residues involved in the formation of compound I. Despite having low similarity among sequences of the family except for a highly conserved GXXDG motif, the general structure of DyPs shares common features as a two-domain protein with unique ferredoxin-like fold, comprising α-helices and anti-parallel β-sheets with the heme ligand located in between the domains. LRET was also suggested as the mechanism for DyPs to oxidize large substrates such as lignin [49].

Bacterial DyPs have been heterologously expressed in *E. coli*, which enables the improvement of expression yields and the possibility of protein engineering [49, 51]. A recent attempt of directed evolution of a bacterial DyP from *Pseudomonas putida* MET94 has led to a variant with significant improvement in activity towards 2,6-dimethoxyphenol and lignin model compounds, as well as higher optimal pH (pH 8.5) and increased tolerance to hydrogen peroxide [51].

2.2 Laccases (EC 1.10.3.2)

Laccases (benzenediol:oxygen oxidoreductases) belong to a diverse enzyme superfamily called multicopper oxidase (MCO), also including ascorbate oxidase, bilirubin oxidase, ferroxidase, nitrite reductase, and ceruloplasmin. A wide range of substrates can be oxidized by laccases through the four-electron reduction of dioxygen and the formation of two water molecules as byproducts [52, 53]. Biological functionalities of laccases are diverse, apart from lignin degradation, including cell wall formation, detoxification, morphogenesis, etc. Laccase enzymes are widespread and can be found in fungi, bacteria, plants, and insects [21, 52]. Ligninolytic fungal laccases have been abundantly found in Basidiomycetes, notably in white-rot fungi [24], while a limited number of bacterial laccases has been reported to be active towards lignin/depolymerized lignin and lignin model compounds, including enzymes from *Pseudomonas* spp., *Rhodococcus* spp., *Amycolatopsis* sp., and *Sphingobium* sp.[54]. Laccases from the white-rot fungus *T. versicolor*, CotA from *Bacillus* sp., and small laccase from *Streptomyces coelicolor* (SLAC) are notable enzymes that have been extensively studied. The redox potentials of laccases are lower than those of peroxidases (0.4–0.8 V instead of 0.8–1.2 V, respectively, versus normal hydrogen electrode (NHE)), and phenolic substrates with lower redox potentials can be oxidized directly by laccases. In the case of non-phenolic compounds with higher redox potentials or larger molecules such as lignin and lignin fragments, laccases can oxidize the substrates through small aromatic compounds acting as mediators (laccase-mediator-system—LMS). Fungal laccases generally have higher redox potentials than bacterial ones and can oxidize lignin substrates such as Kraft lignin without the need for mediators. The most prominent examples are the laccase isoenzymes from *T. versicolor* [55]. A comprehensive survey of the substrate scope of laccases and laccase-like MCOs can be found in a study by Reiss et al. [53], in which the activities of 11 laccases from plant, fungi, and bacteria were tested against more than 90 compounds.

Unlike peroxidases, laccases do not require H_2O_2 or any extra coenzyme for their reaction but oxygen, and instead of the heme prosthetic group, (at least) four copper atoms in the active site play key roles in the catalytic cycle [52, 56] (Fig. 3). The copper atoms are classified based on their spectroscopic features in which the type-1 copper (T1Cu) has a strong absorption at around 600 nm wavelength in the oxidized state, which accounts for the blue color of the purified enzymes. While the type-2 cooper (T2Cu) does not show substantial absorbance feature, the binuclear type-3 (T3Cu) copper sites exhibit a strong absorbance at 330 nm [52, 56]. The T2 copper and the binuclear T3 coppers form a tri-nuclear copper center (TNC) that locates around 13 Å apart from the T1 site. While the T1Cu is coordinated by two His, one Cys, and in many cases, another residue in the axial position (Met in bacterial/plant laccases or Phe/Leu in fungal laccases), the TNC coppers are coordinated by eight His residues, two for the T2Cu and three for each of the T3Cu [52, 56, 57]. The catalytic cycle of a laccase starts with the substrate oxidation taking place at the T1 site where four electrons of the corresponding reductant are donated to the resting oxidized (RO) form of the enzyme. To reduce all four Cu(II) atoms to Cu(I), the electrons first enter the T1 site and are further transferred to the TNC through the Cys-His pathway. A subsequent peroxide intermediate (PI) is then formed after the fully reduced TNC reacts with dioxygen followed by a decay of the PI to a native intermediate (NI) through cleavage of the O–O bond. The cycle is completed when the NI is slowly decaying to the RO form and with a H_2O molecule being released [52, 56].

Most of the fungal and bacterial laccases share the common structural feature of a globular, three β-barrel cupredoxin-like domain in which the T1Cu site is positioned in domain 1 and the TNC is located between domains 1 and 3. A small two-domain laccase from *Streptomyces coelicolor*, named SLAC, was first described by Machczynski et al. [58] whose structure was elucidated and further characterized by Skálová et al. [59] (PDB ID: 3CG8). SLAC's structure is composed of six domains that are arranged in the trimeric form of two-domain units. The T1Cu, in this case, is situated in domain 2, and all copper atoms of TNC are at the interface of domains 1 and 2. LccED, Laccase, and Multicopper Oxidase Engineering Database, has assembled the information about sequences and structures of SLAC-like laccases under the homologous family Hfam39 [31]. Many of the SLAC-like laccases have been found in Actinobacteria, which makes this phylum an interesting target for mining of new laccases for lignin degradation [27–29].

Challenges in using laccases for lignin depolymerization include low redox potentials, especially in many bacterial laccases, and the optimal setup of laccase-mediator systems (LMS). One approach to increase the redox potential of bacterial laccases is to exchange the weakly coordinating axial Met residue at the T1Cu site with non-coordinating Leu or Phe, which are more commonly found in fungal laccases [60]. One of the most studied bacterial laccases is CotA from *Bacillus* spp. which in nature is involved in the formation of pigment in the endospore's coat. The enzyme has been found to be highly thermostable and to have a broad substrate scope. Durao et al. [61] observed an increase of approximately

100 mV in the redox potential of the M520L and M520F variants of CotA from *Bacillus subtilis*, even though the mutated variants suffered from a decrease in catalytic activity. Targeting substrate specificity of CotA, Gupta et al. [62] obtained a variant with an increase of more than 100-fold towards 2,2′-amino-bis (3-ethylbenzothiazoline-6-sulfonic acid (ABTS, a model substrate of laccases and peroxidases) and with even higher thermostability using a combinatorial approach of rational design and directed evolution, focusing on the ABTS binding site of the enzyme. Another CotA from *Bacillus pumilus* was also evolved using targeted mutagenesis, resulting in variants with moderate increase in catalytic efficiency towards ABTS [63]. By removing a methionine-rich helical region of the MCO CueO from *E. coli*, resulting in a more accessible substrate binding site, Kataoka et al. [64] generated an enzyme variant with 30 times increased activity against ABTS. A recent breakthrough in genetical engineering of laccases came from MetGen Oy, a commercial enzyme producer, with the product MetZyme® LIGNO™, a lignin oxidase originated from bacteria that can function at pH 10–11 and at high temperature up to 70 °C [65]. Other types of laccases, including SLAC and fungal laccases, have also been subjected to protein engineering to increase catalytic efficiency, substrate scope, expression, thermostability, as well as pH and salt stability. Many more examples and approaches have been summarized in a recent comprehensive review [60], as well as a review of laccase-related patents from 2009 to 2019 [66].

An alternative to broaden the substrate scope of laccases is to improve the laccase-mediator system (LMS). A LMS of many fungal laccases and 1-hydroxy-benzotriazole (HOBt) has been shown to be able to delignify kraft pulp [67]. Other LMS consisting of *T. versicolor* laccase and ABTS or HOBt could oxidize a phenolic β-O-4 linked lignin dimer (guaiacylglycerol-β-guaiacyl ether, GBG) [68]. Natural laccase mediators originated from the lignin degradation process such as vanillin, syringaldehyde, acetosyringone, *p*-coumaric acid, acetovanillone, etc., have been studied intensively in LMS. A variety of synthetic substrates, namely ABTS, HOBt, promazine, phenothiazine, 2,2,6,6-tetramethylpiperidinyloxy or 2,2,6,6-tetramethylpiperidine 1-oxyl (TEMPO), have also been evaluated in different LMSs with the purpose of developing more affordable, effective, and stable systems [69, 70]. Recently, Albarrán-Velo et al. synthesized and evaluated nitrogenated derivatives of vanillin and syringaldehyde as mediators in LMS of two commercial laccases from *T. versicolor* and *Myceliophthora thermophila* [71].

A survey of the laccase-related patent landscape showed that 20% of the patented application is within lignin removal and modification, followed by 15% in biochemistry and biocatalysis, and 13% in pharma/cosmetics/agrochemicals [66]. Therefore, obtaining new laccases or laccase variants with high redox potentials and substrate scope through data mining or protein engineering coupled with effective mediators in new, low-cost LMS is of high interest for industrial applications of these enzymes.

2.3 Etherases

As β-O-4 ether bonds account for up to 80% of the lignin intermolecular bonds [7, 8], intracellular β-etherases in the β-aryl ether degradation pathway have recently gained attention as candidates for lignin degradation process. Several β-etherases belonging to the glutathione-*S*-transferase superfamily from bacterial species such as *Sphingobium* sp., *Novosphingobium* sp. and recently, one from the white-rot fungi *Dichomitus squalens*, have been characterized [7, 17, 72]. Currently, the number of characterized β-etherases is still limited, and the knowledge about the role and potential of these enzymes in lignin degradation is somewhat lacking. A recent study by Voß et al. [73] has shed more light on the diversity of bacterial β-etherases, and conserved motifs among the enzymes were identified. Using a peptide pattern recognition (PPR) approach for database mining, almost 100 novel putative β-etherase sequences were found by the authors, many of them outside the *Sphingomonadaceae* and *Erythrobacteraceae* families. A subset of 13 new β-etherases with confirmed etherase activity were further biochemically characterized [73]. This study has thereby triggered new possibilities for finding new β-etherases from genomic and metagenomics sequences based on sequence/motif homology searches using, for example, profile Hidden Markov Models (HMMs).

3 Discovery of New Ligninolytic Enzymes

Several routes are available and have been applied so far to discover ligninolytic enzymes from microbial biodiversity (Fig. 4). As presented above, fungi and bacteria have been the main source of such enzymes. In fact, most of the discoveries and enzyme descriptions reported to date are derived from single fungal or bacterial strain isolates or microbial consortia obtained from relevant natural environments (e.g., rotting trees, termite guts, compost piles, etc.), showing growth and/or ligninolytic activity on or in the presence of lignin (Table 1). In addition, strain collections existing in many research groups and containing taxa later described to be active on lignin (e.g., Actinobacteria), can be valuable sources to discover new ligninolytic enzymes. Suitable approaches in their discovery range from simple growth experiments (often long-term due to slow growth) on a broad spectrum of commercially available lignin substrates to advanced conversion assays of culture supernatants using lignin (native or technical) or lignin model substrates (e.g., veratryl alcohol, guaiacylglycerol-β-guaiacyl ether (GGE)) and detection of breakdown products by HPLC (increase in the low molecular weight fraction) or LC–MS (identification of specific aromatic mono- and oligomers) [137–147]. Through genome sequencing of active isolates and co-cultures, followed by bioinformatics-based assembly, annotation and prediction, gene candidates putatively encoding enzymes of known lignin-active enzyme families can be identified in silico. These are then (often in codon-optimized form) cloned in suitable expression systems for enzyme production, purification and functional assessment (see

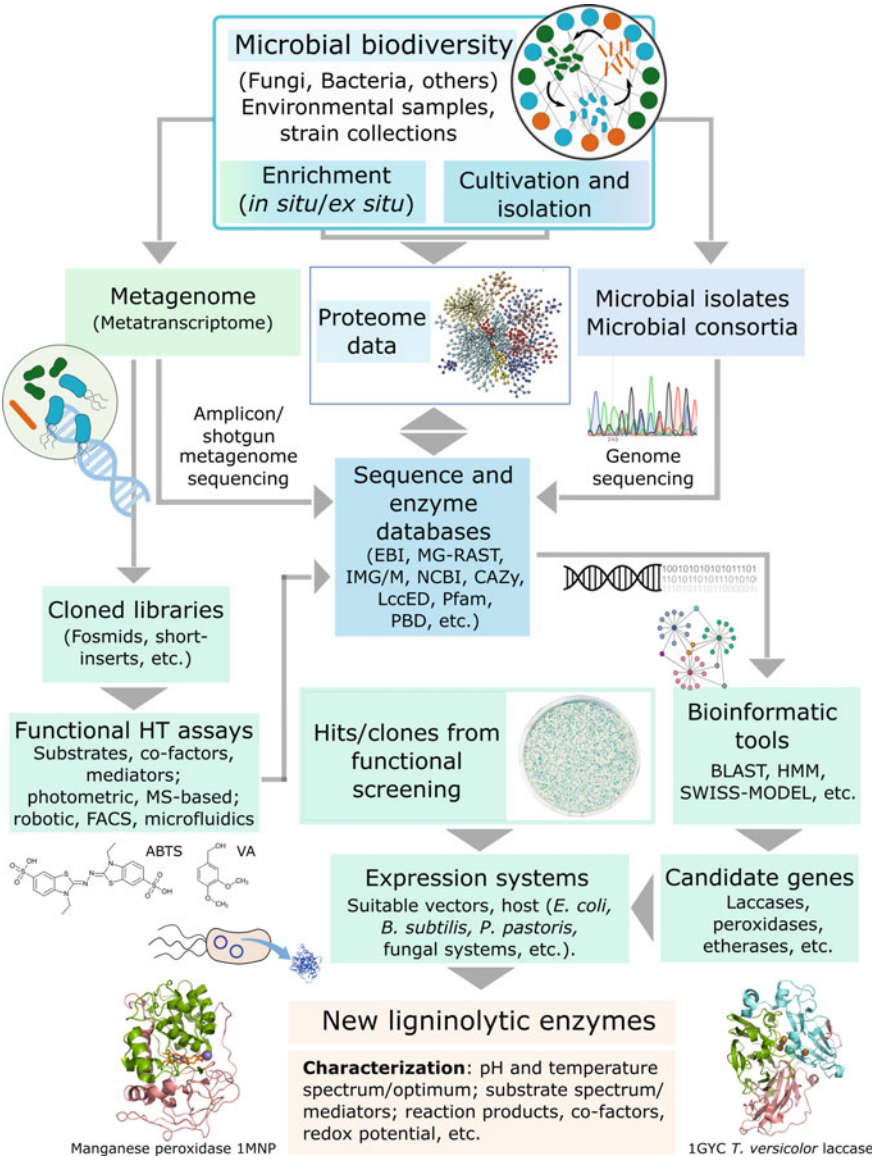

Fig. 4 Discovery pipelines for new ligninolytic enzymes involving cultivation dependent and -independent approaches, as well as sequence- and function-based screening. ABTS, (2,2′-azino-bis (3-ethylbenzothiazoline-6-sulfonic acid)); VA—veratryl alcohol. FACS—fluorescence-activated cell sorting

sub-sections in Sect. 2 for details and examples). Proteome analysis of lignin active culture supernatants can thereby be used as a tool that can accelerate the discovery process through integrating peptide signals with DNA sequence information.

In parallel to the discovery routes involving strain cultivation, in the past two decades enzyme discovery based on environmental metagenomes has developed into a powerful alternative approach to expand the spectrum of novel enzymes, including ligninolytic enzymes. For that route, capable of capturing the metabolic potential of the entire microbial biodiversity, including the vast majority of strains in an environment that cannot be readily cultivated in the lab (estimated to be regularly above 95% of all strains), total DNA of the microbial fraction of samples from a relevant environment is isolated. Suitable natural environments targeted for new ligninolytic enzymes thereby usually contain lignocellulose, like decaying wood, compost piles, animal intestinal content, etc., or represent artificial situations set up to specifically enrich for microbes capable of degrading lignin in situ (e.g., by means of microbial traps filled with lignin substrate and placed e.g. in a compost pile) or ex situ (e.g., IBIDI biofilm flow system inoculated with relevant environmental microbiomes and using lignin substrate as carbon source (manuscript of the authors in preparation). Metagenomic DNA can then be subjected to high-throughput (HT) sequencing. Approaches include, e.g., (i) 16S and 18S rRNA gene or ITS amplicon sequencing for determining the prokaryotic and eukaryotic consortium structure, respectively, (ii) shotgun DNA sequencing for determining the full metabolic potential of the microbial assemblage, and, (iii) if starting with cDNA, reverse-transcribed from total RNA, the metabolically active portion of the metagenome (i.e., metatranscriptome).

Metagenome sequences are regularly stored in public databases like EBI metagenomics, MG-RAST, and IMG/M, which are rapidly growing sources for bioinformatics-based in silico mining for new enzyme candidates of the lignin active families presented above. Important tools applied to utilize sequence-homology (e.g., BLAST), sequence signatures (e.g., profiles Hidden Markov Model (HMM)), and protein structure similarity (e.g., 3D-BLAST, SWISS-MODEL) and link to dedicated databases for relevant enzyme classes (NCBI, CAZy, LccED, eLignin, profiles HMM from Pfam, PDB, etc.) [22, 31, 32, 148]. As for the analysis of genomes, carefully in silico analyzed and selected candidate genes of putative lignin-active enzymes are then cloned in suitable expression systems for enzyme production, purification, and characterization. In silico approaches to discover new enzymes have lately improved a lot to more accurately predict enzyme function based on DNA sequence, increasing the chances of correct functional prediction of gene candidates. However, being dependent on previous results (sequences, annotations, structures), they fail to predict entirely new enzymes with no apparent homology to any existing database entries.

Here, functional metagenomics approaches are complementary as they are purely based on observable function. For functional screening, metagenomic DNA (or cDNA) is used for library cloning, with fosmid cloning or short insert fragment cloning into (broad host-range) expression vectors currently being the most popular techniques. Libraries are usually established in *E. coli* and then transferred to (a

variety of) relevant expression hosts likely to be able to express encoded genes and produce functional enzymes [149, 150]. A range of functional assays for different ligninolytic enzyme classes is available as described in the previous section, which can be adapted for high throughput use, e.g., in microtiter plate format on robotic HT screening workstations using colorimetric, absorbance or HT-MS analysis, or droplet-based screening using FACS or microfluidics based on fluorescence, absorption or light scattering as signals for sorting and isolating positive events (hits). After hit confirmation, identification of the gene(s) responsible for the observed phenotype is usually done by sequencing, sequence analysis, sub-cloning, and heterologous expression of gene candidates in a suitable host strain that can ideally also be used for the up-scaled production and purification of the new ligninolytic enzyme for the purpose of full characterization. This usually involves determination of the range and optimal conditions for enzyme function (e.g., pH, temperature), full substrate spectrum and obtained reaction products, effects of mediators and potential co-factors (also to be considered included in screening assays), redox potential, and ultimately protein structure.

4 Challenges of Enzymatic Lignin Depolymerization for Value-Added Products

As previously mentioned, lignin is a challenging substrate for targeted depolymerization by biocatalysis. In fact, in addition to providing structure and mechanical stability in higher plants, lignin serves the purpose of exactly preventing such decay from occurring in nature. Furthermore, technical processing of lignocellulose, like thermochemical pre-treatments or the pulping processes, have for a long time targeted a high quality of the polysaccharide fraction of the feedstock for the production of cellulose or later the generation of sugars for the biotechnological production of biofuels and bio-based chemicals, leaving the lignin fraction condensed, largely insoluble and chemically modified as a low-value side-product that can barely be used for anything else than thermochemical conversion into char, oil, gases, heat, and power [151]. Exceptions are the soluble lignosulfonates from sulfite pulping and derivable chemical products that play a role in value creation in integrated biorefineries connected to pulping processes. More recently, sulfur-free approaches, like Organosolv processes enable recovery of distinct fractions of cellulose, hemicellulose, and lignin of higher quality and therewith may provide a better basis for value creation beyond energy products from a larger fraction of lignin in the future, including by using enzymes. However, as most of the lignin produced today occurs in highly modified form, development and impact of enzymatic processes in this field are challenged by the need for processing a substrate that is highly recalcitrant and non-natural for enzymes that have not evolved to efficiently degrade it [36].

As presented in the previous section, much progress has been made in the discovery, characterization, heterologous production, and improvement of enzymes active on lignin, and the recent developments in the fields of metagenomics and bioinformatics, triggered by plunging prices for high throughput sequencing since the millennium, can be expected to accelerate this development. Except for the etherases, all ligninolytic enzyme families known today use oxidative radical chemistry for their function. This in principle allows their application also on the bulk of highly modified lignin from large-scale industrial applications, like pulp and paper, if leaving out the key complicating aspects of high condensation level (low share of cleavable ether bonds) and low solubility at enzyme relevant pH of these substrates, as well as the presence of inhibitors of enzyme function, contributing to low yields in enzymatic depolymerization. In any case and as also relevant for chemo-catalytic approaches of lignin depolymerization, this comes with the challenge of highly reactive intermediates that tend to react immediately with other fragments within the substrate mix, leading to re-polymerization in competition with lignin breakdown [152]. Also here, the condensation through the formation of highly resistive C–C linkages needs to be minimized to maintain the possibility of high yield recovery of desired LMW products. Besides the need for preventing similar effects already during biomass pre-treatment and lignin recovery alongside preserving the native, ether-bond rich lignin structure as much as possible, this can be achieved by chemical quenching or rapid physical removal of the reactive intermediates [10]. Chemical quenching can theoretically be achieved by scavengers that convert reactive intermediates to stable molecules before they can cross-link with other lignin fragments. Examples for scavengers explored in thermochemical lignin degradation are phenol, short-chain acids and alcohols, and formaldehyde [153–157]. However, the compatibility of such compounds with enzymatic lignin degradation processes needs to be carefully examined. Membrane technology separating lignin monomers close to their formation provides another option for achieving more efficient lignin depolymerization. In a recently published study involving commercial laccase from *Aspergillus* sp. (Novozym, 51,003), depolymerization into fragments below 1 kDa was effective in a bioreactor with in-situ membrane extraction of reactive fragments of lignin from the bulk medium, providing a first successful proof-of-concept of that approach against detrimental repolymerization [158].

It is clear from the above mentioned that the issue of low conversion yields from enzymatic depolymerization of lignin involves improvements on several levels. One key is that lignocellulose processing in an integrated biorefinery setting needs to take the quality of the lignin into consideration from the start and prevent as much as possible condensation and formation of recalcitrant C–C bonds at the steps of pre-treatment and fractionation. The resulting more native lignin then represents a much better substrate for both chemo- and biocatalytic depolymerization into low molecular weight compounds. This is particularly true for enzymes in environmental microorganisms that have evolved to efficiently attack lignin in its natural form as a source of carbon for their metabolism (see Sect. 4). The efficiency of natural enzymes already known or to be discovered in the future (obtained primarily

through screening on natural lignin) should, therefore, be much higher than on the majority of technical lignins available today. Enzyme and biocatalytic process engineering could then focus on achieving, e.g., tolerances to depolymerization conditions that maximize lignin solubility (e.g., high pH, methanol, ethanol) and minimize re-polymerization, i.e., the tolerance to relevant radical scavengers and optimal implementation in membrane reactors, recovering LMW compounds in parallel to the depolymerization reaction. Innovative membrane technology could thereby through enzyme stabilization, and recycling in addition, serve the need of minimizing enzyme production costs, which is an often referred to challenge in rendering biocatalytic processes economically viable [159]. Based on a more native and bio-accessible lignin substrate through prevention of condensation and other modifications, it can be expected that complexity of the resulting LMW fraction will be lowered. This would ultimately increase the portion of individual compounds in the degradation mix that can be isolated and marketed as high-value chemicals and/or provide a better feedstock for microbial conversion [10] to produce the broad spectrum of chemicals and materials known to be addressable by industrial biotechnology [8].

5 Microbial Lignin Valorization

As presented above, enzymatic ligninolysis by laccases and peroxidases derives monolignin products such as ferulate, *p*-coumarate, caffeate, vanillin, guaiacol, phenol, benzoate, cresol, catechol, syringate, and gallate. In addition to being marketable products themselves, they can be used by a broad range of microorganisms for the convergent transformation, the so-called funneling, into a smaller set of intermediate aromatic metabolites. The current most prominent funneling pathways comprise those towards protocatechuate, catechol, and gallate/3-*O*-methyl-gallate, involving enzymes like decarboxylases, *O*-demethylases, alcohol and aldehyde dehydrogenases, as well as acyl-CoA synthetases and -hydratases/lyases. Dependent on the position of ring-cleavage in meta- or ortho position by a range of different dioxygenases, the resulting muconate, and mesaconate derivatives have different entry points to microbial central carbon metabolism, as recently summarized in excellent review articles [8, 160]. From there, the whole toolbox of microbial hosts, metabolic engineering, systems biotechnology, and synthetic biology is available to target efficient production of fuels, chemicals and materials for a whole range of applications and markets [8]. Relevant fields of strain development include; (i) improving stress tolerance to process-relevant parameters, such as the presence of toxic compounds, extreme pH, high temperature, etc., by means of adaptive laboratory evolution (ALE) and/or reverse engineering, (ii) the general improvement of aromatic compound utilization through, e.g., extending the substrate spectrum and optimizing the conversion routes of aromatic catabolism and their regulation, and (iii) the establishment and improvement of the production of specific chemicals, materials, and fuels ([8], and

references therein). Particularly promising microbial platforms for lignin biotechnology, readily providing relevant aromatics catabolic pathways, natural robustness towards toxic substrates and proven suitability for industrial-scale biotechnology applications, are *P. putida* and *C. glutamicum*. Other platforms of natural degraders of aromatics with good chemical tolerance, e.g., from the clade of the Actinobacteria currently being explored, may also provide viable options in the future. As a key feature towards aromatic tolerance, optimizing the operation of aromatic catabolism at a high level has been suggested [8]. Important chemicals and materials currently being targeted by microbial conversion for production from lignin-derived mono-lignins include cis,cis-muconic acid, organic acids like pyruvate, lactate, and succinate, pyridine-related organic acids, the polymers polyhydroxyalkanoates (PHA) and nylon, lipids with prospects for biofuel application, as well as diverse flavor and fragrance compounds ([8], and references therein).

A common aspect to be considered in all these approaches, however, is the challenge of as of yet comparably low product titers from lignin-based compounds than from glucose or other common substrates. Rendering such processes competitive will, therefore, require a combination of strain engineering and evolution for optimal conversion into products and tolerances to inhibitors, as well as bioprocess development that minimizes inhibition by substrates, inhibitors, and products [160]. In the meantime, and with respect to the large bulk of water-insoluble, condensed lignin from current large-scale industrial lignocellulose processes that also in the future will be hardly usable for enzymatic and microbial utilization, the path of gasification followed by syngas fermentation might develop into a viable alternative for higher value creation form lignin using industrial biotechnology.

6 Conclusions and Outlook

The economic success of future lignocellulosic biorefineries is highly dependent on an efficient valorization of lignin, comprising a major share of its feedstock that is too valuable only to be used for low-value energy applications. This is, however, still challenged by the structural complexity of lignin and its heterogeneity due to its diverse sources and recovery processes. Much progress has lately been made towards better-exploiting lignin through depolymerization into a wide range of value-added products and their subsequent funneling into microbial production processes as documented by recent comprehensive reviews [8, 9, 160, 161]. However, despite of the considerable progress also on discovering and engineering new enzymes active on lignin and the microbial utilization of lignin-derived aromatic compounds into a broad spectrum of valuable products, biotechnological approaches meet great competition in thermochemical and chemo-catalytic approaches. The latter are rapidly developing in parallel, with the advantage of being more adaptable to the current mix of low-quality lignins available from established industrial processes. One important field of development is, therefore,

hybrid approaches of thermochemical and/or chemo-catalytic breakdown of lignin into a larger share of compounds that can be utilized for upgrading by microbial mineralization. This ranges from the production of bio-oils and subsequent microbial utilization of metabolizable compounds therein [162] to gasification of lignin into syngas and subsequent gas fermentation [163]. This will allow more of the lignin feedstock to be converted into products with a higher value than fuels, heat, and power. In the meantime, efforts need to be made to transition lignocellulose processing as it is still predominantly performed today towards better sustainability with respect to the use of toxic chemicals, energy consumption, and preserving value also in the lignin fraction, i.e., preserving as much as possible its native structure for controllable and sustainable depolymerization using enzymes. Developing a broad spectrum of enzymatic and biotechnological pathways to marketable products from lignin and demonstrating their economic viability will provide key arguments in this transition to more sustainable value creation from lignin using biocatalysis.

Acknowledgements This work was supported by the project OXYMOD of the Centre for Digital Life Norway (DLN) under Research Council of Norway grant number 269408, and the EU Horizon 2020 project MetaFluidics with grant agreement number 685474.

References

1. Leisola M, Pastinen O, Axe DD (2012) Lignin-designed randomness. BIO-Complexity 2012 (3). https://doi.org/10.5048/BIO-C.2012.3
2. Sanderson K (2011) Lignocellulose: a chewy problem. Nature 474(7352):S12–S14. https://doi.org/10.1038/474S012a
3. Phillips M (1934) The chemistry of lignin. Chem Rev 14(1):103–170. https://doi.org/10.1021/cr60047a005
4. Upton BM, Kasko AM (2016) Strategies for the conversion of lignin to high-value polymeric materials: review and perspective. Chem Rev 116(4):2275–2306. https://doi.org/10.1021/acs.chemrev.5b00345
5. Ralph J, Lapierre C, Boerjan W (2019) Lignin structure and its engineering. Curr Opin Biotechnol 56:240–249. https://doi.org/10.1016/j.copbio.2019.02.019
6. Li C, Zhao X, Wang A et al (2015) Catalytic transformation of lignin for the production of chemicals and fuels. Chem Rev 115(21):11559–11624. https://doi.org/10.1021/acs.chemrev.5b00155
7. Chio C, Sain M, Qin W (2019) Lignin utilization: a review of lignin depolymerization from various aspects. Renew Sustain Energy Rev 107:232–249. https://doi.org/10.1016/j.rser.2019.03.008
8. Becker J, Wittmann C (2019) A field of dreams: lignin valorization into chemicals, materials, fuels, and health-care products. Biotechnol Adv 37(6):107360. https://doi.org/10.1016/j.biotechadv.2019.02.016
9. Sun Z, Fridrich B, de Santi A et al (2018) Bright side of lignin depolymerization: toward new platform chemicals. Chem Rev 118(2):614–678. https://doi.org/10.1021/acs.chemrev.7b00588
10. Schutyser W, Renders T, Bosch SVd et al (2018) Chemicals from lignin: an interplay of lignocellulose fractionation, depolymerisation, and upgrading. Chem Soc Rev 47(3):852–908. https://doi.org/10.1039/C7CS00566K

11. Zakzeski J, Bruijnincx PCA, Jongerius AL et al (2010) The catalytic valorization of lignin for the production of renewable chemicals. Chem Rev 110(6):3552–3599. https://doi.org/10.1021/cr900354u
12. Shrotri A, Kobayashi H, Fukuoka A (2017) Catalytic conversion of structural carbohydrates and lignin to chemicals. In: Song C (ed) Advances in catalysis, vol 60. Academic, London, pp 59–123. https://doi.org/10.1016/bs.acat.2017.09.002
13. Linger JG, Vardon DR, Guarnieri MT et al (2014) Lignin valorization through integrated biological funneling and chemical catalysis. Proc Natl Acad Sci 111(33):12013–12018. https://doi.org/10.1073/pnas.1410657111
14. Holladay JE, White JF, Bozell JJ et al. (2007) Top value-added chemicals from biomass—volume II—results of screening for potential candidates from biorefinery lignin. https://doi.org/10.2172/921839
15. Guerriero G, Hausman J-F, Strauss J et al (2016) Lignocellulosic biomass: biosynthesis, degradation, and industrial utilization. Eng Life Sci 16(1):1–16. https://doi.org/10.1002/elsc.201400196
16. Chundawat SPS, Beckham GT, Himmel ME et al (2011) Deconstruction of lignocellulosic biomass to fuels and chemicals. Ann Rev Chem Biomol Eng 2(1):121–145. https://doi.org/10.1146/annurev-chembioeng-061010-114205
17. Bugg TDH, Ahmad M, Hardiman EM et al (2011) Pathways for degradation of lignin in bacteria and fungi. Nat Prod Rep 28(12):1883–1896. https://doi.org/10.1039/C1NP00042J
18. Jönsson LJ, Martín C (2016) Pretreatment of lignocellulose: formation of inhibitory by-products and strategies for minimizing their effects. Bioresour Technol 199:103–112. https://doi.org/10.1016/j.biortech.2015.10.009
19. Kamimura N, Sakamoto S, Mitsuda N et al (2019) Advances in microbial lignin degradation and its applications. Curr Opin Biotechnol 56:179–186. https://doi.org/10.1016/j.copbio.2018.11.011
20. Martínez AT, Camarero S, Ruiz-Dueñas. FJ et al (2018) Biological lignin degradation. In: Lignin valorization. Energy and environment series. pp 199–225. https://doi.org/10.1039/9781788010351-fp001
21. Janusz G, Pawlik A, Sulej J et al (2017) Lignin degradation: microorganisms, enzymes involved, genomes analysis and evolution. FEMS Microbiol Rev 41(6):941–962. https://doi.org/10.1093/femsre/fux049
22. Brink DP, Ravi K, Liden G et al (2019) Mapping the diversity of microbial lignin catabolism: experiences from the eLignin database. Appl Microbiol Biotechnol 103(10):3979–4002. https://doi.org/10.1007/s00253-019-09692-4
23. Ceja-Navarro JA, Karaoz U, Bill M et al (2019) Gut anatomical properties and microbial functional assembly promote lignocellulose deconstruction and colony subsistence of a wood-feeding beetle. Nat Microbiol 4(5):864–875. https://doi.org/10.1038/s41564-019-0384-y
24. Pollegioni L, Tonin F, Rosini E (2015) Lignin-degrading enzymes. FEBS J 282(7):1190–1213. https://doi.org/10.1111/febs.13224
25. Asina F, Brzonova I, Voeller K et al (2016) Biodegradation of lignin by fungi, bacteria and laccases. Bioresour Technol 220:414–424. https://doi.org/10.1016/j.biortech.2016.08.016
26. Tian JH, Pourcher AM, Bouchez T et al (2014) Occurrence of lignin degradation genotypes and phenotypes among prokaryotes. Appl Microbiol Biotechnol 98(23):9527–9544. https://doi.org/10.1007/s00253-014-6142-4
27. Saini A, Aggarwal NK, Sharma A et al (2015) Actinomycetes: a source of lignocellulolytic enzymes. Enzyme Res 2015:279381. https://doi.org/10.1155/2015/279381
28. Suriya J, Bharathiraja S, Manivasagan P et al (2016) Enzymes from rare actinobacterial strains. Adv Food Nutr Res 79:67–98. https://doi.org/10.1016/bs.afnr.2016.08.002
29. Fernandes TAR, Silveira WBd, Passos FML et al (2014) Laccases from Actinobacteria—what we have and what to expect. Adv Microbiol 04(06):285–296. https://doi.org/10.4236/aim.2014.46035

30. Majumdar S, Lukk T, Solbiati JO et al (2014) Roles of small laccases from Streptomyces in lignin degradation. Biochemistry 53(24):4047–4058. https://doi.org/10.1021/bi500285t
31. Sirim D, Wagner F, Wang L et al (2011) The laccase engineering database: a classification and analysis system for laccases and related multicopper oxidases. Database (Oxford) 2011: bar006. https://doi.org/10.1093/database/bar006
32. Savelli B, Li Q, Webber M et al (2019) RedoxiBase: a database for ROS homeostasis regulated proteins. Redox Biol 26:101247. https://doi.org/10.1016/j.redox.2019.101247
33. Bugg TDH, Williamson JJ, Rashid GMM (2020) Bacterial enzymes for lignin depolymerisation: new biocatalysts for generation of renewable chemicals from biomass. Curr Opin Chem Biol 55:26–33. https://doi.org/10.1016/j.cbpa.2019.11.007
34. Yoshida T, Sugano Y (2015) A structural and functional perspective of DyP-type peroxidase family. Arch Biochem Biophys 574:49–55. https://doi.org/10.1016/j.abb.2015.01.022
35. Levasseur A, Piumi F, Coutinho PM et al (2008) FOLy: an integrated database for the classification and functional annotation of fungal oxidoreductases potentially involved in the degradation of lignin and related aromatic compounds. Fungal Genet Biol 45(5):638–645. https://doi.org/10.1016/j.fgb.2008.01.004
36. Abdel-Hamid AM, Solbiati JO, Cann IK (2013) Insights into lignin degradation and its potential industrial applications. Adv Appl Microbiol 82:1–28. https://doi.org/10.1016/B978-0-12-407679-2.00001-6
37. Cragg SM, Beckham GT, Bruce NC et al (2015) Lignocellulose degradation mechanisms across the Tree of Life. Curr Opin Chem Biol 29:108–119. https://doi.org/10.1016/j.cbpa.2015.10.018
38. Wong DW (2009) Structure and action mechanism of ligninolytic enzymes. Appl Biochem Biotechnol 157(2):174–209. https://doi.org/10.1007/s12010-008-8279-z
39. Saez-Jimenez V, Rencoret J, Rodriguez-Carvajal MA et al (2016) Role of surface tryptophan for peroxidase oxidation of nonphenolic lignin. Biotechnol Biofuels 9:198. https://doi.org/10.1186/s13068-016-0615-x
40. Ryu K, Kang JH, Wang L et al (2008) Expression in yeast of secreted lignin peroxidase with improved 2,4-dichlorophenol degradability by DNA shuffling. J Biotechnol 135(3):241–246. https://doi.org/10.1016/j.jbiotec.2008.04.007
41. Ryu K, Hwang SY, Kim KH et al (2008) Functionality improvement of fungal lignin peroxidase by DNA shuffling for 2,4-dichlorophenol degradability and H_2O_2 stability. J Biotechnol 133(1):110–115. https://doi.org/10.1016/j.jbiotec.2007.09.008
42. Ilić Đurđić K, Ece S, Ostafe R et al (2020) Flow cytometry-based system for screening of lignin peroxidase mutants with higher oxidative stability. J Biosci Bioeng 129(6):664–671. https://doi.org/10.1016/j.jbiosc.2019.12.009
43. Sharma A (2020) Lignocellulolytic Enzymology. In: Aggarwal NK, Sharma A (eds) Water hyacinth: a potential lignocellulosic biomass for bioethanol. Springer International Publishing, Berlin, pp 21–35. https://doi.org/10.1007/978-3-030-35632-3_3
44. Miyazaki-Imamura C, Oohira K, Kitagawa R et al (2003) Improvement of H_2O_2 stability of manganese peroxidase by combinatorial mutagenesis and high-throughput screening using in vitro expression with protein disulfide isomerase. Protein Eng 16(6):423–428. https://doi.org/10.1093/protein/gzg054
45. Reading NS, Aust SD (2000) Engineering a disulfide bond in recombinant manganese peroxidase results in increased thermostability. Biotechnol Prog 16(3):326–333. https://doi.org/10.1021/bp0000151
46. Saez-Jimenez V, Fernandez-Fueyo E, Medrano FJ et al (2015) Improving the pH-stability of versatile peroxidase by comparative structural analysis with a naturally-stable manganese peroxidase. PLoS ONE 10(10):e0140984. https://doi.org/10.1371/journal.pone.0140984
47. Perez-Boada M, Ruiz-Duenas FJ, Pogni R et al (2005) Versatile peroxidase oxidation of high redox potential aromatic compounds: site-directed mutagenesis, spectroscopic and crystallographic investigation of three long-range electron transfer pathways. J Mol Biol 354 (2):385–402. https://doi.org/10.1016/j.jmb.2005.09.047

48. Garcia-Ruiz E, Gonzalez-Perez D, Ruiz-Dueñas FJ et al (2012) Directed evolution of a temperature-, peroxide- and alkaline pH-tolerant versatile peroxidase. Biochem J 441 (1):487–498. https://doi.org/10.1042/BJ20111199
49. Colpa DI, Fraaije MW, van Bloois E (2014) DyP-type peroxidases: a promising and versatile class of enzymes. J Ind Microbiol Biotechnol 41(1):1–7. https://doi.org/10.1007/s10295-013-1371-6
50. Rahmanpour R, Rea D, Jamshidi S et al (2016) Structure of *Thermobifida fusca* DyP-type peroxidase and activity towards Kraft lignin and lignin model compounds. Arch Biochem Biophys 594:54–60. https://doi.org/10.1016/j.abb.2016.02.019
51. Brissos V, Tavares D, Sousa AC et al (2017) Engineering a Bacterial DyP-type peroxidase for enhanced oxidation of lignin-related phenolics at alkaline pH. ACS Catalysis 7(5):3454–3465. https://doi.org/10.1021/acscatal.6b03331
52. Solomon EI, Heppner DE, Johnston EM et al (2014) Copper active sites in biology. Chem Rev 114(7):3659–3853. https://doi.org/10.1021/cr400327t
53. Reiss R, Ihssen J, Richter M et al (2013) Laccase versus laccase-like multi-copper oxidase: a comparative study of similar enzymes with diverse substrate spectra. PLoS ONE 8(6): e65633. https://doi.org/10.1371/journal.pone.0065633
54. Ravi K, Abdelaziz OY, Nöbel M et al (2019) Bacterial conversion of depolymerized Kraft lignin. Biotechnol Biofuels 12(1):56. https://doi.org/10.1186/s13068-019-1397-8
55. Bourbonnais R, Paice MG, Reid ID et al (1995) Lignin oxidation by laccase isozymes from *Trametes versicolor* and role of the mediator 2,2′-azinobis (3-ethylbenzthiazoline-6-sulfonate) in kraft lignin depolymerization. Appl Environ Microbiol 61(5):1876–1880
56. Jones SM, Solomon EI (2015) Electron transfer and reaction mechanism of laccases. Cell Mol Life Sci 72(5):869–883. https://doi.org/10.1007/s00018-014-1826-6
57. Zhu Y, Zhang Y, Zhan J et al (2019) Axial bonds at the T1 Cu site of *Thermus thermophilus* SG0.5JP17–16 laccase influence enzymatic properties. FEBS Open Bio 9 (5):986–995. https://doi.org/10.1002/2211-5463.12633
58. Machczynski MC, Vijgenboom E, Samyn B et al (2004) Characterization of SLAC: a small laccase from *Streptomyces coelicolor* with unprecedented activity. Protein Sci 13(9):2388–2397. https://doi.org/10.1110/ps.04759104
59. Skalova T, Dohnalek J, Ostergaard LH et al (2009) The structure of the small laccase from *Streptomyces coelicolor* reveals a link between laccases and nitrite reductases. J Mol Biol 385(4):1165–1178. https://doi.org/10.1016/j.jmb.2008.11.024
60. Mate DM, Alcalde M (2015) Laccase engineering: from rational design to directed evolution. Biotechnol Adv 33(1):25–40. https://doi.org/10.1016/j.biotechadv.2014.12.007
61. Durao P, Bento I, Fernandes AT et al (2006) Perturbations of the T1 copper site in the CotA laccase from *Bacillus subtilis*: structural, biochemical, enzymatic and stability studies. J Biol Inorg Chem 11(4):514–526. https://doi.org/10.1007/s00775-006-0102-0
62. Gupta N, Lee FS, Farinas ET (2010) Laboratory evolution of laccase for substrate specificity. J Mol Catal B: Enzym 62(3–4):230–234. https://doi.org/10.1016/j.molcatb.2009.10.012
63. Chen Y, Luo Q, Zhou W et al (2017) Improving the catalytic efficiency of *Bacillus pumilus* CotA-laccase by site-directed mutagenesis. Appl Microbiol Biotechnol 101(5):1935–1944. https://doi.org/10.1007/s00253-016-7962-1
64. Kataoka K, Komori H, Ueki Y et al (2007) Structure and function of the engineered multicopper oxidase CueO from *Escherichia coli*—deletion of the methionine-rich helical region covering the substrate-binding site. J Mol Biol 373(1):141–152. https://doi.org/10.1016/j.jmb.2007.07.041
65. Hämäläinen V, Grönroos T, Suonpää A et al (2018) Enzymatic processes to unlock the lignin value. Front Bioeng Biotechnol 6. https://doi.org/10.3389/fbioe.2018.00020
66. Zerva A, Simić S, Topakas E et al (2019) Applications of microbial laccases: patent review of the past decade (2009–2019). Catalysts 9(12). https://doi.org/10.3390/catal9121023

67. Bourbonnais R, Paice MG, Freiermuth B et al (1997) Reactivities of various mediators and laccases with kraft pulp and lignin model compounds. Appl Environ Microbiol 63 (12):4627–4632
68. Hilgers R, Vincken JP, Gruppen H et al (2018) Laccase/mediator systems: their reactivity toward phenolic lignin structures. ACS Sustain Chem Eng 6(2):2037–2046. https://doi.org/10.1021/acssuschemeng.7b03451
69. Canas AI, Camarero S (2010) Laccases and their natural mediators: biotechnological tools for sustainable eco-friendly processes. Biotechnol Adv 28(6):694–705. https://doi.org/10.1016/j.biotechadv.2010.05.002
70. Christopher LP, Yao B, Ji Y (2014) lignin biodegradation with laccase-mediator systems. Front Energy Res 2. https://doi.org/10.3389/fenrg.2014.00012
71. Albarrán-Velo J, López-Iglesias M, Gotor V et al (2017) Synthesis of nitrogenated lignin-derived compounds and reactivity with laccases. Study of their application in mild chemoenzymatic oxidative processes. RSC Adv 7 (80):50459–50471. https://doi.org/10.1039/c7ra10497a
72. Marinović M, Nousiainen P, Dilokpimol A et al (2018) Selective Cleavage of lignin β-O-4 aryl ether bond by β-etherase of the white-rot fungus *Dichomitus squalens*. ACS Sustain Chem Eng 6(3):2878–2882. https://doi.org/10.1021/acssuschemeng.7b03619
73. Voß H, Heck CA, Schallmey M et al (2020) Database mining for novel bacterial β-etherases, glutathione-dependent lignin-degrading enzymes. Appl Environ Microbiol 86(2). https://doi.org/10.1128/AEM.02026-19
74. Datta R, Kelkar A, Baraniya D et al (2017) Enzymatic degradation of lignin in soil: a review. Sustainability 9(7):1163. https://doi.org/10.3390/su9071163
75. Janusz G, Pawlik A, Świderska-Burek U et al (2020) Laccase properties, physiological functions, and evolution. Int J Mol Sci 21(3):966. https://doi.org/10.3390/ijms21030966
76. Linde D, Pogni R, Cañellas M et al (2015) Catalytic surface radical in dye-decolorizing peroxidase: a computational, spectroscopic and site-directed mutagenesis study. Biochem J 466(2):253–262. https://doi.org/10.1042/BJ20141211
77. Bonnen AM, Anton LH, Orth AB (1994) Lignin-degrading enzymes of the commercial button mushroom *Agaricus bisporus*. Appl Environ Microbiol 60(3):960–965
78. Lankinen VP, Bonnen AM, Anton LH et al (2001) Characteristics and N-terminal amino acid sequence of manganese peroxidase from solid substrate cultures of *Agaricus bisporus*. Appl Microbiol Biotechnol 55(2):170–176. https://doi.org/10.1007/s002530000509
79. Steffen KT, Hofrichter M, Hatakka A (2002) Purification and characterization of manganese peroxidases from the litter-decomposing basidiomycetes Agrocybe praecox and Stropharia coronilla. Enzyme Microb Technol 30(4):550–555. https://doi.org/10.1016/S0141-0229(01)00525-7
80. Bouacem K, Rekik H, Jaouadi NZ et al (2018) Purification and characterization of two novel peroxidases from the dye-decolorizing fungus *Bjerkandera adusta* strain CX-9. Int J Biol Macromol 106:636–646. https://doi.org/10.1016/j.ijbiomac.2017.08.061
81. Fukasawa Y, Osono T, Takeda H (2011) Wood decomposing abilities of diverse lignicolous fungi on nondecayed and decayed beech wood. Mycologia 103(3):474–482. https://doi.org/10.3852/10-246
82. Jong Ed, Field JA, de Bont JAM (1992) Evidence for a new extracellular peroxidase manganese-inhibited peroxidase from the white-rot fungus *Bjerkandera* sp. BOS 55. FEBS Lett 299(1):107–110. https://doi.org/10.1016/0014-5793(92)80111-S
83. Liers C, Arnstadt T, Ullrich R et al (2011) Patterns of lignin degradation and oxidative enzyme secretion by different wood- and litter-colonizing basidiomycetes and ascomycetes grown on beech-wood. FEMS Microbiol Ecol 78(1):91–102. https://doi.org/10.1111/j.1574-6941.2011.01144.x
84. Grąz M, Jarosz-Wilkołazka A (2011) Oxalic acid, versatile peroxidase secretion and chelating ability of *Bjerkandera fumosa* in rich and limited culture conditions. World J Microbiol Biotechnol 27(8):1885–1891. https://doi.org/10.1007/s11274-010-0647-5

85. Enoki M, Watanabe T, Nakagame S et al (1999) Extracellular lipid peroxidation of selective white-rot fungus *Ceriporiopsis subvermispora*. FEMS Microbiol Lett 180(2):205–211. https://doi.org/10.1016/S0378-1097(99)00487-5
86. Heinzkill M, Bech L, Halkier T et al (1998) Characterization of laccases and peroxidases from wood-rotting fungi (Family Coprinaceae). Appl Environ Microbiol 64(5):1601–1606. https://doi.org/10.1128/AEM.64.5.1601-1606.1998
87. Lobos S, Larraín J, Salas L et al (1994) Isoenzymes of manganese-dependent peroxidase and laccase produced by the lignin-degrading basidiomycete *Ceriporiopsis subvermispora*. Microbiology (Reading, England) 140(Pt 10):2691–2698. https://doi.org/10.1099/00221287-140-10-2691
88. Dedeyan B, Klonowska A, Tagger S et al (2000) Biochemical and molecular characterization of a laccase from *Marasmius quercophilus*. Appl Environ Microbiol 66(3):925–929. https://doi.org/10.1128/aem.66.3.925-929.2000
89. Steffen KT, Cajthaml T, Šnajdr J et al (2007) Differential degradation of oak (*Quercus petraea*) leaf litter by litter-decomposing basidiomycetes. Res Microbiol 158(5):447–455. https://doi.org/10.1016/j.resmic.2007.04.002
90. Gramss G, Kirsche B, Voigt K-D et al (1999) Conversion rates of five polycyclic aromatic hydrocarbons in liquid cultures of fifty-eight fungi and the concomitant production of oxidative enzymes. Mycol Res 103(8):1009–1018. https://doi.org/10.1017/S0953756298008144
91. Jarosz-Wilkołazka A, Kochmańska-Rdest J, Malarczyk E et al (2002) Fungi and their ability to decolourize azo and anthraquinonic dyes. Enzyme Microb Technol 30(4):566–572. https://doi.org/10.1016/S0141-0229(02)00022-4
92. Kirk TK, Farrell RL (1987) Enzymatic "combustion": the microbial degradation of lignin. Annu Rev Microbiol 41(1):465–501. https://doi.org/10.1146/annurev.mi.41.100187.002341
93. Sugiura T, Yamagishi K, Kimura T et al (2009) Cloning and homologous expression of novel lignin peroxidase genes in the white-rot fungus *Phanerochaete sordida* YK-624. Biosci Biotechnol Biochem 73(8):1793–1798. https://doi.org/10.1271/bbb.90152
94. Lang E, Eller G, Zadrazil F (1997) Lignocellulose decomposition and production of ligninolytic enzymes during interaction of white rot fungi with soil microorganisms. Microb Ecol 34(1):1–10. https://doi.org/10.1007/s002489900029
95. Arora DS, Gill PK (2001) Effects of various media and supplements on laccase production by some white rot fungi. Bioresour Technol 77(1):89–91. https://doi.org/10.1016/S0960-8524(00)00114-0
96. Baldrian P (2006) Fungal laccases—occurrence and properties. FEMS Microbiol Rev 30(2):215–242. https://doi.org/10.1111/j.1574-4976.2005.00010.x
97. Orth AB, Royse DJ, Tien M (1993) Ubiquity of lignin-degrading peroxidases among various wood-degrading fungi. Appl Environ Microbiol 59(12):4017–4023
98. Vares T, Niemenmaa O, Hatakka A (1994) Secretion of ligninolytic enzymes and mineralization of 14C-ring-labelled synthetic lignin by three *Phlebia tremellosa* strains. Appl Environ Microbiol 60(2):569–575
99. Akpinar M, Urek RO (2014) Extracellular ligninolytic enzymes production by *Pleurotus eryngii* on agroindustrial wastes. Prep Biochem Biotechnol 44(8):772–781. https://doi.org/10.1080/10826068.2013.867870
100. Arora DS, Sandhu DK (1987) Decomposition of angiospermic wood sawdust and laccase production by two Pleurotus species. J Basic Microbiol 27(4):179–184. https://doi.org/10.1002/jobm.3620270402
101. Salame TM, Knop D, Levinson D et al (2012) Release of *Pleurotus ostreatus* versatile-peroxidase from Mn^{2+} repression enhances anthropogenic and natural substrate degradation. PLoS ONE 7(12):e52446. https://doi.org/10.1371/journal.pone.0052446
102. Gramss G, Ziegenhagen D, Sorge S (1999) Degradation of soil humic extract by wood- and soil-associated fungi, bacteria, and commercial enzymes. Microb Ecol 37(2):140–151. https://doi.org/10.1007/s002489900138

103. Kabiersch G, Rajasärkkä J, Ullrich R et al (2011) Fate of bisphenol A during treatment with the litter-decomposing fungi *Stropharia rugosoannulata* and *Stropharia coronilla*. Chemosphere 83(3):226–232. https://doi.org/10.1016/j.chemosphere.2010.12.094
104. Hatakka A (1994) Lignin-modifying enzymes from selected white-rot fungi: production and role from in lignin degradation. FEMS Microbiol Rev 13(2–3):125–135. https://doi.org/10.1111/j.1574-6976.1994.tb00039.x
105. Selinheimo E, Kruus K, Buchert J et al (2006) Effects of laccase, xylanase and their combination on the rheological properties of wheat doughs. J Cereal Sci 43(2):152–159. https://doi.org/10.1016/j.jcs.2005.08.007
106. Kurtz MB, Champe SP (1982) Purification and characterization of the conidial laccase of *Aspergillus nidulans*. J Bacteriol 151(3):1338–1345
107. Marbach I, Harel E, Mayer AM (1984) Molecular properties of extracellular *Botrytis cinerea* laccase. Phytochemistry 23(12):2713–2717. https://doi.org/10.1016/0031-9422(84)83001-0
108. Chefetz B, Chen Y, Hadar Y (1998) Purification and characterization of laccase from *Chaetomium thermophilium* and Its role in humification. Appl Environ Microbiol 64 (9):3175–3179
109. Kiiskinen L-L, Viikari L, Kruus K (2002) Purification and characterisation of a novel laccase from the *Ascomycete melanocarpus albomyces*. Appl Microbiol Biotechnol 59(2–3):198–204. https://doi.org/10.1007/s00253-002-1012-x
110. Froehner SC, Eriksson K-E (1974) Purification and properties of *Neurospora crassa* laccase. J Bacteriol 120(1):458–465
111. Iyer G, Chattoo BB (2003) Purification and characterization of laccase from the rice blast fungus. Magnaporthe grisea FEMS Microbiol Lett 227(1):121–126. https://doi.org/10.1016/S0378-1097(03)00658-X
112. de Gonzalo G, Colpa DI, Habib MHM et al (2016) Bacterial enzymes involved in lignin degradation. J Biotechnol 236:110–119. https://doi.org/10.1016/j.jbiotec.2016.08.011
113. Narnoliya LK, Agarwal N, Patel SN et al (2019) Kinetic characterization of laccase from *Bacillus atrophaeus*, and its potential in juice clarification in free and immobilized forms. J Microbiol 57(10):900–909. https://doi.org/10.1007/s12275-019-9170-z
114. Wang H, Huang L, Li Y et al (2020) Characterization and application of a novel laccase derived from *Bacillus amyloliquefaciens*. Int J Biol Macromol 150:982–990. https://doi.org/10.1016/j.ijbiomac.2019.11.117
115. Koschorreck K, Schmid RD, Urlacher VB (2009) Improving the functional expression of a *Bacillus licheniformis* laccase by random and site-directed mutagenesis. BMC Biotechnol 9:12. https://doi.org/10.1186/1472-6750-9-12
116. Reiss R, Ihssen J, Thöny-Meyer L (2011) *Bacillus pumilus* laccase: a heat stable enzyme with a wide substrate spectrum. BMC Biotechnol 11:9. https://doi.org/10.1186/1472-6750-11-9
117. Hullo M-F, Moszer I, Danchin A et al (2001) CotA of *Bacillus subtilis* Is a copper-dependent laccase. J Bacteriol 183(18):5426–5430. https://doi.org/10.1128/JB.183.18.5426-5430.2001
118. Martins LO, Soares CM, Pereira MM et al (2002) Molecular and biochemical characterization of a highly stable bacterial laccase that occurs as a structural component of the *Bacillus subtilis* endospore coat. J Biol Chem 277(21):18849–18859. https://doi.org/10.1074/jbc.M200827200
119. Jeon S-J, Park J-H (2020) Refolding, characterization, and dye decolorization ability of a highly thermostable laccase from *Geobacillus* sp. JS12. Protein Expr Purif 173:105646. https://doi.org/10.1016/j.pep.2020.105646
120. Roberts JN, Singh R, Grigg JC et al (2011) Characterization of dye-decolorizing peroxidases from *Rhodococcus jostii* RHA1. Biochemistry 50(23):5108–5119. https://doi.org/10.1021/bi200427h
121. Endo K, Hayashi Y, Hibi T et al (2003) Enzymological characterization of EpoA, a laccase-like phenol oxidase produced by *Streptomyces griseus*. J Biochem 133(5):671–677. https://doi.org/10.1093/jb/mvg086

122. Molina-Guijarro JM, Pérez J, Muñoz-Dorado J et al (2009) Detoxification of azo dyes by a novel pH-versatile, salt-resistant laccase from *Streptomyces ipomoea*. Int Microbiol 12 (1):13–21. https://doi.org/10.2436/20.1501.01.77
123. Suzuki T, Endo K, Ito M et al (2003) A thermostable laccase from *Streptomyces lavendulae* REN-7: purification, characterization, nucleotide sequence, and expression. Biosci Biotechnol Biochem 67(10):2167–2175. https://doi.org/10.1271/bbb.67.2167
124. Diamantidis G, Effosse A, Potier P et al (2000) Purification and characterization of the first bacterial laccase in the rhizospheric bacterium *Azospirillum lipoferum*. Soil Biol Biochem 32 (7):919–927. https://doi.org/10.1016/S0038-0717(99)00221-7
125. Givaudan A, Effosse A, Faure D et al (1993) Polyphenol oxidase in *Azospirillum lipoferum* isolated from rice rhizosphere: Evidence for laccase activity in non-motile strains of *Azospirillum lipoferum*. FEMS Microbiol Lett 108(2):205–210. https://doi.org/10.1111/j.1574-6968.1993.tb06100.x
126. Pawlik A, Wójcik M, Rułka K et al (2016) Purification and characterization of laccase from *Sinorhizobium meliloti* and analysis of the lacc gene. Int J Biol Macromol 92:138–147. https://doi.org/10.1016/j.ijbiomac.2016.07.012
127. Masai E, Katayama Y, Nishikawa S et al (1999) Characterization of *Sphingomonas paucimobilis* SYK-6 genes involved in degradation of lignin-related compounds. J Ind Microbiol Biotechnol 23(4–5):364–373. https://doi.org/10.1038/sj.jim.2900747
128. Picart P, de María PD, Schallmey A (2015) From gene to biorefinery: microbial β-etherases as promising biocatalysts for lignin valorization. Front Microbiol 6. https://doi.org/10.3389/fmicb.2015.00916
129. Grass G, Rensing C (2001) CueO is a multi-copper oxidase that confers copper tolerance in *Escherichia coli*. Biochem Biophys Res Commun 286(5):902–908. https://doi.org/10.1006/bbrc.2001.5474
130. Liu X, Yuan Z, Wang J et al (2017) Crystal structure and biochemical features of dye-decolorizing peroxidase YfeX from *Escherichia coli* O157 Asp143 and Arg232 play divergent roles toward different substrates. Biochem Biophys Res Commun 484(1):40–44. https://doi.org/10.1016/j.bbrc.2017.01.081
131. Kalyani DC, Phugare SS, Shedbalkar UU et al (2011) Purification and characterization of a bacterial peroxidase from the isolated strain *Pseudomonas* sp. SUK1 and its application for textile dye decolorization. Ann Microbiol 61(3):483–491. https://doi.org/10.1007/s13213-010-0162-9
132. Lambertz C, Ece S, Fischer R et al (2016) Progress and obstacles in the production and application of recombinant lignin-degrading peroxidases. Bioengineered 7(3):145–154. https://doi.org/10.1080/21655979.2016.1191705
133. McMahon AM, Doyle EM, Brooks S et al (2007) Biochemical characterisation of the coexisting tyrosinase and laccase in the soil bacterium *Pseudomonas putida* F6. Enzyme Microb Technol 40(5):1435–1441. https://doi.org/10.1016/j.enzmictec.2006.10.020
134. Miyazaki K (2005) A hyperthermophilic laccase from *Thermus thermophilus* HB27. Extremophiles 9(6):415–425. https://doi.org/10.1007/s00792-005-0458-z
135. Uthandi S, Saad B, Humbard MA et al (2010) LccA, an Archaeal laccase secreted as a highly stable glycoprotein into the extracellular medium by *Haloferax volcanii*. Appl Environ Microbiol 76(3):733–743. https://doi.org/10.1128/AEM.01757-09
136. Fernandes AT, Damas JM, Todorovic S et al (2010) The multicopper oxidase from the archaeon *Pyrobaculum aerophilum* shows nitrous oxide reductase activity. FEBS J 277 (15):3176–3189. https://doi.org/10.1111/j.1742-4658.2010.07725.x
137. Alcalde M, Bulter T (2003) Colorimetric assays for screening laccases. In: Arnold FH, Georgiou G (eds) Directed enzyme evolution: screening and selection methods. Methods in molecular biology™. Humana Press, Totowa, pp 193–201. https://doi.org/10.1385/1-59259-396-8:193

138. Casciello C, Tonin F, Berini F et al (2017) A valuable peroxidase activity from the novel species *Nonomuraea gerenzanensis* growing on alkali lignin. Biotechnol Rep 13:49–57. https://doi.org/10.1016/j.btre.2016.12.005
139. Chen Y-r, Sarkanen S, Wang Y-Y (2012) Lignin-degrading enzyme activities. In: Himmel ME (ed) Biomass conversion. Humana Press, Totowa, pp 251–268. https://doi.org/10.1007/978-1-61779-956-3_21
140. Kosa M, Ragauskas AJ (2012) Bioconversion of lignin model compounds with oleaginous Rhodococci. Appl Microbiol Biotechnol 93(2):891–900. https://doi.org/10.1007/s00253-011-3743-z
141. Lupoi JS, Singh S, Parthasarathi R et al (2015) Recent innovations in analytical methods for the qualitative and quantitative assessment of lignin. Renew Sustain Energy Rev 49:871–906. https://doi.org/10.1016/j.rser.2015.04.091
142. Morreel K, Dima O, Kim H et al (2010) Mass spectrometry-based sequencing of lignin oligomers. Plant Physiol 153(4):1464–1478. https://doi.org/10.1104/pp.110.156489
143. Prothmann J, Spégel P, Sandahl M et al (2018) Identification of lignin oligomers in Kraft lignin using ultra-high-performance liquid chromatography/high-resolution multiple-stage tandem mass spectrometry (UHPLC/HRMSn). Anal Bioanal Chem 410(29):7803–7814. https://doi.org/10.1007/s00216-018-1400-4
144. Reale S, Di Tullio A, Spreti N et al (2004) Mass spectrometry in the biosynthetic and structural investigation of lignins. Mass Spectrom Rev 23(2):87–126. https://doi.org/10.1002/mas.10072
145. Saito Y, Tsuchida H, Matsumoto T et al (2018) Screening of fungi for decomposition of lignin-derived products from Japanese cedar. J Biosci Bioeng 126(5):573–579. https://doi.org/10.1016/j.jbiosc.2018.05.001
146. Soden DM, O'Callaghan J, Dobson ADW (2002) Molecular cloning of a laccase isozyme gene from *Pleurotus sajor-caju* and expression in the heterologous *Pichia pastoris* host. Microbiology 148(12):4003–4014. https://doi.org/10.1099/00221287-148-12-4003
147. Tekere M, Mswaka AY, Zvauya R et al (2001) Growth, dye degradation and ligninolytic activity studies on Zimbabwean white rot fungi. Enzyme Microb Technol 28(4):420–426. https://doi.org/10.1016/S0141-0229(00)00343-4
148. Levasseur A, Drula E, Lombard V et al (2013) Expansion of the enzymatic repertoire of the CAZy database to integrate auxiliary redox enzymes. Biotechnol Biofuels 6(1):41. https://doi.org/10.1186/1754-6834-6-41
149. Lewin A, Lale R, Wentzel A (2017) Expression platforms for functional metagenomics: emerging technology options beyond *Escherichia coli*. In: Charles TC, Liles MR, Sessitsch A (eds) Functional metagenomics: tools and applications. Springer International Publishing, Cham, pp 13–44. https://doi.org/10.1007/978-3-319-61510-3_2
150. López-Mondéjar R, Algora C, Baldrian P (2019) Lignocellulolytic systems of soil bacteria: a vast and diverse toolbox for biotechnological conversion processes. Biotechnol Adv 37(6):107374. https://doi.org/10.1016/j.biotechadv.2019.03.013
151. Kumar A, Anushree KJ et al (2020) Utilization of lignin: a sustainable and eco-friendly approach. J Energy Inst 93(1):235–271. https://doi.org/10.1016/j.joei.2019.03.005
152. Zeng J, Mills MJL, Simmons BA et al (2017) Understanding factors controlling depolymerization and polymerization in catalytic degradation of β-ether linked model lignin compounds by versatile peroxidase. Green Chem 19(9):2145–2154. https://doi.org/10.1039/C6GC03379B
153. Okuda K, Umetsu M, Takami S et al (2004) Disassembly of lignin and chemical recovery—rapid depolymerization of lignin without char formation in water–phenol mixtures. Fuel Process Technol 85(8):803–813. https://doi.org/10.1016/j.fuproc.2003.11.027
154. Shuai L, Amiri MT, Questell-Santiago YM et al (2016) Formaldehyde stabilization facilitates lignin monomer production during biomass depolymerization. Science 354(6310):329–333. https://doi.org/10.1126/science.aaf7810

155. Gosselink RJA, Teunissen W, van Dam JEG et al (2012) Lignin depolymerisation in supercritical carbon dioxide/acetone/water fluid for the production of aromatic chemicals. Bioresour Technol 106:173–177. https://doi.org/10.1016/j.biortech.2011.11.121
156. Toledano A, Serrano L, Labidi J (2012) Organosolv lignin depolymerization with different base catalysts. J Chem Technol Biotechnol 87(11):1593–1599. https://doi.org/10.1002/jctb.3799
157. Brittain AD, Chrisandina NJ, Cooper RE et al (2018) Quenching of reactive intermediates during mechanochemical depolymerization of lignin. Catal Today 302:180–189. https://doi.org/10.1016/j.cattod.2017.04.066
158. Steinmetz V, Villain-gambier M, Klem A et al (2020) In-situ extraction of depolymerization products by membrane filtration against lignin condensation. Bioresour Technol 311:123530. https://doi.org/10.1016/j.biortech.2020.123530
159. Sheldon RA, Brady D (2018) The limits to biocatalysis: pushing the envelope. Chem Commun 54(48):6088–6104. https://doi.org/10.1039/C8CC02463D
160. Xu Z, Lei P, Zhai R et al (2019) Recent advances in lignin valorization with bacterial cultures: microorganisms, metabolic pathways, and bio-products. Biotechnol Biofuels 12 (1):32. https://doi.org/10.1186/s13068-019-1376-0
161. Kim KH, Kim CS (2018) Recent efforts to prevent undesirable reactions from fractionation to depolymerization of lignin: toward maximizing the value from lignin. Front Energy Res 6. https://doi.org/10.3389/fenrg.2018.00092
162. Davis K, Rover MR, Salvachúa D et al (2019) Promoting microbial utilization of phenolic substrates from bio-oil. J Ind Microbiol Biotechnol 46(11):1531–1545. https://doi.org/10.1007/s10295-019-02208-z
163. Liakakou ET, Vreugdenhil BJ, Cerone N et al (2019) Gasification of lignin-rich residues for the production of biofuels via syngas fermentation: comparison of gasification technologies. Fuel 251:580–592. https://doi.org/10.1016/j.fuel.2019.04.081

Enzymatic Production of Bioactive Peptides from Whey Proteins: Their Active Role and Potential Health Benefits

Alexandra F. A. Salvado, Jorge H. Leitão, and Luis P. Fonseca

Abstract

The primary function of dairy proteins is to provide amino acids to young mammals, being also an essential source of food protein for adults. Besides, milk proteins also confer potential health benefits in the form of bioactive peptides released into the intestine during the digestive process. These bioactive peptides perform regulatory activities in the human body, playing a relevant role in health maintenance. These bioactive peptides have relatively short amino acid sequences (2–30) and are functionally inactive within the structure of the protein parent molecules. Bioactive peptides as additives in "functional foods" are produced in vitro by digestive and microbial enzymes, from fermentation processes or during the processing of protein foods. However, when they are present in a mixture with other peptides, their behavior and properties can be hidden due to antagonistic and or synergistic effects. For this reason, the concentration and purification of bioactive peptides are required before their final formulation. In this chapter, we describe the enzymatic processes involved in the in vitro production of bioactive peptides with particular relevance for those originating from milk and whey proteins. Examples of bioactive peptides used as anticancer, antidiabetic, antihypertensive, antimicrobial, antioxidant, immunomodulatory, and opioid properties are illustrated.

Keywords

Whey proteins · Protein hydrolysis · Proteases · Bioactive peptides · Health benefits

A. F. A. Salvado · J. H. Leitão · L. P. Fonseca (✉)
Bioengineering Department, Instituto Superior Técnico, Institute for Bioengineering and Biosciences, University of Lisbon, Lisbon, Portugal
e-mail: luis.fonseca@tecnico.ulisboa.pt

J. J. G. Moura et al. (eds.), *Enzymes for Solving Humankind's Problems*,
https://doi.org/10.1007/978-3-030-58315-6_15

1 Bioactive Peptides

Peptides are a chain of amino acids covalently linked to each other by peptide bonds. Peptides have shown to have a broad spectrum of activities, such as regulation and biological functions that bring benefits to human health, as well as applications at the level of research, clinical diagnosis, and even at the industrial scale.

Several synthetic peptides have been designed and today are used as antigens, substrates or enzyme inhibitors, in vitro diagnostic probes, affinity ligands of solid supports, and components of molecular electronic devices. Other peptides are released from natural proteins or synthesized by chemical or enzymatic processes, playing an important role in applications in the areas of health and nutrition and medicinal therapy. Peptides that show biological activities are bioactive peptides. When compared to synthetic drugs, peptides with therapeutic or nutraceutical functions have several advantages, such as high activity and specificity, low toxicity, and lower accumulation in human tissues [1].

A large number of bioactive peptides contain peptide chains composed of 2–30 amino acids. For example, aspartame, a dipeptide constituted by one L-aspartic acid and an L-phenylalanine, is mostly used as an artificial sweetener in food and beverages. Other longer peptides show an extensive range of biological activities such as in the regulation of metabolism, cell proliferation, cellular communication, immune system response, hormonal secretion, cell defense, among many others [2]. These bioactive peptides that represent a specific fragment of the primary sequence of animal or vegetable proteins revealed to be suitable as food additives due to their properties as antihypertensive, antioxidant, antimicrobial, among many others.

Several individual steps are involved in the bioactive peptides production and identification starting by the initial choice of a protein source, the release of peptides from protein parent molecules, their isolation and purification before their biological activity assay, and final determination of their amino acid sequence (Fig. 1).

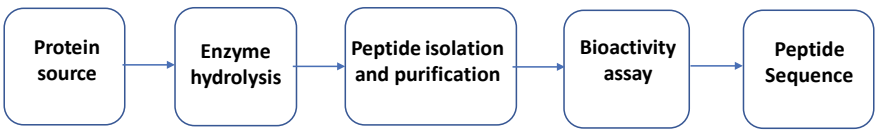

Fig. 1 Schematic diagram of the usual strategy involved in the classical enzymatic production and identification of bioactive peptides

2 Protein Source and Research of Bioactive Peptides

The production of bioactive peptides currently in the market starts with the choice of a protein source followed by hydrolysis with the release of bioactive peptides from the primary sequence of the native proteins. The main precursors of bioactive peptides are mainly proteins of animal origin such as meat, milk (casein and serum proteins), eggs, although proteins from plant sources are also in use, such as soybean proteins, wheat, rice, and others [3]. Recently, considerably more attention has also been devoted to research and testing of new sources of proteins such as fish residues, sponges, algae, and mollusks. Ishak and Sarbon [4] tested the production of bioactive peptides by hydrolysis of shortfin scad (*Decapterus macrosoma*) waste residues with endogenous proteases and addition of Alcalase. Another possible source of these peptides is the design and biosynthesis by recombinant host microorganisms. The most recent studies in this field include the expression of a specific sequence of a peptide by algae in recombinant proteins, being the bioactive peptide released after protein digestion [5]. However, hydrolysis of caseins and whey proteins are the primary sources and references for the discovery of bioactive peptides after the screening of their biological activity [6].

Milk consists of two heterogeneous families of proteins, one insoluble composed of caseins (80% w/w) and the other containing soluble proteins such as serum proteins (20% w/w). Caseins in the milk are organized in micelles and are composed of four caseins: α_{s1} (40%), α_{s2} (10%), β (36%), and k (14%). Whey proteins are a sub-product of cheese making. Whey proteins are constituted mainly by serum proteins, rich in human-essential amino acids, in particular of amino acids with branched side chains, and containing amino acids with sulfur residues [7]. The protein profile of whey proteins includes β-lactoglobulin (β-LG, for short), α-lactoalbumin (α-LA), immunoglobulins (IG), bovine serum albumin (BSA), bovine lactoferrin (BLF), lactoperoxidase (LP), and glycomacropeptides (GMP) [8].

The whey protein concentrate (WPC) is obtained by ultrafiltration (UF) from acid or sweet whey proteins. The pH of acid whey is equal to or less than 5.1, resulting from the addition of an acidic agent to milk, while the pH of sweet whey is equal to or greater than 5.6 obtained after enzymatic coagulation of milk. On the other hand, nowadays, whey protein isolate (WPI) is also available and produced by eliminating fat, cholesterol, carbohydrates, in particular lactose, using UF. Additionally, pure whey proteins such as β-LG, α-LA, BLF, and BSA are already produced at a large-scale and available in the industrial market [7]. The whey proteins and hydrolysates, and their fractionated peptides released from the protein parent molecules, together with other smaller whey components, were identified as responsible for a wide variety of nutritional and physiological effects [9]. These effects include among others (i) physical performance, recovery after exercise and prevention of muscle atrophy; (ii) satiety and weight control; (iii) cardiovascular health; (iv) anticancer activity; (v) wound treatment and recovery; (vi) infection control; (vii) child nutrition and (viii) healthy aging [10].

Hydrolysis of whey proteins produces highly complex protein hydrolysates that can contain hundreds of peptide sequences in which the specific bioactive peptide represents only a single smaller constituent. The identification of these bioactive peptides requires intense labor of specialized technicians using sophisticated purification and characterization techniques. Mass spectrometry (MS) is the preferred analytical method for determining their amino acid sequence once identified the subfractions of protein hydrolysates containing the bioactive peptides [11]. MS techniques, when combined with other analytical methodologies such as liquid chromatography (LC/MS), are widely used to isolate and quantify bioactive peptides derived from protein from food, in the food itself, and biological fluids.

Today, in "functional foods" (designer foods/medicinal and therapeutical foods), the bioactive peptides derived from milk and whey proteins are included as additives functioning as macro/micro essential nutrients or a non-nutritional component, or component whose nutritional value is not listed as essential [12].

While some of these effects remain putative, a considerable number of bioactive peptides received scientific scrutiny and have been validated as beneficial by several laboratories around the world in the face of the growing demand by a highly diverse group of consumers. Nowadays, there are already several bioactive peptides derived from milk and whey proteins commercialized internationally and identified by several authors [13, 14]. These peptides are in the market as additives in various food products but not all with therapeutic effects approved by regulatory agencies such as the FDA. This fact is associated with the absence of documentation that validates its functionality and health benefits or has not undergone clinical validation studies with human volunteers that prove the results obtained in vitro and in vivo testing with animal models [15].

3 Production of Bioactive Peptides

In the global process of industrial production of peptides, it is worth highlighting the existence of several stages to achieve a concentrated and purified final formulation before its commercialization [16]. These include the pre-treatment of the protein solution, protein hydrolysis by control mainly of temperature and pH and the hydrolytic agent concentration, the separation and purification of bioactive peptides, and drying in the final stage of the formulation [17].

Fermentation processes with dairy starter cultures, i.e., with lactic acid bacteria (LAB) and hydrolysis with digestive or microbial proteases, are the most widely used methodologies for releasing bioactive peptides from the primary sequence of natural proteins. However, chemical processes using acid and alkaline catalytic agents and even heat in protein-rich food processing can also release some bioactive peptides [18].

Bioactive peptides for the food industry, rather than those used in the pharmaceutical industry, cannot be characterized at a high cost; otherwise, their use is not economically viable [19]. For this reason, large-scale production of bioactive

peptides used as food additives is preferably obtained by enzymatic hydrolysis from milk and whey proteins with food-grade digestive or microbial proteolytic enzymes, pure or a mixture of proteases, characterized by different specificities and low production cost [20].

The most common method for evaluating and monitoring the release of peptides in the laboratory and on the industrial scale is by quantifying the **Degree of Hydrolysis (DH)**, i.e., the percentage of peptide bonds broken during the hydrolytic process of proteins. According to Agyei et al. [17], DH influences the size of the peptides generated, and peptides with biological functions require DH > 10%. The hydrolysis of proteins produces multiple fragments from the primary sequence of native proteins, and the number of smaller ones increases with DH. These fragments (f) are assayed and then identified by a peptide chain according to the single-letter amino acid code, for instance, containing the abbreviation of natural amino acids f(GALMFWKQESPVICYHRNDT). The production of peptides on an industrial scale continues with challenges in the face of the existence of several bottlenecks due to the absence of technological environment-friendly, and economically efficient processes [20].

3.1 Effect of Industrial Pre-treatment of Proteins

Long hydrolytic processes are required to achieve high DH, more favorable for the production of physiologically active peptides, which increases the probability of microbial contamination. To avoid the addition of bactericides or pasteurization processes, Tavares et al. [21] proposed and tested the pre-treatment of whey protein concentrate (WPC) by microfiltration using a synthetic membrane with a weight exclusion (MWCO) of 20 kDa to reduce microbial loading. Other strategies consist of the research and use of new proteolytic enzymes that are resistant to high temperatures or acid conditions and thus can help eliminate optimal microbial growth conditions during the production of bioactive peptides. Other authors have proposed enzymatic hydrolysis together with high-pressure homogenization because enzyme activity is less sensitive to pressure compared to high temperature, reducing in this way, the cost of industrial production of bioactive peptides [22].

New pre-treatment technologies of protein solutions that do not employ heat or high pressure to minimize microbial contamination have currently been laboratory-tested such as the use of UV, microwaves, ultrasonication, ozone, and application of the pulsed electric field. For example, ultrasonication led to a more significant release of antioxidant peptides from hydrolysates of whey proteins compared to control (untreated whey proteins) in opposition to the use of microwave [23].

A comparison of the quality of industrial and research laboratory-level produced β-LG hydrolysates showed very similar peptide profiles, although with very different biological activities. This unexpected behavior obtained after the release of the peptides generated from the same protein molecule and with the same hydrolytic process is due, according to Li-Chan [24], to conformational changes in the structure of proteins processed at the industrial level. These alterations in protein

structure allow increasing access of endopeptidases to the bonds of the polypeptide chain, therefore facilitating enzymatic hydrolysis. However, protein pre-treatment can also produce protein aggregation and, consequently, hinder the release of peptide bonds from the protein parent molecule(s), for example, due to high-temperature processing [25] and high-pressure [26].

Additionally, processes involving strong acids have an adverse action on Gly (Glycine for short according to the three-letter amino acids code) and Asn amino acids. At the same time, alkaline conditions affect the Cis, Ser, and Thr amino acids, significantly decreasing lysine bioavailability. Furthermore, Lys can be involved in a Maillard reaction when it is present with 1% of lactose or other sugars that remain after hydrolysis [27]. This last modification can significantly affect DH obtained from isolated protein α-LA, either with trypsin or α-chymotrypsin, because these enzymes are unable to perform the hydrolysis of peptide bonds with glycosylated Lys [28]. However, the same authors found that hydrolysis of these peptide bonds with *Bacillus licheniformis* protease (BLP) and subtilisin A was independent of the degree of glycosylation.

In addition to the effect of pre-treatment of native protein solutions, the stability of the peptides subjected to high variations of temperature, pressure, salts, pH, and organic solvents used during hydrolysis or downstream processing should also be evaluated. Stability is an essential factor in ensuring the maintenance of the biological and or physiological activity of bioactive peptides [20]. These stability changes can alter or, at worst, destroy the beneficial bioactivity of the specific peptide. Therefore, the discovery of new bioactive peptides at the level of laboratory research is essential to test conditions close to those one used at the industrial-scale.

3.2 Protein Hydrolysis—The "Classical" Approach

Several physical, chemical, or biological hydrolytic processes release the bioactive peptides from the protein parent molecules. The heat releases bioactive peptides in protein-rich food processing, in the chemical methods acid or alkaline catalytic agents are added, while in biocatalysis enzymes or fermentation processes are used (Fig. 2). However, the classic hydrolytic processes of the protein parent molecules presently in use to generate bioactive peptides are (i) hydrolysis using pure or in mixture digestive enzymes; (ii) fermentation processes using microorganisms with proteolytic activity, and (iii) the hydrolytic action of microbial or vegetable proteases.

3.2.1 Digestive Enzymes

Currently, commercial preparations of food-grade proteases contain a diverse number of endopeptidases divided mainly into six categories, according to amino acid residues and co-factor involved in the catalytic process. Thus, there are serine-, cysteine-, aspartic-, glutamic-, and threonine-proteases, as well as metallic-proteases [29]. The mentioned amino acid residues act as nucleophilic agents attacking peptide

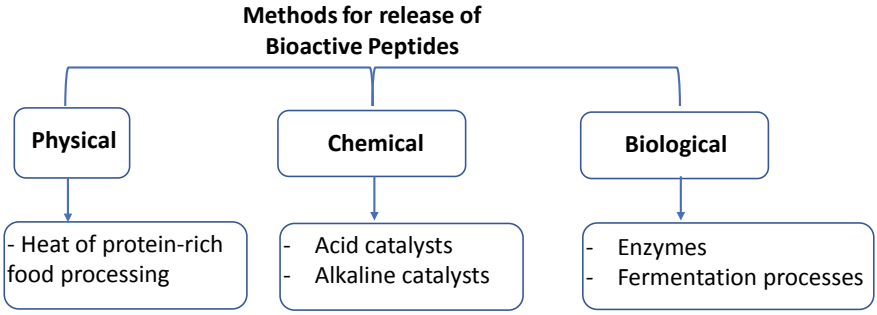

Fig. 2 Methods for release of bioactive peptides from protein parent molecules and used as additives in "functional foods"

bonds, while metallic-proteases use divalent cations such as zinc in the formation of a coordination complex activating water molecules for the catalytic process [30]. According to the above classification and the sequence polypeptide chain where the proteases act ($\mathbf{P}_1$–$\mathbf{P'}_1$), it was also demonstrated that other residues of neighboring amino acids ($\mathbf{P}_2$, $\mathbf{P}_3$, $\mathbf{P'}_2$, $\mathbf{P'}_3$, …) play a critical effect on the hydrolytic process of that specific peptide bond.

Digestive enzymes are commercially available from animal tissues such as porcine or bovine and are by far the most used enzymes for hydrolysis of milk and whey proteins and production of bioactive peptides used as additives in "functional foods" [31]. In this large group of enzymes, trypsin (serine endopeptidase, EC.3.4.21.4), pepsin (aspartic endopeptidase, EC.3.4.23.1), and chymotrypsin (serine endopeptidase, EC.3.4.21.1) are the most relevant.

A significant number of studies have been performed on the hydrolysis of WPC, WPI, and purified proteins, such as α-LA and β-LG. Cheison et al. [32] described the efficiency and specificity of trypsin, obtaining high hydrolysis with β-LG and low hydrolysis with α-LA at 25 °C and pH 8.5 after 2 h. Contrastingly, Acid Protease A hydrolyzed α-LA efficiently at 37.5 °C, and pH 3 after 2 h [33]. Hydrolysis of these protein substrates, for example, with trypsin in the pH range 7–8, chymotrypsin at pH 7.8, and pepsin at pH 2.6 led to DH between 6–22%, but the type of peptides generated was dependent on the specificity of the protease. The difference of the pH values used in hydrolysis is due to the mechanism and charge of the amino acid involved in the active site of the different proteases. However, the pH value is also an essential factor in the susceptibility of the protein parent molecules to proteolytic action, as the dissociation of β-LG dimers occur for pH values between 2 and 7.5. In contrast, the β-LG self-association occurs in the form of dimers or octamers at extreme values of this range [34]. These authors also observed that potassium phosphate buffer at high concentrations causes β-LG dimerization that affects the accessibility of proteases to the polypeptide chain and therefore prevents hydrolysis of peptide bonds inside specific dimer regions.

3.2.2 Microbial Proteases

Proteolytic enzymes of bacterial or fungal origin were also successfully tested to release bioactive peptides from whey proteins, although their use is more limited than digestive enzymes. There is a wide variety of these proteolytic enzymes commercially available such as Proteinase K (alkaline endopeptidase of the EC.3.4.21.64), thermolysin (metallic-endopeptidase EC.3.4.24.27) and subtilisin (serine endopeptidase, EC.3.4.21.62), among many others. Furthermore, mixtures (or cocktails) of proteases are also used for the production of bioactive peptides derived from whey proteins. The advantages of using a cocktail of proteases in contrast to enzymatic preparations with a pure enzyme are due to peptide diversity that can generate increased bioactivity at a reduced cost. Ghosh et al. [35] tested the hydrolysis of whey proteins with the preparation Flavourzyme, commercialized by Novozymes, which contain endo- and exo-peptidases produced by *Aspergillus oryzae*. These authors found that the number of small peptides increased with the concentration of commercial enzyme preparation.

3.2.3 Fermentation Processes

Dairy starter cultures consist of *Lactobacilli* strains that contain various lactic acid bacteria (LAB) with proteolytic activity in the production of bioactive peptides by the hydrolysis of milk proteins. This group of bacteria includes *Lactococcus lactis*, *Lactobacillus helveticus,* and *Lactobacillus delbrueckii var. bulgaricus*, characterized by containing proteases integrated into the cell wall and various intracellular peptidases [36]. The interest in these *Lactobacilli* strains is associated with the fact that they can be isolated from different ecological environments. Although they belong to the same biological family, several studies reported that they hydrolyze proteins differently and therefore produce a wide variety of bioactive peptides from the same protein substrate. Different hydrolysis studies performed on the fraction of milk and whey proteins using *Lactobacilli* strains at 30–37 °C for 24 h led to higher DH for longer fermentation time. However, the bioactive peptides production yield by the *Lactobacilli* strains is relatively small compared to what is possible to achieve with the use of pure enzymes [37]. Therefore, some authors added Prozyme E, a commercial cocktail of proteases, after 5 h of fermentation to increase the efficiency of the fermentation process. However, these fermentation conditions have not proven to be economically viable for the production of pure peptides in large quantities. Nisin, an antibiotic, is a unique exception as it is a natural fermentation product of *Lactococcus lactis* [38].

3.2.4 Plant Proteolytic Enzymes

The current trend in the production of bioactive peptides is to search and test new proteases able to hydrolyze peptide bonds in specific and less well-known sites envisaging the production of almost tailor-made peptides with precise size, for uses in medical therapies and specific diets. Plants have been investigated as alternative sources of peptidases since their peptidases act with different specificity and in a large variety of protein sources. In this research, particular attention focus on aspartic proteases present in the flowers of the *Asteraceae* family, mainly thistle

flowers (*Cynara cardunculus*) and *Arctium minus* [39] that are widely used in the Iberian Peninsula in the manufacture of artisanal cheese [40]. These proteases, named cyprosins or cynarases, break the peptide bonds within the polypeptide chain of whey proteins next to hydrophobic amino acid residues, especially Phe, Leu, Thr, and Tyr, and act mainly in α-LA [41]. These authors used aqueous extracts of *C. cardunculus* in the hydrolysis of WPC, WPI, isolated α-LA protein, and casein macropeptides with DH of 8–16% depending on the ratio enzyme/protein substrate, and hydrolysis time between 1 to 7 h. In turn, Lafarga et al. [42] performed BSA hydrolysis with food-grade enzyme papain (EC.3.4.22.2) extracted from *Carica papaya*. Other proteins of plant origin, such as bromelain extracted from stems (EC.3.4.22.32) and fruit (EC.3.4.22.33) of pineapples, were reported to have the ability to hydrolyze the peptide bond in whey proteins [43].

3.3 Protein Hydrolysis Strategies

3.3.1 Using Free Enzymes in Solution

Soluble digestive enzymes used in an agitated reactor at large-scale is the simplest method to perform protein hydrolysis, and once reached the desired DH, the process is interrupted by disabling the enzyme activity by pasteurization. The next step is the separation of peptides from the enzyme and non-hydrolyzed proteins by an ultrafiltration (UF) process. The synthetic UF membrane is characterized by pore size suitable for the free enzyme and non-hydrolyzed protein substrate to be retained within the membrane module (concentrate) while the peptides generated characterized by a much smaller size cross the membrane into the permeate. This filtration step functions as the first step of isolation and purification in the production process of bioactive peptides. The combination of the agitated reactor with a UF membrane module was the next step to implement a continuous process of hydrolysis of whey proteins and the production of bioactive peptides [31]. This strategy was also tested in the hydrolysis of concentrated protein solutions of Alfalfa (*Medicago sativa*) [44] and wheat gluten [45]. This configuration allows performing hydrolysis continuously, with better control of the reaction, minimizing the loss of protein substrate and free enzyme, and simultaneously, separate the fractions of protein hydrolysates that pass through the membrane into the permeate [46].

The hydrolysis of the proteins results in the release of individual amino acids and small peptides that gradually decrease the pH of the reaction medium as the degree of hydrolysis (DH) increases. To work close to the optimal pH value in an enzymatic process and under more controlled hydrolytic conditions is added as a chemical agent to maintain a constant pH value in the reactor. This pH correction allows the monitoring of DH in real-time, known as the pH–STAT reaction strategy.

Fernández and Kelly [47] compared the pH–STAT strategy with an uncontrolled reaction with a free pH decrease in the hydrolysis of WPI with the commercial proteolytic preparation Protamex®. These authors concluded that under the non-pH

control, the hydrolysis of whey proteins was faster, but in contrast, the pH–STAT strategy was more suitable for trypsin. Additionally, they also reported that the comparison of both hydrolytic strategies of WPI with papain achieved similar DH at the end. However, the profile of peptides and their physical–chemical and bioactive properties were very different.

The pH values during the hydrolytic process have a decisive influence on the profile of the peptides generated by the different proteases [48]. The confirmation of these results by other authors led to the conclusion that the production of bioactive peptides should be controlled, not only temporarily or based on the degree of hydrolysis (DH), but also by bioactivity tests [49].

3.3.2 Using Immobilized Enzymes

The immobilization of enzymes has been extensively studied and tested in the synthesis of peptides. Protein hydrolysis performed with immobilized proteases allows the overcome some difficulties identified on a large-scale and offers several advantages over conventional hydrolysis with soluble digestive enzymes. Several of these advantages can be highlighted (i) enzymatic hydrolysis in softer and controlled conditions, (ii) avoid autolysis activity of the protease itself minimizing the contamination of bioactive peptides released from the protein parent molecules, and (iii) easy separation and recycling of preparation with immobilized enzyme after the hydrolysis step, making the process economically more viable.

The profile of peptides is also associated with the controlled and rapid stop of the protein hydrolysis reaction. However, this is not always easy for the free enzyme without using an aggressive method such as pasteurization, which can affect the quality of the bioactive peptides generated. In contrast, preparation with immobilized protein can be removed easily and quickly from the hydrolytic reaction medium by sedimentation, filtration, or centrifugation, and more recently, when the biocatalysts have paramagnetic properties, a magnetic field was proposed. Inclusively, immobilized protease (e.g., trypsin) combining with ultrasonic probe-based can enhance the assessment of the protein cleavage quickly [50].

Peptide profile differences observed in protein hydrolysates were also justified by the alteration of protein substrate accessibility or affinity to the immobilized enzyme. Therefore, the primary selection criterium for the immobilization of proteases is the choice of macroporous supports to ensure free access of the protein substrate to immobilized proteases. However, the high costs associated with support and the most common methods used in the immobilization of proteases often decrease the economic advantage and has limited its application more intensely in protein hydrolysis and bioactive peptide production.

Ittrat et al. [51] proposed that the use of agricultural waste materials function as cheap alternative supports for protease immobilization. Bassan et al. [52] immobilized trypsin in particles resulting from the processing of the agro-industrial lignocellulosic waste material with great success in the production of bioactive peptides from whey proteins. These authors also found that more than 80% of enzyme activity remained after five cycles of reuse of this preparation with immobilized protease. Other studies highlight the immobilization of trypsin by adsorption and covalent

bond on the surface of spent grains in studies of hydrolysis of α-LA and β-LG [53]. These authors also observed high retention of the activity by multipoint covalent enzyme immobilization to support functionalized with glycidol groups. Other authors also tested this functional group in agarose gel in the immobilization of trypsin, chymotrypsin, and carboxypeptidase A in casein hydrolysis [54]. Remarkably, Pedroche et al. [55] observed an increase in stability of about 4,700 times of trypsin immobilized on the same support in comparison to free enzyme.

Preparations of immobilized proteases were used in the hydrolysis of whey proteins in agitated reactors as well as in packed in columns, which allows operating in continuous flow. This operation mode decreases large-scale operating costs, rapid hydrolysis process, and increased yield of bioactive peptide compared to conventional protein digestion processes in discontinuous mode [56]. The same authors also tested the immobilization of trypsin in a small-scale polymethacrylate monolith with 18-folds reuse, even with greater efficiency in the DH of β-LG in comparison to the reaction system with free trypsin in solution. Szymańska et al. [57] proposed the use of siliceous monoliths with macropores to ensure access of protein substrates to immobilized proteases.

Emerging new processes of immobilization of enzymes include cross-linking of insoluble proteins. These new immobilization processes were applied to the immobilization of proteases, in particular as cross-linked enzyme aggregates (CLEA) and cross-linked enzyme crystals (CLEC). The CLEC proved to be a more robust method in the immobilization of subtilisin and more efficient in protein hydrolysis [58].

3.4 Synthesis of Peptides—The "Rational" Approach

An alternative to the release of bioactive peptides by hydrolysis of the protein parent molecules mainly from milk or whey proteins is the design and rational synthesis of peptides. The methods involved in the rational synthesis of peptides can be classified as chemical (using two possible routes, synthesis in solid phase or liquid phase), DNA-based technology, and enzymatic synthesis (Fig. 3). The most appropriate method for peptide synthesis depends mainly on the length, quantity, and purity of the peptide to produce.

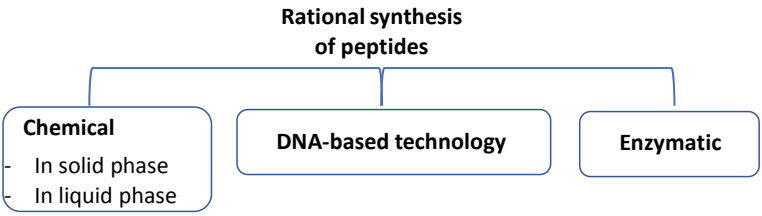

Fig. 3 Synthesis of peptides based on the "rational" approach

3.4.1 Chemical Synthesis

The main application of chemical synthesis of peptides in the laboratory or at a small scale is their use as therapeutic drugs or for diagnosis purposes. There are two variants in the chemical synthesis of peptides, in a liquid phase and a solid phase. Although both protocols are well established for peptide synthesis, this technology has several disadvantages. These disadvantages include (i) racemization of the resulting peptides after the reaction; (ii) the requirement of previous steps to protect of the residues or lateral side-chain of the most sensitive amino acids to maintain peptide functionality; (iii) low overall efficiency and generation of sub-products; iv) toxicity of solvents and protection and deprotection agents, as well as of chemical catalysts used in the reaction synthesis [59].

Peptide synthesis in solid phase is used for the generation of sequences of 10–100 amino acids long, with excellent potential for the development of multifunctional peptides [60]. This strategy requires a solid support to anchor the initial amino acid or small peptide sequence. The chain grows by extension of the N-terminal or C-terminal, step by step, by the sequential incorporation of a new amino acid or small peptide fragment until the synthesis of the desired peptide. The peptide synthesis in solid-phase approaches facilitates cyclic coupling, protection, and deprotection steps of more sensible residues of amino acids, as well as the intermediate purification steps needed until achieving the peptide synthesis with longer sequences. This rational strategy was initially used for active peptide synthesis. Examples are the synthesis of YGLF and YGG identified as fragment sequences f(50–53) and f(18–20), respectively, released from α-LA [61]. The great advantage of this strategy is to implement the automation of the different steps of the global process with increase income and decrease of consumption of reagents [59]. On the other hand, peptide synthesis in the liquid phase is the preferred method for large-scale synthesis of relatively short-chain peptides by direct condensation reaction between different amino acids or smaller peptide fragments using strategies similar to those used in solid-phase reaction.

3.4.2 Recombinant DNA Technology

Another alternative method, according to the rational approach, is based on recombinant DNA technology. This technology approach requires an intense and costly phase of research and development. However, once established a recombinant biosynthesis system of the desired peptide, usually characterized by a long chain, it is possible to obtain it in large quantities via a fermentation process from relatively inexpensive nutrients. Despite significant advances, short sequence biosynthesis remains impractical due to low expression efficiencies and difficulties encountered in the extraction and purification of the biosynthesized peptide [62]. Besides, recombinant DNA expression systems and biosynthesis of the desired peptide typically in bacterial hosts cannot be used for the production of aminated peptides, since these microorganisms do not have the necessary peptidylglycine α-amidating enzyme (α-AE). This disadvantage represents a significant limitation considering the widespread occurrence of amidation processes and their role often crucial in the expression of biological activity by a specific peptide. Another

disadvantage of the genetic engineering approach regards the biosynthesis of peptides integrating unnatural amino acids. These unnatural amino acids are important functional groups currently incorporated into some drugs and pharmacologic compounds.

3.4.3 Enzymatic Synthesis

Special attention was also given to the rational synthesis of bioactive peptides via enzymatic process due to the high stereospecificity associated with enzymes, the softness of reaction conditions, the minimal need of protection of the more sensitive side-chain amino acids, and avoid the racemization of the final peptide in comparison with the chemical synthesis. Like chemical synthesis, enzymatic synthesis of peptides can occur by extension of N- or C-terminal. However, enzymatic synthesis is limited to the synthesis of peptide that not exceed peptide chains with more than 10 amino acids [63].

The most commonly used proteolytic enzymes in this strategy of rational synthesis of peptides are proteases of the serine or cysteine group such as subtilisin, trypsin, chymotrypsin, or papain. However, other hydrolases were also tested, such as lipases and penicillin acylase [64]. Typically, enzymatic synthesis of peptides catalyzes the formation of peptide bonds between amino acids, dipeptides, or small peptide fragments. The first one functions as a donor of an acyl group (e.g., carboxyl) then localized in the part of the N-terminal. In turn, the second one works as an amine group donor associated with the C-terminal of the peptide sequence. Enzyme synthesis of peptides can occur using one of two distinct reaction strategies, i.e., enzyme synthesis under thermodynamic control or kinetic control [65].

The final product yield under thermodynamic control can be increased: (i) using an excess of one of the reagents; (ii) removing one of the final products; (iii) adding an organic solvent to alter the pka of the amine and carboxyl groups; (iv) using a biphasic reaction system, and, more recently; (v) using ionic liquids or anhydrous reaction medium containing a minimum concentration of water.

In the case of peptide synthesis under thermodynamic control occurs in an aqueous reaction medium, then these conditions must favor the removal of the final product (e.g., precipitation) with the consequent displacement of thermodynamic equilibrium. Another strategy is the use of organic solvents that alter the dielectric constant of the reaction medium by lowering the acidity of the carboxyl group and reducing the alkaline strength of the amine group. This effect induces an increased concentration of species with uncharged groups that are more reactive to be involved in the formation of peptide bonds. On the other hand, the use of organic solvents to alter the thermodynamic equilibrium affects the catalytic and stability of the protease negatively. The main disadvantages of this specific strategy are the requirement of a large amount of enzyme and low reaction rates.

In the strategy of enzymatic synthesis of peptides under kinetic control, one activated (e.g., ester) amino acid or a small peptide binds with a second amino acid or small peptide. In this reaction strategy, the synthesis velocity (S) is much higher than the hydrolysis velocity (H), and the S/H ratio should be as high as possible. The activated amino acid or small peptide is used since its conversion into the final

product is thermodynamically more favorable. The advantage of the kinetic control strategy is to require a ratio enzyme to substrate lower than required in the thermodynamic control strategy. The efficiency of the peptide synthesis under kinetic control is also profoundly affected by the pH value and ionic strength. Therefore, the second peptide that is involved in the nucleophilic attack should be uncharged, and hence it is vital to choose the pH in the reaction environment according to the pka of the nucleophile amine group. The addition of co-solvents can also help to dissolve the activated amino acid or small peptide and simultaneously minimize the reaction rate of its hydrolysis and the final product.

3.4.4 Bioinformatic Tools on In Silico Design of Bioactive Peptides

Ideally, the on in silico process of peptide synthesis should reduce the time required for selecting the best hydrolysis conditions for various native proteins and multiple known proteases based in databases like BIOPEP [66] and UniProtKB [67]. The Bioinformatics tools like BIOPEP "enzyme action", ExPASy Peptide Cutter [68], and PoPS [69] algorithm are excellent strategies for enzymatic peptide synthesis. However, the design of peptides based on in silico proteolysis tools cannot guarantee experimental reproducibility considering the complex nature of protein-protease interactions. Furthermore, as the bioinformatics approaches currently used do not consider the possibility of the existence of other peptide sequences than those available in the "in silico hydrolysates", and the lack of database update and some attractive synthesis opportunities might be missed [70].

4 Bioactive Peptides Isolation and Purification Methods

The behavior and bioactive properties of an individual peptide present in a protein hydrolysate may be significantly different compared to when it is isolated due to antagonistic and or synergistic effects when present in a mixture of peptides. After hydrolysis, the target peptides need to be concentrated and purified, which simultaneously facilitates its posterior identification. Peptides have similar physical–chemical properties, but the specific side chains of amino acids composing their primary structure allow their separation according to charge, size, solubility, and hydropathy, i.e., the difference in hydrophobicity versus hydrophilicity of the compound [71]. Peptide purification is a pre-requirement independent of the methods used in its production, whether for specific applications in the food or pharmaceutical industry. Of course, different degrees of purity are required, inclusively higher than 95% for conventional pharmaceutical applications [72]. Selective precipitation, membrane filtration, and different chromatographic processes have been commonly used for peptide fractionation enrichment. Agyei et al. [17] reviewed the methods for the extraction and purification of peptides.

4.1 Precipitation

Selective precipitation of non-hydrolyzed proteins separate them from soluble peptides, and the right conditions depend on protein solubility in a specific precipitating agent. The precipitation used in the first stage of peptide isolation from protein hydrolysates involves the addition of a precipitating agent. These agents are organic solvents such as ethanol or methanol, acids like trichloroacetic acid (TCA), or salts such as ammonia sulfate. Centrifugation or filtration can then be used to separate the insoluble compounds easily.

After this step, the isolation or fractionation of a target peptide is also possible using the selective conditions such as adjusting pH to its isoelectric point where it is insoluble and separates from other soluble peptides.

In some cases, the addition of chemical compounds can produce peptide degradation and changes in its main physical and biological properties. However, precipitation is a relatively fast, low-cost, and easy-to-scale process. Removal of precipitation agents and other contaminants is essential because they can interfere or hinder the purification of the target peptide and its subsequent identification.

4.2 Membrane Modules

UF membrane modules can also be used to separate peptides from non-hydrolyzed proteins without the addition of precipitating agents. The proper selection of membrane pore and physical properties allows some purification of the target peptide [73]. Ultrafiltration (UF) and nanofiltration (NF) processes are commonly used to fractionate mixtures of peptides and amino acids, in this way, improving their biological or functional properties [74].

Arrutia et al. [75] observed a high flux of permeation through the membrane when operating at a pH value of the isoelectric point of the target peptide. On the other hand, the selection of the synthetic material constituting the UF membrane is a relevant factor, as apolar peptides can adsorb on the membrane surface. Another adverse effect occurs by the formation of the polarization layer on the surface of the membrane, significantly decreasing the effective pore size. To prevent these phenomena, Doyen et al. [76] proposed the use of UF membranes combined with electrodialysis processes. In this case, the electrical charge and size are responsible for higher efficiency in the separation of the target peptide. For example, this greater efficiency is due to a higher migration of anionic peptides from the concentrate compartment when the opposite charge electrode (cathode) is localized in the permeate [77].

Membrane technology has several advantages, and among them are (i) no requirement of chemicals addition; (ii) relatively low energy consumption; (iii) low processing costs, and (iv) easy scale-up. These advantages make membrane processes an important separation technology in comparison to chromatographic techniques at industrial-scale applications.

4.3 Chromatographic Techniques

Chromatographic techniques are primarily used in the separation of peptide mainly in the laboratory and at a small scale. The high purity of the target peptide for the pharmaceutic industry is required, but its high added value offsets the high associated costs in its purification when using chromatography (90% of the total cost). Although chromatographic processes allow achieving high separation and selectivity of target peptide, these processes are characterized by low productivity and high operating and investment costs, which make their extensive use at the industrial-scale prohibitively expensive [31]. Ion exchange chromatography (IEC) and size exclusion chromatography (SEC) are some of the chromatographic techniques tested for target peptides purification. In contrast, high-performance liquid chromatography (HPLC) is crucial for peptide identification and production in the laboratory and on a small scale. However, the most efficient process for peptides purification continues undoubtedly to be reverse-phase HPLC chromatography [78].

Salvado [79] carried out the hydrolysis of sweet whey with chymotrypsin for 10 min, at temperature 37 °C and initial pH of 6.7, reducing the protein concentration in about 43% (as assessed by the Bicinchoninic Acid (BCA) assay method). Tricine SDS-PAGE showed the efficiency and selectivity of this hydrolytic process. The soluble k-casein (k-CN) and β-LG were not hydrolyzed under these experimental conditions, as shown by the bands in lanes 3 and 4 in Fig. 4. On the other hand, α-LA was hydrolyzed as the respective band in lane 4 disappear in the gel (Fig. 4). The resulting sweet whey hydrolysate presents several small fragments with a molecular weight in the range 2.8–16.7 kDa and additional lower molecular weight peptides, which are not visible by Coomassie staining after electrophoresis in Tricine SDS polyacrylamide gel (line 4 Fig. 4).

Almost all proteins, fragments, and peptides present in the sweet whey hydrolysate are positively charged at pH 4.5, according to the sample loaded into the isoelectric focusing gel (lane 4 Fig. 5).

After centrifugation, the soluble fraction of the sweet whey hydrolysate at pH 4.5 was loaded into a cationic exchanger column (SP-Sepharose XL™ from GE Health Care). All small fragments and peptides of the sweet whey hydrolysate adsorbed on the anionic support that exchange cations in opposition to what happened with soluble k-casein (k-CN) and β-LG that did not adsorb as the respective stained bands are present in the gel (lane 5 Fig. 4). The elution of the fragments and peptides occurred only with citrate buffer 25 mM pH 4.5 containing 250 or 350 mM of NaCl (Fig. 6).

The different eluent fractions were mixed, and their antimicrobial activity was assessed using the microdilution method. Penicillin–Streptomycin is used as control. The eluent fractions showed microbial inhibition, especially of the *Staphylococcus aureus* strain tested. However, the identification and quantification of peptides with microbial activity require the use of the reverse-phase- HPLC.

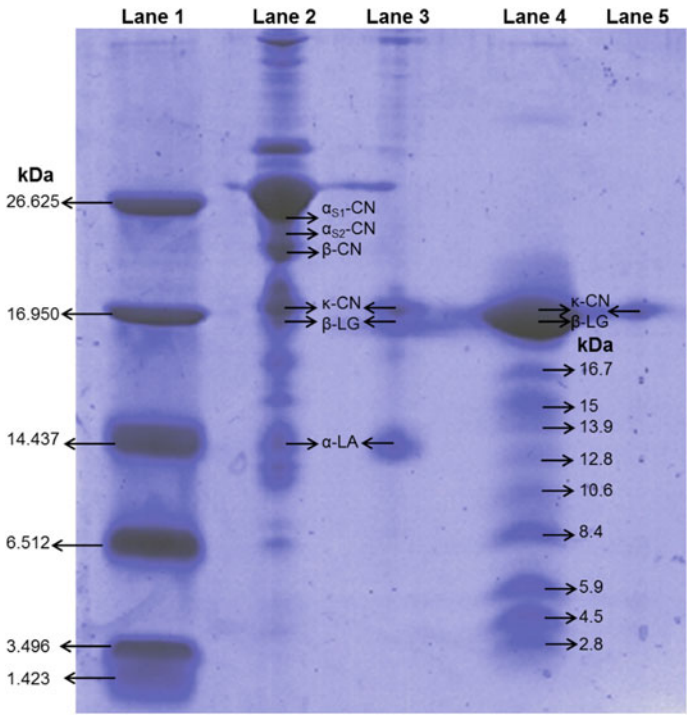

Fig. 4 Photograph of a Coomassie-stained SDS polyacrylamide gel after electrophoresis in Tricine buffer, of samples of HTST skimmed milk (diluted 20×, Lane 2), sweet whey (diluted 20×, Lane 3), sweet whey hydrolysate supernatant (without dilution, Lane 4), and sweet hydrolysate supernatant with citrate buffer 20 mM pH 4.5 come out from cationic exchanger column during adsorption and washing steps (diluted 24×, Lane 5). Lane 1 represents the polypeptide SDS-PAGE molecular weight standards composed of Triosephosphate isomerase (26.625 kDa), Myoglobin (16.950 kDa), α-Lactalbumin (14.437 kDa), Aprotinin (6.512 kDa), Insulin b chain (oxidized, 3.496 kDa), and Bacitracin (1.423 kDa)

Leeb et al. [80] obtained bioactive peptides such as fragment f(9–14) from hydrolysis of β-LG with a yield of 52%, using a chromatography ion exchange adsorption membrane.

Hippauf et al. [81] purified peptides in the chromatography adsorption column mainly by hydrophobic interactions using an activated charcoal focus on peptides containing Trp, such as Ile-Trp or Ala-Trp.

Bhut et al. [82] proposed chromatographic membrane processes that combine a functionalized membrane with ligands (e.g., ionic exchangers) used in protein separation.

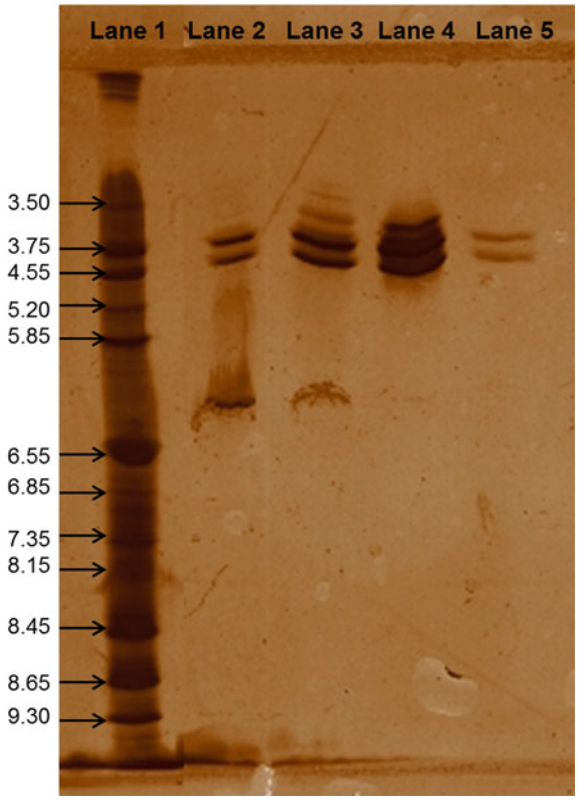

Fig. 5 Photograph of a polyacrylamide gel after isoelectric focusing of samples of HTST skimmed milk (diluted 20×, Lane 2), sweet whey (diluted 20×, Lane 3), sweet whey hydrolysate supernatant (without dilution, Lane 4), and sweet hydrolysate supernatant with citrate buffer 20 mM pH 4.5 come out from cationic exchanger column during adsorption and washing steps (diluted 24×, Lane 5). Lane 1 contains the Broad pI Kit pH 3–10 (GE Healthcare) containing: amyloglucosidase (pI = 3.50); methyl red (pI = 3.75); trypsin inhibitor (pI = 4.55); β-lactoglobulin A (pI = 5.20); bovine carbonic anhydrase B (pI = 5.85); human carbonic anhydrase B (pI = 6.55); myoglobin, acidic band (pI = 6.85); myoglobin, basic band (pI = 7.35); lentil lectin, acidic (pI = 8.15); lentil lectin, middle (pI = 8.45); lentil lectin, basic (pI = 8.65) and trypsinogen (pI = 9.30)

Saiga et al. [83] described an example of the complexity of a peptide purification process. In the first stage, these authors used two sequential chromatography columns, one with cationic exchange resin (AG 50W-X2) followed by a second anionic exchange resin (AG 1-X4). In the second stage, eluted fractions were concentrated in a UF membrane (MW < 500 Da) and finally subjected to purification in a reverse-phase HPLC column.

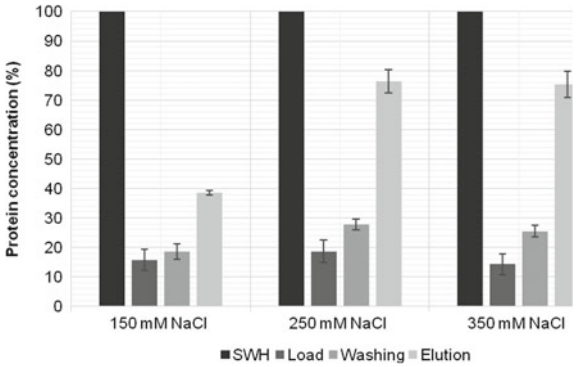

Fig. 6 Percentage of soluble protein concentration obtained in each chromatographic step (Load, Washing, and Elution) using cationic exchanger column (SP-Sepharose XL™) used to adsorb the peptides and fragments present in the sweet whey hydrolysate supernatant, washing steps with citrate buffer 20 mM pH 4.5, and purification by elution with eluents presenting increased concentration of NaCl. The initial soluble concentration (100%) was 1.0 mg/mL

5 Bioactive Peptides Derived from Whey Proteins

In addition to the bioactivity inherent to whey proteins, these proteins also contain peptides that, once released from the primary sequence, present bioactivity often different from that associated with the protein parent molecules. A vast number of authors identified a considerable number of bioactive peptides as fragments of whey proteins. These fragments still can be searched, and a vast number of them are available in specialized databases. For this reason, the following sub-chapters illustrate some important examples that made the bridge between the bioactive peptides with their relevant biological activities, namely anticancer, antidiabetic, antihypertensive, antimicrobial, antioxidant, immunomodulatory, and opioid properties (Fig. 7) [84].

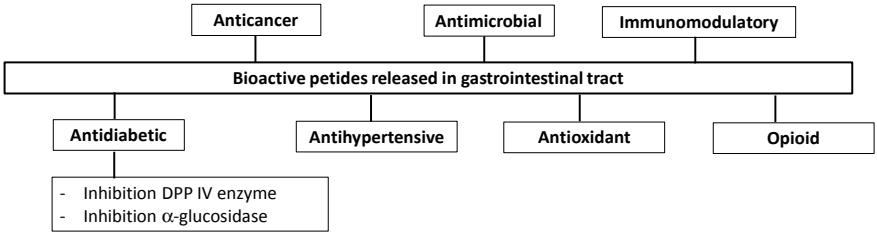

Fig. 7 Different physiological and biological activities of whey protein hydrolysates released in the gastrointestinal tract

5.1 Anticancer Peptides

Cancer accounts for about one-eighth of deaths worldwide and has now become one of the leading causes of mortality. Fortunately, rapid progress in the successful treatment of some cancers, formerly fatal, has changed the situation of cancer patients to survivors with chronic diseases due to the development of successful therapy and using anticancer drugs. The development of new medical therapies based on bioactive peptides showed to possess and bring several significant benefits, including low cytotoxicity, strong specificity, ability to penetrate tumor cells, small size, and easy structural modification [85]. Some whey proteins have played notable roles in cancer therapy by exhibiting activities against cancer cells mainly through cytoplasmic membrane disturbance and apoptosis induction. For example, the multimeric form of α-LA protein accelerates apoptotic processes in the transformed and immature cells while protecting mature epithelial cells. The β-LG protein showed to have the ability to protect against cancer development in an animal model when administered orally. Both BSA and bovine lactoferrin (BLF) prevented the growth of a human cell line responsible for breast cancer, but they are dependent on dosage [86].

Additionally, some fragments released after hydrolysis of whey proteins showed also to play an important role in cancer therapy. One example is the fragment FKCRRWQWRMKKLGAPSITCVRRAF f(17–41) released from bovine lactoferrin, called Lactoferricin. This fragment exhibited cytotoxic activity in several human and rat malignant cell lines, including fibrosarcoma, leukemia, different cancer cells, and neuroblastoma. Additionally, these peptides are at concentrations that do not substantially affect the viability of normal fibroblasts, lymphocytes, epithelial cells, endothelial cells, or erythrocytes [87].

Chen et al. [88] reported that anticancer peptides have a sequence length of 5–30 amino acids with 40–60% content in hydrophobic residues, a specific cationic charge, and a secondary structure in the α-helix form, in particular with a twist on its helical axis. Gabernet et al. [89] found a high percentage of Ala, Gly, Ile, Lys, Arg, and Leu amino acids, while amino acid Lys is responsible for the positive charge.

Chalamaiah et al. [90] recently reviewed the anticancer peptides derived from milk and whey proteins and their related amino acid composition.

5.2 Antidiabetic Peptides

Gaudel et al. [91] reported positive effects with oral administration of whey protein hydrolysates that improved blood glucose clearance, reduced hyperinsulinemia, and restoration of the ability of pancreatic islet to segregate insulin in response to the glucose level in an animal model of obese mice. Additionally, Nongonierma et al. [92] also observed that whey protein hydrolysates with high concentrations of free amino acids and hydrophilic peptides were responsible for increasing the insulinotropic response of BRIN-BD11 cells.

Whey proteins and their hydrolysates showed to affect blood glucose control and insulinotropic response positively in humans when administrated orally, and therefore, can be useful in type 2 diabetes control and therapy [93]. Although not fully understood, the effects of whey proteins and their hydrolysates on glycemia seem to be mediated, in vivo, by stimulating the secretion of intestinal hormones, acting also as inhibitors of the enzymes, dipeptidyl peptidase IV (DPP IV) and α-glucosidase.

Kehinde and Sharma [94] recently reviewed the antidiabetic properties of hydrolysates and peptides from multiple food sources.

5.2.1 Inhibition of the DPP IV Enzyme

Several proteins are considered as precursors of peptide inhibitors of the enzyme DPP IV and thus able to regulate plasma levels of hormones, the glucagon-like peptide 1 (GLP1), and the glucose-dependent insulinotropic polypeptide (GIP), both substrates of DPP IV enzyme [95]. In fact, in silico approaches revealed several encrypted peptides within the amino acid sequences of dietary proteins that could act as DPP IV inhibitors. Peptides identified as DPP IV inhibitors from those protein hydrolysates usually have molecular weights below 2 kDa. Most of them contain Proline amino acid residues and or hydrophobic ones within their sequence, which play a more significant role [96, 97]. Additionally, the inhibitory abilities of peptide seem to result from competitive, un-competitive, or non-competitive modes of inhibition of DPP IV enzyme.

The in vitro evaluation of the synthesized peptide IPA, identified after the digestion of β-LG protein with proteinase K, demonstrated its ability to inhibit the DPP IV enzyme competitively [98]. Similarly, the peptide IPAVFKIDAL released from α-LA was also reported to exhibit competitive inhibition of DPP IV enzyme, which can result from its structural similarity to the enzyme–substrate. Peptides LAHKALCSEKsL and ILDKVGINY released from α-LA also inhibited DPP IV by direct interaction with the active sites of the enzyme. On the contrary, Lacroix and Li-Chan [99] observed that the peptides LKPTPEGDL and LKPTPEGDLEIL released from β-LG showed to be among others, the most potent DPP IV inhibitors identified from whey protein hydrolysates. These peptides seem to act according to the mode of un-competitive inhibition on DPP IV, that is, they probably bind to the enzyme–substrate complex when formed, but outside the active site and thus decreasing the catalytic activity of the DPP IV enzyme.

Additionally, the peptide WLAHKALCSEKLDQ released from α-LA exhibited an un-competitive inhibitory behavior. Besides, peptides WLAHKAL and LCSEKLDQWL were reported as non-competitive inhibitors, binding outside the catalytic center of DPP IV enzyme or to the enzyme–substrate complex. The structure–activity relationships and the exact mechanisms by which whey-derived peptides inhibit the DPP IV enzyme are not yet fully elucidated [95].

Conventional synthetic drugs such as Diprotin A (IPI), Diprotin B (VPL), and Sitagliptin are the most potent inhibitors of DPP IV enzyme. They are more potent than individual peptides present in whey protein hydrolysates. Thus, the above example of bioactive peptides from whey protein hydrolysates cannot replace the

medicines available on the market but might be used as natural supplements in diets and or food-drug medical therapies for the control of type 2 diabetes [99].

Liu et al. [100] recently reviewed the peptides inhibitory properties of DPP IV enzyme from food-derived sources.

5.2.2 Inhibition of α-Glucosidase

Another strategy for the control of type 2 diabetes is the inhibition of carbohydrate hydrolyzing enzymes such as α-glucosidase. The enzyme is bound to the membrane of the epithelial mucosa of the small intestine, decreasing blood glucose levels [101]. WPC and β-LG hydrolysates obtained with serine protease isolated from *Cucurbita ficifolia* inhibited α-glucosidase of *Saccharomyces cerevisiae* [102]. Additionally, in vivo studies showed that the peptides released from whey protein hydrolysates or β-LG and α-LA proteins inhibited α-glucosidase in the intestine of rats by 36, 33, and 24%, respectively, as compared to non-hydrolyzed protein substrates that did not show detectable enzyme inhibition [103]. However, because of the small number of non-saccharide inhibitors of the α-glucosidase, investigations should focus on the identification of peptides responsible for inhibiting this enzyme. These investigations will positively contribute further to our understanding of the in vivo inhibition mechanism and its physiological role.

Wang et al. [104] recently reviewed different properties of bioactive peptides, including α-glucosidase inhibitory peptides from soy protein.

5.3 Antihypertensive Peptides in the Cardiovascular System

Hypertension, also known as high blood pressure, is one of the main risk factors for cardiovascular diseases, a group of heart and blood vessel disorders that include coronary, cerebrovascular, peripheral arterial, rheumatic and congenital diseases of the heart. One of the most studied bioactivities of peptides is the ability to reduce blood pressure. Many antihypertensive peptides are shown to inhibit the angiotensin-converting enzyme (ACE) (also known as peptidyl-dipeptide hydrolase, EC 3.4.15.1). This enzyme plays a fundamental physiological role in renin-angiotensin, kallikrein-kinin, and immune systems. Thus, synthetic ACE inhibitors such as enalapril, lisinopril, captopril, and ramipril have been widely used as drugs with antihypertensive activity. However, these synthetic drugs demonstrated several side effects, such as increased potassium levels, reduced renal function, allergic reactions, rashes, and taste disorders [105].

Several bioactive peptides derived from whey protein were isolated and evaluated for their antihypertensive activity by inhibiting ACE activity and avoiding undesirable side effects. Also, these peptides minimize the cost associated with synthetic drug therapy. Some fragments were released from α-LA and identified, such as LAHKAL f(105–110), KGYGGVSL f(16–23), KGYGGVSLPEW f(16–26), DKVGINYW f(97–104), and DKVGINYf(97–103) [41]. Besides, the fragments LAMA f(22–25), LDAQSAPLR f(32–40), VLDTDYK f(94–100), and VAGTW f(15–19) were released from β-LG, among many others [106].

The ACE inhibitors have sequences ranging 2–12 amino acids in length, with Leu, Ile, Val, Lys, and Arg residues in the C-terminal region, and showed to be responsible for the most significant inhibition [107]. Aromatic residues of amino acid located in the C-terminal such as Trp, Tyr, Phe, and Pro, in any of the three-terminal possible positions, also exhibited inhibitory effects of enzyme activity through interaction with different subsites of the catalytic structure of the ACE [108].

Daliri et al. [109] recently reviewed the antihypertensive properties of peptides released from whey proteins.

5.4 Antimicrobial Peptides

Because of the emergence of new multidrug-resistant bacteria (MDR), there is a need to find and develop new antimicrobial agents. Antimicrobial peptides (AMPs) are a particular subset of peptides that play an important role in the defense mechanisms of numerous organisms. Studies on the structure and sequence of peptides with antimicrobial activity show that they are generally positively charged (cationic), with a high proportion of hydrophobic residues. Antimicrobial peptide sequences include 10–50 amino acids with hydrophobic residues and a cationic and anionic charge (e.g., Lys, Arg, Ala, Leu, among others) in which the latter has a substantial contribution to the amphipathic characteristics of these bioactive peptides [110].

These characteristics allow AMPs to selectively bind to the negatively charged microbial membranes through electrostatic interactions, leading to disturbances in the integrity of the bacterial cytoplasmic membrane. The resulting interaction leads to cytoplasm loss by leakage of cell content by different suggested mechanisms. The damage to the integrity of the lipid bilayer is conceivable to interfere or leading directly or indirectly to cell death [111].

The inhibition of biopolymer synthesis can also result in cell death. For example, peptidoglycan biosynthesis is essential to maintain cell integrity and function. Thus, any disturbance in its synthesis may culminate in the death of the microbial cell that may occur due to the contribution of multiple independent or cooperative mechanisms. Even when acting on the same microbial species, different mechanisms can prevail, depending on environmental factors, the phase of growth, and the presence of immunological responses [112].

The antimicrobial action of AMPs is broad spectrum because they act on bacterial membranes and other more generic intracellular targets such as DNA, unlike most antibiotics that generally are active against specific targets such as proteins. Such characteristic mechanisms of action allow AMPs to avoid the most common resistance mechanism observed for traditional antibiotics and, therefore, the development of resistance is more unlikely [113].

In recent decades, the impact of AMPs released from dairy proteins on human health and the production of new functional food ingredients were subject to intensive research. Bovine or human lactoferrin exhibits antimicrobial activity

against a broad spectrum of gram-positive and gram-negative bacteria, including *Listeria monocytogenes*. The researchers proposed the possibility of incorporating AMPs derived from whey proteins directly into pharmaceuticals and dietary food therapies [114].

Proteolytic fragments derived from whey proteins, lactoferrin, and lysozyme were widely studied concerning the search for their antimicrobial activity. Fragments TPEVDDEALEK f(125–135), KVAGT f(14–18), VRT f(123–125), PEGDI f(50–54), and LPMH f(143–146) were released from β-LG with trypsin or pepsin [115, 116]. For example, proteolytic digestion of β-LG by trypsin released four antimicrobial fragment peptides against gram-positive bacteria corresponding to VAGTWY f (15–20), AASDISLLDAQSAPLR f(25–40), IPAVFK f(78–83), and VLVLDTDYK f(92–100) [117].

Mohanty et al. [118] reviewed the antimicrobial bioactive peptides derived from milk and whey proteins and their mechanism of action.

5.5 Antioxidant Peptides

In recent years, special attention focused on the search for whey-derived peptides with free-radical quenching activities (scavenging) and lipid peroxidation. Free radicals can modify nucleic acid molecules, in particular DNA, proteins, lipids, and cell small molecules. Several authors report that they play a significant role in the occurrence of some diseases, such as cardiovascular diseases, diabetes, and neurological disorders such as Alzheimer´s disease. Also, lipid peroxidation in food products can cause deterioration in food quality, shorten its shelf life, and reduce consumer's acceptability of processed foods. Drug regulatory agencies restricted the use of synthetic antioxidants such as butylated hydroxytoluene (BHT), butylated hydroxyanisole (BHA), propyl gallate (PG), and tert-butylhydroquinone (TBHO) due to their potential toxic effect on humans [119].

Conway et al. [120] suggested that peptides derived from enzymatic hydrolysis of α-LA and β-LG present in WPC were probably responsible for antioxidant activity in comparison with caseins present in skimmed milk. These authors also found that the primary mode of action is related to the peptide chain of amino acid sequence and composition.

The antioxidant fragments INYW f(101–104) and LDQW f(115–118) were released from α-LA, while FNPTO f(151–155), LQKW f(58–61), and LDTDYKK f(95–101) were released from β-LG using thermolysin [121, 122]. The fragments WYSLAMAASDI f(19–29) and YVEEL f(42–46) result from the digestion of β-LG with Corolase PP [123].

Peptides with sequences of 5–11 amino acids, including hydrophobic residues such as Tyr, Trp, Phe, Pro, His, and Val or Leu in the N-terminal, were associated with the most significant antioxidant activity [124]. Other hydrophobic amino acids, such as Pro and His, are also described as essential for antioxidant activity as this activity is related to a high number of ionizable groups and the exposure of hydrophobic groups [125]. There are inexpensive and straightforward methods to

assess antioxidant capacity in vitro. However, they should be used in models based on food and or cellular systems as it is a better approach to identify the antioxidant potential of peptides [121]. In this perspective, the antioxidant activities of peptides present in products derived from whey proteins can satisfy the growing demand for more natural antioxidants to preserve human health and maintain food quality.

Corrochano et al. [126] recently reviewed the antioxidant peptides released from whey proteins and their mechanisms on cellular antioxidant pathways.

5.6 Immunomodulatory Peptides

An increasing number of studies suggest that whey proteins may contain biologically active peptides with immunomodulatory properties encrypted in primary sequences [127]. Theoretically, immunomodulatory peptides can be released from whey proteins during the digestion process in the intestine and can thus affect downstream immune responses and cellular functions. However, the amount and concentration of bioactive peptides generated during digestion in adults are probably too low to induce significant effects on the immune system, especially for an expected therapeutic effect. Bioactive peptide concentrates can be produced on a commercial scale using enzymatic hydrolysis and separation technologies for their enrichment. Additionally, the development of immunomodulatory peptides from whey proteins is currently limited by the lack of characterization of bioactive hydrolysate immunomodulator peptides and the absence of clinical data on the physiological effects of these peptides. Most studies on the immunomodulatory effects of whey proteins, enzymatic hydrolysates, and peptides have as target the specific immune system, evaluating lymphocyte activation and proliferation, cytokine secretion, and antibody production [128].

Wu et al. [129] identified aromatic residues and charged amino acids present in peptide sequences of 2–12 amino acids in length as involved in binding to receptors on the surface of cells involved in the immunologic system and production of immune responses. For example, digestion of whey proteins with trypsin-chymotrypsin demonstrated the ability to generate components involved in immune response in a murine model of *Escherichia coli* infection, inducing increases in IgA concerning the absence of infection [130]. Additionally, hydrolyzed samples of bovine whey protein obtained with commercial enzymes, pepsin, and Corolase PP, and using human gastric and duodenal juices, showed a dosage-dependent inhibition in the proliferation of peripheral blood mononuclear cells in vitro. More recently, the addition of peptides derived from whey protein showed a positive effect on the development of immunomodulatory diets in animal models, both murine and rats [130]. These authors identified several fragments released from β-LG with trypsin and chymotrypsin with immunomodulatory properties such as VAGTWY f(15–20), EILLQK f(55–60), IDALNENK f(84–91), VLVLDTDYKKYLLF f(92–105), ALKALPMHIR f(139–148), and ALPMHIR f(142–148).

Kiewiet et al. [131] recently reviewed immunomodulatory protein hydrolysates and their applications.

5.7 Opioid Peptides

Opioid peptides are short amino acid sequences present in dairy products that play an active role in the nervous system. These peptides have pharmacological similarity with opium (morphine) and exert their activity by binding to specific receptors in the target cell. Typical opioid peptides are all originated from precursor proteins such as endorphins, enkephalins, and dynorphins, and they have the same N-terminal sequence, Tyr-GlyGly-Phe. Opioid peptides derived from other precursor proteins, such as serum proteins, are called "atypical" [132]. That is, they consist of several amino acid sequences where only Tyr is conserved in the N-terminal region. Thus, the N-terminal sequence of "atypical" opioid peptides is Tyr-X-Phe or Tyr-X-X-Phe. It seems that the presence of Tyr and another aromatic amino acid form an essential structural motive involved in connection with opioid receptors. These opioid-like sequences are encrypted in the primary structure of the main whey proteins, in particular in fragments released from α-LA and β-LG such as YGLF f(50–53) and YLLF f(102–105), respectively named α- and β-Lactorphins. Kostyra et al. [132] also identified several atypical" opioid peptides released from BSA, such as ALKAWSVAR f(208–216) and YGFQNA f(399–404).

The roles played by food-derived opioid peptides in central nervous and gastrointestinal systems were recently reviewed by Liu and Udenigwe [133], while Garg et al. [134] recently reviewed the opioid peptides released from food proteins.

6 Conclusions and Perspectives

Enzymatic catalysis is an essential strategy for hydrolysis of milk and whey proteins in useful products such as bioactive peptides. The ability of different enzymes and conditions to generate bioactive peptides were the subject of intensive research worldwide. Several proteolytic enzymes are used to produce products derived from whey proteins presenting a wide range of remarkable biological activities, including antimicrobial, antioxidant, antihypertensive, and antidiabetic activities. The association of this variety of biological activities with several peptide sequences was reviewed in this chapter. Whey proteins are (and will be) an important source for the production and discovery of new bioactive peptides.

Proteins and peptides from milk and whey components continue to be preferred as potential ingredients for functional and nutraceutical foods, and as active medicinal agents. This preference is based on the strong consumer trend in the search for health and well-being. The mechanisms of action of bioactive peptides still need to continue to be fully elucidated.

Future research should focus on new hydrolysis processes of whey proteins under conditions resembling those used on a large scale. Furthermore, the search of less common proteases such as proteolytic enzymes from plants and marine organisms with the potential to release new unique amino acid sequences will undoubtedly be active fields of research. The high cost of purification and actual

synthesis of the specific sequence of peptides leads to the need to improve methodologies for use in large-scale production to ensure higher yields and income of these bioactive molecules.

Cytotoxicity studies to ensure safety and the absence of adverse effects in vivo are required before these products obtain approval from food or pharmaceutical regulatory agencies. The evaluation of different aspects such as dosage, toxicity, and possible side effects by human trials should also be considered, to confirm and validate the established effects of bioactive peptides in vitro. Furthermore, detailed research is needed to provide better knowledge about maintaining bioactivity during gastrointestinal transit, peptide absorption mechanisms, and their destination and place of action in vivo.

Acknowledgements The authors thank Fundação para a Ciência e a Tecnologia (FCT) and IBB —Institute for Bioengineering and Biosciences for funding through project UIDB/04565/2020.

References

1. Daliri EB-M, Oh DH, Lee BH (2017) Bioactive peptides. Foods 6(5):32
2. Manfredi-Lozano M, Roa J, Tena-Sempere M (2018) Connecting metabolism and gonadal function: novel central neuropeptide pathways involved in the metabolic control of puberty and fertility. Front Neuroendocrinol 48:37–49
3. Maestri E, Marmiroli M, Marmiroli N (2016) Bioactive peptides in plant-derived foodstuffs. J Proteomics 147:140–155
4. Ishak NH, Sarbon NM (2017) Optimization of the enzymatic hydrolysis conditions of waste from shortfin scad (*Decapterus macrosoma*) for the production of angiotensin I-converting enzyme (ACE) inhibitory peptide using response surface methodology. Int Food Res J 24(4): 1735–1743
5. Rosales-Mendoza S (2016) Chapter 8, Algae-made nutraceuticals produced using genetic approaches. In: Rosales-Mendoza S (eds) Algae-based biopharmaceuticals. Springer International Publishing, Switzerland, pp 121–141
6. Brandelli A, Dariot DJ, Corrêa APF (2015) Whey a source of peptides with remarkable biological activities. Food Res Int 73:149–161
7. Smithers GW (2015) Whey-ing up the options—yesterday, today and tomorrow. Int Dairy J 48:2–14
8. Nath A, Mondal S, Kanjilal T, Chakraborty S, Curcio S, Bhattacharjee C (2015) Synthesis and functionality of proteinacious nutraceuticals from casein whey-A clean and safe route of valorization of dairy waste. Chem Eng Res Des 97:192–207
9. Dhaval A, Yadav N, Purwar S (2016) Potential applications of food derived bioactive peptides in management of health. Int J Pept Res Ther 22:377–398
10. Morelli G, Accardo A (2015) Peptides in theranostics. In: Kruger G, Albericio F (eds) Advances in the discovery and development of peptide therapeutics. Future Science Ltd., pp 173–184
11. Panchaud A, Affolter M, Kussmann M (2012) Mass spectrometry for nutritional peptidomics: how to analyze food bioactives and their health effects. J Proteomics 75(12): 3546–3559
12. Carrasco-Castilla J, Hernández-Álvarez AJ, Jiménez-Martínez C, Gutiérrez-López GF, Dávila-Ortiz G (2012) Use of proteomics and peptidomics methods in food bioactive peptide science and engineering. Food Eng Rev 4(4):224–243

13. Lacroix IM, Meng G, Cheung IW, Li-Chan EC (2016) Do whey protein-derived peptides have dual dipeptidyl-peptidase IV and angiotensin I-converting enzyme inhibitory activities? J Funct Foods 21:87–96
14. Arif MI (2018) Engineering amidases for peptide C-terminal modification, Ph.D. thesis, Groningen, University of Groningen
15. Nongonierma AB (2016) O'keeffe MB, Fitzgerald RJ (2016) Milk protein hydrolysates and bioactive peptides. In: McSweeney PLH, O'Mahony JA (eds) Advanced dairy chemistry. Springer, New York, pp 417–482
16. Zambrowicz A, Timmer M, Polanowski A, Lubec G, Trziszka T (2013) Manufacturing of peptides exhibiting biological activity. Amino Acids 44:315–320
17. Agyei D, Ongkudon CM, Wei CY, Chan AS, Danquah MK (2016) Bioprocess challenges to the isolation and purification of bioactive peptides. Food Bioprod Process 98:244–256
18. Toldrá F, Reig M, Arcstoy M-C, Mora L (2018) Generation of bioactive peptides during food processing. Food Chem 267(30):395–404
19. Capriotti AL, Cavaliere C, Piovesana S, Samperi R, Laganà A (2016) Recent trends in the analysis of bioactive peptides in milk and dairy products. Anal Bioanal Chem 408(11):2677–2685
20. Lafarga T, Hayes M (2017) Bioactive protein hydrolysates in the functional food ingredient industry: overcoming current challenges. Food Rev Int 33(3):217–246
21. Tavares TG, Amorim M, Gomes D, Pintado ME, Pereira CD, Malcata FX (2012) Manufacture of bioactive peptide-rich concentrates from whey: characterization of pilot process. J Food Eng 110(4):547–552
22. Bamdad F, Bark S, Kwon CH, Suh JW, Sunwoo H (2017) Anti-inflammatory and antioxidant properties of peptides released from β-lactoglobulin by high hydrostatic pressure-assisted enzymatic hydrolysis. Molecules 22(6):949
23. Uluko H, Zhang S, Liu L, Tsakama M, Lu J, Lv J (2015) Effects of thermal, microwave, and ultrasound pretreatments on antioxidative capacity of enzymatic milk protein concentrate hydrolysates. J Funct Foods 18:1138–1146
24. Li-Chan EC (2015) Bioactive peptides and protein hydrolysates: research trends and challenges for application as nutraceuticals and functional food ingredients. Curr Opinion Food Sci 1:28–37
25. Cheison SC, Kulozik U (2017) Impact of the environmental conditions and substrate pre-treatment on whey protein hydrolysis: a review. Crit Rev Food Sci Nut 57(2):418–453
26. De Maria S, Ferrari G, Maresca P (2017) Effect of high hydrostatic pressure on the enzymatic hydrolysis of bovine serum albumin. J Sci Food Agr 97(10):3151–3158
27. Mohan A, Udechukwu MC, Rajendran SR, Udenigwe CC (2015) Modification of peptide functionality during enzymatic hydrolysis of whey proteins. RSC Adv 5(118):97400–97407
28. Deng Y, Wierenga PA, Schols HA, Sforza S, Gruppen H (2017) Effect of Maillard induced glycation on protein hydrolysis by lysine/arginine and non-lysine/arginine specific proteases. Food Hydrocolloid 69:210–219
29. Rawlings ND, Barret AJ, Bateman A (2012) MEROPS: The database of proteolytic enzymes, their substrates and inhibitors. Nucleic Acids Res 40(D1):D343–D350
30. Brew K, Dinakarpadian D, Nagase H (2000) Tissue inhibitors of metalloproteinases: evolution, structure and function. Biochim Biophys Acta (BBA)—Protein Struct M 1477:267–283
31. Korhonen H, Pihlanto A (2006) Bioactive peptides: production and functionality. Int Dairy J 16(9):945–960
32. Cheison SC, Leeb E, Toro-Sierra J, Kulozik U (2011) Influence of hydrolysis temperature and pH on the selective hydrolysis of whey proteins by trypsin and potential recovery of native alpha-lactalbumin. Int Dairy J 21(3):166–171
33. Cheison SC, Bor EK, Faraj AK, Kulozik U (2012) Selective hydrolysis of α-lactalbumin by acid protease A offers potential for β-lactoglobulin purification in whey proteins. LWT-Food Sci Tech 49(1):117–122

34. Cheison SC, Lai MY, Leeb E, Kulozik U (2011) Hydrolysis of β-lactoglobulin by trypsin under acidic pH and analysis of the hydrolysates with MALDI-TOF-MS/MS. Food Chem 125(4):1241–1248
35. Ghosh BC, Prasad LN, Saha NP (2017) Enzymatic hydrolysis of whey and its analysis. J Food Sci Technol 54(6):1476–1483
36. Hayes M, Ross RP, Fitzgerald GF, Stanton C (2007) Putting microbes to work: dairy fermentation, cell factories and bioactive peptides. Part 1: Overview. Biotechnol J 2(4): 426–434
37. Virtanen T, Pihlanto A, Akkanen S, Korhonen H, Stanton C (2007) Development of antioxidant activity in milk whey during fermentation with lactic acid bacteria. J Appl Microbiol 102(1):106–115
38. Dussault D, Vu KD, Lacroix M (2016) Enhancement of nisin production by *Lactococcus lactis* subsp. *lactis*. Probiotics Antimicrob Proteins 8(3):170–175
39. Cimino CV, Colombo ML, Liggieri C, Bruno M, Vairo-Cavalli S (2015) Partial molecular characterization of *Arctium minus* aspartylendopeptidase and preparation of bioactive peptides by whey protein hydrolysis. J Med Food 18(8):856–864
40. Sampaio P, Calado C, Sousa L, Bressler D, Pais MS, Fonseca L (2010) Optimization of the culture medium composition using response surface methodology for new recombinant cyprosin B production in bioreactor for cheese production. Eur Food Res Technol 231(2):339–346
41. Tavares T, Contreras MDM, Amorim M, Martín-Álvarez PJ, Pintado M, Recio I, Xavier Malcata F (2011) Optimisation, by response surface methodology, of degree of hydrolysis and antioxidant and ACE-inhibitory activities of whey protein hydrolysates obtained with cardoon extract. Int Dairy J 21(12):926–933
42. Lafarga T, Aluko RE, Rai DK, O'Connor P, Hayes M (2016) Identification of bioactive peptides from a papain hydrolysate of bovine serum albumin and assessment of an antihypertensive effect in spontaneously hypertensive rats. Food Res Int 81:91–99
43. Pavan R, Sapna Jain S, Kumar A (2012) Properties and therapeutic application of bromelain: a review. Biotechnol Res Int. https://doi.org/10.1155/2012/976203
44. Kapel R, Chabeau A, Lesage J, Riviere G, Ravallec-Ple R, Lecouturier D, Wartelle M, Guillochon D, Dhulster P (2006) Production, in continuous enzymatic membrane reactor, of an anti-hypertensive hydrolysate from an industrial alfalfa white protein concentrate exhibiting ACE inhibitory and opioid activities. Food Chem 98(1):120–126
45. Cui J, Kong X, Hua Y, Zhou H, Liu K (2011) Continuous hydrolysis of modified wheat gluten in an enzymatic membrane reactor. J Sci Food Agric 91:2799–2805
46. Rios GM, Belleville MP, Paolucci D, Sanchez J (2004) Progress in enzymatic membrane reactors—a review. J Membr Sci 242:189–196
47. Fernández A, Kelly P (2016) PH-stat vs. free-fall pH techniques in the enzymatic hydrolysis of whey proteins. Food Chem 199:409–415
48. Carvalho NCD, Pessato TB, Fernandes LGR, de Lima ZR, Netto FM (2017) Physicochemical characteristics and antigenicity of whey protein hydrolysates obtained with and without pH control. Int Dairy J 71:24–34
49. Le Maux S, Nongonierma AB, Barre C, FitzGerald RJ (2016) Enzymatic generation of whey protein hydrolysates under pH-controlled and non pH-controlled conditions: impact on physicochemical and bioactive properties. Food Chem 199:246–251
50. Vale G, Santos HM, Carreira RJ, Fonseca L, Miró M, Cerdà V, Reboiro-Jato M, Capelo JL (2011) An assessment of the ultrasonic probe-based enhancement of protein cleavage with immobilized trypsin. Proteomics 11(19):3866–3876
51. Ittrat P, Chacho T, Pholprayoon J, Suttiwarayanon N, Charoenpanich J (2014) Application of agriculture waste as a support for lipase immobilization. Biocatal Agric Biotechnol 3(3):77–82

52. Bassan JC, de Souza Bezerra TM, Peixoto G, da Cruz CZP, Galán JPM, Vaz ABDS, Garrido SS, Filice M, Monti R (2016) Immobilization of trypsin in lignocellulosic waste material to produce peptides with bioactive potential from whey protein. Materials 9(5):357
53. Rocha C, Gonçalo MP, Teixeira JA (2011) Immobilization of trypsin on spent grains for whey protein hydrolysis. Process Biochem 46(2):505–511
54. Pedroche J, Yust MM, Lqari H, Giron-Calle J, Vioque J, Alaiz M (2004) Production and characterization of casein hydrolysates with a high amino acid Fisher's ratio using immobilized proteases. Int Dairy J 14:527–533
55. Pedroche J, Yusta MM, Mateo C, Fernandez-Lafuente R, Giron-Calle J, Alaiz M (2007) Effect of the support and experimental conditions in the intensity of the multipoint covalent attachment of proteins on glyoxyl-agarose supports: correlation between enzyme-support linkages and thermal stability. Enzyme Microb Technol 40(5):1160–1166
56. Mao Y, Cernigoj U, Zalokar V, Štrancar A, Kulozik U (2017) Production of β-lactoglobulin hydrolysates by monolith based immobilized trypsin reactors. Electrophoresis 38(22–23):2947–2956
57. Szymanska K, Pietrowska M, Kocurek J, Maresz K, Koreniuk A, Mrowiec-Bialon J, Widłak P, Magner E, Jarzebski A (2016) Low back-pressure hierarchically structured multichannel microfluidic bioreactors for rapid protein digestion-proof of concept. Chem Eng J 287:148–154
58. Amorim Fernandes JF, Mcalpine M, Halling P (2005) Operational stability of subtilisin CLECs in organic solvents in repeated batch and in continuous operation. Biochem Eng J 24 (1):11–15
59. Guzmán F, Barberis S, Illanes A (2007) Peptide synthesis: chemical or enzymatic. Electron J Biotechnol 10(2). https://doi.org/10.2225/vol10-issue2-fulltext-13
60. Kimmerlin T, Seebach D (2005) 100 years of peptide synthesis: ligation methods for peptide and protein synthesis with applications to beta-peptide assemblies. J Pept Res 65(2):229–260
61. Nurminen ML, Sipola M, Kaarto H, Pihlanto-Leppälä A, Piilola K, Korpela R, Tossavainen O, Korhonen H, Vapaatalo H (2000) Alpha-lactorphin lowers blood pressure measured by radiotelemetry in normotensive and spontaneously hypertensive rats. Life Sci 66(16):1535–1543
62. Sewald N, Jakubke H-D (2009) Peptides: chemistry and biology. Wiley-VCH Verlag GmBH & Co, KGaA, Weinheim
63. Kumar D, Bhalla TC (2005) Microbial proteases in peptide synthesis: approaches and applications. Appl Microbiol Biot 68(6):726–736
64. Chen F, Zhang F, Wang A, Li H, Wang Q, Zeng Z, Wang S, Xie T (2010) Recent progress in the chemo-enzymatic peptide synthesis. Afr J Pharm Pharmacol 4(10):721–730
65. Nuijens T, Quaedflieg PJLM, Jakubke H-D (2012) Hydrolysis and synthesis of peptides. In: Drauz K, Gröger H, May O (eds) Enzyme catalysis in organic synthesis. Wiley-VCH Verlag GmBH & Co. KGaA, Weinheim
66. BIOPEP (http://www.uwm.edu.pl/biochemia/index.php/pl/biopep)
67. UniProtKB (http://www.uniprot.org/)
68. ExPASy Peptide Cutter (http://web.expasy.org/peptide_cutter)
69. PoPS algorithm is available at http://mathbio.nimr.mrc.ac.uk/~ffranca/POPS and at the mirror site http://www.cs.vu.nl/~ibivu/programs/popswww
70. Udenigwe CC (2014) Bioinformatics approaches, prospects and challenges of food bioactive peptide research. Trends Food Sci Technol 36(2):137–143
71. Fernández A, Zhu Y, FitzGerald RJ, Riera FA (2014) Membrane fractionation of a β-lactoglobulin tryptic digest: effect of the membrane characteristics. J Chem Technol Biot 89(4):508–515
72. Agyei D, Danquah MK (2011) Industrial-scale manufacturing of pharmaceutical-grade bioactive peptides. Biotechnol Adv 29(3):272–277

73. Coutte F, Lecouturier D, Firdaous L, Kapel R, Bazinet L, Cabassud C, Dhulster P (2017) Recent rends in membrane bioreactors. In: Pandey A, Larroche C, Soccol C (eds) Current developments in biotechnology and bioengineering. Elsevier, Amsterdam, pp 279–311
74. Mundi S, Aluko RE (2014) Inhibitory properties of kidney bean protein hydrolysate and its membrane fractions against renin, angiotensin converting enzyme, and free radicals. Austin J Nutri Food Sci 2(1):1–11
75. Arrutia F, Rubio R, Riera FA (2016) Production and membrane fractionation of bioactive peptides from a whey protein concentrate. J Food Eng 184:1–9
76. Doyen A, Udenigwe CC, Mitchell PL, Marette A, Aluko RE, Bazinet L (2014) Anti-diabetic and antihypertensive activities of two flaxseed protein hydrolysate fractions revealed following their simultaneous separation by electrodialysis with ultrafiltration membranes. Food Chem 145:66–76
77. Holder A, Merath C, Kulozik U, Hinrichs J (2015) Impact of diffusion, transmembrane pressure and the electrical field on peptide fractionation using cross-flow electro membrane filtration. Int Dairy J 46:31–38
78. Adebiyi AP, Adebiyi AO, Yamashita J, Ogawa T, Muramoto K (2008) Purification and characterization of antioxidative peptides from unfractionated rice bran protein hydrolysates. Inter J Food Sci Technol 43:35–43
79. Salvado AFA (2015) A comparative study between the correlation of the in silico and in vitro hydrolysis of whey proteins. M.Sc. thesis, Instituto Superior Técnico, University of Lisbon
80. Leeb E, Holder A, Letzel T, Cheison SC, Kulozik U, Hinrichs J (2014) Fractionation of dairy based functional peptides using ion-exchange membrane adsorption chromatography and cross-flow electro membrane filtration. Int Dairy J 38(2):116–123
81. Hippauf F, Lunow D, Borchardt L, Henle T, Kaskel S (2014) Extraction of ACE inhibiting dipeptides from protein hydrolysates using porous carbon materials. Carbon 77:191–198
82. Bhut BV, Weaver J, Carter AR, Wickramasinghe SR, Husson SM (2011) The role of polymer nanolayer architecture on the separation performance of anion-exchange membrane adsorbers: I. Protein separations. Biotechnol Bioeng 108(11):2645–2653
83. Saiga A, Tanabe S, Nishimura T (2003) Antioxidant activity of peptides obtained from porcine myofibrillar proteins by protease treatment. J Agric Food Chem 51:3661–3667
84. Mann B, Athira S, Sharma R, Kumar R, Sarkar P (2019) Bioactive peptides from whey proteins. In: Deeth HC, Bansad N (eds) Whey proteins—from milk to medicine. Academic, London, pp 519–547
85. Barras D, Widmann C (2011) Promises of apoptosis-inducing peptides in cancer therapeutics. Curr Pharm Biotechnol 12(8):1153–1165
86. Pepe G, Tenore GC, Mastrocinque R, Stusio P, Campiglia P (2013) Potential anticarcinogenic peptides from bovine milk. J Amino Acids 2013:1–7
87. Mader JS, Salsman J, Conrad DM, Hoskin DW (2005) Bovine lactoferricin selectively induces apoptosis in human leukemia and carcinoma cell lines. Mol Cancer Ther 4(4):612–624
88. Chen W, Ding H, Feng P, Lin H, Chou KC (2016) IACP: a sequence-based tool for identifying anticancer peptides. Oncotarget 7(13):16895
89. Gabernet G, Müller AT, Hiss JA, Schneider G (2016) Membranolytic anticancer peptides. Med Chem Commun 7(12):2232–2245
90. Chalamaiah M, Yu W, Wu J (2018) Immunomodulatory and anticancer protein hydrolysates (peptides) from food proteins: a review. Food Chem 245:205–222
91. Gaudel C, Nongonierma AB, Maher S, Flynn S, Krause M, Murray BA, Kelly PM, Baird AW, FitzGerald RJ, Newsholme PA (2013) Whey protein hydrolysate promotes insulinotropic activity in a clonal pancreatic β-cell line and enhances glycemic function in *ob/ob* mice. J Nutr 143(7):1109–1114
92. Nongonierma AB, Gaudel C, Murray BA, Flynn S, Kelly PM, Newsholme P, FitzGerald RJ (2013) Insulinotropic properties of whey protein hydrolysates and impact of peptide fractionation on insulinotropic response. Int Dairy J 32(2):163–168

93. Patil P, Mandal S, Tomar SK, Anand S (2015) Food protein-derived bioactive peptides in management of type 2 diabetes. Eur J Nutr 54(6):863–880
94. Kehinde BA, Sharma P (2018) Recently isolated antidiabetic hydrolysates and peptides from multiple food sources: a review. Crit Rev Food Sci Nutr 60(35):1–20
95. Power O, Nongonierma AB, Jakeman P, FitzGerald RJ (2014) Food protein hydrolysates as a source of dipeptidyl peptidase IV inhibitory peptides for the management of type 2 diabetes. Proc Nutr Soc 73(1):34–46
96. Nongonierma AB, FitzGerald RJ (2014) Susceptibility of milk protein-derived peptides to dipeptidyl peptidase IV (DPP-IV) hydrolysis. Food Chem 145:845–852
97. Lacroix IM, Li-Chan EC (2014) Isolation and characterization of peptides with dipeptidyl peptidase-IV inhibitory activity from pepsin-treated bovine whey proteins. Peptides 54:39–48
98. Tulipano G, Cocchi D, Caroli AM (2012) Comparison of goat and sheep beta-lactoglobulin to bovine beta-lactoglobulin as potential source of dipeptidyl peptidase IV (DPP-4) inhibitors. Int Dairy J 24(2):97–101
99. Lacroix IME, Li-Chan ECY (2012) Dipeptidyl peptidase-IV inhibitory activity of dairy protein hydrolysates. Int Dairy J 25(2):97–102
100. Liu R, Cheng J, Wu H (2019) Discovery of food-derived dipeptidyl peptidase IV inhibitory peptides: a review. Int J Mol Sci 20(3):463
101. Kahn SE, Cooper ME, Del Prato S (2014) Pathophysiology and treatment of type 2 diabetes: perspectives on the past, present, and future. Lancet (London, England) 383(9922): 1068–1083
102. Konrad B, Anna D, Marek S, Marta P, Aleksandra Z, Józefa C (2014) The evaluation of dipeptidyl peptidase (DPP)-IV, α-glucosidase and angiotensin converting enzyme (ACE) inhibitory activities of whey proteins hydrolyzed with serine protease isolated from Asian pumpkin (*Cucurbita ficifolia*). Int J Pept Res Ther 20(4):483–491
103. Lacroix IME, Li-Chan ECY (2013) Inhibition of dipeptidyl peptidase (DPP)-IV and α-glucosidase activities by pepsin-treated whey proteins. J Agric Food Chem 61(31):7500–7506
104. Wang R, Zhao H, Pan X, Orfila C, Lu W, Ma Y (2019) Preparation of bioactive peptides with antidiabetic, antihypertensive, and antioxidant activities and identification of α-glucosidase inhibitory peptides. Food Sci Nutr 7:1848–1856
105. Bougatef A, Nedjar-Arroume N, Ravallec-Plé R, Leroy Y, Guillochon D, Barkia A, Nasri M (2008) Angiotensin I-converting enzyme (ACE) inhibitory activities of sardinelle (*Sardinella aurita*) by-products protein hydrolysates obtained by treatment with microbial and visceral fish serine proteases. Food Chem 111(2):350–356
106. Pihlanto-Leppälä A (2000) Bioactive peptides derived from bovine whey proteins: opioid and ACE-inhibitory peptides. Trends Food Sci Technol 11(9–10):347–356
107. Pan D, Cao J, Guo H, Zhao B (2012) Studies on purification and the molecular mechanism of a novel ACE inhibitory peptide from whey protein hydrolysate. Food Chem 130(1): 121–126
108. García-Mora P, Martín-Martínez M, Bonache MA, González-Múniz R, Peñas E, Frias J, Martinez-Villaluenga C (2017) Identification, functional gastrointestinal stability and molecular docking studies of Lentil peptides with dual antioxidant and AngiotensinI converting enzyme inhibitory peptides. Food Chem 221:464–472
109. Daliri EB-M, Lee BH, Park B-J, Kim S-H, Oh D-H (2018) Antihypertensive peptides from whey proteins fermented by lactic acid bacteria. Food Sci Biotechnol 27(6):1781–1789
110. Sah BNP, Vasiljevic T, McKechnie S, Donkor ON (2017) Antioxidative and antibacterial peptides derived from bovine milk proteins. Crit Rev Food Sci Nutrition 58(5):726–740
111. Yeaman MR, Yount NY (2003) Mechanisms of antimicrobial peptide action and resistance. Pharmacol Rev 55(1):27–55
112. Choi H, Lee DG (2012) Synergistic effect of antimicrobial peptide arenicin-1 in combination with antibiotics against pathogenic bacteria. Res Microbiol 163(6–7):479–486

113. Seo MD, Won HS, Kim JH, Mishig-Ochir T, Lee BJ (2012) Antimicrobial peptides for therapeutic applications: a review. Molecules 17(10):12276–12286
114. Théolier J, Fliss I, Jean J, Hammami R (2014) Antimicrobial peptides of dairy proteins: from fundamental to applications. Food Rev Int 30(2):134–154
115. Demers-Mathieu V, Gauthier SF, Britten M, Fliss I, Robitaille G, Jean J (2013) Antibacterial activity of peptides extracted from tryptic hydrolyzate of whey protein by nanofiltration. Int Dairy J 28(2):94–101
116. Théolier J, Hammami R, Labelle P, Fliss I, Jean J (2013) Isolation and identification of antimicrobial peptides derived by peptic cleavage of whey protein isolate. J Funct Foods 5 (2):706–714
117. Kamau SM, Lu RR, Chen W, Liu XM, Tian FW, Shen Y, Gao T (2010) Functional significance of bioactive peptides derived from milk proteins. Food Rev Int 26(4):386–401
118. Mohanty D, Jena R, Choudhury PK, Pattnaik R, Mohapatra M, Saini MR (2016) Milk derived antimicrobial bioactive peptides: a review. Int J Food Prop 19(4):837–846
119. Zhang J, Zhang H, Wang L, Guo X, Wang X, Yao H (2009) Antioxidant activities of the rice endosperm protein hydrolysate: identification of the active peptide. Eur Food Res Technol 229(4):709–719
120. Conway V, Gauthier SF, Pouliot Y (2013) Antioxidant activities of buttermilk proteins, whey proteins, and their enzymatic hydrolysates. J Agric Food Chem 61(2):364–372
121. Sadat L, Cakir-Kiefer C, N'Negue MA, Gaillard JL, Girardet JM, Miclo L (2011) Isolation and identification of antioxidative peptides from bovine α-lactalbumin. Int Dairy J 21 (4):214–221
122. Contreras MM, Hernández-Ledesma B, Amigo L, Martín-Álvarez PJ, Recio I (2011) Production of antioxidant hydrolyzates from a whey protein concentrate with thermolysin: optimization by response surface methodology. LWT—Food Sci Tech 44(1):9–15
123. Hernández-Ledesma B, Amigo L, Recio I, Bartolomé B (2007) ACE-inhibitory and radical-scavenging activity of peptides derived from beta-lactoglobulin f(19–25). Interactions with ascorbic acid. J Agric Food Chem 55(9):3392–3397
124. Jiang B, Zhang X, Yuan Y, Qu Y, Feng Z (2017) Separation of antioxidant peptides from pepsin hydrolysate of whey protein isolate by ATPS of EOPO copolymer (UCON)/ Phosphate. Sci Rep 7(1):13320
125. Zhou DY, Zhu BW, Qiao L, Wu HT, Li DM, Yang JF, Murata Y (2012) In vitro antioxidant activity of enzymatic hydrolysates prepared from abalone (Haliotis discus hannai Ino) viscera. Food Bioprod Process 90(2):148–154
126. Corrochano AR, Buckin V, Kelly PM, Giblin L (2018) Invited review: whey proteins as antioxidants and promoters of cellular antioxidant pathways. J Dairy Sci 101(6):4747–4761
127. Santiago-López L, Hernández-Mendoza A, Vallejo-Cordoba B, Mata-Haro V, González--Córdova A (2016) Food-derived immunomodulatory peptides. J Sci Food Agric 96 (11):3631–3641
128. Gauthier SF, Pouliot Y, Saint-Sauveur D (2006) Immunomodulatory peptides obtained by the enzymatic hydrolysis of whey proteins. Int Dairy J 16(11):1315–1323
129. Wu W, Zhang M, Sun C, Brennan M, Li H, Wang G, Lai F, Wu H (2016) Enzymatic preparation of immunomodulatory hydrolysates from defatted wheat germ (*Triticum vulgare*) globulin. Int J Food Sci Tech 51(12):2556–2566
130. Jacquot A, Gauthier SF, Drouin R, Boutin Y (2010) Proliferative effects of synthetic peptides from β-lactoglobulin and α-lactalbumin on murine splenocytes. Int Dairy J 20 (8):514–521
131. Kiewiet MBG, Faas MM, de Vos P (2018) Immunomodulatory protein hydrolysates and their application. Nutrients 10(7):904–926
132. Kostyra E, Sienkiewicz-Szlapka E, Jarmolowska B, Krawczuk S, Kostyra H (2004) Opioid peptides derived from milk proteins. Polish J Food Nutr Sci 13(Suppl. 1):25–35

133. Liu Z, Udenigwe C (2018) Role of food-derived opioid peptides in the central nervous and gastrointestinal systems. J Food Biochem 43(1):e12629
134. Garg S, Nurgali K, Mishru VK (2016) Food proteins as source of opioid peptides—a review. Curr Med Chem 23(9):893–910